

REPRODUCIBILITY OF THE ORIGINAL PAGE IS POOR.

JPL Contract 953311

(NASA-CR-128337) OUTER PLANET ENTRY PROBE  
SYSTEM STUDY. VOLUME 2: SUPPORTING  
TECHNICAL STUDIES Final Report (Martin  
Marietta Corp.) Aug. 1972 519 p CSCL 22A

N72-33827

63/30

Unclas  
43497

# Outer Planet Entry Probe System Study

Final Report

**Volume II**  
**Supporting**  
**Technical Studies**

August 1972

JPL Contract 953311

Volume II

Supporting  
Technical  
Studies

August 1972

---

**OUTER PLANET  
ENTRY PROBE SYSTEM  
STUDY**

**FINAL REPORT**



**R. S. Wiltshire  
Program Manager**

**MARTIN MARIETTA CORPORATION  
P. O. Box 179  
Denver, Colorado 80201**



*Survivable Saturn Atmosphere Probe*

#### ACKNOWLEDGEMENTS

---

The following Martin Marietta Corporation, Denver Division, personnel participated in this study, and their efforts are greatly appreciated:

Raymond S. Wiltshire	Study Leader, Program Manager
Allen R. Barger	Science Integration
Eugene A. Berkery	Telecommunications, Data Handling, Power, and ACS, Lead
Dennis V. Byrnes	Navigation
Philip C. Carney	Mission Analysis
Patrick C. Carroll	Systems
Revis E. Compton, Jr.	Telecommunications
Robert G. Cook	Mechanical Design
Douglas B. Cross	Mission Analysis
Ralph F. Fearn	Propulsion
Robert B. Fischer	Mission Analysis
Thomas C. Hendricks	Mission Analysis
John W. Hungate	Systems, Lead
Carl L. Jensen	Thermal Analysis
Melvin W. Kuethe/ Rufus O. Moses	Mechanical/Structural/Probe Integration, Lead
Kenneth W. Ledbetter	Science, Lead
Paula S. Lewis	Mission Analysis
John R. Mellin	Structures
Jack D. Pettus	Data Link Analysis
Robert J. Richardson	Receiver Systems
Arlen I. Reichert	Propulsion
E. Doyle Vogt	Mission Analysis, Lead
Donald E. Wainwright	Systems
Clifford M. Webb	Thermal Analysis
Charles E. Wilkerson	Data Handling



## FOREWORD

---

This final report has been prepared in accordance with requirements of Contract JPL-953311 to present data and conclusions from a six-month study for the Jet Propulsion Laboratory by Martin Marietta Aerospace, Denver Division. The report is divided into the following volumes:

Volume I - Summary

Volume II - Supporting Technical Studies

Volume III - Appendixes

## CONTENTS

---

	<u>Page</u>
I. INTRODUCTION . . . . .	I-1
II. ENVIRONMENTAL MODELS . . . . .	II-1
A. Jupiter . . . . .	II-1
B. Saturn, Uranus, and Neptune Model Atmospheres . . . . .	II-7
C. RF Attenuation . . . . .	II-10
D. References . . . . .	II-14
III. SCIENCE INVESTIGATIONS . . . . .	III-1
A. Objectives and Questions . . . . .	III-1
B. Relevant Measurements and Performance Criteria . . . . .	III-2
C. Instruments and Measurement Techniques . . . . .	III-7
D. Entry and Descent Science Mission Analysis . . . . .	III-28
E. References . . . . .	III-32
IV. MISSION DESIGN CONSIDERATIONS . . . . .	IV-1
A. Mission Profile . . . . .	IV-3
B. Launch and Interplanetary Trajectories . . . . .	IV-4
C. Approach Orbit Determination . . . . .	IV-12
D. Planetary Encounter . . . . .	IV-24
E. Dispersion Analysis . . . . .	IV-37
F. Planetary Entry . . . . .	IV-48
G. Missions to Other Planets . . . . .	IV-60
H. References . . . . .	IV-69 and IV-70
V. JUPITER STUDIES . . . . .	V-1
A. Parametric Analysis . . . . .	V-1
B. Nominal Jupiter Probe System Definition . . . . .	V-121
C. Probe-Dedicated Alternative Jupiter Probe System Definition . . . . .	V-187
D. Spacecraft/Radiation/Compatible Jupiter Probe System Definition . . . . .	V-226 thru V-256
VI. SATURN STUDIES . . . . .	VI-1
A. Parametric Analysis . . . . .	VI-1
B. Saturn Probe System Definition . . . . .	VI-27 thru VI-61

VII.	URANUS STUDIES . . . . .	VII-1
A.	Parametric Analysis . . . . .	VII-1
B.	Saturn Probe Applicability for Uranus . . . . .	VII-18 thru VII-34
VIII.	NEPTUNE STUDIES . . . . .	VIII-1
A.	Science Analysis . . . . .	VIII-1
B.	Mission Analysis Parametrics . . . . .	VIII-3
C.	Neptune Parametric Analysis Summary . . . . .	VIII-6
IX.	PROGRAM EVALUATION . . . . .	IX-1
A.	Feasibility . . . . .	IX-1
B.	Commonality . . . . .	IX-17 thru IX-29

#### FIGURE

---

II-1	Pressure vs Temperature for the Jupiter Model Atmospheres . . . . .	II-2
II-2	Pressure vs Altitude for the Jupiter Model Atmospheres . . . . .	II-3
II-3	Equatorial Flyby Trajectories Workshop Nominal and Upper-Limit Proton Models . . . . .	II-6
II-4	Equatorial Flyby Trajectories Workshop Nominal and Upper-Limit Electron Models . . . . .	II-6
II-5	Pressure vs Temperature for Saturn Nominal Atmosphere . . . . .	II-7
II-6	Altitude Pressure Profile for Saturn Nominal Atmosphere . . . . .	II-8
II-7	Pressure vs Temperature for Uranus Nominal Atmosphere . . . . .	II-9
II-8	Pressure vs Temperature for Neptune Nominal Atmosphere . . . . .	II-9
II-9	Zenith Atmosphere Attenuation for Jupiter . . . . .	II-11
II-10	Zenith Attenuation for Saturn Nominal Atmosphere . . . . .	II-12
II-11	Zenith Attenuation for Uranus Nominal Atmosphere . . . . .	II-13
III-1	Digital Accelerometer System . . . . .	III-8
III-2	Accelerometer Electrical Interfaces . . . . .	III-12
III-3	Turbulence Accelerometer Measurements . . . . .	III-13
III-4	Viking-Derived Pressure Transducer . . . . .	III-14
III-5	Pressure Transducer Electrical Interconnection . . . . .	III-16
III-6	Viking Temperature Gage . . . . .	III-17
III-7	PAET Temperature Gage . . . . .	III-18
III-8	Temperature Gage Dimensions - Viking . . . . .	III-21

III-9	Temperature Gage Electrical Interface . . . . .	III-21
III-10	Mass Spectrometer Inlet System . . . . .	III-22
III-11	Typical Magnetic Sector Mass Spectrometer Mattauch-Herzog Geometry - Viking . . . . .	III-23
III-12	Quadrupole Mass Spectrometer Analyzer Schematic - PAET .	III-23
IV-1	Titan III/Centaur Performance Data . . . . .	IV-5
IV-2	Launch Energy Contours for Jupiter Missions . . . . .	IV-7
IV-3	$V_{HP}$ Variations with Arrival Date . . . . .	IV-10
IV-4	$V_{HP}$ Effects at Jupiter . . . . .	IV-11
IV-5	Optimization of Trip Time for 1979 Launch to Jupiter . .	IV-13
IV-6	Comparison of Launch Opportunities . . . . .	IV-13
IV-7	Impact Plane and Uncertainty Ellipse . . . . .	IV-15
IV-8	Geocentric Declination of Planets and Spacecraft . . . .	IV-19
IV-9	Approach Tracking at Saturn . . . . .	IV-22
IV-10	Relay Link Parameters . . . . .	IV-25
IV-11	Rotation Rate Matching at Planets . . . . .	IV-28
IV-12	Comparison of Deflection Modes for Nominal Jupiter Mission . . . . .	IV-32
IV-13	Comparison of Deflection $\Delta V$ Requirements . . . . .	IV-33
IV-14	Link and $\Delta V$ Requirements for Orbiter Missions . . . . .	IV-35
IV-15	Cone, Clock, and Cross-Cone Angles . . . . .	IV-39
IV-16	Spacecraft-Probe Look Direction Dispersions, Uranus Mission . . . . .	IV-39
IV-17	Dispersions Resulting from Different Measurement Types (Saturn/JST 77 Mission) . . . . .	IV-46
IV-18	Deceleration to Subsonic Speeds . . . . .	IV-52
IV-19	Typical Jupiter Entry Parametrics . . . . .	IV-53
IV-20	Jupiter Entry Decelerations . . . . .	IV-55
IV-21	Saturn Entry Decelerations . . . . .	IV-55
IV-22	Uranus Entry Decelerations . . . . .	IV-55
IV-23	Neptune Entry Decelerations . . . . .	IV-55
IV-24	Maximum Deceleration Comparisons for Jupiter, Saturn, Uranus and Neptune . . . . .	IV-56
IV-25	Maximum Dynamic Pressure Comparisons for Jupiter, Saturn, Uranus and Neptune . . . . .	IV-57
IV-26	Velocity Attitude Profile . . . . .	IV-58
IV-27	Interplanetary Trajectories for JS Missions . . . . .	IV-62
IV-28	Interplanetary Trajectories for JU Missions . . . . .	IV-63
IV-29	Interplanetary Trajectories for SUN Missions . . . . .	IV-64
IV-30	Jupiter Entry Geometry . . . . .	IV-65
IV-31	Saturn Entry Geometry . . . . .	IV-66
IV-32	Uranus Entry Geometry . . . . .	IV-67
IV-33	Neptune Entry Geometry . . . . .	IV-68
V-1	Program Parametric Analysis Flow Diagram . . . . .	V-1
V-2	Pressure Descent Profile Parametrics - Jupiter Cool/Dense Atmosphere . . . . .	V-3

V-3	Effects of Drogue Parachute and Staging	
	Pressure on Descent Profile . . . . .	V-4
V-4	Ballistic Coefficient and Instrument Sampling	
	Time Effects on Measurement Performance in	
	Cool/Dense Atmosphere . . . . .	V-6
V-5	Measurements per Kilometer Profiles for Various	
	Sampling Times - Cool/Dense Model . . . . .	V-7
V-6	Pressure Descent Profile Parametrics - Jupiter	
	Nominal Atmosphere . . . . .	V-9
V-7	Descent Times to Various Pressures in Both	
	Jupiter Model Atmospheres . . . . .	V-10
V-8	Ballistic Coefficient and Instrument Sampling	
	Time Effects on Measurement Performance in	
	Jupiter Nominal Atmosphere . . . . .	V-11
V-9	Effect of Flight Path Angle on Entry Time . . . . .	V-13
V-10	Entry Accelerometer Performance . . . . .	V-14
V-11	1972 Noise Figure State of the Art for Tunnel	
	Diodes and Transistor Amplifiers . . . . .	V-21
V-12	Spacecraft Recovery System Temperature . . . . .	V-22
V-13	RF Power Required vs Entry Flight Path Angle . . . . .	V-26
V-14	Spacecraft Antenna Requirements for	
	Point Design 8 . . . . .	V-27
V-15	Bit Error Probability . . . . .	V-31
V-16	Direct Earth Link Communications Geometry . . . . .	V-36
V-17	Data Handling Subsystem, General Purpose	
	Approach . . . . .	V-39
V-18	Data Handling Subsystem, Special Purpose	
	Approach . . . . .	V-41
V-19	Power and Pyrotechnic Subsystems . . . . .	V-43
V-20	ACS Block Diagram . . . . .	V-48
V-21	Probe Major Assemblies . . . . .	V-51
V-22	Jupiter Entry Loads . . . . .	V-52
V-23	Aeroshell Weights . . . . .	V-53
V-24	Aeroshell Weights . . . . .	V-54
V-25	Hypersonic Ballistic Coefficient vs	
	Aeroshell Radius . . . . .	V-55
V-26	Equipment Deck Weight vs Planetary Entry	
	Deceleration . . . . .	V-57
V-27	Descent Probe Outer Structure Weight vs	
	Planetary Entry Deceleration . . . . .	V-57
V-28	Base Cover Weight vs Entry Deceleration . . . . .	V-58
V-29	Main Parachute Diameter vs Ballistic Coefficient . . . . .	V-60
V-30	Main Parachute Weight vs Diameter . . . . .	V-61
V-31	Secondary Parachute Diameter vs Ballistic	
	Coefficient . . . . .	V-62
V-32	Secondary Parachute Weight vs Diameter . . . . .	V-63

V-33	Atmospheric Pressure Variations for Parachute Deployment . . . . .	V-65
V-34	Parachute Deployment Dispersions . . . . .	V-66
V-35	Heat Shield Mass Fraction vs Ballistic Coefficient and Initial Entry Angle . . . . .	V-67
V-36	Size Adjustment Factor . . . . .	V-67
V-37	Adjustment Factor for Entry Latitude and Entry from Orbit . . . . .	V-67
V-38	Solid Rocket Motors/Monopropellant Hydrazine Systems . . . . .	V-74
V-39	Total Motor Weight and Propellant Weight vs Probe Deflection Velocity . . . . .	V-78
V-40	Mission Phases and Events . . . . .	V-81
V-41	Probe Thermal Control Subsystem Design . . . . .	V-84
V-42	Jupiter Probe Equipment Temperature Limits . . . . .	V-86
V-43	Effects of Temperature on Battery Capacity . . . . .	V-87
V-44	Battery Dry Storage Charge Retention Characteristics . . . . .	V-87
V-45	Basic Cruise/Coast Thermal Model Schematic . . . . .	V-89
V-46	Cruise/Coast Thermal Radioisotope Heater Requirement . . . . .	V-91
V-47	Comparison of Cruise/Coast Parametric Probe Configuration . . . . .	V-92
V-48	Basic Descent Probe Thermal Model Schematic . . . . .	V-93
V-49	Minimum Compartment Probe Descent Temperature vs Insulation Thickness and Weight . . . . .	V-94
V-50	Comparison of Descent Parametric Probe Configurations . . . . .	V-96
V-51	Descent Thermal Analysis of Scaled Probe Configuration . . . . .	V-97
V-52	Descent Thermal Analysis of Vented Probe Configuration . . . . .	V-98
V-53	Instantaneous Probe Heat Leak . . . . .	V-100
V-54	Jupiter Atmospheric Models Temperature vs Descent Pressure . . . . .	V-101
V-55	Descent Thermal Analysis of Jupiter Cool/Dense and Nominal Atmosphere . . . . .	V-102
V-56	Descent Thermal Analysis of High Power RF Transmitter for 6 to 7 $R_J$ and Possible Direct-Link Communications . . . . .	V-103
V-57	Radiation Sensitivity to Latitude . . . . .	V-104
V-58	Typical Tolerance of Semiconductor Devices to Electron Irradiation . . . . .	V-106
V-59	Typical Tolerance of Semiconductor Devices to Proton Irradiation . . . . .	V-107
V-60	Bulk Radiation Effects on NPN Power Transistors at $10^{11}$ N/cm <sup>2</sup> . . . . .	V-109

V-61	Radiation Sensitivity of Thermosetting Resins . . . . .	V-111
V-62	Relative Radiation Stability of Elastomers . . . . .	V-112
V-63	Relative Radiation Resistance to Thermoplastic Resins . . . . .	V-113
V-64	Entry Probe Parts/Materials Evaluation Plan . . . . .	V-114
V-65	Weight vs Entry Angle . . . . .	V-117
V-66	RF Power vs Entry Angle . . . . .	V-117
V-67	Weight vs Latitude . . . . .	V-117
V-68	Radiation vs Latitude . . . . .	V-117
V-69	Pressure Depth for Science Objectives . . . . .	V-118
V-70	Pressure Depth vs RF Power . . . . .	V-118
V-71	Pressure Depth Impact on Thermal Control . . . . .	V-118
V-72	Spacecraft-Probe-Mission Candidates for the Titan IIIIE/Centaur/Burner II . . . . .	V-120
V-73	Time and Velocity vs Descent Radius . . . . .	V-124
V-74	Nominal Jupiter Probe Mission Description . . . . .	V-127
V-75	Pictorial Sequence of Events . . . . .	V-130
V-76	Functional Block Diagram for the Nominal Jupiter Probe . . . . .	V-133
V-77	Data Profile for the Nominal Jupiter Probe . . . . .	V-134
V-78	System Power Profile for the Nominal Jupiter Probe . . . . .	V-135
V-79	Probe-to-Spacecraft Communications Range for the Nominal Mission . . . . .	V-137
V-80	Nominal Jupiter Probe Aspect Angle . . . . .	V-138
V-81	End of Mission Attenuation for Jupiter Cool/Dense Atmosphere . . . . .	V-139
V-82	Relative Power Required for Jovian Descent, Nominal Probe . . . . .	V-140
V-83	Communications Functional Diagram . . . . .	V-143
V-84	Spacecraft Antenna Requirements for the Nominal Mission . . . . .	V-144
V-85	Acquisition/Tracking/Data/Spacecraft Receiver Diagram . . . . .	V-146
V-86	Jupiter Survivable Probe - Task I Configuration II . . . . .	V-153
V-87	Configuration Breakdown . . . . .	V-155
V-87a	Probe Descent . . . . .	V-161
V-88	Descent Probe Structure . . . . .	V-162
V-89	Aeroshell Structure . . . . .	V-164
V-90	Relationship of Ballistic Coefficient to Pressure Attitude at $M = 0.7$ . . . . .	V-166
V-91	Deflection Propulsion Motor . . . . .	V-171
V-92	Jupiter Probe Attitude Control System . . . . .	V-172
V-93	Launch to Descent Thermal History of the Nominal Jupiter Probe . . . . .	V-175

V-94	Radioisotope Heater Sizing Based on Probe Thermal Coating Selection . . . . .	V-177
V-95	Thermal Analysis Entry, Descent Power Profile for Nominal Jupiter Probe . . . . .	V-179
V-96	Nominal Jupiter Mission, Descent Temperature and Pressure Profiles . . . . .	V-180
V-97	MOPS Spacecraft/Jupiter Probe Integration . . . . .	V-182
V-98	Time and Velocity vs Descent Radius (Cool/Dense Atmosphere) . . . . .	V-190
V-99	Time and Velocity vs Descent Radius (Nominal Atmosphere) . . . . .	V-191
V-100	Probe-Dedicated Alternative Mission Description . . . . .	V-194
V-101	Data Profile for the Probe-Dedicated Jupiter Mission . . . . .	V-198
V-102	Power Profile for Probe-Dedicated Jupiter Mission . . . . .	V-200
V-103	Probe Aspect Angle for the Jupiter Probe- Dedicated Mission . . . . .	V-201
V-104	Spacecraft Antenna Requirements for the Jupiter Probe-Dedicated Mission . . . . .	V-203
V-105	Trajectory Geometry for the Jupiter Probe-Dedicated Mission . . . . .	V-206
V-106	Alternative Jupiter Probe-Dedicated Mission Configuration . . . . .	V-211
V-107	Attitude Control Subsystem . . . . .	V-216
V-108	Launch to Descent Thermal History of Probe- Dedicated Jupiter Mission Probe . . . . .	V-219
V-109	Launch to Descent Thermal History of Probe- Dedicated Jupiter Mission with Partially Sealed Probe Improved Thermal Control . . . . .	V-220
V-110	Launch to Descent Thermal History of Probe- Dedicated Jupiter Mission with Nitrogen Gas Partially Sealed Probe Improved Thermal Control . . . . .	V-221
V-111	Radioisotope Heater Sizing Based on Probe Thermal Coating Selection . . . . .	V-223
V-112	Probe-Dedicated Mission Descent Temperature and Pressure Profiles . . . . .	V-225
V-113	Radiation-Compatible Alternative Mission Definition . . . . .	V-229
V-114	Data Profile for Spacecraft-Radiation- Compatible Jupiter Mission . . . . .	V-233
V-115	Power Profile for Spacecraft-Radiation- Compatible Jupiter Mission . . . . .	V-233
V-116	Trajectory Geometry for the Spacecraft- Radiation-Compatible Mission . . . . .	V-239
V-117	Jovian Magnetosphere Noise Temperature Distance Geometry . . . . .	V-240



V-118	Radiation-Compatible Mission Noise Temperature . . . . .	V-242
V-119	Probe Definition of Spacecraft-Radiation-Compatible Jupiter Mission . . . . .	V-247
V-120	Launch to Descent Thermal History of Spacecraft-Radiation-Compatible Alternative Jupiter Probe . . . . .	V-254
V-121	Radioisotope Heater Sizing Based on Thermal Coating Selection Probe . . . . .	V-256
V-122	Spacecraft-Radiation-Compatible Alternative Mission Descent Temperature and Pressure Profiles . . . . .	V-254
VI-1	Saturn Pressure Descent Profile Parametrics . . . . .	VI-3
VI-2	Uranus Pressure Descent Profile Parametrics . . . . .	VI-4
VI-3	Descent Time for Saturn and Uranus vs Ballistic Coefficient . . . . .	VI-5
VI-4	Instrument Sampling Time Effects on Measurement Performance for Saturn and Uranus . . . . .	VI-6
VI-5	Saturn and Uranus Entry Accelerometer Performance . . . . .	VI-8
VI-6	End of Mission Attenuation for Saturn Nominal Atmosphere . . . . .	VI-12
VI-7	Spacecraft Receiving System Noise Temperature for Saturn Mission . . . . .	VI-13
VI-8	Probe-to-Spacecraft Communications Range for the Saturn Mission . . . . .	VI-15
VI-9	Saturn Probe Aspect Angle . . . . .	VI-16
VI-10	Spacecraft Antenna Requirements for the Saturn Mission . . . . .	VI-18
VI-11	Radioisotope Heater Requirement and Probe Coast Equilibrium Temperature for Saturn Probe . . . . .	VI-22
VI-12	Saturn Atmospheric Models Temperature vs Descent Pressure . . . . .	VI-23
VI-13	Nominal Saturn Mission Descent Temperature and Pressure Profiles . . . . .	VI-24
VI-14	Saturn Probe Descent Parametric Thermal Response . . . . .	VI-25
VI-15	Instantaneous Saturn Probe Atmospheric Heat Leak . . . . .	VI-26
VI-16	Saturn Mission Description . . . . .	VI-31
VI-17	Data Profile for Saturn Probe . . . . .	VI-35
VI-18	Power Profile for Saturn Probe . . . . .	VI-35
VI-19	Saturn Probe Configuration . . . . .	VI-41
VI-20	Alternative Saturn Probe Configuration . . . . .	VI-45
VI-21	Heat Shield Mass Fraction vs Entry Angle for Planet Saturn . . . . .	VI-48
VI-22	Heat Shield Mass Fraction vs Entry Angle for Planet Uranus . . . . .	VI-48

VI-23	Launch to Descent Thermal History of the Saturn Probe . . . . .	VI-55
VI-24	Mariner Jupiter Saturn Spacecraft . . . . .	VI-57
VI-25	Spacecraft Probe Integration Configuration . . . . .	VI-59
VII-1	End of Mission Attenuation for Uranus Nominal Atmosphere . . . . .	VII-4
VII-2	Spacecraft Receiving System Noise Temperature for the Uranus Mission . . . . .	VII-6
VII-3	Probe-to-Spacecraft Communications Range for the Uranus Mission . . . . .	VII-7
VII-4	Uranus Probe Aspect Angle . . . . .	VII-8
VII-5	Spacecraft Antenna Requirements for the Uranus Mission . . . . .	VII-9
VII-6	Uranus Atmospheric Models, Temperature vs Descent Pressure . . . . .	VII-13
VII-7	Radioisotope Heater Requirement and Probe Coast Equilibrium Temperature for the Uranus Probe . . . . .	VII-15
VII-8	Nominal Uranus Mission Descent Temperature and Pressure Profiles . . . . .	VII-15
VII-9	Uranus Probe Descent Parametric Thermal Response . . . .	VII-16
VII-10	Uranus Probe Instantaneous Battery Heating Requirement . . . . .	VII-17
VII-11	Uranus Probe Instantaneous Probe Atmospheric Heat Leak . . . . .	VII-17
VII-12	Uranus Mission Description . . . . .	VII-24
VII-13	Data Profile for the Uranus Probe . . . . .	VII-27
VII-14	Power Profile for the Uranus Probe . . . . .	VII-28
VII-15	Launch to Descent Thermal History of the Uranus Probe . . . . .	VII-34
VIII-1	Neptune Pressure Descent Profile . . . . .	VIII-2
VIII-2	Neptune Mission (JUN 79) . . . . .	VIII-4
IX-1	1972 Noise Figure State of the Art for Tunnel Diodes and Transistor Amplifiers . . . . .	IX-3
IX-2	Turnstile/Cone Descent Antenna . . . . .	IX-5

# TABLE

II-1	Cloud Locations in Various Model Atmospheres . . . . .	II-1
II-2	Workshop Radiation Fluences . . . . .	II-5
II-3	Artificial Radiation Environment . . . . .	II-5
III-1	Measurements Relevant to Objective . . . . .	III-2
III-2	Instruments Related to Measurements . . . . .	III-4
III-3	Performance Criteria . . . . .	III-4
III-4	Digital Accelerometer System Characteristics . . . . .	III-9
III-5	Pressure Gage Characteristics . . . . .	III-15
III-6	Temperature Gage Characteristics . . . . .	III-20
III-7	Neutral Mass Spectrometer Characteristics . . . . .	III-24
III-8	Isotopes and Hydrozen Compounds Less than 40 amu for Mass Spectrometer Analysis . . . . .	III-25
III-9	Properties of Lower Modeled Clouds . . . . .	III-31
III-10	Establishment of Design Limit Pressure . . . . .	III-31
IV-1	Summary of Reference Missions . . . . .	IV-2
IV-2	DSN Tracking Data Summary . . . . .	IV-17
IV-3	Planetary Ephemeris and Mass Uncertainties (1 $\sigma$ ) . . . .	IV-17
IV-4	Variation of Control Uncertainty with Jupiter Launch Date . . . . .	IV-20
IV-5	Control Uncertainties at Jupiter, Saturn, and Uranus for DSN Tracking Only . . . . .	IV-20
IV-6	Effect of QVLBI Measurement on Control Uncertainties . .	IV-21
IV-7	Effect of Optical Tracking on Control Uncertainties . .	IV-21
IV-8	Effect of Tracking Arc Length on Control Uncertainties Near Zero Declination . . . . .	IV-23
IV-9	Effect of Deflection Radius on Control Uncertainties . .	IV-24
IV-10	Comparison of Insertion $\Delta V$ Requirements . . . . .	IV-36
IV-11	Entry Dispersions (3 $\sigma$ ) for Execution Error Levels on Jupiter Nominal Mission . . . . .	IV-42
IV-12	Dispersion Contributions from Orbit Determination and Execution Errors . . . . .	IV-43
IV-13	Entry Dispersions as Functions of Deflection Radius . .	IV-44
IV-14	Entry Dispersions as Functions of Entry Angle . . . . .	IV-44
IV-15	Entry Dispersions as Functions of Deflection Mode . . .	IV-45
IV-16	Entry Dispersions as Functions of Navigation Types . . .	IV-46
IV-17	Entry Dispersions as Functions of Spacecraft Periapsis (Jupiter Nominal Mission) . . . . .	IV-47
IV-18	UD208 Input Data . . . . .	IV-48
IV-19	Ablative Mass Fractions . . . . .	IV-50
IV-20	Design Mission Entry Parameters . . . . .	IV-59
IV-21	Comparison of Planetary Constants . . . . .	IV-60
IV-22	Comparison of Planetary Encounters for Candidate Missions . . . . .	IV-61
V-1	Science Data Rates for Mission Variations . . . . .	V-21
V-2	Constraints for Program Parametric Point Designs . . . .	V-19

V-3	Telecommunication Subsystem Parameters for the Parametric Point Designs . . . . .	V-25
V-4	Original Probe Telemetry Design Control Table . . . . .	V-34
V-5	Probe Telemetry Design Control Table for Nominal Probe Direct Link . . . . .	V-35
V-6	Data Management Functional Requirements . . . . .	V-40
V-7	Tolerance Summary . . . . .	V-49
V-8	Jovian Entry Probe Base Heating . . . . .	V-68
V-9	Ablator Materials Considered and Properties . . . . .	V-70
V-10	Unit Weight of Ablator Required to Protect Base Cover Structure to 300°F Maximum during Planetary Entry . . . . .	V-70
V-11	Jupiter Probe Propulsion System Parameter Comparisons . . . . .	V-77
V-12	Mission Parametric Effects on Probe Propulsion System . . . . .	V-79
V-13	Launch Weights for Parametric Point Designs . . . . .	V-115
V-14	Pressure Depth vs RF Power . . . . .	V-119
V-15	Deflection Mode Velocity Requirements . . . . .	V-119
V-16	Nominal Instrument Characteristics (Viking-Derived) . . . . .	V-122
V-17	Nominal Jupiter Probe Instrument Sampling Times and Data Rates . . . . .	V-123
V-18	Nominal Descent Measurement Performance . . . . .	V-125
V-19	Nominal Jupiter Probe Mission Summary . . . . .	V-128
V-20	Nominal Jupiter Sequence of Events . . . . .	V-131
V-21	Nominal Jupiter Probe Weight Summary . . . . .	V-132
V-22	Probe Telemetry Link Design for the Nominal Jupiter Probe . . . . .	V-141
V-23	Telecommunications RF System for the Nominal Jupiter Probe . . . . .	V-145
V-24	Nominal DHS Sequence of Events . . . . .	V-148
V-25	Nominal Power Requirements . . . . .	V-150
V-26	Physical Characteristics of the Pyrotechnic Subsystem . . . . .	V-156
V-26a	Pyrotechnic Events . . . . .	V-161
V-27	Nominal Jupiter Probe Weight Breakdown . . . . .	V-167
V-28	MOPS Spacecraft Nominal Jupiter Probe Weight Breakdown . . . . .	V-186
V-29	Alternative Instrument Characteristics . . . . .	V-188
V-30	Alternative Jupiter Probe-Dedicated Instrument Sampling Times and Data Rates . . . . .	V-188
V-31	Alternative Descent Measurement Performance in Both Atmospheres . . . . .	V-192
V-32	Alternative Jupiter Probe-Dedicated Mission Summary . . . . .	V-195
V-33	Sequence of Events for Probe-Dedicated Jupiter Mission . . . . .	V-197

V-34	Weight Summary for Probe-Dedicated Jupiter Mission . . . . .	V-199
V-35	Probe Telemetry Link Design, Probe-Dedicated Jupiter Mission . . . . .	V-204
V-35a	Telecommunications RF Subsystem for the Probe Dedicated Mission . . . . .	V-205
V-36	System Noise Temperature for the Jupiter Probe-Dedicated Mission at 1 GHz . . . . .	V-207
V-37	Weight Breakdown for the Probe-Dedicated Alternative Jupiter Probe . . . . .	V-214
V-38	Radiation Compatible Alternative Jupiter Probe Instrument Sampling Times and Data Rates . . . . .	V-227
V-39	Radiation Compatible Alternative Mission Summary . . . . .	V-230
V-40	Sequence of Events for Spacecraft-Radiation-Compatible Jupiter Mission . . . . .	V-232
V-41	Weight Summary for Spacecraft-Radiation-Compatible Jupiter Mission . . . . .	V-234
V-42	Probe Telemetry Link Design, Spacecraft-Radiation-Compatible Jupiter Mission . . . . .	V-236
V-42a	Telecommunications RF Subsystem for the Spacecraft-Radiation-Compatible Jupiter Mission . . . . .	V-237
V-43	Weight Breakdown for Spacecraft-Radiation-Compatible Jupiter Probe . . . . .	V-249
VI-1	Probe Telemetry Link Design for the Saturn Probe . . . . .	VI-19
VI-2	Saturn Probe Instrument Sampling Times and Data Rates . . . . .	VI-29
VI-3	Saturn Probe Descent Measurement Performance . . . . .	VI-29
VI-4	Saturn Mission Summary . . . . .	VI-32
VI-5	Sequence of Events for the Saturn Probe . . . . .	VI-34
VI-6	Weight Summary for Saturn Probe . . . . .	VI-36
VI-7	Telecommunications RF Subsystem for the Saturn Mission . . . . .	VI-38
VI-8	Heat Pulse Ablator Analysis . . . . .	VI-49
VI-9	Unit Weight of Ablator Required to Protect Base Cover Structure to 300°F Maximum during Planetary Entry . . . . .	VI-49
VI-10	Weight Breakdown for the Saturn Probe . . . . .	VI-50
VII-1	Probe Telemetry Link Design for the Uranus Probe . . . . .	VII-11
VII-2	Uranus Probe Instrument Sampling Times and Data Rates . . . . .	VII-21
VII-3	Uranus Probe Descent Measurement Performance . . . . .	VII-22
VII-4	Uranus Mission Summary . . . . .	VII-25
VII-5	Sequence of Events for the Uranus Probe . . . . .	VII-27
VII-6	Uranus Probe Weight Summary . . . . .	VII-28
VII-7	Saturn/Uranus Probe Comparisons . . . . .	VII-29
VII-8	Telecommunications RF Subsystem for the Uranus Mission . . . . .	VII-31
VIII-1	Neptune Probe Descent Measurement Performance . . . . .	VIII-3

IX-1	EMR Transmitter Characteristics . . . . .	IX-2
IX-2	Attitude Control System Availability . . . . .	IX-12
IX-3	Thermal Control . . . . .	IX-14
IX-4	Mechanical Subsystem Components . . . . .	IX-14
IX-5	Deflection Propulsion Solid Propellant Motor . . . . .	IX-15
IX-6	GN <sub>2</sub> Cold Gas System Component Selection . . . . .	IX-15
IX-7	Comparison of Science Mission Characteristics . . . . .	IX-18
IX-8	Comparison of Similar Missions at Candidate Planets . .	IX-19
IX-9	Telecommunications Subsystem Characteristics . . . . .	IX-22
IX-10	Commonality Comparisons . . . . .	IX-25

## I. INTRODUCTION

---

This volume contains discussions of the technical studies and detailed descriptions of four different probe systems. The report is arranged to present the environment, science investigations, and general mission analysis considerations first, because these efforts establish the science and mission constraints that lead to system design criteria. These data are followed by discussions of the studies pertaining to the planets Jupiter, Saturn, Uranus, and Neptune. Except for Neptune, each planet discussion is divided into two parts: (1) parametric activities and (2) probe definition for that planet, or the application of a given probe for that planet. The Neptune discussion is limited to parametrics in the area of science and mission analysis. Each of the probe system definitions consists of system and subsystem details including telecommunications, data handling, power, pyrotechnics, attitude control, structures, propulsion, thermal control, and probe to spacecraft integration. The first configuration is discussed in detail and the subsequent configuration discussions are limited to the differences. Finally, the volume includes discussions of the hardware availability to support a probe system and commonality of science, missions, and subsystems for use at the various planets.

The organization of Volume I, Summary, is by topics similar to this volume which serves as a detailed reference to the summary volume.

## II. ENVIRONMENTAL MODELS

---

### A. JUPITER

#### 1. Jupiter Atmospheric Models

The Jupiter models used in this study were taken from Reference II-1, a NASA monograph written principally by T. N. Divine and F. D. Palluconi of the Jet Propulsion Laboratory. The statement of work specifies use of two models, specifically, the cool/dense and the nominal. Figure II-1 gives the pressure versus temperature profiles for each, showing that at 30 bars, the difference in temperature is 240°K. Also shown, is the location of the clouds, better specified by Table II-1. Figure II-2 completes the description by connecting pressure with altitude for each model.

Appendix E, Vol III, of this report gives a detailed breakdown of the components of each atmosphere, as well as computer listings of atmospheric parameters with a fine altitude resolution.

*Table II-1 Cloud Locations in Various Model Atmospheres*

ATMOSPHERE	CLOUD	PRESSURE RANGE, bars	
		CLOUD TOP	CLOUD BASE
Jupiter C/D	NH <sub>3</sub>	0.833	1.42
Jupiter C/D	H <sub>2</sub> O	10.0	32.3
Jupiter Nom	NH <sub>3</sub>	0.30	0.469
Jupiter Nom	H <sub>2</sub> O	1.80	2.76
Saturn Nom	NH <sub>3</sub>	0.727	1.12
Saturn Nom	H <sub>2</sub> O	3.94	6.92
Uranus Nom	CH <sub>4</sub>	0.49	0.93
Uranus Nom	NH <sub>3</sub>	4.80	6.69
Uranus Nom	H <sub>2</sub> O	32.2	48.4
Neptune Nom	CH <sub>4</sub>	1.43	3.47
Neptune Nom	NH <sub>3</sub>	17.1	22.8



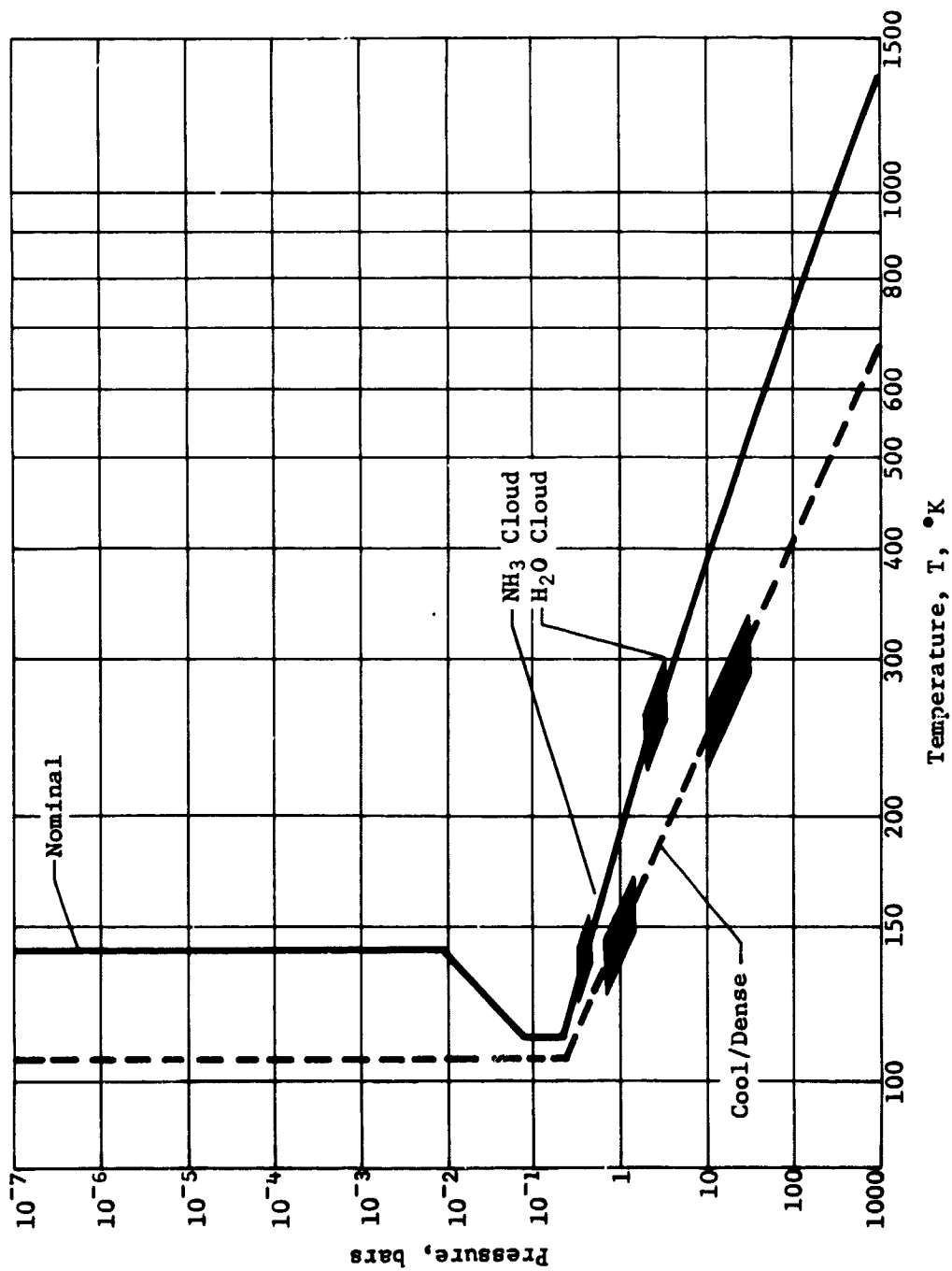


Figure II-1-1 Pressure vs Temperature for the Jupiter Model Atmospheres

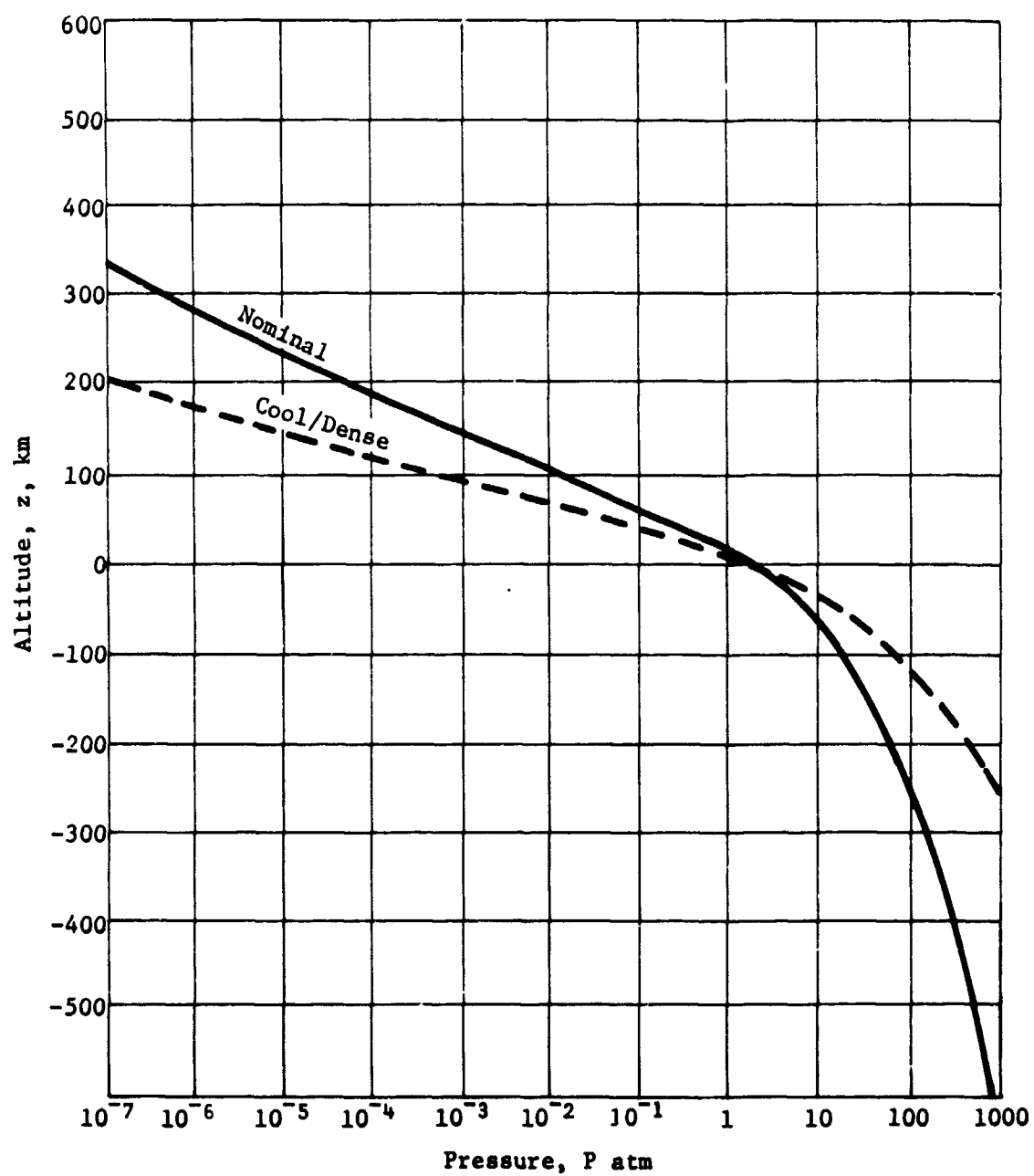


Figure II-2 Pressure vs Altitude for the Jupiter Model Atmospheres

## 2. Radiation

Jupiter proton and electron natural radiation environment models were generated by the Jupiter Radiation Belt Workshop in mid-summer 1971 and were recently updated as the Post Workshop Models which are unpublished. Six Jupiter missions, at inclinations ranging from  $3^\circ$  to  $87^\circ$ , were evaluated by JPL for both of these radiation models. The resulting proton and electron integrated radiation fluences for the workshop model are shown in Table II-2. Figures II-3 and II-4 (Ref II-1) show typical proton and electron fluences for a low inclination mission as a function of Jupiter radii, and the protection afforded by shielding up to 16 gram/cm<sup>2</sup>. From these figures, it is seen that at one Jupiter radius, shielding is relatively ineffective for probe application.

The spacecraft (S/C) and probe itself provide artificial radiation fields as a result of the radioisotope thermoelectric generators (RTGs), which are power sources on the S/C, and radioisotope heater units on the probe. Throughout the mission, the artificial devices emit gamma rays and energetic neutrons. The RTGs and the heaters on the probe impose artificial environments on the probe, as shown in Table II-3. Assuming 1 neutron = 0.5 protons, it is seen that the artificial radiation environment for a mission as long as 3180 days for Uranus is generally between the upper limit and nominal limit for the natural radiation environments.

Table II-2 Workshop Radiation Fluences

Jupiter Mission	Mission Description					Radiation Fluences, cm <sup>-2</sup>		
	Entry Angle, γ, deg	Latitude, deg	R <sub>p</sub> , km	Eccentricity	Arg of R <sub>p</sub> , deg	Inclination, deg	Electron (3 MeV Equiv)	
							Nominal	Upper Limit
1	-30	2.7	54,053	1.02974	183.8	3.32	1.25 × 10 <sup>11</sup>	6.73 × 10 <sup>11</sup>
2	-10	4.6	69,604	1.03854	171.1	9.55	1.39 × 10 <sup>11</sup>	7.38 × 10 <sup>11</sup>
3	-30	27.9	54,053	1.02974	169.5	29.93	3.84 × 10 <sup>10</sup>	2.11 × 10 <sup>11</sup>
4	-10	31.4	69,604	1.03854	166.5	72.18	3.75 × 10 <sup>9</sup>	1.95 × 10 <sup>10</sup>
5	-30	69.9	54,033	1.02734	50.8	87.19	2.82 × 10 <sup>10</sup>	1.67 × 10 <sup>11</sup>
6	-42.6	86.1	39,229	1.01996	3.1	87.19	9.93 × 10 <sup>5</sup>	2.53 × 10 <sup>8</sup>
							5.28 × 10 <sup>8</sup>	3.18 × 10 <sup>11</sup>

Table II-3 Artificial Radiation Environment

Radiation Source	Dose Rates		Dose for Jupiter Mission		Dose for Saturn Mission		Dose for Uranus Mission	
	Gamma, rad/hr	Neutrons, n/cm <sup>2</sup> /sec	Gamma, rad	Neutrons, n/cm <sup>2</sup>	Gamma, rad	Neutrons, n/cm <sup>2</sup>	Gamma, rad	Neutrons, n/cm <sup>2</sup>
Pioneer RTGs	1 × 10 <sup>-2</sup>	3.6 × 10 <sup>2</sup>	1.6 × 10 <sup>2</sup>	2.1 × 10 <sup>10</sup>	3 × 10 <sup>2</sup>	3.9 × 10 <sup>10</sup>	5.7 × 10 <sup>2</sup>	7.4 × 10 <sup>10</sup>
TOPS RTGs	5.6 × 10 <sup>-2</sup>	2 × 10 <sup>3</sup>	9.1 × 10 <sup>2</sup>	1.2 × 10 <sup>11</sup>	1.7 × 10 <sup>3</sup>	2.2 × 10 <sup>11</sup>	3.2 × 10 <sup>3</sup>	4.1 × 10 <sup>11</sup>
MOPS RTGs	4.9 × 10 <sup>-2</sup>	1.7 × 10 <sup>3</sup>	8 × 10 <sup>2</sup>	1 × 10 <sup>11</sup>	1.5 × 10 <sup>3</sup>	1.9 × 10 <sup>11</sup>	2.8 × 10 <sup>3</sup>	3.5 × 10 <sup>11</sup>
Probe Heaters	--	1.2 × 10 <sup>3</sup>	--	7.1 × 10 <sup>10</sup>	--	1.3 × 10 <sup>11</sup>	--	2.5 × 10 <sup>11</sup>
Spacecraft data calculated from North American Rockwell Report SD 71-770, November 1971. Jupiter Mission = 680 days; Saturn Mission = 1261 days; Uranus Mission = 2386 days.								

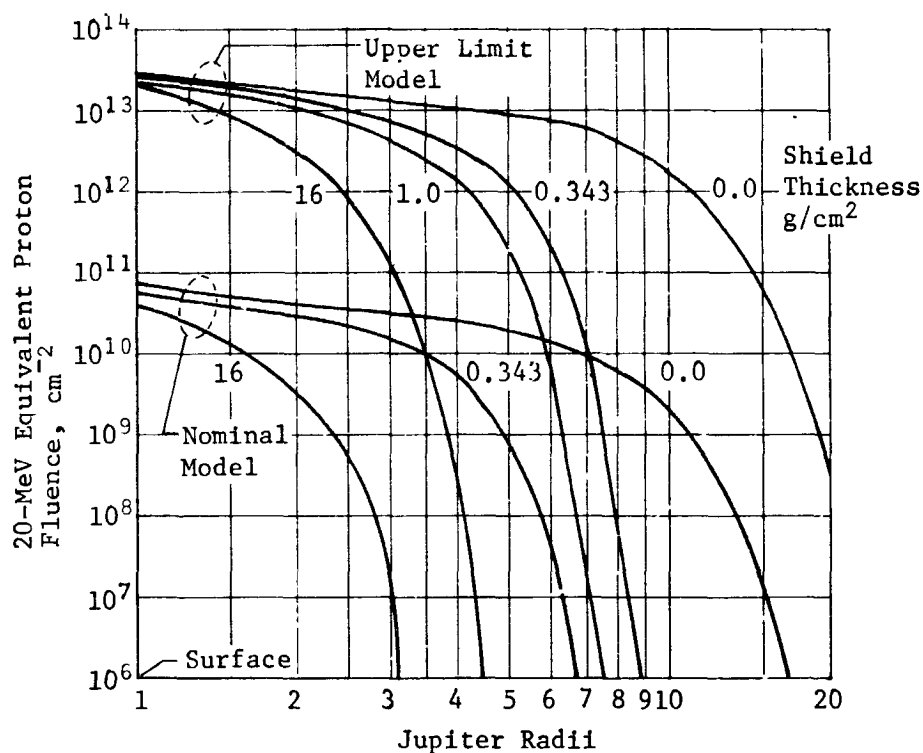


Figure II-3 Equatorial Flyby Trajectories Workshop  
Nominal and Upper-Limit Proton Models

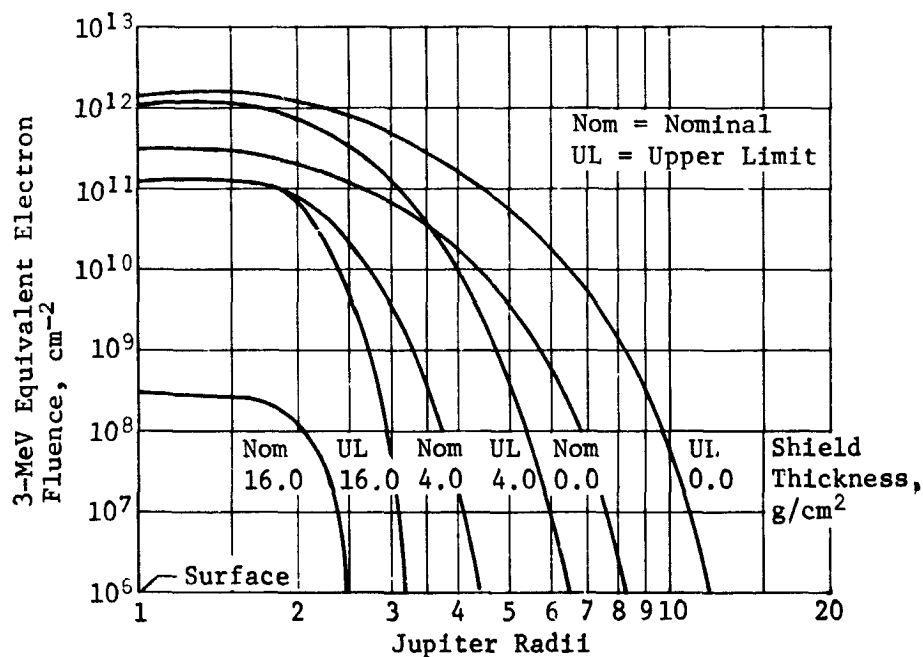


Figure II-4 Equatorial Flyby Trajectories Workshop  
Nominal and Upper-Limit Electron Models

B. SATURN, URANUS, AND NEPTUNE MODEL ATMOSPHERES

The models for the atmospheres of Saturn, Uranus, and Neptune were taken from the NASA monographs, References II-3 and II-4. Only the nominal model for each atmosphere was specified by the statement of work. Figures II-5 through II-8 show temperature versus pressure profiles for each planet, and a pressure versus altitude graph for Saturn. Cloud locations are shown on the plots and are also detailed in Table II-1.

Appendix E, Vol III, of this report gives a detailed breakdown of the atmospheric constituents, as well as computer listings of atmospheric parameters with a fine altitude resolution.

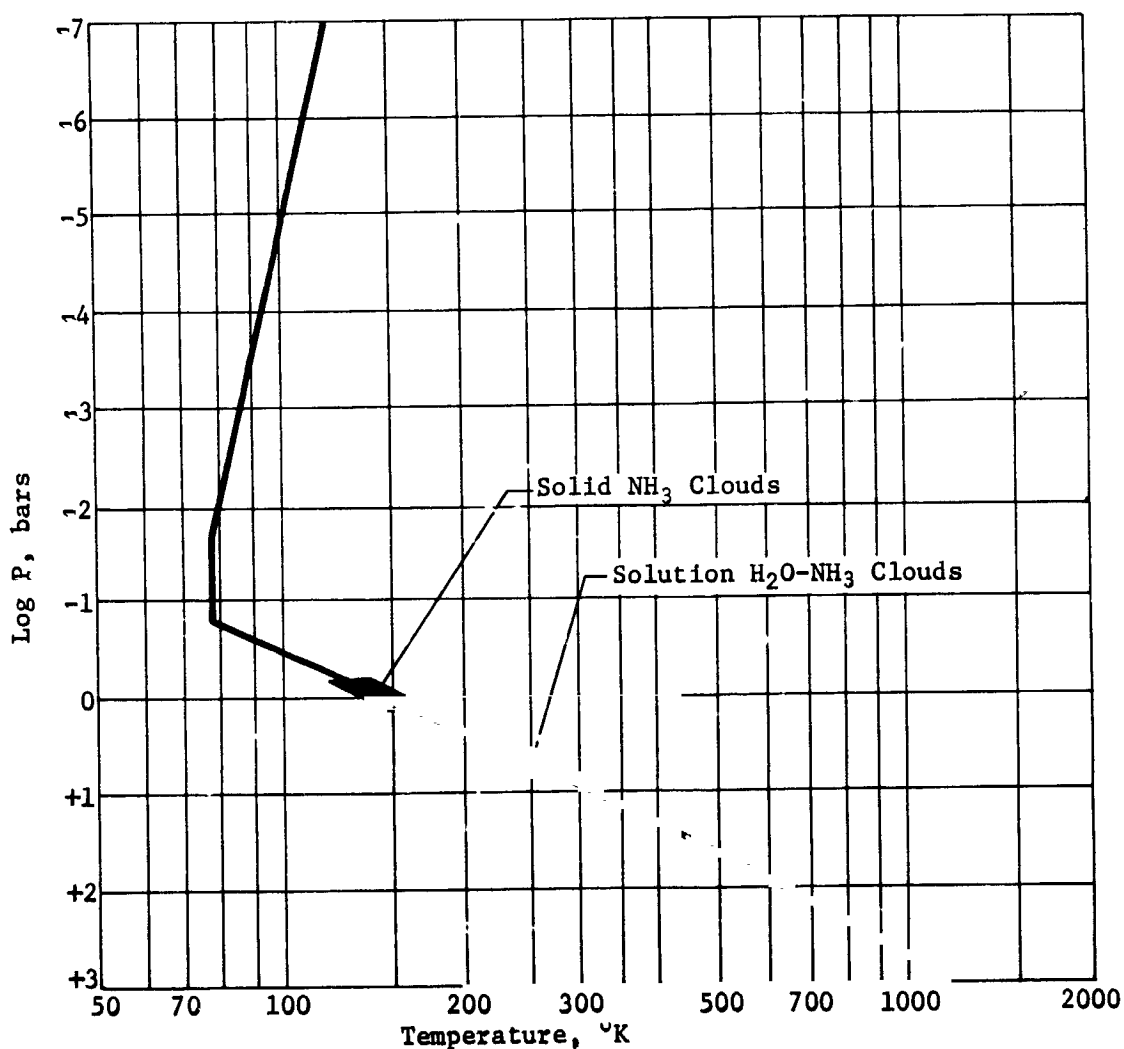


Figure II-5 Pressure vs Temperature for Saturn Nominal Atmosphere

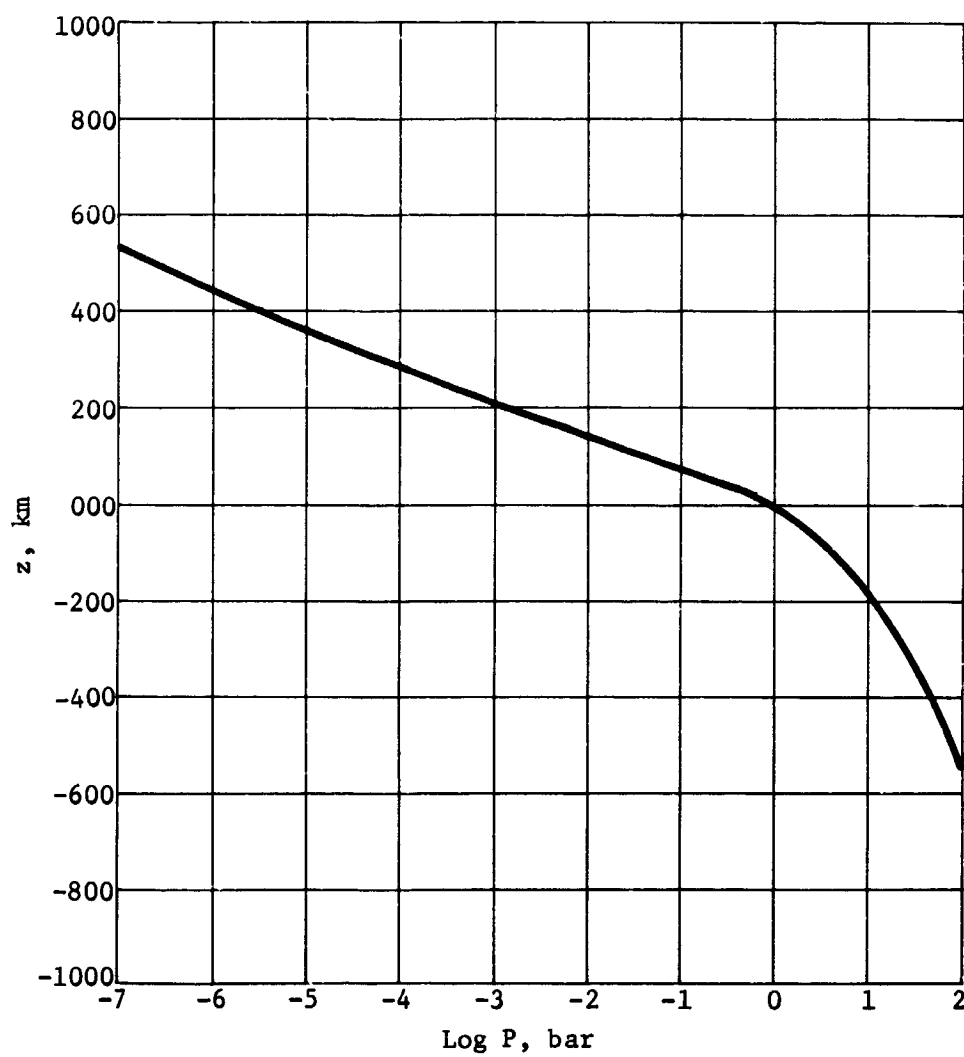


Figure II-6 Altitude Pressure Profile for Saturn Nominal Atmosphere

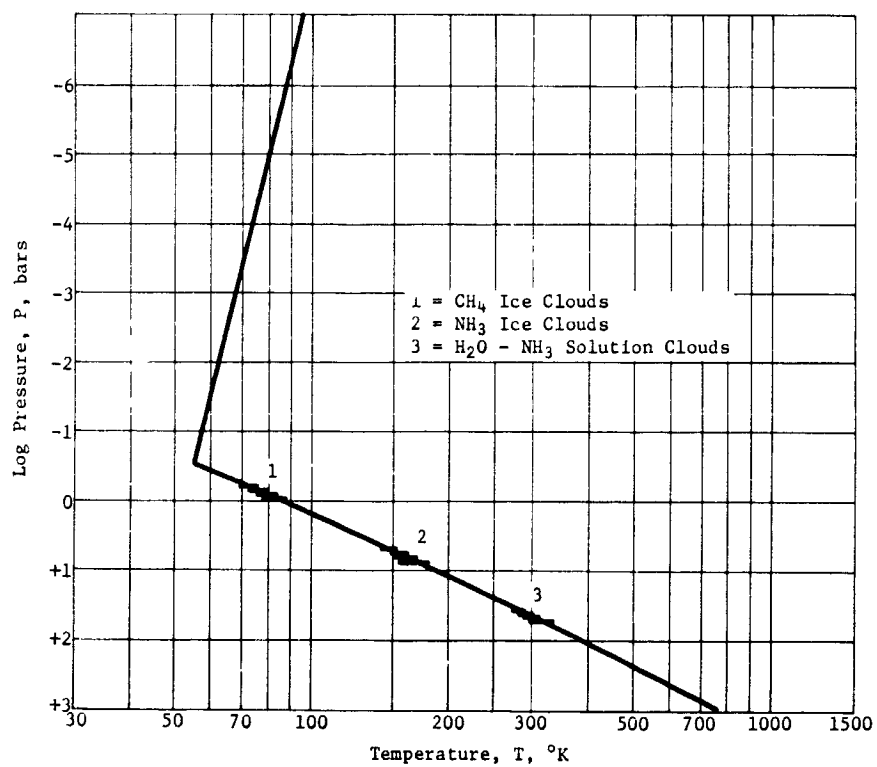


Figure II-7 Pressure vs Temperature for Uranus Nominal Atmosphere

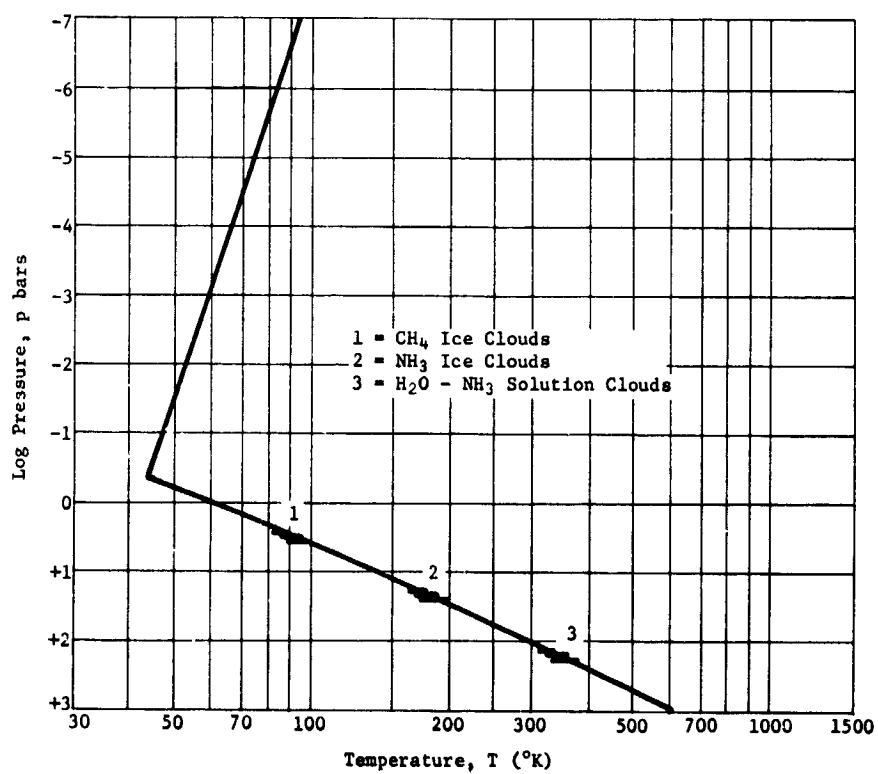


Figure II-8 Pressure vs temperature for Neptune Nominal Atmosphere



### C. RF ATTENUATION

The techniques used to determine microwave losses in the planet atmosphere are basically those used on the previous contract (Ref II-5). Improvements have been made to some of the calculations; details are described in Vol III, Appendix A. Only the results are summarized here.

The atmospheres of the three planets are very similar in content, being composed primarily of hydrogen and helium. The main sources of absorption are pressure broadening of absorption lines in the polarizable gasses (ammonia and water) and absorption in the clouds. Absorption is a function of elevation, look vector aspect angle, and the operating frequency. A second source of RF signal loss is defocusing loss caused by ray refraction in the dense atmosphere. Defocusing loss is independent of frequency but is a function of the aspect angle. Defocusing losses for the three planets of interest are very small ( $< 0.5$  dB), since all missions use axial beam antennas during descent and the trajectory is designed to minimize the probe aspect angle to  $20^\circ$  or less. The total attenuation from the planet atmosphere is the sum of absorption and defocusing loss.

Zenith attenuation for the three planets is shown in Figures II-9 through II-11. As seen in Figure II-9, RF loss for the nominal atmosphere is quite low compared to the cool/dense atmosphere with the 30 bars nominal curve coincident with the 10 bars cool/dense curve. Total loss increases approximately as  $\sec \psi$  for aspect angles away from zenith, up to  $20^\circ$ . For a depth of 7 bars atmosphere loss for Saturn is slightly greater than for Uranus. Comparison of Figures II-10 and II-11 indicates the similarity of atmosphere loss. For depths greater than 20 bars, Uranus has the greater loss, but below that depth Saturn's loss is slightly greater.

Atmosphere attenuation is the major loss factor in the RF link during descent and, as seen from the curves, can be quite high if the design depth and RF frequency are high. In order to have atmosphere effects minimized, the depth, aspect angle, and frequency must be kept to minimum values. Each mission was designed with this fact in mind in order to have missions optimized from the standpoint of RF power required and still achieve the science objectives.

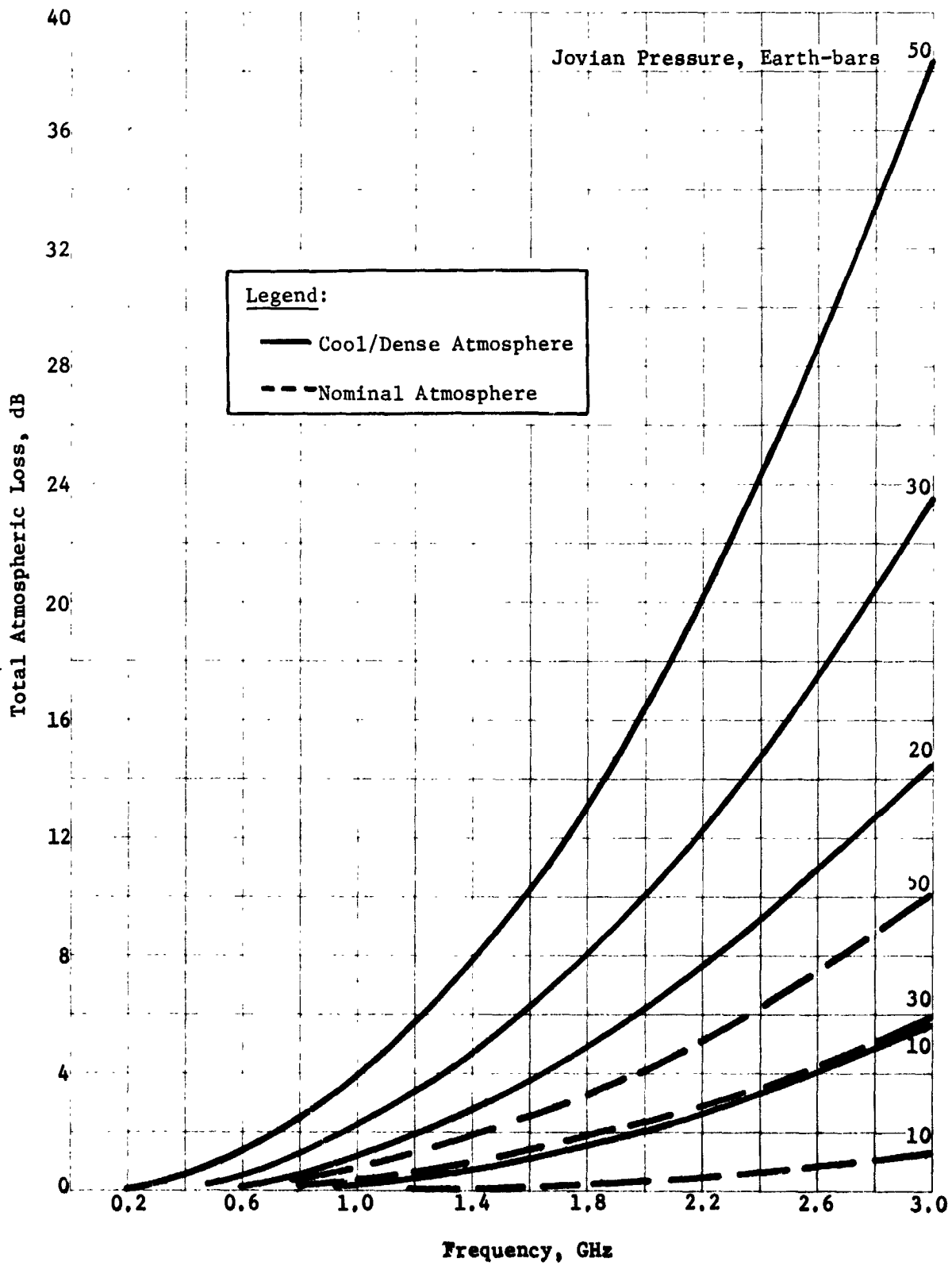


Figure II-3 Zenith Atmosphere Attenuation for Jupiter

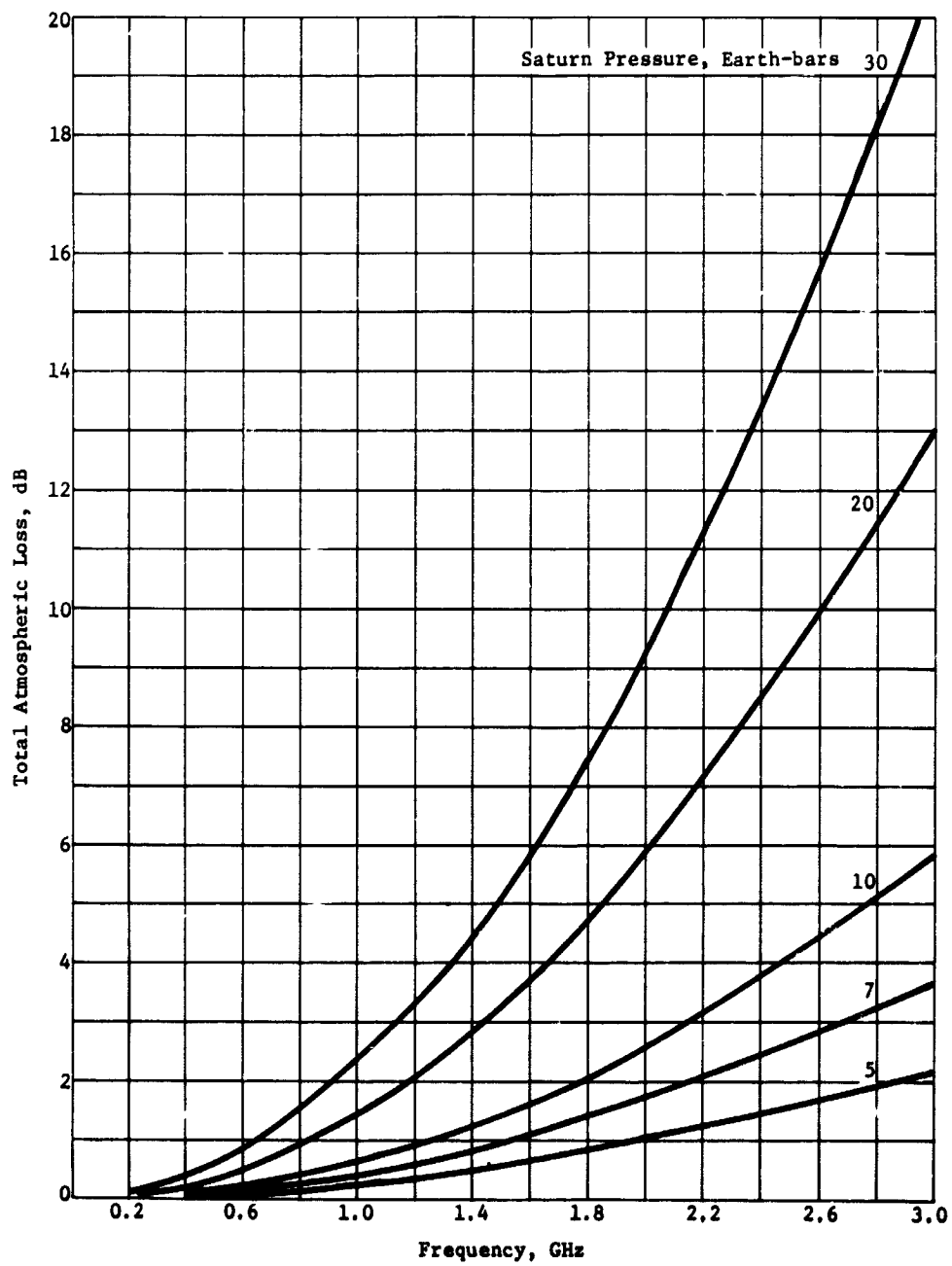


Figure II-10 Zenith Attenuation for Saturn Nominal Atmosphere

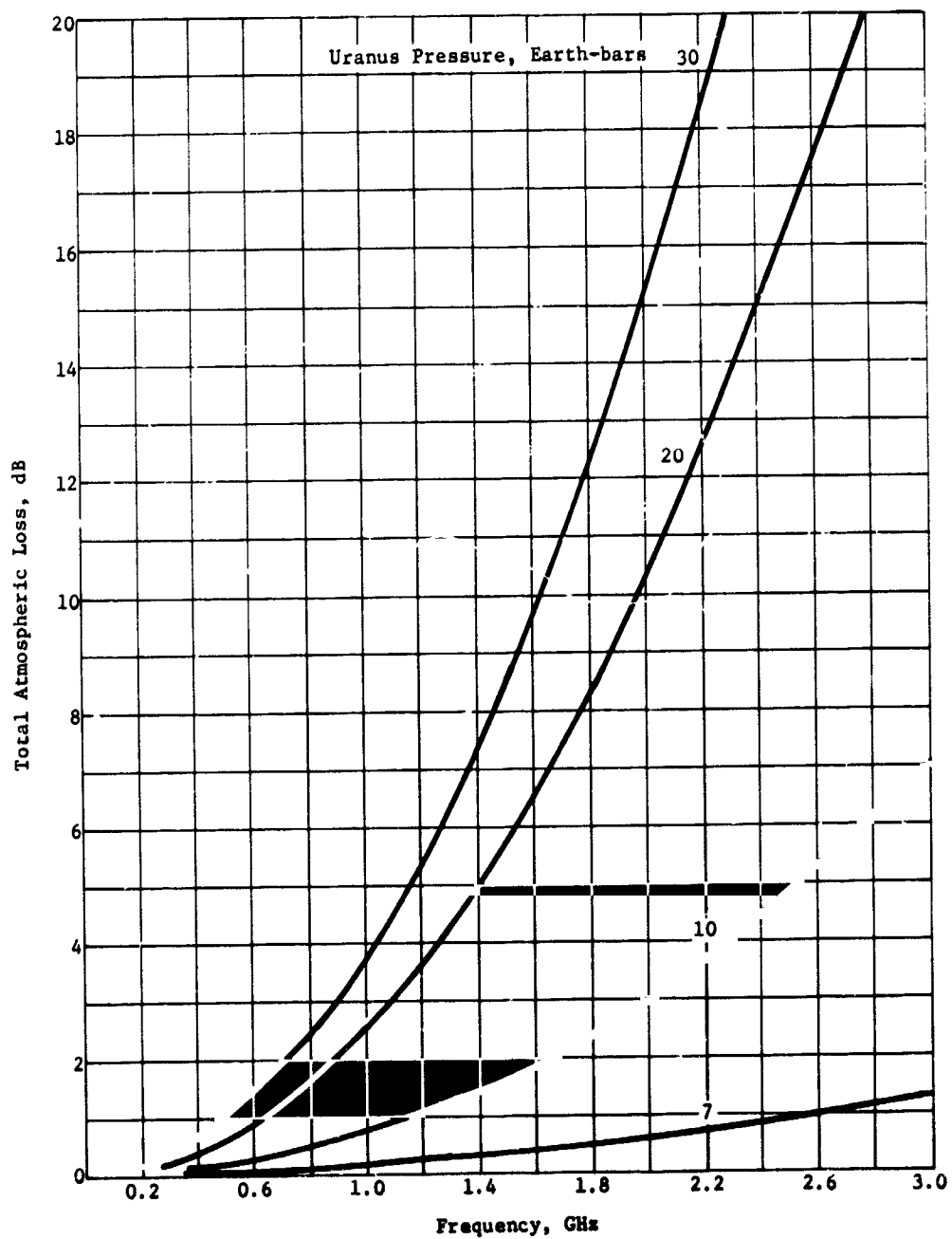


Figure II-11 Zenith Attenuation for Uranus Nominal Atmosphere

D. REFERENCES

- II-1. *The Planet Jupiter (1970)*. NASA Space Vehicle Design Criteria (Environment) NASA SP-8069, August 1971.
- II-2. R. H. Parker: *Interim Report on Jupiter Radiation Belt Workshop*. JPL Interoffice Memo, July 23, 1971.
- II-3. *The Planet Saturn (1970)*. NASA Space Vehicle Design Criteria (Environment), Preliminary Copy, October 1970.
- II-4. F. D. Palluconi: *Preliminary Model Atmospheres for the Planets Uranus and Neptune*. JPL Section Document 131-17, November 4, 1971.
- II-5. S. J. Ducsai, Program Manager: *Jupiter Atmospheric Entry Mission Study, Final Report*, Martin Marietta Corporation Report No. 71-1, JPL Contract 952811, April 1971.

## 1.1. SCIENCE INVESTIGATIONS

The science instrument payload was specified by JPL at the beginning of the study to be the SAG Exploratory payload consisting of 4 instrument types: a neutral mass spectrometer, temperature gauge, pressure gauge, and accelerometer triad (Ref III-1). The primary science activities during the course of the study were to: (1) establish measurements and performance criteria consistent with this payload, based upon data from the previous study (Ref III-2) and discussions with consulting scientists; (2) provide specific instrument characteristics to subsystem areas and to establish the word content of each instrument measurement and interface with the data handling system; (3) determine the descent profiles and instrument sequencing and evaluate the measurement performance with respect to the criteria.

### A. OBJECTIVES AND QUESTIONS

The primary objective of a first generation survivable probe to a Jovian planet is to penetrate the atmosphere to a depth sufficient to obtain representative reliable measurements of the bulk composition. For this study, this was specified to be at least 2 bars of pressure and, if possible, down to 30 bars. Actually, the design pressure limit for end of mission for fixed objectives varies with the model atmosphere.

The basic science questions that the nominal probe mission will attempt to answer were taken from the previous study (Ref III-2) which referenced a JPL document (Ref III-3). These questions are

- 1) What are the relative abundances of hydrogen, deuterium, helium, neon, and other elements, and what are their isotopic compositions?
- 2) What are the present-day atmospheric composition and altitude profiles of pressure, temperature, and density, and what effect do they have on the radiation balance?
- 3) What are the chemical composition and vertical distribution of the clouds?
- 4) What is the level of turbulence in the atmosphere?

From these questions, a set of measurements can be defined to provide answers.

B. RELEVANT MEASUREMENTS AND PERFORMANCE CRITERIA

1. Relevant Measurements

To obtain satisfactory answers to the basic science questions by means of the SAG Exploratory instruments, a list of seven measurements of observables is presented in Table III-1.

*Table III-1 Measurements Relevant to Objectives*

- 1) Determine the relative abundances of H and He in the lower atmosphere (below the turbopause).
- 2) Determine the isotopic ratios H/D,  $\text{He}^3/\text{He}^4$ ,  $\text{Ne}^{20}/\text{Ne}^{22}$ ,  $\text{C}^{12}/\text{C}^{13}$ ,  $\text{Ar}^{36}/\text{Ar}^{40}$  and others in the lower atmosphere.
- 3) Determine the concentration profiles of the minor atmospheric constituents, particularly Ne, A,  $\text{CH}_3$ ,  $\text{CH}_4$ ,  $\text{NH}_3$ , and  $\text{H}_2\text{O}$ , down to the design limit.
- 4) Determine the temperature versus pressure and time profiles from above the cloud tops down to the design limit with sufficient precision to determine whether the lapse rate is adiabatic.
- 5) Determine the atmospheric mean molecular weight and identify the major contributing gases.
- 6) Obtain an indication of the vertical distribution and structure of the cloud layers with respect to pressure and temperature, and the chemical composition of each layer.
- 7) Obtain an indication of the magnitude and frequency of any atmospheric turbulence from above the cloud tops down to the design limit.

In general, there is no exact one-to-one correspondence between the questions and observable measurements. Some questions require many kinds of measurements, while a single measurement may contribute to several questions. The questions themselves are strongly interrelated and an answer to one requires at least a partial answer to others.

The first four measurements listed in the table are those that determine the bulk composition and general atmospheric properties. They can be measured directly by the exploratory instruments, and thus are the primary measurements. Included in these measurements are the abundances of total hydrogen and helium to give the important H/He ratio, as well as abundance measurements for several isotopes in the 1 to 40 amu mass spectrometer range. The mass spectrometer also will be set to detect minor constituent compounds, which will be measured down to the design pressure limit. Also included are measurement profiles of pressure and temperature made by the respective gauges from cloud tops to the design pressure limit. The temperature measurement is required to determine the lapse rate in the atmosphere.

Table III-2 shows the relation of the instruments to the measurements in terms of direct or related measurements. The first four measurements are the only ones that can be taken directly. The fifth measurement, that of determining the mean molecular weight of the bulk atmosphere, can be accomplished primarily from mass spectrometer data with assistance from the other instruments; it is also a primary measurement.

The last two measurements cannot be directly made by any of the exploratory payload instruments, but indications can be obtained by all the instruments; these measurements are considered secondary. Variations that may occur in temperature and pressure, as the probe passes through a cloud layer, will be detected as will the mass spectrometer measurements of the constituents that compose the cloud. Thus, an indication of cloud structure can be obtained.

The primary function of the accelerometer triad is to measure decelerations that occur during the entry phase of the mission, but the dynamic range of the instrument can be selected such that it will also measure the large-scale turbulence magnitudes in the descent phase of the mission. The accelerometers will directly measure turbulence but this is shown to be a related measurement in Table III-2 because they may not be able to obtain detailed small scale turbulence, resulting in a gross overall turbulence analysis. Temperature and pressure readings that may vary with turbulence will also be used.

## 2. Performance Requirements

For the relevant measurements to be useful for mission design and evaluation, criteria must be established with which the instrument performance can be compared to assure that the particular design will satisfy the objectives. Both depth of penetration (pressure) and number of measurements are important. Table III-3 presents



Table III-2 Instruments Related to Measurements

INSTRUMENT MEASUREMENT	TEMPERATURE GAUGE	PRESSURE GAUGE	ACCELEROMETER TRIAD	NEUTRAL MASS SPECTROMETER
H/He Ratio	R	R	R	D
Isotopic Ratios	N	N	N	D
Minor Constituents	R	R	N	D
Temperature/Pressure	D	D	R	R
Mean Molecular Weight	R	R	R	R
Cloud Layering	R	R	R	R
Turbulence	R	R	R	N
D = Direct Measurement				
R = Related Measurement				
N = Little or No Relation				

Table III-3 Performance Criteria

MEASUREMENT	PRESSURE DEPTH	MINIMUM SAMPLING REQUIRED
H/He Ratio	1 bar Minimum	4 Measurements at Different Pressures
Isotopic Ratios	1 bar Minimum	4 Measurements at Different Pressures
Minor Constituents	To Design Limit	2 Per Scale Height below Cloud Tops
Temperature	To Design Limit	1 Per °K
Pressure	To Design Limit	2 Per Kilometer below Cloud Tops
Mean Molecular Weight	5 bars Minimum	4 Measurements at Different Pressures
Cloud Layering	To Design Limit	2 Measurements Inside Each Cloud
Turbulence	To Design Limit	1 Per Kilometer below Cloud Tops

the established criteria for each measurement. These were influenced by the previous study (Ref III-2), the JPL Assessment Report (Ref III-4), and discussions with a panel of science consultants which included Dr. Richard Goody, Dr. Donald Hunten, Dr. Michael McElroy, Dr. Robert Vogt, Mr. Harvey Allen, Dr. George Wetherill, and Dr. Alan Barrett.

The mass spectrometer has three separate constraints imposed upon its measurements, one of which will govern the design. For the H/He ratio, isotopic ratios, and mean molecular weight determination, four measurements are required with the stipulation that they be at slightly different pressures over the first few bars of descent pressure. This is primarily for redundancy, but also to enable determination of any major variation with altitude, if it occurs. Secondly, to enable measurement of the minor constituents, a sampling of at least two measurements per scale height from the top of the first cloud down to the design limit is required. In addition, the mass spectrometer measurements of minor constituents will give information on cloud composition; thus there should always be two (for redundancy) full 1-40 amu sweeps while the probe is inside each cloud in all the model atmospheres.

The temperature gage has a requirement to determine the temperature profile as the probe descends. To obtain a detailed profile, the panel of science consultants agreed that one measurement/°K would be sufficient. However, the desire is also to be able to accurately determine the lapse rate in the atmosphere. To do this may require the temperature measurements to have a relative accuracy of 1% of the vertical temperature gradient (0.02 °K/km for Jupiter) as well as an absolute accuracy of 1% of the value.

The accelerometers will obtain entry deceleration data, and measure large-scale turbulence. The technique for this is discussed in the Section C, however, the criterion given here is for the descent measurements, and is to complete one turbulence measurement every kilometer below cloud tops. At Saturn, Uranus, and Neptune the turbulence is not expected to be as significant as for Jupiter.

For the pressure measurement, the criterion is to make two measurements/km below the top of the first modeled cloud, which is between 0.3 and 0.84 bars in all models. In addition to determining pressure descent profiles, the pressure transducers may

be able to detect turbulence; thus the one measurement/km also applies, although overruled by the first requirement. Also, both the pressure and temperature gages are required to make a minimum of two measurements inside each cloud, but this too is satisfied by the former requirements.

### 3. Targeting Considerations

a. *General* - For a first generation entry probe into any of the Jovian planets, the entry site on the planet should be selected such that it is both relevant to the desired objectives and typical of the planet as a whole in order to permit extrapolation of the results to other locations. The lack of optical or ionospheric instruments simplifies the landing site selection considerations for all of the outer planets, making lightside or darkside entries essentially equivalent, with the exception of Uranus, which will be discussed later. However, it would be unacceptable to enter exactly on the terminator because the processes occurring here may cause atmospheric variations that the instruments could not separate from normal conditions. Thus, a corridor 6° wide centered on the terminator should be avoided.

b. *Jupiter* - In addition to the above, the Great Red Spot of Jupiter should be avoided as atypical. It would be desirable to avoid shear layers and very high velocity turbulence by entering at a quiescent site. In general, these exist at the center of a zone or belt. The belts shift in latitude from year to year but the average latitudes for the centers are:

North or South Equatorial Current	$\pm 4^\circ$
North Equatorial Belt	$+ 12^\circ$
North Component of South Equatorial Belt	$- 10^\circ$
North or South Temperate Belt	$\pm 30^\circ$

c. *Saturn* - Here avoidance of the rings may cause a few sites to be unattainable. The only belt on the planet that appears discernable is a light one that has its center at about 15° N latitude. Actually, any latitude on the planet is acceptable.

d. *Uranus* - Since this planet is inclined 98° to its orbital plane and because it currently (and for the next ~ 15 years) has its north pole pointing in the general direction of the Sun, all of

the solar energy input is in the northern hemisphere. This means that a large gradient in conditions probably exists between light-side and darkside; thus entry sites on the lightside at least  $20^\circ$  from the terminator are desirable. No other constraints exist because belts are not discernable.

e. *Neptune* - No constraints exist on entry sites except to avoid the terminator.

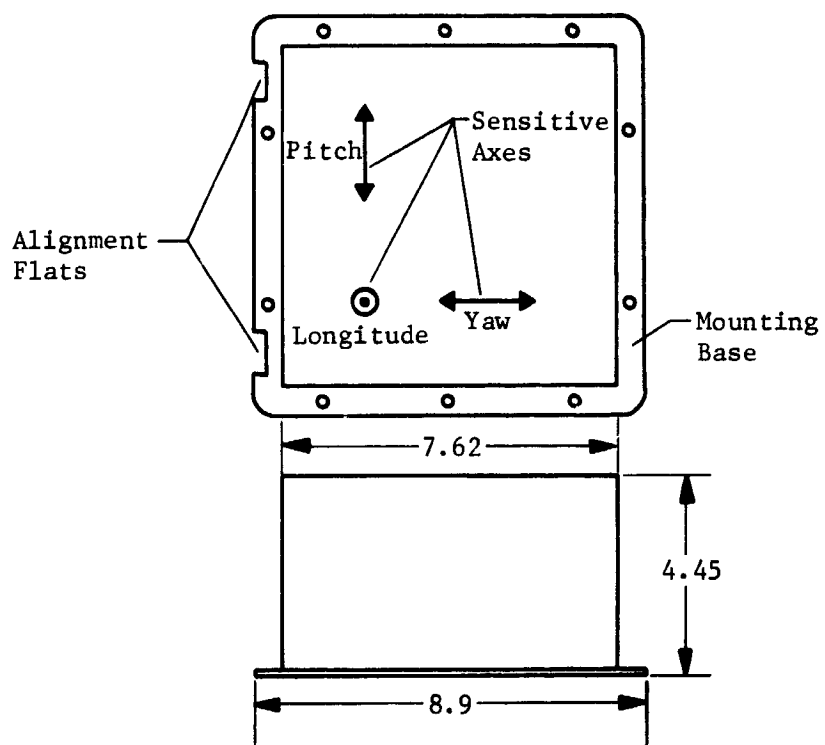
### C. INSTRUMENTS AND MEASUREMENT TECHNIQUES

This section presents the SAG Exploratory instruments proposed for use to make the measurements given in the preceding section. In particular, the physical and electrical characteristics are given to provide input for subsystem areas. Also, the word composition of the data from each instrument will be given to provide input to the data handling system.

#### 1. Digital Accelerometer Triad System

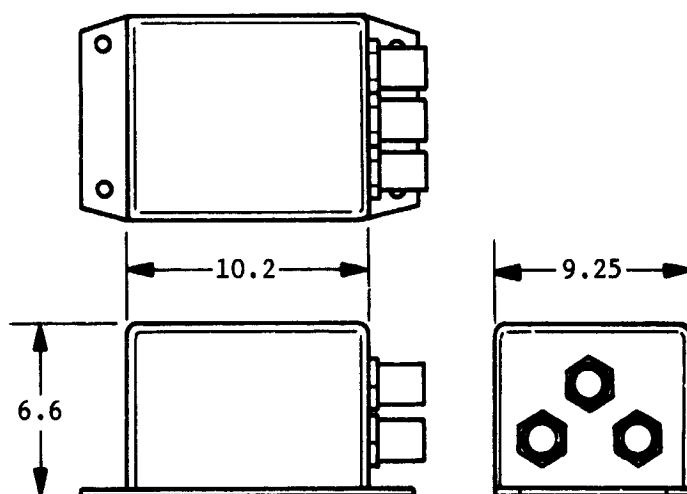
The accelerometer used on both Viking and PAET is the Bell Aerospace Model IX System, consisting of one longitudinal and two cross-axis pendulous, force rebalance acceleration transducers accompanied by an analog-to-digital converter. Although rated for a range from  $10^{-4}$  g to only 200 g, a discussion with Bell Aerospace Company (Ref III-5) revealed that to obtain a range of  $10^{-2}$  g to 1600 g would require only a small modification in the flexure of the pendulous proofmass, and with new uses of hybrid microelectronics the package will be smaller than that currently in use for Viking. The digital accelerometer system consists of four parts: the analog accelerometer, pulse rate converter, on-board processor, and an entry g sensor, all packaged in two separate components shown in Figure III-1. The characteristics of the system are shown in Table III-4. Ranges are given for those characteristics that are mission-dependent.

a. *Entry Accelerometer Measurements* - During the entry phase of the mission, which lasts only 30-80 seconds, the accelerometers must measure the entry g-load with sufficient accuracy to enable



(a) Analog Accelerometer System Combined, 3-Axis Package

Note: Dimensions in cm



(b) Pulse Rate Converter and Onboard Processor

Figure III-1 Digital Accelerometer System (Ref III-6)

Table III-4 Digital Accelerometer System Characteristics

<u>Item</u>	<u>Characteristics</u>
1.	Weight, kg - AA 0.57; PRC 0.98; Total 1.55
2.	Size, cm - AA 8.9 x 7.62 x 4.45; PRC 10.2 x 9.25 x 6.6
3.	Volume, cm <sup>3</sup> - AA 258.5; PRC 655; Total 916.0
4.	Power Required - 2.8 Watts
5.	Warmup Time - 30 sec
6.	Sampling Interval - Entry - 0.1 to 0.4 sec Descent - 8 to 15 sec sweep*
7.	Data Bits per Sample - Entry - 30 Descent - 60
8.	Data Bit Rate - Entry 100-200 bps Descent - 4-7.5 bps
9.	Temperature Limits - 230°K to 370°K
10.	Heat Dissipated - 2.8 Watts Maximum
11.	Onboard Processing Required - Yes*, for descent.
12.	Operational Altitudes - Entry to end of mission
13.	Sensitivity 10 <sup>-2</sup> to 1600g axial; 10 <sup>-2</sup> to 125g lateral
14.	Location - Longitudinal axis (Fig. III-1) aligned along probe axis.

\*For measurements in the turbulent area, onboard processing is required to give average value, peak value, and number of zero crossings to yield frequency and amplitude of turbulence during each sweep.

AA = Analog Accelerometer

PRC = Pulse Rate Convertor

reconstruction of the g-load versus time curve, especially at the peak g point. From this, the atmospheric structure can be determined from the following equations:

$$V = V_E + \int_0^t a_s dt$$

$$\rho = -2 \frac{m}{C_D A} \frac{a_s}{V^2}$$

$$h = \int_t^{t_e} (V \sin \gamma) dt$$

$$P = \int_h^{\infty} \rho g dh$$

$$T = \frac{P}{R\rho}$$

where:

$a_s$  = deceleration along the flight path

$V_E$  = entry velocity

$m$  = mass of the vehicle

$A$  = area of the vehicle

$V$  = velocity as  $f(t)$

$C_D$  = drag coefficient

$\rho$  = atmospheric density

$h$  = altitude

$t_e$  = total entry time

$\gamma$  = flight path angle

P = atmospheric pressure

T = atmospheric temperature

R = specific gas constant

The density will be determined to the same accuracy as the acceleration and entry velocity can be measured. The temperature determination assumes that the specific gas constant has been determined by an independent gas composition measurement further down in the atmosphere. Accelerometers with an accuracy of 0.1% of reading are required, i.e., about 1.6 g axial at full scale.

The axial accelerometer is sampling at a rate of 10 samples/sec for Jupiter and 5 samples/sec for the other Jovian planets, while the lateral accelerometers are sampling at a rate exactly half of each of these. Each data word consists of 10 bits and is an analog measurement that has been converted to a digital signal. The electrical interface for this conversion is shown in Figure III-2. For Jupiter, the resultant bit rate is 200 bps during entry, and for the other planets, it is 100 bps. Since the probe is undergoing communications blackout, all of the entry accelerometer data must be stored to be later interleaved with real time data transmitted during descent. The accelerometers are turned on several minutes before entry because of trajectory uncertainties, and if the zero data measured during this time were stored, it would quickly exceed the storage capability. Thus, a g-sensor is required to determine when a nonzero measurement is first made and storage can begin. The storage requirements for entry accelerometer data vary from about 5400 bits to about 8800 bits. This is interleaved and transmitted during descent times of from 33 to 43 min, which results in bit rates for transmission of stored data from 2.2 to 4.4 bps.

b. *Descent Turbulence Accelerometer Measurements* - After the parachute is deployed, a signal is sent to the accelerometer processor to instruct it to switch the measurement mode to descent, simultaneously with the deployment of the temperature gage. In this mode of operation, the accelerations from turbulence will be much lower in magnitude and more random in direction than during entry.



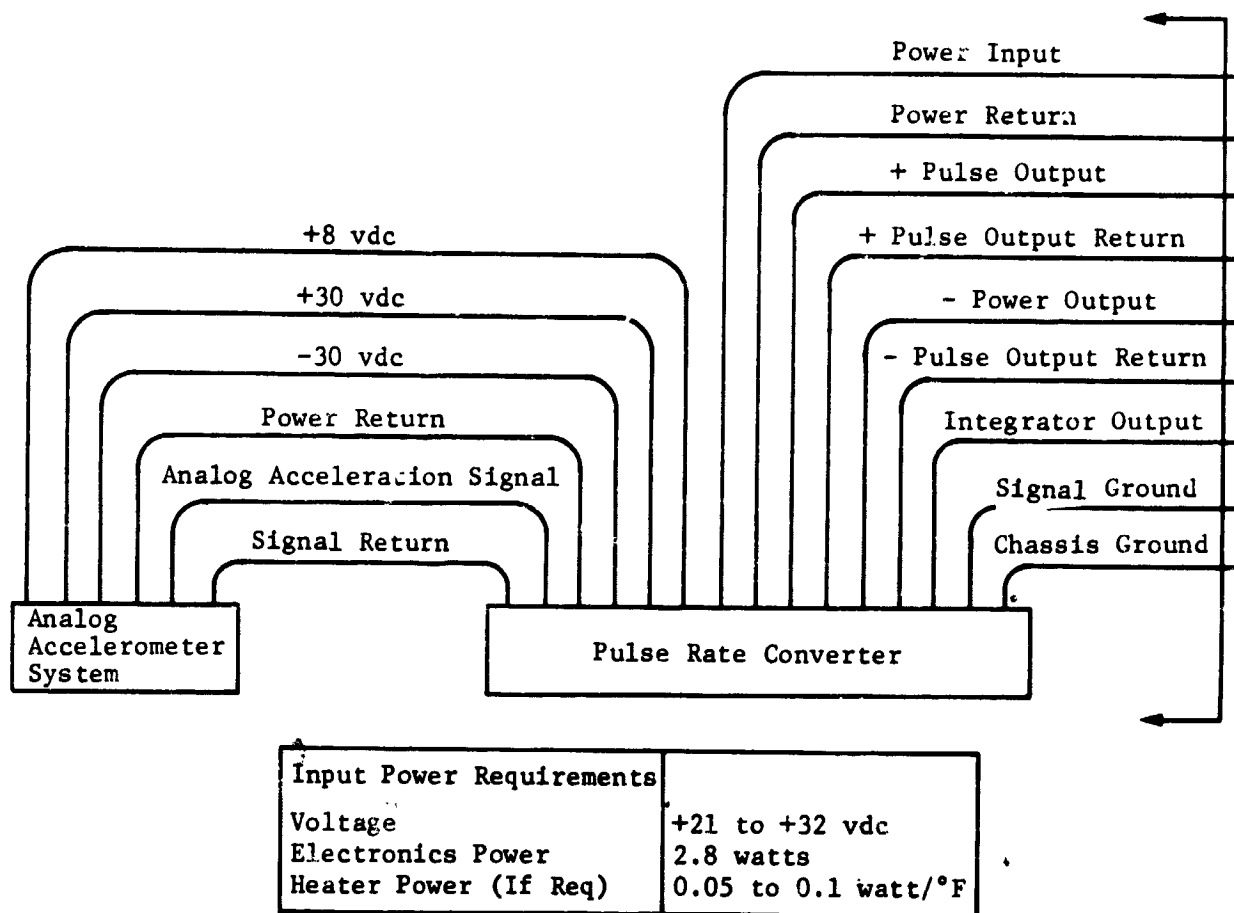


Figure III-2 Accelerometer Electrical Interfaces

The desire is to determine the magnitude and frequency of the probe acceleration response to turbulence variations. This is done by making an analog sweep of 8- to 15-sec duration and through the use of onboard processing, determine the average value of turbulence, the peak value of turbulence, and the number of average crossings. This is schematically pictured in Figure III-3. This technique is used for the axial accelerometer and a combination of the two lateral accelerometers so that the result is a separate measurement of vertical and horizontal turbulence. Each word is again a 10-bit word so that each measurement consists of a total of 60 bits. With sampling times for a single sweep as shown above, the bit rate can vary from 4 to 7.5 bps. With the exception of the first few tens of seconds, during which acquisition occurs, the data is telemetered in real time.

In conclusion, the accelerometers appear to be state-of-the-art even for the larger range required for Jupiter entry. However, an analysis needs to be performed to determine if an increase in structural rigidity is necessary for the *lateral* accelerometers in order to withstand the 1600g cross-axis entry load.

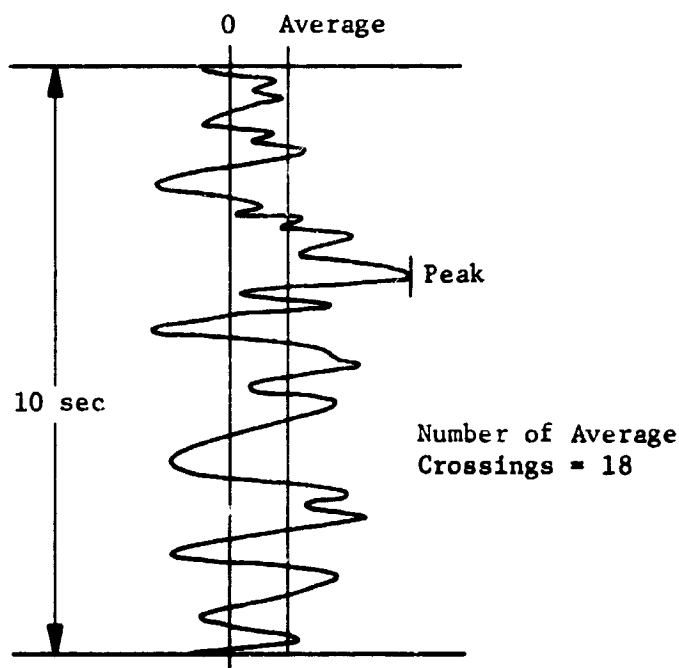


Figure III-3 Turbulence Accelerometer Measurements

## 2. Pressure Gage

Both the Viking pressure gage and the PAET pressure gage were considered for use, with modification, for the entry probe. The comparative characteristics for both are given in Table III-5. It can be seen that the PAET instrument is slightly lighter in weight but significantly smaller in volume, which translates into supporting system weight savings. Power requirements are also significantly less.

Two instruments are required to cover the pressure range under consideration. One should have a range from a few millibars to about one bar, and the second from this point down to the design pressure limit. Both can be vibrating diaphragm-type instruments, but the diaphragm for the high range instrument must be improved over that used on PAET.

Figure III-4 shows a drawing of a Viking-type pressure transducer. The PAET gage would look identical except for having smaller dimensions as given in Table III-5. Figure III-5 shows the electrical connections to the pressure. Each pressure word is taken

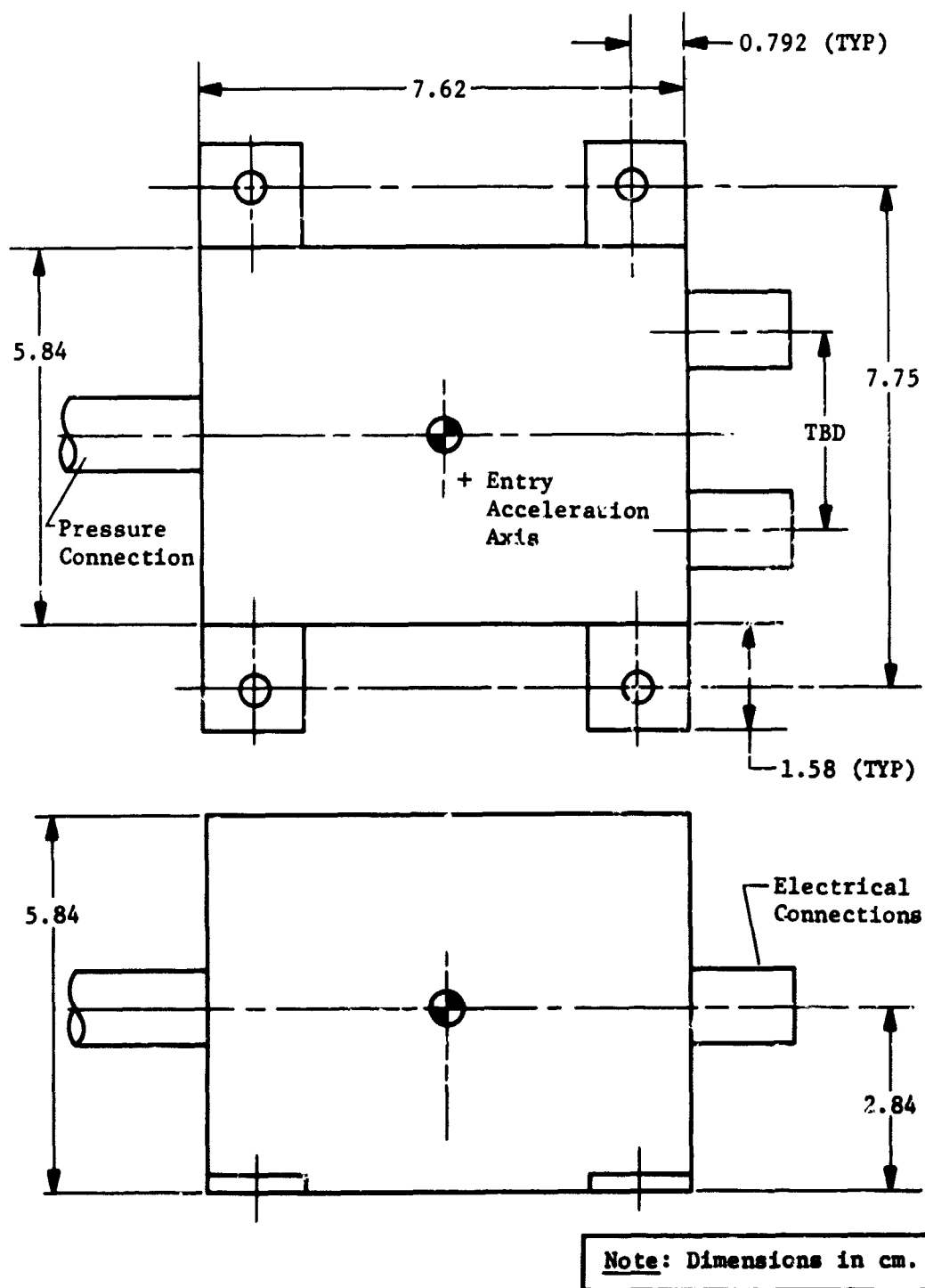


Figure III-4 Viking-Derived Pressure Transducer (Ref III-7)

Table III-5 Pressure Gage Characteristics

(All entries typical for each pressure transducer).

	VIKING DERIVED	PAET DERIVED
1. Weight	0.385 kg	0.34 kg
2. Size (cm)	7.62 x 5.84 x 5.84	4.92 x 5.0 x 5.0
3. Volume	262 cm <sup>3</sup>	123 cm <sup>3</sup>
4. Power Required	1.4 watts	0.65 watts
5. Warmup Time	30 sec	Same
6. Sampling Interval	3 to 6 sec	Same
7. Data Bits per Sample	10 bits	Same
8. Data Bit Rate	1.7 to 3.3 bps	Same
9. Temperature Limits	-20°F to 125°F	Same
10. Heat Dissipated	1.4 watts	0.65 watts
11. Onboard Processing Required	No	No
12. Operational Altitudes	Chute deployment to design pressure	Same
13. Sensitivity	5 x 10 <sup>-2</sup> to 1 bar & 1 to 30 bars	Same
14. Location/Orientation:	Located to limit sensor tube to 8 in. (20.3 cm) overall with approximately 1 in. (2.54 cm) projected from outer shell of descent probe. Sensor tube to be ~ 90° to probe surface with opening ~ 90° to descent path; the base of the instrument should be mounted perpendicular to the entry acceleration axis.	

to be 10 bits, thus the bit rate for 3- to 6-sec sampling intervals ranges from 1.7 to 3.3 bps. The instruments will sample simultaneously near the range crossover pressure ( $\sim 1$  bar), but only the most reliable will be transmitted.

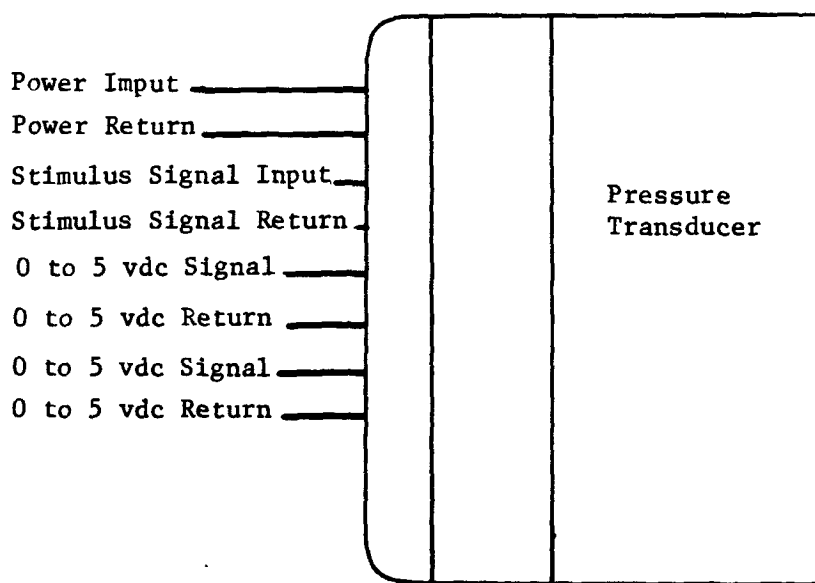


Figure III-5 Pressure Transducer Electrical Interconnections

### 3. Temperature Gage

The Viking parachute phase temperature gage is very similar to the PAET instrument as can be seen by comparing Figure III-6 to Figure III-7. Both sensors are thermocouples deployed by means of a pyrotechnically activated spring. The required temperature range for each of the planets is tabulated.

Jupiter	100 to 400°K
Saturn	70 to 350°K
Uranus	50 to 250°K
Neptune	40 to 190°K

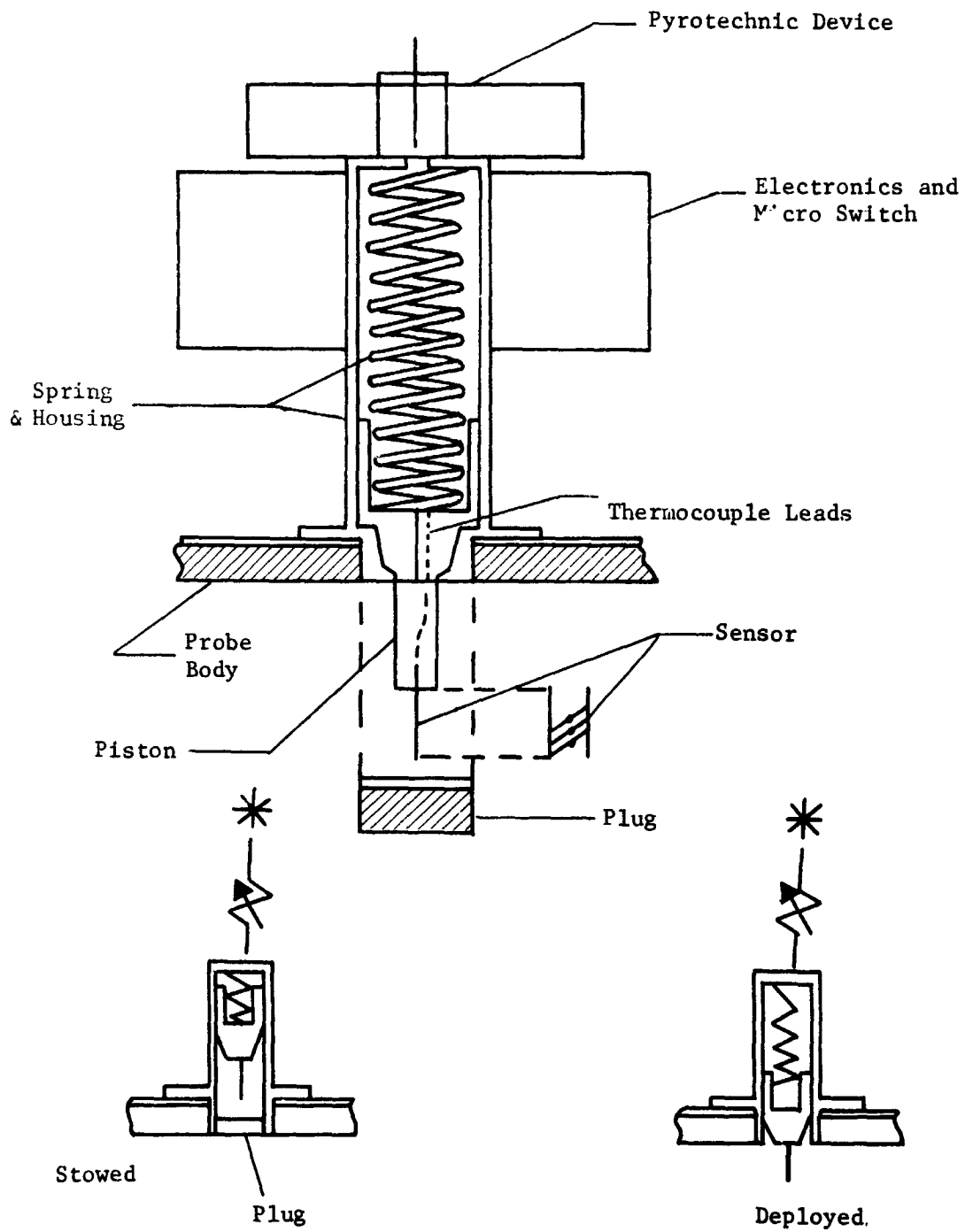


Figure III-6 Viking Temperature Gage (Ref III-8)

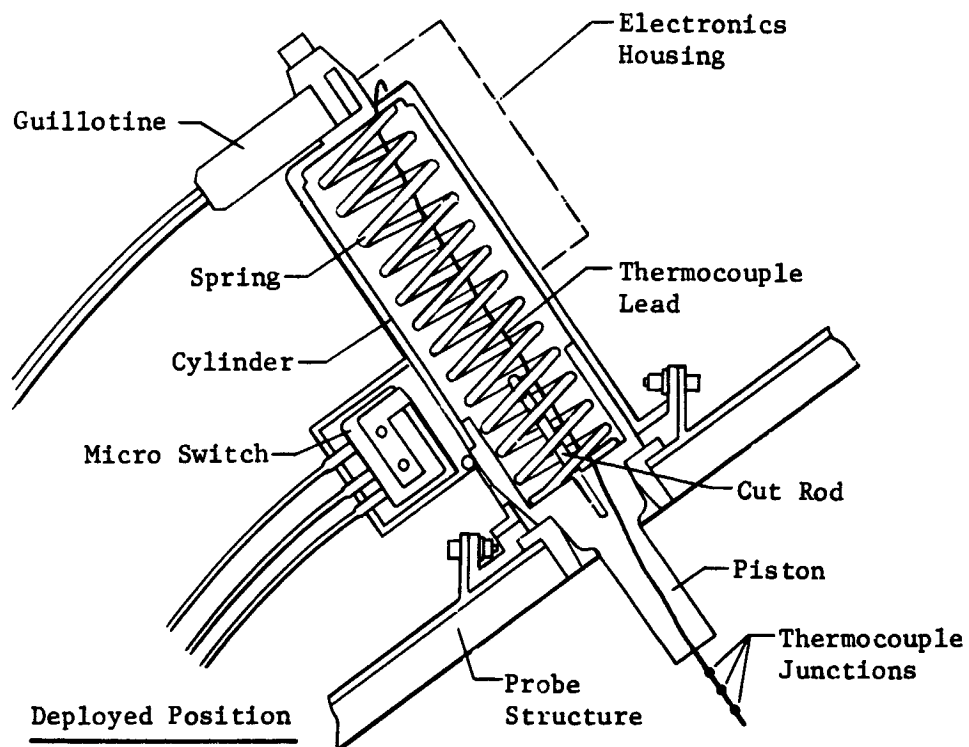


Figure III-7 PAET Temperature Gage (Ref III-9)

The Viking temperature gage has a range of 100 to 400°K, and thus is applicable, without modification, to Jupiter entries. Minor modifications must be made for the remainder of the planets. The thermocouple measurements should have an accuracy of  $\pm 1\%$ , but if more accurate measurements are necessary, a platinum resistance wire sensing element could be used. Temperature gradients can be determined with an accuracy that is nearly the same as the measurement resolution if no evaporating or condensing droplets interfere. Thermocouples generally have a rapid temperature equalization with the ambient atmosphere, lessening the condensation problem. In the deployed position, the temperature sensor protrudes 1 in. from the probe body. For typical velocities encountered at the varying densities of descent in the primarily hydrogen atmosphere, the maximum thickness of the boundary layer is about 0.37 in.

The characteristics of the temperature gage used in this study are shown in Table III-6 and the dimensions given in Figure III-8. Figure III-9 shows the electrical interfaces. The data words are again 10-bit and the sampling times are simultaneous with the pressure gage measurements varying from 3 to 6 sec/sample. This results in a bit rate which varies from 1.7 to 3.3 bps. The instrument will begin sampling with the other descent instruments as soon as the aeroshell is released and the sensor is deployed.

#### 4. Neutral Mass Spectrometer

The neutral mass spectrometer is the primary instrument in the SAG Exploratory payload making direct composition measurements of the planetary atmosphere. The mass spectrometer inlet design necessary does not match that of the Viking entry mass spectrometer or the Viking lander GCMS. It more closely resembles that of the PAET entry vehicle, but that inlet system was designed for a maximum atmospheric pressure of 1 atm. Therefore, the design used here, while similar to both Viking and PAET, most closely resembles one being proposed for the Pioneer Venus which must descend to 100 atm of pressure. The analyzer, however, can be either the Viking magnetic sector or the PAET quadrupole.

The inlet system is of the remote sampling design. The gases from the ambient atmosphere enter through a small tube (0.05 in. dia) and through a porous sintered leak into a sample volume of less than 1 cm<sup>3</sup> (Figure III-10). One-shot valves, initially closed, seal the system in vacuum until ready to begin measurement. The



Table III-6 Temperature Gage Characteristics

<u>Item</u>	<u>Characteristics</u>
1. Weight -	0.45 kg
2. Size (cm) - Electronics	7.92 x 3.12 x 1.76
	- Sensor: 5.34 dia x 3.81 long
3. Volume -	426 cm <sup>3</sup>
4. Power Required -	1.4 watts
5. Warmup Time -	5 min
6. Sampling Interval -	3-5 sec
7. Data Bits per Sample -	10 bits
8. Data Bit Rate -	1.7 to 3.3 bps
9. Temperature Limits -	-40°F (233.2°K) to + 125°F (324.8°K)
10. Heat Dissipated -	1.4 watts
11. On Board Processing Required -	No
12. Operational Pressures -	0.1 to 30 bars
13. Sensitivity -	100°K to 400°K
14. Location/Orientation -	After deployment, the sensor element should extend a minimum of 1 in. (2.54 cm) from the descent probe external surface ~ 90° to the surface, and ~ 90° to the descent path

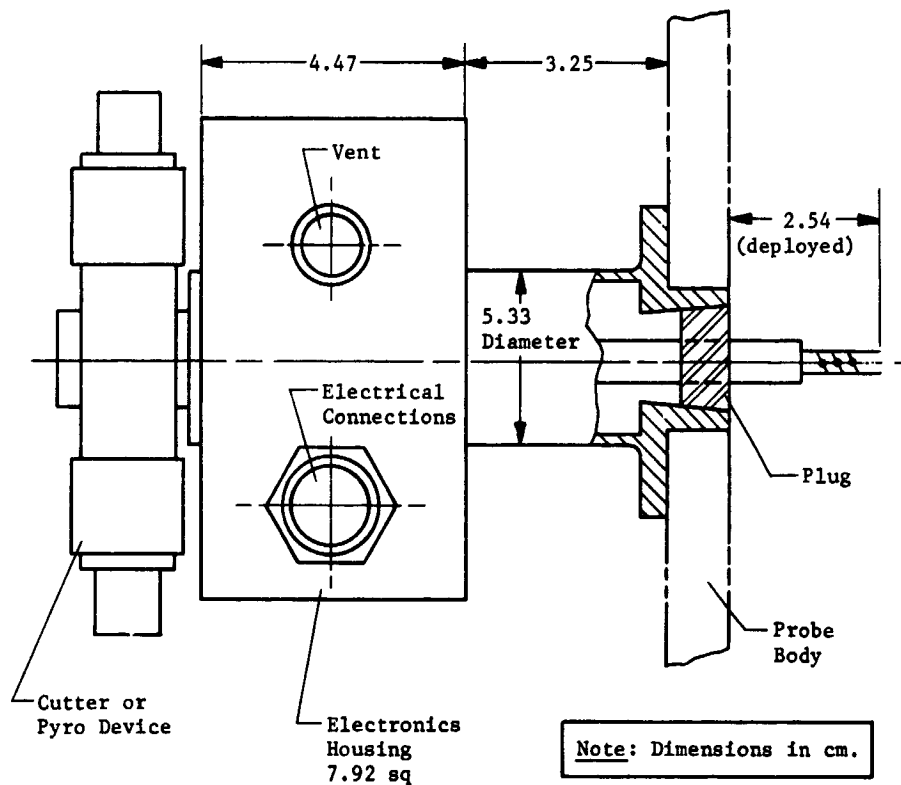


Figure III-8 Temperature Gage Dimensions--Viking

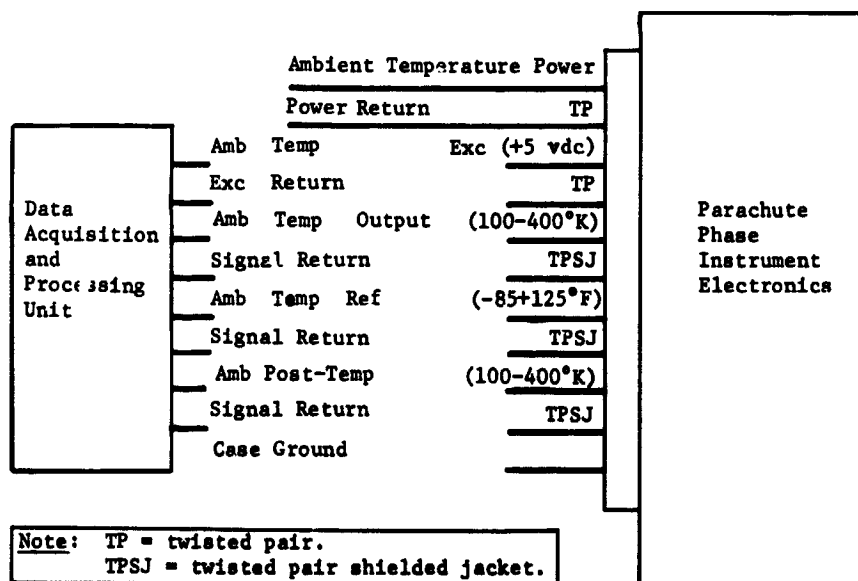
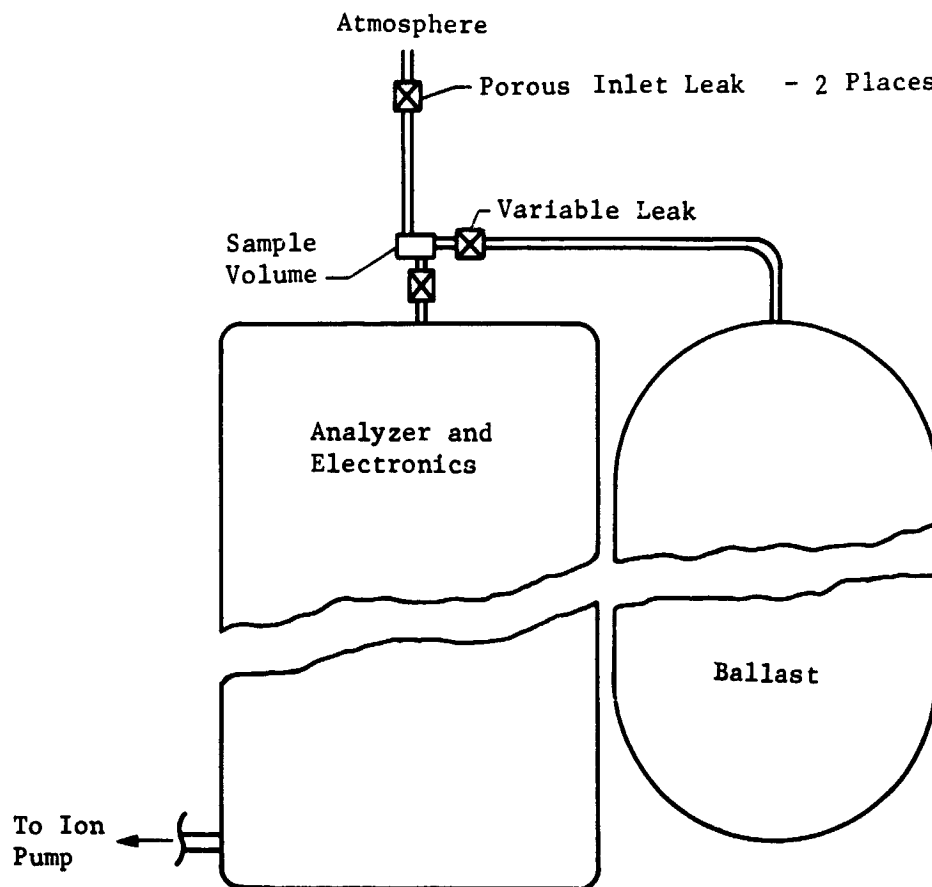


Figure III-9 Temperature Gage Electrical Interface

flow through the initial leak increases with increasing atmospheric pressure, raising the pressure in the sample volume. A constant pressure of about 1 torr must be maintained in the sample volume to maintain a steady flow rate into the mass spectrometer, and consequently, a constant pressure of  $\leq 10^{-5}$  torr inside the analyzer. This is accomplished by the use of a variable leak in a line from the sample volume to an evacuated ballast volume. The inlet system will require an electrical heater coil around the tubes and leaks to prevent condensations of ammonia and water and blockage of the flow. The power for this is included in that given for the spectrometer system.



*Figure III-10 Mass Spectrometer Inlet System*

The neutral particles entering the mass spectrometer are ionized and accelerated. Both the Viking-type magnetic sector and PAET-type quadrupole were investigated. The magnetic sector instrument shown in Figure III-11 is a double focusing-type with an electrostatic analyzer that provides both energy filtering and spatial focusing, providing precise mass resolution. The mass separation is brought about by the magnetic field as in a conventional mass spectrometer.

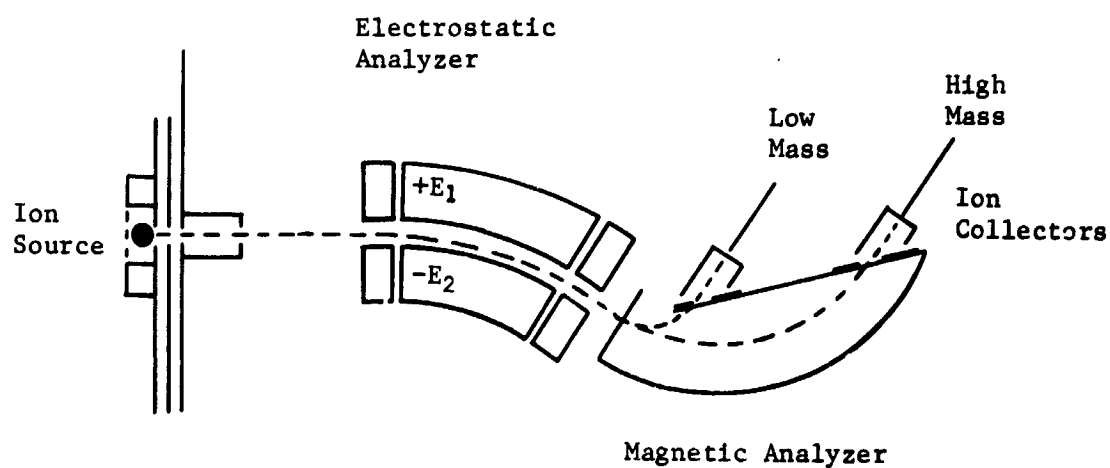


Figure III-11 Typical Magnetic Sector Mass Spectrometer  
Mattauch-Herzog Geometry--Viking

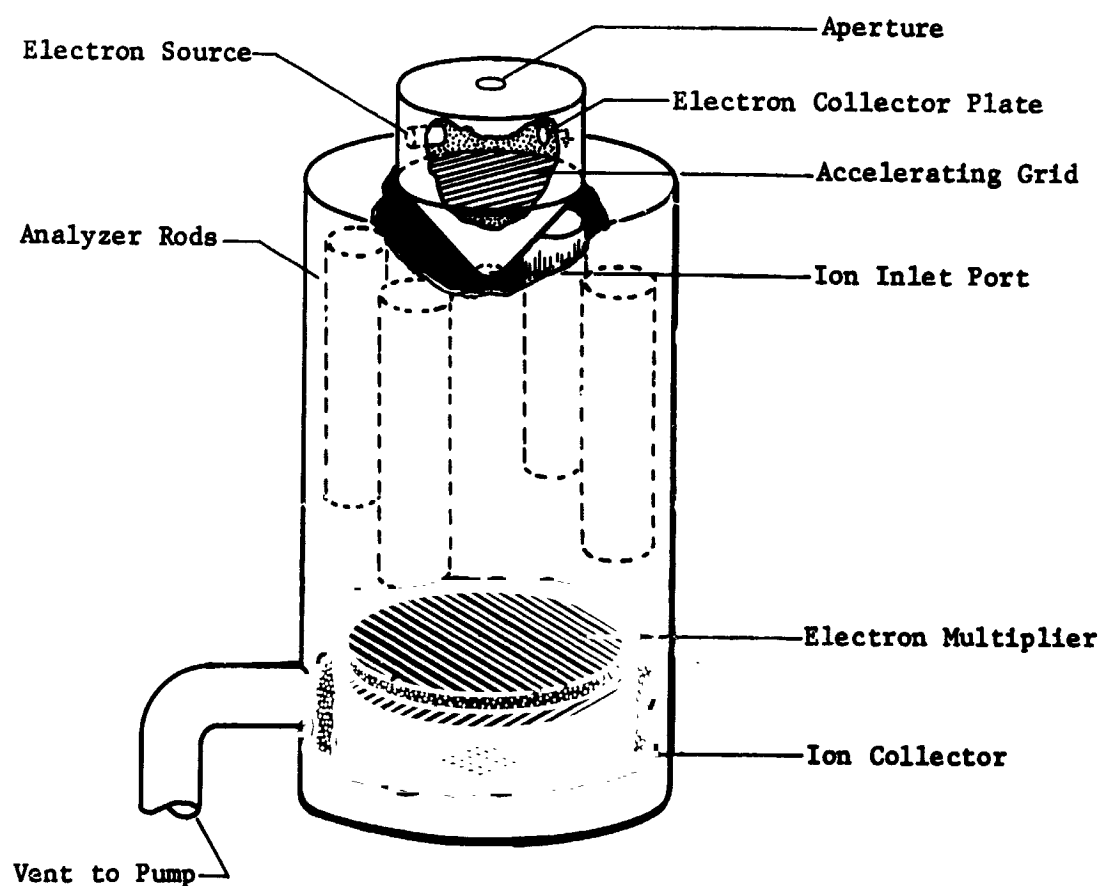


Figure III-12 Quadrupole Mass Spectrometer Analyzer Schematic--PAET

Table III-7 Neutral Mass Spectrometer Characteristics

	Nominal Jupiter Probe	Alternate Jupiter Probe & All Others
1. Weight - Analyzer	2.27 kg	1.81 kg
Electrical	2.72 kg	2.72 kg
Pump	0.45 kg	0.45 kg
Inlet System	0.45 kg	0.45 kg
2. Size - Analyzer (cm)	10.2 dia x 22.9 long	7.6 dia x 20.3 long
Electrical (cm)	12.7 x 15.3 x 17.8	Same
Pump (cm)	7.62 x 7.62 x 7.62	Same
Ballast Volume (cm)	8.9 dia x 19.1 long	7.6 dia x 10.9 long
3. Volume - Analyzer	1868 cm <sup>3</sup>	934 cm <sup>3</sup>
Electrical	3445 cm <sup>3</sup>	Same
Pump	443 cm <sup>3</sup>	Same
Ballast Volume	1000 cm <sup>3</sup> pressure tank	500 cm <sup>3</sup> pressure tank
4. Power required	16 watts	14 watts
5. Warmup times	5 min.	Same
6. Sampling Interval	30-70 sec	Same
7. Data Bits per Sample	400 bits	Same
8. Data Bit Rate	6-14 bps	Same
9. Temperature Limits	-20°C to 50°C	Same
10. Dynamic Range	10 <sup>6</sup> (1-40 amu)	Same
11. Onboard Processing Required	No	No
12. Operational Pressures	0.1 to 30 bars	0.1 to 13 bars
13. Sensitivity (without multiplier)	10 <sup>-6</sup> amf/torr	Same
14. Location/Orientation - aperture at lowest point on descent capsule to sample undisturbed atmosphere. Inlet system requires a sample volume $\leq 1$ cm <sup>3</sup> with lines to analyzer and ballast volume.		

Table III-8 Isotopes and Hydrogen Compounds Less than  
40 amu for Mass Spectrometer Analysis

Mass No.	Formula	Name
1	H	Hydrogen
2	D	Deuterium
2	H <sub>2</sub>	Diatomic Hydro en
3	HD	Deuterated Hydrogen.
3	He	Helium Isotope
4	He	Helium Isotope
7	Li	Lithium Isotope
9	Be	Beryllium Isotope
11	B	Boron Isotope
12	C	Carbon Isotope
13	C	Carbon Isotope
14	N	Nitrogen Isotope
14	CH <sub>2</sub>	Carbon Dihydride
15	CH <sub>3</sub>	Carbon Trihydride
16	CH <sub>4</sub>	Methane
17	NH <sub>3</sub>	Ammonia
18	H <sub>2</sub> O	Water
19	DHO	Deuterated Water
20	Ne	Neon Isotope
20	HF	Hydrogen Fluoride
22	Ne	Neon Isotope
26	C <sub>2</sub> H <sub>2</sub>	Acetylene
27	HCN	Hydrogen Cyanide
28	C <sub>2</sub> H <sub>4</sub>	Ethylene
30	CH <sub>2</sub> O	Formaldehyde
30	C <sub>2</sub> H <sub>6</sub>	Ethane
32	SiH <sub>4</sub>	Silane
34	H <sub>2</sub> S	Hydrogen Sulfide
36	HCl	Hydrogen Chloride
36	Ar	Argon Isotope
38	HCl	Hydrogen Chloride (Isotopic)
38	Ar	Argon Isotope
40	Ar	Argon Isotope

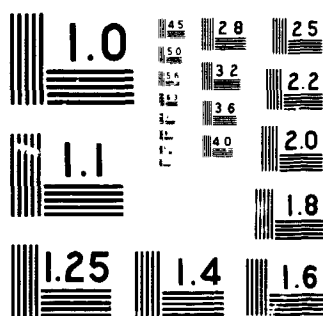
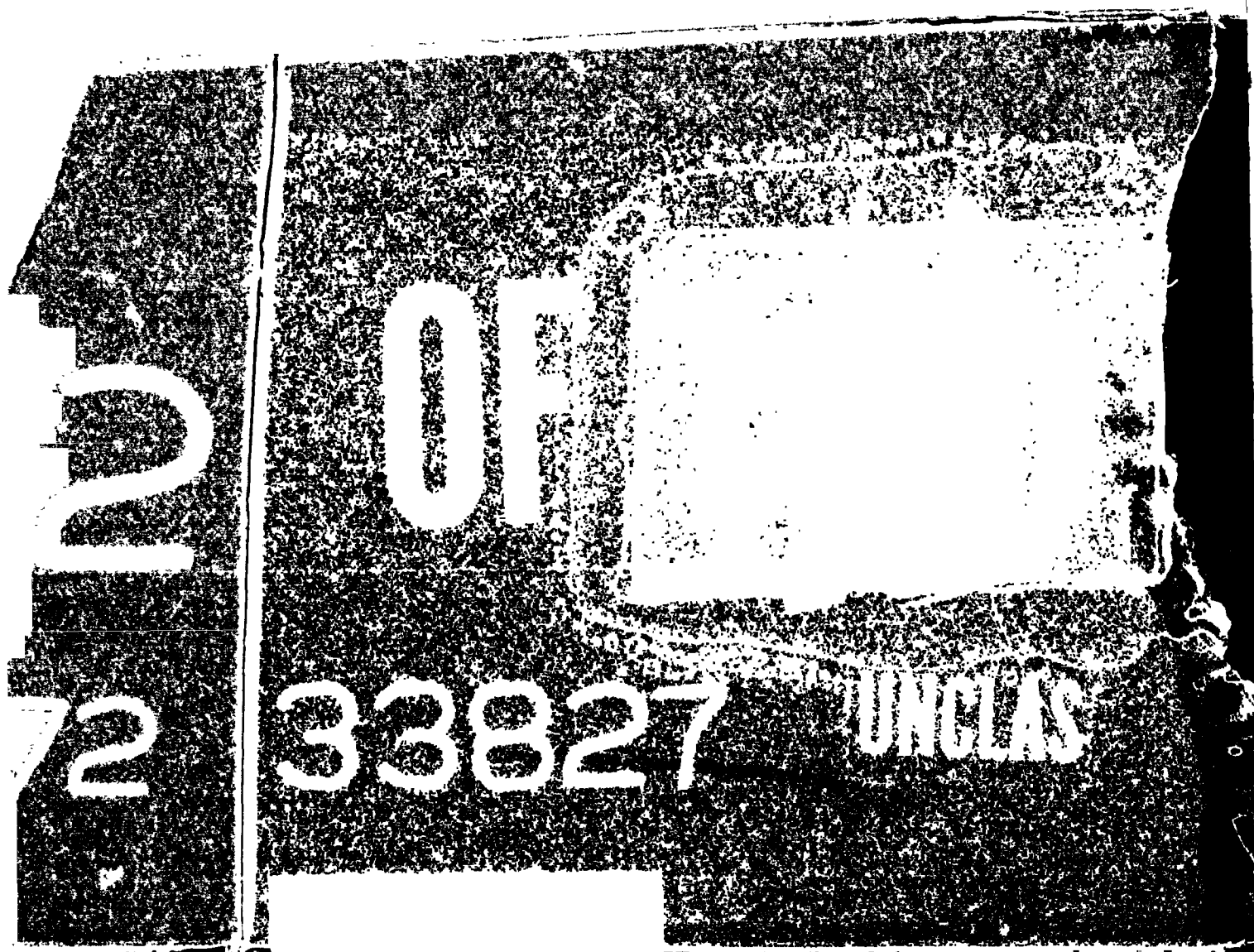
The quadrupole analyzer, shown in Figure III-12, consists of four parallel cylindrically hyperbolic electrodes upon which a dc voltage and RF field are superimposed. Ions, other than those within a limited charge to mass ratio range, traversing the length of the analyzer, are thrown into unstable trajectories and are removed from the ion stream. The desired ion group travels the full length of the analyzer and are collected by the detector. Mass scanning is accomplished by varying the field applied to the rods.

Attention has been focused on the question of using a quadrupole or magnetic sector mass spectrometer in space science applications for several years. Each time a comparison is made, it is in response to a very narrow application and this makes it more difficult to obtain an objective set of data for tradeoff studies. This uncertainty is not accidental but rather results from the proposition that there is no overwhelming advantage for the sole use of either type of instrument. Each flight instrument selection must result from a detailed comparison of the mission objectives, environments, and power-weight-volume constraints to the characteristics of the mass spectrometer in question.

The magnetic sector instrument offers the higher potential scientific return of the two types provided that high mass ( $\geq 100$  amu) is one of the desired objectives. The high mass range requires increasing the magnetic strength and weight. The scan electronics for this type of instrument are well known, reliable and accurate over a large mass range. Further, this type of instrument design has a proven capability on numerous rocket flights.

The quadrupole has been used primarily for Earth satellite and rocket borne instruments and has a proven capability over a mass range of 1-60 amu. To date, the quadrupole instruments have been lighter and require less volume than the equivalent magnetic sector instruments. The electronic system, although very complex for high mass range, can be simplified for the mass range 1-60 amu. The quadrupole scan does offer one definite advantage in that the scans are linear and this simplifies the data collection system. The quadrupole analyzer provides the additional capability of taking either positive or negative ion spectra with only electronic switching.

Table III-7 lists the characteristics for mass spectrometers with both types of analyzers. Actually for the nominal Jupiter probe, neither type was specified, but the volumes were designed for the Viking magnetic sector. After telephone conversations with various



MICROCOPY RESOLUTION TEST CHART  
NATIONAL BUREAU OF STANDARDS-1963

quadrupole mass spectrometer manufacturers, the volume of the analyzer was reduced for the remainder of the missions under consideration and specified to be a quadrupole. The ballast volume was 1 liter for the nominal mission which descends to 30 bars and only 0.5 liter for the others with a maximum depth of 13 bars.

The mass range considered is from 1 to 40 amu. This is sufficient to measure the constituents which compose greater than 99.9% of the expected Jovian atmospheres. Table III-8 lists the isotopes and hydrogen compounds having mass numbers less than 40 amu that could conceivably exist in these atmospheres. Some, but not all, of the isotopic variations of the compounds are also listed. In addition, other nonhydrogen compounds, such as  $N_2$ , CO, or NO might exist, filling in some of the vacant mass numbers in Table III-8. This is justification for the continuous sweep to 40 amu. Note that there is a possible conflict for several of the mass numbers, particularly 2, 3, 14, 20, 30 and 36. As a maximum, the data-bit requirement would be 10 bits for detector current and 6 additional bits for mass number. A convenient data compression approach would be to use a "zero" to indicate a detector current below threshold and a "one" to indicate that a measurable peak exists. The detector current bits would only be required following an indication of threshold. The actual number of masses that will exceed the detectability threshold will probably be less than 20; thus, providing for 10 bits per mass number, or 400 bits/sample is a conservative estimate of actual requirements. The sampling times vary from 30 to 70 sec for the 1-40 amu sweep; thus the bit rate ranges from about 6 to 14 bps.

For the interface with the data handling system (DHS), the instrument will require a sequence of on-commands before its measurement period. As a minimum, the DHS would only have to supply the first of these with the remainder produced internally using the DHS clock signals. The initial on signal is required roughly 5 min before aeroshell release. Before aeroshell release, the detection circuitry will be electrically calibrated. Calibration using known amounts of the elements should be expected.

The analyzer section of the mass spectrometer is state of the art and available. The inlet system requires further test and evaluation to verify the design. The response time between gas entering the first leak from the ambient atmosphere and reaching the analyzer is about 30 sec, however recent experimental results indicate that the sample volume should be reduced to as much as  $0.1 \text{ cm}^3$  in which case the response time could be reduced to  $\leq 10$



quadrupole mass spectrometer manufacturers, the volume of the analyzer was reduced for the remainder of the missions under consideration and specified to be a quadrupole. The ballast volume was 1 liter for the nominal mission which descends to 30 bars and only 0.5 liter for the others with a maximum depth of 13 bars.

The mass range considered is from 1 to 40 amu. This is sufficient to measure the constituents which compose greater than 99.9% of the expected Jovian atmospheres. Table III-8 lists the isotopes and hydrogen compounds having mass numbers less than 40 amu that could conceivably exist in these atmospheres. Some, but not all, of the isotopic variations of the compounds are also listed. In addition, other nonhydrogen compounds, such as  $N_2$ , CO, or NO might exist, filling in some of the vacant mass numbers in Table III-8. This is justification for the continuous sweep to 40 amu. Note that there is a possible conflict for several of the mass numbers, particularly 2, 3, 14, 20, 30 and 36. As a maximum, the data-bit requirement would be 10 bits for detector current and 6 additional bits for mass number. A convenient data compression approach would be to use a "zero" to indicate a detector current below threshold and a "one" to indicate that a measurable peak exists. The detector current bits would only be required following an indication of threshold. The actual number of masses that will exceed the detectability threshold will probably be less than 20; thus, providing for 10 bits per mass number, or 400 bits/sample is a conservative estimate of actual requirements. The sampling times vary from 30 to 70 sec for the 1-40 amu sweep; thus the bit rate ranges from about 6 to 14 bps.

For the interface with the data handling system (DHS), the instrument will require a sequence of on-commands before its measurement period. As a minimum, the DHS would only have to supply the first of these with the remainder produced internally using the DHS clock signals. The initial on signal is required roughly 5 min before aeroshell release. Before aeroshell release, the detection circuitry will be electrically calibrated. Calibration using known amounts of the elements should be expected.

The analyzer section of the mass spectrometer is state of the art and available. The inlet system requires further test and evaluation to verify the design. The response time between gas entering the first leak from the ambient atmosphere and reaching the analyzer is about 30 sec, however recent experimental results indicate that the sample volume should be reduced to as much as  $0.1 \text{ cm}^3$  in which case the response time could be reduced to  $\leq 10$

sec. Appendix N of Volume III gives the theoretical equations for response time relations. There is also a problem involved because of the fact that the masses of the primary constituents exist in two different groups, specifically 1-4 amu and 15-18 amu. The leak rates through the sintered plug could be appreciably different, distorting the measurements. This is a laboratory experimental-type problem and will require a solution before actual flight.

A laboratory model of this proposed inlet system has been built under pressure, and will soon undergo tests in a simulated Venus atmosphere. Several laboratory experiments have been identified by this study which need to be performed to aid in understanding the application of this system to the Jovian atmospheres. In particular, they are: (1) determination of extent of mass discrimination by the molecular inlet leak through the analysis of known amounts of two gases with widely separated masses, (e.g.  $H_2$  and  $N_2$ ) with consideration of the effect of variations in inlet system temperature; (2) understanding of the condensation problem in the inlet system by analysis of a gas with high concentrations of ammonia and/or water at different temperatures; (3) investigation of the pumping problems associated with the high concentration of inert helium in the Jovian atmospheres; (4) complete analysis of a simulated Jovian atmosphere containing  $H_2$ , He,  $NH_3$ ,  $CH_4$ , and  $H_2O$ .

#### D. ENTRY AND DESCENT SCIENCE MISSION ANALYSIS

##### 1. Science Sequence of Events

The sequence of science events for all of the entry probe missions is approximately the same, with the times and pressures for occurrences varying. The instruments are turned on at least 5 min before entry for warmup, with time increments due to trajectory uncertainties added to this. The accelerometers begin sampling data but not storing it. The g-sensor associated with the accelerometer processor will sense the beginning of entry and command the data handling system to begin storing the deceleration data from all 3 axes.

On the missions investigated, entry may last from 19 to 79 sec, terminating when the probe, with a ballistic coefficient of  $102 \text{ kg/m}^2$  ( $0.65 \text{ slug/ft}^2$ ) reaches Mach 0.7. This may occur at a pressure level of from 33 to 92 millibars in the design missions, although it can occur later for high flight path entries. (Table V-1.) At this point a large parachute, with ballistic coefficient of approximately  $15 \text{ kg/m}^2$ , is deployed; this slows the probe to terminal velocity. The entry accelerometers are still taking data. The probe falls for 10 sec to stabilize its horizontal oscillations and reach terminal velocity and then releases the aeroshell, which falls out of the way. After a 2-sec delay, pyrotechnics deploy the temperature gage, first ejecting the plug, and uncovering the mass spectrometer inlet aperture, releasing the vacuum. The accelerometers are switched over to the turbulence measurement mode and the full extent measurements begin. These events are pre-programmed since the spacecraft has not yet acquired the probe.

For descents into Saturn, Uranus, and Neptune, much higher ballistic coefficients are required than for Jupiter which means a smaller parachute. For these missions, after a delay of about 3 additional sec, the main parachute is released and a secondary or drogue parachute is deployed. All four instruments are now collecting data in the descent mode and storing it with the entry accelerometer data. After approximately 90 sec, the spacecraft acquires the probe and data transmission begins, sending all the data subsequently collected back in real time and interleaving the stored data.

The descent parametrics for each planet, including selection of ballistic coefficients and instruments sampling times are detailed in the chapters discussing the various planet parametrics. They are selected on a basis of the measurement performance meeting the criteria. Three distinct points in the descent are important to measure the performance: (1) the point during descent where the temperature begins to increase, generally 2 to 4 min after chute deployment, is important for the temperature measurement; (2) the first encounter with clouds, which varies from 2 to 8 min after deployment, is important for all instruments; (3) immediately after drogue chute deployment, at several bars of pressure on deep descents. End of mission pressure varies from 7 to 30 bars.

## 2. Design Limit Descent Pressure Depth

The section discussing performance criteria earlier in this chapter listed the terminal pressure requirements of several measurements as the design limit. The design limit pressure is that point in a descent profile where all of the requirements have been met by the actual performance, within an overall set of constraints. In this study, this overall constraint was to descend to 2 to 30 bars depending upon the "risk and cost effect" of the higher pressures.

The measurement that controls the depth is that determining the composition of the lowest (above 30 bars) cloud in the given atmosphere, with the mass spectrometer. For each planet and atmosphere considered, the particular cloud, its pressure range and density range are shown in Table III-9. The specific requirement is to obtain two full mass spectrometer sweeps inside the cloud. The number of measurements is a function of both ballistic coefficient and instrument sampling time. Measurements made all the way through the cloud would be desirable, but not necessary.

Using the selected ballistic coefficients for the various planets (see parametrics sections), specifically  $0.09 \text{ slug/ft}^2$  ( $14.13 \text{ kg/m}^2$ ) for Jupiter and  $0.70 \text{ slug/ft}^2$  ( $109.9 \text{ kg/m}^2$ ) for the other planets, and a mass spectrometer sampling time of 60 sec, the first column of values in Table III-10 shows the pressure depths required to obtain two mass spectrometer sweeps inside the cloud.

However, note in Table III-9 that the cloud densities at the cloud top are extremely low compared to those at the cloud base. Therefore, if the two mass spectrometer measurements are required to be made at points in the cloud where the cloud density is at least  $1.0 \text{ mg/liter}$ , the resultant pressure limits are as shown in the second column of Table III-10. This requirement affords a better opportunity for the measurement of minor constituents by the mass spectrometer.

The last column of Table III-10 shows the design limit pressure used in this study. For Jupiter, since the probe must be designed for the worst-case cool/dense atmosphere, a descent to 13 bars in the cool/dense atmosphere will govern the design. The equivalent descent time in the nominal atmosphere allows the probe to reach 7.5 bars. The design limit pressure for Saturn was moved to 7 bars because this allows the probe to pass completely through the water cloud without detriment to the mission.

Table III-9 Properties of Lower Modeled Clouds

Atmosphere	Cloud	Pressure Range, bars	Density Range, mg/liter
Jupiter C/D	H <sub>2</sub> O	10.0 - 32.3	0.41 - 39.2
Jupiter Nominal	H <sub>2</sub> O	1.80 - 2.76	0.074 - 2.02
Saturn Nominal	H <sub>2</sub> O	3.94 - 6.92	0.074 - 4.82
Uranus Nominal	NH <sub>3</sub>	4.80 - 6.69	0.1 - 1.12
Neptune Nominal	NH <sub>3</sub>	17.1 - 22.8	0.4 - 3.60

Table III-10 Establishment of Design Limit Pressure

Atmosphere Model	Pressure for 2 Measurements in Cloud, Bars	Pressure for 2 Measurements Where $\rho < 1$ mg/l in clouds, Bars	Design Limit Pressure, Bars
Jupiter C/D	11.6	13	13
Jupiter Nominal	2.2	3	7.5
Saturn Nominal	4.4	6	7
Uranus Nominal	5.3	7	7
Neptune Nominal	18.1	20	20

E. REFERENCES

- III-1. *Preliminary SAG Payload and Mission Recommendations for Jupiter Entry Probes.* JPL Section Document 131-15, 20 September, 1971.
- III-2. S. J. Ducsay, Program Manager: *Jupiter Atmospheric Entry Mission Study.* Final Report, Vol II, III, MMC Report No. 71-1, JPL Contract 952811, April 1971.
- III-3. *Science Criteria for Jupiter Entry Missions.* JPL Section Report 131-07 December 31, 1969.
- III-4. *A 1971 Assessment of the Feasibility of a Jupiter Atmospheric Entry Mission.* JPL Advanced Technical Studies Office, September 1971.
- III-5. Murry Meldrum: Bell Aerospace Company, Telecon.
- III-6. *Bell Aerospace Inertial Instruments.* Bell Aerospace Company, Buffalo N.Y.
- III-7. *Absolute Pressure Transducer.* Viking Specification Document PD7400069, November 1969.
- III-8. *Temperature Transducers.* Viking Specification Document, PD7400086, September 1971.
- III-9. Preliminary Description of PAET Instruments for April Design Review, March 28, 1969.

#### IV. MISSION DESIGN CONSIDERATIONS

This chapter provides a general overview of the mission planning considerations involved with probe missions to the outer planets. The general subjects included in this summary are launch and interplanetary trajectory selection, approach orbit determination results, approach trajectories and deflection maneuver analysis, critical mission dispersion studies, and entry trajectory characteristics. In addition, data summarizing various swingby missions to outer planets are presented.

Most of the data presented is of a parametric nature, supporting the mission planning decisions that led to the final mission designs presented in Chapter V. By presenting mission design considerations in a separate chapter, it is possible to compare the mission characteristics to the different planets conveniently. Thus, in the discussion of deflection maneuver requirements, the deflection  $\Delta V$  trends for the four candidate planets are compared side by side; entry peak decelerations for the four planets are discussed in a similar manner.

Many missions have been analyzed during the course of this study. Table IV-1 lists the missions most often referred to in subsequent discussions. Missions A, B, C, I, and J are the system design missions described fully in Chapter V. Missions D, E, and F, Jupiter probe-dedicated missions, similar to Mission 1 but launched in different years, were studied to determine the impact of launch year. Mission G is an "optimal" Jupiter orbiter mission analyzed for the problems introduced by including a probe on an orbiter mission. The data for this mission was obtained from Reference IV-1. Mission H is a low inclination approach trajectory consistent with a JS 77 mission. All of the data listed in Table IV-1 refers to the nominal design of the specific mission. In many cases, parametric studies were made about this nominal design and, thus in certain sections, mission parameters will differ from those given in the Table.

Table IV-1 Summary of Reference Missions

Mission Index	Mission Title	Launch Date	Jupiter Arrival	Planetary Arrival	$C_3$ km <sup>2</sup> /sec <sup>2</sup>	Total Trip Time, day	VHP, km/sec	Periapsis, Planet Radii	Entry Angle, deg	Deflection Radius, $\times 10^6$ km	$\Delta V$ , m/sec
A.	Jupiter Nominal <sup>1</sup>	11/7/79	9/17/81	9/17/81	105	680	8.47	2.00	-20	10	221
B.	Jupiter Probe-Dedicated <sup>1</sup>	11/7/79	9/17/81	9/17/81	105	680	8.47	2.00	-15	30	71
C.	Jupiter Radiation-Compatible <sup>1</sup>	11/7/79	9/17/81	9/17/81	105	680	8.47	6.00	-15	30	256
D.	Jupiter 1978	10/10/78	8/10/80	8/10/80	122	670	8.33	2.00	-20	10	221
E.	Jupiter 1980	12/5/80	10.12/82	10/12/82	98	676	8.69	2.00	-20	10	221
F.	Jupiter 1982	1/4/82	11/10/83	11/10/83	95	675	8.63	2.00	-20	10	221
G.	Jupiter Probe/Orbiter	10/29/79	12/1/81	12/8/81	105 <sup>2</sup>	764	7.27	2.00	-20	10	221
H.	Saturn/Fast JS 77	9/5/77	3/16/79	12/8/80	111	1190	14.87	2.02	-20	10	141
I.	Saturn/JST 77 <sup>1</sup>	9/4/77	4/16/79	2/16/81	107	1261	13.66	2.33	-25	10.15	170
J.	Uranus/JU 79 <sup>1</sup>	11/6/79	6/19/81	5/19/86	113	2386	13.62	2.42	-60	9.75	170
K.	Neptune/JUN 79 <sup>1</sup>	11/6/79	6/19/81	3/12/90	113	3779	15.46	3.00	-20	10	95

<sup>1</sup>Missions used for systems designs<sup>2</sup>PLA < 36° constraint ignored



A. MISSION PROFILE

To give perspective to the subjects discussed in the following sections, it is helpful to examine the general profile of a typical probe mission. The mission begins with a launch from the Eastern Test Range (ETR) at Cape Kennedy. The prime launch vehicle under consideration is the Titan III five-segment (Titan IIIE) with Burner II. Spacecraft under consideration have included the Pioneer spacecraft and a Mariner class spacecraft. The Pioneer spacecraft is a spin-stabilized vehicle weighing 248 kg (547 lb). The Mariner-type vehicle is three-axis stabilized and weighs approximately 500 kg (1100 lb). The spacecraft is launched into a 100-nautical-mile parking orbit and after a short coast is injected onto the interplanetary trajectory.

After the interplanetary cruise, which may include a swingby of an intermediate planet, the spacecraft approaches the target planet. Tracking is initiated for a final midcourse maneuver which refines the spacecraft trajectory toward its desired value. The midcourse is generally performed 13 days before the deflection maneuver. In the deflection maneuver, the probe is separated from the spacecraft and placed on a trajectory intersecting the target entry site. The probe-spacecraft relative geometry is established to achieve an effective communication link during the critical entry phase of the mission.

The probe remains dormant for a coast period of 10 to 50 days. Then, on the order of an hour before entry, the spacecraft acquires the probe signal. Engineering data on the status of the probe and instruments are transmitted. The probe then enters the planetary atmosphere, and probe transmission is terminated at the sensing of 0.1 g.

Following the sensing of 0.1 g, the descent antenna is activated. As the probe descends through the atmosphere measurements are taken and transmitted to the spacecraft for relay to the Earth. The mission ends at pressures of about 10 to 30 bars and descent times of about half an hour.

## B. LAUNCH AND INTERPLANETARY TRAJECTORIES

Opportunities for Earth-Jupiter transfer occur approximately every 13 months when the Earth and Jupiter are in superior conjunction. Transfers divide naturally into two types: Type I transfers with central angles of less than  $180^\circ$ ; Type II with central angles greater than  $180^\circ$  and having longer flight times. This study has been limited to the analysis of Type I trajectories in the time period 1978 to 1982. This chapter presents the parametric data from which the interplanetary trajectory may be selected.

### 1. Launch Energy

Fixing the launch and arrival dates essentially determines the Earth-Jupiter transfer. Given those dates, the heliocentric position vectors of Earth at launch and Jupiter at arrival are determined. By Lambert's theorem (Ref IV-2), those two vectors and the time interval required to traverse them determine the heliocentric conic that closely approximates the actual flight path on the mission. The geocentric hyperbola may then be computed so that, at departure from Earth, the velocity of the spacecraft relative to the Earth (called the hyperbolic excess velocity,  $V_{HE}$ ) plus the orbital velocity of the Earth,  $\vec{V}_{EL}$ , matches the velocity,  $\vec{V}_L$ , of the heliocentric conic at launch:

$$\vec{V}_{HE} = \vec{V}_L - \vec{V}_{EL} \quad [B-1]$$

The variable normally used to discuss launch energy is  $C_3$ , the *vis viva* energy, defined as the square of the magnitude of the hyperbolic excess velocity or

$$C_3 = V_{HE}^2 \quad [B-2]$$

which represents twice the energy per unit mass of the spacecraft. An alternative variable used to describe launch energies is the characteristic velocity,  $V_{CH}$ , which represents the velocity needed at the injection radius  $R_I$  to have the equivalent energy, or

$$V_{CH}^2 = V_{HE}^2 + \frac{2\mu}{R_I} \quad [B-3]$$

For a given launch vehicle, the amount of payload that can be injected into interplanetary trajectories is a function of the launch energy--the smaller the required energy, the larger the possible payload.

Figure IV-1 illustrates the payload capability for the launch vehicles considered in this study: The reference Titan IIIE five- and seven-segment vehicles, both with and without Burner II stages, and updated performance data for the Titan IIIE five-segment vehicle with Burner II. The data indicated are taken from Reference IV-3 and IV-4, respectively. It should be noted that the seven-segment vehicle is no longer being considered for development, but is included here for comparison purposes. The performances for standard Titan vehicles are based on a launch azimuth of  $115^\circ$ , while the updated Titan vehicle performance is evaluated at an azimuth of  $90^\circ$ . Performance data for all vehicles assume a 185-km parking orbit. The payload in all cases refers to probe, spacecraft, spacecraft modifications, and adapters. Generally, a Pioneer spacecraft weighing about 249 kg would be launched by a standard five-segment Titan/Centaur, while a MOPS (modified Outer Planet Spacecraft) or, Mariner class spacecraft, weighing about 589 kg would require either a seven-segment vehicle or the five-segment Burner II vehicle. Adding the weight of a typical probe and spacecraft modifications to these weights demonstrates that launch energies much greater than  $C_3 = 130 \text{ km}^2/\text{sec}^2$  are not realizable. For certain combinations, the maximum  $C_3$  obtainable is even less than this limit.

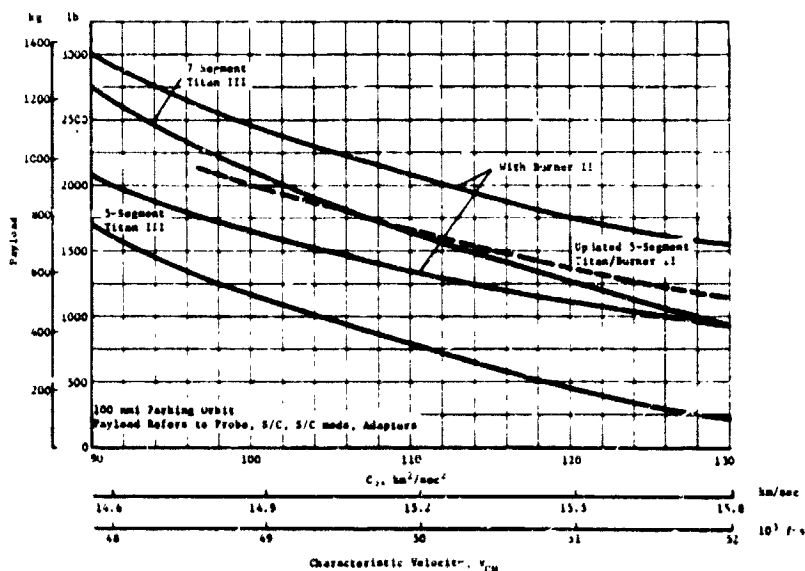


Figure IV-1 Titan III/Centaur Performance Data

Figure IV-2 provides the  $C_3$  contours for launch years 1978, 1979, 1980, and 1981-82, during which years, it should be noted, the launch energy requirements decrease progressively. Using these figures, reasonable selections of launch date/arrival date (LD/AD) and, equivalently, the interplanetary trajectory can be made.

Many of the reference missions defined in Table IV-1 are noted on the figures, indicated by the mission indices provided in the table. Special attention should be given to Missions A, D, E and F as these are the "equivalent" probe missions for the years 1979, 1978, 1980, and 1982, respectively, upon which launch year comparisons will be made.

#### Launch Constraints

LD/AD selection must consider other requirements in addition to launch energy. A primary restriction involves the range safety constraint. Given a launch site, the launch azimuth essentially determines the ground trace of the trajectory. The standard launch profile includes azimuths from  $\Sigma_L = 90^\circ$  to  $\Sigma_L = 115^\circ$ .

Because Cape Kennedy is at  $28.5^\circ$  latitude, the maximum declination of the launch asymptote,  $V_{HE}$ , would be  $DLA = 28.5^\circ$  for

$\Sigma_L = 90^\circ$ , and  $DLA = 36^\circ$  for  $\Sigma_L = 115^\circ$ . The range safety constraint can therefore be translated into the requirement that the DLA must be less than  $36^\circ$  in absolute value. The contours of  $DLA = 36^\circ$  are indicated in Figure IV-2. The constraint is most restrictive for 1978 Type I launches, eliminating nearly half the available period. By 1980 and 1982, it is of little consequence.

A second launch constraint is frequently imposed on the DLA to avoid possible problems in navigation for the midcourse maneuver. The uncertainty in the declination of the spacecraft is given by

$$\Delta\delta = \frac{\Delta r_s / r_s}{\tan \delta}$$

[B-4]

where  $\delta$  is the geocentric declination of the spacecraft, and  $\Delta r_s$  and  $r_s$  are the uncertainty and mean value of the spin axis radius of the station taking the measurement (Ref IV-5). Thus, the navigation process is degraded when the spacecraft trajectory is near zero declination. The spacecraft will be on the

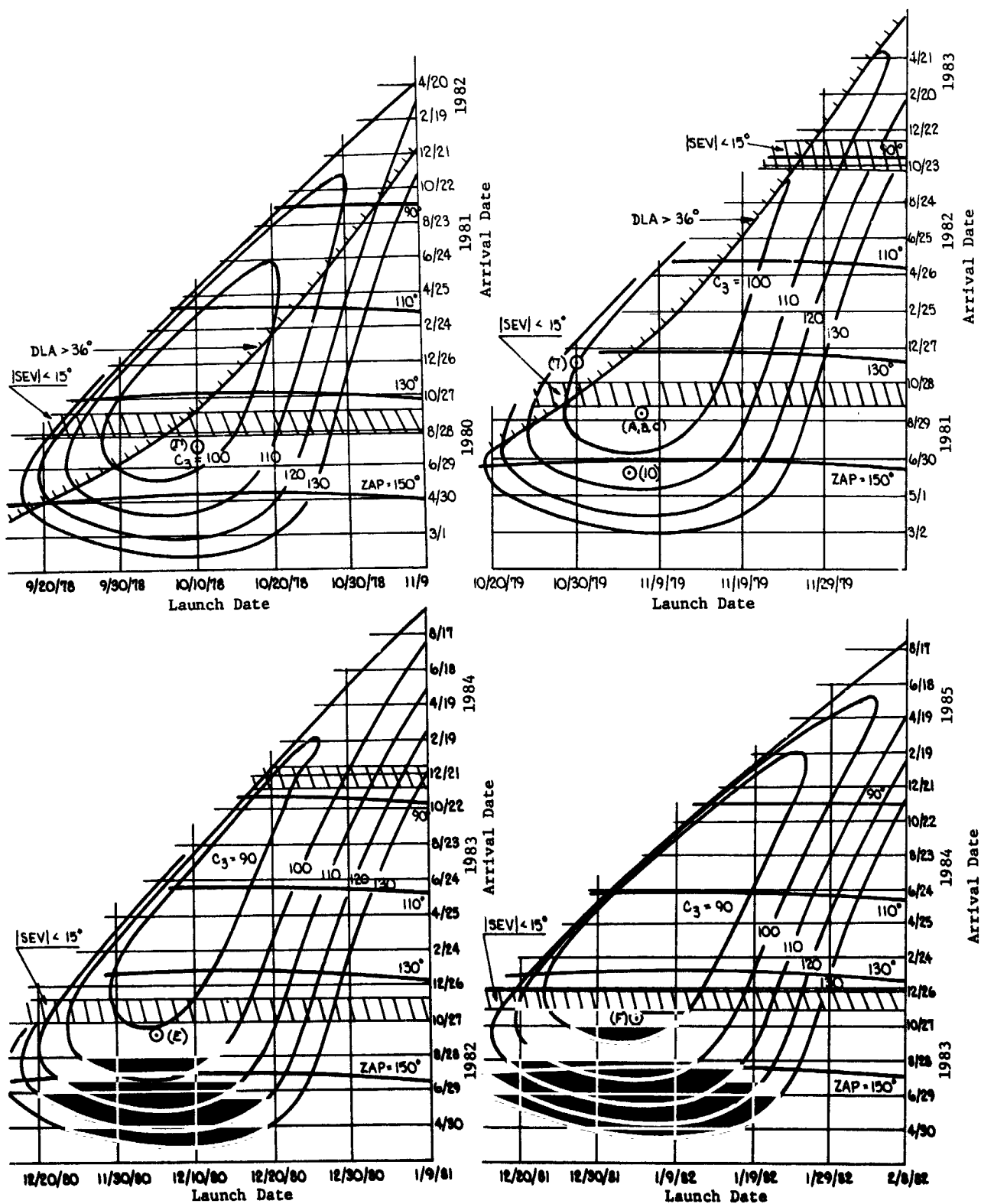


Figure IV-2 Launch Energy Contours for Jupiter Missions

launch asymptote two to three days after launch and will therefore have the declination of the asymptote at that time. If the declination is near zero, the critical tracking for the first midcourse would then be impaired. Therefore, the navigation constraint

$$|DLA| > 2^\circ$$

[B-5]

is noted on Figure IV-2 but is considered somewhat soft. Two relatively minor constraints are applied to parking orbit coast time and daily launch windows. Generally, parking orbit time,  $\Delta t_p$ , (at 185-km orbit) must be less than 1 hr and hopefully under 0.5 hr.

$$\Delta t_p \leq 1 \text{ hr}$$

[B-6]

The daily launch window defined by launches over the range of azimuths  $\Sigma_L = 90^\circ$  to  $\Sigma_L = 115^\circ$  be at least 1 hr.

$$\Delta t_w \geq 1 \text{ hr}$$

[B-7]

These constraints are checked to ensure that they are not violated.

### 3. Arrival Constraints

Arrival constraints are placed on missions to avoid possibly poor geometries at that critical time. Because the launch period for Jupiter missions is generally a month or two and the trip time to Jupiter is greater than 1½ years, the arrival constraints can usually be written as a function of arrival date only, with the launch date assumed to be in the middle of the allowable launch period.

The most critical arrival constraint is an observability limitation. At the time of arrival at Jupiter, the spacecraft must be visible from Earth. If the Sun is between Earth and Jupiter at this time, the critical tracking and communication tasks could not be performed. Therefore, the SEV angle (angle from the Sun to Earth to Vehicle or Jupiter) at arrival must be bounded away from zero. The recommended constraint is

$$|SEV| > 15^\circ$$

[B-8]

A second constraint is imposed to avoid poor navigation at approach to the planet. Because of relation of Equation [B-4], the navigation process is degraded if the spacecraft arrives at Jupiter when the geocentric declination of Jupiter is near zero. Therefore, the constraint is applied

$$\delta_J \neq 0^\circ \quad [B-9]$$

However, a new navigation technique known as Quasi-Very Long Baseline Interferometry (QVLBI) has recently been discovered that permits effective tracking of the spacecraft even when this constraint is violated (Ref IV-6). Thus, the constraint can be de-emphasized if this technique can be used. Arrival dates resulting in poor navigation,  $\delta_J = 0$ , are also noted in Figure IV-2.

A key parameter defining the arrival geometry is the hyperbolic excess velocity at the planet,  $\vec{V}_{HP}$ , defined by

$$\vec{V}_{HP} = \vec{V}_A - \vec{V}_{PA} \quad [B-10]$$

where  $\vec{V}_A$  is the velocity on the interplanetary transfer conic at arrival, and  $\vec{V}_{PA}$  is the orbital velocity of the planet at arrival.

For Jupiter missions, the magnitude of this vector varies between approximately 5 and 13 km/sec, as indicated in Figure IV-3(b).

The major impact of  $\vec{V}_{HP}$  magnitude is on coast time from deflection to periapsis;  $\vec{V}_{HP}$  affects entry velocity only very slightly.

The results of both these variations are indicated in Figure IV-4.

Of more importance is the direction of the  $\vec{V}_{HP}$  vector relative to the Sun and Earth. Let  $\vec{V}_{JS}$  and  $\vec{V}_{JE}$  represent the vectors from Jupiter to the Sun and Earth, respectively, at the arrival time.

The ZAE angle is defined as the angle between the  $\vec{V}_{HP}$  and  $\vec{V}_{JE}$  vectors, as indicated in Figure IV-3(b). The ZAE value fixes the geometry of the approach relative to Earth. Therefore, for example, it contributes to the efficacy of approach orbit determination. Values of ZAE near  $90^\circ$  generally lead to a degradation of the tracking process as the accelerative effects of the target planet are in the plane normal to the Earth-spacecraft line, and the effects on tracking are reduced. However, with a planet as

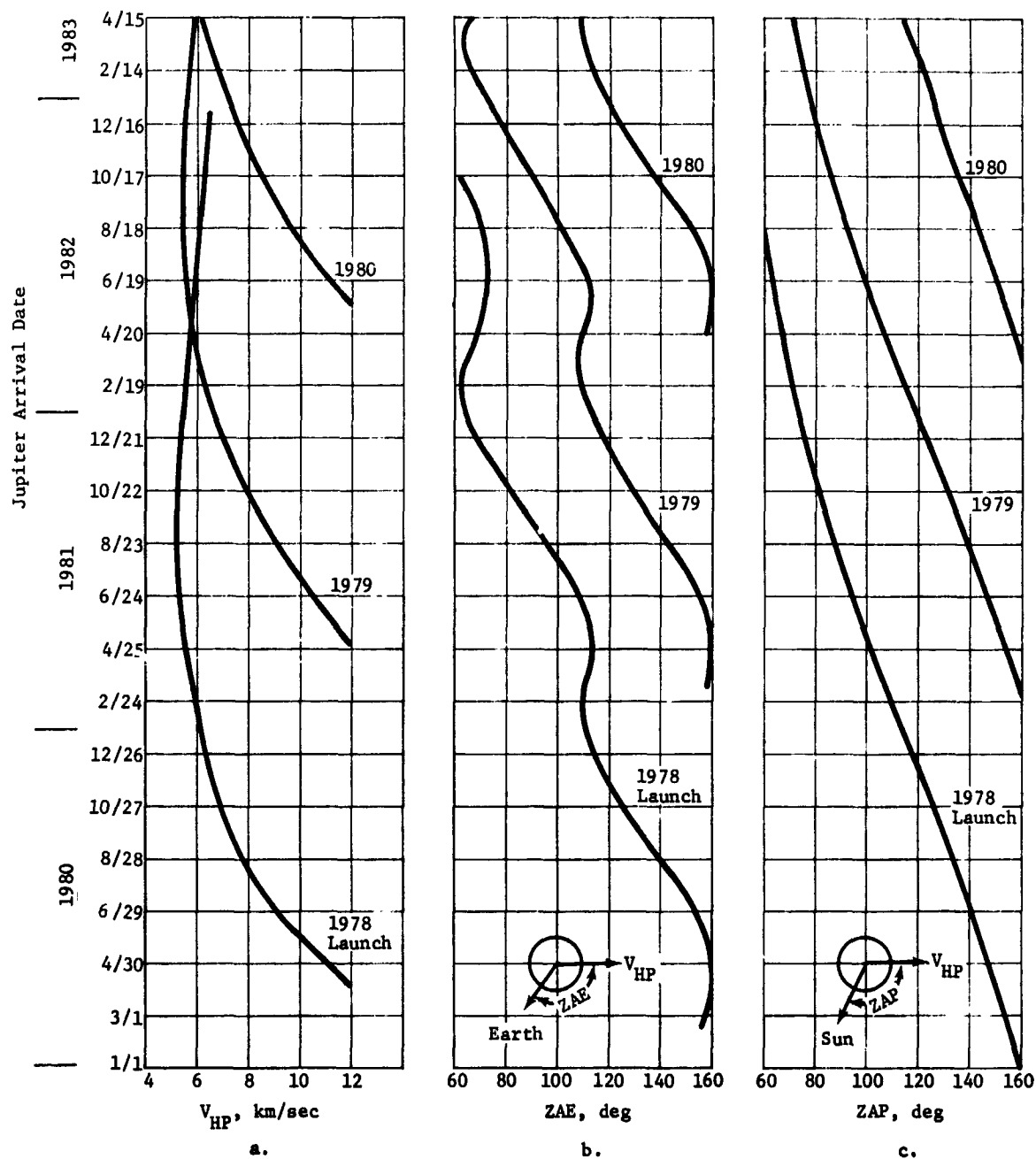


Figure IV-3  $V_{HP}$  Variations with Arrival Date



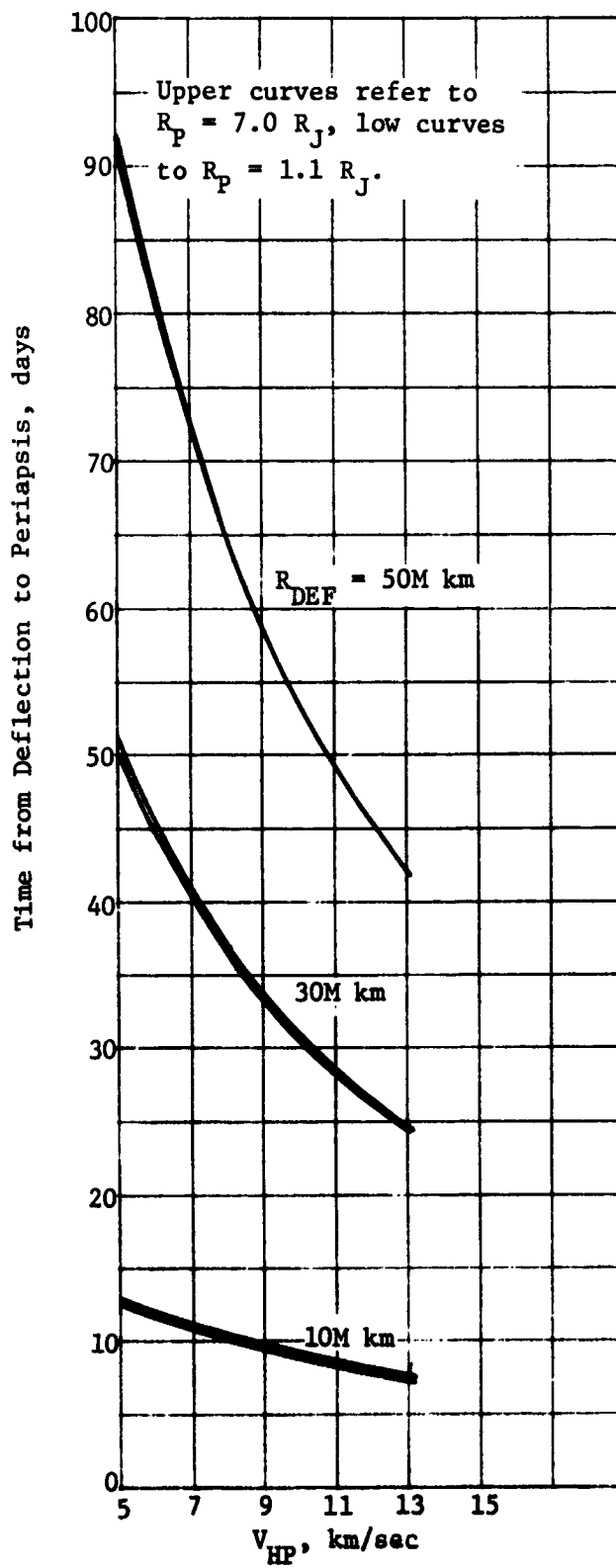
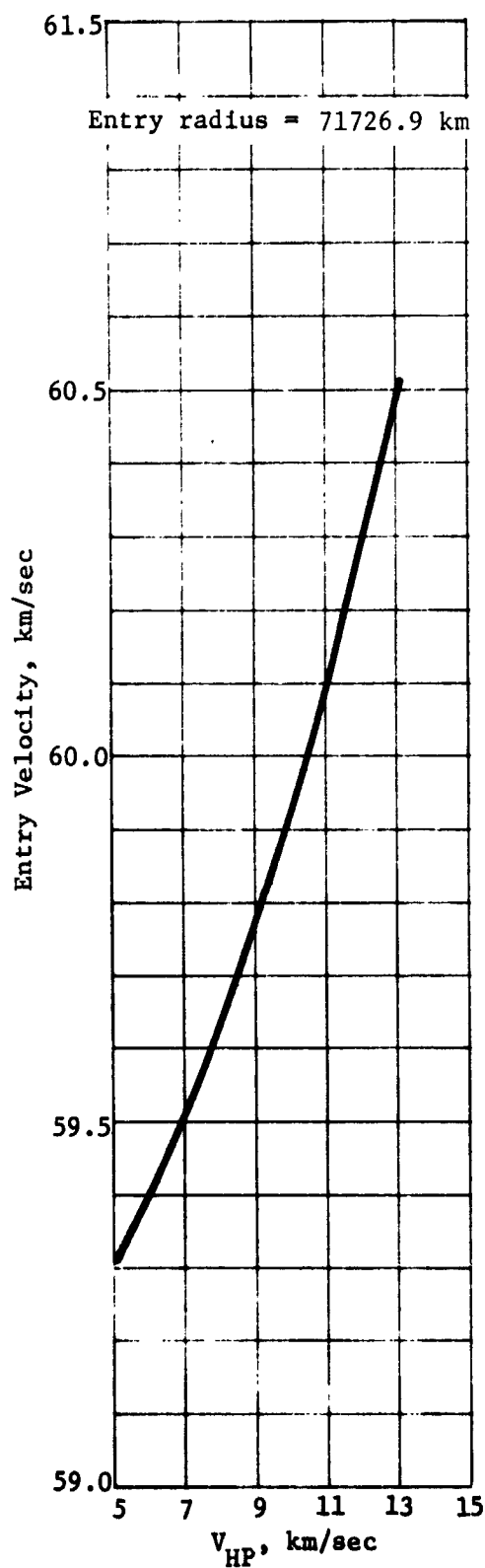


Figure IV-4  $V_{HP}$  Effects at Jupiter

large as Jupiter, accelerative effects are large enough to reduce the effect of this condition. Values of ZAE, as functions of the arrival date, are given in Figure IV-3(b). For reference purposes, the  $C_3$  contours indicate the dates where the following constraint is violated.

$$|ZAE - 90^\circ| > 5^\circ$$

[B-11]

The ZAP angle is defined as the angle between the  $V_{HP}$  and the  $V_{JS}$  vectors, as indicated in Figure IV-3. This parameter determines the lighting conditions of the approach trajectory.

#### 4. Launch Opportunity Comparisons

The data presented in the previous subsections may be combined to determine general conclusions. Figure IV-5 plots available payload (probe, spacecraft, spacecraft modifications, and spacecraft-launch vehicle adapter) versus trip time for the 1979 launch opportunity. The result is that for a 20-day launch period satisfying the range safety constraint, the optimal trip time is slightly less than 700 days. This corresponds to missions arriving at Jupiter just before Jupiter is occulted by the Sun. The payload is based on the standard performance data for the five-segment Titan with the Burner II stage.

Figure IV-6 provides a comparison of the four launch opportunities between 1978 and 1982. The payloads are based on 20-day launch periods for the reference missions noted for each opportunity in Figure IV-2, assuming the standard performance data for the Titan IIID/Burner II vehicle. The progressive improvement with each year is clear. Several reference weights are also indicated on the figure to aid interpretation of the results.

### C. APPROACH ORBIT DETERMINATION

The purpose of the approach orbit determination is to estimate the knowledge and control uncertainties at the probe deflection point. These uncertainties partially determine the dispersions that must be accounted for in the mission. (See Section E.)

#### 1. Procedure and Ground Rules

The approach orbit determination sequence for the missions can be summarized as follows: tracking is performed to the point 13 days before the deflection maneuver, at which time a final mid-course maneuver is performed. Mapping of this uncertainty covariance forward to the probe deflection time determines the control covariance. Continued tracking to the time of probe

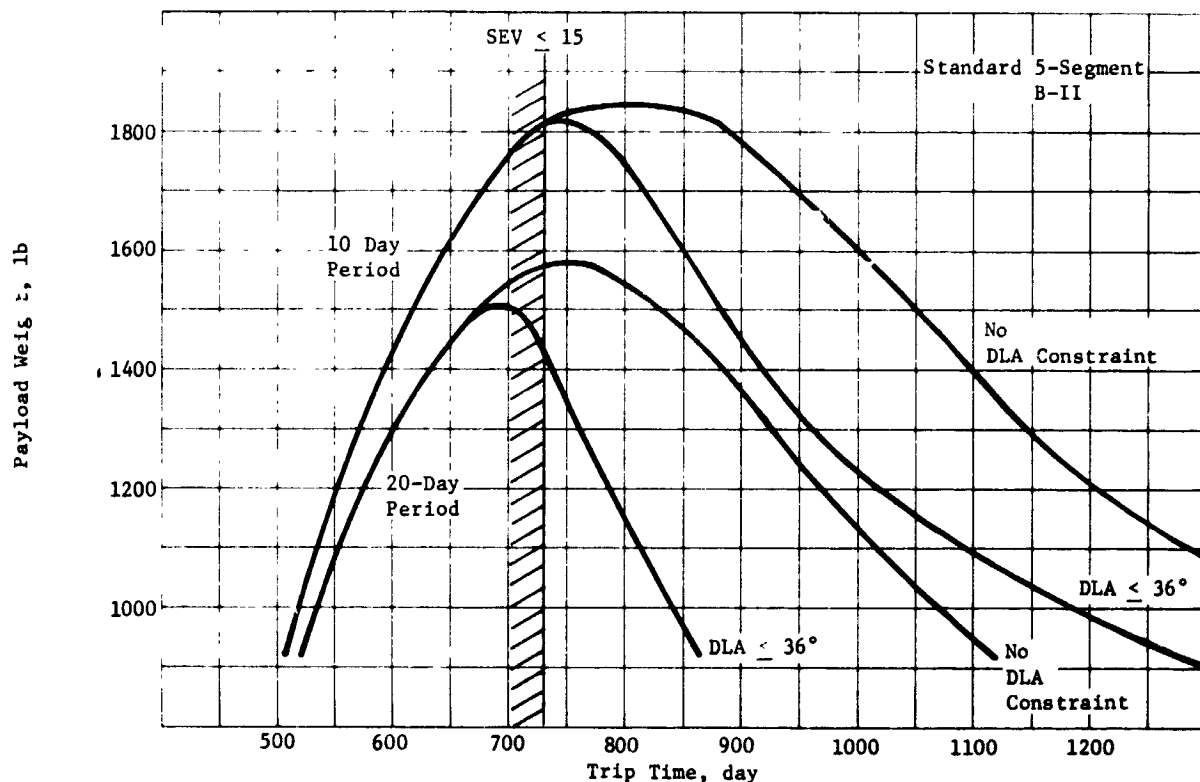


Figure IV-5 Optimization of Trip Time for 1979 Launch to Jupiter

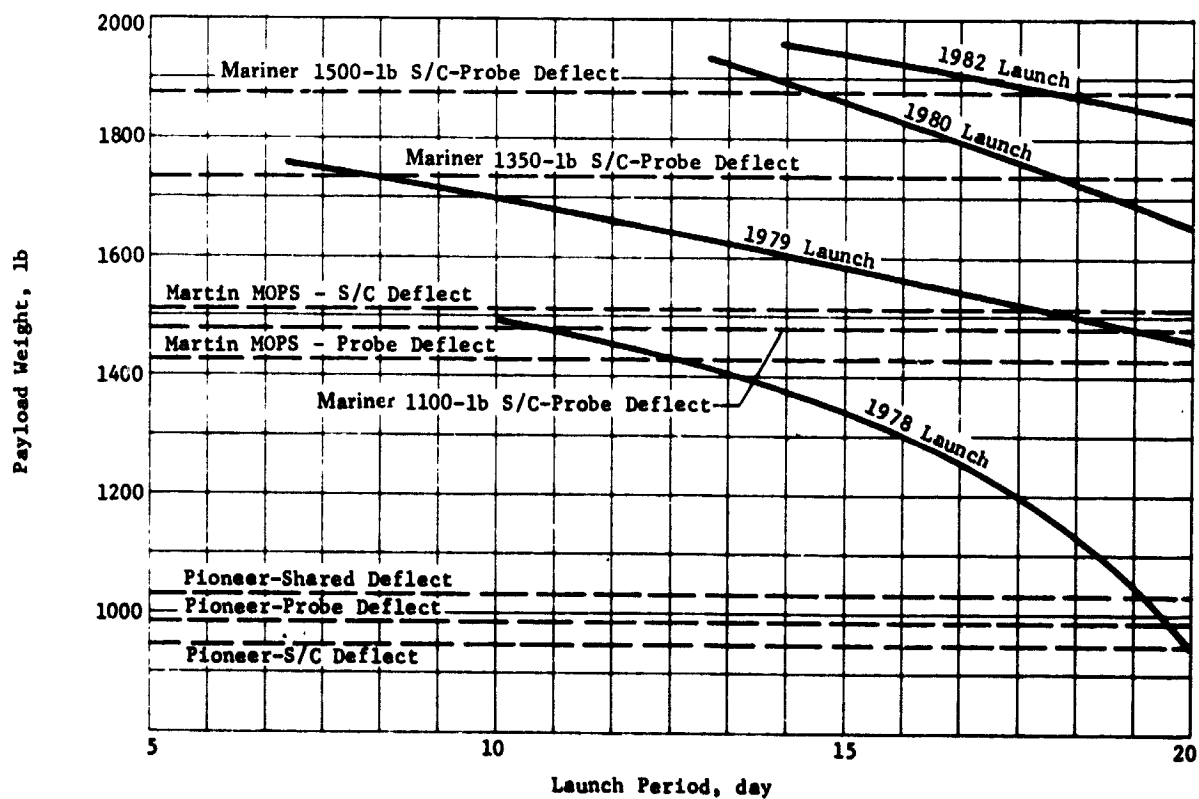


Figure IV-6 Comparison of Launch Opportunities

deflection results in the knowledge covariance. For the missions considered in this study, the additional tracking does not produce much of a decrease in this covariance. The knowledge covariance is generally only 5 to 10% smaller than the control if a sufficient amount of tracking has been performed for the mid-course maneuver. Thus, data will be presented only in terms of control uncertainties. In all cases, tracking is performed by the Deep Space Network (DSN).

The navigation analyses concentrated on three of the missions summarized in Table IV-1 of this chapter. Jupiter studies were largely based on the Jupiter Nominal mission (Mission A) which has the same approach trajectory as the alternative Jupiter missions, Missions B and C. Saturn studies were performed for Mission H, the Saturn/Fast JS 77. It represents somewhat of a "worst case" trajectory for Saturn as the geocentric declination of Saturn passes through zero 30 days before deflection, or 40 days before Saturn encounter. Tracking at Uranus was analyzed using the approach trajectory consistent with the JU 79 mission, Mission J. Brief assessments were made of the comparable Jupiter missions for other years, Missions D, E, and F.

The mathematical model use to simulate the navigation and guidance sequence is discussed in detail in Ref IV-15. Briefly, at any point along the spacecraft trajectory, probabilistic dispersions are described by control and knowledge covariances. The control covariance,  $P_c$ , defines uncertainties between the nominal (or desired) trajectory and possible actual trajectories. The knowledge covariance,  $P_k$ , defines uncertainties between the actual trajectory and possible estimates of that trajectory. The knowledge covariance is linearly propagated between measurements. At measurements, the knowledge covariance is reduced by the new information content of that measurement.

It is inconvenient to describe the trajectory uncertainties by giving the 6 x 6 covariances in terms of Cartesian coordinates. Usually, these uncertainties are translated into the more intuitive quantities of impact plane and time-of-flight uncertainties. The impact plane is defined as the plane centered at the target body normal to the approach asymptote  $\hat{S}$ . (See Fig. IV-7.) The impact parameter,  $\hat{B}$ , is the vector from the center of the planet to the point at which the asymptote pierces the impact plane. The  $\hat{T}$  axis in the plane is defined by

$$\hat{T} = \frac{\hat{S} \times \hat{K}}{|\hat{S} \times \hat{K}|} \quad [B-12]$$

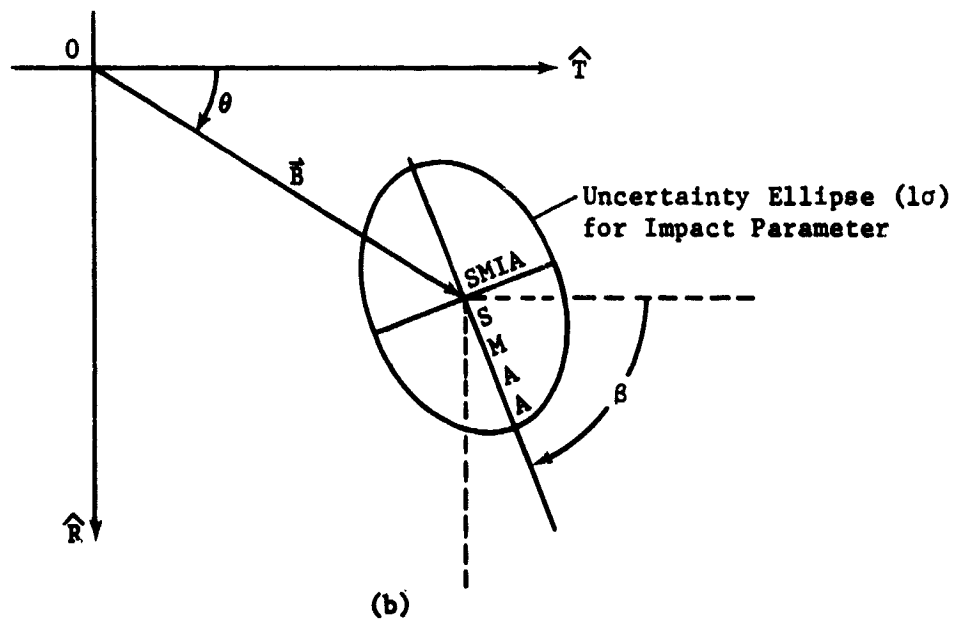
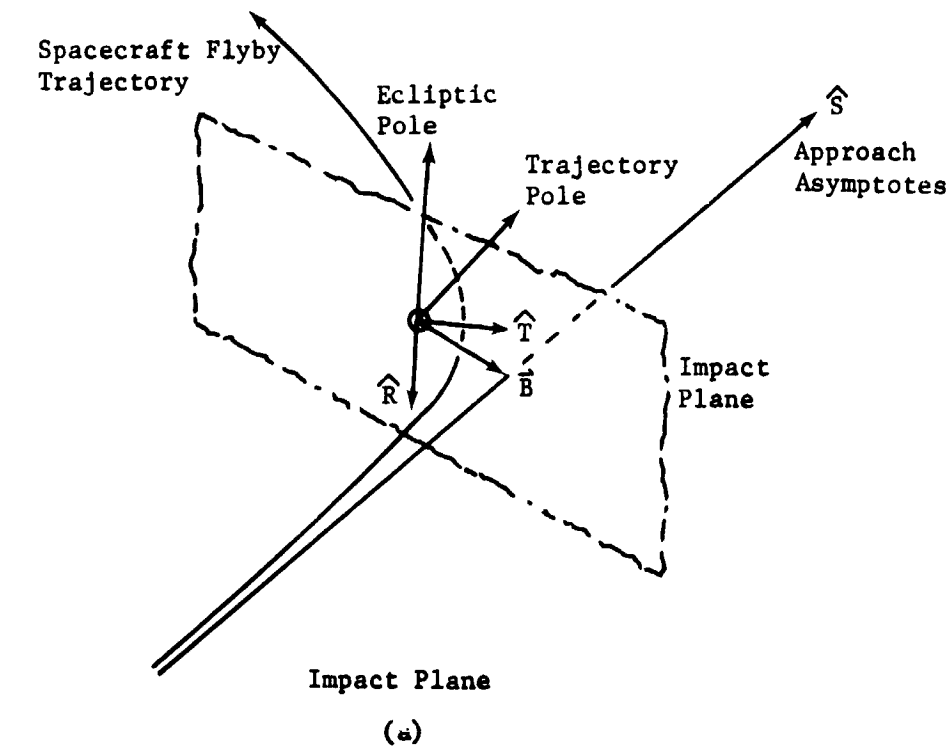


Figure IV-7 Impact Plane and Uncertainty Ellipse

where  $\hat{K}$  is the normal to the ecliptic plane. The  $\hat{R}$  axis completes The RST right-hand system

$$\hat{R} = \hat{S} \times \hat{T}$$

[B-13]

The angle  $\theta$  is the angle from the  $\hat{T}$  axis to the  $\vec{B}$  vector.

The distribution of dispersed trajectories can be described by an ellipse centered about the nominal impact point (Fig. IV-7(b)). Ellipse size is specified by the semi-major (SMAA) and semi-minor (SMIA) axes. The orientation is given by the angle  $\beta$ . Time-of-flight uncertainty is then the uncertainty in the time at which the impact plane is pierced.

The principal variables affecting the navigation and guidance analysis are tracking-station location uncertainties, tracking-station measurement noise, and planetary mass and ephemeris uncertainties. The coordinate system used is the ecliptic equinox.

The DSN tracking data used in the study are in Table IV-2. Equivalent station location errors are three times larger than the most optimistic predictions for the late 1970s (Ref IV-5), but are realistic in light of recent estimates for Viking 1975. The Doppler and range data noise are taken from Reference IV-7, supplied by the contractor. The measurement noise of 0.3 mm/sec for a 1-min count time is simulated by taking 10 measurements per day and using a Doppler uncertainty of 0.025 mm/sec ( $1\sigma$ ).

Additional data types appear necessary to alleviate tracking problems at the outer planets. When an approach trajectory has near-zero geocentric declination, as the case for the nominal trajectories at Jupiter and Saturn, it may be necessary to introduce QVLBI measurements (Ref IV-6). These measurements are modeled as near-simultaneous range measurements from two tracking stations widely separated in latitude. The noise level for these measurements is 3 to 6 meters. Some cases with optical tracking are considered and for these, the optical tracking is modeled with star-planet angle (SPA) and apparent planet diameter (APD) measurements. The noise level for these measurements is 10 arc-sec. Optical measurements are simulated by making one APD measurement and three simultaneous SPA measurements each 24 hours during those periods of time that optical tracking is being used.

The planetary ephemeris and mass uncertainties are based on References IV-8 and IV-9. The values are given in Table IV-3.

Table IV-2 DSN Tracking Data Summary

Tracking Stations	Equivalent Station Location Errors (1 $\sigma$ )	
Madrid	Distance from earth spin axis, m	1.5
	Longitudinal distance, m	3.0
Canberra	Distance parallel to spin axis, m	2.0
Goldstone	Station longitude correlation	0.97
Doppler noise: 0.5m, $5 \times 10^4$ sec count time = 0.3 mm/sec for 1-min count time		
Range noise: 150 m		

Table IV-3 Planetary Ephemeris and Mass Uncertainties (1  $\sigma$ )

Error	Jupiter	Saturn	Uranus
In-orbit track, km	500	750	10,000
Radial, km	300	750	10,000
Out-of-plane, km	100	250	2,000
Mass	$1.4 \times 10^{-5} M_J$	$1.14 \times 10^{-4} M_S$	$3.7 \times 10^{-3} M_U$

## 2. Approach Orbit Determination

The covariances at the time of deflection, which result from the approach orbit determination phase of the mission, are functions of approach trajectory, length of tracking arc, type of tracking data, and radius of deflection.

a. *Approach Trajectory* - The geocentric equatorial declination at approach has a very important effect on orbit determination. It is important because Doppler tracking degenerates for small values of this parameter according to the formula

$$\Delta \delta = \frac{\Delta r_s / r_s}{\tan \delta}$$

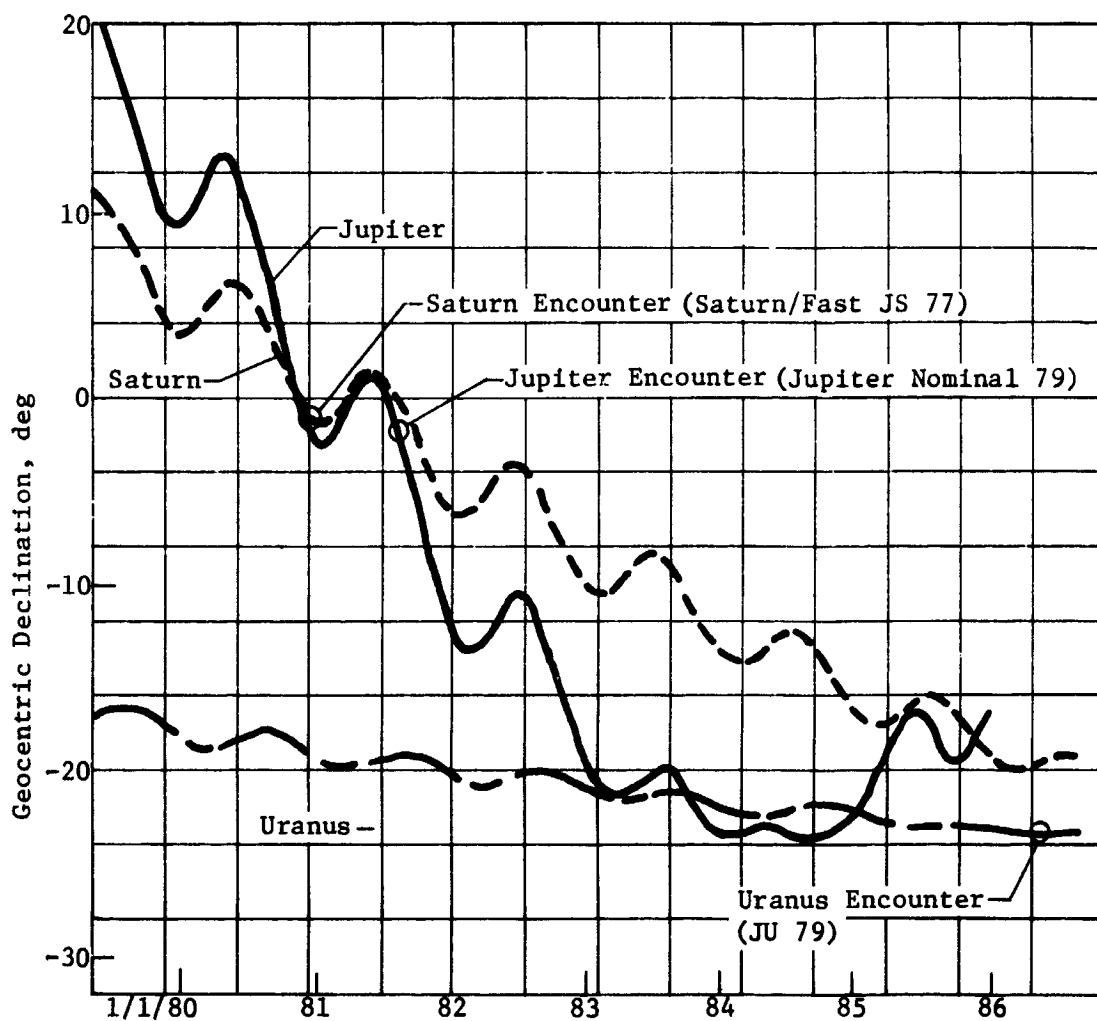
where  $\delta$  is the declination,  $r_s$  is the distance of the tracking station from the spin axis of the Earth, and  $\Delta\delta$  and  $\Delta r_s$  are the respective uncertainties in those parameters.

Figure IV-8 illustrates the variation of the geocentric equatorial declination of Jupiter, Saturn, and Uranus over an interval of about six years covering the region of interest for this study. Also shown are the spacecraft declinations for the Jupiter and Saturn approaches. The Uranus approach remains essentially constant at  $-23^\circ$  declination. Table IV-4 gives the control uncertainties for the Jupiter reference trajectories for 1978, 1979 (nominal probe optimal mission), 1980, and 1982. It is seen that indeed for the 1979 mission, the near zero declination geometry results in degradation of the orbit determination.

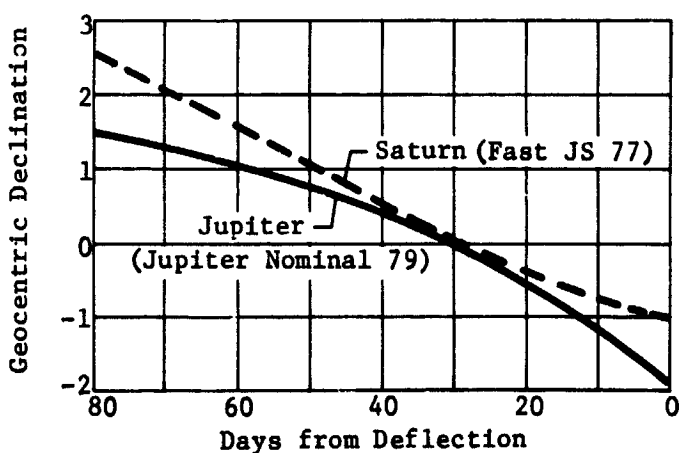
*b. Tracking Data Type* - When tracking data for Jupiter, Saturn, and Uranus are compared, it is seen that the uncertainties are progressively larger. Table IV-5 shows data for the approach orbit determination at the three planets using only ground-based DSN tracking. The increase in uncertainties with increasing distance from the Earth is due primarily to the increasing size of the ephemeris errors for the more distant outer planets.

The QVLBI-type of measurement can partially alleviate the problem at Jupiter and Saturn as it shown in Table IV-6. Both long and short tracking arcs are shown for Saturn as well as two noise levels for the QVLBI measurements. At Uranus, however, zero declination is not a problem; the tracking difficulty is due almost entirely to the very large ephemeris errors. Ground-based tracking is unable to observe any significant gravitational effect of the planet on the trajectory until quite near the planet ( $R \lesssim 10^6$  km). Thus, to reduce the uncertainties to reasonable levels, some sort of onboard optical tracking system will be necessary at Uranus. Table IV-7 compares ground-based tracking only, to ground-based plus optical tracking for both Saturn and Uranus. It is seen that significant improvements are made at both planets, although the time-of-flight error for Uranus remains quite large. Figure IV-9(a) shows the B-plane dispersions at Saturn with range/Doppler tracking only, with the addition of QVLBI, and optical tracking. Figure IV-9(b) shows the effect of a QVLBI measurement as tracking proceeds along a 30-day arc.





(a) Geocentric Declination of Planets



(b) Geocentric Declination of Spacecraft

Figure IV-8 Geocentric Declination of Planets and Spacecraft

Table IV-4 Variation of Control  
Uncertainty with  
Jupiter Launch Date

CONTROL UNCERTAINTY AT DEFLECTION					
YEAR	SMAA km	x	SMIA km	x	TOF sec
1978	972	x	287	x	46
1979	1511	x	311	x	46
1980	714	x	256	x	44
1982	458	x	242	x	44

Table IV-5 Control Uncertainties at Jupiter,  
Saturn, and Uranus for DSN Tracking  
Only

CONTROL UNCERTAINTY AT DEFLECTION					
PLANET	SMAA km	x	SMIA km	x	TOF sec
Jupiter					
Nominal 79	1511	x	311	x	46
Saturn/ Fast JS 77	2178	x	760	x	40
Uranus/ JU 79	9407	x	2411	x	1003
For 80-day tracking arc.					
Probe deflection radii are Jupiter 30M km, Saturn 10M km, Uranus 5M km.					

Table IV-6 Effect of QVLBI Measurement on Control Uncertainties

PLANET	CONTROL UNCERTAINTY AT DEFLECTION				
	SMAA km	X	SMIA km	X	TOF sec
Jupiter Nominal 79 (80-day arc)--					
range/range-rate	1511	x	311	x	46
with QVLBI	1289	x	308	x	49
Saturn/Fast JS 77 (80-day arc)--					
range/range-rate	2178	x	760	x	40
with QVLBI	1100	x	759	x	40
Saturn/Fast JS 77 (30-day arc)--					
range/range-rate	3943	x	1067	x	138
with QVLBI - 3m noise	1600	x	1055	x	70
with QVLBI - 6m noise	3010	x	1063	x	122
For the 80-day arc, the QVLBI measurement is after 20 days					
For the 30-day arc, the QVLBI measurement is after 5 days					
Both tracking arcs at Saturn terminate at 10M km radius					

Table IV-7 Effect of Optical Tracking on Control Uncertainties

PLANET	CONTROL UNCERTAINTY AT DEFLECTION				
	SMAA km	X	SMIA km	X	TOF sec
Saturn/Fast JS 77					
range/range-rate	3943	x	1067	x	138
with optical	468	x	234	x	39
Uranus/JU 79					
range/range-rate	9407	x	2411	x	1003
with optical	1277	x	424	x	440
For 30-day tracking arc					

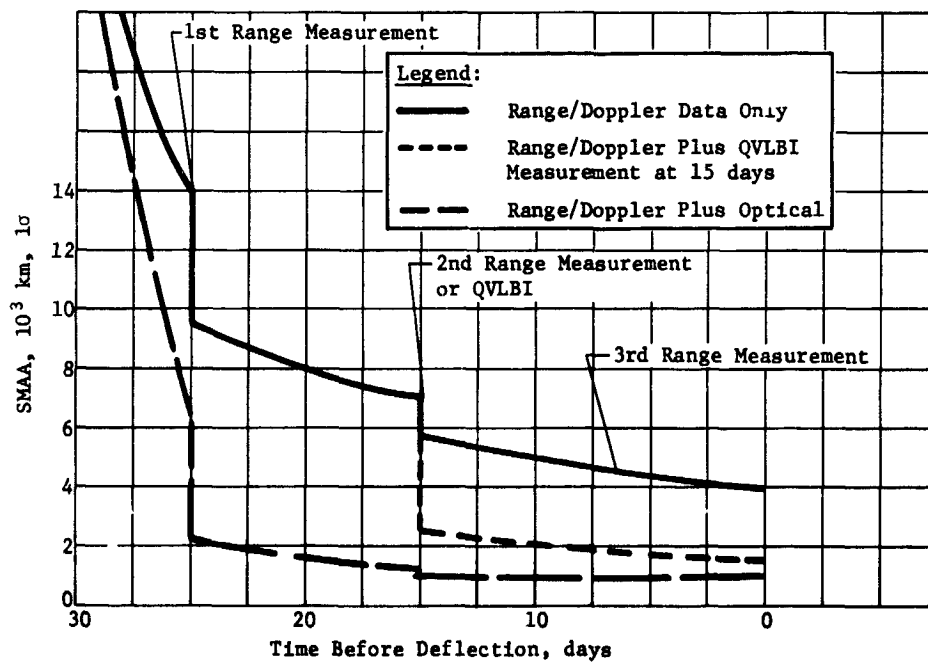
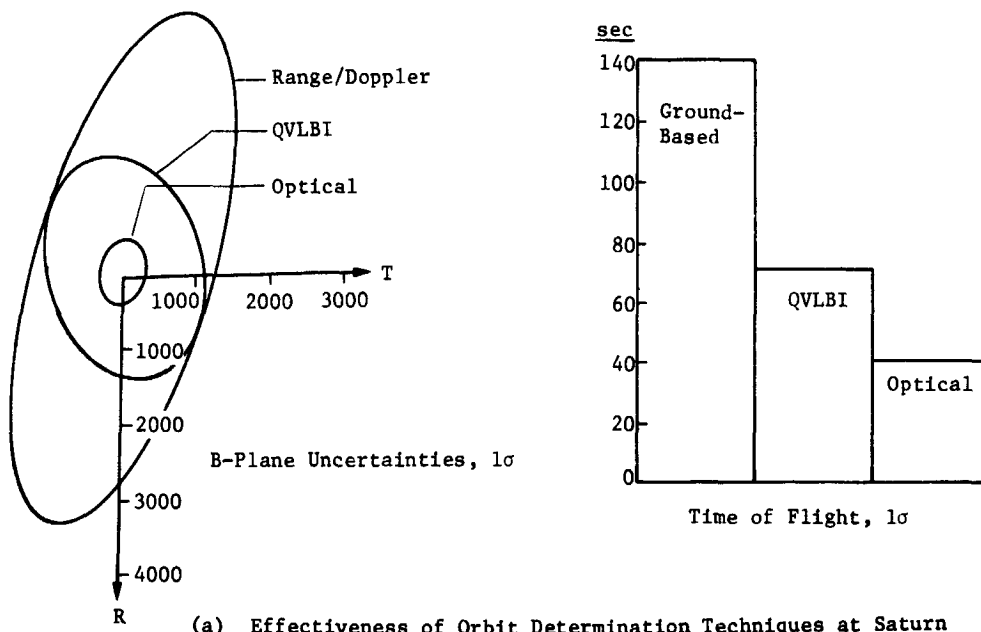


Figure IV-9 Approach Tracking at Saturn

c. *Tracking Arc Length* - Generally, a 30- to 40-day tracking arc is sufficient for ground-based tracking to reduce the uncertainties to a level consistent with the measurement and dynamic error models assumed. However, this is not the case for the nominal Jupiter and Saturn approach trajectories due to the zero declination problem. For both trajectories, zero declination is reached about 30 days before deflection (Fig. IV-7) so that a 30- to 40-day tracking arc produces significantly worse results than an 80-day arc. This is shown in Table IV-8. If short tracking arcs are required for these trajectories, then an additional data type may be necessary, either QVLBI or optical measurements.

*Table IV-8 Effect of Tracking Arc Length on Control Uncertainties Near Zero Declination*

PLANET	CONTROL UNCERTAINTY				
	SMAA km	X	SMIA km	X	TOF sec
Jupiter <sup>1</sup> (80-day arc)	1511	x	311	x	46
Jupiter <sup>1</sup> (30-day arc)	2613	x	459	x	147
Saturn <sup>2</sup> (80-day arc)	2178	x	760	x	40
Saturn <sup>2</sup> (30-day arc)	3943	x	1067	x	138
Ground-based range/range-rate tracking only					
<sup>1</sup> Jupiter Nominal 79					
<sup>2</sup> Saturn/Fast JS 77					

d. *Radius of Deflection* - Increasing the deflection radius generally increases trajectory uncertainties. This is to be expected since being nearer to the target planet leads to greater accelerations on the trajectory, which can be picked up by the navigation algorithm. The increasing uncertainty with radius, however, is rather small compared to the variation in uncertainty due to length of tracking arc or additional data types. Data for Jupiter, Saturn, and Uranus are shown in Table IV-9.

Table IV-9 Effect of Deflection Radius on Control Uncertainties

PLANET (deflection radius)	CONTROL UNCERTAINTY				
	SMAA km	X	SMIA km	X	TOF sec
Jupiter <sup>1</sup> (10M km)	1509	x	207	x	38
(20M km)	1566	x	236	x	42
(30M km)	1511	x	311	x	46
(50M km)	1315	x	361	x	66
Saturn <sup>2</sup> (10M km)	2178	x	760	x	40
(20M km)	2198	x	770	x	67
(30M km)	2253	x	767	x	85
Uranus <sup>3</sup> (5M km)	9407	x	2411	x	1003
(10M km)	9438	x	2421	x	1011
(15M km)	9441	x	2422	x	1013
<sup>1</sup> Jupiter Nominal 79					
<sup>2</sup> Saturn/Fast JS 77					
<sup>3</sup> Uranus/JU 79					

#### D. PLANETARY ENCOUNTER

The planetary encounter phase of the mission is taken to mean that part of the mission characterized by conic trajectories for the probe and spacecraft. The prime problems associated with planetary encounter include the design of the communication relay link, the selection of the approach trajectory, and the analysis of the deflection maneuver. These three problems are obviously not independent of each other but must be worked in an integrated fashion; they will, however, be discussed in the order stated as much as possible. An analysis of the problem of designing the encounter phase when a probe and orbiter mission are combined will then be given. This section will be limited to deterministic considerations only, the following section will discuss dispersion effects.

# 1. Design of Relay Link

The design of the relay link has a dominant influence on the entire planetary encounter phase. It affects the selection of the approach trajectory whenever that option is available. It places major design requirements on the deflection maneuver. It also is a prime consideration in the investigation of probe/orbiter missions.

The key parameters associated with the relay link analysis are illustrated in Figure IV-10. During the pre-entry phase, the probe is assumed to move on a conic trajectory in the attitude required at entry for zero relative angle of attack. During the entry phase, the probe rotates so its axis is radial relative to the center of the planet. During the descent phase, the probe is on a parachute descending along a radius vector as that vector rotates about the center of the planet at the angular rotation rate of the planet. Definitions of the relevant parameters follows.

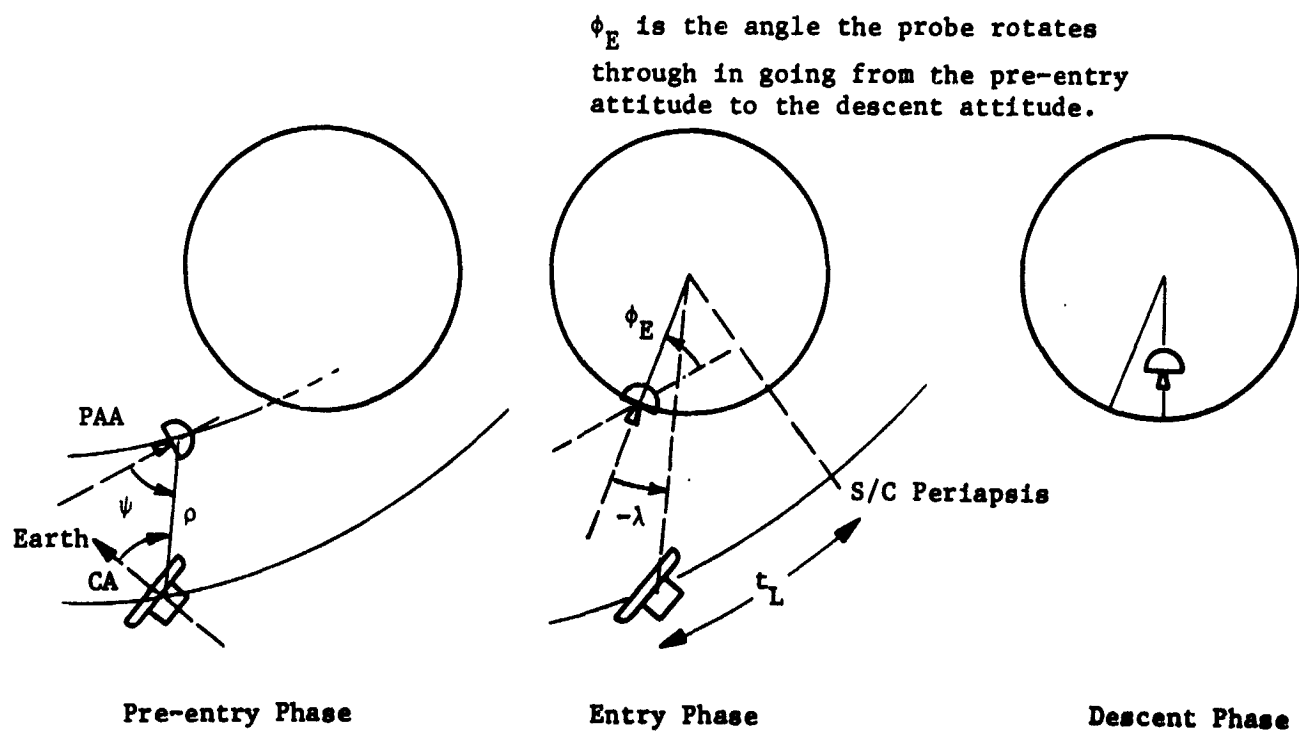


Figure IV-10 Relay Link Parameters

*Probe Aspect Angle (PAA),  $\psi$*  - The angle between the axis of the probe and the probe-to-spacecraft range. The PAA time history has a discontinuity at entry corresponding to the instantaneous rotation of the probe from pre-entry to descent attitude. The PAA would optimally be identically zero; practically this is not possible. The larger the values of the PAA, the more power is required for the probe antenna.

*Relay or Communication Range ( $\rho$ )* - The distance between the probe and spacecraft. This optimally is kept as small as possible.

*Lead Angle ( $\lambda$ )* - The angle between the spacecraft radius and the probe radius (projected into the spacecraft plane, if necessary) at entry. If  $\lambda$  is negative, the probe leads the spacecraft at entry; if positive, the spacecraft leads.

*Lead Time ( $t_L$ )* - The time from entry to spacecraft periapsis passage. If  $t_L$  is positive (the usual case) entry occurs before the spacecraft has passed periapsis.

*Cone Angle (CA) Clock Angle (CLA)* - The CA and CLA are here referenced to Earth and Canopus. The CA is the angle included by the Earth-spacecraft-probe alignment. The CLA then locates that direction relative to Canopus. A detailed illustration is provided in Section E of this chapter.

The probe aspect angle and the relay range are the two parameters most related to the link performance, and these should be held to as small values as possible. Generally, however, the probe aspect angle is the more important consideration; probe power requirements are generally reduced as the probe aspect angle is reduced.

During the descent phase, the probe is moving at the same angular rate as the planet. Thus, if the spacecraft were directly overhead at entry ( $\lambda = 0$ ) and moved at the same angular rate as the planet's rotation rate, the probe aspect angle would be zero. The attempt to achieve this is rotation rate matching. The angular rate of the spacecraft  $\dot{\theta}$  is given by  $r^2 \dot{\theta} = h$ , where  $h$  is the angular momentum of the spacecraft (determined by the approach velocity,  $V_{HP}$ , and the periapsis radius,  $R_p$ ). Since  $r$  is a function of time, the rotation rate of the spacecraft may be computed as a function of time for varying periapsis radii.



The results of such a study for the planets under investigation is provided in Figure IV-11. The rotation rate of each planet is indicated on the figures. To assess the sensitivity of the results, the rotation rates encountered when the approach velocity is varied is indicated for the  $1.5 R_p$  trajectory for each planet. It should be noted that the results given here are for equatorial entries only; the effective rotation rate of the probe is decreased as the latitude moves away from zero.

The selection of an effective communication geometry for a given mission requires an iterative search. The descent time for missions considered in this study are generally about half an hour for all planets. Thus, the rotation rate matching should be done to obtain equal rates averaged over this interval of time. Suppose for definiteness, the flyby periapsis is constrained to be  $2 R_J$  for a Jupiter mission. Then, it appears that the lead time should be about 1.3 hr to obtain effective rate matching. However, the nominal PAA, although staying roughly constant through the mission, might be at a large value. Thus, it may be desirable to decrease the lead time, which would result in the spacecraft angular rate being greater than that of the probe, and choose a lead angle that would have the probe initially leading the spacecraft at such a value that during descent the spacecraft would overtake the probe.

The inclination of the probe and spacecraft trajectories must also be considered in designing the link. The optimal arrangement is to have the probe and spacecraft trajectories both equatorial. If the probe enters at a nonzero latitude, during the descent it will rotate on a contour of constant latitude. The spacecraft trace is a great circle; therefore, the relative inclination of the two orbits must be chosen with care. This is especially critical with Uranus missions. Since Uranus pole is approximately in the ecliptic plane, it is generally impossible to obtain equatorial flybys. (The approach velocity  $V_{HP}$  at Uranus is typically along the pole and since the flyby orbit plane must contain this vector, low inclination orbits are impossible.)

The finalized communication geometries for each of the design missions are provided in Figures V-74, V-100, V-113, VI-16, and VII-12. A typical Neptune geometry is given in Figure VIII-2.

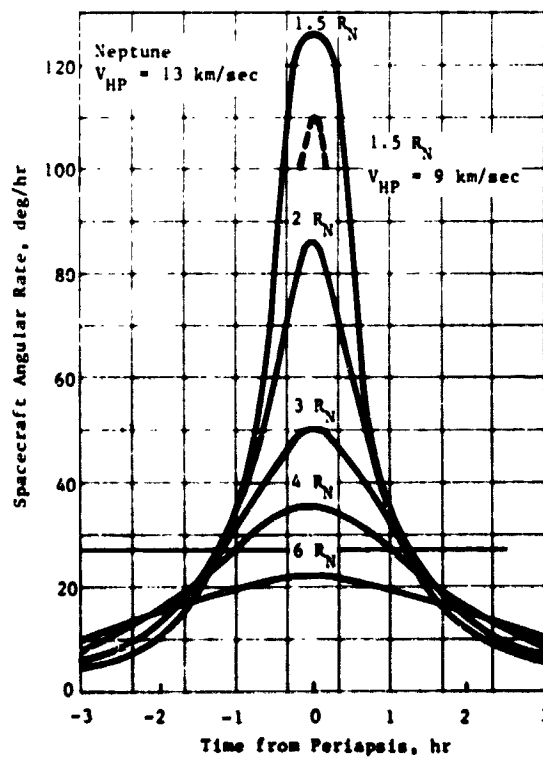
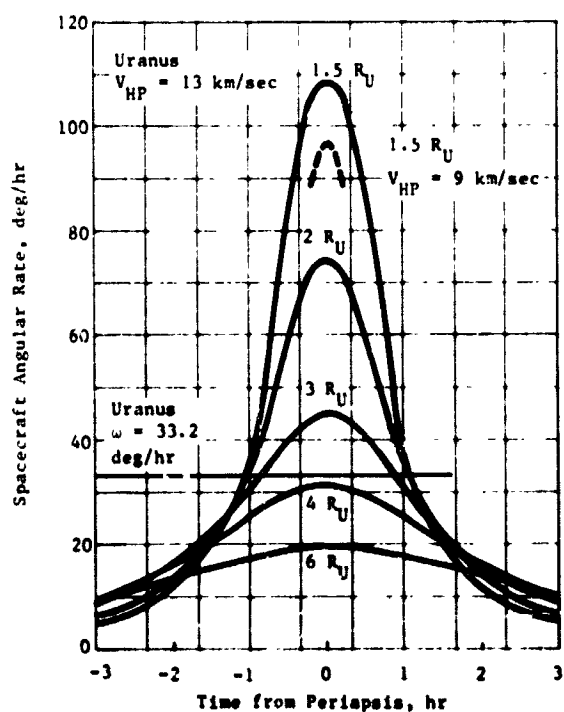
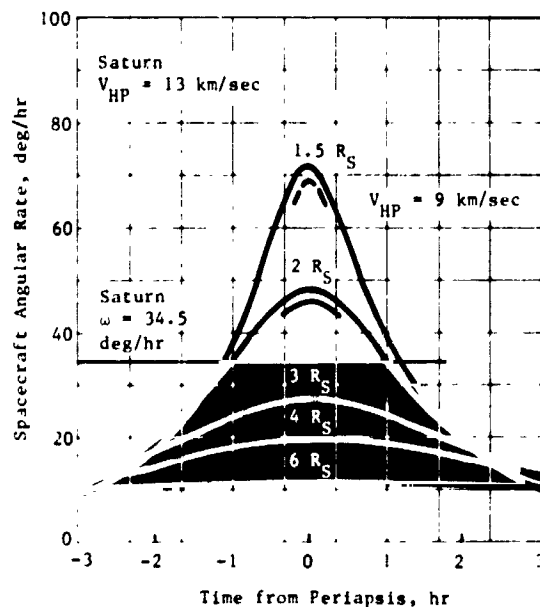
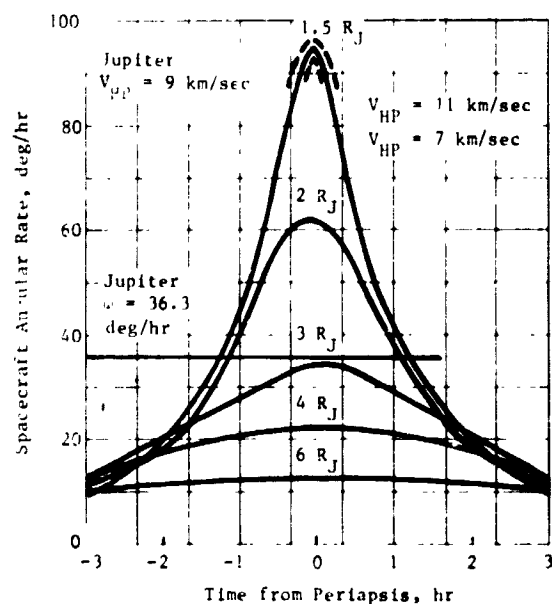


Figure IV-11 Rotation Rate Matching at Planets

## 2. Selection of Approach Trajectory

For many missions, the selection of the approach trajectory is constrained by considerations other than those of the probe mission. Thus, for missions involving gravity-assist swingbys, satellite encounters, or orbiter requirements, there may be little freedom in the selection of the spacecraft approach trajectory. For probe-dedicated missions, however, the flyby geometry may be selected to obtain advantageous results.

The rotation rate matching data (Fig. IV-11) is applicable for such an analysis. The periapsis radii that result in effective rate matching for small lead time missions of descent times near 30 min are about  $2.7 R_J$ ,  $2.5 R_S$ ,  $3.5 R_U$ , and  $5.0 R_N$  for Jupiter, Saturn, Uranus, and Neptune, respectively. The optimal periapsis radius is actually also dependent upon the approach velocity,  $V_{HP}$ , and the probe entry angle, and would involve some iteration to determine. Using the first guess of the optimal periapsis radius, the contours of possible entry sites and possible subperiapsis points would be constructed. (Similar to Fig. IV-30 thru IV-33). The time for the spacecraft to move from the entry site to periapsis would be computed and used as the first estimate of optimal lead time. The rotation rate matching figure would be consulted and a better guess on the spacecraft periapsis radius made. The process would be continued until convergence at the optimal value. Thus, there really is no standard optimum periapsis radius; it is very much a function of approach velocity, entry angle, and descent time. The values given above are thus to be used as reasonable approximations of the optimum.

## 3. Deflection Maneuver Parametrics

The deflection maneuver must accomplish three objectives: (1) place the probe on a trajectory intersecting the desired entry site, (2) orient the probe for zero relative angle of attack at entry, (3) establish an effective relay link between the probe and spacecraft.

The communication geometries that lead to effective links have been discussed in the previous two sections. This section will compare three modes for performing the deflection maneuver and then give parametric data on deflection  $\Delta V$  requirements.

a. *Comparison of Deflection Modes* - Three modes for implementing the deflection maneuver have been identified for analysis. Each can be used to acquire a given entry site and a desired communication geometry. The resulting trajectories for both the probe and spacecraft are almost identical for the three modes. The significant difference is in the deflection,  $\Delta V$ , rotations required, and the procedure used to effect the maneuver.

The first mode is the probe deflection mode. Here, the spacecraft is targeted to fly by the planet at the desired periapsis and inclination. At the deflection point, the  $\Delta V$  magnitude and direction are determined so as to deflect the probe to the entry site and establish the desired communication geometry between the probe and spacecraft. The probe must be aligned independently for the required attitude for zero angle of attack. The  $\Delta V$  and rotation generated can be executed in two distinct sequences depending on the type of thrusters used by the probe.

- 1) *Axial Thrusters* - The spacecraft is first rotated off Earth lock to orient, spinup, and release the probe so its axis is in the direction of deflection  $\Delta V$ . Deflection velocity is fired by the probe. The probe is then precessed, using an attitude control system (ACS), to obtain the attitude required for entry. The spacecraft reacquires Earth lock after probe release.
- 2) *Nonaxial Thrusters* - The spacecraft rotates off Earth lock, spins up, and releases the probe for zero angle of attack. A single thruster aligned in the required  $\Delta V$  direction (or a combination of thrusters whose net effect is in the same direction), then fires the deflection  $\Delta V$  to accomplish the maneuver. This thrust must not destroy the attitude of the probe. The difficulty in implementing this scheme makes it inferior to the first scheme.

The first mode, therefore, requires that the probe either have a  $\Delta V$  precession and ACS capabilities, or a very sophisticated  $\Delta V$  capability.

The second mode is the shared deflection. The spacecraft is again targeted to flyby conditions. In this mode, the probe  $\Delta V$  is constrained to the direction required for zero angle of attack. The magnitude is chosen so that the probe trajectory intersects the desired entry site. The spacecraft must then be accelerated to establish the required communications geometry. This correction

is applied in the direction of spacecraft velocity to minimize perturbations to the spacecraft trajectory. The implementation sequence for this mode follows.

- 1) The spacecraft rotates off Earth lock, spins up, and releases the probe for the zero angle of attack.
- 2) The probe then fires its axial thruster for its deflection  $\Delta V$ .
- 3) The spacecraft is then rotated to align it in the direction of its velocity.
- 4) After applying the correction velocity, the spacecraft is re-oriented toward Earth.

Thus, the probe is only required to generate the axial thrust; the spacecraft handles the other maneuvers.

The third mode of deflection, spacecraft deflection, has the simplest probe requirements of the candidate modes. The spacecraft trajectory is initially targeted to impact the entry site. The probe is spun up and released for zero angle of attack. The spacecraft is then deflected away from the planet to establish communication geometry and required flyby radius. Thus, the spacecraft performs all the maneuvers, and the probe is kept as simple as possible.

The deflection sequences for the three modes when applied to the nominal Jupiter mission are given in Figure IV-12. A comparison of  $\Delta V$  requirements for a variety of Jupiter missions is given in Figure IV-13.

*b. Comparison of Deflection  $\Delta V$  Requirements* - Deflection  $\Delta V$  requirements are given for a wide range of parametrics in Figure IV-13. The important trends will be summarized here.

*Deflection Radius* - The  $\Delta V$  requirements are reduced drastically as deflection radius is increased. This is apparent from the significant downward slopes of all the curves even when plotted on a logarithmic scale as in Figure IV-13.

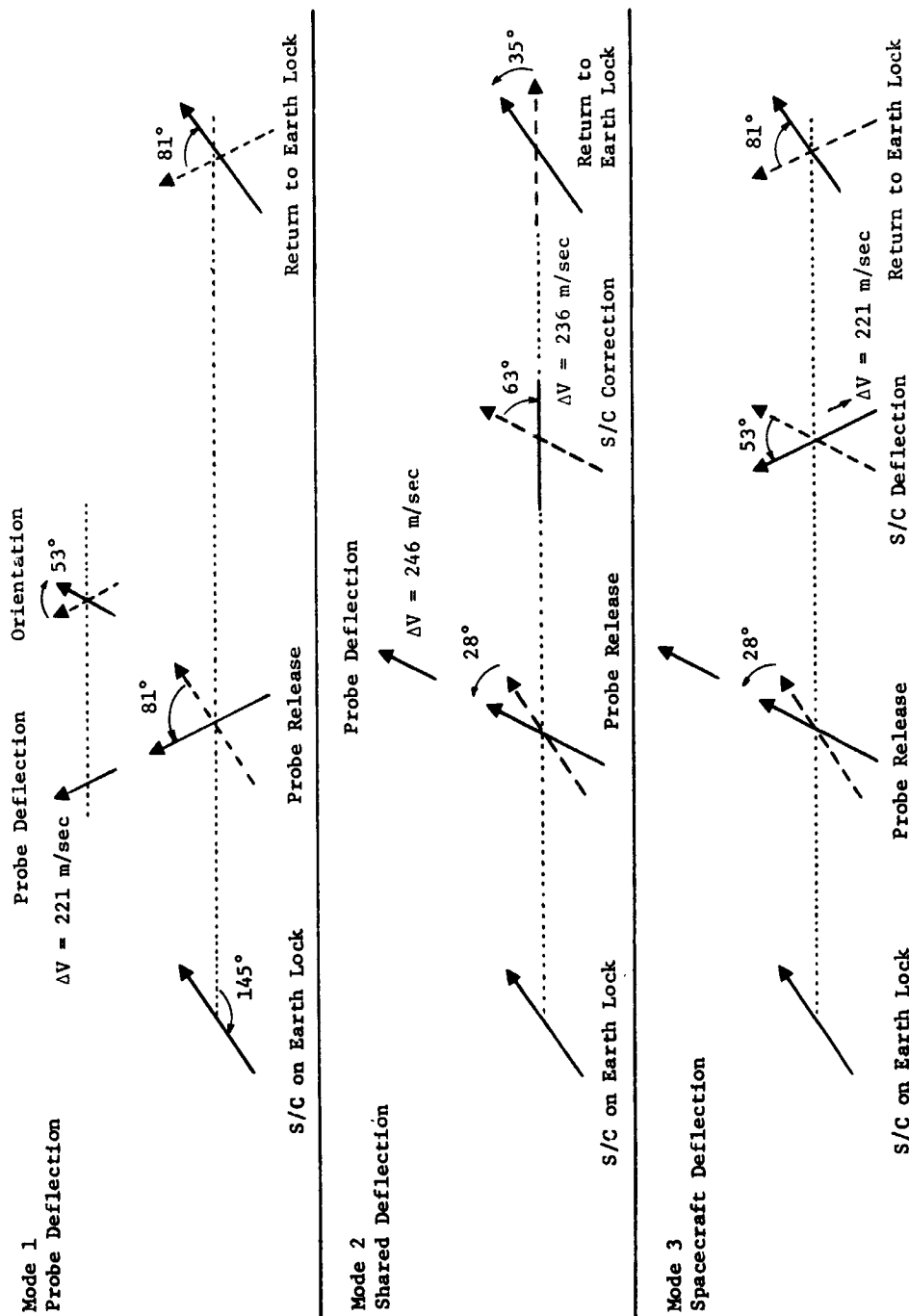


Figure IV-12 Comparison of Deflection Modes for Nominal Jupiter Mission

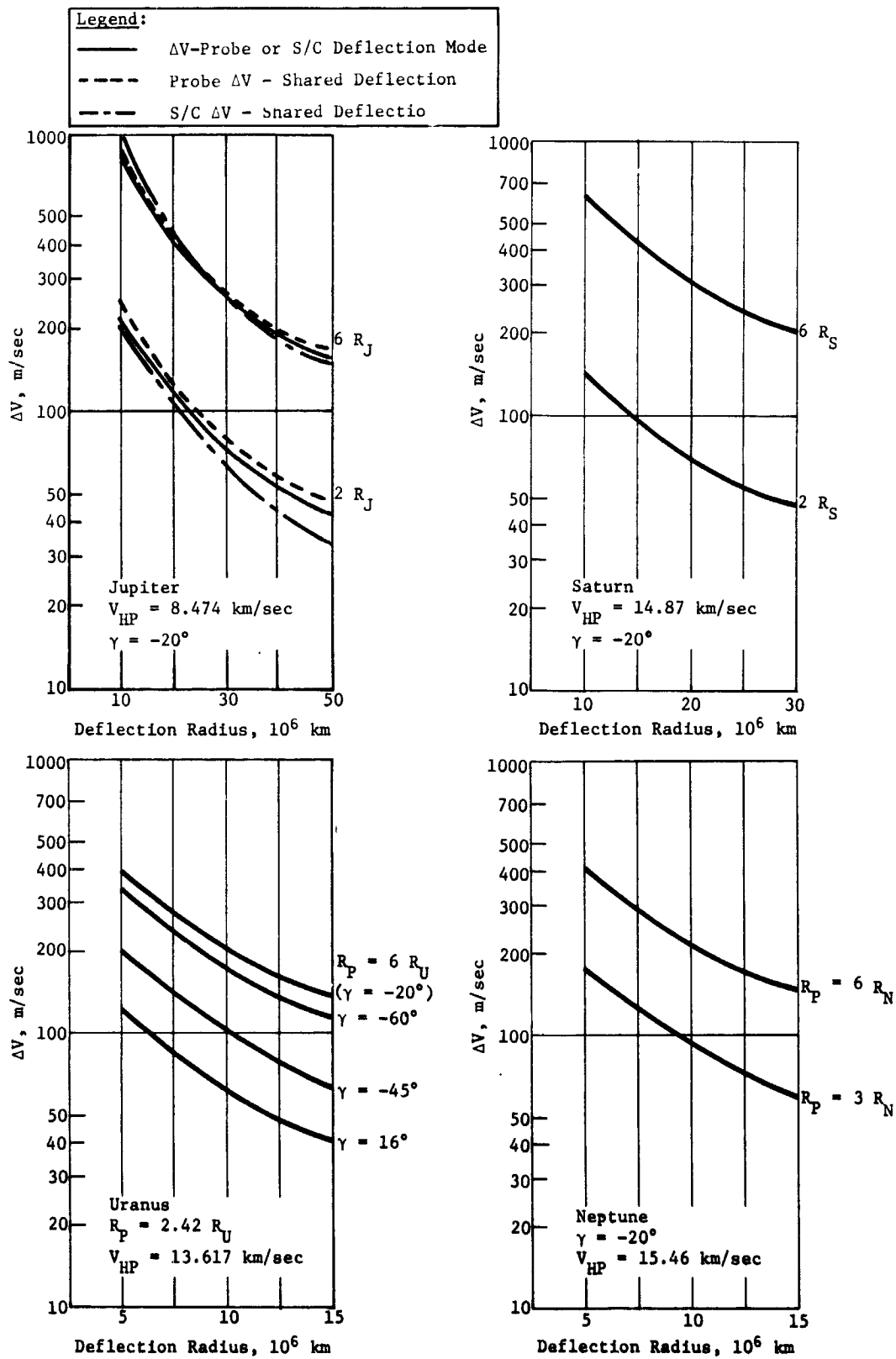


Figure IV-13 Comparison of Deflection  $\Delta V$  Requirements

*Spacecraft Periapsis* - The  $\Delta V$  requirements are about linearly proportional to the spacecraft periapsis; doubling the periapsis radius doubles the  $\Delta V$  requirement for a fixed deflection radius.

*Entry Angle* - The  $\Delta V$  requirements increase with entry angle as indicated for Uranus. For the Jupiter nominal mission ( $2 R_J$  periapsis,  $10 \times 10^6$  km deflection radius), the  $\Delta V$  requirements increased from 205 to 221 to 249 m/sec, respectively, as the entry angle increased from  $-10^\circ$  to  $-20^\circ$  to  $-30^\circ$ .

*Approach Velocity* - The  $\Delta V$  requirements increase only slightly with approach velocity  $V_{HP}$ . For the Jupiter nominal mission ( $2 R_J$  periapsis,  $10 \times 10^6$  km deflection radius,  $-20^\circ$  entry angle, the  $\Delta V$  increased from 214 to 221 to 225 m/sec as the  $V_{HP}$  was increased from 5 to 8.47 to 11 m/sec.

*Deflection Mode* - A comparison of the  $\Delta V$  requirements for the three deflection modes is provided in Figure IV-13. The  $\Delta V$  requirements for the probe in probe deflection and the spacecraft in spacecraft deflection are identical. Generally for shared deflection, the probe  $\Delta V$  is slightly higher than this value and the spacecraft  $\Delta V$  is slightly lower.

*Planetary Comparisons* - The  $\Delta V$  requirements are approximately proportional to the mass of the planet as indicated. Thus, reasonable deflection radius ranges appear to be 10-50 million km for Jupiter, 10-30 million km for Saturn, and 5-15 million km for Uranus and Neptune.

#### 4. Probe/Orbiter Mission Design

An interesting option for a Jupiter mission is to combine a probe mission with an orbiter mission. In this option, the probe mission must be totally completed before periapsis so that the spacecraft can be inserted into orbit at that time. Sufficient margin must be included in the phasing period (the time interval between end of probe mission and orbit insertion) to allow for operational procedures.

An optimal Jupiter orbiter mission for 1979 (Ref IV-1) having a periapsis radius of  $2 R_J$  was selected for the analysis of the sequencing problem. A probe mission involving a probe entering



at an entry angle of  $-20^\circ$  was integrated into the basic orbiter mission. Deflection maneuvers were performed at  $10 \times 10^6$  km leading to a variety of lead times (and thereby phasing periods). The resulting probe aspect angle (PAA) time histories and  $\Delta V$  requirements are illustrated in Figure IV-14.

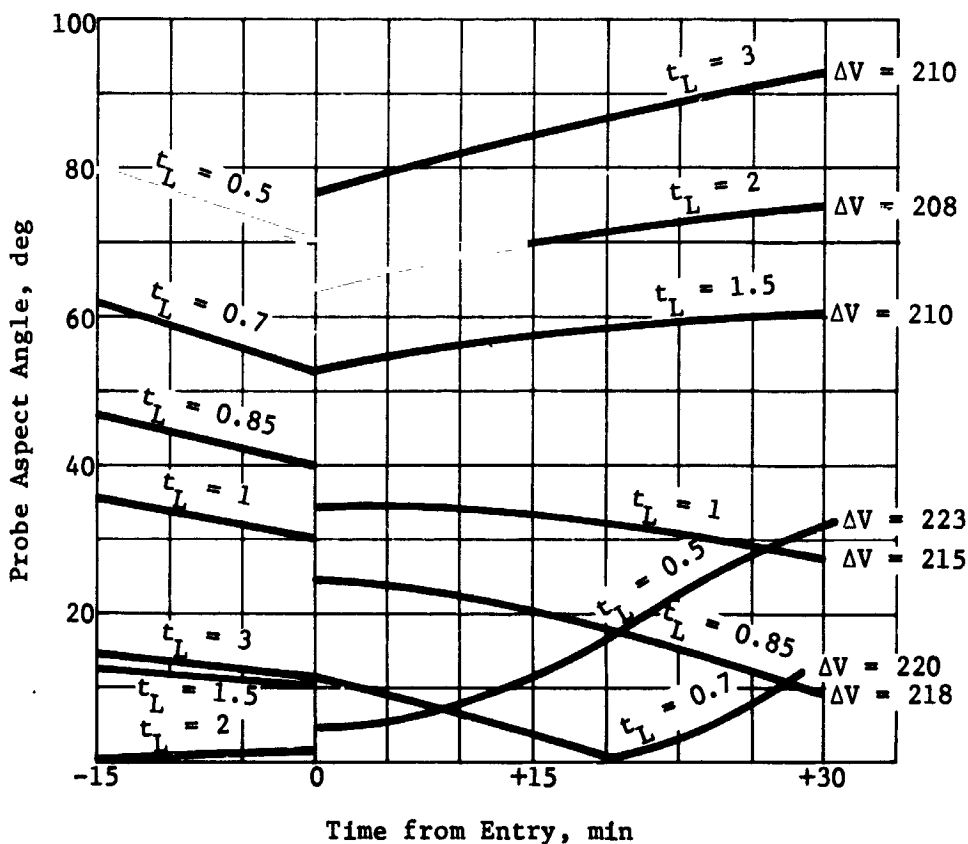


Figure IV-14 Link and  $\Delta V$  Requirements for Orbiter Missions

The optimal lead time for a simple probe mission is seen to be  $t_L = 0.7$  hr. This results in a descent probe aspect angle which starts at  $12^\circ$ , passes through zero, and ends at  $13^\circ$ . However, since descent is approximately 0.5 hr, the phasing period for this mission is only 0.2 hr. To obtain a phasing period of 1 hr significantly degrades the communication geometry; a lead time of 1.5 hr is required and this results in probe aspect angles of  $53^\circ$  to  $60^\circ$ . Thus, a definite penalty in communication geometry must be paid to obtain a compatible probe/orbiter mission.

A second penalty involves the added weight required for the insertion (or retro)  $\Delta V$  maneuver. The retro  $\Delta V$  requirements for a variety of possible orbits are summarized in Table IV-10. The nominal Jupiter mission is the 1979 mission chosen for detailed analysis. The Jupiter orbiter mission is the optimal mission discussed above. The apoapsis radii of 5.9 and 26.4  $R_J$  allow encounters with the Jovian satellites Io and Callisto, respectively. As indicated in the table, the retro  $\Delta V$  for the nominal mission differs from the optimal  $\Delta V$  by less than 200 m/sec. The retro  $\Delta V$  for the reference missions in 1978, 1980, and 1982 were also computed and varied from the nominal 1979 mission by less than 10%.

Table IV-10 Comparison of Insertion  $\Delta V$  Requirements

MISSION	$V_{HP}$ , km/sec	PERIAPSIS, $R_J$	POAPSIS, $R_J$	RETRO $\Delta V$ , km/sec
Nominal Jupiter	8.474	2.0	2.0	5.134
Nominal Jupiter	8.474	2.0	5.9	6.519
Nominal Jupiter	8.474	2.0	26.4	2.186
Nominal Jupiter	8.474	2.0	100.0	1.219
Jupiter Orbiter	7.270	2.0	100.0	1.038

For the impact on launch weight, the  $\Delta V$  requirement was converted to a weight penalty for the Jupiter orbiter mission. For a Pioneer class spacecraft (initial weight of 600 lb), adding the  $\Delta V$  capability would increase the spacecraft weight by about 115 lb and would require about 265 lb in propellant. For a Mariner class spacecraft (initial weight of 1100 lb), the increase in spacecraft weight would be about 210 lb and the propellant weight would be 480 lb ( $I_{sp} = 230$ , propellant mass fraction = 0.7). Adding

this extra weight in the later opportunities (1980, 1982) may be feasible, but in the earlier launch years the extra payload requirements seriously reduce the launch period (see Section B of this chapter).

## E. DISPERSION ANALYSIS

Errors and uncertainties are inherent in any mission. Unavoidable errors in navigation and guidance processes lead to uncertainties in spacecraft state at the deflection point. Execution errors in the deflection maneuver itself cannot be escaped. These errors and their resulting dispersions must be considered in mission design.\*

Parameters whose dispersions are most critical fall naturally into two classes -- entry parameters and communication parameters: entry parameters are variables associated with probe entry, such as entry site, flight path angle, angle of attack, or time of entry; dispersion in these parameters can affect the science return of the mission. Communication parameters are quantities describing the communication link between probe and spacecraft, such as probe aspect angle, communication range, range rate, or range direction. Dispersions in communication parameters must be accounted for in the design of the link to ensure that science data can be returned to Earth.

### 1. Communications Link Dispersions

a. *Cone, Clock, and Cross-Cone Angles* - The direction that the spacecraft must look to see the probe is generally described in terms of cone angle (CA) and clock angle (CLA) referenced to the Earth and Canopus (Fig. IV-15). Cone angle is the angle included by the Earth-to-spacecraft-to-probe alignment. Clock angle is the angle between the Canopus meridian and the cone meridian measured clockwise looking toward Earth. The Canopus meridian is the great circle defined by the Earth-spacecraft axis and the Canopus direction. The cone meridian is the great circle defined by the Earth-spacecraft axis and the spacecraft probe direction.

---

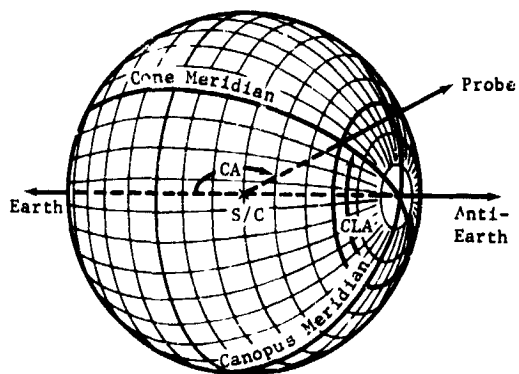
\* The dispersion results reported in this section were generated using a Monte Carlo analysis which combines the effects of both navigation uncertainties and deflection execution errors to produce the final dispersion. The computer program and analytic technique are summarized in Appendix I.

It is inconvenient to describe dispersions in spacecraft-probe look direction in terms of cone and clock angles. Figure IV-15 illustrates the problem. Location A has a nominal look direction of  $CA = 120^\circ$  and  $CLA = 75^\circ$  with circular dispersions about that point of  $10^\circ$  radius. In terms of cone angle and clock angle, dispersions would be  $\Delta CA = \pm 10^\circ$  and  $\Delta CLA = \pm 12^\circ$ , which adequately describe the area the spacecraft antenna must cover. However, suppose the same distribution is now moved to point B defined by a nominal cone angle of  $CA = 180^\circ$ . Now, dispersions in cone angle and clock angle are given by  $\Delta CA = \pm 10^\circ$  and  $\Delta CLA = \pm 180^\circ$ . Thus, the definition of dispersions in clock angle breaks down when the nominal cone angle is close to  $180^\circ$ .

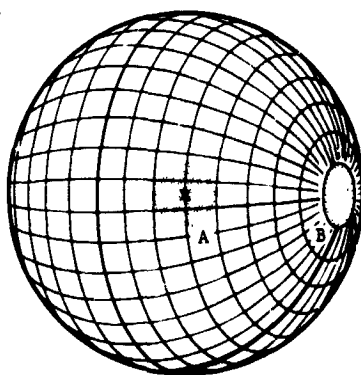
This problem can be eliminated by describing dispersions in spacecraft-probe look directions in terms of cone angle and cross-cone angle (XCA). Given the nominal look direction, the cone meridian can be constructed as usual. The cross-cone circle is the great circle normal to the cone meridian at the nominal probe point. As seen from the spacecraft, the cone and cross-cone axes appear to be Cartesian coordinates. Cross-cone dispersions remain well defined for all values of nominal cone and clock angles. Cross-cone and clock angle dispersions are approximately related by  $\Delta XCA = \Delta CLA \sin CA$ .

Dispersions in terms of cone and clock angles and in terms of cone and cross-cone angles are given in Fig. IV-16 for the Uranus mission of this study. Ellipses are plotted at times 37, 30, 10, and 0 min before nominal entry time and at actual entry time, respectively, for the points 1 through 5. The dramatic difference between the clock angle dimension and the cross-cone angle dimension is caused by the fact the nominal cone angle here is about  $160^\circ$ . For most of the missions, the cone angle is nearer  $90^\circ$  and the clock and cross-cone plots are nearly identical.

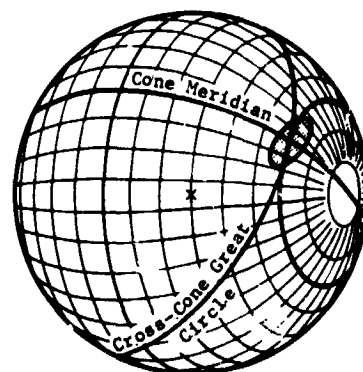
*b. Timing Uncertainties* - The active phase of the mission for the probe is initiated by a timer on the probe which activates an operational sequence fixed time interval,  $\Delta T_p$ , following the deflection maneuver. This operational sequence includes turning on the probe transmitter and the science instruments. The spacecraft must acquire the probe signal and transmit the relevant engineering data before communications blackout on the pre-entry antenna. Furthermore, the science instruments and particularly the accelerometers must be operating before entry so that the entry decelerations may be sensed.



a. Definition of CA & CLA



b. Dispersions in CA & CLA.



c. Definition of XCA

Figure IV-15 Cone, Clock, and Cross-Cone Angles

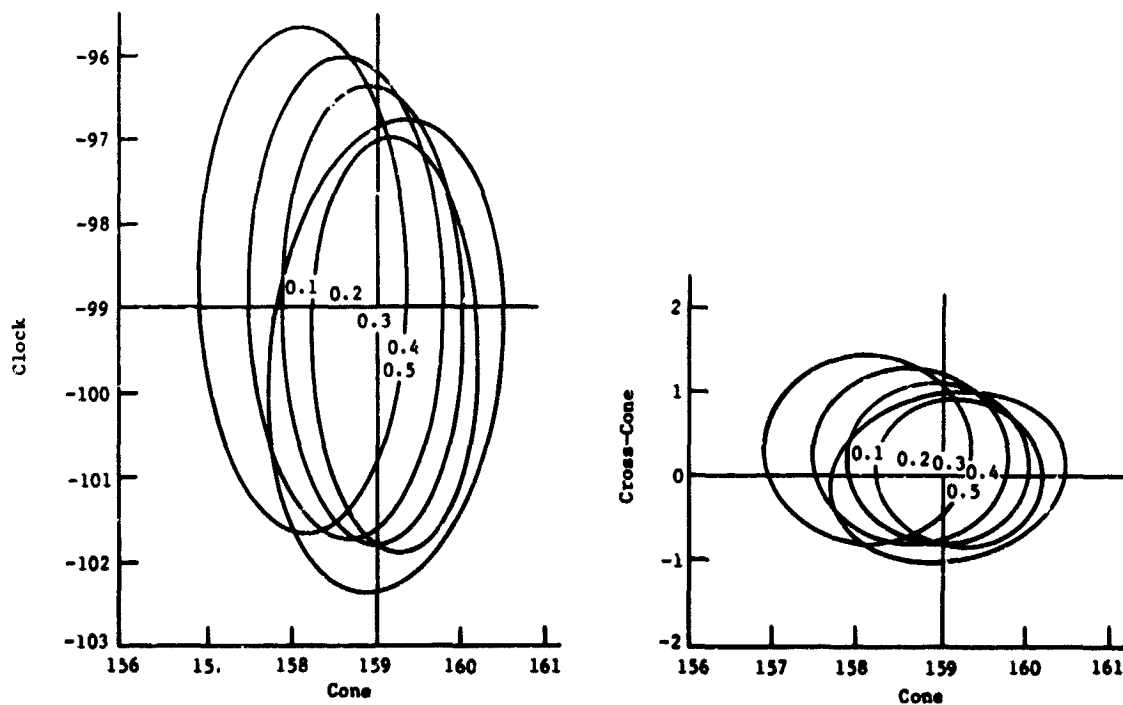


Figure IV-16 Spacecraft-Probe Look Direction Dispersions, Uranus Mission

Suppose that there were no uncertainty in the entry time. Then, if  $\Delta T_0$  were the time interval required for these operations between probe activation and probe entry, the timer could be based on a dormant time (time from deflection of probe activation) of

$$\Delta T_D^* = \Delta T_C - \Delta T_0 \text{ if no coast time uncertainty}$$

where  $\Delta T_C$  is the nominal coast time or time from deflection to entry. However, there is an uncertainty in the time interval from deflection to entry caused by uncertainties in the spacecraft state at deflection and deflection execution errors. Let  $\Delta t_u$  be the 3  $\sigma$  uncertainty in entry time. The probe activation (and probe acquisition time) must be set to

$$\Delta T_D = \Delta T_D^* - \Delta t_u = \Delta T_C - \Delta T_0 - \Delta t_u$$

where  $\Delta T_0$  is about 12 min for the complex probe and 6 min for the simple probe. Thus, the 3  $\sigma$  time of entry uncertainty, which is generally from 6 to 40 min, plays a critical role in determining the time of probe acquisition.

c. *Atmospheric Uncertainties* - The difficulty in modeling atmospheric uncertainties such as turbulence introduces problems into the communication parameter dispersion analysis. For this reason, certain assumptions must be made for the descent portion of the mission. The prime assumption is that the probe attitude while on the parachute is within  $\pm 20^\circ$  of vertical. This dispersion dominates the lead angle dispersions which never exceeded about  $8^\circ$ . This uncertainty is then superimposed upon the nominal probe aspect angle time history to determine requirements on the probe RF system.

A similar model is used to determine the spacecraft look direction dispersions (CA/XCA dispersions). Here the CA/XCA ellipse at actual entry of the probe (distinguished from nominal entry time) is assumed to grow 10% from entry to end of mission. The linearly increasing ellipses are then superimposed upon the nominal time history of the CA/XCA directions to determine spacecraft antenna size and direction requirements.

The range, Doppler, and Doppler rate dispersions at entry and descent are totally dominated by the variations in the nominal values of these parameters. These, of course, must be considered in the design of the relay link system.

## 2. Deflection Dispersion Trends

A quantitative discussion of the deflection dispersion trends is given in this section. For each individual study, the variations in the dispersions ( $3\sigma$ ) of nine critical mission parameters are presented. Dispersions are given for entry parameters of entry time (time from deflection to actual entry of the probe), entry flight path angle, entry angle of attack, and entry site (in terms of angular uncertainties in downrange (DR) and crossrange (XR)). Dispersions ( $3\sigma$ ) are supplied for communication parameters of entry lead angle, spacecraft-to-probe look direction at entry (in terms of the cone angle (CA) and cross-cone angle (XCA) defined in the previous section) and spacecraft-probe range rate.

a. *Execution Error Levels* - The execution errors of the deflection maneuver are modeled as arising from three sources:

- 1)  $\Delta V$  proportionality error. This is an error in the magnitude of the delivered deflection  $\Delta V$ . Normally the  $3\sigma$  uncertainty for this error is about 1% for solid rocket engines.
- 2)  $\Delta V$  pointing error. This is an error in the direction of the net delivered  $\Delta V$  from the commanded direction. The magnitude of this error is varied over the range  $1^\circ$  to  $3^\circ$  ( $3\sigma$ ).
- 3) Probe orientation error. This is an error in the orientation of the probe for the zero angle of attack. This error was varied over the same range as the  $\Delta V$  pointing error.

The  $\Delta V$  pointing error dominates the  $\Delta V$  proportionality error as the pointing error produces a  $\Delta V$  component error normal to the nominal direction of approximately 1.7%, 3.5%, and 5.2% for pointing errors of  $1^\circ$ ,  $2^\circ$ , and  $3^\circ$  ( $3\sigma$ ). The probe orientation error affects only the entry angle dispersions. Table IV-11 presents the dispersions resulting from four different levels of execution errors about the Nominal Jupiter Mission. The deflection radius for this mission is  $10^7$  km and the deflection  $\Delta V$  is 221 m/sec. The last three cases are all run with proportionality errors of 1% ( $3\sigma$ ) and probe orientation errors of  $2^\circ$ . Navigation uncertainties were included in all cases. For the first case, no execution errors of any size were used.

Table IV-11 Entry Dispersions (3 $\sigma$ ) for Execution Error Levels on Jupiter Nominal Mission

$\Delta V$ POINTING ERROR (3 $\sigma$ ), deg	ENTRY TIME, min	ENTRY ANGLE, deg	ANGLE OF ATTACK, deg	LEAD ANGLE, deg	ENTRY SITE		SPACECRAFT PROBE LOOK		
					DOWNRANGE, deg	CROSSRANGE, deg	CA, deg	XCA, deg	DOPPLER, m/sec
No Errors	2.58	0.23	0.42	0.32	0.51	0.17	0.97	0.34	0.16
1.5	5.72	0.93	2.98	3.05	1.74	0.55	7.36	0.46	2.09
2.0	7.98	1.08	3.08	4.40	2.02	0.75	10.89	0.64	3.11
3.0	10.33	1.25	3.21	5.77	2.35	0.96	14.35	0.78	4.06

b. *Navigation Uncertainties vs Execution Errors* - The entry dispersions are produced by both errors in the spacecraft state at deflection caused by navigation uncertainties and errors in the delivered deflection  $\Delta V$  caused by implementation errors. Table IV-12 compares the relative contributions by these two error sources for missions at Jupiter, Uranus and Saturn. The execution errors (3  $\sigma$ ) in all cases are 1% proportionality, 2° pointing, and 2° orientation. The navigation uncertainties for Jupiter and Saturn assumed Doppler/range tracking only; the Uranus mission assumed optical tracking. For each mission, dispersions are given for navigation only and for the combined effects of both navigation and execution errors. It is seen that at Jupiter, the dispersions are totally dominated by execution errors. At Saturn, navigation and execution errors have about an equal effect. At Uranus navigation errors begin to dominate. In fact with Earth-based tracking, 1% of the probes would miss the planet. Even using optical tracking, the navigation errors have a significant contribution to the net dispersions.

c. *Deflection Radius Effects* - The selection of the deflection radius must consider the impact of dispersions. As shown in Section C of this chapter, the navigation uncertainties increase as the deflection radius increases. Since the deflection  $\Delta V$  magnitude decreases as the deflection radius is increased, the contribution due to execution errors also decreases. However, this is compensated for by the effect that increase the coast time from deflection to entry increases the time interval over which dispersions will grow.



Table IV-12 Dispersion Contributions from Orbit Determination and Execution Errors

MISSION	Model	ENTRY TIME, min	ENTRY ANGLE, deg	ANGLE OF ATTACK, deg	LEAD ANGLE, deg	ENTRY SITE		SPACECRAFT-PROBE DIRECTION		
						DR, deg	XR, deg	CA, deg	XCA, deg	DOPPLER, m/sec
Jupiter Nominal	No Exec	2.58	0.23	0.42	0.32	0.51	0.17	0.97	0.34	0.16
	With Exec	7.98	1.08	3.08	4.40	2.02	0.75	10.89	0.64	8.56
Saturn Fast JS 77	No Exec	4.50	2.79	1.66	2.50	4.56	2.09	1.21	0.71	0.76
	With Exec	6.58	3.41	3.75	3.25	5.60	2.30	5.16	1.28	1.02
Uranus JU 79	No Exec	22.54	4.44	1.75	3.79	6.40	2.52	0.95	0.52	0.18
	With Exec	22.89	6.08	3.37	6.60	8.46	8.04	1.40	0.98	0.25

Table IV-13 illustrates the trades in deflection radius. Here four missions which had used several values for deflection radius are compared. The execution errors ( $3\sigma$ ) are 1% proportionality and  $2^\circ$  pointing and  $2^\circ$  orientation for all missions. The general trend is that although the dispersions generally increase as the deflection radius increases, the size of the growth is very much mission-dependent.

d. *Entry Angle* - The variations in dispersions as functions of the entry angle are illustrated in Table IV-14. Both missions assume execution errors of 1% proportionality,  $2^\circ \Delta V$  pointing, and  $2^\circ$  orientation. The Jupiter trajectories are all deflected at 10 million km; the Uranus missions are deflected at 5, 10, and  $10 \times 10^6$  km for the entry angles  $-15^\circ$ ,  $-45^\circ$ , and  $-60^\circ$ , respectively. The Jupiter missions assume range/Doppler tracking while the Uranus missions assume optical tracking.

The general trend is predictable: the shallower the entry angle, the larger the entry parameter dispersions. The Uranus mission at  $-15^\circ$  had four probes (of 100 samples) missing the planet. For Uranus missions, it is, therefore, especially important to consider dispersions when selecting the entry site (entry angle).

Table IV-13 Entry Dispersions as Functions of Deflection Radius

MISSION	DEFLECTION RADIUS, 10 <sup>6</sup> km	$\Delta V$ , m/sec	ENTRY TIME, min	ENTRY ANGLE, deg	ANGLE OF ATTACK, deg	LEAD ANGLE, deg	ENTRY SITE		SPACECRAFT-PROBE DIRECTION		
							DR, deg	XR, deg	CA, deg	XCA, deg	DOPPLER, m/sec
Jupiter Nominal	10 30	221 73	7.98 11.83	1.08 1.33	3.08 3.39	4.40 6.47	2.02 2.50	0.75 0.76	10.89 10.68	0.64 0.58	3.10 4.28
Jupiter Radiation- Compatible	30	256	38.42	6.02	5.60	6.91	11.46	2.00	7.54	0.41	4.39
Saturn Fast JS 77	10 20 30	141 70 47	6.58 7.12 7.02	3.41 3.38 3.41	3.75 3.80 3.81	3.25 3.38 3.40	5.60 5.59 5.62	2.30 2.40 2.39	5.16 5.13 5.29	1.28 1.29 1.30	1.02 1.00 1.02
Uranus JU 79	5 10	337 170	22.51 22.89	5.92 6.08	2.80 3.37	6.51 6.60	8.00 8.46	4.83 8.04	0.99 1.40	0.88 0.98	0.24 0.25

Table IV-14 Entry Dispersions as Functions of Entry Angle

MISSION	ENTRY ANGLE, deg	MISSES OF 100 CASES	ENTRY TIME, min	ENTRY ANGLE, deg	ANGLE OF ATTACK, deg	LEAD ANGLE, deg	ENTRY SITE		S/C-PROBE DIRECTION		
							DR, deg	XR, deg	CA, deg	XCA, deg	RANGE RATE, km/sec
Jupiter Nominal	-10 -20 -30	0 0 0	8.04 7.98 8.01	2.64 1.08 0.87	3.65 3.08 3.02	5.07 4.40 3.75	5.03 2.02 1.63	0.45 0.75 0.90	10.99 10.89 5.66	0.49 0.64 0.64	3.69 3.11 2.37
Uranus JU 79	-15 -45 -60	4 0 0	24.07 22.59 22.89	12.80 5.80 6.08	3.66 3.10 3.37	11.83 5.56 6.60	18.98 7.86 8.46	2.37 3.69 8.04	1.40 1.67 1.40	0.81 1.44 0.98	1.18 0.35 0.25

e. *Deflection Modes* - A dispersion analysis was made of the three deflection modes as applied to the nominal Jupiter mission. The results are summarized in Table IV-15. Execution errors of 1% proportionality, 2°  $\Delta V$  pointing, and 2° orientation were held constant for all three modes. The spacecraft deflection mode is far superior to the other two modes in terms of entry parameter dispersions. This is because no  $\Delta V$  execution errors are added to the probe state at deflection. The shared deflection has slightly larger dispersions than the probe deflection because its probe  $\Delta V$  (246 m/sec) is slightly greater than the probe deflection  $\Delta V$  (221 m/sec).

Table IV-15 Entry Dispersions as Functions of Deflection Mode

DEFLECTION MODE	DEFLECTION $\Delta V$ , m/sec	ENTRY TIME, min	ENTRY ANGLE, deg	ANGLE OF ATTACK, deg	LEAD ANGLE, deg	ENTRY SITE		S/C-PROBE DIRECTION		
						DR, deg	XR, deg	CA, deg	XCA, deg	RELAY DOPPLER, km/sec
Spacecraft	221	2.68	0.21	2.35	5.02	0.18	0.54	9.27	0.87	4.04
Probe	221	7.98	1.08	3.08	4.40	2.02	0.74	10.89	0.64	3.10
Shared	246/236	7.80	1.55	4.12	5.96	2.87	0.80	10.75	1.01	4.10

The communication parameter dispersions are approximately the same for the spacecraft and probe deflection modes. The communication parameter dispersions are slightly larger for the shared deflection because execution errors are added twice in that mode.

f. *Navigation Types* - For Jupiter missions, the dispersions are essentially determined by execution errors. For Saturn and Uranus missions, navigation uncertainties play an important role in the generation of dispersions. Table IV-16 compares the dispersions resulting from several different types of tracking. In all cases, execution errors are 1% proportionality, 2°  $\Delta V$  pointing, and 2° probe orientation. The Saturn results are based on the 30-day tracking arc comparisons reported on in Section C of this chapter. Recall that the Saturn approach in the JS mission is near zero geocentric declination, and therefore QVLBI measurements are very effective. The progressive decrease in dispersions is marked as QVLBI and optical measurements are added to the standard range/Doppler measurements. The "perfect" navigation case represents the situation if there were no navigation uncertainties in the mission: the dispersions are resulting only from execution errors. These results are illustrated in Figure IV-17 for a visual comparison.

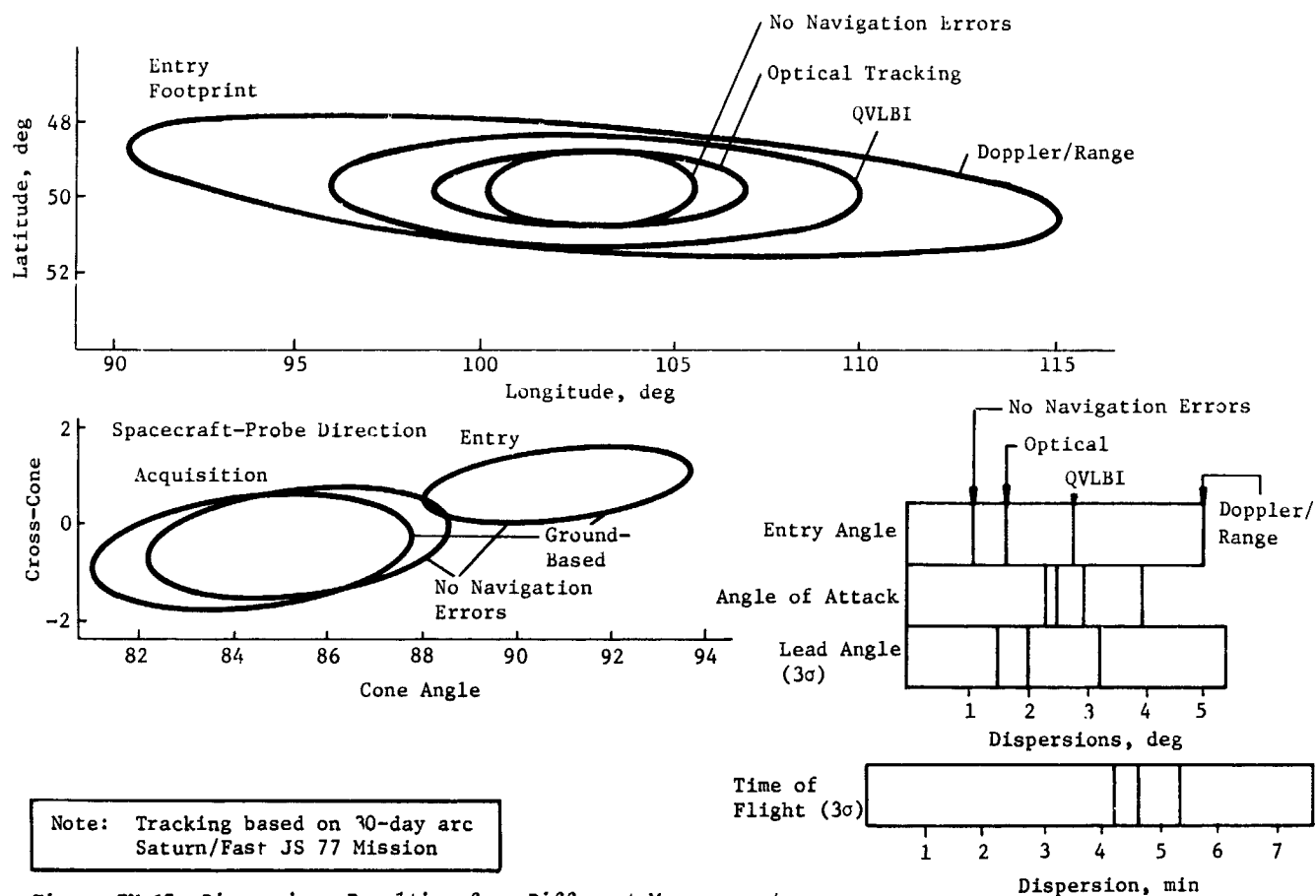


Figure IV-17 Dispersions Resulting from Different Measurement Types (Saturn/JST 77 Mission)

Table IV-16 Entry Dispersions as Functions of Navigation Types

MISSION	NEW TYPE	ENTRY TIME, min	ENTRY ANGLE, deg	ANGLE OF ATTACK, deg	LEAD ANGLE, deg	ENTRY SITE		S/C-PROBE DIRECTION		RANGE RATE km/sec
						DR, deg	XR, deg	CA, deg	XCA, deg	
Saturn JST 77	Range/Doppler	7.59	5.04	4.00	5.43	12.70	1.57	3.04	0.80	1.60
	QVLBI	5.34	2.84	2.95	3.19	7.18	1.56	2.21	0.78	0.96
	Optical	4.60	1.70	2.55	2.05	4.28	1.26	1.99	0.64	0.67
	Perfect	4.17	1.14	2.37	1.64	2.88	1.21	1.83	0.76	0.60
Uranus JU 79	Range/Doppler	59.37	37.86	16.07	42.05	79.48	43.91	9.89	1.46	1.67
	Optical	22.89	6.08	3.37	6.60	8.46	8.04	1.40	0.98	0.25
	Perfect	1.61	3.75	2.78	4.97	8.12	4.81	0.94	0.85	0.17

The results for Uranus are even more significant. Using standard range/Doppler tracking, the uncertainties in state at deflection are so large that even at a steep entry angle, one probe (out of 100 samples) missed the planet. Therefore, the dispersions indicated here result from the first 100 samples that did hit the planet. Going to optical tracking reduces all of the parameters dramatically except for time of flight error which is still large. The "perfect" tracking is indicated again for comparative purposes.

- g. *Spacecraft Periapsis* - Increasing spacecraft periapsis affects dispersions mainly through the proportional increase in deflection  $\Delta V$ , that is, increasing periapsis results in a larger  $\Delta V$  which then results in larger dispersions because of the proportionality execution error (see Table IV-17). These execution errors are partially counterbalanced in dispersions in certain parameters because of altered geometric effects. Thus, the dispersions in the spacecraft look direction are decreased by increasing spacecraft periapsis because even though the positional errors of the probe are increased, the greater distance between the probe and spacecraft results in smaller angular variations. The lead angle and Doppler dispersions increase only slightly for the larger spacecraft periapsis because of the slower spacecraft motion on the larger periapsis trajectory. The other parameters increase by approximately the ratio of the deflection  $\Delta V$ .

Table IV-17 *Entry Dispersions as Functions of Spacecraft Periapsis (Jupiter Nominal Mission)*

MISSION	SPACE- CRAFT PERI- APSIS	DEFLECTION RADIUS 10 <sup>6</sup> km	$\Delta V$ , m/ sec	ENTRY TIME, min	ENTRY ANGLE, deg	ANGLE OF ATTACK, deg	LEAD ANGLE, deg	ENTRY DR, deg	SITE XR, deg	SPACECRAFT PROBE DIRECTION		
										CA, deg	XCA, deg	DOPPLER, m/sec
JUPITER	2R <sub>J</sub>	30	73	11.83	1.33	3.39	6.47	2.50	0.76	10.68	0.58	4.28
Nominal	6R <sub>J</sub>	20	256	38.42	6.02	5.60	6.91	11.46	2.00	7.54	0.41	4.39

- h. *Entry Latitude* - Varying the entry latitude has no effect on dispersions as long as the inclination of the probe and spacecraft trajectories is chosen to allow the change in entry latitude to be obtained without varying the entry angle. Then the dispersions for the mission parameters are identical for changes in latitude except for possible orientations in entry site footprints or space-probe look direction ellipses. If entry angle is changed to vary the entry latitude, the effects are those described in subsection IV.E.2.d.

## F. PLANETARY ENTRY

The entry phase of the mission is initiated at a pressure level of  $10^{-7}$  atmospheres, continues through vehicle deceleration, and terminates when the vehicle reaches a velocity of  $M = 0.7$  at which time the aeroshell is staged. Typically, the entry phase lasts no longer than one minute; however, during this time, the probe experiences severe deceleration loads, dynamic pressures, and heating.

Selection of the entry angle, ballistic coefficient, staging altitude (or equivalently pressure), and their effect on the probe's entry environment is considered. Entries into the nominal atmosphere at Jupiter, Saturn, Uranus and Neptune were investigated for ballistic coefficients of 78.5, 157.1 and 235.6 kg/m<sup>2</sup> (0.5, 1.0, and 1.5 slug/ft<sup>2</sup>), and for inertial entry angles  $\gamma_{IE}$  ranging from  $-10^\circ$  to  $-60^\circ$ . The effects of variation in the atmospheric model was studied for Jupiter. All other planets studied considered only the nominal atmospheric model as defined in Appendix E. All of the entry data presented in this section were generated using Martin Marietta's UD208 entry program, modified to model ablation of the aeroshell's heat shield. For completeness, a brief description of the UD208 program is given including program options, typical input and output, and a discussion of the mass ablation model.

*Description of Entry Trajectory Program* - The UD208 program numerically integrates a trajectory through a planetary atmosphere to determine pertinent trajectory and aerodynamic parameters.

Inputs into the program are divided into the five categories listed in Table IV-18 along with representative category inputs.

Table IV-18 UD208 Input Data

VEHICLE DATA	INITIAL STATE
Reference Area	Altitude
Reference Length	Velocity
Nose Radius	Flight Path Angle
Weight	Inclination
PLANET DATA	AERODYNAMIC DATA
Radius	Lift vs Mach Number
Rotation Rate	Drag vs Mach Number
Gravitational Constant	Aeroshell Mass Ablation Model
Harmonics	
ATMOSPHERIC DATA	
Temperature and Pressure profiles vs Altitude	

The outputs of the program include histories of the following parameters: altitude, velocity (relative and inertial), flight path angle (relative and inertial), deceleration, Mach number, dynamic pressure, and geocentric latitude and longitude.

In order to generate time histories of the above variables, several assumptions are involved. These include the atmospheric model, mass ablation model, and the lift and drag coefficients defined as a function of Mach number. The atmospheric models used in this study, which include temperature, pressure, and density profiles as a function of altitude, are obtained from References IV-10, -11, -12, -13.

The entry velocities, particularly at Jupiter, are sufficiently high that a substantial portion of the heat shield is ablated. The mass ablation model incorporated in UD208 is described in Equation F-1.

$$M(t) = M_E \left\{ 1 - \frac{M_A}{M_E} \left[ f \left( \frac{V_R(t)}{V_{Re}} \right) \right] \right\} \quad [F-1]$$

where

$M_E$  = mass at entry

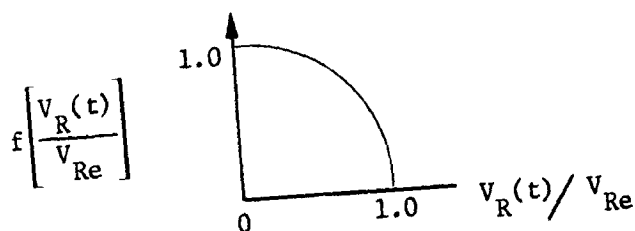
$M_A$  = total mass ablated

$V_R(t)$  = velocity at time,  $t$ , relative to the planetary atmosphere

$V_{Re}$  = relative velocity at entry

$f \left[ \frac{V_R(t)}{V_{Re}} \right]$  = fraction of total mass ablated as a function of the instantaneous velocity ratio  $V_R(t)/V_{Re}$

The function  $f \left[ V_R(t)/V_{Re} \right]$  is determined from empirical data available for entry simulations into the Jovian atmosphere and relates the fraction of total mass ablated to the instantaneous velocity ratio,  $V_R(t)/V_{Re}$ . The same functional relationship is assumed to be valid at Saturn, Uranus, and Neptune, and is used in their respective entry simulations. The general shape of the ablation curve is similar to the one shown below. The specific shape is determined from data presented in Reference IV-14.



At entry where the ratio of  $V_R(t)/V_{Re}$  is unity, Equation F-1 yields  $M_e$ , no mass yet ablated. When  $V_R(t) \ll V_{Re}$  the value of  $f[V_R(t)/V_{Re}]$  is unity and the total system mass approaches  $M_e - M_A$ , the mass at entry minus the total of the mass ablated.

The different ablative mass fractions,  $M_A/M_e$ , determined from Reference IV-14, are given in Table IV-19.

Table IV-19 Ablative Mass Fractions

MASS FRACTION	JUPITER	SATURN	URANUS	NEPTUNE
$\frac{M_{ABLATED}}{M_{ENTRY}}$	0.25	0.095	0.03	0.019

As indicated by the ablative mass fractions, entry into the Jovian atmosphere presents the most severe environment considered where one quarter of the mass is ablated during entry.

Aerodynamic research on hypersonic entries of sphere cone configurations has shown that for the configurations considered in this study, a good approximation to the variation of drag coefficient with Mach number is shown in the tabulation.

Mach No.	100	5	3	2	1.5	1.0	0.5	0
$C_D$	1.51	1.51	1.53	1.52	1.48	1.25	1.02	1.0

The UD208 program has the capability of accepting such tabular data.

To provide adequate sampling of the planetary atmosphere by the science instruments aboard the probe requires staging the aeroshell from the probe at a pressure level of 100 mb. Staging of the descent probe at subsonic velocities is desirable to take advantage of subsonic parachute technology.



Figure IV-18 shows how the staging conditions (stage above 100 mb at  $M = 0.7$ ) are affected by entry angle, ballistic coefficient and model atmosphere. As both ballistic coefficient and entry angle are increased, the altitude when  $M = 0.7$  decreases. This trend is consistent for the four outer planets studied. A Jovian entry into a cool/dense atmosphere presents the most severe restriction in selecting the ballistic coefficient. Therefore, any ballistic coefficient chosen, which results in adequate staging at Jupiter, is also acceptable at any of the other three outer planets. Also shown on Figure IV-18 are the altitudes corresponding to 100 mb for the five model atmospheres considered in this study.

Many parametric studies were performed in which ballistic coefficients, entry angles, and model atmospheres were varied. A condensation of this data given to indicate trends is shown in Figure IV-19. Shown on this figure are four graphs which apply to Jupiter; however, it is indicative of trends also observed at Saturn, Uranus, and Neptune. Graph (a) gives an indication of how the peak g-loading varies with model atmosphere and ballistic coefficient. Observations are as follows:

- 1) peak g-loading increases linearly with entry angle in the range from  $-10^\circ$  to  $-30^\circ$ ;
- 2) changes in ballistic coefficient between 0.4 and 1.4 has little effect on the maximum deceleration for the same entry angle;
- 3) entry into the cool/dense atmosphere results in peak deceleration which is approximately 50% larger than a corresponding entry into the nominal atmosphere. Unlike maximum decelerations, the maximum dynamic pressure varies directly with ballistic coefficients for similar entry angles and this is shown on Graph (b). The time histories of axial deceleration for different entry angles are shown in Graph (c). Both the shape and maximum value (time of occurrence and magnitude) is a function of entry angle. The time histories of dynamic pressure are shown for different ballistic coefficients in Graph (d).

All of the data shown in Figure IV-19 applies to equatorial entries in the direction of planetary rotation. Entering at latitudes other than equatorial results in increased relative entry velocity and an increase in peak decelerations. Entering at the pole of Jupiter requires an entry flight path angle of  $-41^\circ$  (see Figure IV-20 for the geometry) and results in a peak deceleration of 3500 g. The corresponding equatorial entry results in a peak deceleration of 2700 g, which is approximately 30% less than the polar entry.

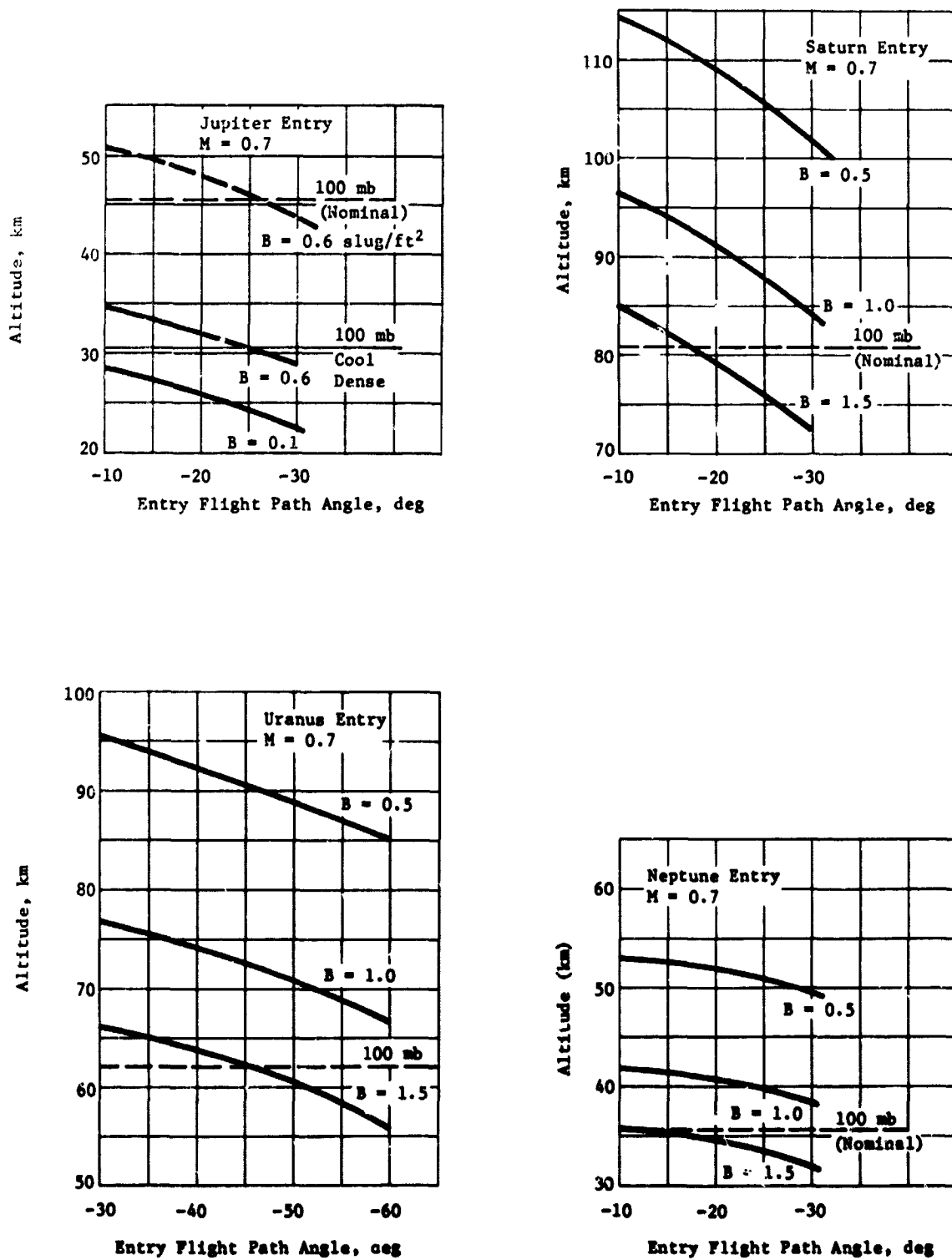


Figure IV-18 Deceleration to Subsonic Speeds

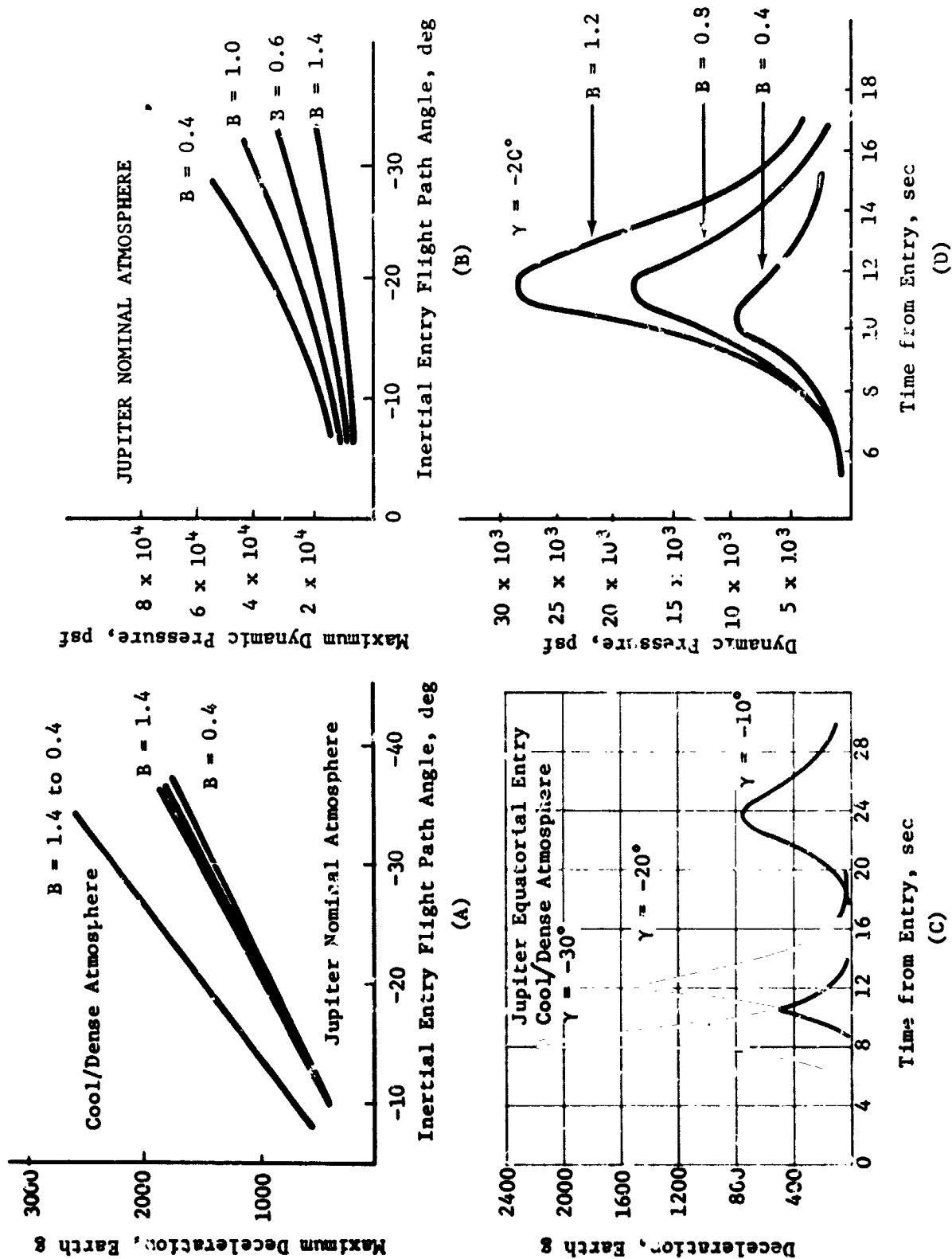


Figure IV-19 Typical Jupiter Entry Parametrics

Deceleration profiles for entry into the nominal Saturn atmosphere for both equatorial and polar entries is shown in Figure IV-21. Again the maximum decelerations for the polar entry are approximately 30% greater (320 vs 240 g) than for equatorial entry. The Saturn entry trajectories were simulated using the nominal atmosphere with an entry angle of  $-20^\circ$ . Decelerations experienced by the probe as it enters the Uranus atmosphere for  $\gamma_{IE} = -60^\circ$  and  $\gamma_{IE} = -45^\circ$  are plotted in Figure IV-22. Because of the relatively steep entry angles and the fact that the approach geometry precludes equatorial entry with rotation to reduce the relative entry velocity, the maximum decelerations at Uranus are roughly equivalent to those shown for Saturn. The deceleration time histories of entry into Neptune are shown in Figure IV-23. For comparison purposes, plots of maximum deceleration versus flight path angle for all four planets is shown in Figure IV-24. For an entry flight path angle of  $-20^\circ$ , the maximum decelerations for entry into the nominal atmospheres of Jupiter, Saturn, Uranus, and Neptune are 980, 250, 100, and 200 g, respectively. Maximum dynamic pressure versus entry flight path angle is plotted for entries into Jupiter, Saturn, Uranus and Neptune atmospheres in Figure IV-25.

The attitude velocity profile for the entry phase has a characteristic shape which descends vertically along a constant velocity line until the probe experiences the atmospheric forces that tend to decelerate it. Changes in velocity occur more rapidly than changes in altitude in this region. In the final descent phase, the weight of the probe is equalized by the drag and the probe descends vertically through the atmosphere. The four plots in Figure IV-25 illustrate altitude velocity profiles for Jupiter, Saturn, Uranus, and Neptune. Indicated on each graph are the altitudes and velocities at which maximum deceleration and staging occur. Figure IV-26(a) illustrates the effect the atmospheric model has on staging and maximum g altitude. Considering the nominal and cool/dense atmospheres for similar entry conditions, the variation in the altitude of maximum g is 30 km. A similar comparison of staging altitude results in a variation of 17 km. Figure IV-26(b) is the altitude velocity profile for varying ranges of ballistic coefficients for Jupiter entry. Increasing the ballistic coefficient tends to reduce the altitude for a given velocity. Saturn and Uranus velocity profiles are given on Figures IV-26(c) and IV-26(d).

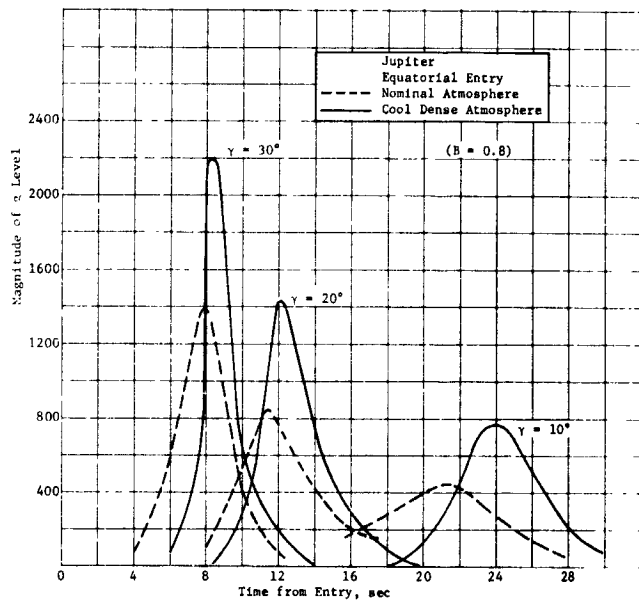


Figure IV-20 Jupiter entry decelerations

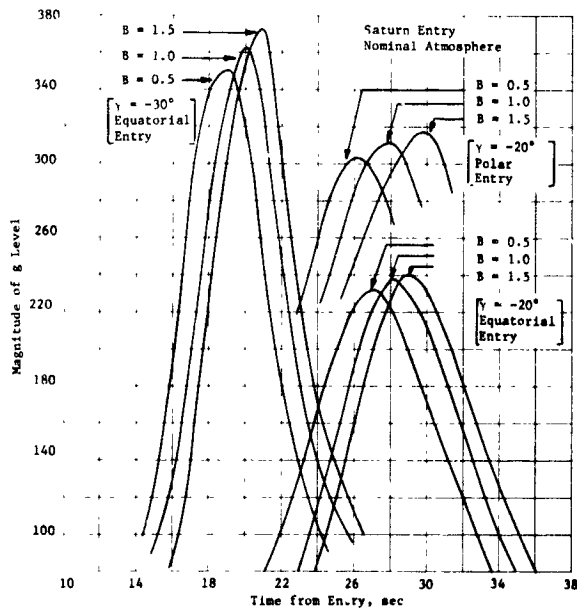


Figure IV-21 Saturn entry decelerations

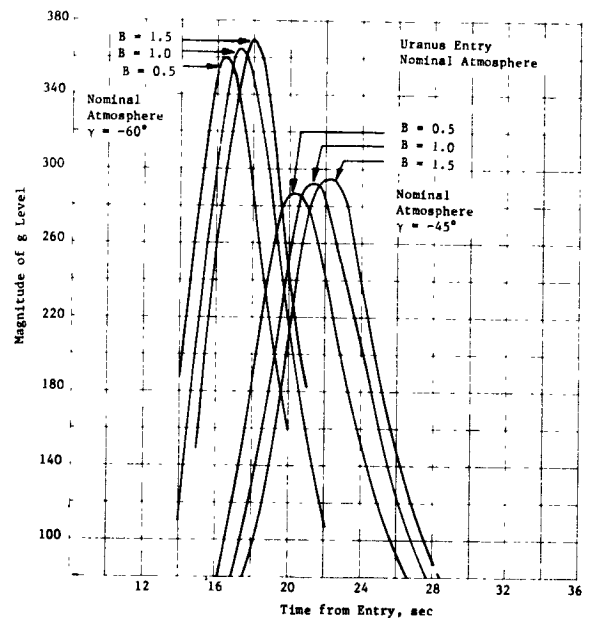


Figure IV-22 Uranus entry decelerations

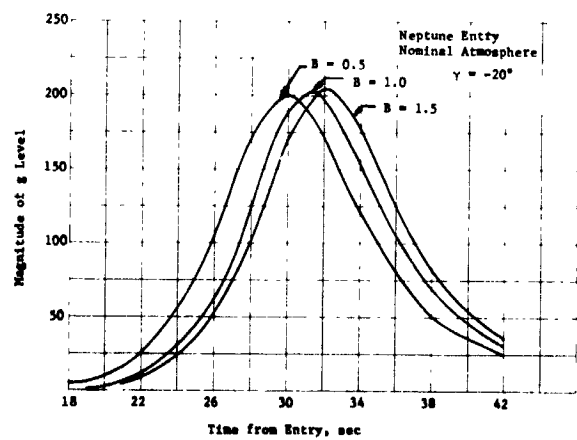


Figure IV-23 Neptune entry decelerations

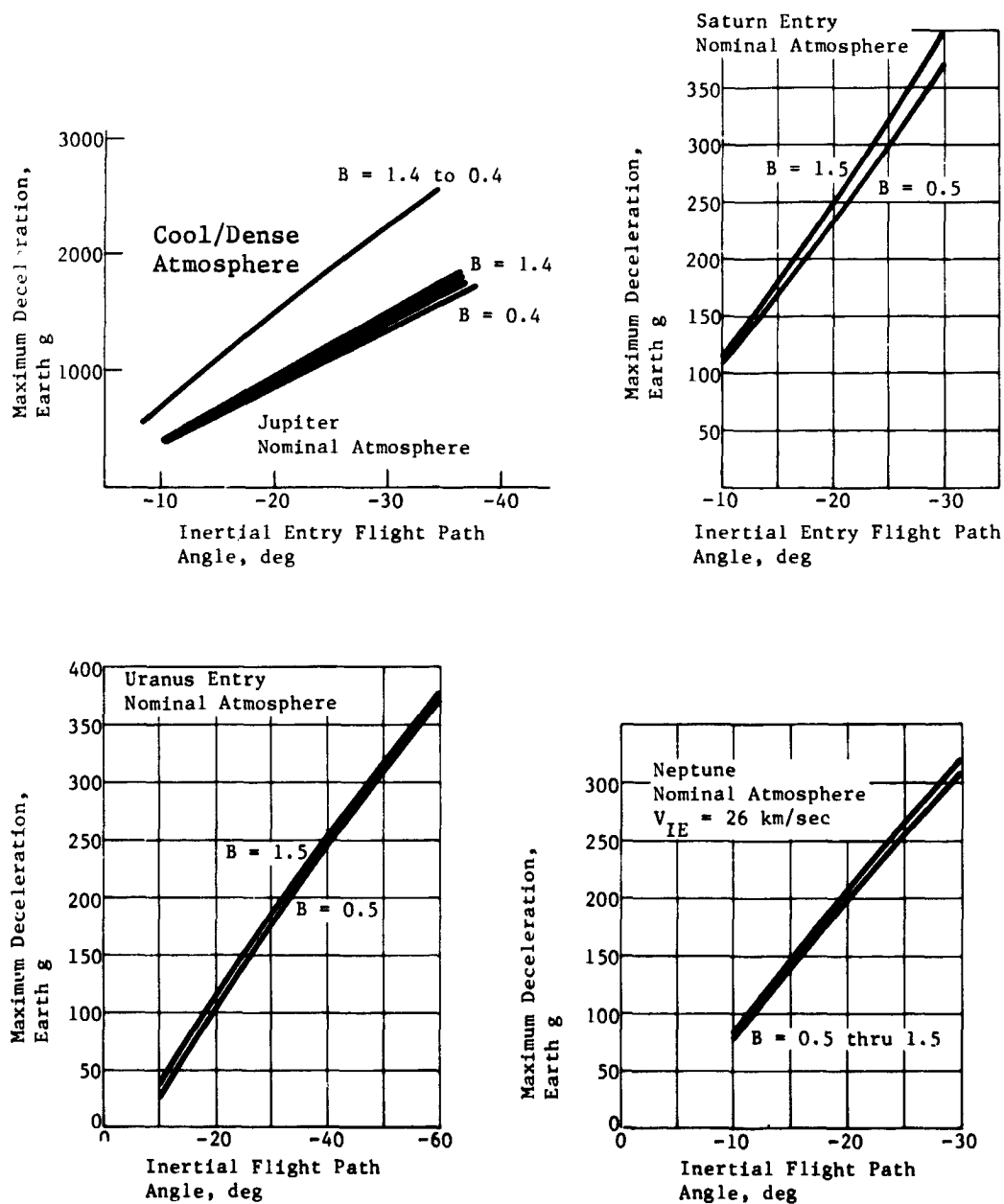


Figure IV-24 Maximum Deceleration Comparisons for Jupiter, Saturn, Uranus and Neptune

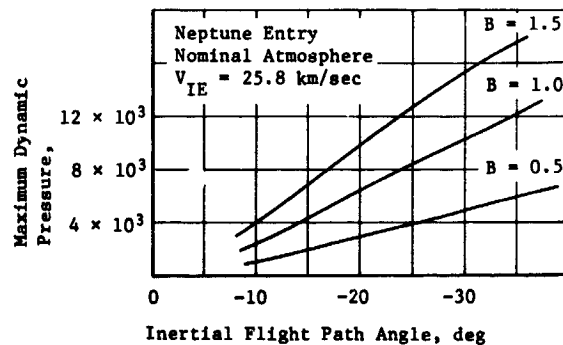
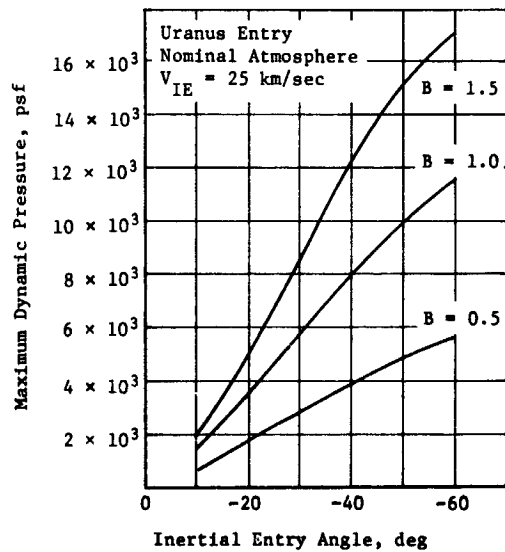
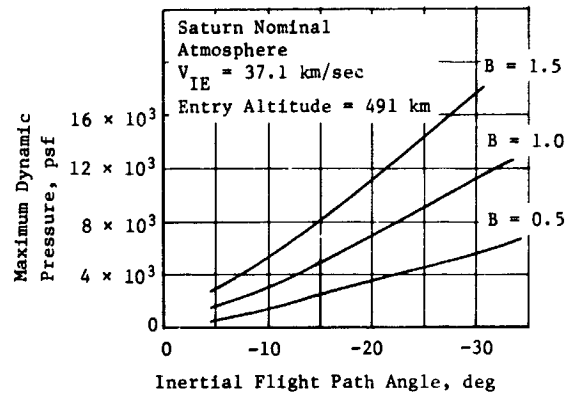
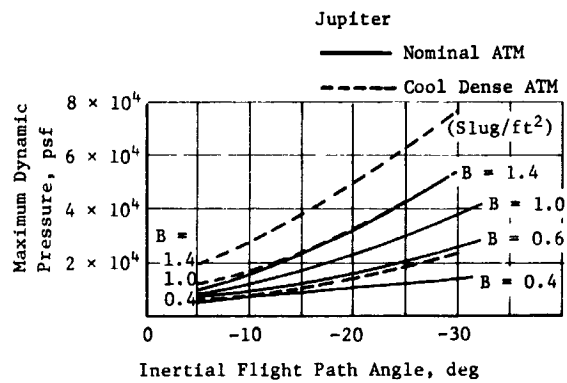
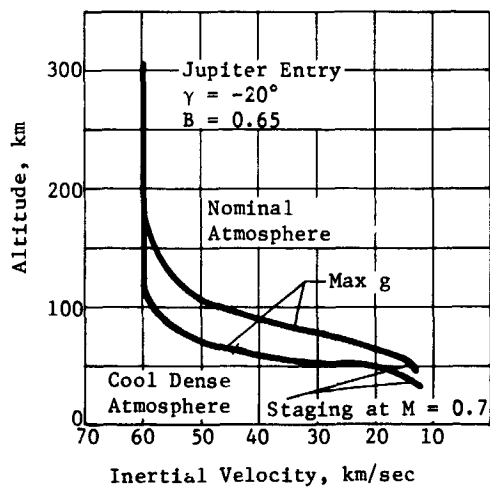
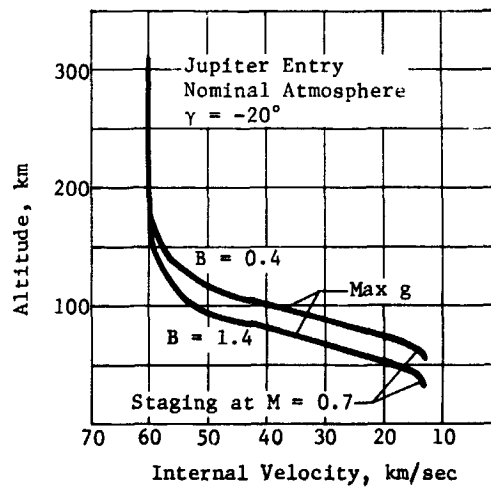


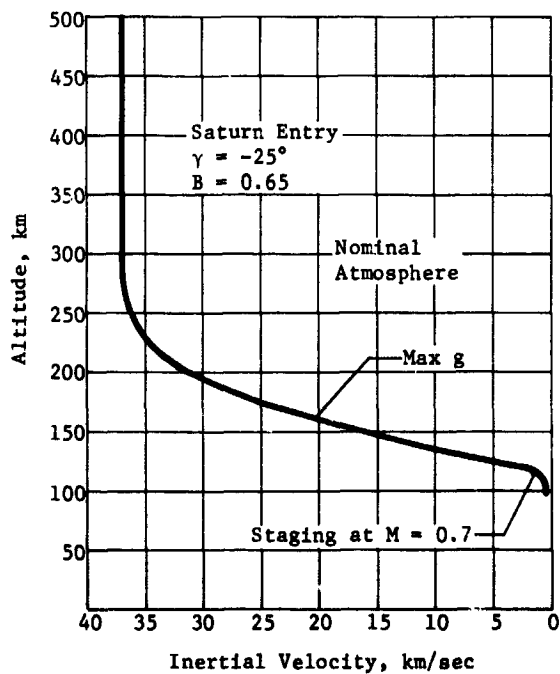
Figure IV-25 Maximum Dynamic Pressure Comparisons for Jupiter, Saturn, Uranus and Neptune



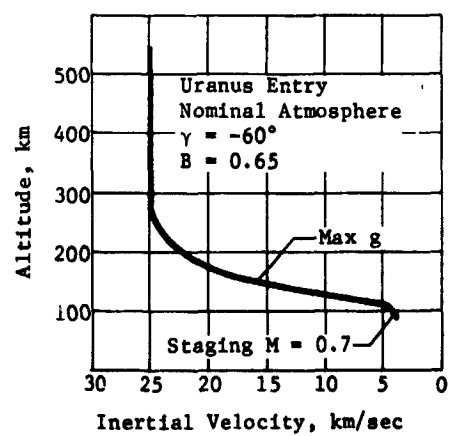
(a)



(b)



(c)



(d)

Figure IV-26 Velocity Altitude Profiles



From this parametric analysis, it is obvious that a probe entering the Jupiter atmosphere will encounter an extremely hostile aerothermodynamic environment; therefore, entry parameters that will minimize the severity of the environment should be selected. This was a contributing factor in the selection of shallow entry angles ( $-15^\circ$  to  $-20^\circ$ ) for the Jupiter reference missions. For the ballistic coefficients under consideration, shallow entry angles are also preferred if the aeroshell is to be staged above 100 mb.

Entry into the atmospheres of Saturn, Uranus, and Neptune places less of a restriction on the entry angle and ballistic coefficient selection than for Jupiter.

The high entry angle at Uranus ( $-60^\circ$ ) was primarily selected from landing site and dispersion considerations. A brief summary of the entry parameters for the five design missions is given in Table IV-20.

Table IV-20 Design Mission Entry Parameters

	JUPITER NOMINAL	JUPITER PROBE DEDICATED	JUPITER RADIATION COMPATIBLE	SATURN JST 77	URANUS JU 79
Entry Velocity (inertial), km/sec	60	60	60	37.1	25
Entry Altitude, km	304.6	304.6	304.6	491.0	531
Design Atmosphere	Cool/ Dense	Cool/ Dense	Cool/ Dense	Nominal	Nominal
Maximum Deceleration, g	1500	1650	1500	300	357
Time of Maximum g, sec	12.0	12.0	12.0	22.5	19.0
Altitude of Maximum g, km	65.0	65.0	65.0	158.0	138.0
Time of $M = 0.7$ , sec	34.0	34.0	34.0	78.5	54.5
Altitude of $M = 0.7$ , km	32.0	32.0	32.0	98.5	78.6
Inertial Entry Angle, deg	-20	-20	-20	-25	-60
Entry Ballistic Coefficient, $\text{kg/m}^2$	102.05	102.05	102.05	102.05	102.05
Maximum Dynamic Pressure, $\text{NT/m}^2$	$1.0 \times 10^6$	$1.1 \times 10^6$	$1.0 \times 10^6$	$2.8 \times 10^5$	$3.5 \times 10^5$

## G. MISSIONS TO OTHER PLANETS

Probe missions may eventually be made to all the outer planets. These may be based on gravity assist trajectories such as the JS 77 mission or gravity assist/solar electric propulsion trajectories such as the Sun 81-83 missions. The purpose of this chapter is to compare the parameters affecting mission design for these planets and to illustrate the interplanetary and planetary approach trajectories for selected missions receiving current attention.

Table IV-21 presents a comparison of the critical mission analysis parameters for each of the planets under consideration. Of special interest for probe entry missions is the relative size of the gravitational constants and escape velocities which set a lower bound on entry velocities. Also, the similarity in the rotation rates for the different planets should be noted.

*Table IV-21 Comparison of Planetary Constants*

PLANET	JUPITER	SATURN	URANUS	NEPTUNE
Gravitational Constant, $\text{km}^3/\text{sec}^2$	126.7	37.93	5.788	6.891
Escape Velocity, $\text{km}/\text{sec}$	60	37	22	25
Equatorial Radius, $\text{km}$	71422	59800	26468	24857
Rotation Rate, $\text{deg}/\text{hour}$	36.3	34.5	33.2	28.3
Obliquity*	3.1	26.7	97.9	29
*Obliquity here refers to inclination between planet equator and planet orbit plane.				

Table IV-22 summarizes the encounters at individual planets for the candidate swingby missions. The first four missions are ballistic trajectories using gravity assists; the last three missions are solar electric propulsion missions with planetary swingbys. The data summarized here is taken from Reference IV-1.

Figures IV-27 through IV-29 illustrate the nominal interplanetary trajectories for the candidate missions. The figures present projections of the trajectories into the ecliptic plane. The direction to the vernal equinox,  $\gamma$ , is noted on the figures.

Finally, the entry conditions corresponding to the various encounters at each planet are plotted in Figures IV-30 through IV-33. Contours of entry angles of  $-30^\circ$ ,  $-20^\circ$ , and  $-10^\circ$  are plotted on the figures for each approach. The terminator is also indicated.

Table IV-22 Comparison of Planetary Encounters for Candidate Missions

DEPARTURE, ENCOUNTER, AND FLYBY PARAMETERS							
MISSION		EARTH	JUPITER	SATURN	URANUS	NEPTUNE	PLUTO
JS 77	LD/AD	9/4/77	4/18/79	2/16/81			
	V <sub>HP</sub>	105 (C <sub>3</sub> )	10.62	13.66			
	R <sub>P</sub>			2.33			
	ZAP-ZAE			169.7-173.6			
	INC			76.8			
JSP 78	LD/AD	10/10/78	4/11/80	11/10/81			9/11/89
	V <sub>HP</sub>	109.6 (C <sub>3</sub> )	11.36	12.85			11.95
	R <sub>P</sub>		16.9	18.7			
	ZAP-ZAE		153.0-161.3	178.3-178.1			162.9-164.0
	INC		6.02	96.72			
JUN 79	LD/AD	11/6/79	6/19/81		5/19/86	3/12/90	
	V <sub>HP</sub>	102.4 (C <sub>3</sub> )	10.58		13.62	15.49	
	R <sub>P</sub>		9.9		2.4		
	ZAP-ZAE		150.7-161.4		175.5-174.3	166.1-167.9	
	INC		0.33		5.12		
JUN 80	LD/AD	12/8/80	5/19/82		10/24/87	4/27/92	
	V <sub>HP</sub>	112.2 (C <sub>3</sub> )	12.78		10.97	12.39	
	R <sub>P</sub>		26.0		3.7		
	ZAP-ZAE		156.4-161.0		166.4-168.8	171.2-172.9	
	INC		1.05		5.13		
SUN 81	LD/AD	11/24/81		3/8/85	1/20/89	1/11/93	
	V <sub>HP</sub>			10.26	12.44	13.31	
	R <sub>P</sub>			5.5	16.0		
	ZAP-ZAE				174.2-175.5	176.2-176.3	
	INC			6.05	34.6		
SUN 82	LD/AD	12/6/82		3/20/86	2/25/90	7/6/94	
	V <sub>HP</sub>			10.43	11.35	11.82	
	R <sub>P</sub>			9.1	21.5		
	ZAP-ZAE				178.0-176.4	177.1-177.0	
	INC			7.18	37.9		
SUN 83	LD/AD	12/18/83		4/1/87	6/27/91	7/19/96	
	V <sub>HP</sub>			10.59	9.96	9.92	
	R <sub>P</sub>			16.6	29.5		
	ZAP-ZAE				170.9-170.6	171.6-171.7	
	INC			8.97	36.8		
<b>Note:</b> 1. Reference plane is ecliptic. 2. R <sub>P</sub> given in planet radii.							

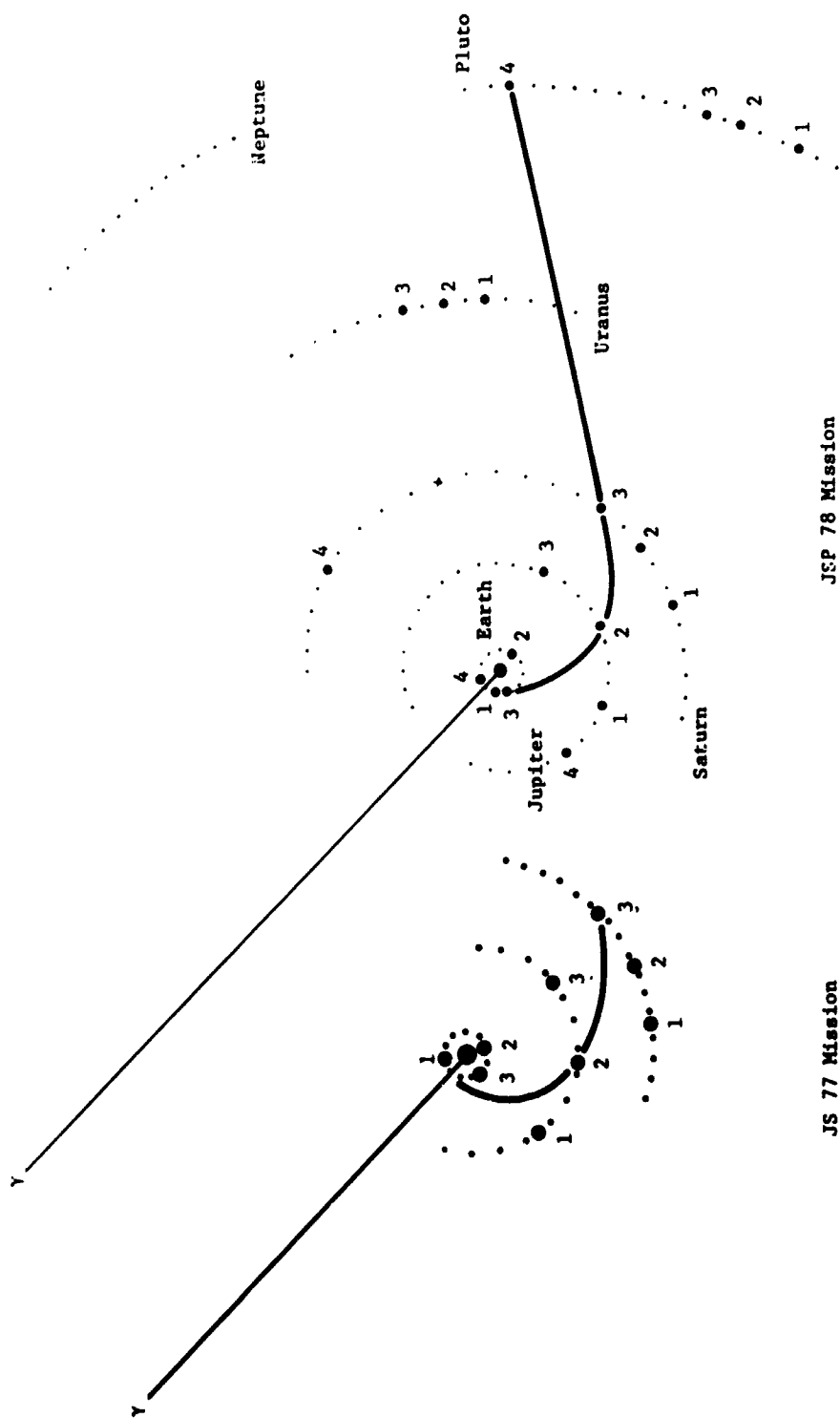


Figure IV-37 Interplanetary Trajectories for JS Missions

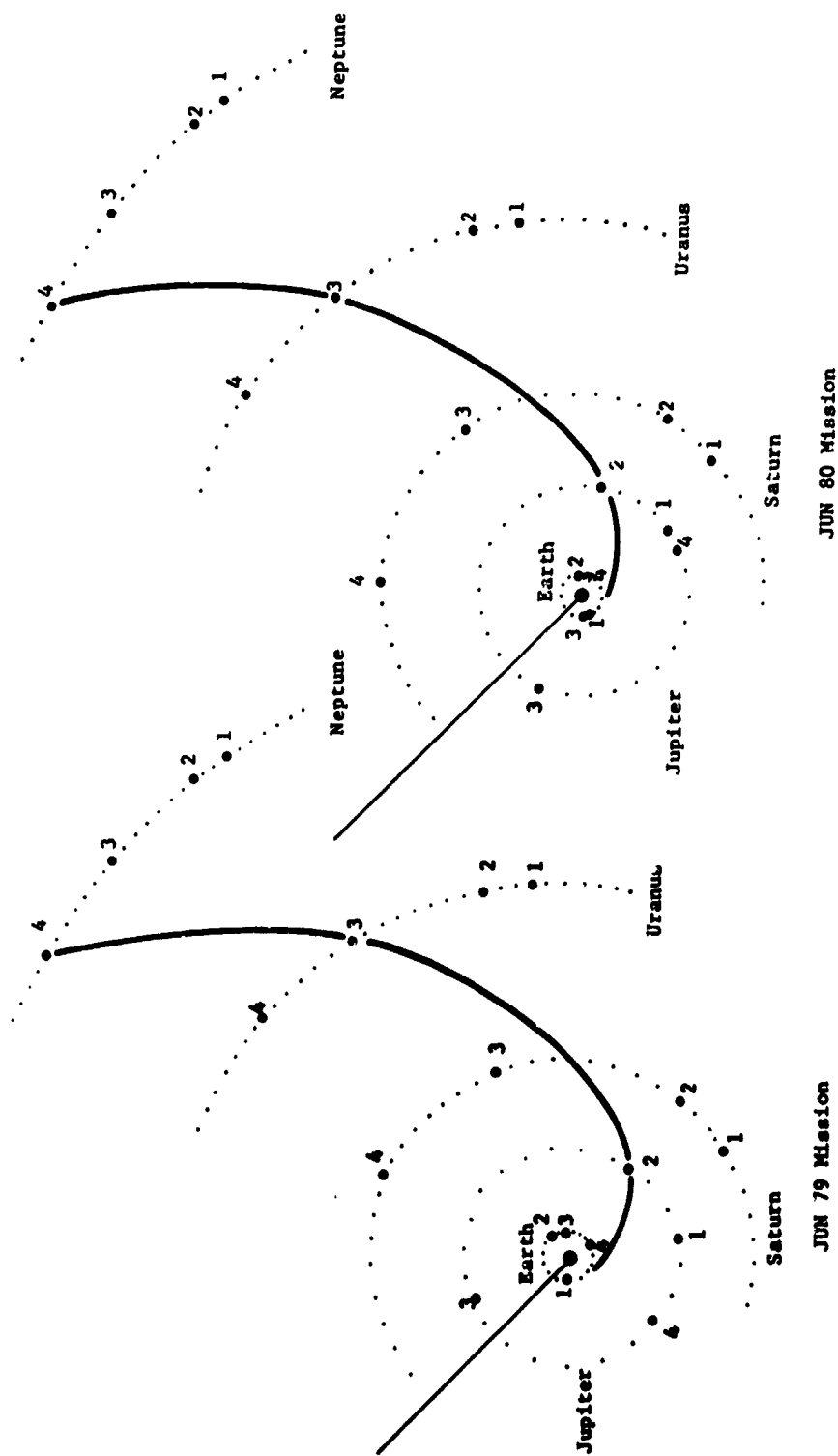


Figure IV-28 Interplanetary Trajectories for JU Missions

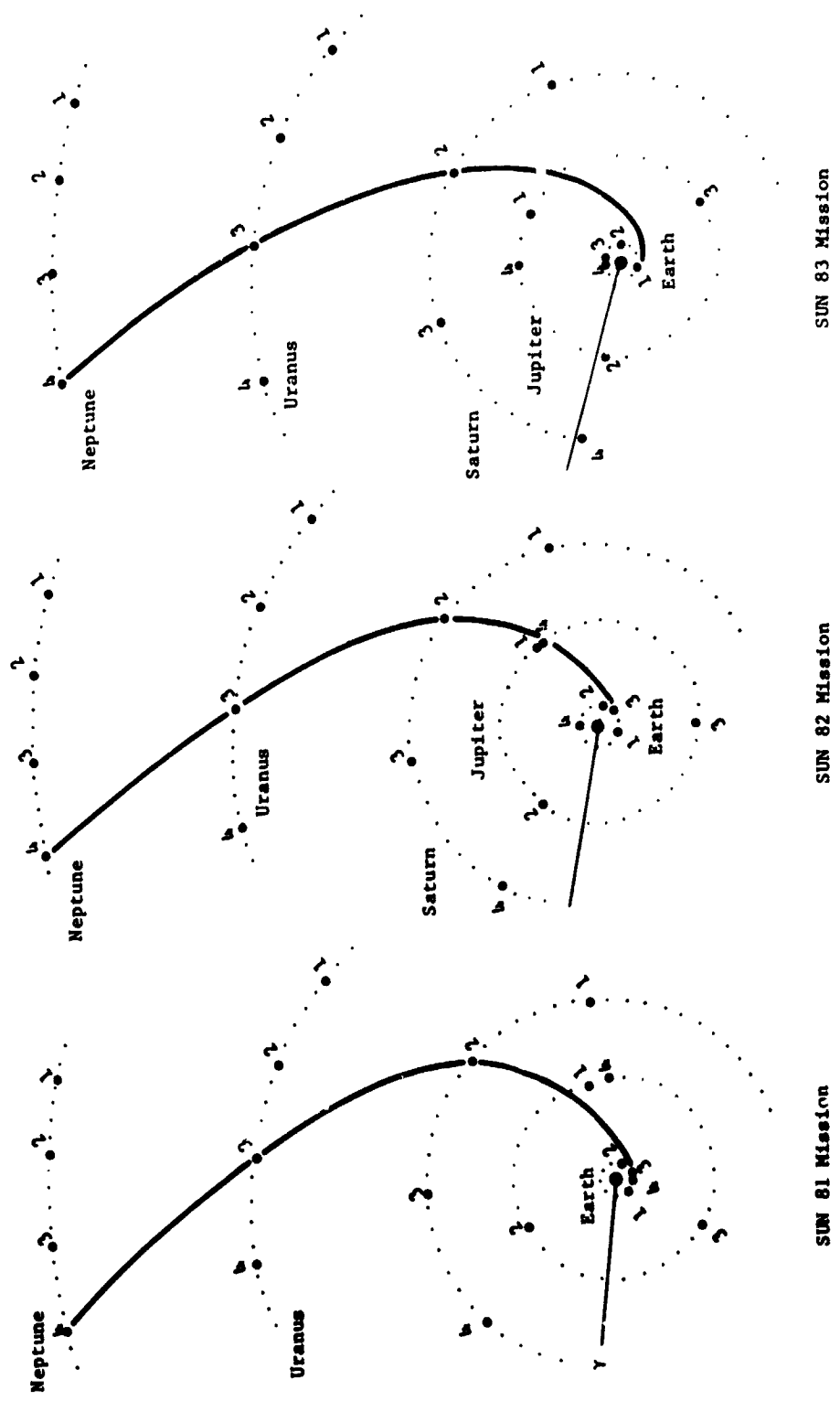


Figure IV-29 Interplanetary Trajectories for SUN Missions

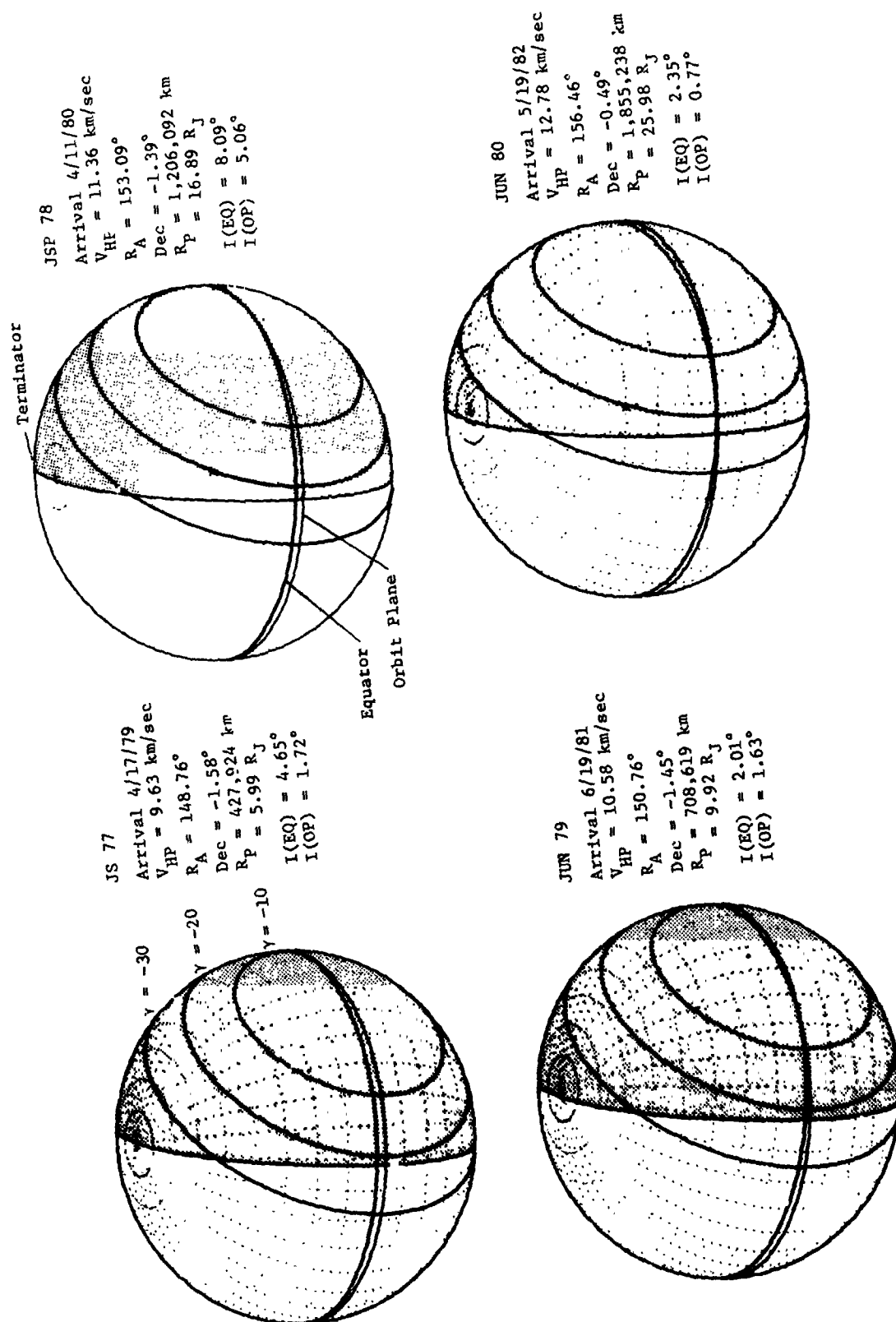


Figure IV-30 Jupiter Entry Geometry

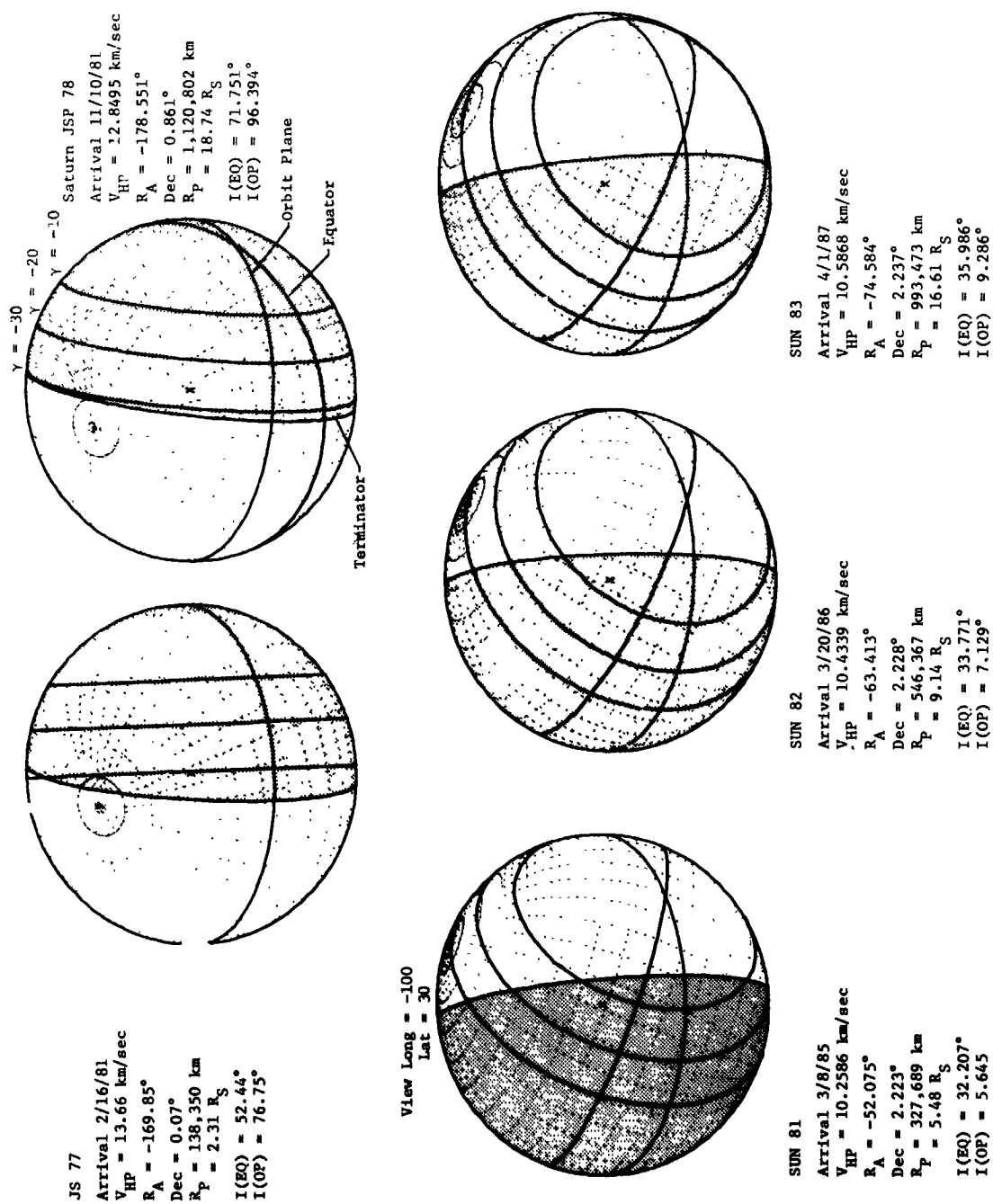


Figure IV-31 Saturn Entry Geometry



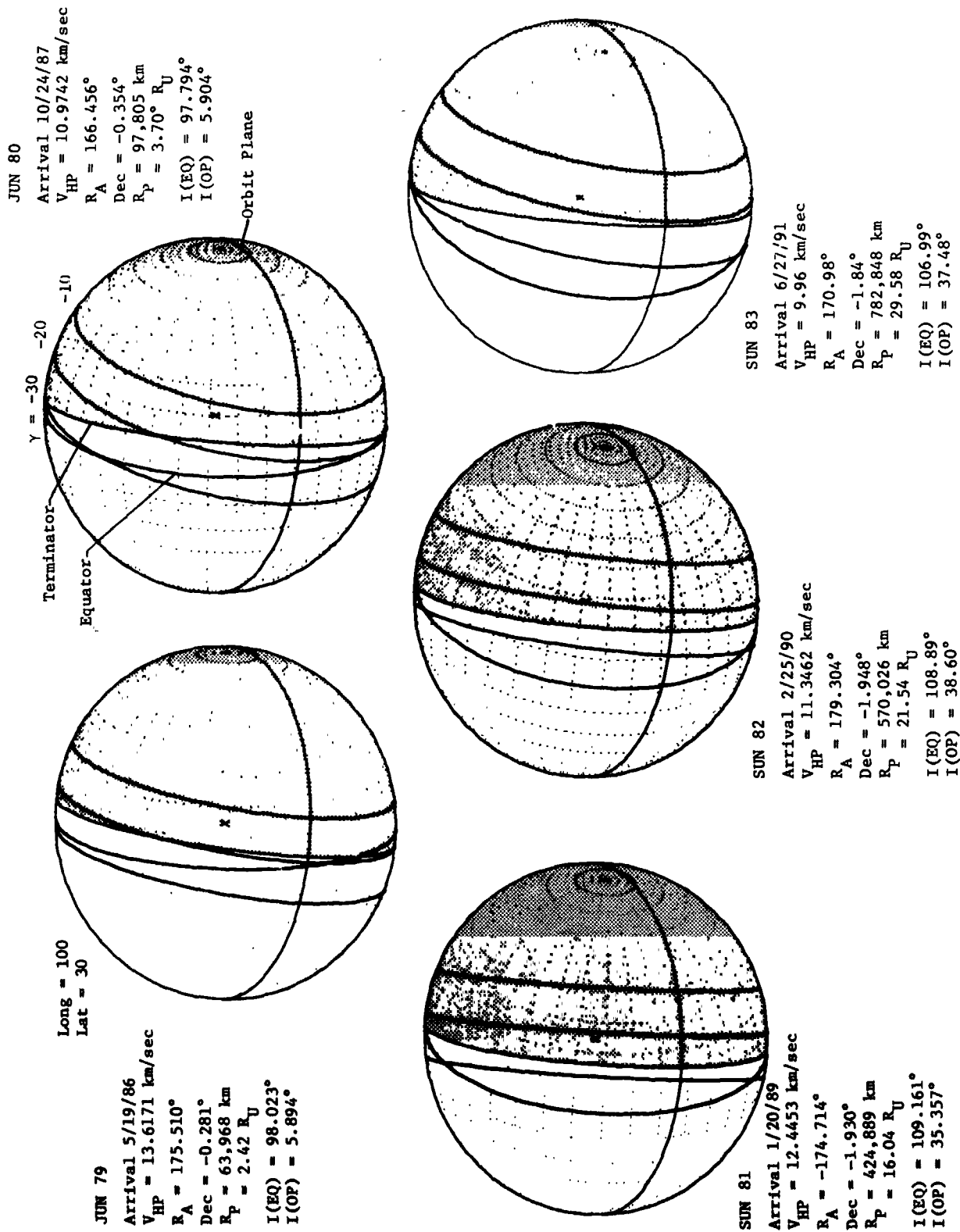


Figure IV-32 Uranus Entry Geometry

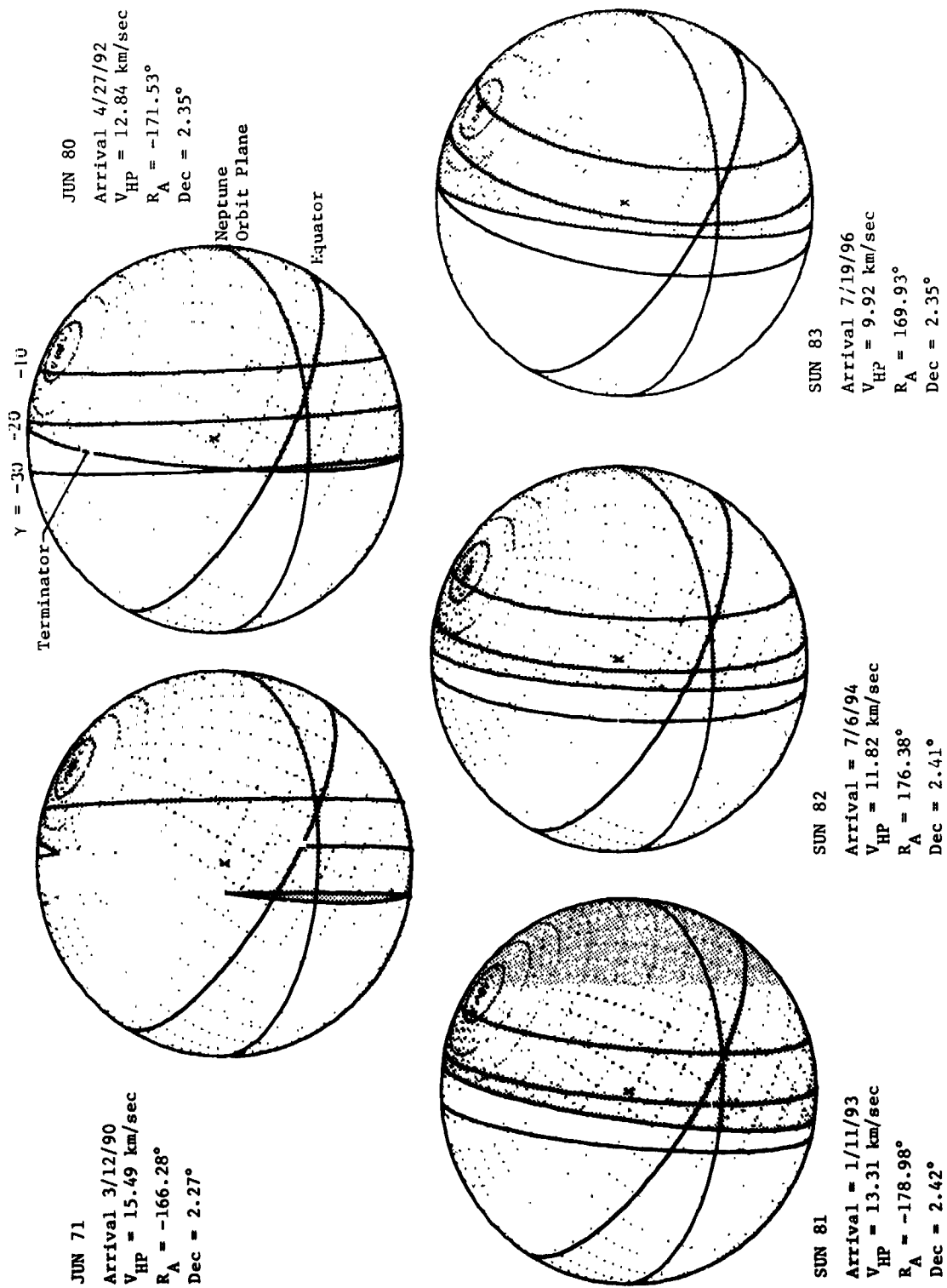


Figure IV-33 Neptune Entry Geometry

H. REFERENCES

- IV-1 Personal communication from J. Beckman, Jet Propulsion Laboratory to D. Vogt, Martin Marietta Corporation, 13 April 1972.
- IV-2 R. H. Battin: *Astronautical Guidance*. McGraw Hill Book Company, New York, 1964.
- IV-3 *Titan III/Centaur Family Launch Vehicle Definition for a Jupiter Entry Mission Study*. Jet Propulsion Laboratory, January 4, 1970.
- IV-4 "Updated Performance for Centaur D-1T and GT Concepts." Enclosure E, *Minutes of Second Meeting OPGT Spacecraft - Launch Vehicle Interface Panel*, Jet Propulsion Laboratory, December 21, 1971.
- IV-5 D. W. Curkendall and R. R. Stephenson: "Earthbased Tracking and Orbit Determination." *Astronautics and Aeronautics*, May 1970.
- IV-6 D. W. Curkendall and J. P. McDaniel: "An Investigation of the Effects of the Major Earth-Based Navigation Error Sources for an Outer Planet Mission." AAS Preprint 71-118, June 28, 1971.
- IV-7 *Brief Summary of DSN Capabilities for Jupiter Atmospheric Probe Mission (1978 Launch Opportunity)*. Jet Propulsion Laboratory Document 131-11, 30 March 1970.
- IV-8 W. G. Melbourne: "Planetary Ephemerides." *Astronautics and Aeronautics*, May 1970.
- IV-9 Personal Communication from W. J. Klepczynski, Naval Observatory, to H. A. Garcia, Martin Marietta Corporation, June 1971.
- IV-10 NASA Space Vehicle Design Criteria document for the Planet Jupiter (1970). NASA SP-8069, August 1971 (See SOW (b)(6)(B)).
- IV-11 NASA Space Vehicle Design Criteria document for the Planet Saturn (1970). (See SOW (C)(4)(b)).
- IV-12 JPL Section Document 131-17, Preliminary Model Atmospheres for the Planets Uranus and Neptune. 4 November 1971.

- IV-13 Constants and Related Information for Astrodynamic Calculations, 1968, by Melbourne, Mulholland, Sjogren, and Sturms. (JPL) NASA Technical Report 32-1306, July 15, 1968.
- IV-14 M. E. Tauber: *Head Protection for Atmospheric Entry into Saturn, Uranus, and Jupiter*. AAS paper 71-145.
- IV-15 D. Vogt et al.: *Computer Program for Mission Analysis of Lunar and Interplanetary Missions*, NASA Contract NAS5-11795, Goddard Space Flight Center, 1971.

## V. JUPITER STUDIES

The Jupiter studies consisted of defining a nominal Jupiter probe based upon nominal constraints and varying each major constraint, individually, to determine its sensitivity. From this sensitivity data, two sets of constraints were established and used to define two alternative Jupiter probes. This data along with other science, mission, and subsystem parametric analyses, are included in this chapter. Some comparisons are made between parameters for the Jupiter studies and similar parameters for Saturn, Uranus, and Neptune, especially in the area of missions.

### A. PARAMETRIC ANALYSIS

The program parametric analysis, identified above, is shown in detail in Figure V-1. Each constraint for the nominal Jupiter probe was varied, incrementally, using the alternative constraints of the program parametrics and the impact assessed in such terms as weight, RF power, bit rate,  $\Delta V$ , etc. These analyses are discussed in the following pages.

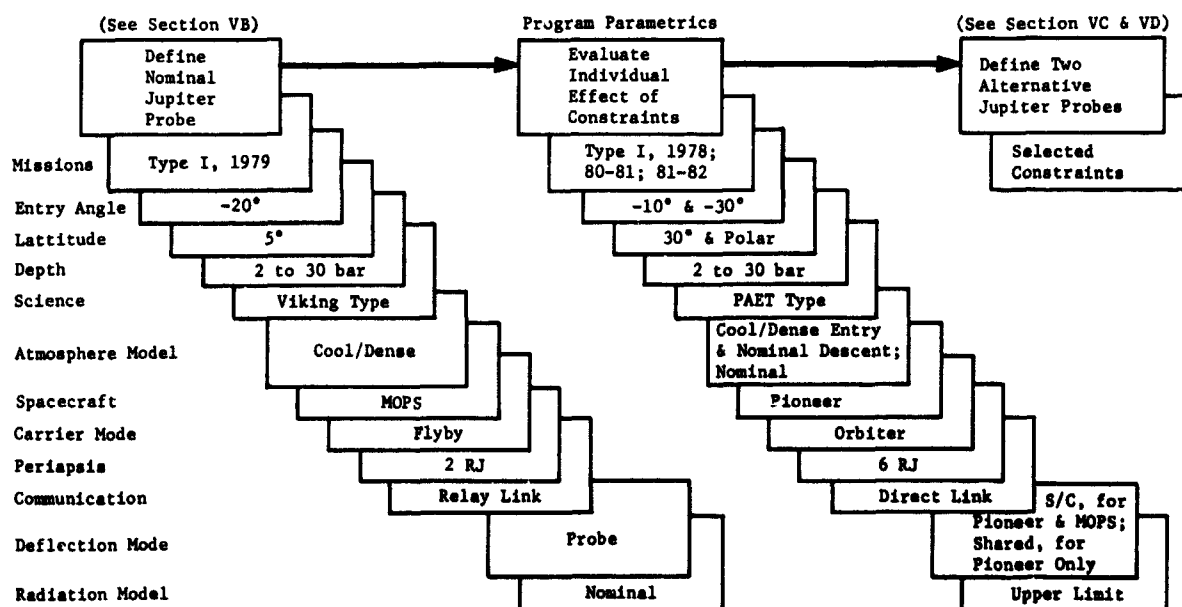


Figure V-1 Program Parametric Analysis Flow Diagram

## 1. Science Performance Analysis

a. *Descent Profile Parametrics* - The major parametrics performed in the science area were to establish a descent profile that would satisfy the objectives of the mission by making the necessary measurements within the criteria. The parameters involved are: (1) the main parachute ballistic coefficient, (2) the drogue or secondary parachute ballistic coefficient, if one is necessary, (3) the pressure at parachute staging, if required, (4) the design limit pressure, and (5) the sampling times for each instrument. The total descent time is also considered because of the limited time the flyby spacecraft is available to establish relay communications link. Also, for Jupiter, the model atmosphere for descent is bounded by two distinct models: the JPL nominal and cool/dense. The above parameters are considered separately in each model.

Investigating first the cool/dense model, Figure V-2 shows the variation in pressure descent profile with changes in main parachute ballistic coefficient. The abscissa represents time from entry, the parachute being deployed at 34 seconds from entry where the vehicle has slowed to Mach 0.7. In the cool/dense model entry profile, this moment occurs at 92 millibars at an altitude of about 32 km.

The range of the ballistic coefficients considered were from 0.05 slug/ft<sup>2</sup> (7.85 kg/m<sup>2</sup>) to 0.25 slug/ft<sup>2</sup> (39.25 kg/m<sup>2</sup>) for the main parachute (B<sub>1</sub>) and from 1.0 (157.0) to 2.4 (376.8) for the secondary parachute (B<sub>2</sub>) with staging pressures from 3 to 15 bars. The size and weight of the main parachute system establishes the lower limit for B<sub>1</sub>, while the descent time and velocity and resultant measurement performance constrain the larger values.

In Figure V-2 the drogue parachute ballistic coefficient and the staging pressure are held constant to show the effect of the main parachute ballistic coefficient independently. In Figure V-3 the main parachute ballistic coefficient is held constant to show the effects of the other two parameters. The effect of the drogue parachute ballistic coefficient is minimal. Even with a staging pressure as high as 3 bars, the difference between the total descent time for a B<sub>2</sub> of 1.50 slug/ft<sup>2</sup> (235.5 kg/m<sup>2</sup>) and 2.0 slug/ft<sup>2</sup> (314.0 kg/m<sup>2</sup>) is about 2 minutes, or <10%; this difference decreases with increasing staging pressure. However, the effect of the staging pressure itself is significant, the difference in descent times between staging at 5 bars and at 12 bars being more than 10 minutes.

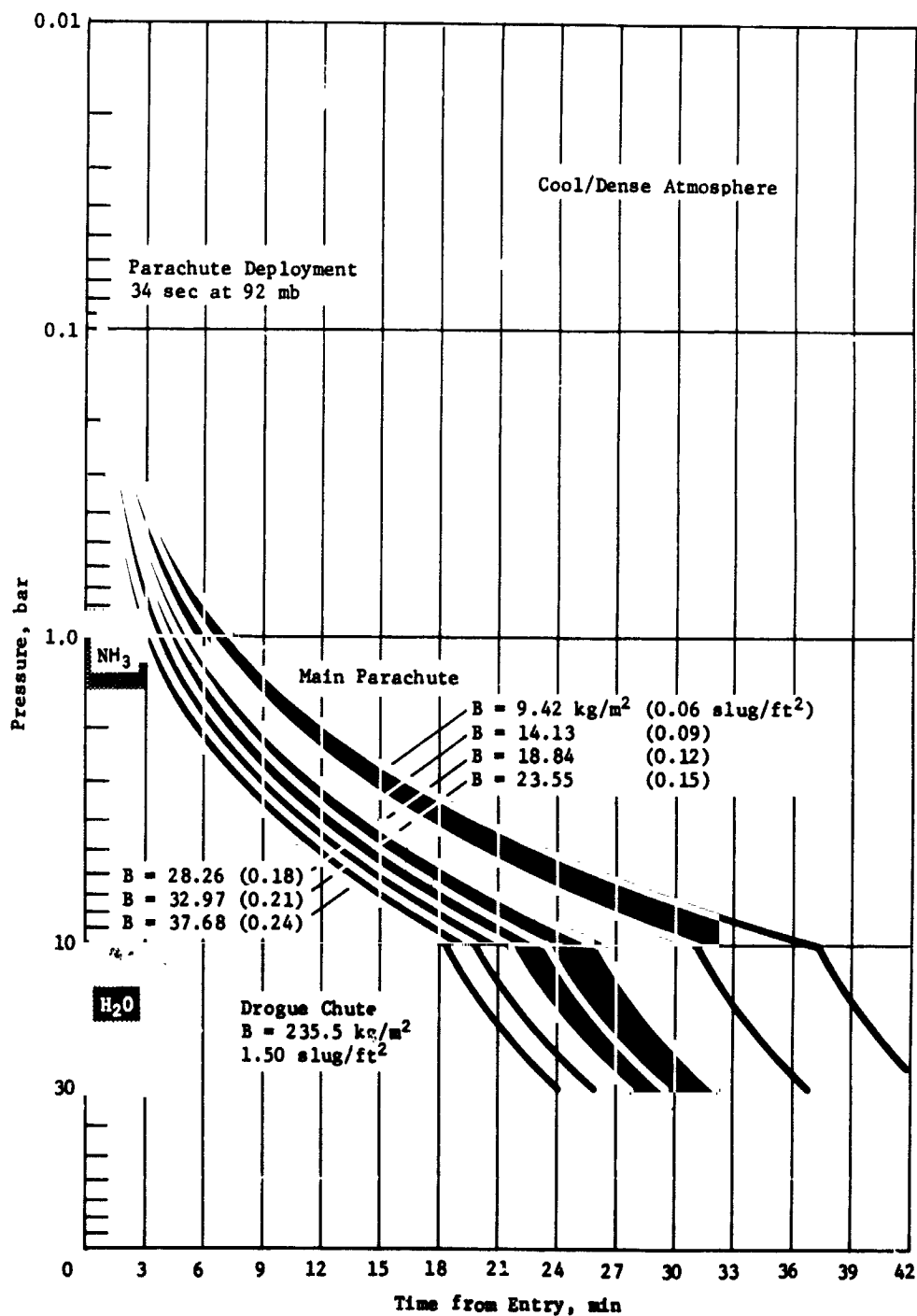


Figure V-2 Pressure Descent Profile Parametrics - Jupiter  
Cool/Dense Atmosphere

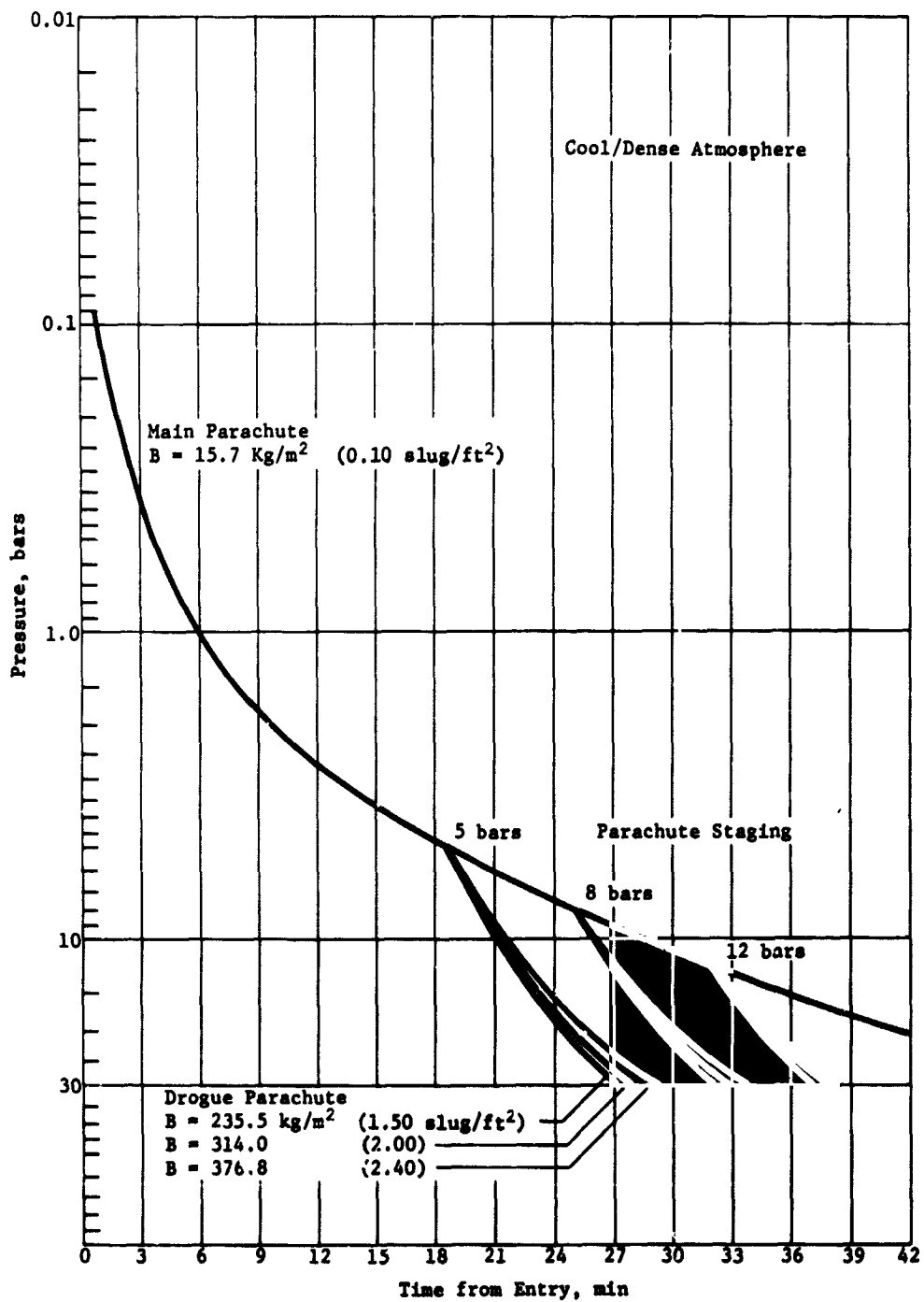


Figure V-3 Effects of Drogue Parachute and Staging Pressure on Descent Profile



Selection of a particular descent profile involves investigation of the variation of the measurement performance of a given instrument with both ballistic coefficient and instrument sampling times. Figure V-4 shows these parametrics for the four instruments and the governing measurement criteria for each. The performance for the temperature measurement is checked against the criteria at the first nonisothermal in the descent profile in (a) of Figure V-4. Since terminal velocity decreases with altitude, and performance therefore improves, this is the worst case point in the descent for a fixed ballistic coefficient. The performance for the pressure and turbulence accelerometer measurements in (c) and (d) of Figure V-4 are checked at the top of the ammonia cloud, which is at about 0.8 bars in the cool/dense atmospheric model, and again the performance will improve with depth. The measurement that governs the mass spectrometer operation is that of obtaining two full sweeps inside the ammonia cloud in each model, as shown in (b) of Figure V-4.

A second point at which the measurement performance of the temperature, pressure, and accelerometer instruments must be compared against the criteria is at parachute staging where the ballistic coefficient changes abruptly. This is shown in Figure V-5 for a specific combination of ballistic coefficients and staging at 10 bars. With a  $B_1$  of 0.12 slug/ft<sup>2</sup> (18.84 kg/m<sup>2</sup>), it can be seen from (c) and (d) of Figure V-4 that a pressure gage sampling time of 5 seconds and an accelerometer sampling time of 10 seconds will exceed the requirements by greater than 30%. However, from Figure V-5 it can be seen that the 5-second sampling time results in a performance of 2.06 measurements/km immediately after parachute staging, while the 10-second sampling time obtains 1.03 measurements/km at the same point; a factor of only 3% over criteria. Likewise the temperature gage performance increases from 0.97 measurements/°K to 3.7 just before parachute staging, and then falls to 1.06 measurements/°K after staging. Thus, to select a profile for cool/dense atmospheric descent requires investigation of measurement performance at two distinct points.

In Chapter III, Section D of this report, the necessary pressure depth of penetration into each model atmosphere was discussed and it was concluded that descending to 30 bars was not essential. To obtain the required measurements in the water cloud, a depth of 13 bars is necessary in the cool/dense atmosphere. The pressure depth in the nominal atmosphere for an equivalent descent time is about 7.5 bars. This eliminates the necessity for a dual parachute descent, as for all ballistic coefficients studied, the time to the above pressure level was less than 45 minutes.

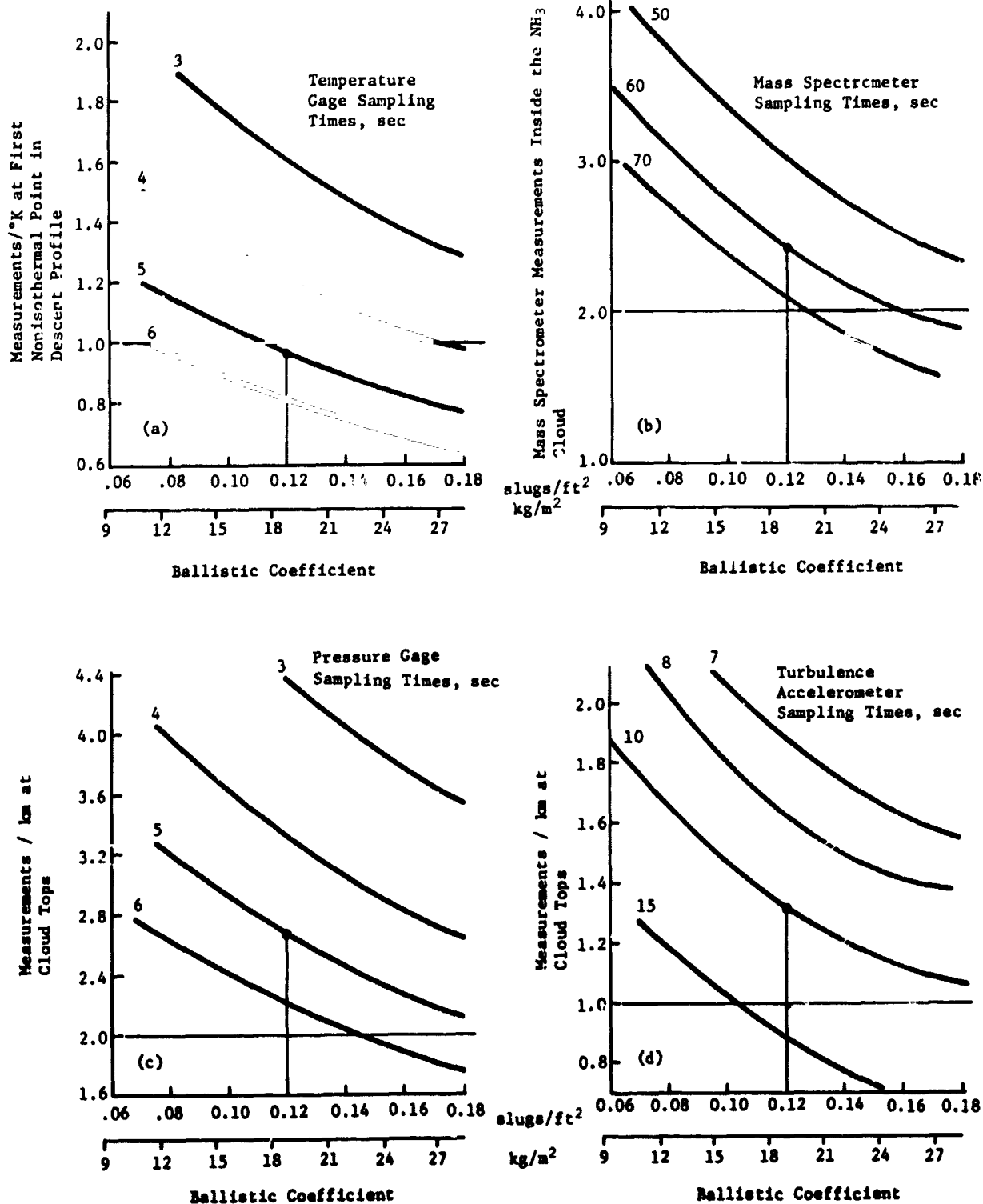


Figure V-4 Ballistic Coefficient and Instrument Sampling Time Effects on Measurement Performance in Cool/Dense Atmosphere

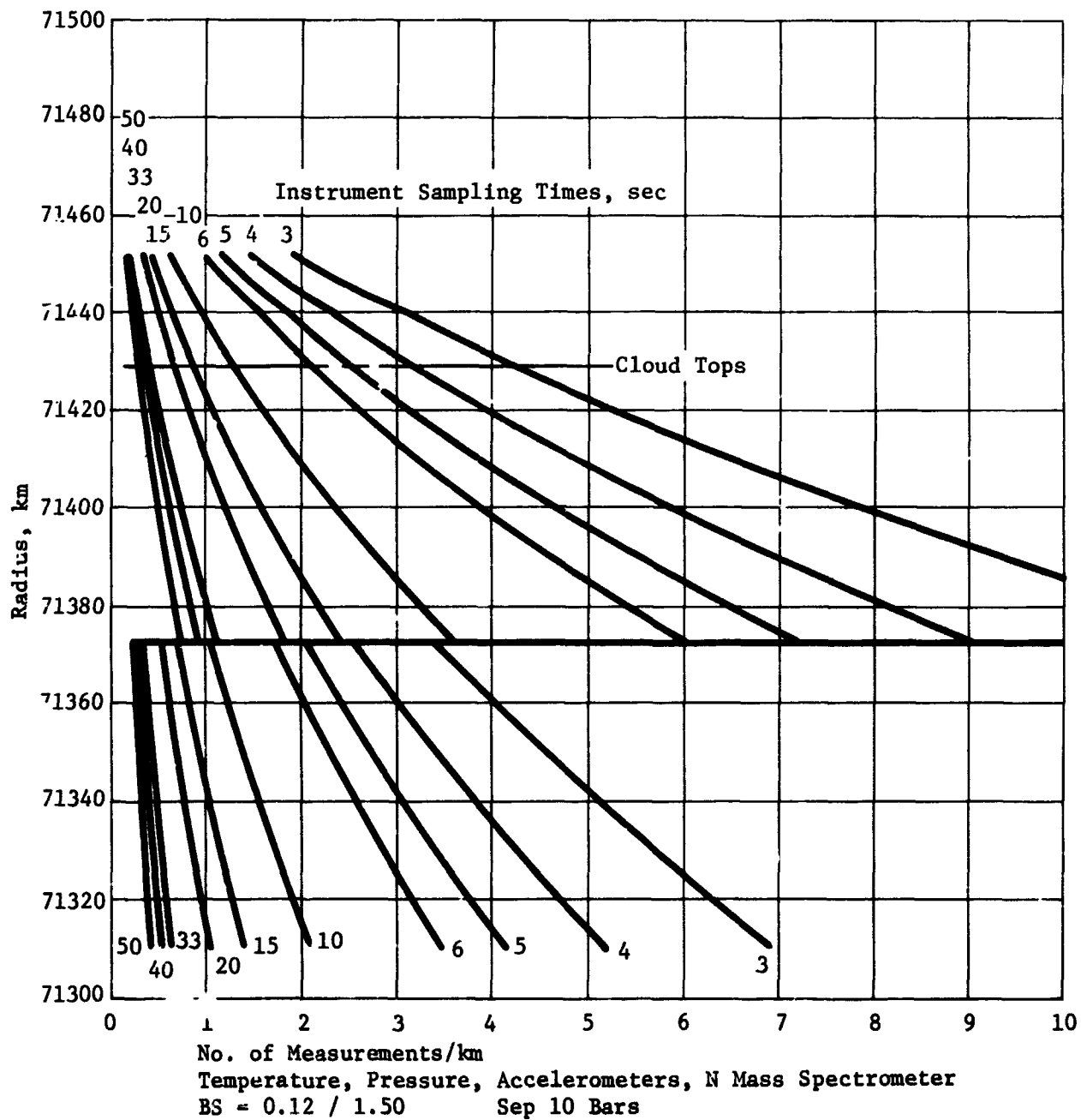


Figure V-5 Measurements per Kilometer Profiles for Various Sampling Times - Cool/Dense Model

Figure V-6 shows the variation in pressure descent profile with changes in parachute ballistic coefficient for a single stage descent in the nominal model atmosphere. The parachute is deployed 39.5 seconds from entry which corresponds to a pressure of 86 millibars and an altitude of about 47.7 km. The range of values that were considered for B is the same as that for the cool/dense atmosphere.

The gradient of pressure with respect to distance in the nominal atmosphere is smaller; thus the clouds exist higher in altitude and lower in pressure, and the pressure gradient across them is less. This means that to obtain equivalent measurement performance in the nominal as in the cool/dense, the velocity with respect to pressure must be less and the time to descend to a given pressure level is longer, for a given ballistic coefficient. This is summarized by Figure V-7.

Figure V-8 presents the instrument sampling time parametrics for the nominal atmosphere. By comparing this with the equivalent figure for cool/dense (Fig. V-4), it can be noted that for a given value of B, the sampling times must be shorter to satisfy performance requirements. The cross-hatched area shown is a design region limited on the left by parachute size and weight and on the right by large data rates. Because there is no parachute staging, then the points in the descent where these graphs are comparing the performance to the criteria are the only critical points. Furthermore, because the nominal atmosphere is the worst-case for measurement performance, a probe designed to meet the criteria in the nominal will also satisfy it in the cool/dense, and in any combination in between.

From Figure V-8, a value of B of 0.09 slug/ft<sup>2</sup> (14.13 kg/m<sup>2</sup>) results in a design point centrally located in the design region and allows a mass spectrometer sampling time of 40 seconds for the 1 to 40 amu sweep. A temperature gauge sampling time of 3.5 seconds satisfies the criteria and the pressure gauge is set to measure simultaneously with the temperature, despite exceeding the requirements. A 10-second sweep by the turbulence accelerometers gives 1.01 measurements/km.

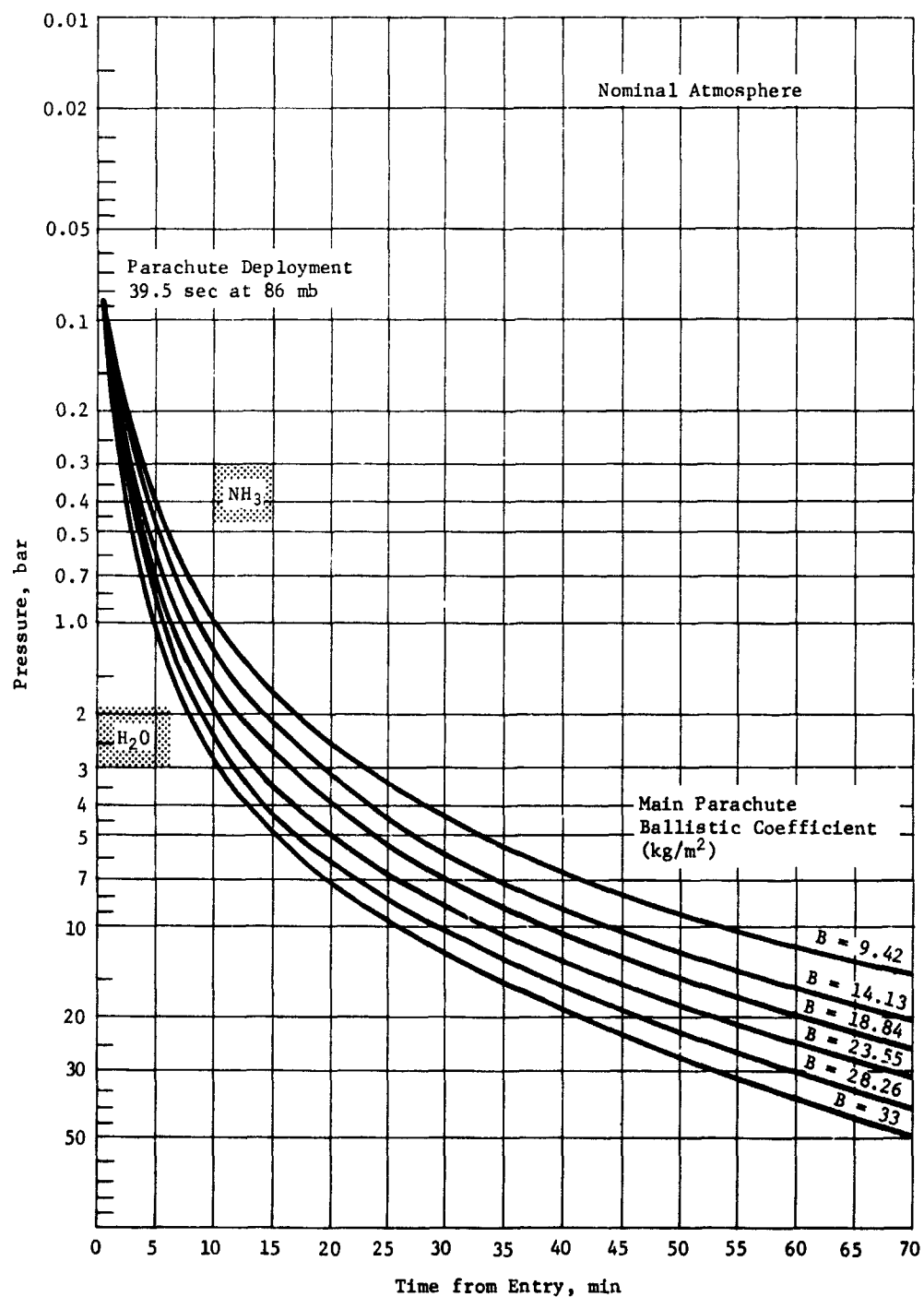


Figure V-6 Pressure Descent Profile Parametrics - Jupiter  
Nominal Atmosphere

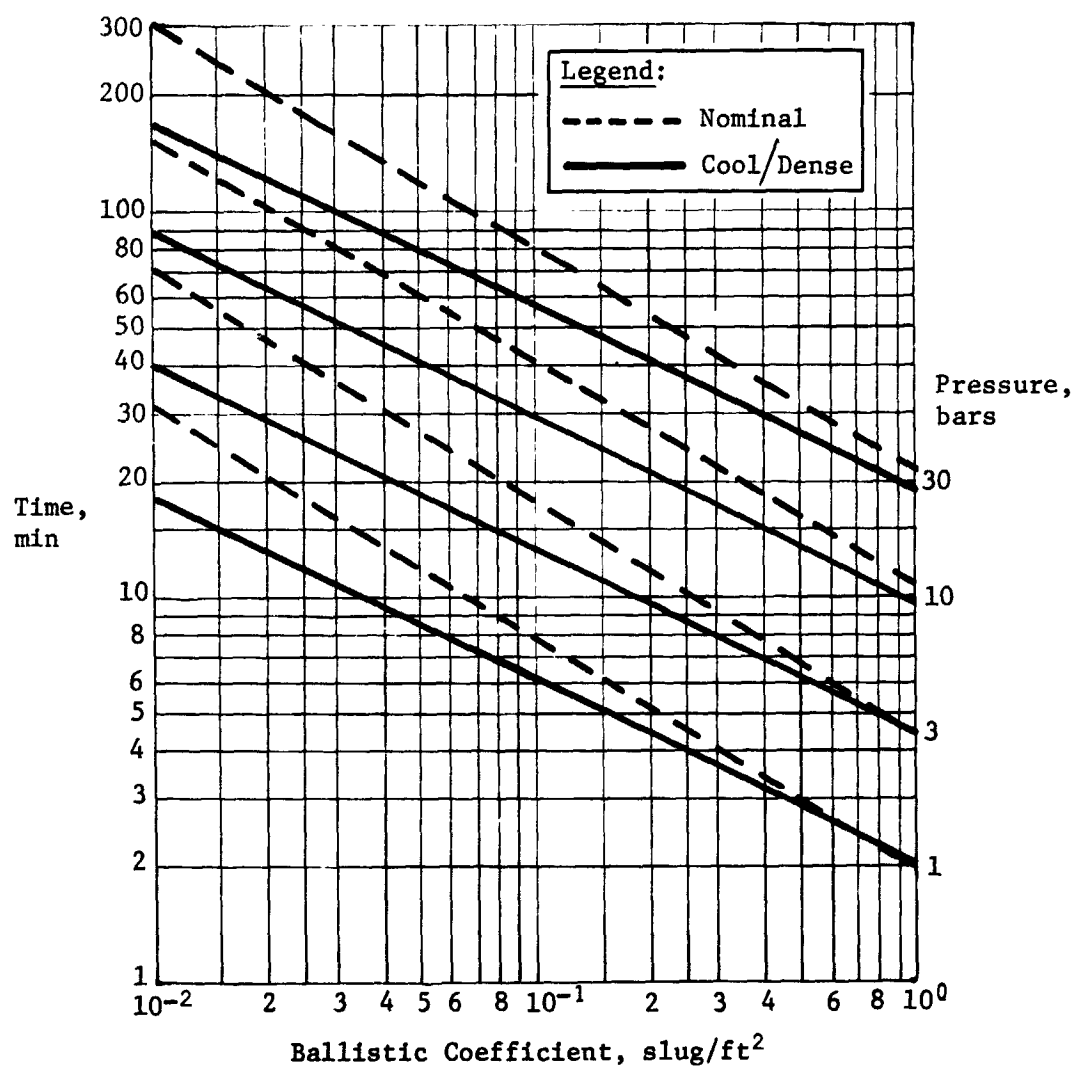


Figure V-7 Descent Times to Various Pressures in Both Jupiter Model Atmospheres.

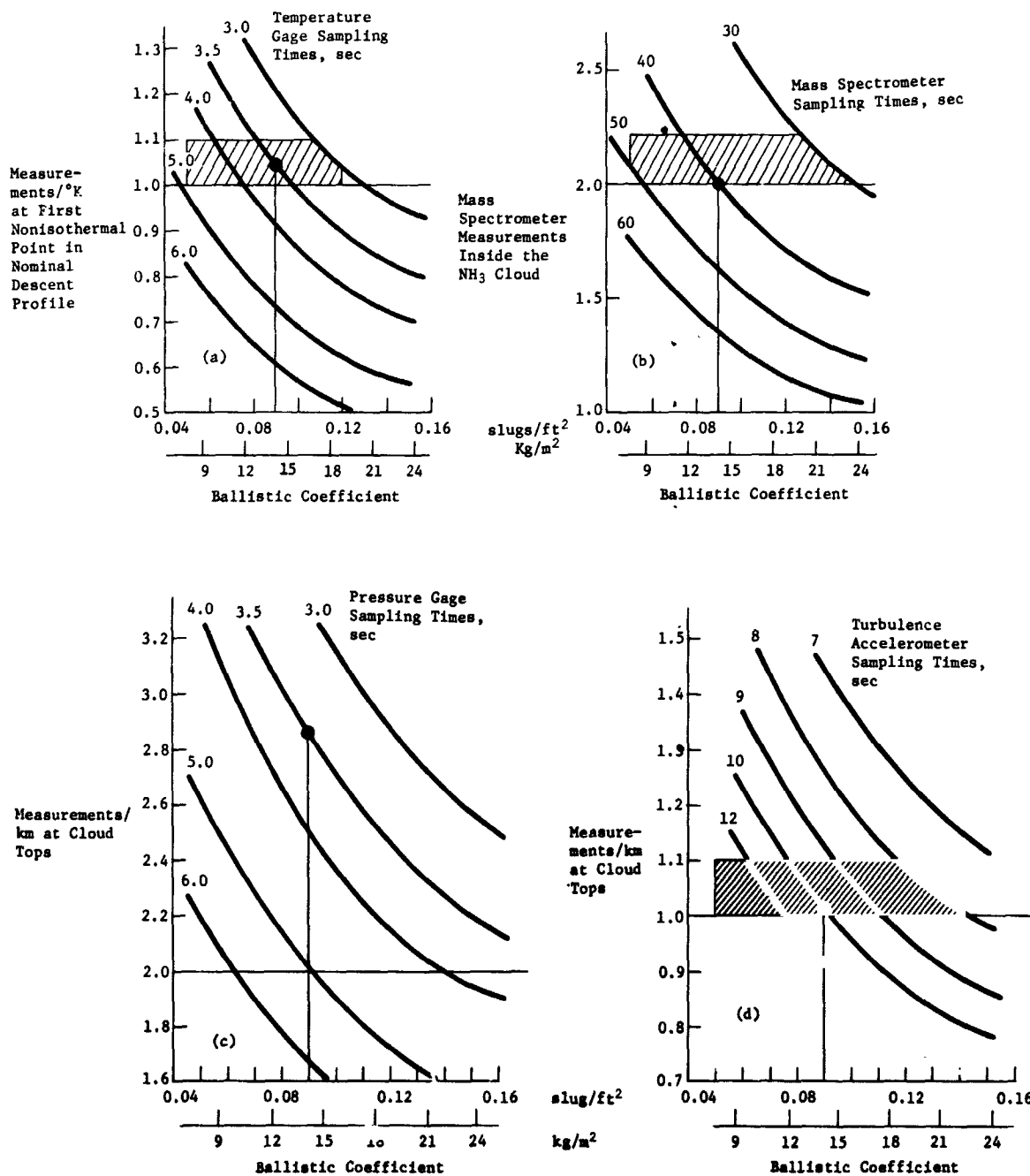


Figure V-8 Ballistic Coefficient and Instrument Sampling Time Effects on Measurement Performance in Jupiter Nominal Atmosphere.

b. *Science Analysis Variations with Mission* - During the parametric analysis portion of the study, the effects of varying flight path angle and model atmosphere on science data rate were investigated. These are summarized in Table V-1. The effect of model atmosphere on entry and descent times has already been discussed in a previous section. From the last two lines in this table, it can be seen that for the same ballistic coefficient and descent pressure, the science data rate can be approximately the same regardless of the descent time; it can be slightly less for the nominal descent if both entry phases are in the same atmosphere.

Table V-1 *Science Data Rates for Mission Variations*

Atmosphere (Entry/Descent)	$\gamma_E$ , deg	Entry Time, sec	Descent Time, sec	Science Bit Rate, bps	Pressure at First Measurement, mb
CD/CD*	10	67	2012	24.7	95
CD/CD	20	34	2002	21.2	111
CD/CD	30	23	1982	20.1	141
CD/CD	42	19	1964	19.7	175
CD/Nom	20	34	2613	25.6	105
Nom/Nom	20	39.5	2619	26.0	96
CD/CD	20	34	1795	27.0	108

b = 0.12  
to  
30 bars

b = 0.09  
to  
10 bars

\*CD = Cool/Dense

The entry flight path angle affects the entry phase directly by changing the time to reach Mach 0.7 and the descent phase indirectly by changing the attitude at which Mach 0.7 is reached, thus varying the starting point in the atmosphere for this descent phase. The variation in entry time is shown in Figure V-9 over a range of flight path angles from 10° to 45°. The time changes by a factor of greater than 3. The entry accelerometers are measuring during this period at a collective rate of 200 bps; thus the entry time has a definite effect on the total science data rate. This effect is shown in the first four lines of Table V-1.

The last column in Table V-1 shows the variation in atmospheric pressure when the first descent instrument measurement is made. This occurs 12 to 15 seconds after the parachute is deployed, which allows time to release the aeroshell, deploy the temperature gage, and release the mass spectrometer covers. The pressure changes 16 to 20 millibars during this period. Therefore, the altitude at which Mach 0.7 and parachute deployment occurs decreases with increasing flight path angle thus increasing the pressure level where descent measurements can begin.



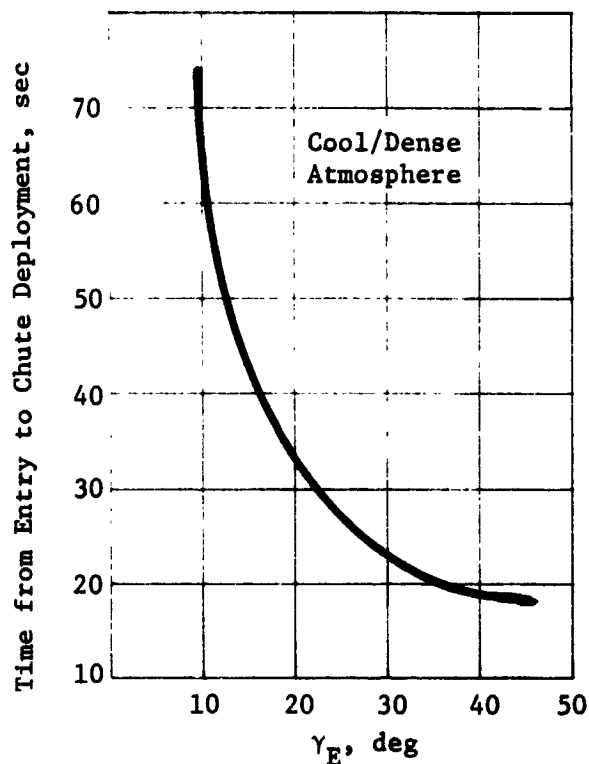


Figure V-9 Effect of Flight Path Angle on Entry Time

c. *Entry Accelerometer Performance* - The primary function of the accelerometer triad is to collect the entry g-load information with sufficient accuracy to be able to reproduce the g-curve, in particular the sharp maximum point on the curve, with the data. This can be used to reconstruct the atmosphere. However, the g-load may go from 10% of its peak value through peak and back to 10% in only a few seconds; thus an analysis was made to ensure that the Viking axial accelerometer sampling rate of 10 samples/sec would give an adequate number of points along the curve to reproduce the steep slope. Figure V-10 is a plot of the expected g-load curves based on each of the cool/dense and nominal model atmospheres and calculated by an entry dynamics computer program. Superimposed upon this are marks that represent individual axial accelerometer measurements. The cool/dense model is the worst-case, reaching a peak of over 1500 g from 100 g in 2.2 seconds, and yet the number of points is adequate. See Chapter IV. F. for other entry conditions.

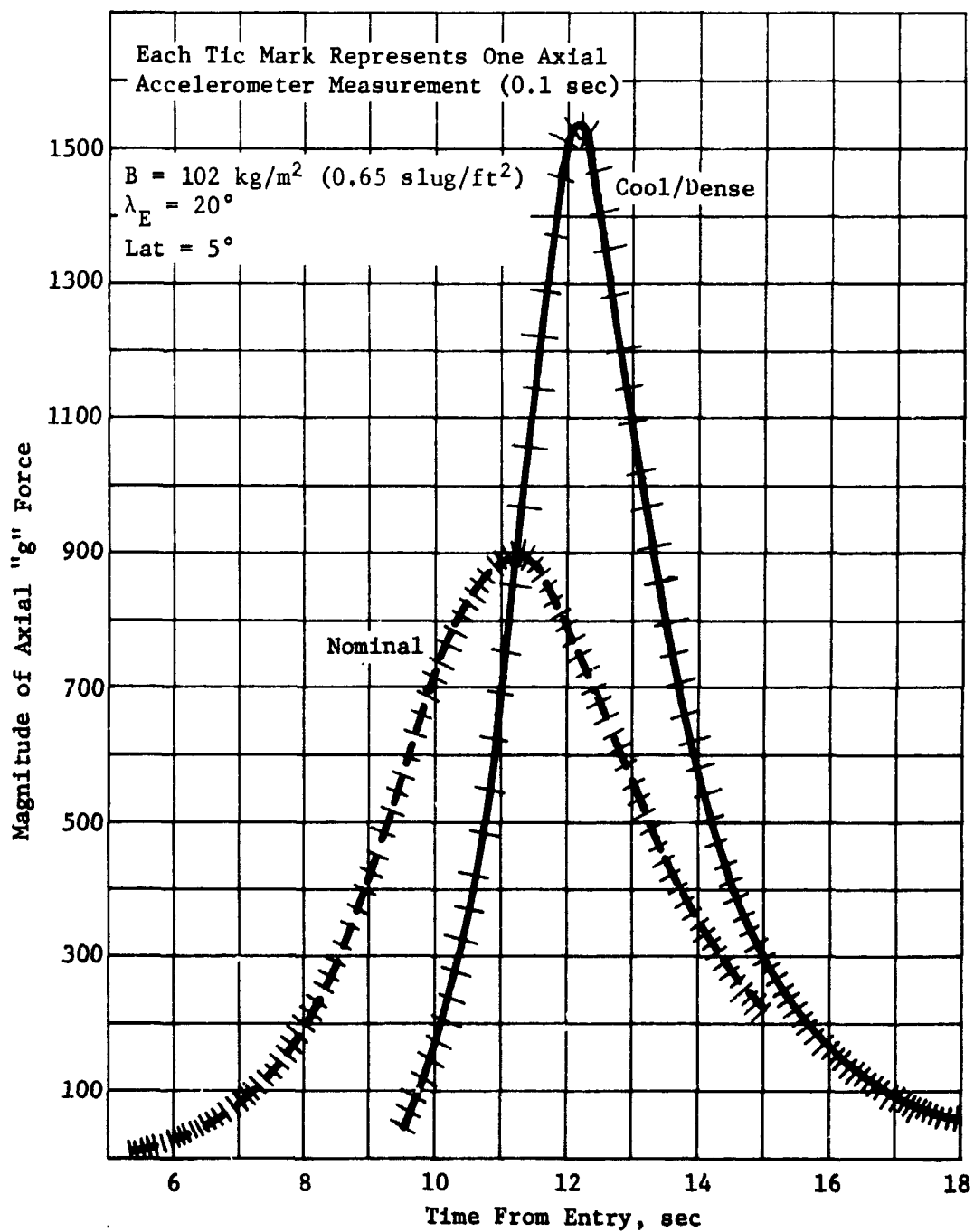


Figure V-10 Entry Accelerometer Performance

## 2. Mission Analysis

The detailed mission analysis and design studies are provided in Chapter IV where comparisons of missions to the different planets may be made conveniently. For completeness, a qualitative summary of the important results, as they apply to Jupiter missions is given in this section.

*a. Interplanetary Trajectory Selection* - The most critical consideration in selecting the interplanetary trajectory (or the launch and arrival dates) for Jupiter probe missions is payload capability. For a typical launch opportunity (1979) a flight time of slightly less than 700 days maximizes the payload capability for a fixed launch energy and period. This result is based on two constraints: the declination of the launch asymptote (DLA) must be less than  $36^\circ$  and the Sun-Earth-vehicle angle at arrival must be greater than  $15^\circ$ . This results in optimal missions arriving at Jupiter just before the Sun occults the view to Jupiter.

The payload capability improves each year in the period 1969-1982. This results not only from a progressive increase in the width of the launch energy contours each year, but also a continual reduction in the area eliminated by the DLA constraint.

For the 1979 mission opportunity, the Burner II stage is required in addition to the Titan 5-segment launch vehicle to have a 20-day period for a MOPS or Mariner class spacecraft. The Burner II stage is not required for a Pioneer class spacecraft.

*b. Approach Trajectory Selection* - The relative geometry between the probe and spacecraft trajectories optimally would have the spacecraft directly overhead as the probe descends through the atmosphere. This would first require that the probe and spacecraft trajectory inclinations be chosen in concert. Generally, the probe trajectory should be a posigrade, low inclination trajectory to minimize the probe's relative velocity at entry and thereby reduce entry effects; the spacecraft should also have a posigrade, low inclination trajectory.

A second consideration involves the selection of the spacecraft periapsis radius. While in terminal descent, the probe rotates with the atmosphere at Jupiter's rotation rate of  $36.6 \text{ deg/hr}$  (equatorial). For the spacecraft to match this angular rate it should have a periapsis radius of about  $2.0$  and  $2.5 R_J$  for mission duration times of one hour and a half hour, respectively.

c. *Navigation and Guidance Considerations* - The uncertainty in the state of the spacecraft at deflection is essentially due to the navigation uncertainties at the time of the last midcourse maneuver. A detailed analysis of the navigation results is given in Chapter IV. The navigation uncertainty for the 1979 mission using Doppler only is characterized by a one-sigma semi-major axis (SMAA) uncertainty in the impact plane of 1600 km ( $30 \times 10^6$  km deflection radius). Adding ranging measurements and then quasi very long baseline interferometry (QVLBI) measurements reduces this to 1500 km and 1400 km, respectively. Deflecting at radii further from the planet requires tracking further from the planet which results in less effective tracking. In going from 10 to 50 million km the uncertainties are roughly doubled. Finally, the navigation characteristics vary from year to year as the geocentric declinations of Jupiter at arrival vary. The SMAAs go from 950 to 1500 to 700 to 450 as the launches proceed from 1978 through 1981-1982 with corresponding geocentric declination at arrival of  $10^\circ$ ,  $0^\circ$ ,  $-21^\circ$ ,  $-26^\circ$ , respectively.

d. *Deflection Maneuver Parametrics* - The purpose of the deflection maneuver is three-fold: (1) to place the probe on a trajectory intersecting the selected entry site, (2) to orient the probe for zero relative angle of attack at entry, and (3) to establish an effective communication link between the probe and spacecraft during the critical descent phase of the mission (b. above). The standard means of accomplishing these objectives is probe deflection wherein the probe is separated from the spacecraft, fires a  $\Delta V$  which accomplishes (1) and (3) above, and then reorients itself by a precession maneuver to the attitude required in (2).

The  $\Delta V$  requirements are such that the deflection radius (the distance from the planet when the maneuver is performed) is generally between 10 and 50 million km. For a spacecraft periapsis radius of  $R_J$  and an entry angle of  $-20^\circ$ , the  $\Delta V$  requirement varies from 221 to 73 to 44 m/sec as the deflection radius increases from 10 to 30 to 50 million km, respectively. The  $\Delta V$ s increase by a factor of 3.5 if the spacecraft periapsis is raised to  $6 R_J$ .

Increasing the deflection radius also increases the coast time resulting in a longer length of time during which the probe is away from the protective environment of the spacecraft and during which dispersions may grow. The coast time is approximately a linear function of deflection radius varying from 9.5 to 34.6 to 61.4 days as the deflection radius is increased from 10 to 30 to 50 million km.

e. *Dispersion Parametrics* - The uncertainty in the spacecraft state at deflection caused by navigational errors and the error in the delivered  $\Delta V$  caused by execution errors result in dispersions that must be accounted for in the design of the probe mission. Dispersions in entry site and entry flight path angle affect science return and interpretation. Dispersions in angle of attack at entry affect science as well as structural, thermal, and aerodynamic design. Dispersions in entry time affect mission sequencing. Dispersions in the relative geometry of the probe and spacecraft determine requirements on the communication link.

For Jupiter missions, dispersions are dominated by execution errors and navigation uncertainties have little impact. Execution errors contribute to approximately 95% of the total dispersions associated with any of the parameters discussed above.

The dispersions are of course a function of the level of execution errors. The proportionality error of 1% ( $3\sigma$ ) is dominated by the less well-defined pointing error in the delivered  $\Delta V$  which is generally assumed to be about  $2^\circ$  ( $3\sigma$ ). Using entry angle as a typical example,  $3\sigma$  dispersions of  $0.2^\circ$ ,  $0.9^\circ$ ,  $1.1^\circ$ , and  $1.3^\circ$  result from assuming  $\Delta V$  pointing errors ( $3\sigma$ ) of  $0^\circ$ ,  $1.5^\circ$ ,  $2.0^\circ$ , and  $3.0^\circ$ , respectively, while holding the navigation uncertainties and proportionally errors (1%) constant (for the nominal mission).

The dispersions are also proportional to the length of the coast arc between deflection and entry and proportional to the magnitude of the deflection  $\Delta V$ . Therefore, there is a complicated trade in increasing the deflection radius which lowers the deflection  $\Delta V$  and increases the coast time.

f. *Comparison of Deflection Modes* - Two alternative deflection modes have been identified in addition to the probe deflection mode discussed in d. on the preceding page. The modes are:

- 1) Shared deflection (planar) - The probe is released in the attitude required for zero relative angle of attack. The  $\Delta V$  magnitude is then chosen so that when fired in the axial direction, the probe impacts the entry site. The spacecraft is then corrected to establish the desired communication geometry;
- 2) Spacecraft deflection - The initial spacecraft trajectory is targeted to impact the desired entry site. The probe is released in the attitude required for zero relative angle of attack. The spacecraft then rotates to a new direction and fires a  $\Delta V$  which deflects it for the desired flyby radius and communication geometry.

The deflection  $\Delta V$  requirements for the probe and spacecraft deflection modes are essentially identical as they are mirror images of each other. The two  $\Delta V$ s required by the shared deflection are of approximately the same magnitude as the probe or spacecraft deflection mode  $\Delta V$ . Thus, for the nominal mission, the  $\Delta V$  required for the probe (in probe deflection) or spacecraft (in spacecraft deflection) is 221 m/sec while the probe  $\Delta V$  is 246 m/sec and the spacecraft  $\Delta V$  is 236 m/sec in the shared deflection mode.

According to dispersion comparisons of the three modes, the spacecraft deflection is best and shared deflection is worst. Entry dispersions (entry angle, entry site, etc) are smallest for the spacecraft deflection as no deflection  $\Delta V$  execution errors are added to the probe trajectory. The communication parameter dispersions for shared deflection are largest because execution errors have been added to both the probe and spacecraft in that mode. Anytime a  $\Delta V$  maneuver is performed, resulting dispersions are approximately proportional to the size of the maneuver.

*g. Entry Trajectory Parametrics* - The critical entry parametric studies deal with (1) the selection of the entry ballistic coefficient which permits deceleration to less than Mach 0.7 above 100 mb for the staging of the aeroshell (2) the behavior of the peak accelerations and maximum dynamic pressures with a variety of entry conditions.

A ballistic coefficient of 102.1 kg/m<sup>2</sup> (0.65 slug/ft<sup>2</sup>) results in speeds below Mach 0.7 at 100 mb in the cool/dense model and 90 mb in the nominal atmosphere for an entry angle of -20°. To meet the staging requirements at an entry angle of -30° for the cool/dense atmosphere requires a ballistic coefficient of 0.5 slug/ft<sup>2</sup>.

The peak *g* experienced at entry angles of -10°, -20°, and -30° are 675, 1500, and 2250 *g*, respectively, in the cool/dense atmosphere and 450, 920, and 1450 *g*, respectively, in the nominal atmosphere (equatorial entry). Thus, the cool/dense model has *g* levels roughly 50% higher than the nominal atmosphere. Entering at higher latitudes increases the peak *g* as the relative velocity is increased. Thus, entering at latitudes of 0°, 30°, and 90° latitude results in peaks of 1500, 1650, and 1800 *g*, respectively, for an entry angle of -20° in the cool/dense atmosphere. The peak *g* level is essentially independent of the ballistic coefficient; however, increasing the ballistic coefficient delays the time at which the peak *g* is achieved.

The max q is a function of ballistic coefficient. Entering with a ballistic coefficient of 1.0 slug/ft<sup>2</sup> at entry angles of -10°, -20°, and -30° results in max q of 10, 22, and 40 x 10<sup>3</sup> psf, respectively, in the cool/dense atmosphere and 6.6, 14.7, and 26.6 x 10<sup>3</sup> psf, respectively, in the nominal atmosphere. The dynamic pressure increases linearly with ballistic coefficient.

### 3. System Integration

The guidelines for implementation of the program parametric analysis are given in Table V-2. The table shows the constraints for the reference configuration (nominal Jupiter probe discussed in Chapter V, Section B) and the set of constraints for elevel point designs. Three significant program parametric analyses, not shown in the table, are (1) mission candidate analysis, (2) direct link communication analysis and (3) deflection mode analysis. These analyses, however, are supplemented by other mission, science, and subsystem analyses and discussed throughout this chapter.

Table V-2 Constraints for Program Parametric Point Designs

Constraint	Configuration											
	Ref	1	2	3	4	5	6	7	8	9	10	11
R <sub>P</sub> (R <sub>J</sub> )	2	2	2	2	2	2	2	2	6	2	2	2
R <sub>EJ</sub> (x 10 <sup>6</sup> km)	10	10	10	10	10	10	10	10	30	10	10	10
γ <sub>E</sub> (-deg)	20	10	30	42.6	20	20	20	20	20	20	20	20
Latitude (deg)	5	5	5	90	5	5	5	5	5	5	5	5
Atmosphere E	CD	CD	CD	CD	CD	Nom	CD	CD	CD	CD	CD	CD
Atmosphere D	CD	CD	CD	CD	Nom	Nom	CD	CD	CD	CD	CD	CD
Deflection Mode	P	P	P	P	P	P	P	P	P	S/C	S/C	S
Spacecraft	TOPS	MOPS	MOPS	MOPS	MOPS	MOPS	Pion	MOPS	MOP <sup>c</sup>	Pion	MOPS	Pion
Descent (bar)	30	30	30	30	10	10	30	30	30	30	30	30
<b>Legend:</b> CD = Cool/Dense; Nom = Nominal; P = Probe; S = Shared; E = Entry; D = Descent; Pion = Pioneer												

#### 4. Telecommunication Subsystem

a. *Introduction* - The parametric analyses were intended to determine the effects of variations in trajectory parameters on the design of the probe. Major trajectory parameters such as periapsis radius and entry angle affect RF power requirements significantly. The parametric studies used as a basis the nominal Jupiter probe as described in Section B of this chapter.

b. *General* - Considerable effort was expended in determining if an optimum operating frequency exists since several losses are directly proportional to frequency and others are inversely proportional to frequency. The analysis is discussed in Volume III, Appendix B. Results of the frequency selection indicate that an optimum frequency does not exist, but, in general, the lower frequencies are affected less by the RF link variables. For this reason, the original operating frequency at S-band (2.3 GHz) was abandoned in favor of a frequency near 1 GHz. Other pertinent information resulting from the frequency study and applicable to the parametric designs is shown in Figures V-11 and V-12. The average receiver noise figure and effective noise temperature is shown in Figure V-11. The average curve was used for all mission studies and is typical for transistor amplifiers. Figure V-12 depicts the noise temperature of the receiving system as a function of frequency. System noise temperature is the sum of the receiver temperature shown in Figure V-11 and the antenna noise temperature also shown in Figure V-12 along with the total system curve.

Attenuation of RF signals for the Jupiter cool/dense and nominal atmospheres are shown in Figure II-9 and the analysis is discussed in detail in Volume III, Appendix A. Jovian atmosphere loss is primarily a result of absorption by the clouds and atmosphere gasses. As seen in the figure, loss is much less for the nominal atmosphere.

Several types of antennas are required for the various missions depending on beamwidth and frequency. Antenna designs are discussed in detail in Volume III, Appendix D. The spacecraft antenna for narrow beamwidths ( $<20^\circ$ ) uses a parabolic dish of conventional design. For missions that require high gain, a dish antenna provides a compact design. Circular polarization is required because the probe is spin-stabilized. Missions that require a spacecraft antenna with a wide beamwidth and low gain can use a helical antenna. A helix provides the proper polarization and is a more efficient design for low gain and large beamwidth.



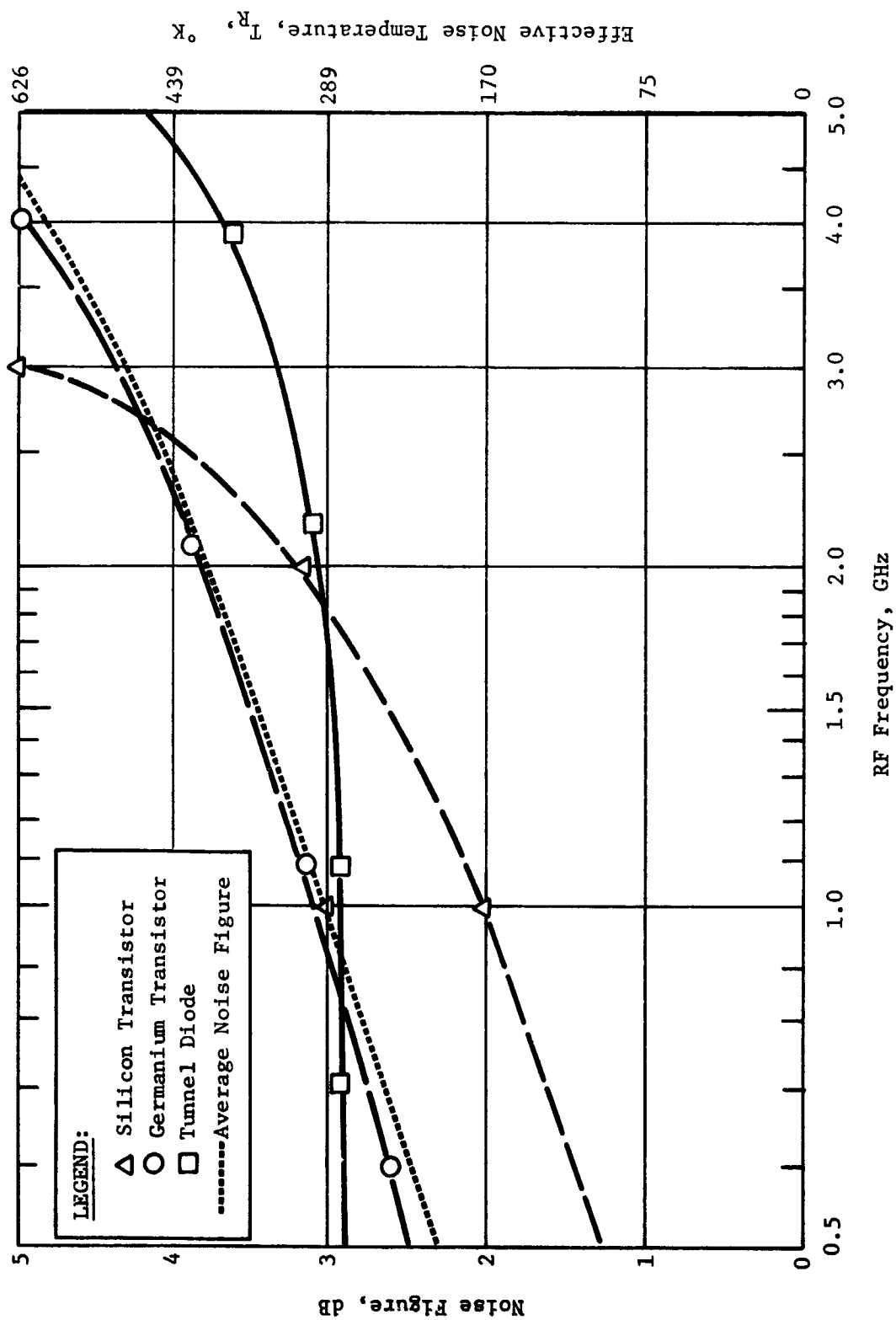


Figure V-11 1972 Noise Figure State of the Art for Tunnel Diodes and Transistor Amplifiers

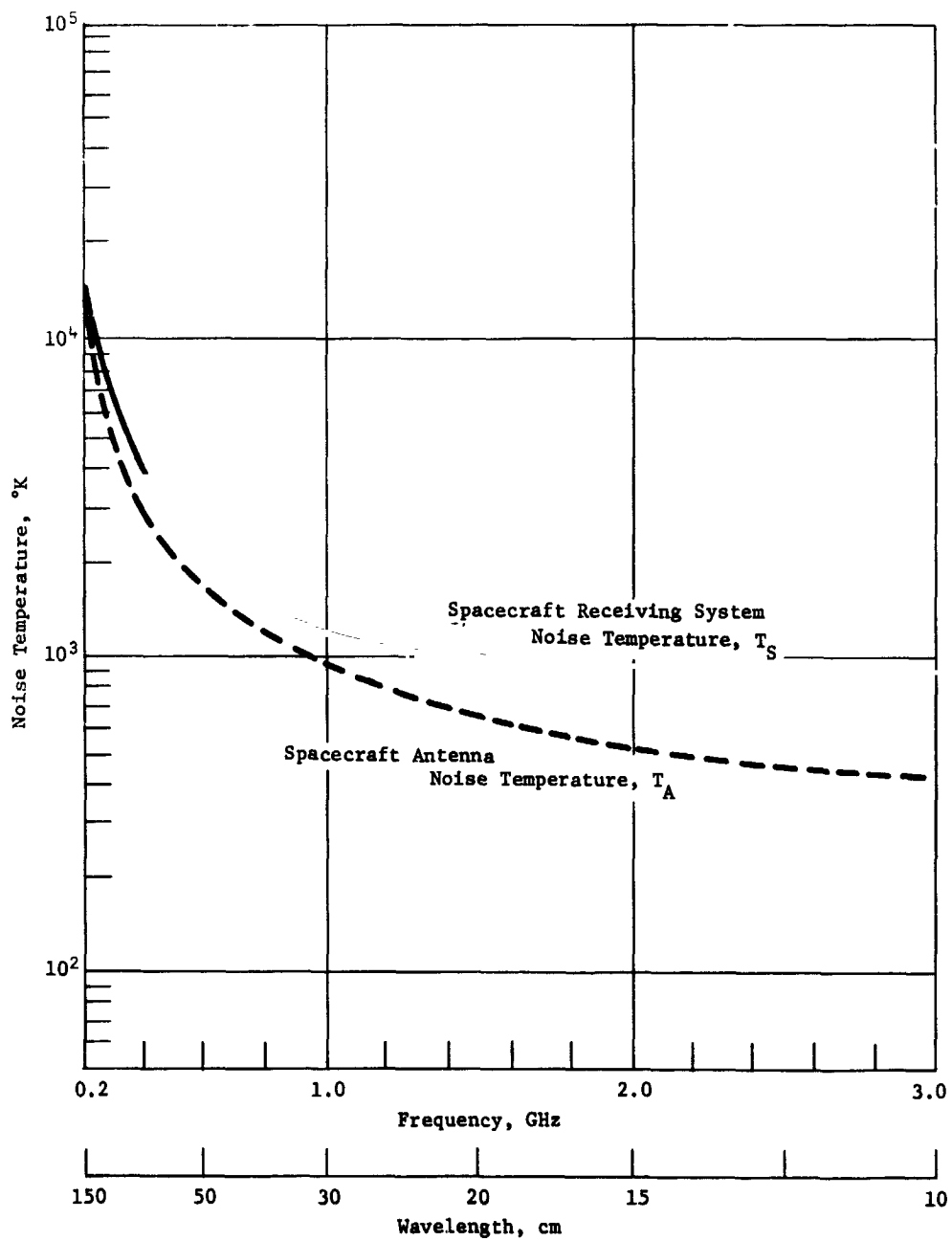


Figure V-12 Spacecraft Receiving System Temperature

Probe pre-entry antennas must have a butterfly pattern that results from a large probe aspect angle prior to entry. For the parametric designs at 1 GHz, a spiral design on a cone was selected. The cone dimensions are too large at 0.86 GHz and an annular slot antenna was chosen which can be placed under the deflection motor. The main drawback to this design is that the antenna is linearly polarized and cross-polarization loss will exist for all look vectors occurring during the probe mission. Since pre-entry communications has a secondary priority, design of a compact, circularly polarized antenna with a butterfly pattern is not considered warranted. The link margin is above zero during preentry and will overcome any polarization loss.

The probe descent antenna uses a turnstile design over a flared cone to provide circular polarization, a large axial pattern, and a compact design. The flare angle and cone depth can be adjusted to achieve the desired beamwidth.

The probe transmitter uses solid state design with an overall efficiency of 45%. Several vendors were contacted to determine 1975 state of the art and upper limits on RF power at UHF. Vendor response is discussed in detail in Chapter IX, Section A.4. An 80-W unit is estimated to be packaged in 2500 cm<sup>3</sup> (150 in.<sup>3</sup>) and weighs 2.7 kg (6 lb). Further investigation into transmitter packaging and weight reductions will be made in future studies. Vendors did not have off-the-shelf hardware in the exact frequency and power ranges of interest on this program.

The transmitter is switched from the pre-entry antenna to the descent antenna during planet entry. An RF coaxial switch reliability performs this function. For power levels up to 20 W, a solid-state switch may be used. Above 20 W, a mechanical switch is required. This is a routine performance for space vehicles and RF switches are the most reliable way to transfer power from one antenna to another. Typical isolation is greater than 50 dB, maximum, insertion loss is 0.3 dB, and standing wave ratio is 1.25:1. See Chapter IX, Section A.4 for complete details on the RF switch.

Requirements for the spacecraft receiver are not critical and a solid-state design using transistors or tunnel diodes may be used. Average noise figures for the receiver front end are shown in Figure V-11 as a function of frequency. Receivers are packaged in 380 cm<sup>3</sup> (23 in.<sup>3</sup>) and weigh 0.9 kg (2 lb). Oscillator stability is maintained if the operating temperature range is -40 to +70°C (-40 to 158°F).

c. *Parametric Point Designs* - Several point designs were investigated to determine the design of the telecommunication subsystem. Configurations that affect RF power requirements are listed in Table V-2 as designs 1, 2, 3, 5, and 8. Each design will be discussed in the following paragraphs.

Designs 1 and 2 varied the entry angle  $\pm 10^\circ$  about the reference mission value of  $20^\circ$ . RF power requirements were determined for the two entry flight path angles at 1 GHz and a bit rate of 28 bps. Spacecraft and probe antennas were optimized for each design. Major design parameters for the two designs are shown in Table V-3 for Configurations 1 and 2. The total RF power required for the conditions given in the table is plotted in Figure V-13. As seen in the figure, higher flight path angles resulted in lower RF power required because probe dispersions were smaller and a smaller spacecraft beamwidth could be used.

Design 3 was the polar entry ( $90^\circ$  latitude) design as seen in Table V-3. RF power of 29 W is required. Probe dispersions were not severe and a  $30^\circ$  spacecraft antenna can be used. The mission is almost identical to the nominal mission from the RF subsystem standpoint.

Design 5 shown in Table V-3 is identical to the nominal mission for all RF parameters except for using the nominal atmosphere model during entry and descent. As seen from Figure II-9, atmosphere loss for the nominal model at 10 bar is 2.8 dB less than the loss for the cool/dense model at 30 bar. The end-of-mission descent depth of 10 bar was chosen for this design from the standpoint of science requirements. As seen from the table, the total RF power required is 12.4 W which is 2.6 dB lower than the power required for the nominal mission. The purpose of this point design was to determine the effects on RF power if the probe were designed for the cool/dense atmosphere and the mission actually encountered a nominal atmosphere. As seen in the table, an additional RF link margin of 2.6 dB would be realized and data would be satisfactorily communicated to the spacecraft for descent to a depth greater than 10 bar. The limit on transmission would depend on the designed burst pressure of the probe and the time when an additional atmosphere loss of 2.6 dB was encountered. Configuration 4 as described in Table V-2 was not analyzed from the communications standpoint because whether or not the probe is transmitting during entry is not mission-critical because RF blackout will occur anyway. The nominal atmosphere model during descent for design 4 then becomes identical to design 5 as far as the communications subsystem is concerned.

Table V-3 Telecommunication Subsystem Parameters for the Parametric Point Designs

Parameter	Point Design Configuration					
	Nominal	1	2	3	5	8
Periapsis Radius, $R_P$ , $R_J$	2	2	2	2	2	6
Ejection Radius, $R_{RJ}$ , $10^7$ km	1	1	1	1	1	3
Entry Path Angle, $\gamma_E$ , -deg	20	10	30	42.6	20	20
Atmosphere	CD	CD	CD	CD	Nom	CD
Descent Depth, bar	30	30	30	30	10	30
Entry Antenna Beamwidth, deg	35	40	20	2	35	30
Entry Antenna Gain, dB	13.5	12.3	16.4	16.4	13.5	14.8
Descent Antenna Beamwidth, deg	120	120	125	120	120	120
Descent Antenna Gain, dB	5	5	4.7	5	5	5
Spacecraft Antenna Beamwidth, deg	45	70	40	30	45	20/15
Spacecraft Antenna Gain, dB	11.3	7.6	12.3	15	11.3	18.3/21
Total RF Power, W	22.8	37.9	17.6	29	12.4	81/36
Invariant Parameters:		Legend for Jupiter Atmospheres:				
Frequency = 1 GHz		CD = Cool/Dense				
Bit Rate = 28 bps		Nom = Nominal				
System Temperature = 1280°F						
$E_b/N_o = 8.9$ dB						
Signal-to-Noise Ratio = 10 dB						
Tone Bandwidth = 15 Hz						

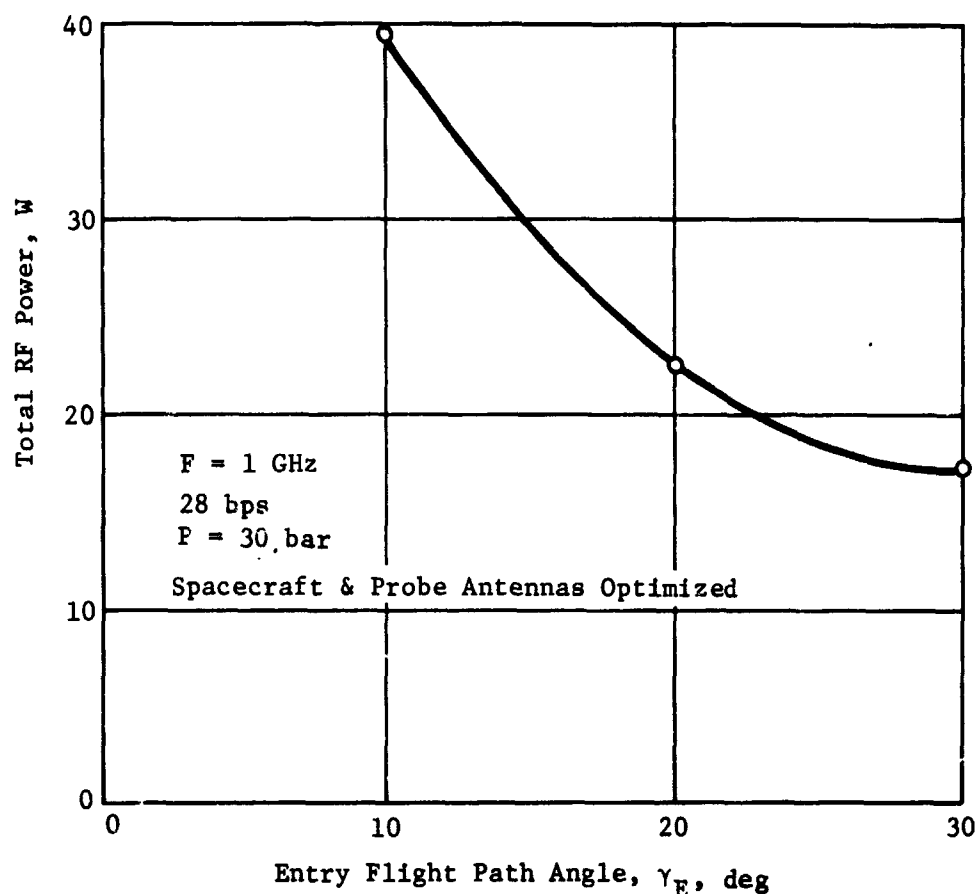
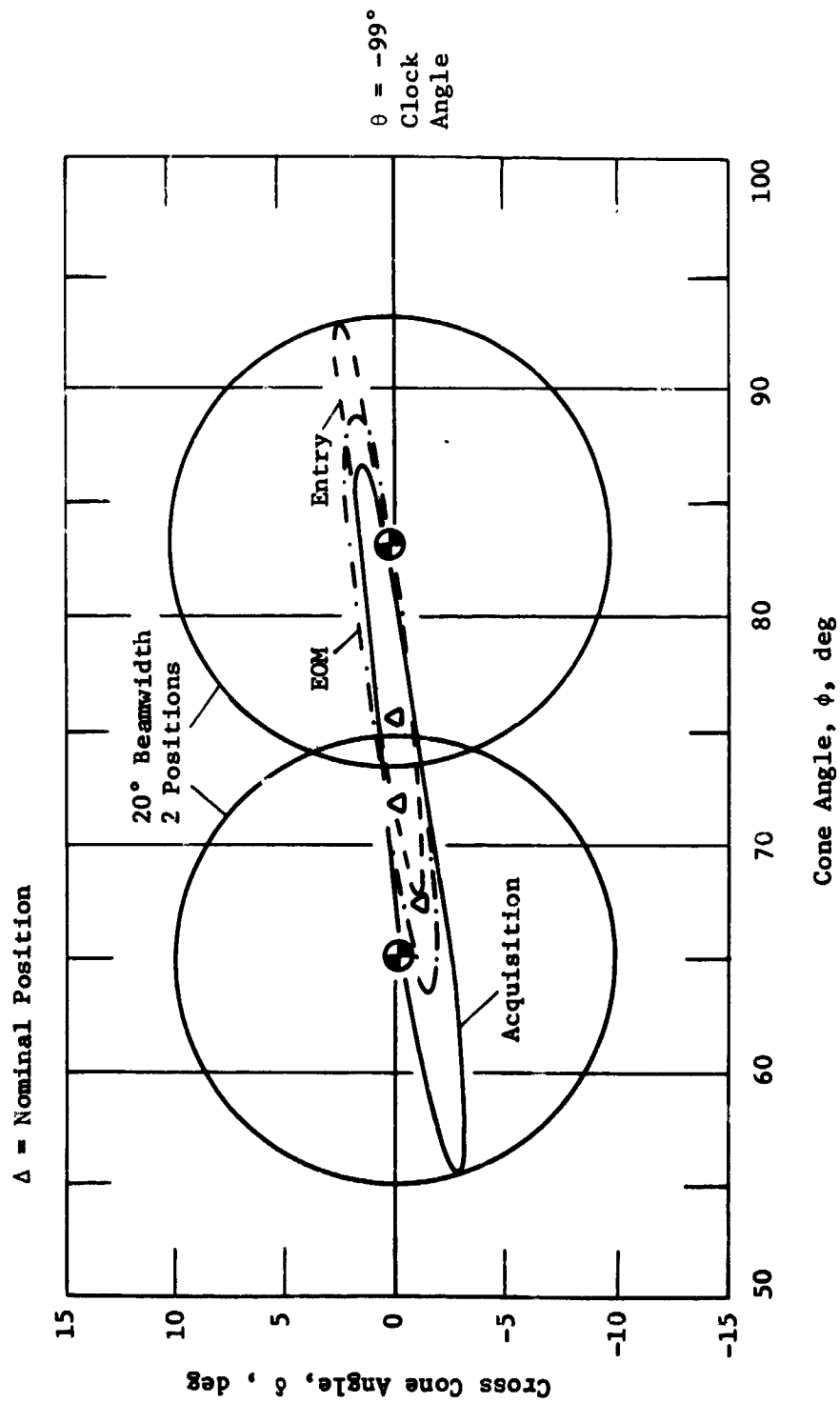


Figure V-13 RF Power Required vs Entry Flight Path Angle

Configurations 6 and 7 did not affect the telecommunications subsystem because the only variations from the nominal probe mission were the spacecraft type, as seen in Table V-2. MOPS is three-axis stabilized and Pioneer is spun stabilized and would require a despun probe tracking antenna platform.

Point design 8 is a mission with spacecraft periapsis at  $6 R_J$ .

Space loss becomes a significant factor in the RF link and probe dispersions were large in cone angle as seen in Figure V-14. The first design attempt used a  $35^\circ$  spacecraft antenna beamwidth, which will encompass the probe dispersion ellipses shown in Figure V-14. The RF power required was 315 W. The second attempt considered a  $20^\circ$  spacecraft antenna beamwidth as shown in the illustration. The antenna is positioned at two locations and has a receiver capable of searching in cone angle with an AGC loop and logic circuits. At acquisition the probe is somewhere in the dispersion ellipse.



V-27

Figure V-14 Spacecraft Antenna Requirements for Point Design 8

The antenna is moved to the first sector position and the logic circuit records the AGC voltage. The same steps are repeated for the second position and the antenna is positioned at the point with the highest AGC voltage. Elevation (cross cone) angle variations are very small and position searches in that direction are unnecessary.

A Monte Carlo analysis was performed on 100-sample missions with selected missions tracked in position from acquisition to entry. The results indicate that a probe in the left half of the ellipse at acquisition will enter in the left half and not move to some other random position. This fact is very helpful because the final position of the probe will be known at entry, based on probe location at acquisition. Additional position searches will not be necessary after the initial search technique.

As seen in Table V-3, using a 20° spacecraft antenna beamwidth results in a requirement of 81 W, which is the upper limit on RF power at 1 GHz for 1975 state of the art. Therefore, a third attempt was made at RF power reduction by a further increase of spacecraft antenna gain. A 15° beamwidth with 3-position search was next considered. This increased the spacecraft antenna gain by almost 3 dB and, as seen in the table, the RF power required drops to 36 W. The frequency must not be lower than 1 GHz or the antenna dish size will exceed the 1.52 m (60 in.) maximum envelope restriction under the payload fairing. The sector search technique is the same as described previously for two positions. Total search time will be longer with more complex logic circuits in the receiver.

Point designs 9, 10, and 11, as described in Table V-2, only involved variations in the deflection technique and type of spacecraft. The results did not affect the communications geometry. As mentioned previously, the Pioneer spacecraft is spun stabilized and a despun antenna platform is required. All other communications parameters are the same as for the reference (nominal) mission.

*d. Spacecraft Receiver Tracking and Acquisition* - The design of the spacecraft receiver is a function of the modulation technique, coding, Doppler uncertainty and Doppler rate. The modulation technique was selected for the purpose of evaluation rather than optimization. PSK modulation has been thoroughly studied for many applications and evaluated in a previous study. Although PSK would provide the lowest power link, it is subject to phase disturbances in the planetary atmospheres which are largely unknown. Binary FSK modulation was therefore chosen as a less susceptible approach. This type of modulation has problem areas associated with acquisition and tracking. The possibility of receiving and recording a



broadband corresponding to the frequency uncertainty was considered and discarded because of the large storage requirements on the spacecraft and the ultimate difficulty of demodulating and decoding the signal at the ground terminal. As a result, the principal efforts on the development of the spacecraft receiver configuration were directed at specifying and defining the method of tracking and acquisition. The final approach by which the data are relayed to the ground terminal may select one of several alternatives: recording a narrow predemodulation bandwidth or demodulation with or without decoding. A full evaluation of these alternatives involves basic communication research and is also influenced by spacecraft capability and is considered beyond the scope of this contract.

The problem of acquisition was initially studied with the intent to acquire and track the data tones. First approaches considered methods for combining the two data signals both before demodulation and after demodulation. The former was considered in systems which used a beat oscillator frequency midway between the two data tones and the use of two beat oscillator frequencies located at equal frequency distances from the two tones. These predetection combination methods would make maximum use of the received signal but have been discarded because the difficulty in establishing that phase coherency of the summed output signals could be achieved. Tracking and acquisition of combined post-detection signals had to be discarded because of insufficient signal-to-noise ratio. This approach is further compromised by use of coding which decreases signal power and increases bandwidth. There is an obvious trade-off for this approach as the data rate decreases, uncoded data would provide sufficient power density in a narrow band to allow acquisition and tracking of the data signal. Also, since many of the probe missions require RF power outputs which are well below the present state-of-the-art capability, increasing the power could decrease the complexity of the spacecraft receiver as compared with the approach selected in this study. It is reasonable to consider that a flight design will provide excess margin wherever possible rather than the minimum power required by the analysis of the mission. In view of the above considerations, a link that provided a constant tone signal in addition to the binary FSK tones was finally selected as a realizable system. The basis of the evaluation is derived directly from Reference 1.

The above referenced paper considers the acquisition of a signal with frequency changing linearly with time with 99% probability of acquisition and 1% probability of false alarm. Although the reference considers a data signal, the analysis is based on a tone and is therefore appropriate to the analysis of a binary FSK system with a tracking and acquisition tone.

The analysis of the tracking error uses classical techniques. A signal-to-noise ratio  $S/N|_T = 10$  dB is provided for the tracking loop. No evaluation of the effects of noise on tracking or of the characteristics of the acquisition transient was made; however, with the above signal-to-noise ratio and the general conservatism of the design, no problem is anticipated in realizing this design. Details of the above analyses may be found in Appendix C of this report.

*e. Error Correction Detection Coding* - A noncoherent FSK system, and especially a binary system, will give poor performance when compared to that attainable according to the Shannon Theory. In attempting to offset this deficiency, error correcting codes must be used.

Convolutional codes are easiest to implement and provide the best performance; therefore, only convolutional codes were considered in this study. Either long or short constraint length codes may be used depending upon the amount of processing if any to be done on the spacecraft. The options range from digitally sampling the received signal and recording the data for relay to Earth to fully detecting and decoding the signal on-board the spacecraft. It was decided, therefore, to assume use of a short constraint length  $K = 8$  and rate  $\frac{1}{2}$  ( $V = 2$ ) code and 3-bit soft decision coding ( $Q = 8$ ) using a maximum likelihood decoder. Therefore, the following approach was taken to estimate the required  $E_b/N_0$  for the desired bit error rate of 5 parts in  $10^5$ : (1) determine the coding gain at this same error rate for a coherent PSK channel; (2) assume that the coding gain for binary FSK will be equally as good.

Figure V-15, which is taken from Figure 2 of Reference 2, was used to determine coding gain for the proposed coding and decoding algorithm which yielded a value of 5.1 dB. The uncoded  $E_b/N_0$  for binary FSK at a bit error rate of  $5 \times 10^{-5}$  is 13 dB. Subtracting 5.1 dB from 13 dB yields 7.9 dB as the value for  $E_b/N_0$  for a coded binary FSK signal. One dB was added to this to cover contingencies resulting in a final value of  $E_b/N_0$  of 8.9 dB for the probe-to-spacecraft relay.

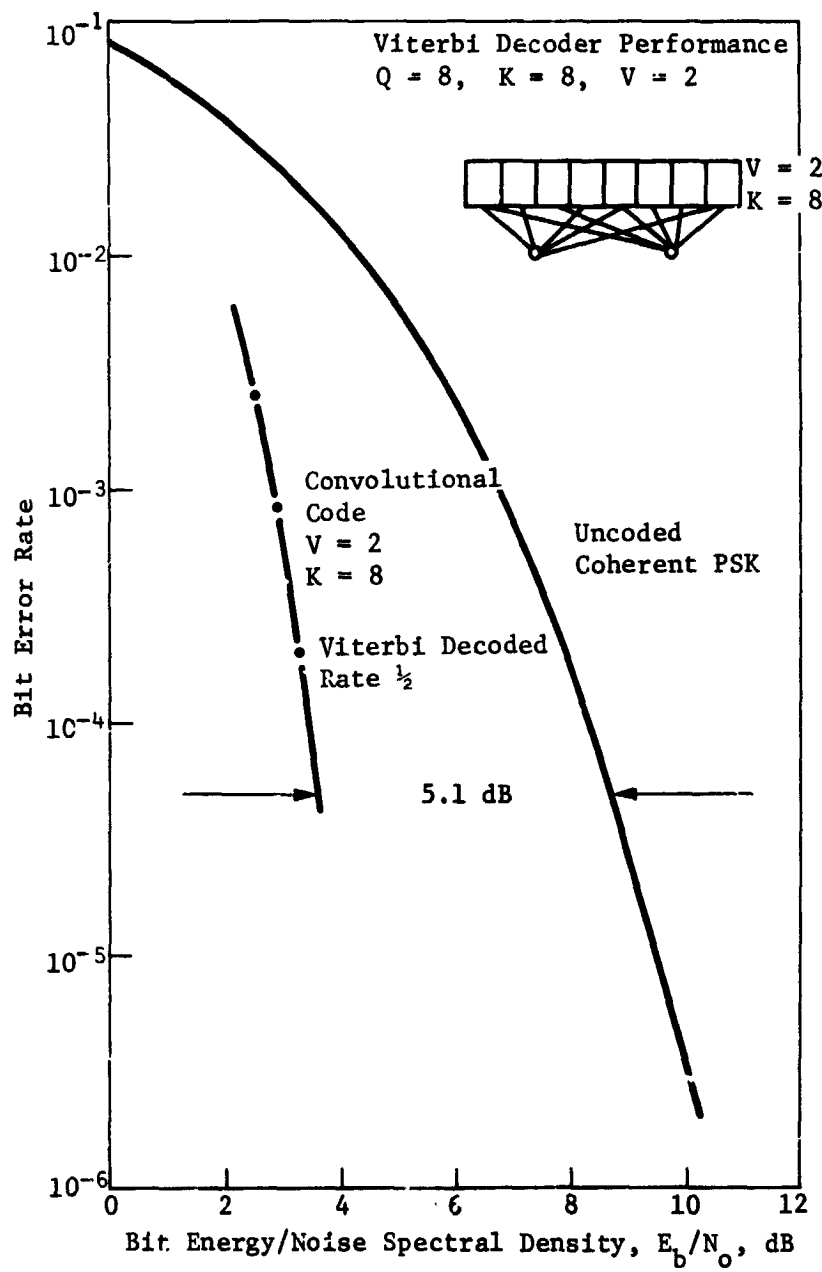


Figure V-15 Bit Error Probability

f. *Direct Communications Link to Earth* - The direct link study of the original contract (Ref 3) was used as a basis from which extrapolations were made, as necessary, to the conditions of the nominal reference probe mission. The fact that the direct link would require a steeper entry than that imposed on the original study was ignored, as required by the statement of work. Therefore, acceptable sub-Earth point geometry was assumed for the direct link to Earth from Jupiter.

*Original Study Criteria* - In order to set the criteria for the direct link study, certain ground rules from the original study are summarized. Dispersions to the probe aspect angle were  $3.6^\circ$  at entry and end of mission. Probe aspect angle varied  $33.5^\circ$  during the mission from entry to a depth of 17 bar, which required 0.93 hr. Targeting was designed to keep the probe as close to the sub-Earth point as possible.

Communications frequency was constrained to the DSN (deep space net) frequency of 2.3 GHz (S-band) with a coded noncoherent modulation format using 32-ary FSK (frequency shift keying) with a 1/5-th rate, constraint length 8 convolutional encoder. Predetection recording, noncoherent detection, and Viterbi decoding were assumed at the DSN ground station. The post-entry bit rate was 20 bps with no preentry communications. The probe used a high gain (22 dB) steerable phased array antenna radiating 15 W of RF power. Noncoherent signaling was chosen over coherent since it avoids losses resulting from power in the carrier. The savings exceeds the loss because less efficient detection for low data rates gives an advantage to noncoherent signaling at these low rates.

For a bit error rate (BER) of  $5 \times 10^{-5}$  with 32 FSK and  $K = 8$  code, an  $E_b/N_o$  of 7.4 dB was used. Convolutionally encoded with Viterbi decoding results in an improvement of 2.5 dB by holding the data rate constant and reducing power, or  $E_b/N_o = 4.9$  dB. Demodulation losses of 1.6 dB were used for the MFSK signaling format because of imperfect frequency and symbol synchronization tracking (Ref 4). This is a conservative estimate for iterative processing of predetection recording. The expected performance is degraded by this loss, resulting in an equivalent  $E_b/N_o$  of 6.5 dB for the design link.

A steerable high gain antenna was required to hold the transmitter to a reasonable power level. The antenna size was limited by available space on the probe; size is inversely proportional to the frequency. An array was chosen on the original study (Ref 3, Vol II, p VII-95). Pointing information was derived from the up-link signal from Earth which permits the use of a self-focusing array that gives rapid acquisition and flexible tracking. Frequency search and acquisition was achieved by an element of the array. The maximum gain is 22 dB with gain decreasing as  $\cos \phi$  for scanning off boresight. The antenna array with RF power amplifiers at each element weighed 23 kg (51 lb).

RF link calculations for the described conditions of the original study are depicted in Table V-4 (Ref 3, Vol II, p VII-100) for a noncoherent system. The DSN dish antenna has a maximum gain of  $61.4 \pm 0.4$  dB with a feed system capable of handling transmission and reception at 2.3 GHz. The zenith noise temperature is  $23 \pm 3^\circ\text{K}$  which is augmented by  $4^\circ$  to account for Jovian disk noise in the main beam and  $6^\circ$  for Earth ionosphere noise resulting from scanning  $65^\circ$  off zenith (Ref 5). Adding these items gives a total DSN antenna noise temperature of  $33 \pm 3^\circ\text{K}$ . Jovian atmospheric and defocusing losses were 2.6 dB for a depth of 17 bar at 2.3 GHz using the original nominal atmosphere model. Adverse tolerances for the receiving antenna gain results from pattern asymmetry and cross-polarization. Probe antenna pointing losses result from the  $3\sigma$ -aspect angle dispersions. Communications range from Earth to Jupiter is 6.36 AU or  $9.54 \times 10^8$  km with a round trip transmission time of 100 min. Receive circuit losses include a recorder loss of 1 dB. A safety margin of 2.6 dB over the total adverse tolerance was selected (Table V-4, Line 21) resulting in a probe transmitter RF power of 15 W required for the direct S-band link.

*Updated Direct Link Calculation* - Parameters of the previous study, where applicable, were used to calculate the RF power for a direct Earth link for the nominal mission trajectory. Several conditions resulted in differences in link parameters. The nominal mission for the present study uses binary FSK modulation and extends to a depth of 30 bar in a cool/dense atmosphere. These were the two major link differences.  $E_b/N_o$  for BFSK is 8.9 dB with a 1-dB recording loss, and a Doppler offset loss during entry of 1 dB. Parameters for the revised direct link study are listed in Table V-5 with changed values noted with an asterisk. Probe aspect angle varied  $13^\circ$  during the mission with a  $3\sigma$  dispersion of  $3.6^\circ$  as seen in Figure V-16. The phased array maintains the beam center towards Earth; therefore, position dispersion is the only source of antenna pointing error. Atmospheric loss for 30 bar depth increased from 2.4 to 13.8 dB.

Table V-4 Original Probe Telemetry Design Control Table

Planet: Jupiter		Modulation: 32-ary FSK	
Mission: Direct Link (Mission F)		Frequency: 2.3 GHz	
Parameter	Nominal Value	Adverse Tolerance	Remarks
1. Total Transmitter Power, dBW	11.8	0.4	15 W
2. Transmitting Circuit Loss, dB	-0.5	0.5	
3. Transmitting Antenna Gain, dB	22.0	0	Phased array
4. Transmitting Antenna Pointing Loss, dB	0	0.3	$3\sigma = 3.6^\circ$
5. Space Loss, dB	-279.2	0	$9.5 \times 10^8$ km
6. Planet Atmosphere & Defocus Loss, dB	-2.4	0.2	17 bar, nominal
7. Polarization Loss, dB	0	0.5	
8. Receiving Antenna Gain, dB	61.4	0.4	210-ft DSN
9. Receiving Antenna Pointing Loss, dB	0	0	
10. Receiving Circuit Loss, dB	-1.1	0	
11. Net Circuit Loss, $\Sigma(2 + 10)$ , dB	-199.8	1.9	
12. Total Received Power (1 + 11), dBW	-188.0	2.3	
13. Receiver Noise Spectral Density, $N_o$ , dBW	-212.8	0.4	$T_S = 33 \pm 3^\circ K$ $NF_c = 0.47$ dB
Data Channel			
14. Fading Loss, dB	0	0	
15. Processing Loss, dB	0	0	
16. Received Data Power (12 + 14 + 15), dBW	-188.0	2.3	
17. Data Bit Rate, $1/T_b$ , dB	13.0	0	$T_b = 20$ bps
18. Threshold $E_b/N_o$ , dB	6.5	0	
19. Threshold Data Power (13 + 17 + 18), dBW	-193.3	0.4	
20. Performance Margin (16 - 19), dB	5.3	2.7	
21. Nominal Over Adverse Value (20 - 20 adv), dB	2.6		
Conditions: 1. Data taken from original study, Mission F (Ref 3, Vol II, p VII-100) 2. Noncoherent coded system 3. Predetection recording, noncoherent detection 4. Viterbi decoding 5. Convolutional encoder, $M = 32$ , $V = 5$ , $Q = 8$ 6. $BER = 5 \times 10^{-5}$ for 32-ary FSK with $K = 8$ code			

Table V-5 Probe Telemetry Design Control Table for Nominal Probe  
Direct Link

Planet: Jupiter		Modulation: BFSK	
Mission: Direct Link		Frequency: 2.3 GHz	
Parameter	Nominal Value	Adverse Tolerance	Remarks
1. Total Transmitter Power*, dBW	25.1	0	400 W
2. Transmitting Circuit Loss, dB	-0.5	0.5	
3. Transmitting Antenna Gain, dB	22.0	0	Phased array
4. Transmitting Antenna Pointing Loss, dB	0	0.3	$\Delta\psi = 3.6^\circ$
5. Space Loss, dB	-279.2	0	$9.5 \times 10^8$ km
6. Planet Atmosphere & Defocus Loss*, dB	-13.8	0.2	Cool/dense
7. Polarization Loss, dB	0	0.5	
8. Receiving Antenna Gain, dB	61.4	0.4	210-ft dish
9. Receiving Antenna Pointing Loss, dB	0	0	
10. Receiving Circuit Loss*, dB	-0.1	0	
11. Net Circuit Loss, $\Sigma(2 \rightarrow 10)$ *, dB	-210.2	1.9	
12. Total Received Power (1 + 11)*, dBW	-185.1	1.9	
13. Receiver Noise Spectral Density, $N_o$ , dBW	-212.8	0.4	$T_S = 33 \pm 3^\circ\text{K}$ $NF_S = 0.47$ dB
Data Channel			
14. Fading Loss, dB	0	0	
15. Processing Loss*, dB	-1.0	0	
16. Received Data Power (12 + 14 + 15)*, dBW	-186.1	1.9	
17. Data Bit Rate, $1/T_b$ *, dB	14.5	0	$T_b = 28$ bps
18. Threshold $E_b/N_o$ *, dB	8.9	1.0	BFSK, entry
19. Threshold Data Power (13 + 17 + 18)*, dBW	-189.4	1.4	
20. Performance Margin (16 - 19)*, dB	3.3	3.3	
21. Nominal Over Adverse Value (20 - 20 adv)*, dB	0		
Conditions: 1. Changes to the original study parameters (Table V-4) denoted by an asterisk 2. Noncoherent coded system 3. Predetection recording, noncoherent detection 4. Viterbi decoding 5. Convolutional encoder, $M = 2$ , $V = 2$ , $Q = 8$ 6. $BER = 5 \times 10^{-5}$ for binary FSK with $K = 8$ code			

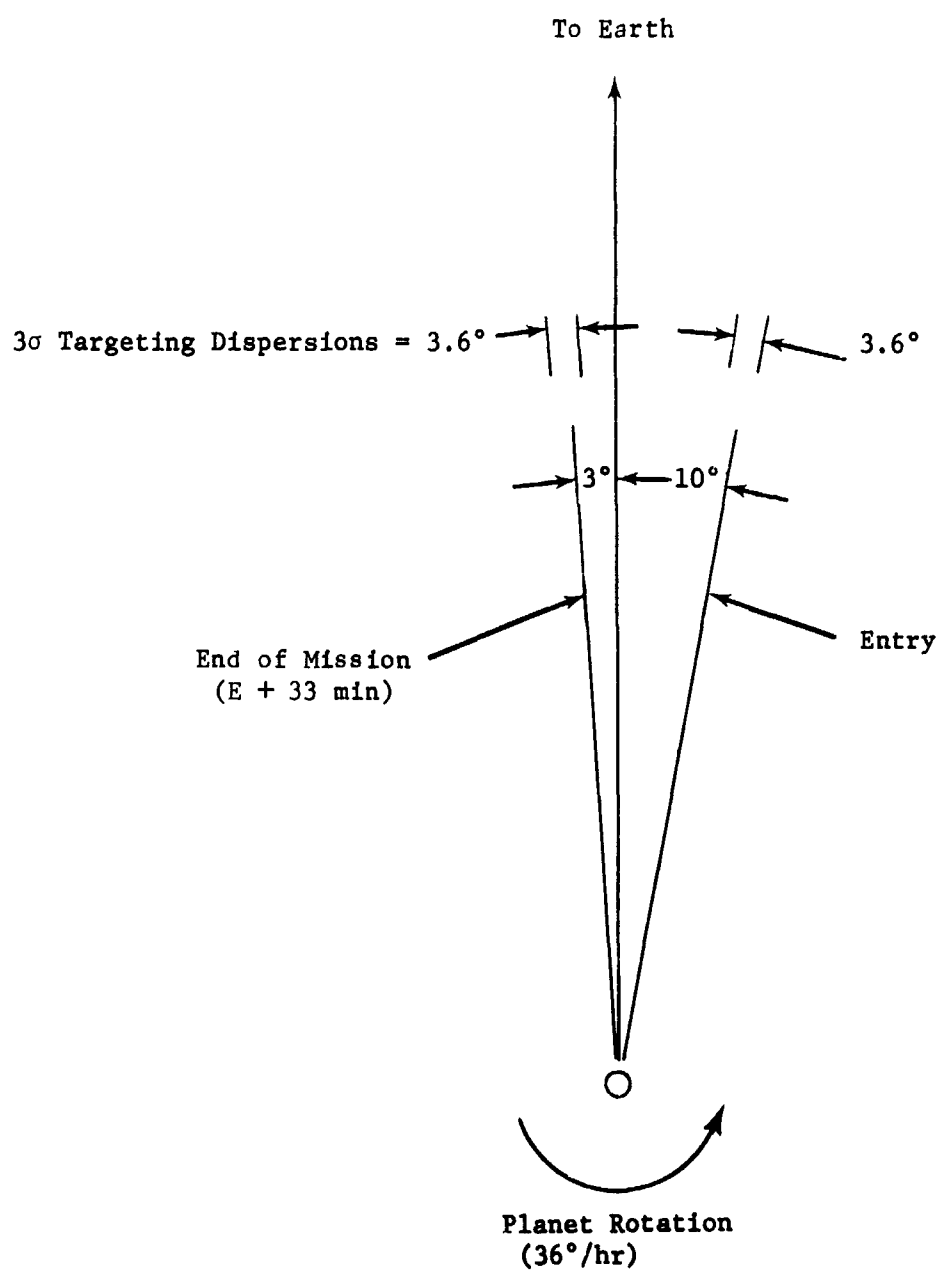


Figure V-16 Direct Earth Link Communications Geometry



The bit rate for the nominal mission is 28 bps which is 1.5 dB higher. Threshold  $E_b/N_o$  is 8.9 dB which results in a 3.9 dB higher threshold data power than originally. Total received power is 2.9 dB higher and the net circuit losses are 10.4 dB higher with the increased atmospheric loss the main factor. Performance margin was set to equal the adverse tolerance, in keeping with standard JPL philosophy.

The resulting RF power is 400 W which is 13.3-dB higher than the power of 15 W determined on the original study (Table V-4). The 11.4 dB difference is attributed to atmosphere loss and is the major factor in the power disparity. The nominal mission adjusted to a depth of 17 bar results in a transmitter power of 18.6 dBW, or 72.2 W. The higher power is attributed mainly to the new cool/dense atmosphere model. If an upper limit of 40 W at S-band were considered, a depth of 13 bar could be reached before atmosphere absorption reduced the RF link margin below zero.

In conclusion, a direct link to Earth is not practical for a mission depth of 30 bar at S-band. Lowering the frequency will reduce atmosphere loss and RF power required, but the probe array antenna size becomes prohibitive. Decreasing the mission depth to 13 bar, or less, results in a viable mission at S-band from the communications standpoint. RF power levels will be 40 W, or less, as the depth is reduced above 13 bar. These levels are within the S-band transmitter state of the art and avoid the possibility of encountering antenna and transmitter RF breakdown problems.

#### g. References

1. S. Georgiev: *A Feasibility Study of An Experiment for Determining The Properties of the Mars Atmosphere*. Final Report, Vol III, Subsystem and Technical Analysis, Contract NAS2-2970, Avco Corporation, Lowell, Mass; NASA CR-73005, Appendix G, September 1966.
2. S. Z. H. Taqvi: "Some Interesting Simulation Results of the Viterbi Decoder." *National Telemetry Conference 1971 Record*, pp 240 through 246.
3. *Jupiter Atmospheric Entry Mission Study Final Report*, Vol II. Contract JPL 952811, Martin Marietta Corporation, Denver, Colorado, MCR-71-1(II), April 1971, pp VII-84 through VII-106.
4. H. D. Chadwick and J. C. Springett: "The Design of Low Data Rate MFSK Communication Systems." *IEEE Transactions*, COM-18, No. 6, December 1970.
5. *DSN Standard Practice*, JPL. Document No. 910-5, March 1970.

## 5. Data Handling Subsystem (DHS)

The configuration of the data handling subsystem was based on studies of probe requirements for Venus and the outer planets. Consideration was given to two general types of systems: the Adaptive Control and Data Processing Group (ACDPG) and Control and Data Processing Unit (CDPU). The ACDPG (Fig. V-17) consists of a computer and a Processor Interface Unit (PIU) which includes all the functional blocks except the computer. The selected computer is a nonredundant version of the Advanced Onboard Processor (AOP) which is being considered by Martin Marietta for outer planet spacecraft. It employs a plated wire memory and bipolar (non-MOS) LSI circuits. By use of a system like the ACDPG, an increase of approximately 5.5 kg and 4 W over the CDPU version could be traded off against savings in weight and power in attitude control and the instruments. Since the AOP computer is designed for redundancy functions, it may be expected that an additional 10 to 30% decrease in weight and power could be achieved for the computer.

The evaluation of the CDPU involved a rather pragmatic evaluation of mission viability which considered the fluctuating instrument designs with consequent changes in interface requirements, development costs, schedule, and practical reliability aspects. The major functional requirements of the data management subsystem are shown in Table V-6. Except for the entry accelerometer instrument, there are no significant storage requirements. For any specific atmosphere, there is a fixed sequence and format. Consequently, the decision-making capability and processing complexity of the subsystem tend to be minimized. The decision as to the locale of the various functions must consider the variability of the science processing requirements during the development of the instruments as well as the significant differences between instruments. The high radiation, g-stress and long-life environment, as well as the value of partial data return, provide a basis for a decentralized data handling subsystem. The remaining functions that are necessarily common to all functions (i.e., formatting and sequencing) should be well protected from failure by redundancy. A decentralized subsystem should be cost and schedule effective through the development program.

The design of a data handling subsystem (Fig. V-18) that primarily serves to provide formatting, sequencing, and encoding may be implemented from available qualified components, integrated circuits, and piece parts. Selection of such devices will be heavily influenced by established reliability and radiation resistance.

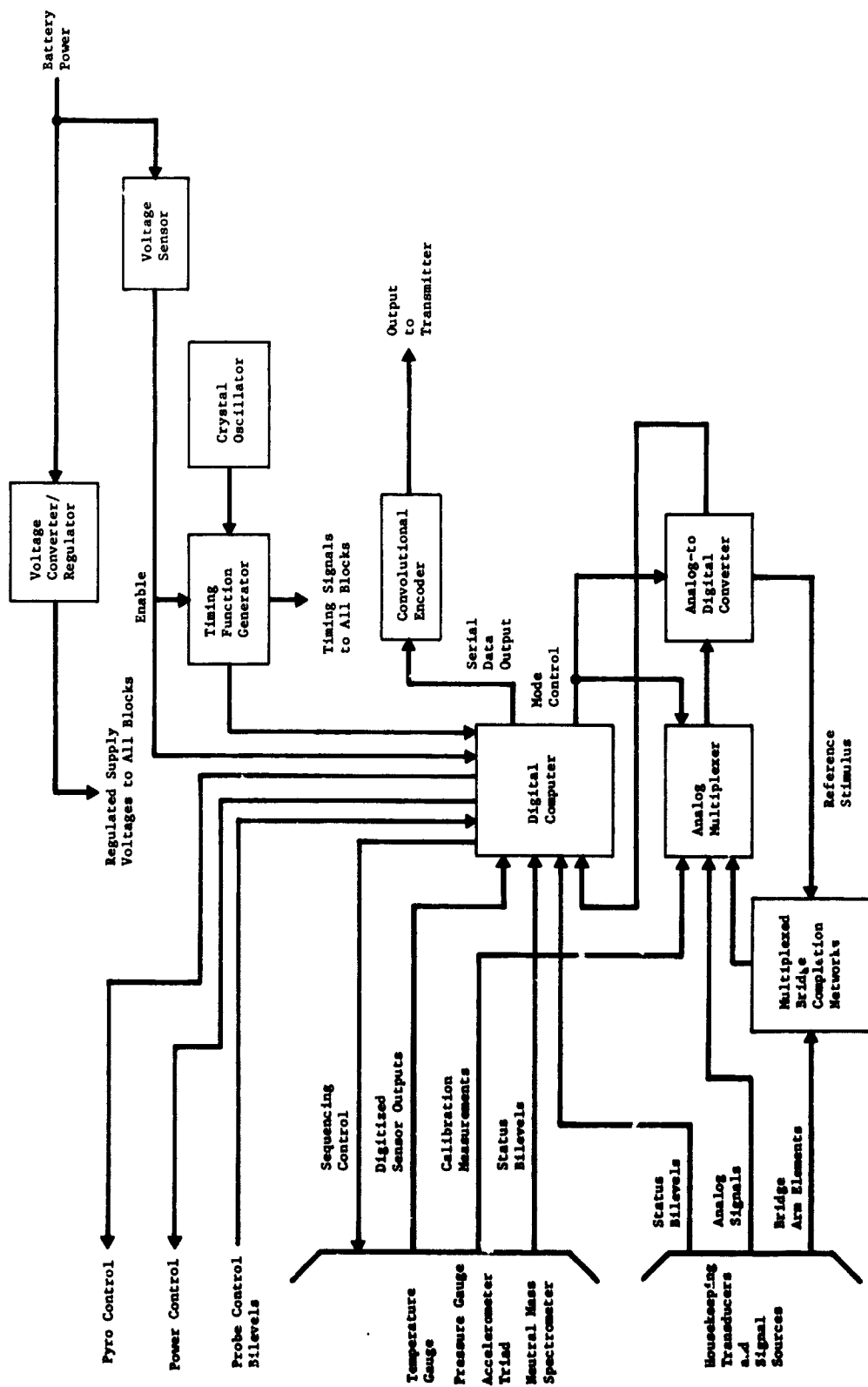


Figure V-17 Data Handling Subsystem, General Purpose Approach

Table V-6 Data Management Functional Requirements

Function	Application	Function Locale	Comments
Timing	Sequencing	DHS	Hardwire/Programmable
	Synchronization	DHS	Sync Bus
Data Storage	Accelerometer	DHS	Blackout Data
	Engineering	DHS	Probe Readiness
Data Processing	Accelerometer	Inst	Turbulence
	NMS	Inst	Analog/Digital Conversion
	Pressure	DHS/Inst	Analog/Digital Conversion
	Temperature	DHS/Inst	Analog/Digital Conversion
	Engineering	DHS	Analog/Digital Conversion
Sequencing/Format	Preentry Probe Readiness	DHS	Ccast Timer/Battery Initiate
	Data Transmission	DHS	Engineering Data
	Postentry Black	DHS	G Switch Initiate
	Probe Readiness	DHS	Engineering/Accelerometer Data
	Data Transmission	DHS	Descent Format

Consideration of atmospheric variability indicate a need for adaptive functions in the subsystem that could conceivably optimize the data return. With the present instrument package, the advantages of optimization with respect to the data return and probe design do not appear to be significant. Furthermore, the information available (i.e., temperature and pressure) are not sufficiently well known to make a valid format decision at the required altitudes.

As a result of the above considerations and comparisons, the recommended approach is the special purpose CDP. The alternative configuration may be reconsidered if there is extensive elaboration of the instrument payload, or a more flexible in-flight programmable system is required. A more complete description of this subsystem may be found in Volume III, Appendix H.

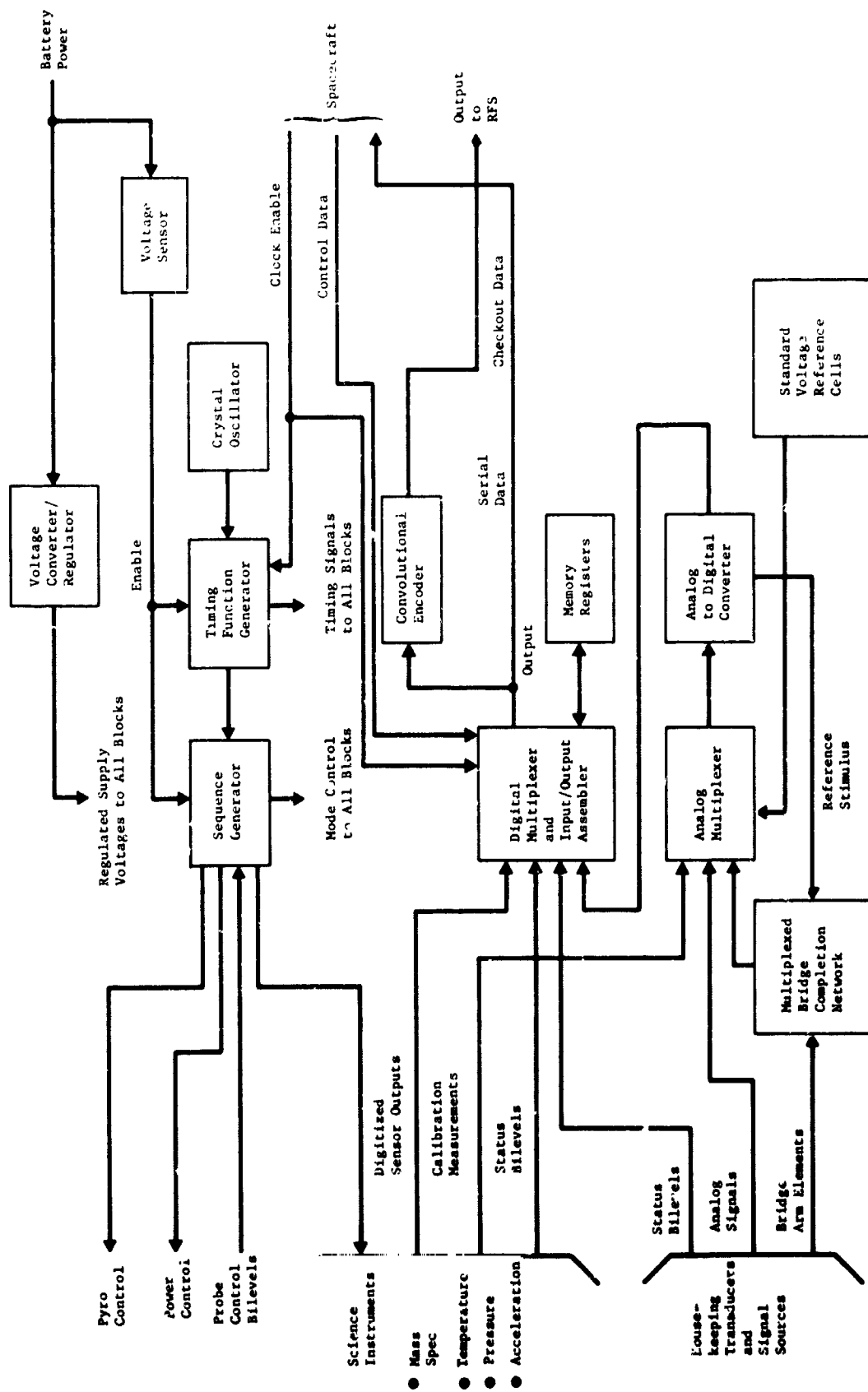


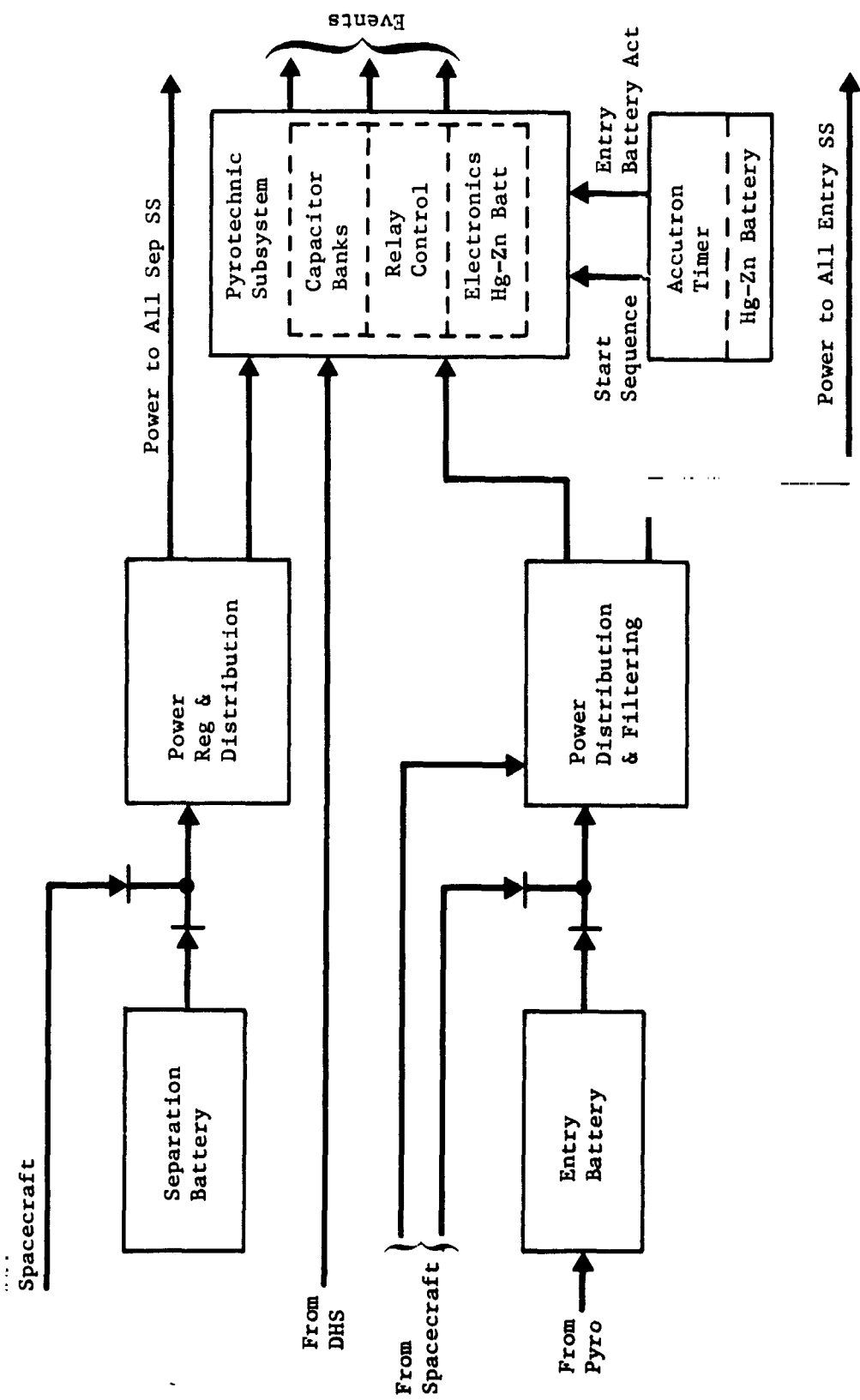
Figure V-18 Data Handling Subsystem, Special Purpose Approach

## C. Power and Pyrotechnic Subsystem

The power subsystem consists of two sections (Fig. V-19) that reflect the differing requirements during the post-separation and the entry/descent periods. Power during separation will be provided by a centralized conditioning unit to supply the power for attitude control, vehicle engineering and other electronics active at this time. During the entry and descent phase of probe operation, battery power will be distributed by a relay controlled power distribution unit and isolated by power separation filters. Primary power will be provided by remote activated pile construction silver zinc primary cells. Energizing the probe separation battery will be accomplished by the probe electronics but will be implemented with spacecraft power and signal. Energizing the second battery before entry will be implemented by the probe pyrotechnic electronics which will be (briefly) powered by a long-life mercury-zinc battery. This event will be initiated by a coast (Accutron) timer that has a self-contained power source (mercury-zinc). Although this approach requires two additional low power batteries, the disparity between the voltage level required for the pyrotechnics (40 V) and the timer (1.6 V) make a single battery impractical.

The subsystem configuration is essentially a result of the battery selection. The remote activated battery does not maintain capacity when activated for more than 24 hours. Consequently, the two active phases of the probe mission each require a separate battery. Since the ACS system is required only during the post-separation phase, reliability considerations suggest the complete isolation of the post-separation power bus from the entry power bus. The two power systems were then configured to meet the differing electrical and environmental requirements.

Selection of the battery was based on studies of outer planet probe requirements for several programs. The tradeoff evaluation used a nominal Jupiter probe mission for life, required wet stand, and temperature profiles. Consideration was given to secondary Ag-Zn batteries flown on float charge, discharge and open circuit. Nickel-cadmium (Ni-Cad) batteries were evaluated in float and discharge conditions for the cruise mode (530 days). All of these approaches would require some battery development and extensive testing for the mission. Expected development and testing by the 1975 time period for long-life batteries will probably emphasize Ni-Cad batteries which have established capability.



V-43 *Figure V-19 Power & Pyrotechnic Subsystems*

However, these batteries would exact a considerable weight penalty on the probe design. The above approaches would also require the spacecraft to perform considerable battery conditioning before probe separation, and would increase the complexity of the spacecraft/probe interface. The remote activated Ag-Zn batteries have established dry-stand capability (91 months) which is comparable to Uranus mission requirements. The reliability of these units has been established. The major problem is the short wet-stand capability caused by the probability of sneak paths in the fill manifold. Solution of this problem and known modifications to the separator material could extend the wet stand to 30 days (i.e., comparable to manual fill Ag-Zn primary batteries). The shorting problem in the fill manifold appear solvable with a low cost development program and several possible approaches are described in the literature and in Volume III, Appendix G. The pile construction battery, while not in extensive use in this country for the ampere-hour capability required by the probe missions ( $\approx 5$  amp-hr), would provide an approximate 50% reduction in weight. Inasmuch as the state of the art of communications subsystem will allow RF power considerably in excess of present requirements, it is expected the power requirements for this major load will increase in order to provide more data or a greater reliability margin. In view of the above considerations, the remote-activated Ag-Zn pile construction battery is recommended for the outer planet entry probe design.

The selection of the Hg-Zn batteries for the Accutron timer and the initial entry pyrotechnic event was not based on a rigorous evaluation. Some brief considerations were given to other type power sources but the Hg-Zn battery appears to provide a higher energy density for the Jupiter mission. The requirements of the Saturn mission may also be met by the Hg-Zn battery based on extrapolated degradation data ( $\approx 7\%$ /year). Although this appears to be a reasonable estimate and consistent with the emphasis of this study, justification of this estimate on a qualitative basis (i.e., test data) was not obtainable in the primarily commercial documentation of this component. The approximate 7-year wet stand required by the Uranus mission may necessitate a re-evaluation of power sources for this low energy application. Prime candidates for this purpose are the low power RTG sources now under development in Pacemaker programs. These designs could fulfill the energy demand but development would be required because of their characteristic low voltage which would entail possibly prohibitive power conditioning losses. In any event, the size and weight of these various components are all small and do not constitute a major concern in the present state of outer planet entry probe design.



The alternative choices for the pyrotechnic system design are limited to battery bus and capacitor bank activation approaches. Since use of the battery bus would lead to serious noise and transient problems, and would probably require a third power distribution system and an additional low power battery, the charged capacitor bank approach, was selected. A more complete description of the trade-off evaluations for the power and pyrotechnic subsystems may be found in Volume III, Appendix G of this report.

## 7. Attitude Control Subsystem (ACS)

The general attitude control problem requires separation of the probe from a 3-axis stabilized spacecraft, spinup to 10 rad/sec ( $\approx 100$  rpm), development of a delta velocity impulse accurately oriented in space ( $\approx 1^\circ$  error), and then maneuver to the final entry attitude. If the spacecraft deflection mode is used, spinup to 5 rpm is the only requirement. For a mission using the Pioneer spacecraft, spinup is provided by the spacecraft. The latter two cases both allow reduction in complexity and cost of the attitude control design.

Several alternative design approaches were considered to implement the attitude control requirements. The principal consideration in the survey of possible systems was simplicity, reliability, and use of available components, since these aspects have a direct impact on cost. A few of these alternatives are briefly discussed below.

*a. Offset Thrust* - The described conditions for the mission profiles that require attitude control indicate that two attitude positions are required: (1) the orientation for the delta velocity impulse and (2) the final position for entry. It has been considered that if the delta velocity impulse could be applied at an angle with respect to the spin axis, the probe could be separated with spin in the entry orientation and no attitude maneuver would be required. This approach could be implemented in one of two ways: (1) a combination of axial thrust and an impulse at right angles to the spin axis; (2) use of an offset solid rocket motor with a firing time that is small compared to the time of rotation. However, both of these approaches would require precise timing functions that would have to be derived from at least a Sun sensor. Furthermore, the effect of offset tolerances and the transverse component of thrust would produce unacceptable attitude errors and further attitude corrections would be required.

b. *Stored Momentum* - This approach would make use of a small fly-wheel operated at high speed. The angular momentum vector of the wheel would be that required to correct the position of the angular momentum vector of the probe from the delta velocity impulse direction to the final position. The wheel would be positioned before separation and then spun up. Once positioned, the wheel would be released on free gimbals. The probe would then be spun up, released, and the solid rocket motor fired. Subsequent to the completion of the delta velocity impulse, the wheel could be locked to the probe spin axis and eventually stopped with respect to the probe frame of reference by frictional means resulting in complete transfer of wheel angular-momentum to the probe. The problems arising with this approach are basically: (1) the possibility of undesirable transfer of momentum from the wheel to the probe before or during the delta velocity impulse; (2) the presence of high energy storage in the wheel could result in the probe eventually achieving an attitude  $180^\circ$  from the desired attitude. The first problem area is the most serious. The "free" gimbals would be stressed during the delta velocity impulse. Consideration was given to providing some drive to a gimbal-oriented along the spin axis in order to overcome the biased friction because of the probe spin. However, even if this approach were considered feasible, an expensive development and qualification program would be required for a precision gimbal development.

c. *Open-Loop Control* - This system would consist of a stored series of timed precession impulses. Since the orientation of the probe and the final attitude is well known, the attitude maneuver could be precisely specified. The final error would then include disturbance to the angular momentum vector caused by the delta velocity impulse. This approach could not be used for missions that required attitude trim before firing the solid rocket motor. This method was discarded because it is not feasible to meet the knowledge requirements on probe spin rate and phase and at least a Sun sensor would be required. Since these sensors are presently available to yield Sun aspect angle as well as Sun crossing time for phasing, a closed-loop system could be used that would provide greater reliability and probably lower cost when testing and less critical requirements are considered.

d. *Simple Close-Loop, Single-Axis Maneuver* - This approach is a natural outgrowth of the open-loop system described above. It would use a Sun sensor that provides a measurement of solar aspect as well as Sun crossing time. The maneuver sequence would consist of firing a preprogrammed set of precession impulses immediately following the delta velocity impulse maneuver. These

pulses could be offset in phase so that essentially a two-axis maneuver could be achieved, although only the maneuver angle with respect to the Sun line (i.e., solar aspect angle) could be measured. Subsequent to the initial maneuver, some time (order of several hours) would elapse while the damper removed residual nutation. A measurement of solar aspect angle would then provide information for further maneuvers.

e. *Closed Loop, Two-Axis Maneuver* - This configuration (Fig. V-20) uses a Sun sensor to measure solar aspect angle and Sun crossing time and a Jupiter sensor to measure Jupiter crossing time. The sequence of the maneuver would be similar to the single-axis system described above. Immediately following the delta velocity impulse maneuver, a preprogrammed series of pulses would orient the probe near its final position. Then, after a waiting period of several damper time constants, measurements are made of solar aspect angle and the angle between the Sun and Jupiter measured about the spin axis of the probe. These measurements are then used to develop subsequent precession programs to finalize the probes position. Because of residual nutation, it is not considered desirable to continuously drive the probe to minimize the final error. For this reason, the maneuver will take place in a series of steps as described above. With this approach there are certain constraints on the relative position of the Sun and Jupiter as discussed below. This system, using attitude sensors, may also be used to trim probe attitude before the delta velocity impulse. Since it represents a minor increment in complexity over a single-axis system and has inherent greater flexibility and capability, it has been the system that has received the major consideration. For missions in which the single-axis system may be a preferred choice, it would be a minor consideration to reduce the two-axis maneuver system to a single-axis maneuver system.

f. *Error Budget* - Table V-7 shows a summary of the tolerances, misalignments, and resultant error budget consistent with the analysis of rigid body motion and the constraints delineated in the introduction of this section. For a more complete description of the attitude control subsystem and analysis, refer to Volume III, Appendix F of this report. In this table, items (13) and (12) express expected errors with and without an ACS trim maneuver before delta velocity impulse thrusting. The velocity dispersions have significant effects on trajectory dispersions and result in higher communication power and longer acquisition time. Since one degree is the nominal error budget contribution of this subsystem to the velocity dispersion, the trim maneuver is included in the mission profile.

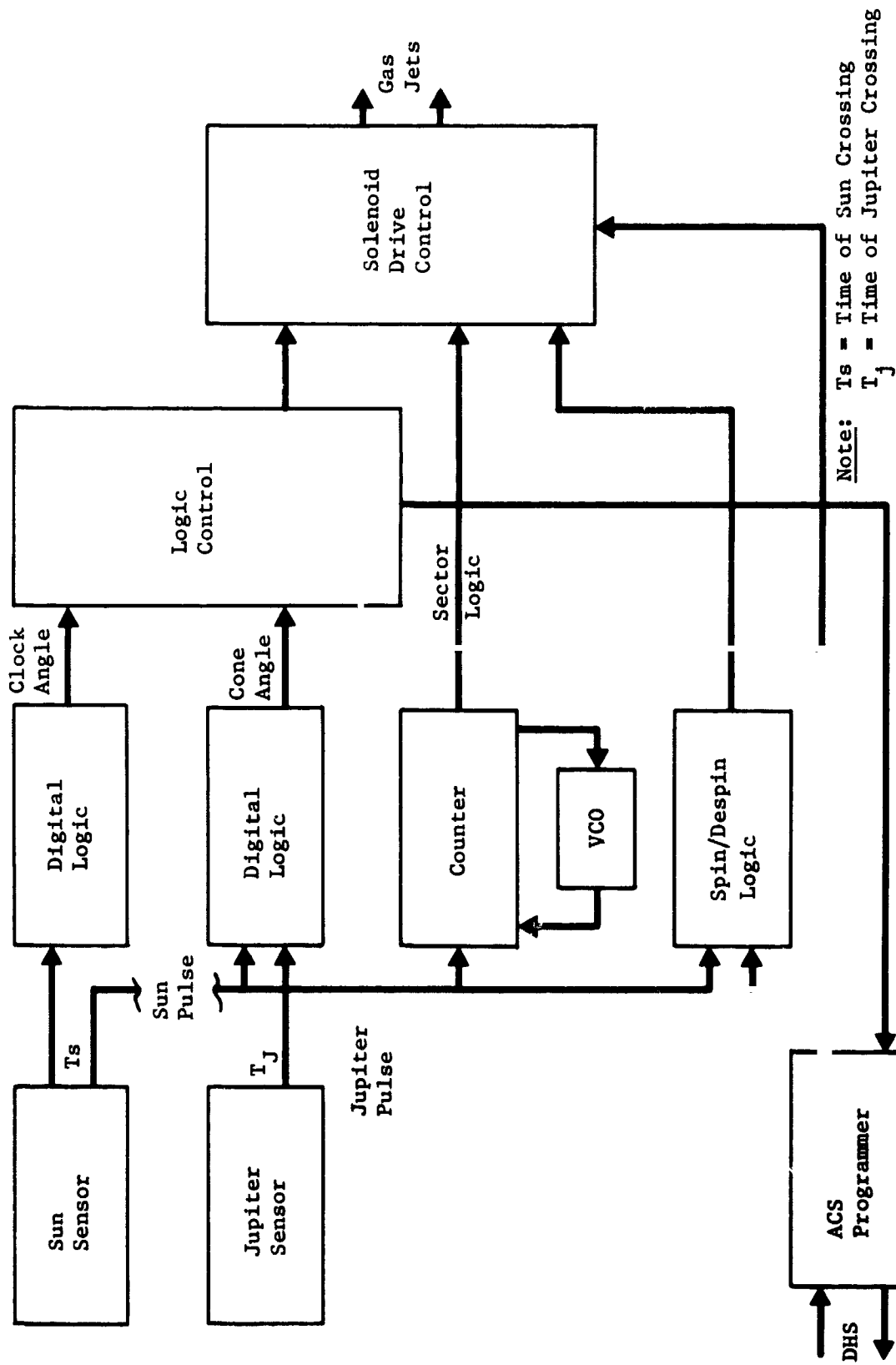


Figure V-20 ACS Block Diagram

Table V-7 Tolerance Summary

<u>Structural Tolerances (3<math>\sigma</math>)</u>	
Nozzle/flange, cm	0.0254
Flange, cm	0.0762
Mounting surface, deg	0.1
CG location, cm	0.038
Thrust vector, deg	0.1
Axial thrust offset (RSS), cm	0.144
Spin thrust offset (RSS), cm	0.102
<u>Probe Parameters</u>	
Spin rate, $W_s$	10 rad/sec (0.5 rad/sec Pioneer mission)
Spin torque, m	4.07 Newton-meters
Spin inertia, $I_s$	12.2 kg-m <sup>2</sup>
Thrust, F	810 Newtons
Thrust period, $t_F$	15 sec
Tipoff rate, $W_t$	0.5 deg/sec
Drift period, $t_D$	0.5 sec
$I_s/I_t - 1$	0.2
<u>Error Source</u>	
	<u>Error, deg</u>
(1) Tipoff error (at 0.5 rad/sec), $W_t I_t / W_s I_s$	0.8
(2) Drift error, $W_t t_D$	0.25
(3) Spinup (tipoff error) (P vector)	0.85
(4) Combined (2) & (3)	1.06
(5) Spinup (tipoff error) (nutation)	0.63
(6) Spinup (misalignment) (P vector)	0.125
(7) Spinup (misalignment) (nutation)	0.125
(8) Combined (5) & (7) (nutation)(RSS)	0.66
(9) Velocity dispersion (nutation)	0.014
(10) Velocity dispersion (misalignment)	0.905
(11) Velocity dispersion [combined (9) & (10)]	0.905
(12) Velocity dispersion [combined (11) & (4)] RSS	1.39
(13) Velocity dispersion [combined (11) & 0.5° ACS error] RSS	1.040

## 8. Structures Subsystem

*a. Structural Design* - The structural component configuration of the planetary probe is shown in Figure V-21. The major components are the entry probe body assembly, the descent probe, aft cover, service module, and the deflection motor assembly. The largest loads seen by the service module and the propulsion motor are those produced by the launch phase of space flight, and assumed to be approximately 10 g. The remainder of the probe structure undergoes the loads of planetary entry. These have been evaluated parametrically for entry into the atmosphere of the planet Jupiter. The results are shown in Figure V-22. It can be seen from this figure that the decelerating loads vary from approximately 450 g at low entry angles in the nominal atmosphere, to approximately 2250 g at 30° entry angle in the cool/dense atmosphere. Polar entry in the cool/dense atmosphere at a 42° entry angle (for comparison) results in a deceleration load of 3876 g. Corresponding values of dynamic pressure vary from approximately 7000 to 36,000 psf for the same entry conditions above, and 62,000 for polar entry.

*Aeroshell Structure* - The aeroshell structure (structure behind the heat shield) is designed by the aerodynamic pressure loads acting on this structure, while the remainder of the entry probe is designed by inertia loads imposed on the structure by the mass of the various components comprising the probe. The aeroshell is designed as a pressure vessel that resists an external (collapsing) pressure equal to the aerodynamic pressure acting normal to the surface of the aeroshell. Parametric analyses of the aeroshell have been performed to determine the weight of this structure as a function of aeroshell diameter and dynamic pressure. These parametric analyses have been performed for both aluminum and titanium construction materials and for both semi-monocoque and honeycomb-type construction. Results show that the lighter weights of aeroshell structure generally result from aluminum or titanium semi-monocoque construction for the pressure range of interest. Figures V-23 and V-24 present the results of these analyses for semi-monocoque construction. Using these curves, the dynamic pressure of the atmospheric entry must be converted to local pressure normal to the structure. To accomplish this conversion, it is practical to assume that the nose cone shape is a pointed cone of 60° half angle with attached shock wave. This assumption is only approximately correct, but gives essentially correct aeroshell weight data. For this 60° half angle cone configuration, the pressure coefficient,  $C_p$ , has a value of 1.38. Thus, the correct pressure to use to enter Figures V-23 and V-24 is determined by converting dynamic pressure from Figure V-22 (in psf) to pressure in psi and multiplying by 1.38.

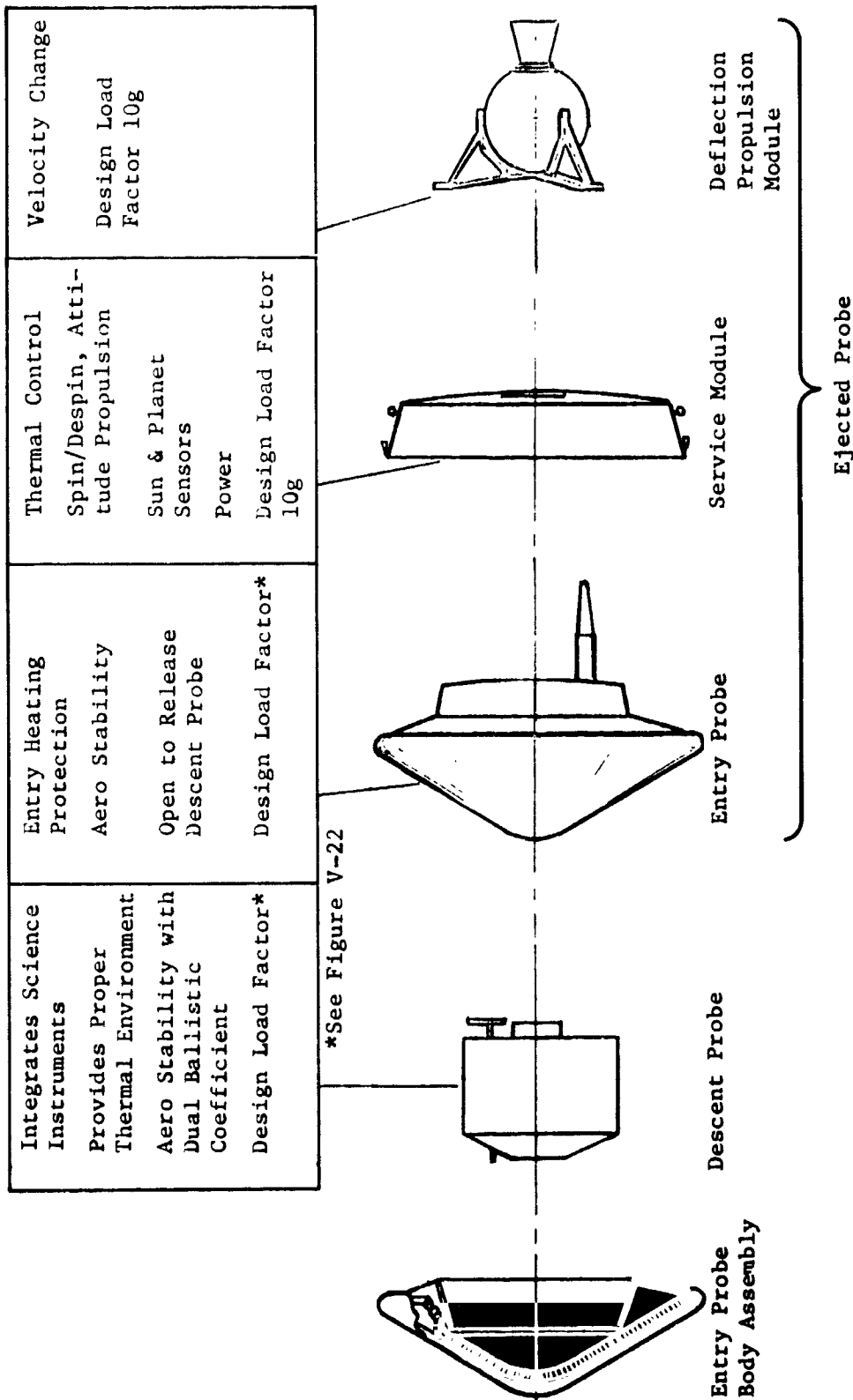


Figure V-21 Probe Major Assemblies

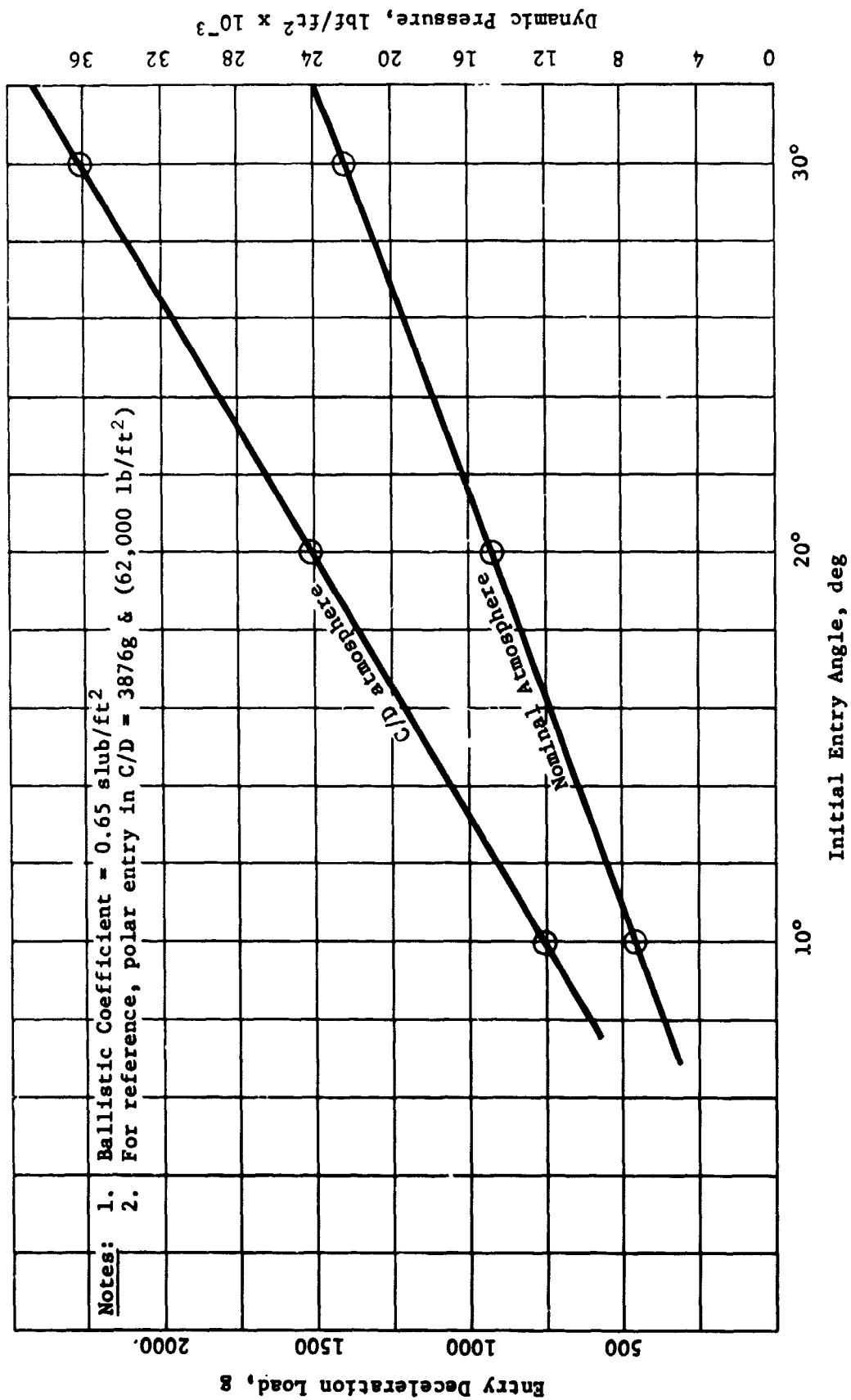


Figure V-22 Jupiter Entry Loads



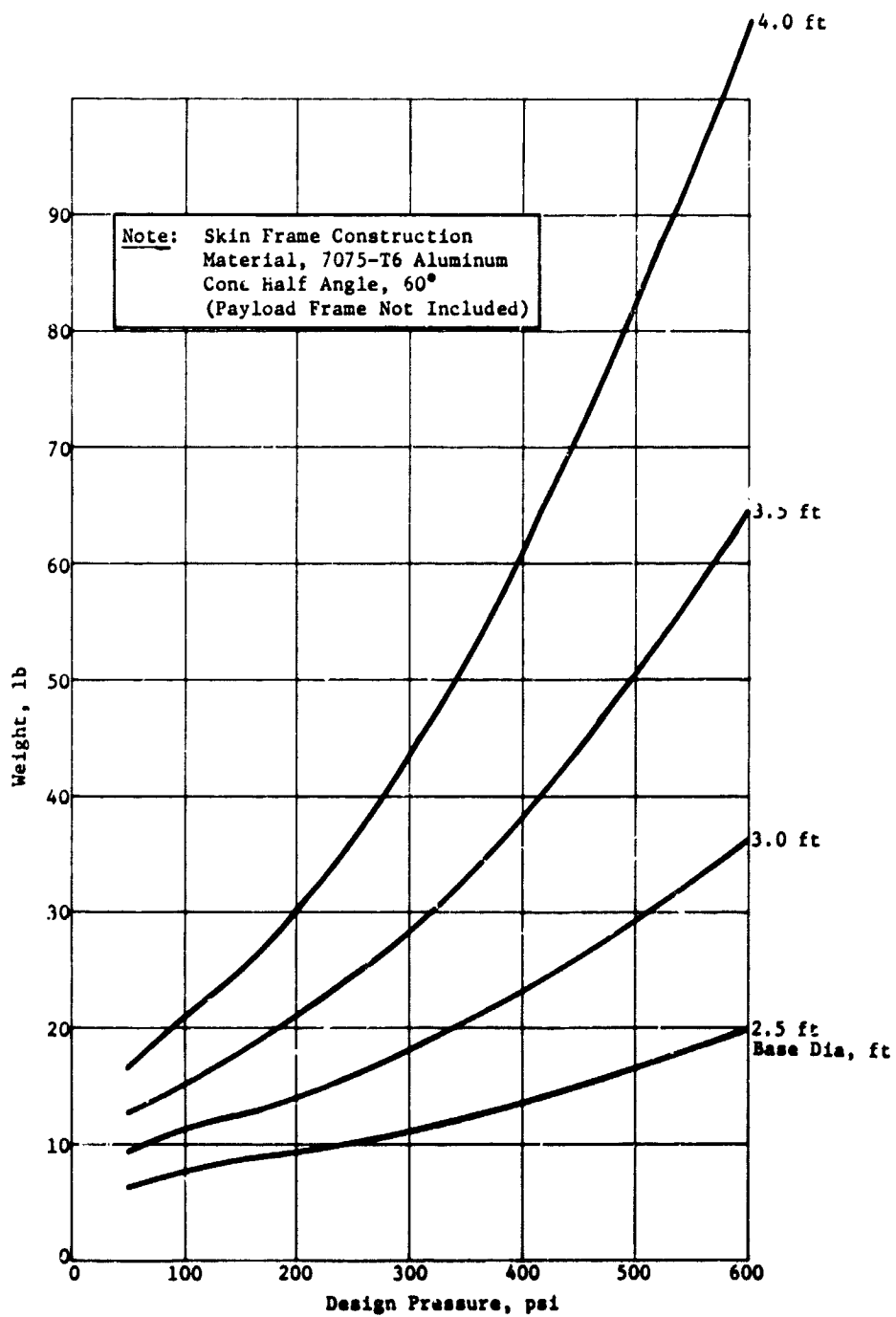


Figure V-23 Aeroshell Weights

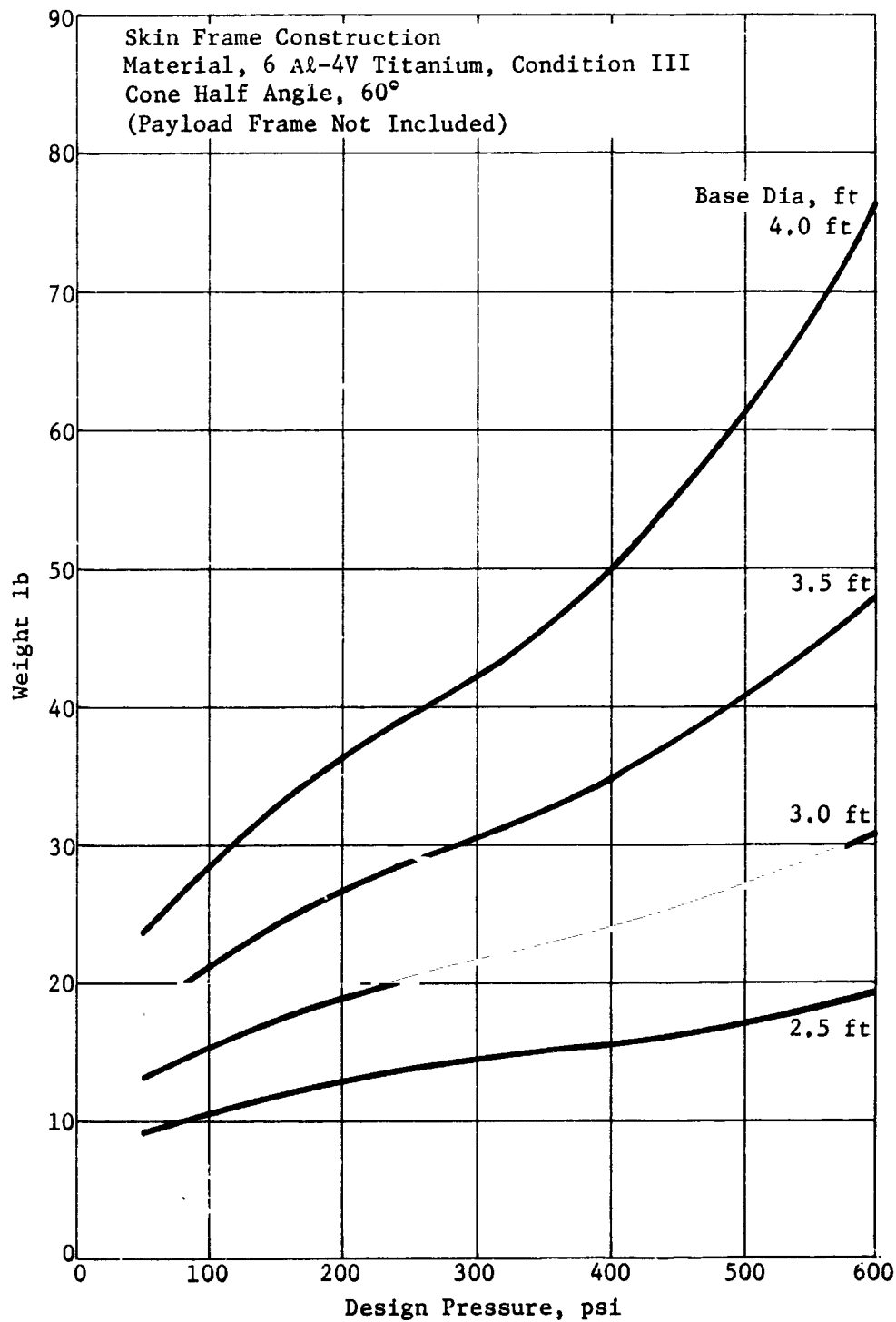


Figure V-24 Aeroshell Weights

The diameter of the aeroshell structure is determined through an iterative process. The proper diameter aeroshell can be derived directly from Figure V-25, once the mass of the entry body is known and the desired ballistic coefficient has been established. However, the iterative process involves assuming a weight for the aeroshell and for the heat shield (The remaining components are largely known.) and totaling the entry mass of the entry probe. From this estimated probe mass, the curves of aeroshell weight and heat shield weight can be entered repetitively to improve the mass estimates and establish the correct probe mass.

*Descent Probe Structure* - The descent probe structural weight is determined from the deceleration loads at entry. Figure V-26 and V-27 present the parametric weights data for the descent probe. In deriving these data, the descent probe diameter has been fixed at 18.5 in. Probe studies to date indicate that descent probe will not vary very much in size for the anticipated science component complement, and will typically lie in the range of 17.0 to 19.0 in. Thus, the descent probe structural weight is largely sensitive to planetary entry deceleration loads and to the mass of components mounted on the equipment platform, and not to size factors.

It should be noted that the descent probe equipment deck is supported at the aft end of the sidewall of the probe rather than at the forward end. This was done in order to distribute the deck load into the probe wall before transferring the load into the aeroshell and the heat shield. Since the heat shield material (graphite) is a relatively brittle material, it is desired to load the heat shield as uniformly as possible such as not to cause cracking. Future analyses may show that the problem is not severe, and if so, weight may be saved in the descent probe shell by locating the equipment deck near the forward end of the descent probe.

The descent probe weight curves are based on the use of 7075-T6 aluminum alloy throughout, with a factor of safety of 1.5. The sidewalls of the descent probe is based on the use of 10 longerons, evenly spaced around. The remainder of the probe is monocoque.

*Base Cover Structure* - The weight of the aft cover for the aeroshell, like the descent probe, is a function of the inertia loading encountered during planetary entry. The aft cover is designed as four separate pieces capable of hinging open after completion of entry, and as such does not have complete circumferential structural continuity. The weight of the aft cover is shown parametrically in Figure V-28 for various entry decelerations. This analysis, like that for the descent probe, is based on the use of 7075-T6 aluminum alloy, and a factor of safety of 1.5.

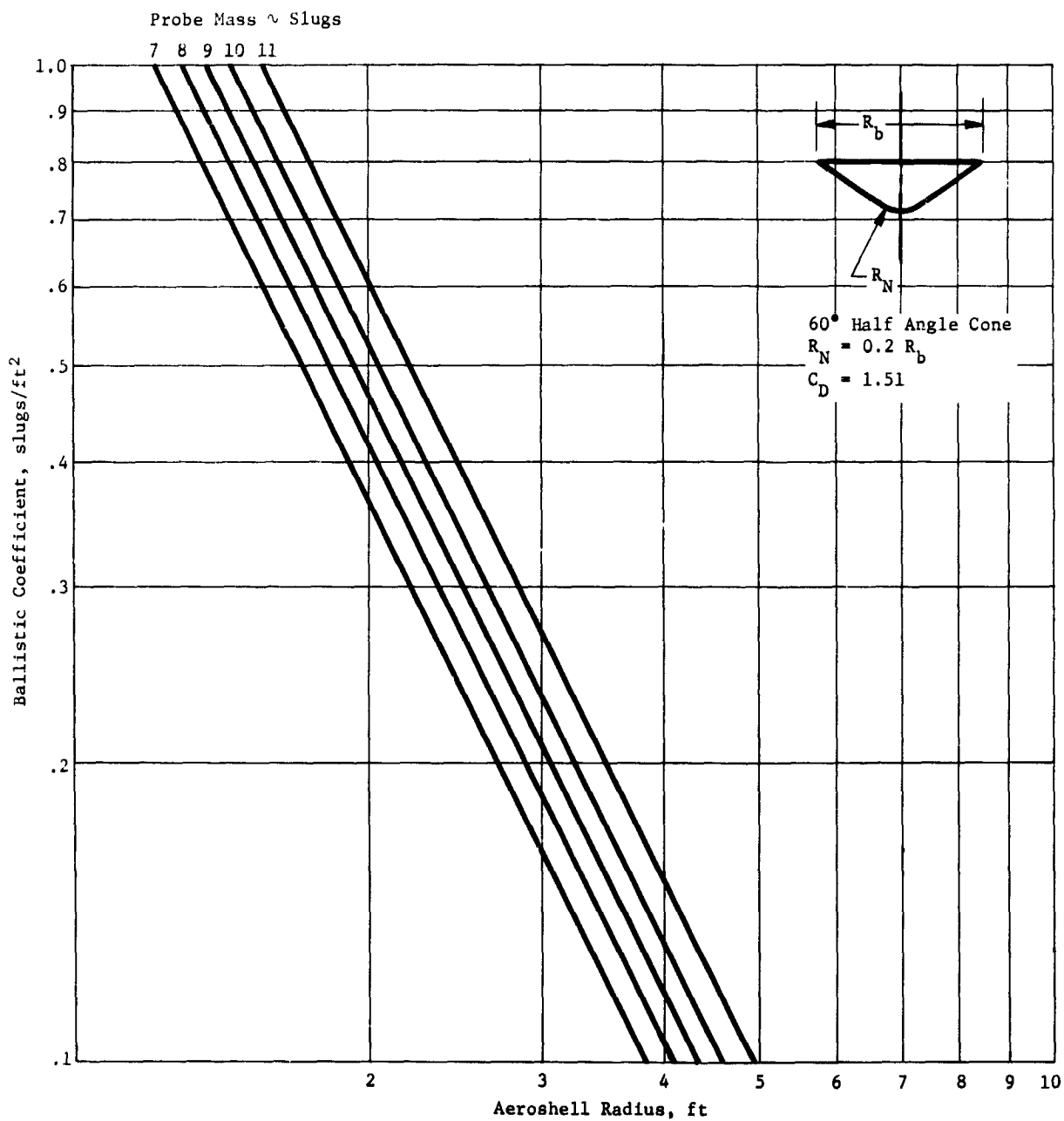


Figure V-25 Hypersonic Ballistic Coefficient vs Aeroshell Radius

\*7075-T6 Alum. Alloy, Factor of Safety = 1.5

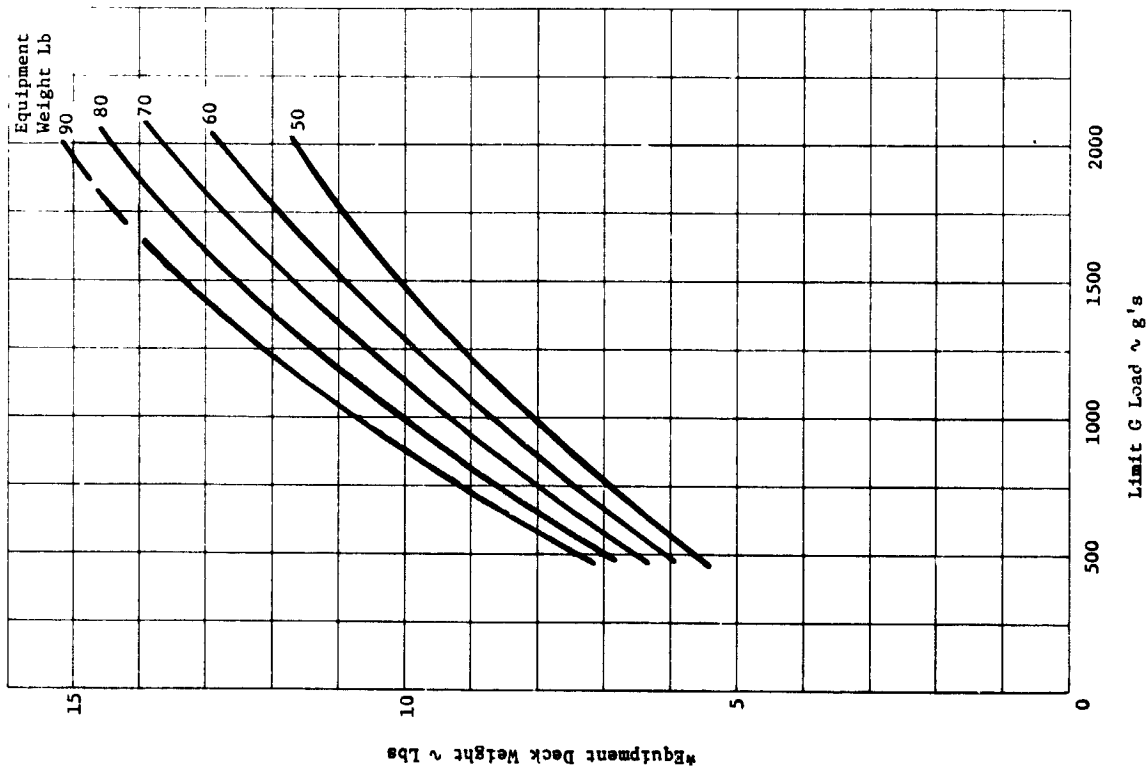


Figure V-26 Equipment Deck Weight vs Planetary Entry Deceleration

\*7075-T6 Alum. Alloy, Factor of Safety = 1.5

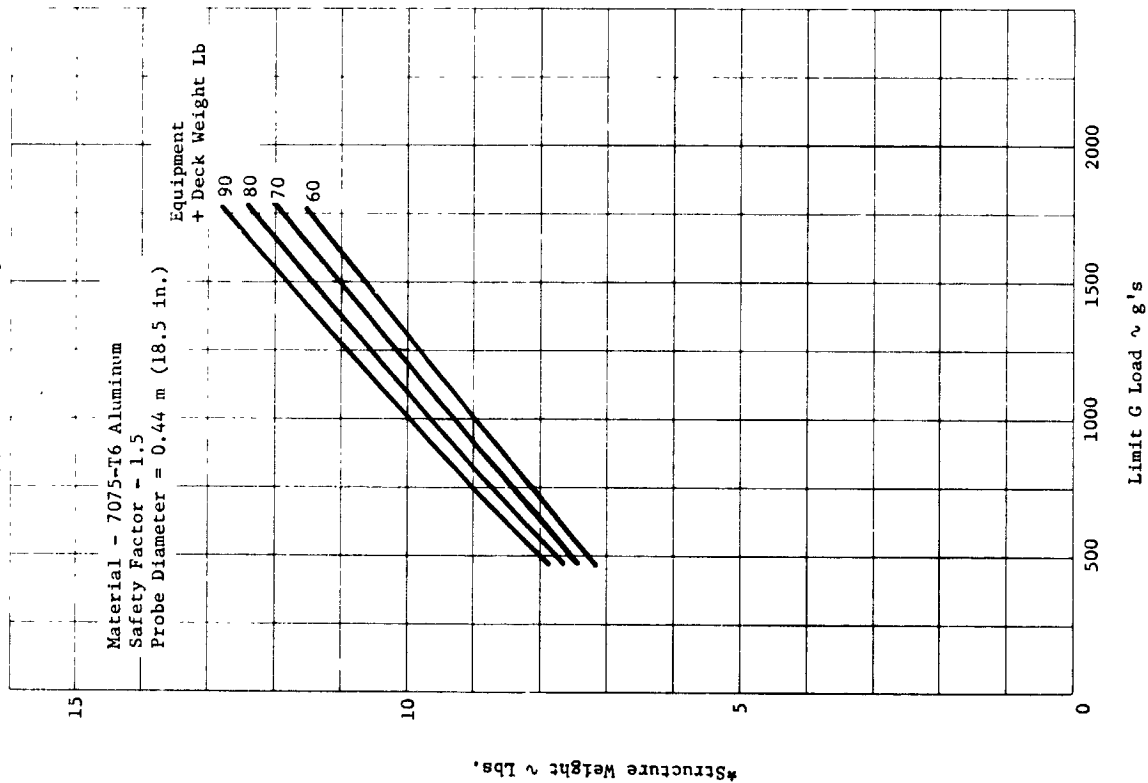


Figure V-27 Descent Probe Outer Structure Weight vs Planetary Entry Deceleration

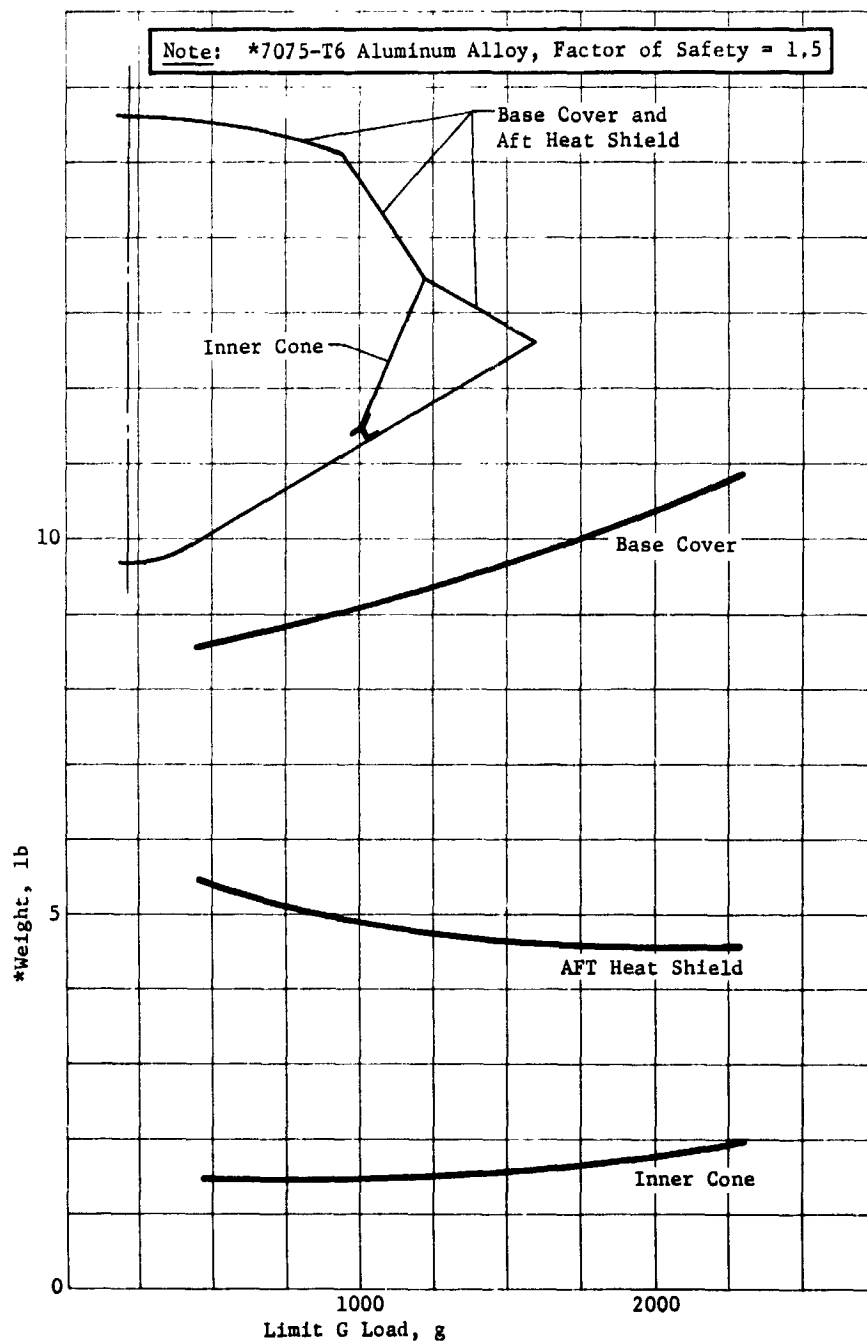


Figure V-28 Base Cover Weight vs Entry Deceleration

*v. Paracnute Aerodecelerator Subsystem* - A parachute decelerator system provides the desired descent ballistic coefficient for the desired descent rate of the probe through the atmosphere. The parachute also provides the necessary separation force to remove the descent probe from the aeroshell after completion of the planetary entry phase. The required parachute designs have been evaluated parametrically to facilitate selection of a parachute decelerator configuration for the descent probes. Figures V-29 thru V-32 present the results of the study. Figures V-29 and V-30 are for relatively large paracnutes providing ballistic coefficients of the order of 7.8 to 31.4 kg/m<sup>2</sup> (0.05 to 0.2 slug per ft<sup>2</sup>). These parachute diameters are large compared to the size of the descent probe body; therefore the drag of the probe body itself, as it contributes to ballistic coefficient, has been ignored. The performance for this decelerator has been based on a disc-gap-band type parachute, and the weights data presented includes the complete system. For purposes of configuration design, the packaging density of the complete parachute is assumed to be approximately 560 kg/m<sup>3</sup> (35 lb/ft<sup>3</sup>). The mortar tube length-to-diameter ratio is approximately 1.25.

The smaller secondary parachute decelerator data of Figures V-31 and V-32 are presented for the case where a two-stage parachute descent system is desired, with a higher ballistic coefficient for the second parachute stage. It is also suitable for a single-stage descent using a higher ballistic coefficient. For the generation of data for these figures, the drag of the descent probe body itself is a high enough contributor to the ballistic coefficient that it cannot be ignored. It is therefore included in the calculations. It should be noted that the data is useful for the secondary parachute selection only for a descent probe diameter of approximately 0.43 to 0.48 m (17 to 18 in.); however, unless the scientific instrument complement for the descent probe is changed, the descent probe is typically about that size. Also, the minimum parachute diameter to be selected is somewhere in the vicinity of 0.27 m (0.90 ft) as this is the (somewhat arbitrary) stability limit.

To determine the parachute size for either parachute, the desired descent probe ballistic coefficient and the descent probe mass are entered on Figures V-29 and V-31. The parachute size is read from the figures directly. Having selected the parachute size, the parachute weight is derived from Figure V-30 or V-32 as applicable.

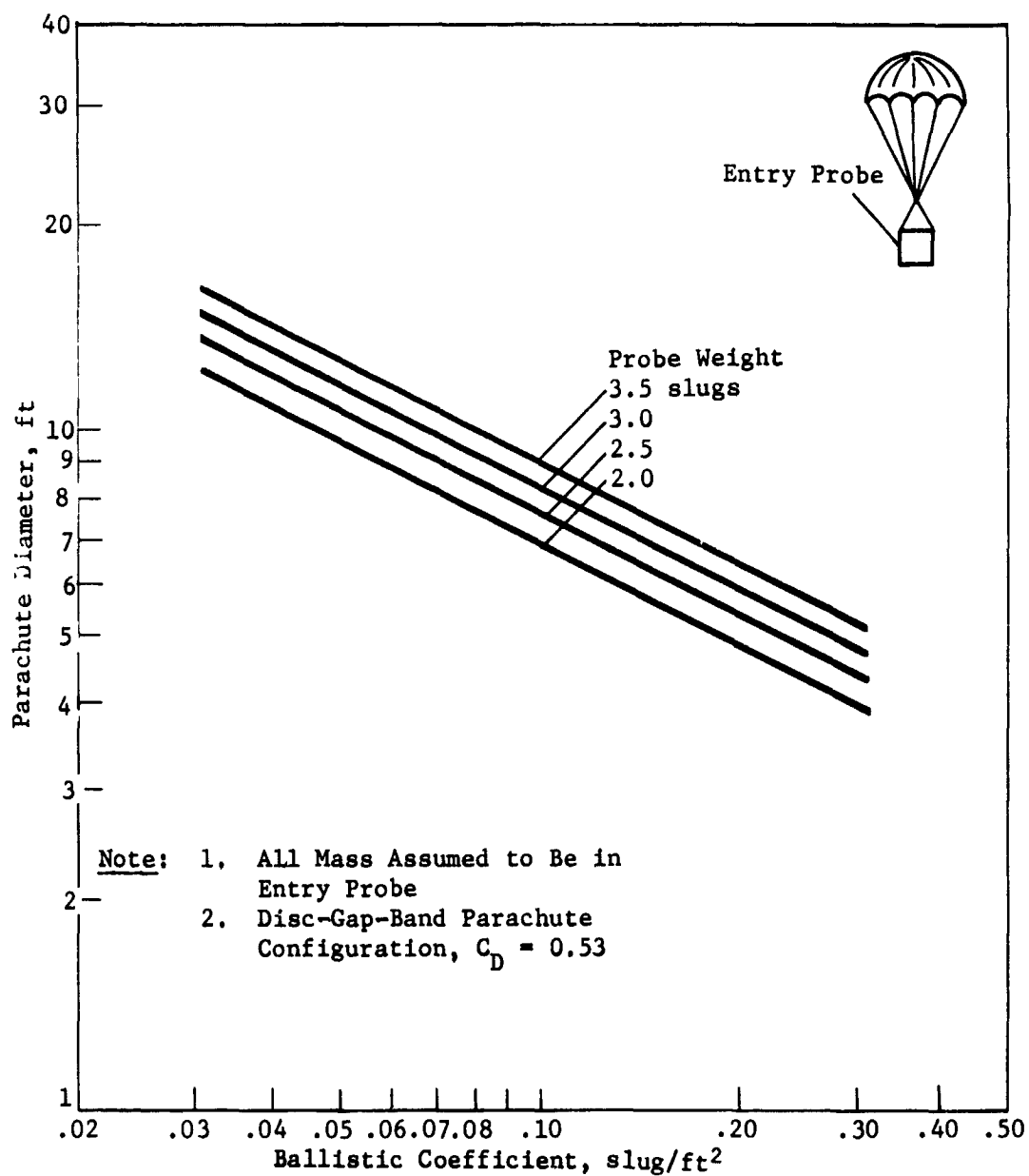


Figure V-29 Main Parachute Diameter vs Ballistic Coefficient



Deployment  $q = 75 \text{ lb/ft}^2$ , No Reefing

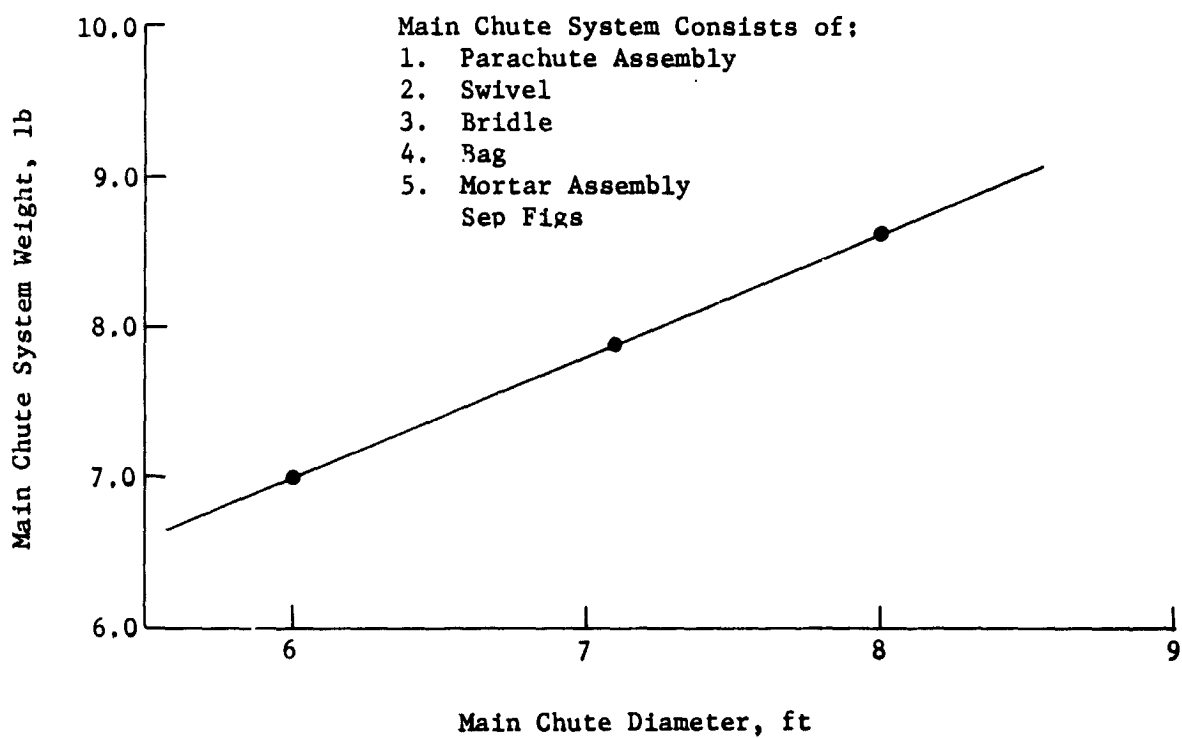


Figure V-30 Main Parachute Weight vs Diameter

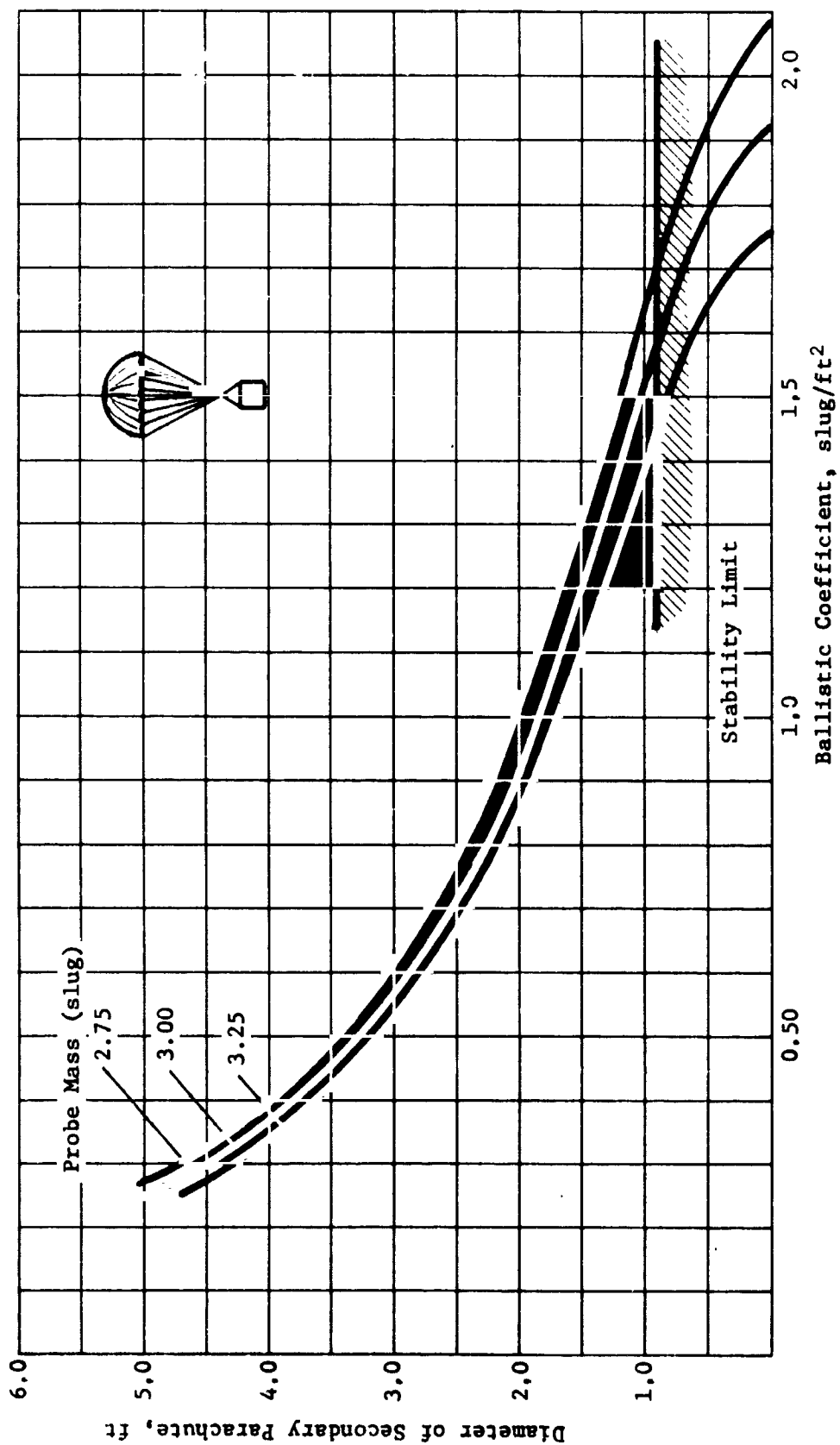


Figure V-31 Secondary Parachute Diameter vs Ballistic Coefficient

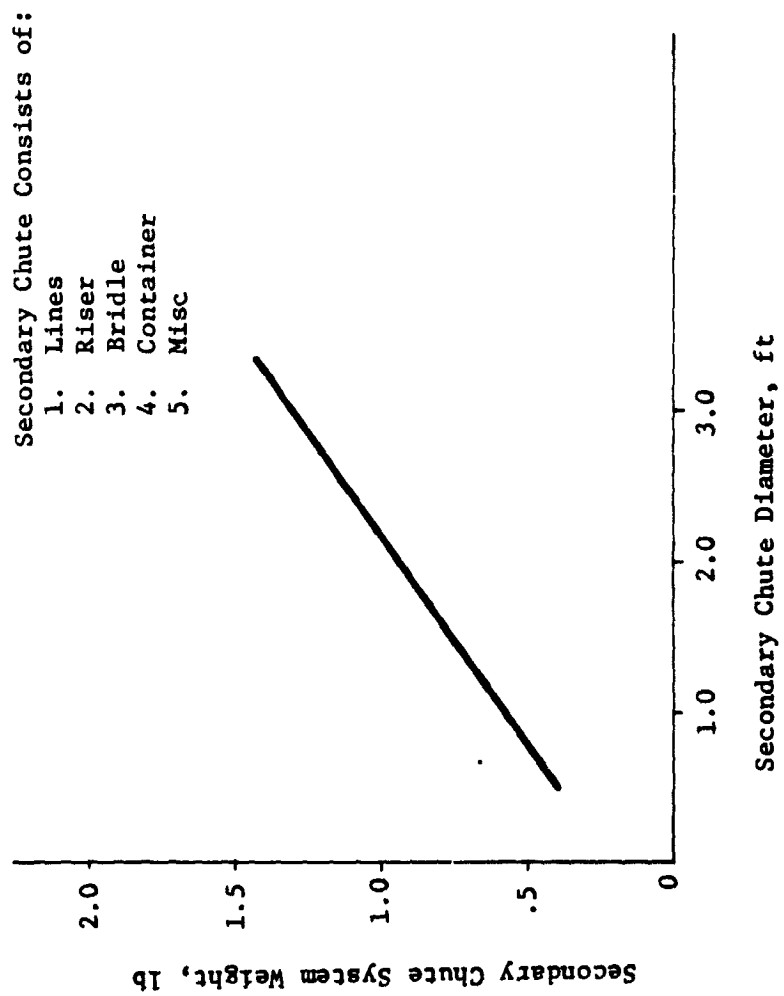


Figure V-32 Secondary Parachute Weight vs Diameter

In the interest of evaluating parachute deployment effects, a parachute deployment sensitivity study was performed. The results of this study are shown in Figures V-33 and V-34. Figure V-33 evaluates the planetary atmospheric pressure at parachute opening versus entry ballistic coefficient and entry angle, assuming the parachute deploys upon decelerating to Mach 0.7. It can be seen that the pressure varies over a pressure range of 50 to 150 millibars over the range of parameters of interest. Figure V-34 investigates the currently proposed method of deploying the parachute using a g-switch and a timer. It is assumed that the planned entry angle is  $20^\circ$  with a potential dispersion of  $\pm 5^\circ$ . It is also assumed that the parachute deployment timer is triggered by an accelerometer as entry deceleration builds up to a value of 100 g, and the parachute is deployed 31.5 seconds later. The resulting variation in atmospheric pressure at parachute deployment is shown in Figure V-34 for the considered dispersions in entry angle and atmosphere. The point values indicated on the figure for Mach number and dynamic pressure are only approximate, as these are interpolated values from machine program runs. It can be seen that the pressure at deployment varies from approximately 50 to 150 millibars.

c. *Heat Shield Evaluation* - The nose cone heat shield analyses performed for this study were based on the results of previous studies\*† which showed entry heating pulses peaking for Jupiter atmospheric entry at approximately  $90 \text{ kw/cm}^2$  for a  $90^\circ$  entry angle, and decreasing downward with decreasing entry angles to approximately  $20 \text{ kw/cm}^2$  for the proposed  $20^\circ$  entry angle. The heat shield protection against this heating for Jupiter planetary entry probes is shown in Figures V-35 thru V-37. Figure V-35 represents the basic data for heat shield protection based on a probe having a nose cone base diameter of 1.6 meters (5.25 ft). This figure presents the mass fraction of the combined heat shield ablator and backface insulation as related to the total mass of the entry body. Also shown is the mass fraction of ablator lost (dotted curves) at entry. Figures V-36 and V-37 present adjustment data to correct the data from Figure V-35 for different size probes and for different entry conditions. To determine the mass fraction of the heat shield, the desired entry ballistic coefficient and initial entry angle are entered on Figure V-35. This mass fraction includes the ablator lost at entry, residual ablator, and the low density carbonaceous thermal insulator between the heat shield and the supporting structure. For the selected point design of a probe, the reference mass fraction is corrected by multipliers selected from Figures V-36 and V-37.

---

\*M. E. Tauber: *Heat Protection for Atmospheric Entry into Saturn, Uranus, and Neptune*. Preprint No. AAS-71-145, 17th Annual AAS Meeting, June 28-30, 1971.

†M. E. Tauber and R. M. Wakefield: *Forebody Heat Shield Weight Estimate for Jupiter Entry Supplement*. JPL Section Document 131-12-S1, July 15, 1970.

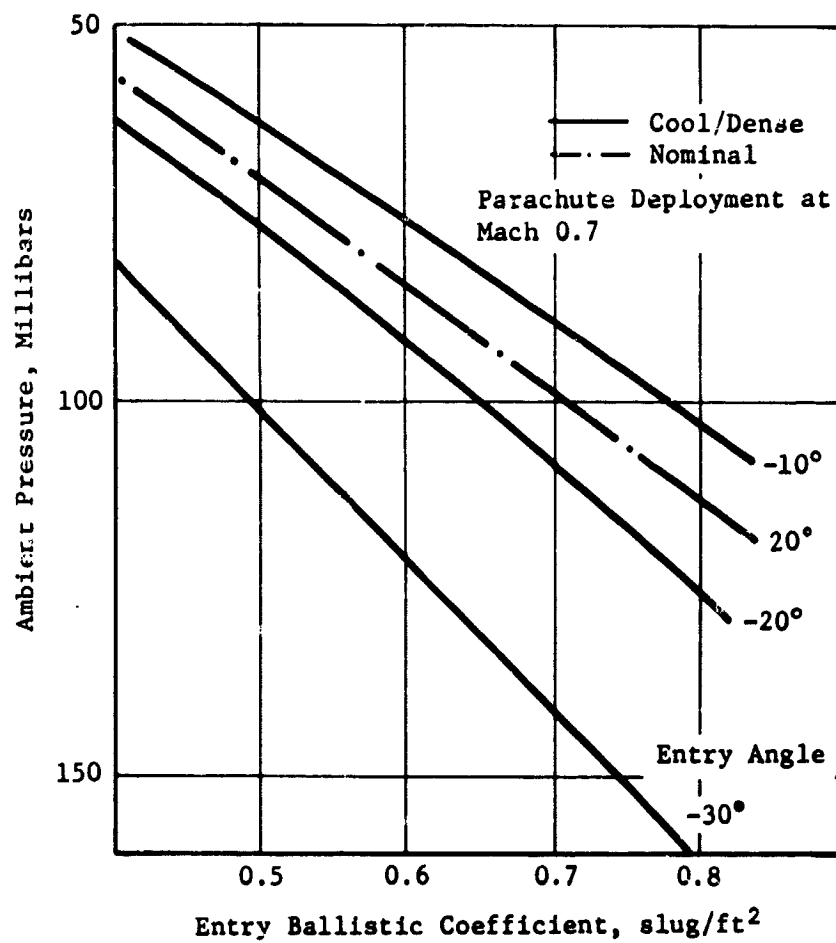


Figure V-33 Atmospheric Pressure Variations for Parachute Deployment

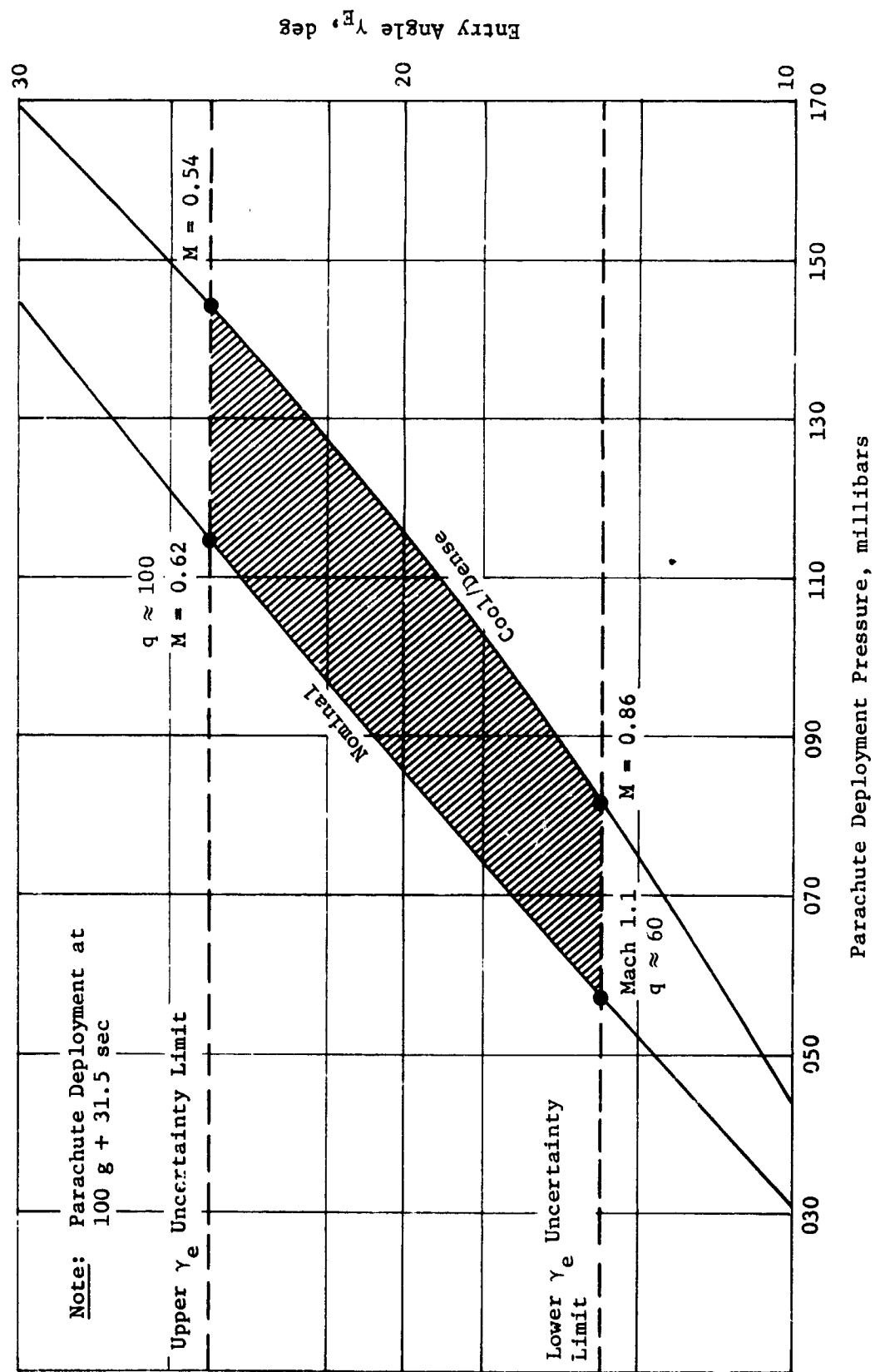


Figure V-34 Parachute Deployment Dispersions

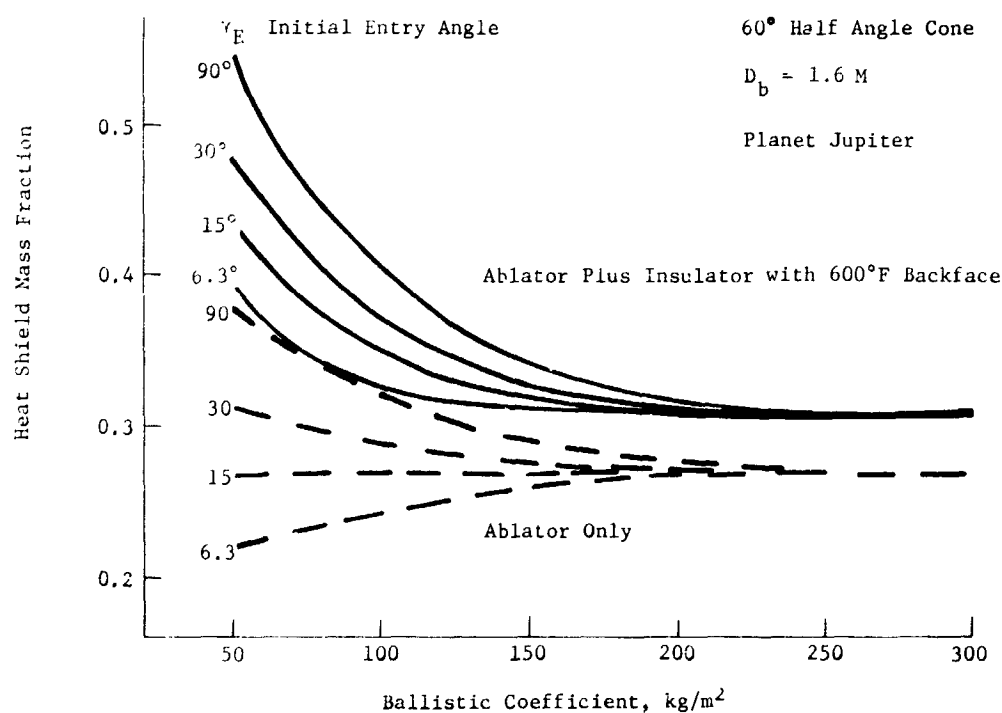


Figure V-35 Heat Shield Mass Fraction vs Ballistic Coefficient and Initial Entry Angle

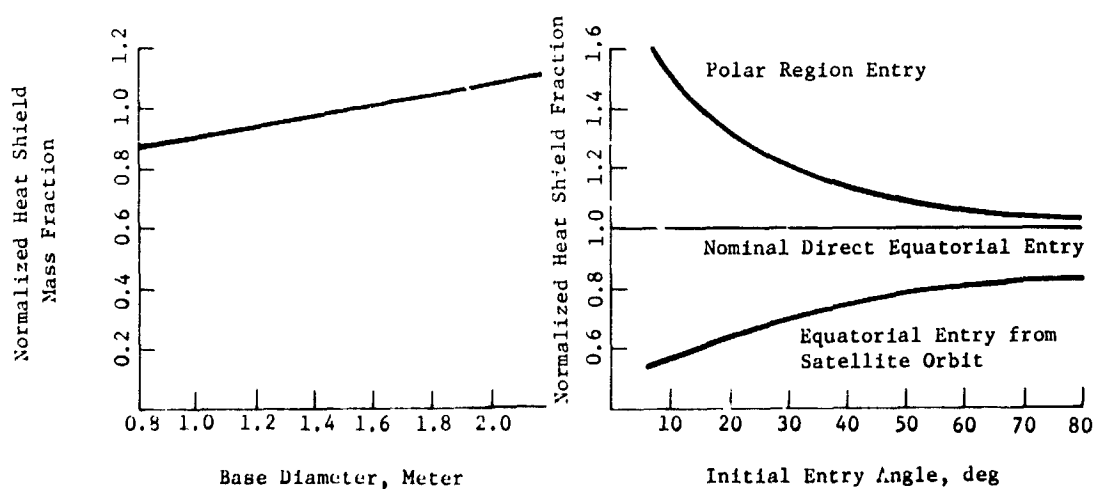


Figure V-36 Size Adjustment Factor

Figure V-37 Adjustment Factor for Entry Latitude and Entry from Orbit

The base heating protection for the Jupiter entry probe is based on an estimate of base heating flux of 2% of the peak forebody heating. This value is based on preliminary data developed by J. D. Stephenson.\*

The Jovian entry analyses done by Stevenson actually indicate a base heating of less than 1.65%, so the 2% value may possibly be conservative. Although heating will vary across the base, it is felt that for this study, an assumption of uniform heating will result in a reasonable weight estimate.

Table V-8 presents a summary of probe base area peak heating rate, total heating and time of heating pulse assuming a triangularly shaped entry heating pulse.

Table V-8 Jovian Entry Probe Base Heating

Planet	$\gamma_E$	Peak Heating Rate, Btu/ft <sup>2</sup> -sec	Total Heat, Btu/ft <sup>2</sup>	Time of Heating Pulse, sec
Jupiter	-60			
	-30	615	1700	5.5
	-20	412	1620	7.9
	-10	210	1550	14.7

Base heating rates and total integrated heating for Jupiter are obtained from M. G. Tauber and R. M. Wakefield.† The Jovian entry heating time history for a -15° entry is shown in Figure B-1a. The total integrated heating for this entry is 90 kw sec/cm<sup>2</sup> 2% of this is 1.8 kw sec/cm<sup>2</sup> or 1585 Btu/ft<sup>2</sup>. This heating is ratioed for other entry angles based upon a ballistic coefficient of 100 kg/m<sup>2</sup> from Figure B-6. Peak heating rates are taken from Figure B-2a at the 100 kg mass cone flank heating curve.

\*J. D. Stephenson: *Radiative and Convective Heating Predictions for the Afterbody Regions of a Jovian Entry Probe*. Symposium on Hypervelocity Radiating Flow Fields for Planetary Entries, Jet Propulsion Laboratory, January 14-15, 1972.

†M. E. Tauber and R. M. Wakefield: *Forebody Heat Shield Weight Estimate for Jupiter Entry Supplement*. JPL Section Document 131-12-S1, July 15, 1970.



The heating in the base region will require ablative protection in all cases for reasonable afterbody unit weights. For example, a 0.050-in. aluminum smear thickness would increase in temperature 700°R in the mildest environment (-10° Uranus entry).

A group of ablators and their pertinent properties are summarized in Table V-6. A formula for making preliminary estimates of ablator weight is

$$\frac{W}{A} = \left( \frac{\psi \beta}{0.214 \psi + T} \right)^{\frac{1}{2}}$$

(Ref) MDAC Report F-738 *Advanced Logistics Spacecraft System*. Vol 5, October 1967

where:

$$\frac{W}{A} = \text{weight/unit area, lb/ft}^2$$

$$\psi = \left( \frac{Q}{\theta \sigma \epsilon} \right)^{\frac{1}{4}}$$

$$\beta = 2.42 \frac{K P \theta}{C_P}$$

T = backface temperature limit, °R

K = conductivity, Btu/ft-sec °R

P = density, lb/ft<sup>3</sup>

θ = heating period - sec = 2 Q/ḡ

C<sub>P</sub> = specific heat Btu/lb °R

σ = Stephen Boltzmann constant = 0.48 x 10<sup>-12</sup> Btu/ft<sup>2</sup> sec (°R)<sup>4</sup>

ḡ = peak heating rate, Btu/ft<sup>2</sup> sec

Q = total heat Btu/ft<sup>2</sup>

Table V-9 Ablator Materials Considered and Properties

Ablator Material	Density, lb/ft <sup>3</sup>	Limit Btu/ft <sup>2</sup> -sec	Virgin K Btu/ft-sec °R	Emissivity	Specific Heat Btu/lb °R
Carbon Phenolic	90	None	$100 \times 10^{-6}$	0.9	0.35
ESA 5500 M3	70	None	$36 \times 10^{-6}$	0.9	0.3
ESA 3560	30	100	$18 \times 10^{-6}$	0.8	0.3
SLA 561	15	50	$7.2 \times 10^{-6}$	0.8	0.3
Quartz Phenolic	110	None	$60 \times 10^{-6}$	0.8	0.27

Table V-10 presents the weight/unit area to protect an aluminum base structure to 760°R (300°F) with all applicable ablators.

Table V-10 Unit Weight of Ablator Required to Protect Base Cover Structure to 300°F Maximum during Planetary Entry

Planet	$\gamma_E$	Ablator Required, lb/ft <sup>2</sup>				
		Carbon Phenolic	ESA 5500-MB	ESA 3560	SLA 561	Quartz Phenolic
Jupiter	-30	1.01	0.55			0.95
	-20	1.18	0.65			1.12
	-10	1.56	0.86			1.47

#### 9. Propulsion Subsystem

Studies were made of the probe propulsion subsystem requirements to accomplish the mission pre-entry deflection (delta velocity) maneuver and probe attitude control. The three potential mission deflection maneuvers under consideration were (1) probe deflection, (2) spacecraft deflection, and (3) shared deflection.

In the probe deflection mode, the spacecraft points the probe in the proper direction for the deflection maneuver and the probe provides spin attitude stabilization and the deflection delta velocity required for planetary entry. The probe then processes to a new attitude for planetary entry. The spacecraft deflection mode requires that the spacecraft perform the entire probe entry requirements. In this case, the spacecraft is initially on a planetary entry course. The spacecraft points the probe in the proper attitude for entry, separates from the probe, and then flies away to its new flyby trajectory. The probe merely spins itself for attitude stabilization in the initial-separation pointed direction. The shared deflection is a mode in which the spacecraft points the probe to an orientation that is common for both the deflection velocity vector and planetary entry by the probe. The spacecraft provides a deflection velocity of its own after separation. Thus, for both the probe deflect mode and for the shared deflect mode, the probe must provide both probe deflection delta velocity and probe attitude control. In both of these cases, the probe attitude control system must provide a probe spinup velocity of approximately 10.5 rad/sec (100 rpm) before ignition of the deflection motor, and then a despin to approximately 0.52 rad/sec (5 rpm). Additionally, for the probe deflect case, the probe must provide a precession maneuver, before despin, to position the probe for entry. For the spacecraft deflect mode, the probe merely provides spinup to 5 rpm after separation from the spacecraft.

The propulsion subsystem candidates considered for the probe design include monopropellant (hydrazine), bipropellant, cold gas, and solid propellant type systems. These candidates were traded off against each other and the selections finally made were a solid rocket motor to provide the probe  $\Delta V$ , and a  $\text{GN}_2$  cold gas system to provide the relatively-small auxiliary-propulsion requirements. A monopropellant hydrazine system employing catalytic thrusters both for  $\Delta V$  and the auxiliary propulsion functions was found to be a worthy competitor, but it is significantly heavier than the solid/cold gas combination. The selected system is applicable regardless of whether the deflection mode is by probe deflect or by shared deflect mode. For the spacecraft deflect mode, the probe need have only a simple spin system to spin the probe for entry; a cold gas system suffices nicely for this task. The following sections present the general rationale which led to the foregoing selections, and the pertinent supporting analyses.

a. *System Weight* - One of the major factors influencing the selection of the type of propulsion system to be used is the system weight, which is particularly critical for the Jupiter probe because the proposed launch vehicle is marginal for this mission. If weights are not held to an absolute minimum, the mission simply can not be performed without going to a larger, more expensive launch vehicle.

The probe  $\Delta V$  maneuver and the auxiliary propulsion functions place entirely different requirements on the probe propulsion system. Therefore, these were studied somewhat independently, and are discussed separately in the following paragraphs.

b.  *$\Delta V$  Propulsion* - Through a series of probe analysis/design iterations, the requirement eventually evolved for a probe weighing approximately 330 lbm at separation from the mother spacecraft, and requiring a  $\Delta V$  of approximately 220 m/sec for optimum Jupiter entry. A first cut approximation of the total impulse required for this maneuver may be obtained directly from Newton's first law by ignoring the decreasing spacecraft mass during the  $\Delta V$  burn, i.e.,

$$I_t \approx \frac{W}{g} \Delta V = 33,000 \text{ N sec. (7420 lbf sec.)}$$

Actually, the required total impulse will be somewhat less than this value, but this is sufficiently accurate to provide the basis for selecting the general type of propulsion system best suited for this maneuver. For the solid, cold gas, and liquid propellant systems considered, all are equally capable of providing the probe  $\Delta V$  requirements ( $I_t \sim 7400 \text{ lbf sec}$ ). All three types of systems

can be easily designed to provide any thrust level/burn-time relationship that might be required. The probe deflection maneuver does not place particularly stringent constraints on the thrust level/burn time of the propulsion system. An exceedingly high thrust might be undesirable because of the resultant high g-load imposed on the probe, and the possibility of greater trajectory errors caused by thrust misalignment, but the thrust requirement is really not particularly restrictive. Likewise, an extremely low thrust level conceivably could lead to burn times too long to be accommodated within the mission time lines, but again, this is not a real restriction. Therefore, considering only the fundamental propulsion output characteristics, such as thrust, burn time and delivered impulse, no particular advantage (or disadvantage) is evident for one type of system versus another. However, when the propulsion system specific impulse is taken into consideration, and the system weights are brought into focus, the preferred systems quickly become self-evident.

The two principal factors influencing propulsion system weight are the specific impulse,  $I_{sp}$ , attainable with the selected propellant (which directly affects the propellant weight), and the system inert weight (also a function of the type of propellant selected). In a detailed weights analysis, the system inert weight is estimated from a preliminary design of the entire system, but for the gross analysis being performed here, sufficient accuracy is obtained by employing a mass ratio  $\lambda$  (ratio of propellant weight to total system weight) that has been found to be typical for the selected propellant.

c. *Solid Propellant Motor* - A cursory review of state-of-the-art solid rocket motors reveals that an  $I_{sp}$  of (2814 Nsec/kg) (287 sec) is readily achievable with composite propellants that contain moderate percentages of powdered aluminum. Several different rocket motor manufacturers produce propellants having this level of performance. For the probe  $\Delta V$  maneuver requiring  $I_t$  approximately (33,000 Nsec) (7400 lb-sec), the total quantity of propellant required at this  $I_{sp}$  is  $\sim 11.8$  kg (26 lbm).

To provide a reasonably accurate estimate of the solid motor inert weight, data obtained from several different manufacturers were plotted as shown in Figure V-38. A conservative estimate of the mass fraction as a function of motor size is provided by the heavy dashed curve (a compromise between the data provided by Hercules and the mass fractions achieved in motors recently fabricated by Thiokol). From the plot, it is evident that a motor containing (11.8 kg) (26 lbm) propellant should have a mass fraction of approximately 0.8, and therefore would weigh approximately (14.7 kg) (32.5 lbm) loaded.

d. *Liquid Propellant System* - Presumably, either a bipropellant system or a monopropellant system can be easily designed to satisfy the Jupiter probe propulsion requirements. An earth storable bipropellant system can provide a specific impulse slightly higher than that of the solid propellant motor, but it will have a somewhat lower mass fraction (higher total weight) as shown in Figure V-38. Since it will be somewhat more complex (less reliable) and does not offer a weight advantage over the solid motor, it really is not a serious contender for this application.

The monopropellant hydrazine system cannot compete successfully with the solid propellant motor strictly on the basis of weight (both its  $I_{sp}$  and mass fraction are lower), but it is a contender because it offers other advantages. Also, by combining the  $\Delta V$  propulsion requirements and the auxiliary propulsion requirements into a single integrated system, some weight advantages do accrue.

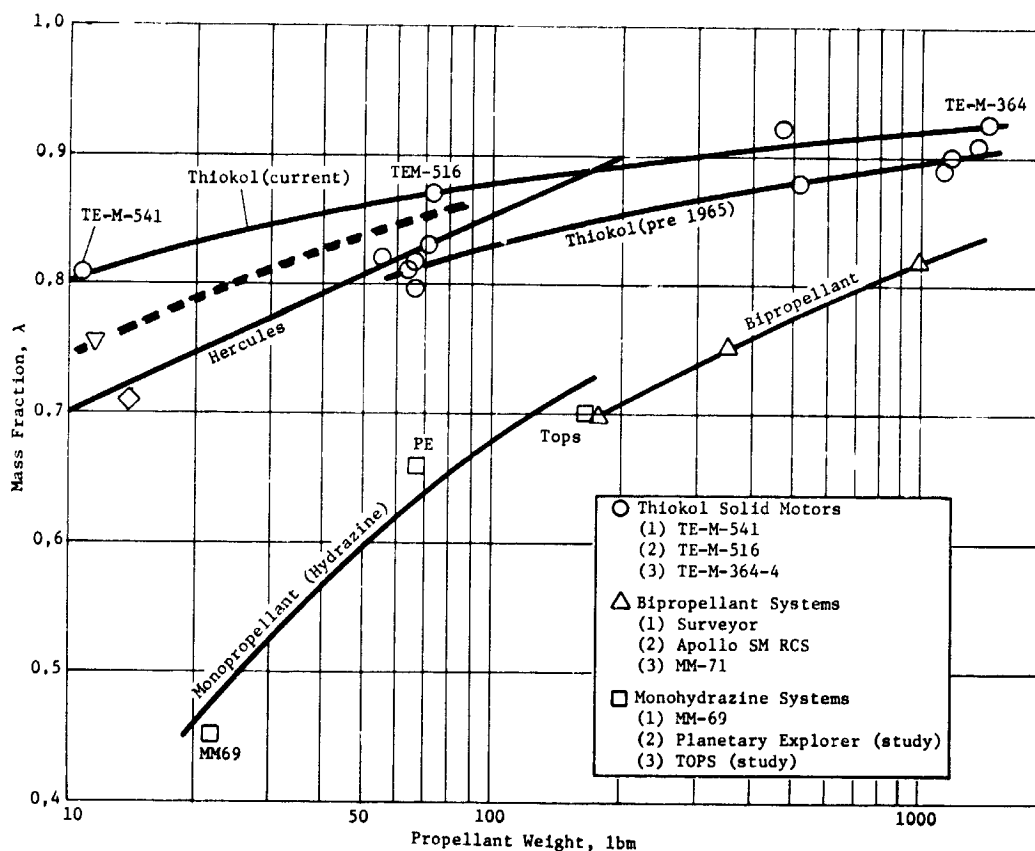


Figure V-38 Solid Rocket Motors/Monopropellant Hydrazine Systems

Monopropellant hydrazine catalytic thrusters consistently provide an  $I_{sp}$  of  $\sim 2260$  Nsec/kg (230 sec), resulting in a required propellant weight of  $\sim 14.5$  kg (32 lbm) (nearly the same as the total system weight for the solid motor). Mass fraction of the hydrazine system probably cannot be estimated as accurately as that for the solid motor because of the many variations in system redundancy provisions and other detailed features, but the mass fraction curve presented in Figure V-38 provides a basis for an initial estimation. This curve is based on actual mass fractions achieved in one existing system (MM69), plus designs developed for two system studies (TOPS and Planetary Explorer). It should be noted, however, that the  $\lambda$  shown actually applies to an integrated  $\Delta V$ /ACS system, rather than a  $\Delta V$  system alone. For a 14.5 kg (32 lbm) propellant load,  $\lambda$  is estimated to be  $\sim 0.53$ , leading to a total system weight of  $\sim 27.1$  kg (60 lbm).

*e. Cold Gas System* - Very little analysis is required to show a cold gas system is not competitive with the chemical systems at the level of total impulse required for  $\Delta V$  propulsion. The quantity of  $GN_2$  required  $I_{sp}$  only 72 would be in excess of 45.3 kg (100 lbm), and the weight of the pressure vessel required to contain the  $GN_2$  would add another 49.8 to 58.9 kg (110 to 130 lbm). For this reason the cold gas system was dropped as a contender for the  $\Delta V$  propulsion function early in the study.

f. *Auxiliary Propulsion* - To size the auxiliary propulsion system, it is necessary to know the moment of inertia of the probe,  $I_z$  (about its spin axis), the thruster moment arm, the angular velocities to be achieved, and the (precession) angle through which the probe must be reoriented before Jupiter entry. From preliminary layouts of the probe,  $I_z$  was determined to be  $\sim 12.2 \text{ kg/m}^2$  ( $9 \text{ slug-ft}^2$ ), and the maximum allowable moment arm,  $\sim 0.457 \text{ m}$  ( $1.5 \text{ ft}$ ). Probe dynamic considerations dictated the need to spin up the probe to  $\sim 10.5 \text{ rad/sec}$  ( $100 \text{ rpm}$ ) prior to accomplishing the  $\Delta V$ , precessing the probe to the proper entry angle, and then despinning to  $\sim 0.52 \text{ rad/sec}$  ( $5 \text{ rpm}$ ) before Jupiter atmospheric entry. For proper entry, the required probe precession angle was found to be of the order of  $0.89 \text{ rad}$  ( $51^\circ$ ).

To accomplish the spinup and despin functions, a thruster impulse of  $534 \text{ Nsec}$  ( $120 \text{ lbf-sec}$ ) is required, and to accomplish the precession maneuver, the required impulse is  $\sim 244 \text{ Nsec}$  ( $55 \text{ lbf-sec}$ ), bringing the total to  $777 \text{ Nsec}$  ( $175 \text{ lbf-sec}$ ). A very small impulse is also required to accelerate the service module to  $0.46 \text{ m/sec}$  ( $1.5 \text{ ft/sec}$ ) just before entry, but this requirement is insignificant compared to the spin and precession requirements. Assumption of a required total impulse of  $800 \text{ Nsec}$  ( $180 \text{ lbf-sec}$ ) provides a conservative estimate upon which the propulsion system design may be based. For this level of impulse, the cold gas system is a strong contender, even though the propellant mass fraction is relatively small. For this application, the total quantity of propellant required is very small; consequently, the system weight is small even though the mass fraction is relatively low. To provide an impulse of  $800 \text{ Nsec}$  ( $180 \text{ lbf-sec}$ ), using a  $\text{GN}_2$  cold gas system for which  $I_{sp} = 706 \text{ Nsec/kg}$  ( $72 \text{ sec}$ ), the quantity of  $\text{GN}_2$  required is  $\sim 1.13 \text{ kg}$  ( $2.5 \text{ lbm}$ ). Allowing an additional 30%  $\text{GN}_2$  to account for leakage and residuals, and providing  $1.93 \text{ kg}$  ( $4.25 \text{ lbm}$ ) for the storage vessel and  $7.2 \text{ lbm}$  for valves and other system components, the total system weight becomes  $6.65 \text{ kg}$  ( $14.7 \text{ lbm}$ ). Thus the system mass fraction is only  $0.22$ , but the total system weight is still not excessive.

g. *Propulsion System Selection Rationale* - As noted previously, the requirement exists for two distinctly different propulsion functions, one involving a relatively large single impulse to effect probe deflection for Jupiter entry, the other a series of relatively small impulses to accomplish probe spinup, despin, and precession, plus final service module ejection. The small impulses conceivably could be provided by several distinct propulsion systems, but it is much more logical to attempt to group them together into a single auxiliary propulsion system. The single impulse bits required for the spinup, despin and module deflection maneuvers presumably could be provided equally well by solid, liquid, or gaseous systems, but the multiple small bits required for the

precession maneuver can not be provided by a conventional solid propellant motor. Possibly, this latter requirement could be satisfied by use of a "cap-pistol" solid propellant system, but this concept has never reached a very high state of development, so was not considered seriously in this study. The precession maneuver, on the other hand, is an ideal application for the cold gas system. It is capable of producing literally thousands of very low, completely reproducible, impulse bits simply by the proper on-off control of the thruster solenoid valve. The cold gas system is relatively heavy because of its low specific impulse, but this is not extremely important because of the small quantity of propellant gas involved.

The auxiliary propulsion requirement places constraints on the propulsion system somewhat different from those of the  $\Delta V$  requirement. The spinup maneuver must take place in the immediate vicinity of the spacecraft to minimize angular tip-off errors after separation. The exhaust products of the spinup nozzles must not contaminate or damage the spacecraft. Cold gas suits this requirement well.

In selection of the deflection motor, a factor to be considered is performance flexibility; i.e., the ability of the system to accommodate changes in performance requirements that may evolve during the spacecraft development and testing phases. In this regard, liquid and gas systems offer significant advantages. Thrust level can be changed over a moderate range by modifying only the thrust chamber without disturbing the rest of the system. Total impulse can be altered by changing only the size of the propellant tankage, or possibly by off-loading the propellant, without disturbing the other system components. It can be controlled precisely by controlling the thruster burn time. Solid propellant motors on the other hand, must be designed and qualified for a fixed total impulse and thrust/burn time relationship. However, the total impulse of the solid propellant motor is typically repeatable from motor to motor within a range of  $\pm 3/4\%$ .

Solid propellant motors inherently possess a high reliability because of their extreme simplicity, and their relatively advanced state of the art. Typical of the reliability estimates made by solid motor fabricators is that provided to Martin Marietta by Aerojet General. Based on various component tests ranging in number from 122 to 2878, and a total number of failures of only 5, a best estimate of motor reliability for this particular application is 0.997. Liquid (and gaseous) propellant systems tend to be less reliable than solid propellant motors because of their greater complexity, but this deficiency can usually be at least partially compensated for by providing redundancy for the critical system components (principally, valves).



The selected propulsion system is a spherical solid propellant motor for the deflection delta velocity maneuver combined with a cold gas attitude control system. The principal driver in the selection is that of minimum system weight, since reliability is not very different for the systems considered. The characteristics of the selected system are as compared with a monopropellant hydrazine system, performing both deflection delta velocity and attitude stabilization as shown in Table V-11. The weight advantage of the selected system is significant, and the fixed total impulse of the solid propellant deflection motor does not constitute a major disadvantage if the mission parameters can be established in advance of motor design. Figure V-39 is a parametric presentation of weights for a spherical rocket motor using a dual nozzle exhaust such as has been chosen for the probe studies.

Table V-11 Jupiter Probe Propulsion System Parameter Comparisons

	TRAJECTORY CORRECTION AND ATTITUDE CON-ROL		
	SOLID	COLD GAS	MONOPROPELLANT-HYDRAZINE
Specific Impulse, sec	287	72	230
Mass Fraction	0.76*	0.18	0.55
Propellant Weight, lbm	26.0	2.5	32
System Weight, lbm	32.5	14.7	62
0-g Effects	None	None	PMD required
Reliability	0.997	0.997	0.995
Total Impulse Control	Fixed	Variable	Variable
*Not including second nozzle			

b. *Mission Parametric Change Effects* - During the course of the nominal Jupiter design and the Jupiter mission parametric effects evaluation, the propulsion system resultant changes were computed. These results are shown in Table V-12. It can be seen from the table that mission parameters such as entry angle and planetary atmospheric variations both affect the probe weight and the desired deflection delta velocity for planetary entry; these effects, in turn, affect the size of the propulsion system. The largest effect is on the probe solid propellant deflection motor; the rocket motor weight comparisons are indicated. Also shown are the total impulse requirements of the attitude control system.

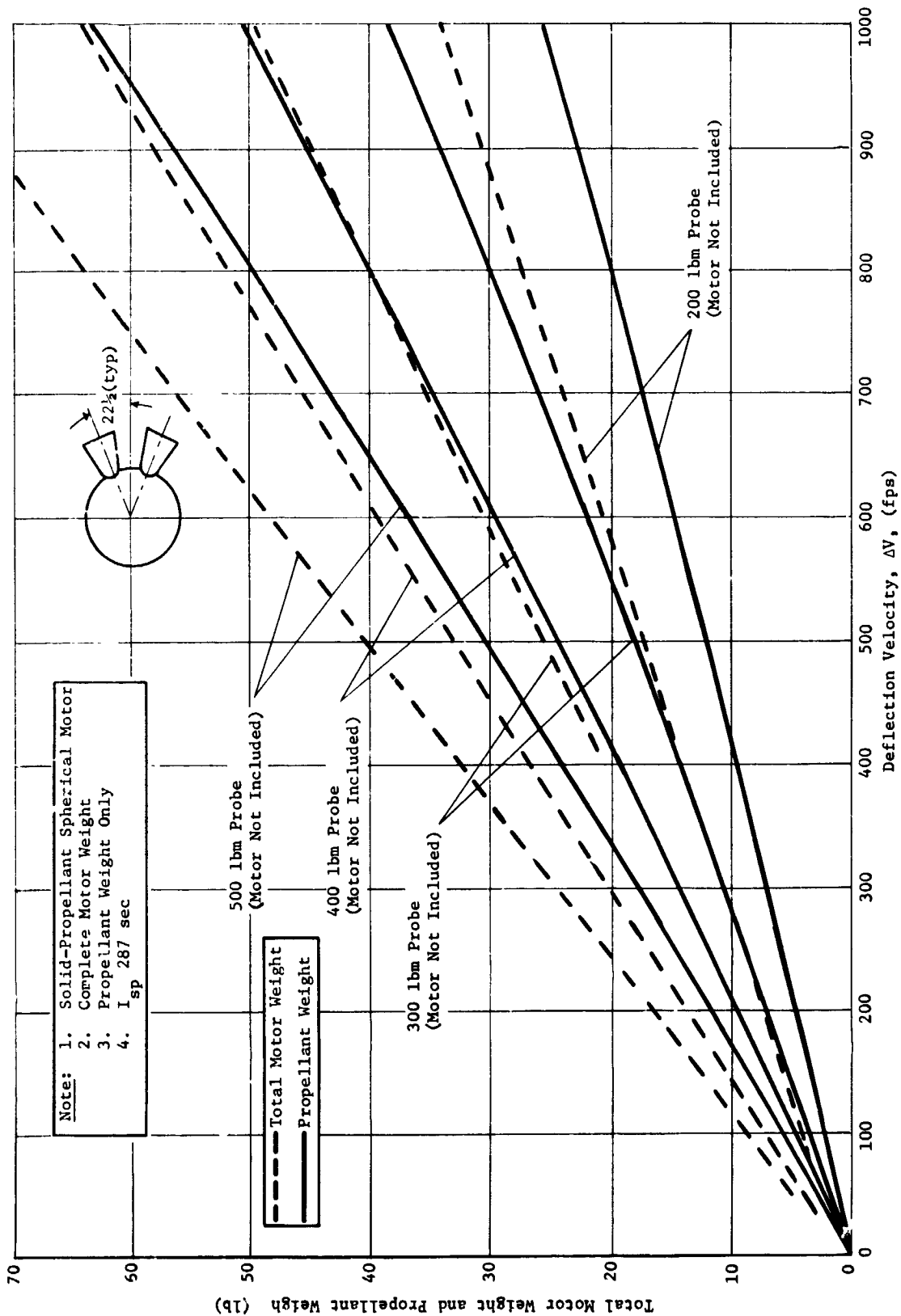


Figure V-39 Total Motor Weight and Propellant Wt. vs Probe Deflections Velocity

Although the impulse requirements vary with mission, the attitude control system weight changes vary little. The weight of the gas to provide the impulse for spin, despin, and precess is only of the order of 2.5 pounds, and the gas bottle 3.5 pounds. Thus, the net effect of changing ACS impulse by 50% results in a total probe weight change of several pounds. The real change in weight occurs when the mission is changed from a probe deflect to a spacecraft deflect or shared deflect mode. For the spacecraft deflect mode, almost the entire ACS system is eliminated (only a simple spin up system is required) and the deflection motor is eliminated entirely. The shared deflection is the poorest performance case, since not only does the probe have to do a near maximum propulsion job, but the spacecraft also must perform a deflection delta velocity maneuver of approximately 200 m/s.

Table V-12 Mission Parametric Effects on Probe Propulsion System

ATMOSPHERE	C/D	C/D	C/D	C/D	Nom	Pioneer S/C	Pioneer Shared
ENTRY ANGLE, deg	10	20	30	Polar	20	Deflection Mode	Deflection Mode
Deflection Velocity, m/s	205	221	255	301	221	0	246**
Probe Entry Mass, lb	305.7	330.0	363.2	465.1	305.7	251*	
$\Delta V$ Rocket Motor Weight, lb	32	35.5	45.0	65.0	34.3		
$\Delta V$ Propellant, lb	23.0	27.0	34.0	51.0	25.0		
ACS System Total Impulse, sec	153	182	198	272	150	0	79
* 67 lbm spacecraft modification for $\Delta V$							
** 201 m/s required for spacecraft $\Delta V$							

#### 10. Thermal Control Subsystems

Thermal control for outer planet probes must be provided to ensure that all probe systems will be maintained within acceptable temperature limits throughout all phases of the mission. For the purposes of analyzing the thermal control subsystem, the entry probe study missions were divided into three phases.

1) *Spacecraft Cruise* - Duration of the mission from launch to near Jupiter spacecraft separation during which time the probe is housed under an environmental cover, shadowed from direct solar impingement except for brief midcourse maneuvers, and in a power-off storage mode;

2) *Probe Coast* - Duration of the mission from near Jupiter spacecraft separation to pre-entry activation of the probe systems during which time the probe is in a brief power-up mode for separation and checkout, and then deactivated for the duration of the coast phase. (The probe/spacecraft environmental cover will have been jettisoned and the probe directly exposed to solar radiation during this phase.);

3) *Entry and Descent* - Duration of the mission beginning about one hour before actually entering the planet atmosphere until the end of the design mission during which time the probe systems are activated for checkout before entry and left in a power-on standby mode. The probe systems then become operational at entry and function throughout the science return descent portion of the mission (see Fig. V-40).

The most critical probe temperatures, from a standpoint of thermal design, are the temperatures at the end of probe coast and the maximum internal equipment temperature experienced at the end of descent in a Jupiter nominal atmosphere or the minimum internal equipment temperature experienced during descent in a Jupiter cool/dense atmospheric encounter.

For nominal Jupiter atmospheric encounters, the primary thermal problem is one of gaining too much thermal energy from the atmosphere environment during descent. For passive thermal design, the desirable probe entry temperature would be just safely above the lower operating probe temperature limit (some initial atmospheric cooling to be considered), and thus allowing optimum leeway for equipment temperature rise during descent.

For cool/dense Jupiter atmospheric encounters, the primary thermal problem is one of losing too much thermal energy to the atmosphere environment during descent. For this atmosphere, therefore, elevation of the probe coast entry temperature to maximum levels without exceeding upper temperature limits and allowing optimum leeway for temperature decrease would be desirable. The maximum probe coast temperature is limited by the upper storage temperature limit of the dry stand remotely activated descent batteries. Since the upper battery storage limit is less than the upper operational probe temperature limit, less leeway is available for probe cooling in the cool/dense atmosphere than for probe heating in the nominal atmosphere.

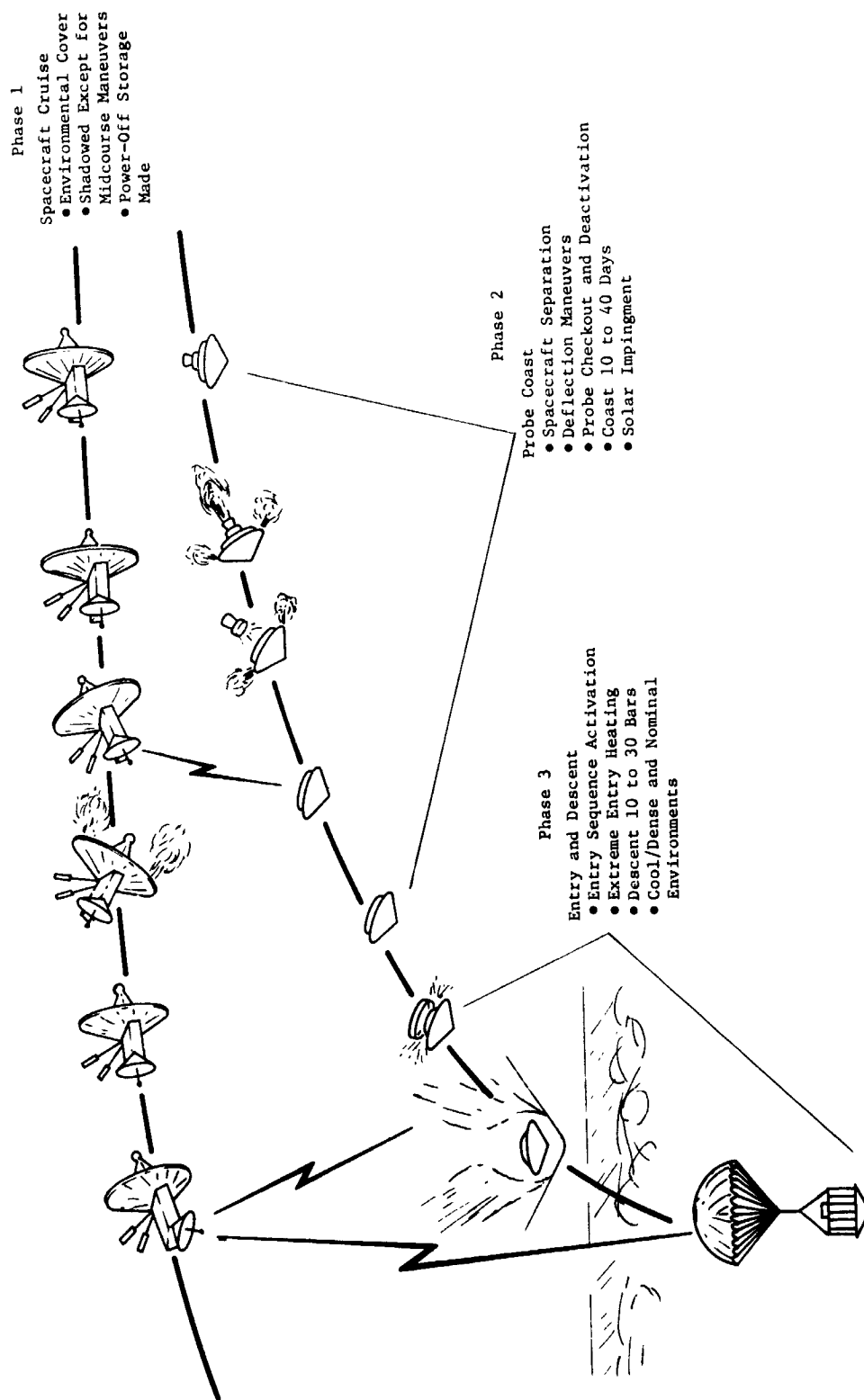


Figure V-40 Mission Phases and Events

a. *Thermal Control Selection* - The selection of an adequate thermal control approach considered simplicity, reliability, and minimum weight as the most important parameters. The basic thermal design recommended is as follows:

1) *Radioisotope Heaters* - These heaters would be located in the service area surrounding the aeroshell and provide guard heating for the descent probe capsule during spacecraft cruise and the probe coast phases of the mission. The purpose of the heaters would be to maintain adequate probe storage temperatures during cruise and provide a satisfactory entry temperature for the atmospheric descent portion of the mission.

2) *Multilayer Insulation* - A multilayer insulation blanket would completely encapsulate the probe during spacecraft cruise and probe coast phases of the mission. Its purpose would be to conserve the internal heating provided by the radioisotope heaters and isolate the probe from the space environment.

3) *Environmental Spacecraft Cover* - An environmental cover would be provided during the spacecraft cruise to protect the probe and multilayer insulation from meteoroid and micrometeoroid damage and to supply a low  $\alpha/\epsilon$  thermal coating for possible direct solar impingements.

4) *Thermal Coatings* - Thermal coatings would be provided on the forward and aft end of the probe to modulate the internal heating required and, in addition, to amplify the solar radiation encountered during the probe coast phase. Moderately low emissivities would be appropriate for conserving isotope heater power and a high  $\alpha/\epsilon$  on the probe aft would provide some probe solar heating before entry.

5) *Deflection Motor Blanket and Heater* - Because the probe deflection motor (if required) would be external from the probe primary multilayer insulation blanket, a second multilayer blanket and heater would be provided for motor thermal control. Since the probe deflection motor is fired immediately after spacecraft separation, a thermostatically control electrical resistance heater powered by the spacecraft could be used. In addition, the multilayer blanket surrounding the deflection motor could be mounted to a lightweight fiberglass frame and which would remain with the spacecraft.

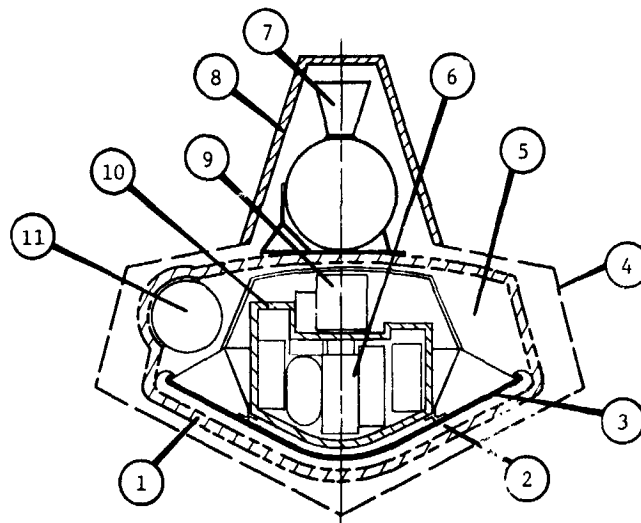
6) *Graphite Ablator and Fibrous Aeroshell Insulation* - Heat shield ablator materials would be provided for probe entry. A backing of fibrous insulation would be required to protect the aeroshell structure and, in turn, isolate the descent probe capsule from the entry heat pulse. No detailed design work was performed for the heat shield; its development is the subject of a separate study.

7) *Internal Probe Low Density Foam Insulation* - The descent probe capsule would be provided with internal foam insulation adjacent to structural probe shell to provide thermal isolation of the internal components from the descent atmospheric environment. An internal insulation would be desired over external insulation because of the packaging and attachment problems of external insulation and probe access and structural interface difficulties. A schematic of the basic thermal control subsystem is presented in Figure V-41.

b. *Thermal Control Alternate Concepts* - In addition to the basic passive thermal control subsystem just outlined, several alternative design concepts may be applicable for outer planet probe missions. Incorporation of their design would depend on individual mission definition and objectives. These alternative thermal control concepts are as follows.

1) *Phase Change Material* - The most critical component from a standpoint of electrical heat dissipation is the RF transmitter. If transmission efficiencies, mission uncertainties, or large communication distances became critical such that large temperature rises would be anticipated for the transmitter, the use of a wax-type phase change material would be recommended. This material melts at about 310°K and can absorb approximately 30 W-hr of the electrical heat dissipation per pound of material.

2) *Nitrogen Gas Environmental Control* - For the vented probe design configuration, the thermal control concept relies on sufficient probe thermal inertia and internal power generation to survive the more severe cool atmospheric encounters. If the probe mass, power, and descent time became critical from the standpoint of maintaining acceptable internal probe equipment temperatures, an alternative thermal design would be used of a nitrogen gas supply to substitute for the intake of Jovian atmospheric gasses at the beginning of the descent. The advantage of nitrogen gas is its low thermal conductivity (approximately 0.035 W/m°K) compared to the Jovian atmosphere (approximately 0.180 W/m°K). Under normal conditions, the Jovian atmosphere inside the probe degrades the performances of the internal probe foam insulation. The presence of a nitrogen gas, however, would not degrade the insulation performance and thus allow improved probe thermal control to maintain internal probe temperatures.



COMPONENT	MATERIAL	THERMAL CONTROL APPROACH
1. External Probe Insulation	Multilayer, ~70 Layers	Radiation: Moderate Low $\epsilon$ , High $\alpha/\epsilon$ on Tail
2. Heat Shield	ATJ Graphite	Ablation
3. Aeroshell	Titanium	Fibrous Carbon Felt Insulation
4. Environmental Cover	Aluminum	Radiation: High $\epsilon$ , Low $\alpha$
5. Service Module	Various	Radioisotope Heaters
6. Science, Communications, Data Handling, Power (Battery)	Various	Internal Low Density Foam Insulation and Minimized Structural Penetrations
7. Deflection Motor	Solid Propellant	Spacecraft Heater and Insulation Blanket
8. Deflection Motor Insulation	Multilayer, ~70 Layers	Radiation: Low $\epsilon$
9. Parachute	Dacron	Thermal Environment of Adjacent Components
10. Internal Probe Insulation	Low Density Foam	Low-K Material Specification
11. Attitude Control System	Valves and Propellants	Thermal Environment Controlled by Service Module Components and Heaters

Figure V-41 Probe Thermal Control Subsystem Design



The use of one or two bars of nitrogen gas initially inside the probe would delay the impact of the atmosphere environment and allow an increased margin of thermal protection during descent.

For nitrogen gas environmental control, the probe would be either precharged before entry or pressurized from a storage bottle at a rate designed to match the increase in descent pressure. Since the vented probe design precludes any significant external collapse pressure, the atmospheric gasses would be allowed to enter the probe when the descent pressure matched the  $N_2$  gas pressure. The performance of the foam insulation would not degrade immediately, but would rather respond to the properties of the gas mixture. For a mixture of nitrogen and the Jovian gasses ( $He/H_2$ ), the heavier nitrogen would be expected to dominate the gas mixture and weight the thermal conductivity.

*c. Probe Equipment Temperature Limits* - The probe equipment temperature limits established for probe thermal design are presented in Figure V-42. The overall probe allowable operating and storage temperature limits are identified and include the RF transmitter, the aggregate internal probe equipment, the equipment located on the aeroshell and service module, and the deflection propulsion system. The atmospheric descent probe is divided into the RF transmitter and internal equipment. Because of the high electrical thermal dissipation in the transmitter, this component is identified separately throughout all thermal analyses.

The limits of the internal equipment are bounded by the primary probe descent batteries at both the lower operating temperature limit (272°K) and the upper storage temperature limit (300°K). The lower operating temperature limit of the batteries is established by the effect of temperature on battery capacity. Figure V-43 shows battery energy density as a function of discharge rate and temperature for typical remotely activated silver-zinc batteries. Also of importance is the upper allowable storage limit of the descent batteries. Since these batteries are dry stored for the duration of the long spacecraft cruise, the charge retention characteristics of the battery cells can degrade with prolonged excessive temperature levels. Figure V-44 presents typical dry storage charge retention characteristics as a function of temperature and storage time. Since the battery storage limit is important from a standpoint of the maximum probe entry temperature allowable, any additional development activities should evaluate these characteristics.

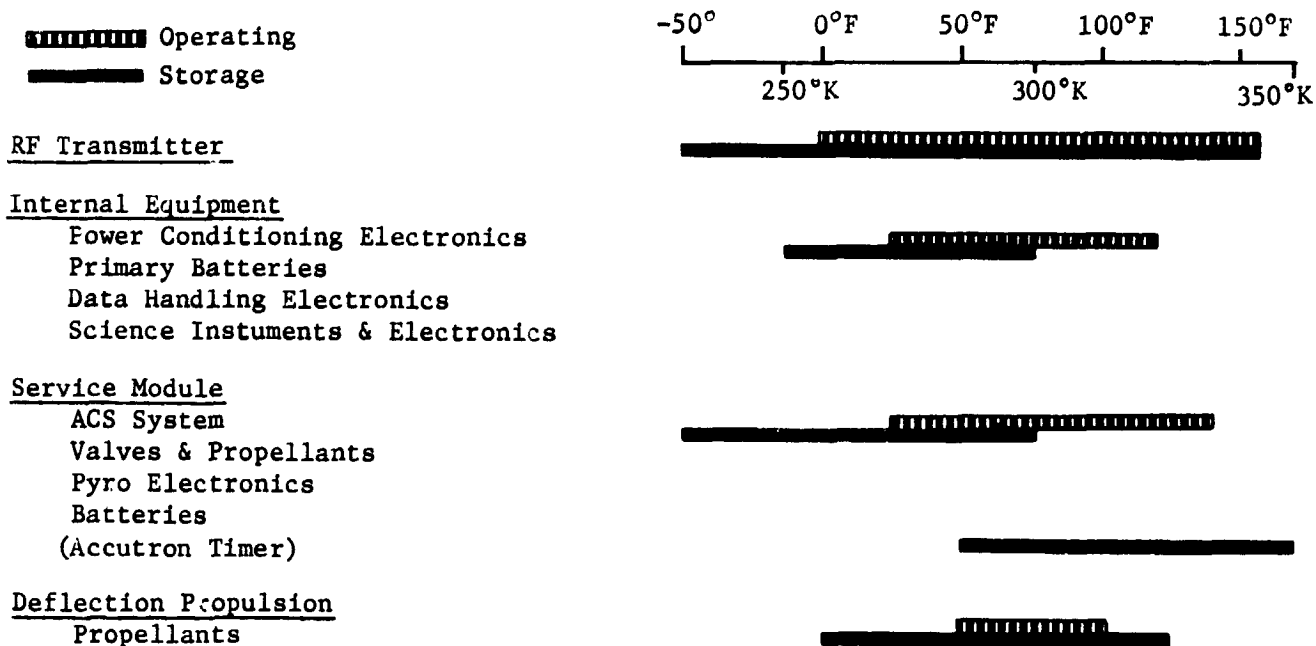


Figure V-42 Jupiter Probe Equipment Temperature Limits

The limits of the internal equipment are also bounded by the neutral mass spectrometer at the upper operating temperature limit (320°K) and by the neutral mass spectrometer at the lower storage limit (250°K). The lower storage temperature is not of significance for probe thermal design since temperature levels are not anticipated below the lower operational temperature limit (272°K). The upper operational temperature limit is important only for warm atmospheric encounters and is not as critical as the lower operational temperature limit during cold encounters.

The temperature limits in the service module are also bounded by the battery discharge and charge retention characteristics. The ACS valves and propellant limit the lower storage and the upper operating temperature conditions. The probe thermal design is such that service module temperatures should be between the lower operating and upper storage limits of the batteries at all times.

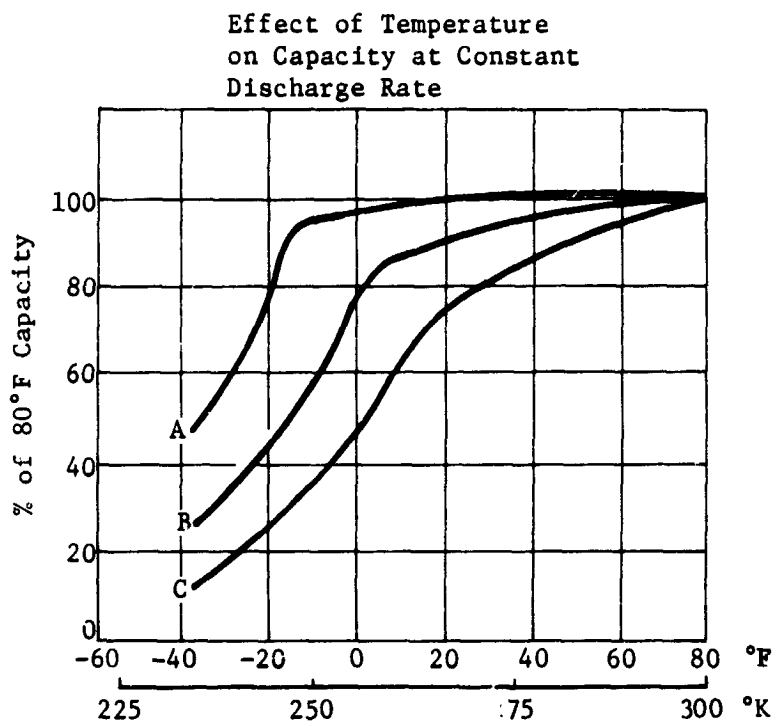


Figure V-43 Effect of Temperature on Battery Capacity

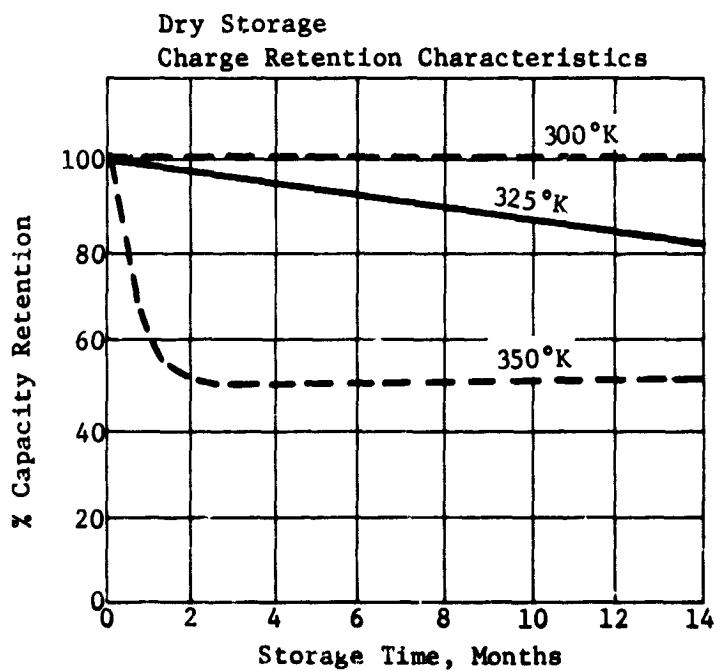


Figure V-44 Battery Dry Storage Charge Retention Characteristics

A probe Accutron timer is also located in the service module, but shown separately because of its higher operating temperature range. What is important, however, is the allowable drift of timers absolute temperature. For the timer to function within expected accuracy levels, a steady temperature must be maintained. For this reason, the location selected for the accutron timer is adjacent to the radioisotope heating units.

The temperature limits applied to the deflection propulsion are presented and represent an allowable temperature range for the propellants. Again, it is not the temperature range that is of the most importance, but the absolute operating temperature itself. Since a "burn to completion" solid has been selected for the deflection maneuver, the temperature dependent output and control characteristics must be established for precise design.

d. *Spacecraft Cruise/Frobe Coast Thermal Analysis* - Thermal control during the spacecraft cruise and probe coast phases of the mission is supplied by internal radioisotope heater power, multilayer insulation, and thermal coatings. To determine the radioisotope heater requirements for the Jupiter probe missions, a finite-element thermal model was constructed and used to perform parametric analysis. Since the equipment temperature at the end of coast is the pivotal design temperature, the subsystem thermal control was selected to establish this temperature and allow minimum probe temperature changes between spacecraft release and entry for the parametric studies.

The finite-element probe cruise and coast model consisted of 16 nodes and 23 associated conductors. Figure V-45 presents a schematic showing the resistance-capacitance thermal network representing the probe model. The nominal mission Jupiter probe design was used to construct the model and determine appropriate conductor values. The structural heat leak paths included the deflection propulsion motor attachments, the ACS thrusters and feed line penetrations, the pre-entry probe antenna, and the MLI joint at the circumference of the probe.

To determine probe heat losses and radioisotope heater power requirements, the multilayer insulation blanket presented the biggest design uncertainty. For insulation performance, two applicable data sources on multilayer insulation were obtained and evaluated. An analytical expression was then developed to represent the effective thermal conductivity of the insulation and incorporated into the analysis (Appendix J, Vol III). To account for the miscellaneous blanket penetrations required to attach and hold the

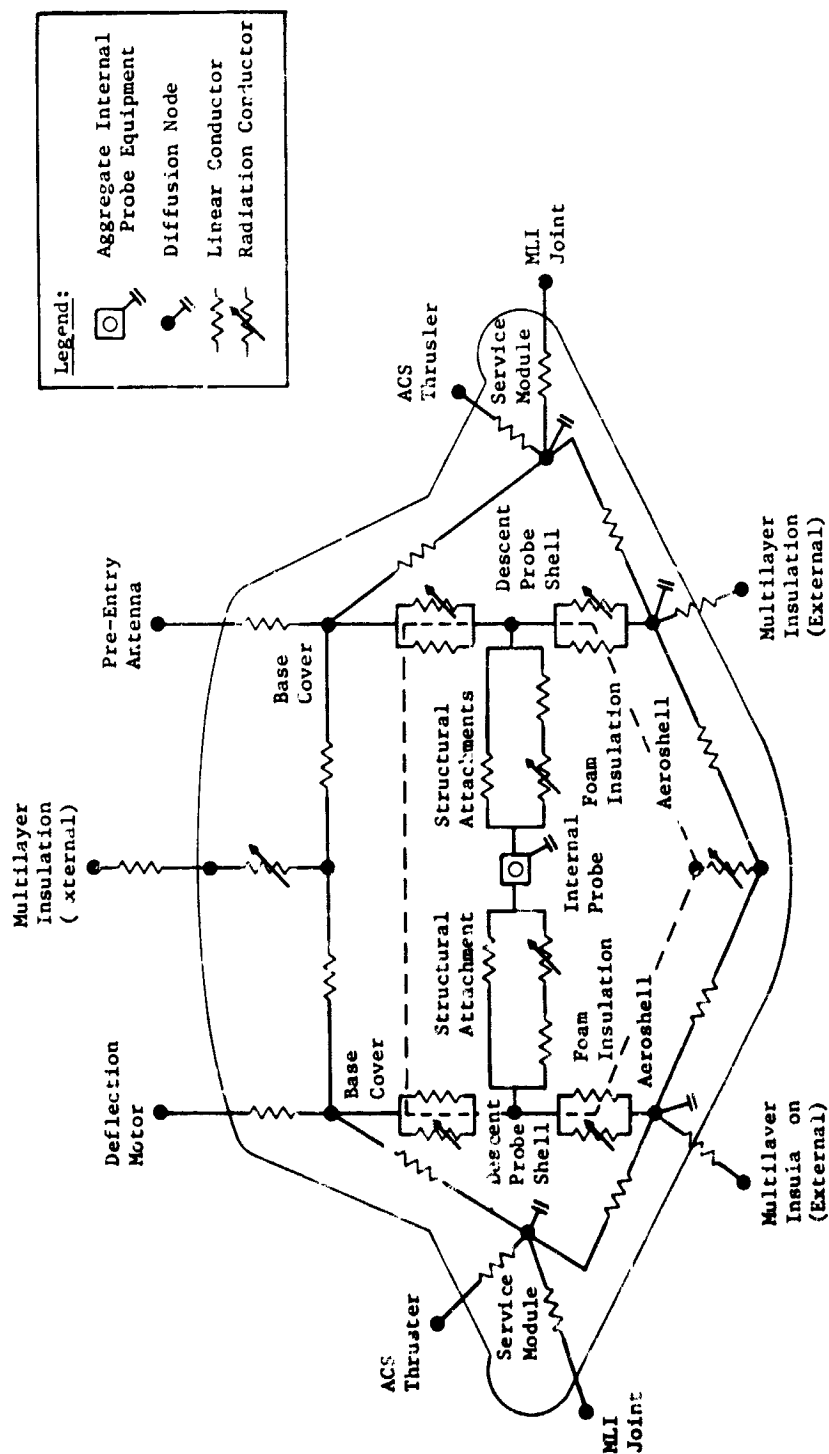


Figure V-45 Basic Cruise/Coast Thermal Model Schematic

insulation in place, the theoretical multilayer insulation conductivity was increased by 50%. This approach may be somewhat conservative but allows leeway in the thermal design for possible later contingencies. Note that the MLI joint was considered separately in the thermal analysis.

Three probe configurations were considered for determining the amount of isotope heater power that may be required. The heating requirement was computed as a function of desired interior probe temperature and is presented in Figure V-46. The multilayer insulation thickness chosen was 1.5 cm, or approximately 70 layers of insulation. This insulation thickness was selected to achieve a reasonable compromise between heater power and insulation bulk and used for all probe analyses.

The cruise/coast probe configurations analyzed are shown schematically in Figure V-47. Although the nominal Jupiter mission consists of a complex probe (probe deflection and attitude control capabilities for spin, precession, and despin), several additional configurations were of interest. The alternative probe configurations investigated considered spacecraft deflection that eliminated the probe deflection propulsion motor and a third probe design that considered a minimal ACS system for low rpm spinup only; thus also eliminated the service module (simple probe).

The thermal coatings selected for cruise/coast parametric analysis allowed a minimum degree of temperature change between spacecraft release and entry (9.8 day coast time for nominal probe). Analysis indicates that approximately eight days are required for the probe to approach two-thirds of its equilibrium temperature after spacecraft release and this design allows smaller uncertainty in the probe coast entry temperature. For the analysis presented, thermal coating values of  $\alpha/\epsilon = 0.20/0.80$  were chosen for the probe forward section (nose) and values of  $\alpha/\epsilon = 0.25/0.25$  were chosen for the probe aft section (tail). The effective multilayer insulation conductivity for this analysis was approximately  $8.5 \times 10^{-4}$  W/m<sup>2</sup>K.

The results presented in Figure V-46 show that a temperature increase of approximately 5°K would be anticipated from spacecraft separation to probe/coast equilibrium. Refinements in later analyses (probe-dedicated alternative Jupiter mission study) show that the effect of the environmental cover ( $\alpha/\epsilon = 0.20/0.80$ ) will raise the probe temperature on the spacecraft 10°K higher than anticipated. Parametric descent analyses show that coast/entry temperatures as high as 297°K would be desired for atmospheric descent, but the long spacecraft cruise phase at these temperature levels may not be. An alternative to the design, therefore, would be selection of thermal coatings that would maintain a

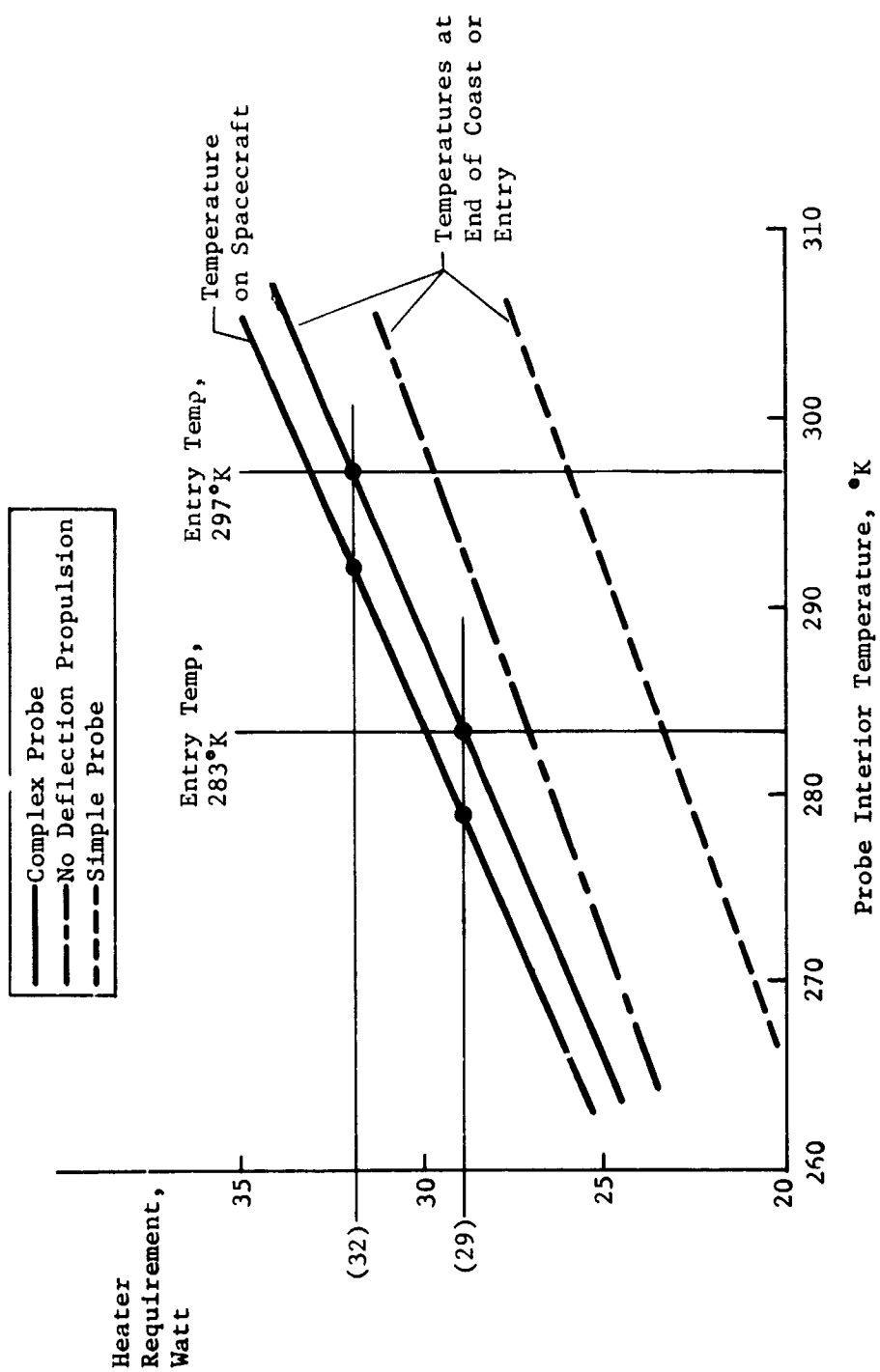


Figure V-46 Cruise/Coast Thermal Control - Radioisotope Heater Requirement

spacecraft probe equilibrium temperature 10 to 20°K lower than the required coast equilibrium temperature, and then use spacecraft power to heat the probe to its probe/coast equilibrium temperature before spacecraft release.

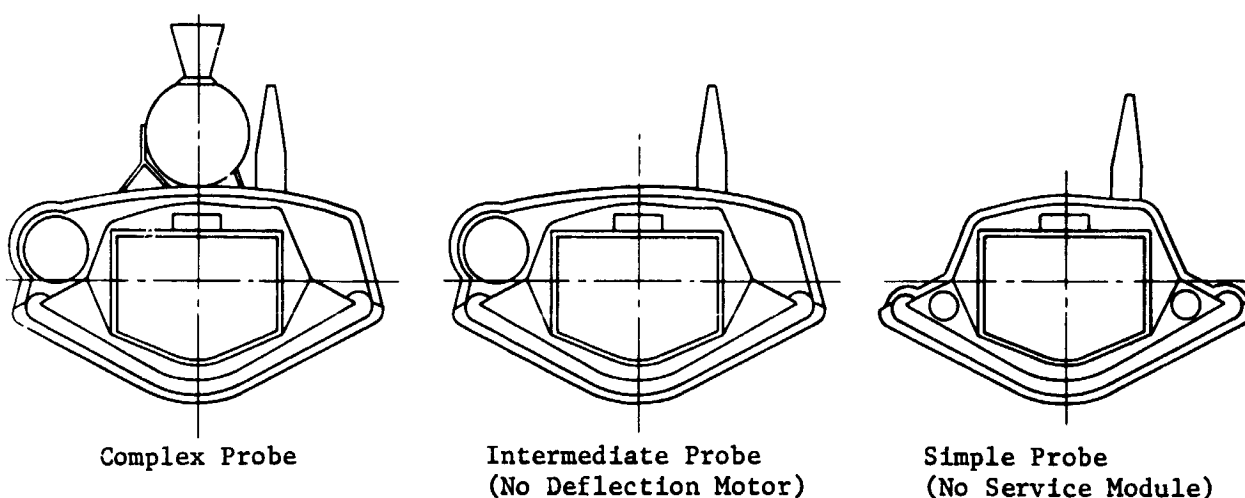


Figure V-47 Comparison of Cruise/Coast Parametric Probe Configurations

e. *Descent Probe Thermal Analysis* - Thermal control for the atmospheric descent portion of the mission relies on the probe/coast entry temperature, internal probe foam insulation, and sufficient probe thermal inertia to survive the descent environment encountered. For the Jupiter studies, two basic probe configurations were evaluated (sealed and vented). Based on the vented probe design, two Jupiter model atmospheres were used (cool/ dense and nominal) to evaluate the mission descent design parameters. In addition, an alternative Jupiter mission was considered where a more powerful RF transmitter could be used for 6 to 7  $R_J$  and possible direct-link communication distances.

To perform the descent probe parametric studies, a descent probe thermal model was constructed consisting of 18 nodes and 28 associated conductors. Figure V-48 presents a schematic depicting the resistance-capacitance thermal network. The nominal Jupiter mission probe design was used as a baseline to determine probe mass properties, thermal/structural details, and the equipment power profile.



Care was exercised to account for all heat losses through penetrations in the foam insulation. Likewise the design of the structural details minimized heat leak paths by avoiding metallic contacts to the probe shell wherever possible. The primary insulation penetrations represent the equipment platform structural supports and the parachute canister attachments.

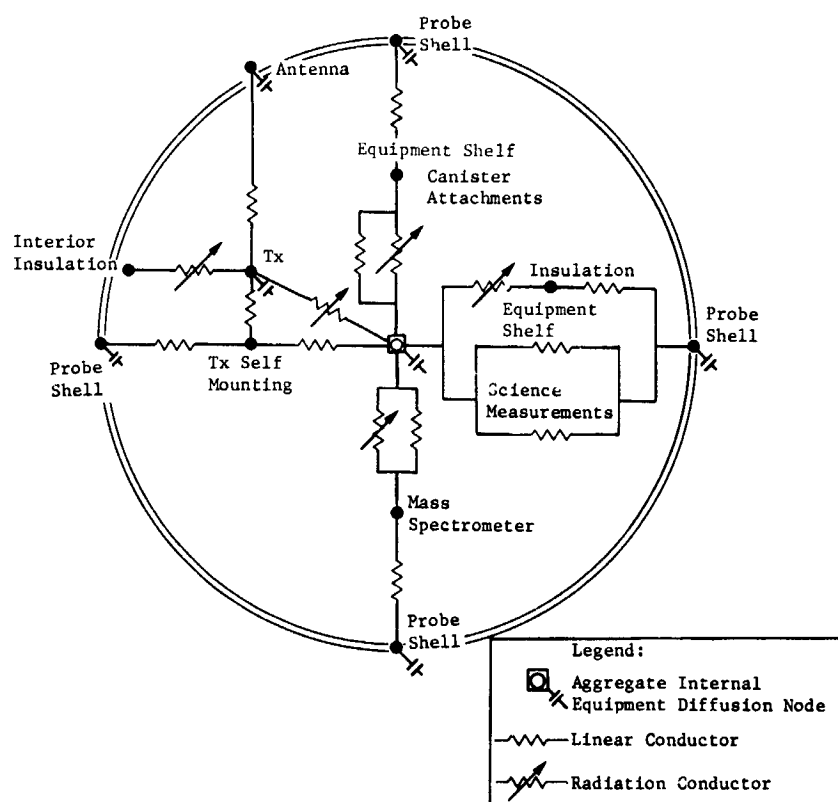
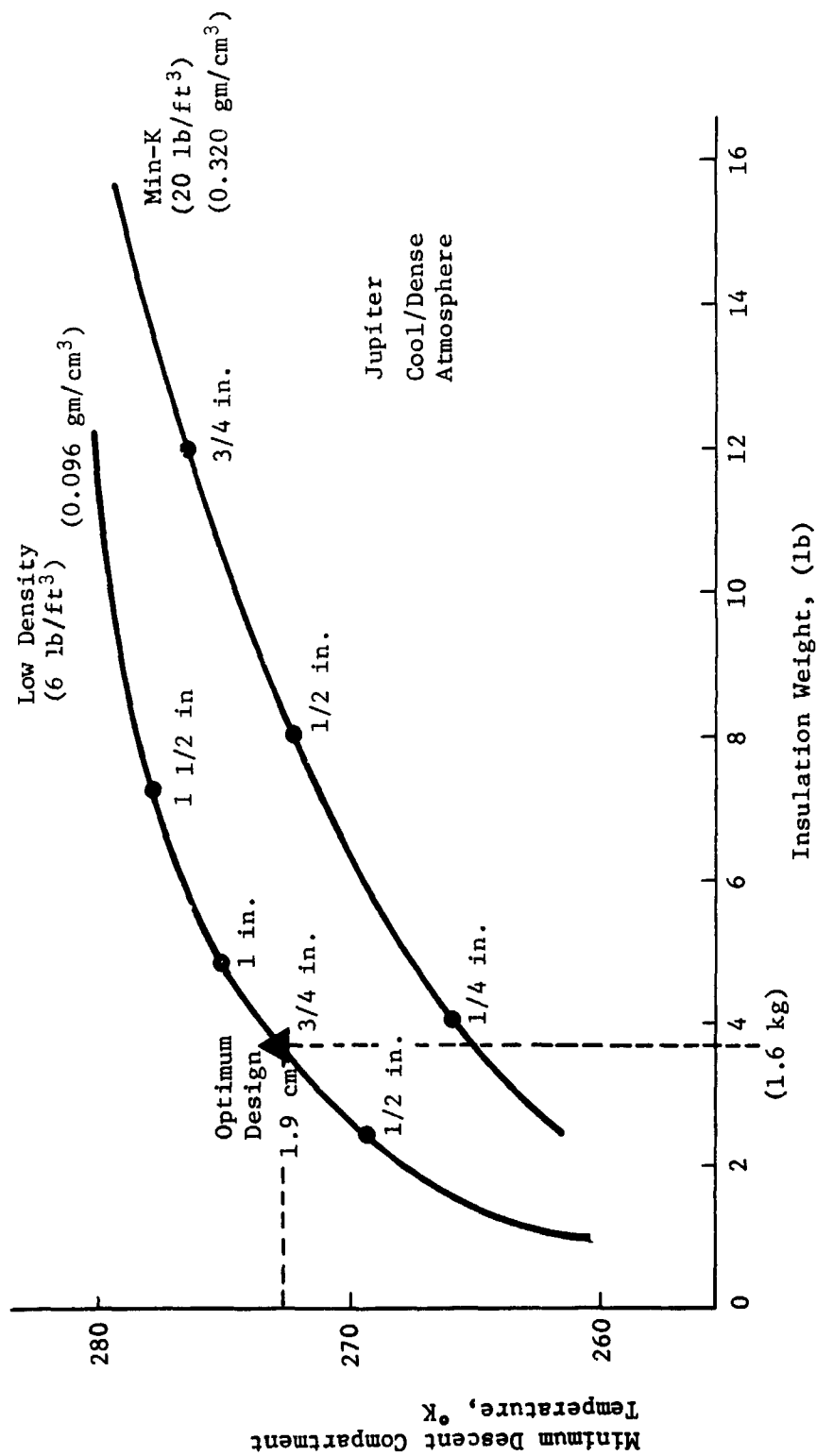


Figure V-48 Basic Descent Probe Thermal Model Schematic

To determine the amount of internal foam insulation desired for probe design, the nominal Jupiter mission and the vented probe combination was used to parametrically evaluate insulation thickness against minimum compartment probe descent temperatures. Results from this study are presented in Figure V-49. An initial descent probe/coast compartment temperature of 283°K was assumed as was a 42-minute pre-entry communication period and a 33-minute cool/dense atmospheric descent to 30 bars pressure. Two insulation types were considered and are plotted as insulation weight against minimum compartment temperature. For the low density foam insulation, conservative insulation properties were assumed

Note: Vented Probe Results  
Based on Initial Compartment  
Probe Temperature of 283°K.



Jupiter  
Cool/Dense  
Atmosphere

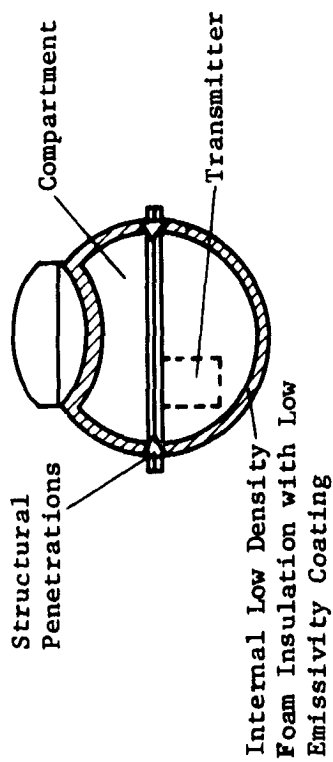
Figure V-49 Minimum Compartment Probe Descent Temperature  
vs Installation Thickness and Weight.

with the insulation conductivity set equal to the conductivity of the atmospheric-gas within the probe ( $\sim 0.18 \text{ W/m}^2\text{K}$ ). As an alternative insulation, a Johns-Manville Min-K insulation that has superior insulation properties in He/H<sub>2</sub> gas mixtures (thermal conductivity approximately  $0.10 \text{ W/m}^2\text{K}$ ) was investigated. Results show that no weight advantage exists because of the higher densities required for those insulations. For the low density insulation, a minimum compartment temperature design point of  $272^\circ\text{K}$  corresponds to 1.9 cm (0.75 in.) thickness and 1.63 kg (3.6 lb) of insulation. Although this design point allows little leeway for exceeding allowable lower limits, the probe/coast entry temperature can be increased for descent margin. The low density insulation was assumed to be  $0.096 \text{ gm/cm}^3$  ( $6.0 \text{ lb/ft}^3$ ).

The two basic descent probe configurations considered for this study were a sealed probe (Configuration 1) and a vented probe (Configuration 2). A schematic of the two probe configurations is presented in Figure V-50. To compare the two designs, identical probe missions were analyzed where each probe had 1.9 cm of low density foam insulation and each performed a 33-minute descent to 30 bars pressure in a cool/dense Jupiter atmosphere. Identical probe mass properties and equipment power profiles were assumed.

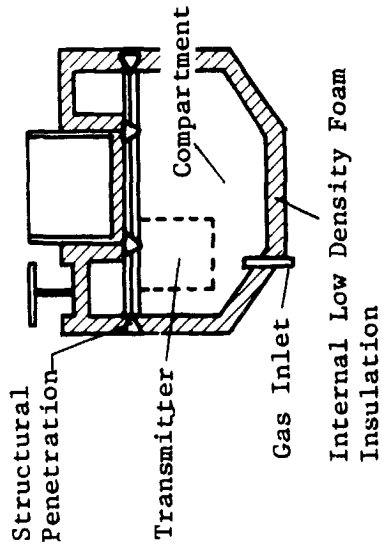
Results for the sealed probe design are presented in Figure V-51. These results present two equipment shelf designs and demonstrate the superiority of aluminum material. A temperature difference of only  $22^\circ\text{K}$  is required to stabilize the RF transmitter for that design. Since the probe is sealed, no degradation in insulation performance occurs (thermal conductivity  $0.035 \text{ W/m}^2\text{K}$ ) and no internal free convection is present. In addition, a low emissivity coating (emissivity 0.06) was assumed on the interior of the probe, which further reduced the insulation heat leak by minimizing radiation coupling with the internal equipment. Analysis shows that the sealed descent probe configuration is very efficient at maintaining the internal probe equipment.

Results for the vented probe design are presented in Figure V-52. The original Task 1 results represent the insulation parametric study results with 1.9 cm of low density foam insulation. Also presented are updated results that include the aluminum self-design and increased probe entry temperature. The higher entry temperature of  $297^\circ\text{K}$  was desired to ensure that the minimum allowable temperature limit would not be exceeded during descent.



**Sealed Probe**

- Excellent Thermal Isolation
- Spherical Shape
- Payload Adapter Required
- Pyro Vent Valve Required



**Vented Probe**

- Adequate Thermal Isolation
- Cylindrical Shape
- Efficient Packaging of Equipment
- Lighter Weight

Figure V-50 Comparison of Descent Parametric Probe Configurations

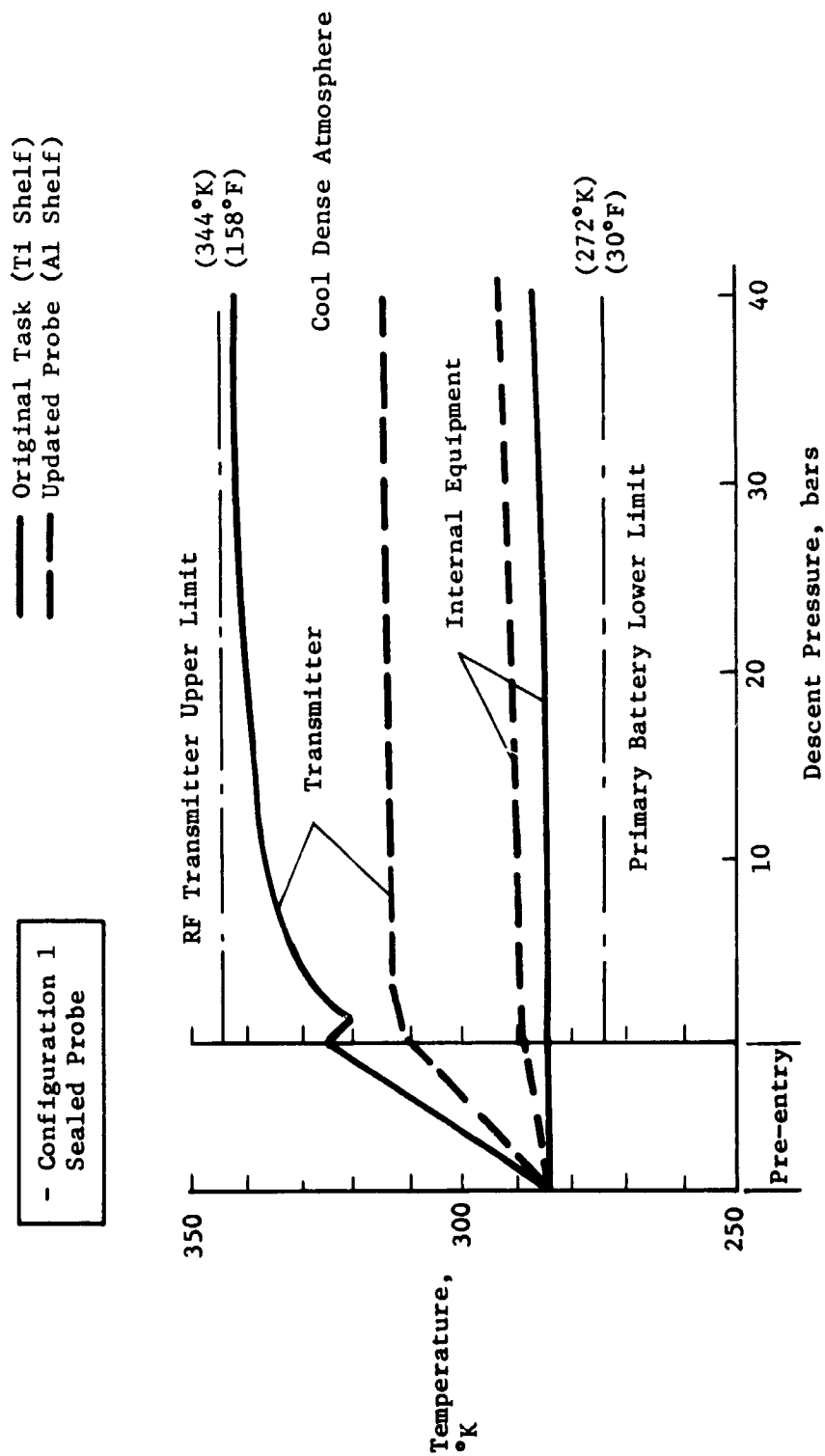


Figure V-51 Descent Thermal Analysis of Sealed Probe Configuration

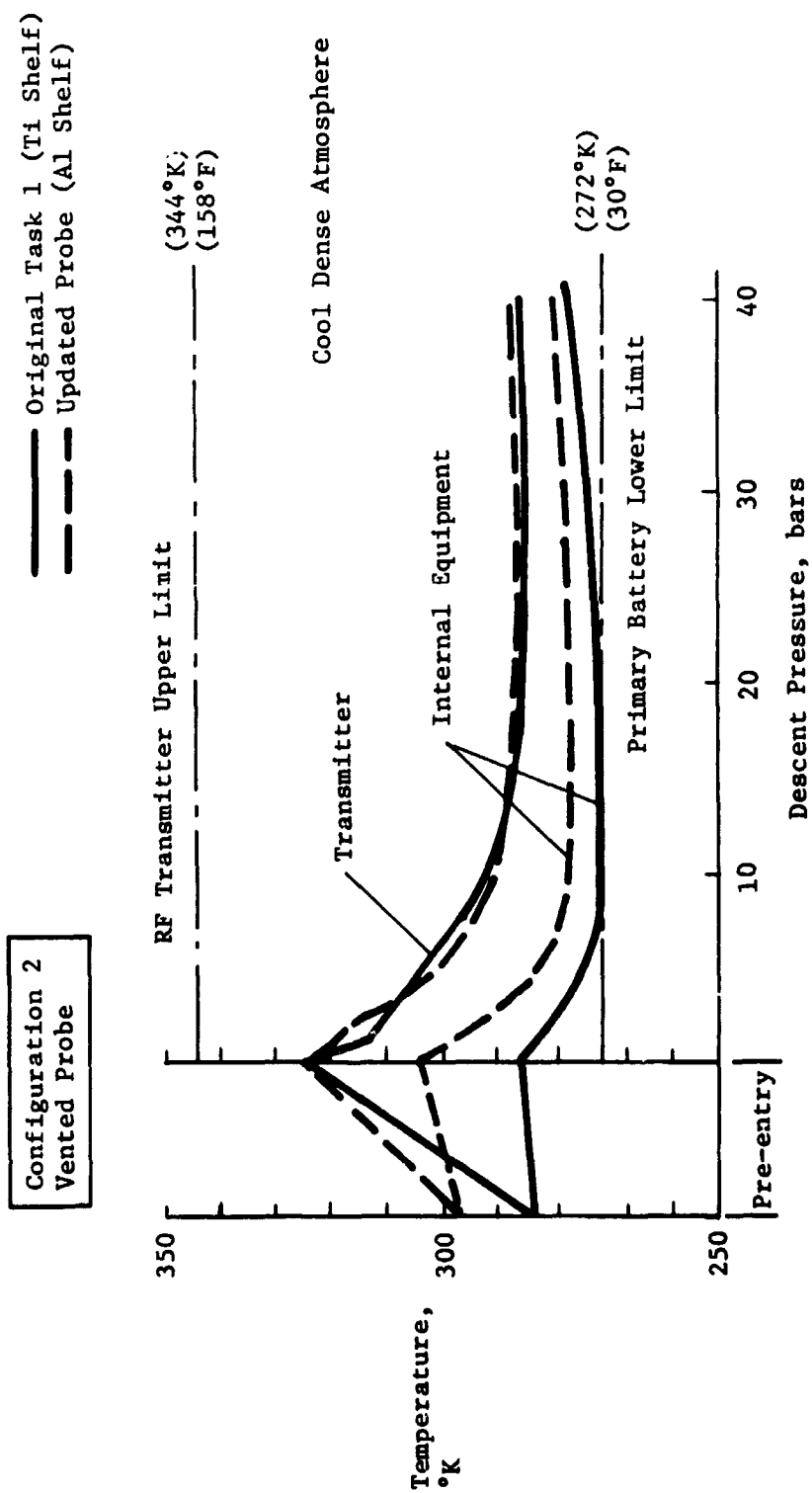


Figure V-52 Descent Thermal Analysis of Vented Probe Configuration

The vented descent probe configuration demonstrates the marked effect of atmospheric gas inside the probe. Degradation in the performance of the insulation thermal conductivity and strong coupling effects of internal free convection on the probe walls results in an increase in insulation heat leak by a factor of approximately an order of magnitude. The instantaneous heat leaks for the sealed and vented probe designs are presented in Figure V-53.

Although the sealed probe is more efficient thermally than the vented probe design, the vented probe was selected as the mission study probe configuration on the basis of its increased equipment package density and the savings of structural weight. Analyses show that the vented probe can provide sufficient thermal control to maintain internal probe temperature limits within allowable temperature limits. The use of the sealed probe configuration would be desired for deeper descent pressures where longer missions and more hostile atmospheric temperatures would be encountered.

Between the two Jupiter atmospheres considered for Jupiter probe mission studies (Fig. V-54), the more severe from a standpoint of thermal control is the cool/dense atmosphere. A comparison of both atmospheric encounters is presented in Figure V-55. The Jupiter mission science objectives produce different descent rates in each atmosphere. For comparable scientific return, the cool/dense requires a 33-minute descent to 30 bars pressure while the nominal atmosphere requires a 43-minute descent to 10 bars pressure. The vented probe design was considered for both missions and each probe used 1.9 cm of low density foam insulation.

For the cool/dense atmospheric descent, an initial probe entry temperature of 297°K was desired for optimum probe equipment temperature margin. The minimum probe temperature occurred at approximately 13 bars and considerable leeway for additional descent was available. For the nominal atmosphere descent, an initial probe entry temperature of 283°K was selected. This entry temperature allowed a reasonable margin to maintain the probe equipment above minimum temperature limits during descent and below the maximum allowable internal equipment temperature at 10 bars pressure. On the basis of previous cruise/coast parametric analyses, 32 W of radioisotope heater power would be required for the cool/dense atmosphere mission entry temperature of 297°K and 29 W of radioisotope heater power for the nominal atmosphere mission entry temperature of 283°K. For the nominal atmosphere encounter, the internal equipment temperature was rising sharply at the end of the desired descent (10 bars) and an extended mission would exceed temperature limits at approximately 14 bars.

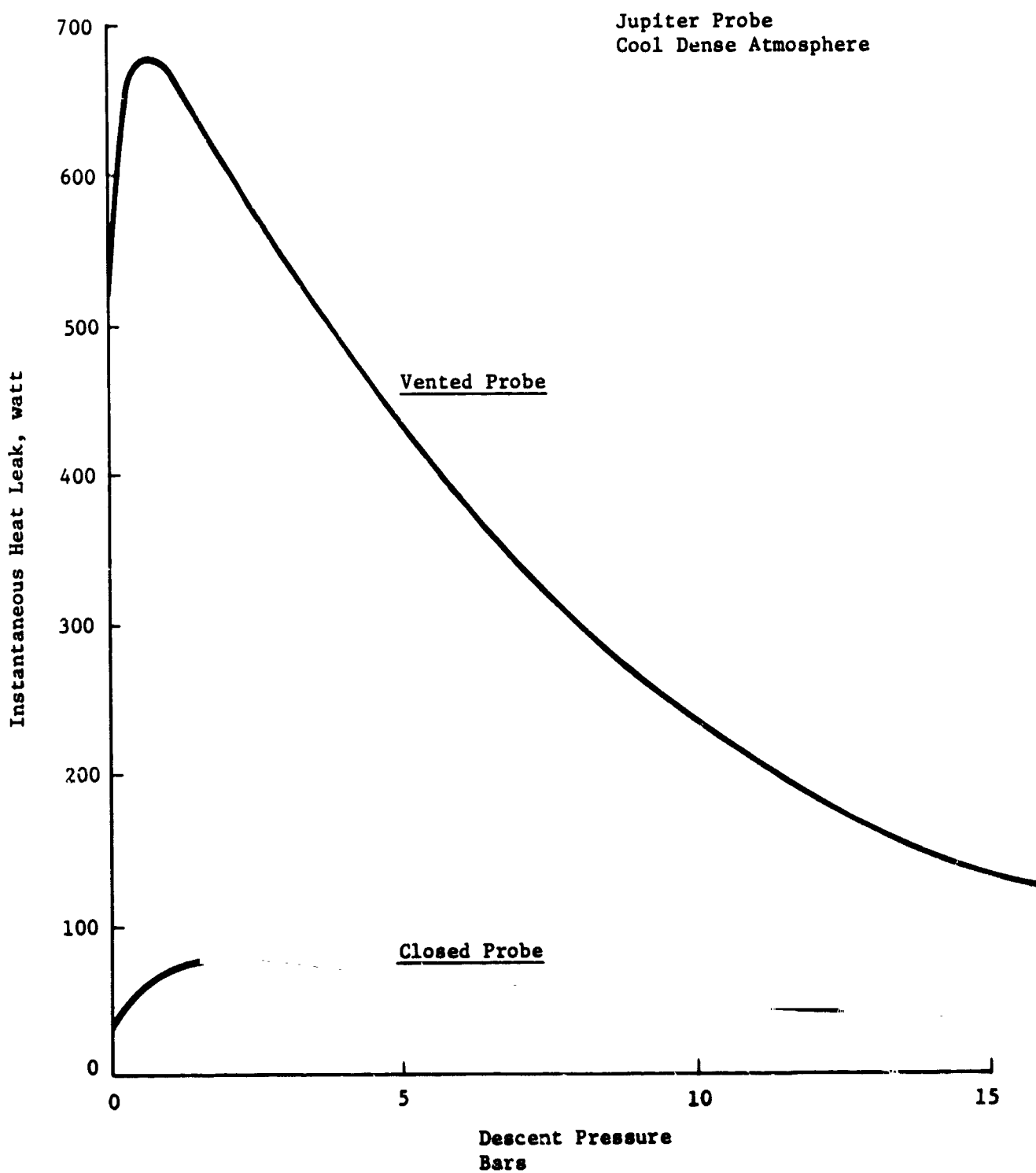


Figure V-53 Instantaneous Probe Heat Leak

V-100



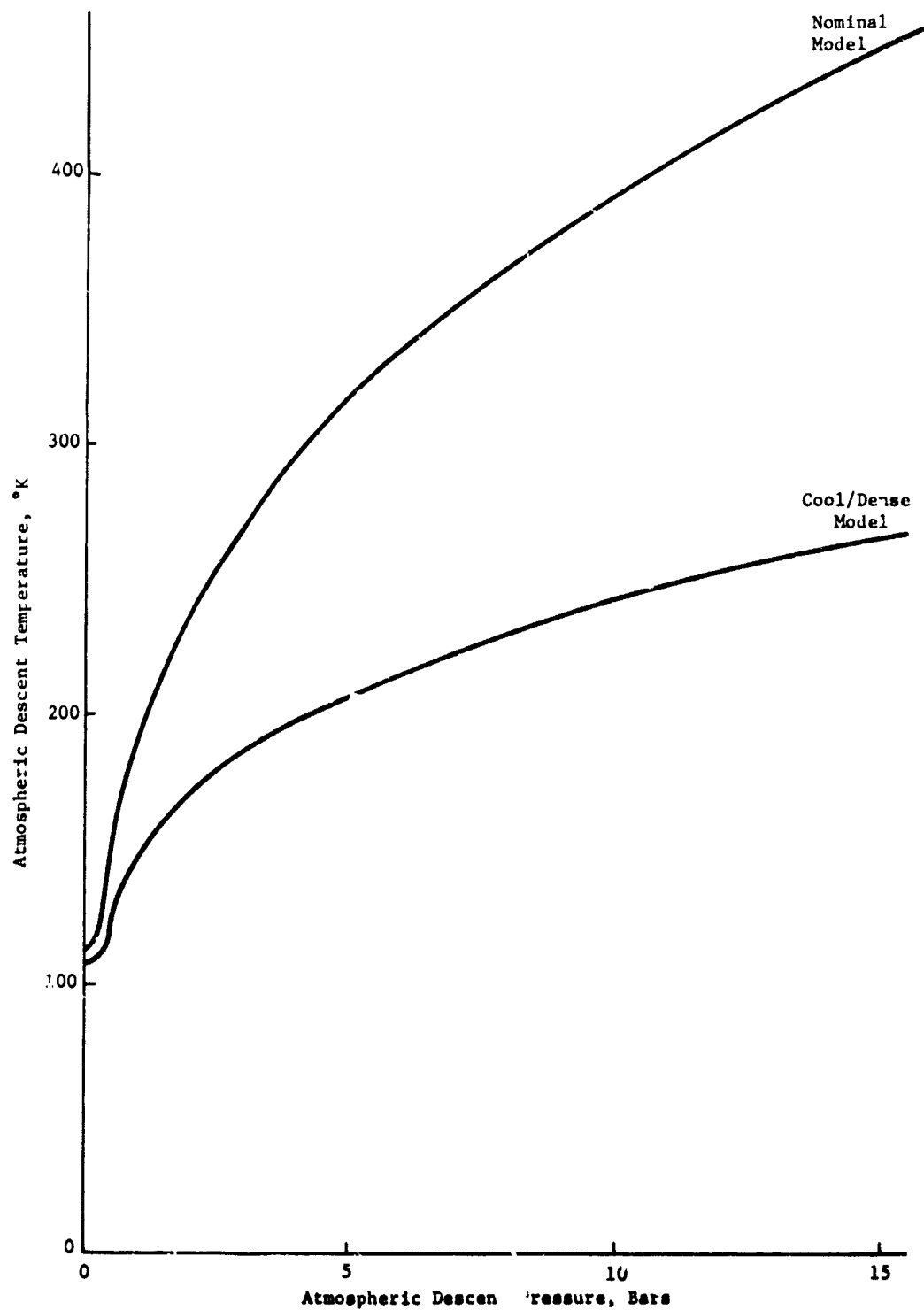


Figure V-54 Jupiter Atmospheric Models - Temperature vs Descent Pressure

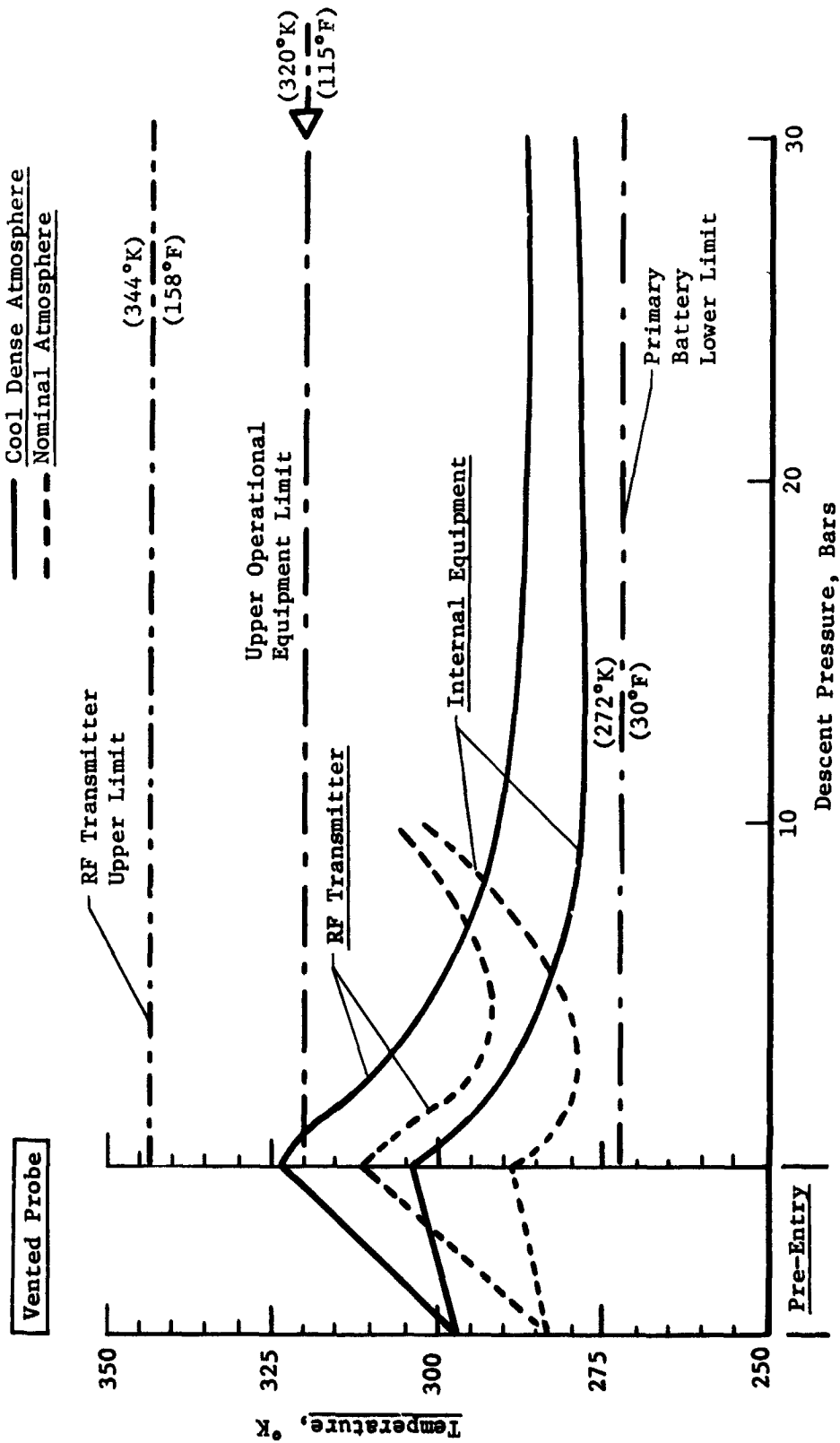


Figure V-55 Descent Thermal Analysis of Jupiter Cool/Dense and Nominal Atmospheres.

An alternative probe mission configuration investigated included a more powerful 40-W RF transmitter for possible direct link and 6 to 7  $R_J$  communication distances. Results for this configuration are presented in Figure V-56 and included mission descents in either the cool/dense or nominal Jupiter atmosphere. Analysis shows that basic probe thermal control is adequate to maintain the probe equipment within allowable temperature limits for these missions. A lower initial probe entry temperature of 283°K was desired, however, for the cool/dense atmosphere descent to maintain the RF transmitter below its upper allowable operating limit. An alternative fix for the RF transmitter could have been the use of phase change material that would melt at about 310°K and absorb approximately 30 W-hr of energy per pound of material.

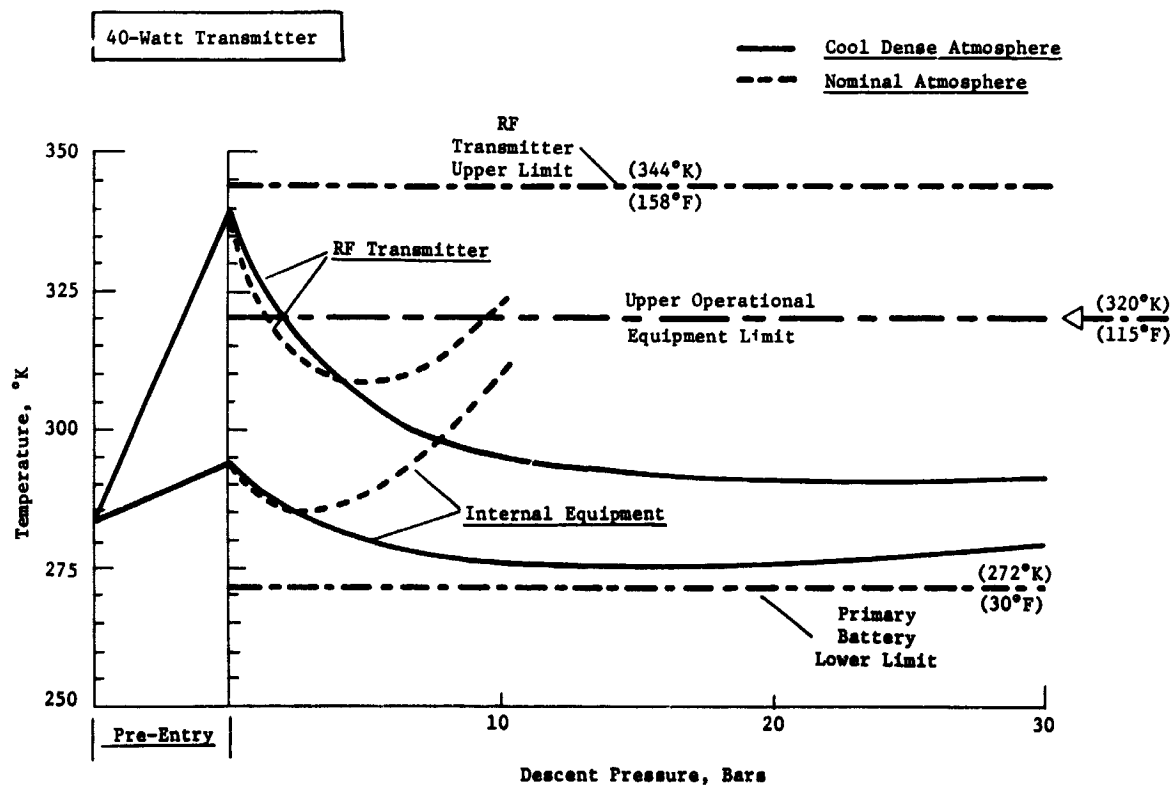


Figure V-56 Descent Thermal Analysis of High Power RF Transmitter for 6 to 7  $R_J$  and Possible Direct-Link Communications.

# 11. Subsystems Sensitivity to Radiation

Radiation effects will occur in most materials. The significance of these effects depends on the degree to which the critical performance characteristics of the material are involved. The pertinent literature available and current studies represent a tremendous volume of information on radiation effects and will not be unnecessarily rephrased here. Radiation problem areas of the probe are related to electronic/electrical degradation and chemical decomposition with associated loss of strength and outgassing. The expected radiation to which the components will be subjected is illustrated in Figure V-57.

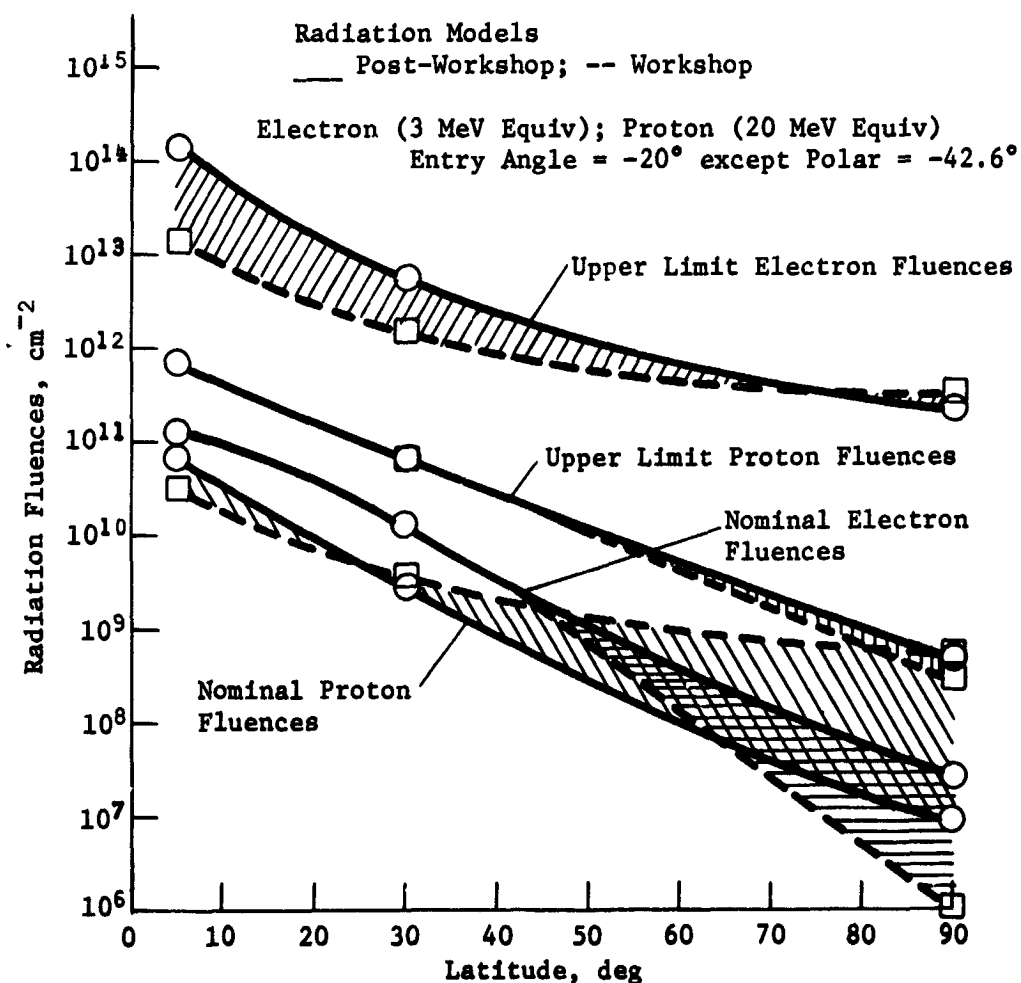


Figure V-57 Radiation Sensitivity to Latitude

a. *Electronic/Electrical Performance* - The principal effects of radiation on semiconductor electronics are the bulk damage effects and the radiation surface induced effects. Bulk damage disrupts the crystal lattice and causes a decrease in carrier lifetime in the base region of the device. This effect is independent of whether the device is active or not. Surface effects are more predominant when the device is under simultaneous electrical and radiation stress. This effect is mainly due to the interaction of ionized gas and ionized impurities with the semiconductor surface. A summary of expected radiation damage caused by proton fluences is illustrated in Figures V-58 and V-59 which were extracted from Reference 1. It is clear from this data that the electronic degradation caused by radiation at Jupiter is a serious design consideration. The critical devices that may be used in an entry probe are power transistors, power diodes, silicon controlled rectifiers, and analog IC circuitry. The scientific instruments with the possible exception of a thermionic cathode in the mass spectrometer do not appear to be susceptible to other than the electronic degradation mentioned above.

The design solutions for reducing the probability of failure caused by radiation involves selection of nonsensitive device types, testing and selecting parts where sensitive device types must be used, derating, redundancy and shielding in approximately that order.

Relays have been selected as a substitute for SCR and power distribution transistors. There are problem areas with relays in the pyrotechnic area caused by contact bounce and the high entry g-stress. The latter problem can be reduced by maintaining hold currents on the latching relays during entry and possibly hardwiring the accelerometer which is activated during entry through suitable buffer resistors. The contact bounce problem will require further study (see Vol III, Appendix G, this report). A major effort to digitize all circuitry must be made. The difficulty of designing effective redundant analog circuitry is well known. Where analog circuits are used, failure sensing approaches must be employed (i.e., loop gain sensing, pilot tones, test condition, etc). The remaining sensitive elements, power transistors, and power diodes remain a difficult area to solve. The entry power subsystem has been dispersed to the degree possible to minimize the stress on these devices. Nevertheless, the transmitter and mass spectrometer power conditioning represent significant hazards. Failure detecting devices for power equipment usually involves analog circuitry and may reduce reliability rather than improve it. Redundancy for this circuitry is frequently ineffective except at the cost of considerable weight and acceptance of

**Figure V-58** Typical Tolerance of Semiconductor Devices to Electron Irradiation

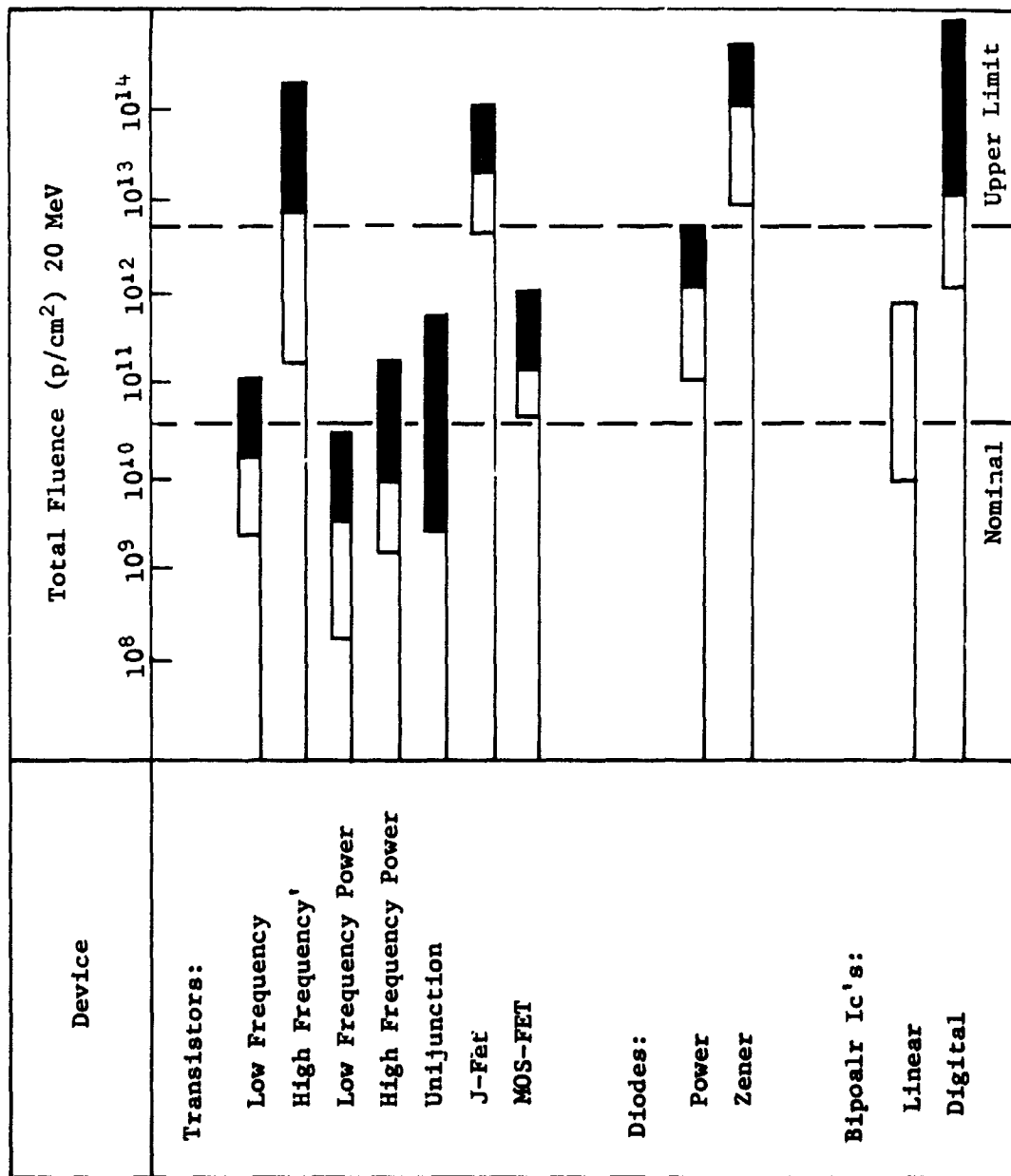


Figure V-59 Typical Tolerance of Semiconductor Device to Proton Irradiation.

heavy power margins for failed circuits. Fuses are a consideration but must be studied with respect to the high g-stress environment. Selection of power transistors would be required; the sensitivity of power transistors to radiation decreases with increased beta and cut-off frequency (Fig. V-60). The use of high temperature environments for annealing out bulk damage is considered ineffective for the mission profile under consideration because of the short annealing periods available. Ultimately it may be necessary to group the power devices together and provide heavy shielding. This will undoubtedly create a difficult but not insurmountable problem because coupling between elements from different circuits in a compact shielded package. Use of shielding must, in general, be a last resort caused by the cost of weight on the probe and the uncertainties with respect to the effectiveness of shielding in the Jupiter environment.

Studies of shielding effectiveness are in progress at Martin Marietta and elsewhere. There are areas of uncertainty in the precise knowledge of the proton radiation attenuation obtained by shielding and the degradation due to the proton radiation over the spectrum of energy levels and densities that theoretically exist in the Jupiter Van Allen belts. In addition the nature, energy distribution, and damage caused by the secondary radiation generated in the shield and interior of the probe is primarily speculative at this time. The Pioneer X, presently enroute to Jupiter, may resolve some of these uncertainties and provide more reliable design constraints.

The effect of radiation on organic compounds influences the electronic design in the areas of adhesives and plastics. The reduction of structural strength of the electronic devices and mounting surfaces must be evaluated with respect to the high g-stress entry environment. Loss of insulating properties caused by fracture or change of electrical properties is an obvious consideration. Electrical breakdown caused by outgassing products is a solvable problem in an adequately insulated design.

*b. Pyrotechnics* - According to Reference 9, after being irradiated, these devices are more sensitive to being ignited, operate at a lower temperature, and contain more energy. Premature operation might be expected because of the radiation environment. However, this is not a proven fact, and there is strong opinion that pyrotechnic devices may satisfactorily withstand the environment and be useable on the descent probe. Additional studies and tests are required to establish positive feasibility of pyrotechnic device on the entry probe.



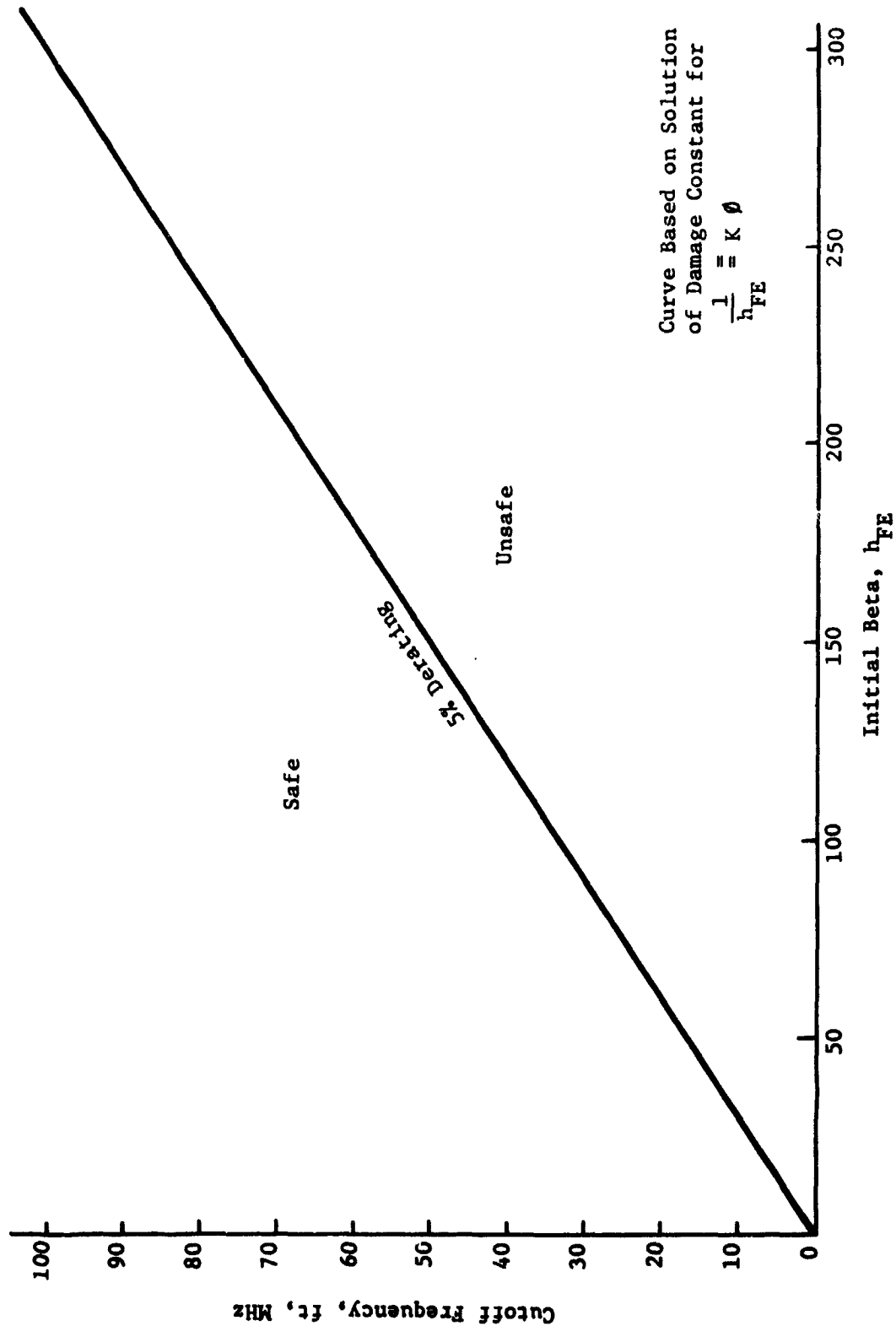


Figure V-60 Bulk Radiation Effects on NPN Power Transistors at  $10^{11} \text{ n/cm}^2$

c. *Propulsion* Reference 9 notes that solid propellants are damaged by radiation at approximately the same levels as pyrotechnics. Their damage consists of quicker ignition and propellant weight loss, which causes faster burning and reduced impulse. For the probe, the solid motors would be used at spacecraft-to-probe separation, before exposure to a high radiation dose.

d. *Materials* - The effect of nuclear radiation on organic materials is shown in Figures V-61 through V-63. The successful usage of organic materials on the entry and descent probe will be established by selection of appropriate materials for design. For metallic materials used in the probe, there is no problem.

e. *Summary* - In summary, the design of a radiation resistant probe would follow methods previously established. A flow chart which illustrates an organized approach for the design of radiation resistant subsystems is presented in Figure V-64. The problem at Jupiter appears to be considerably more severe than previously encountered in space system design and the survivability of the probe has not been established. The feasibility evaluation is further compromised by the uncertainties in the radiation model and the radiation effects.

f. *References*

1. *Preliminary Radiation Effect Considerations for Jupiter Entry Probes*. JPL Section Document 131-18.  
  
J. B. Barengoltz: *Jupiter Radiation Test Levels and Their Expected Impact on an Encounter Mission*. Attachment to JPL Document 131-18.
2. *Power Conditioning Equipment for a Thermoelectric Outer Planets Spacecraft*. General Electric Company. August 1970 (N70-39509).
3. J. Hungate: *Radiation Hazard to the Jupiter Turbopause Probe and Potential Solutions*. Martin Marietta Corporation (Memo October 4, 1971).
4. W. Pich, A. G. Holms-Siedle: *Permanent Radiation Effects in COSMOS Integrated Circuits*. Radio Corporation of America, 1969.
5. A. G. Holm-Siedle, K. H. Zaininger: *Designing MOS Systems for Radiation Environments*. Radio Corporation of America, 1969.

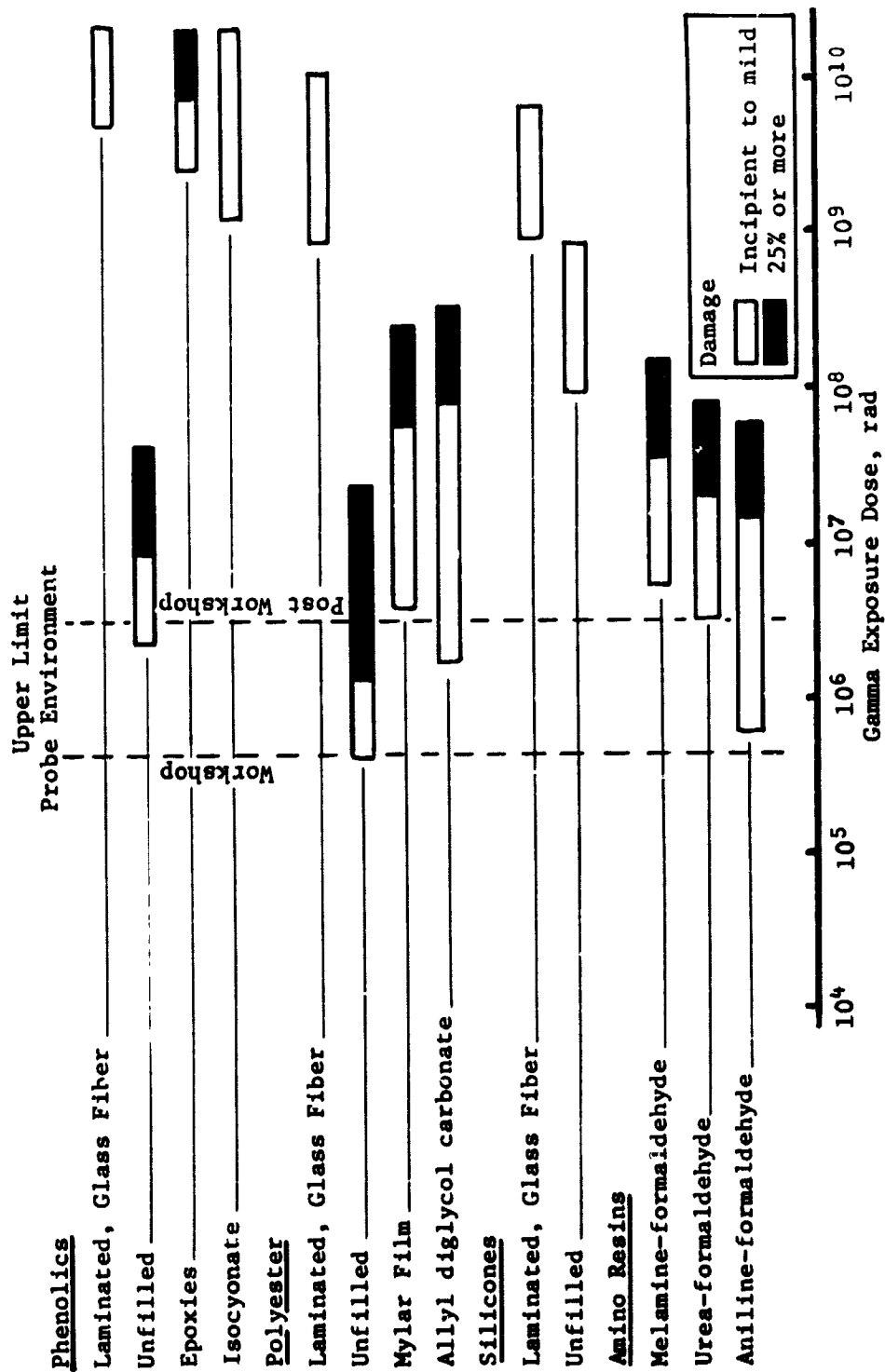


Figure V-61 Radiation Sensitivity of Thermosetting Resins

Legend:		DAMAGE	UTILITY OF PLASTIC
	Incipient to mild		Nearly always usable
	Mild to moderate		Often satisfactory
	Moderate to severe		Limited use
	Incomplete data		

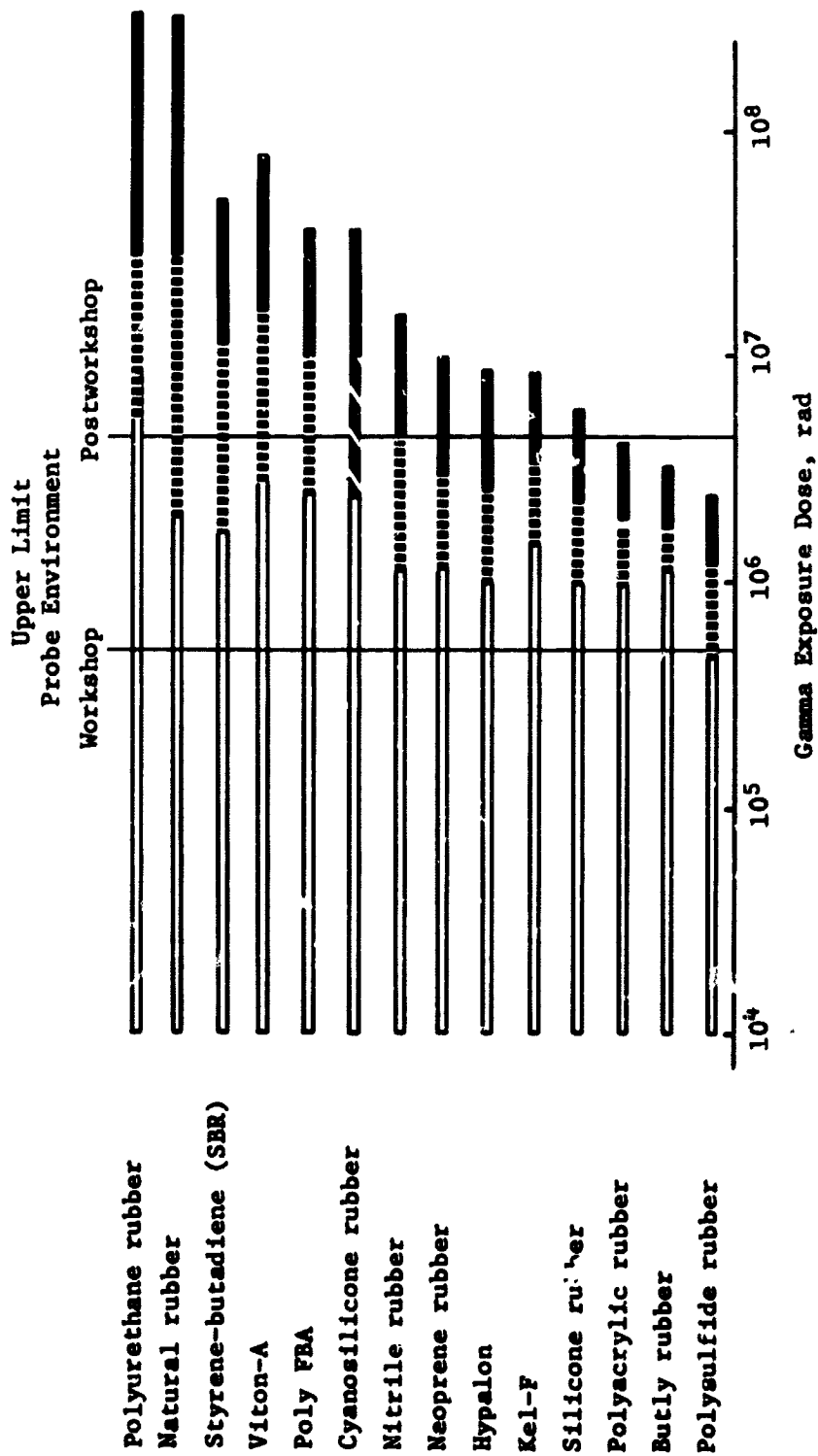


Figure V-62 Relative Radiation Stability of Elastomers

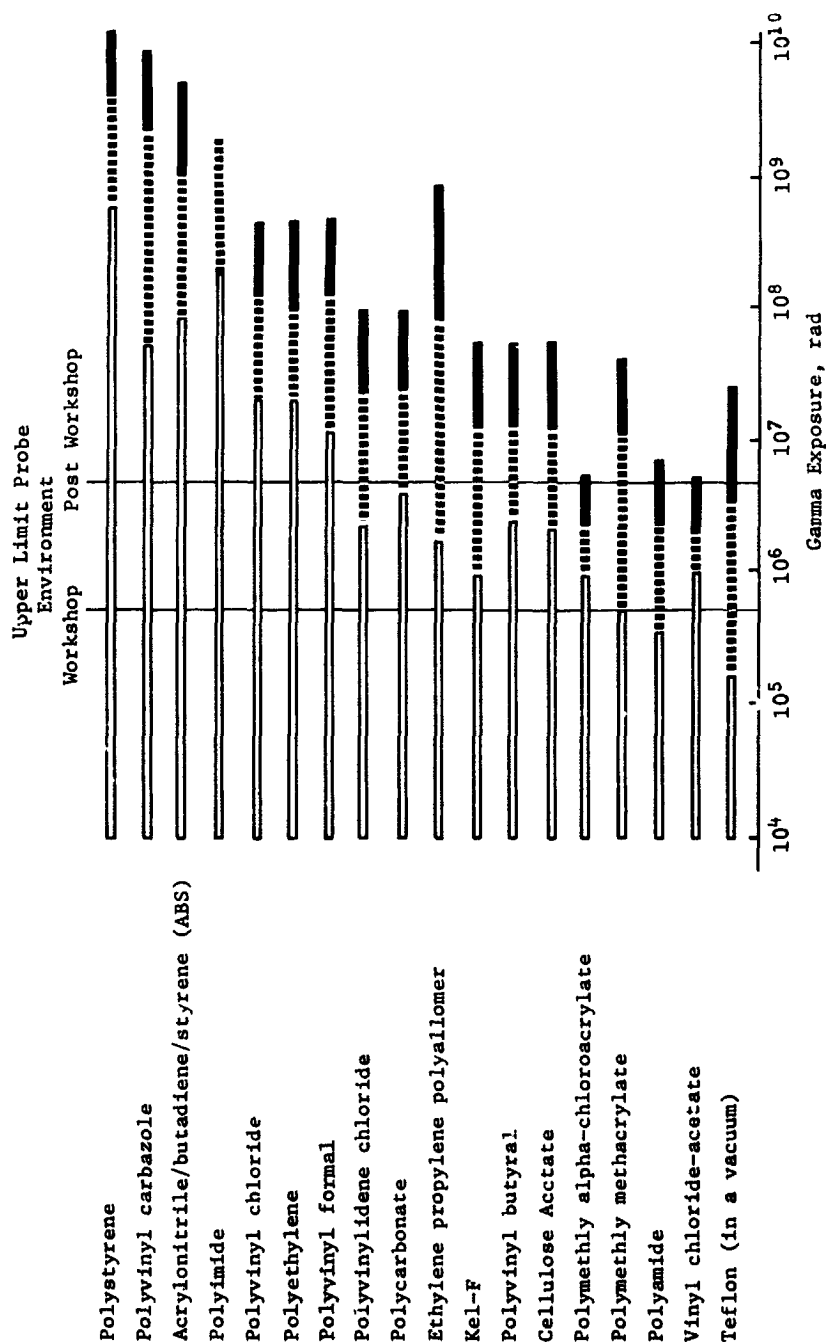
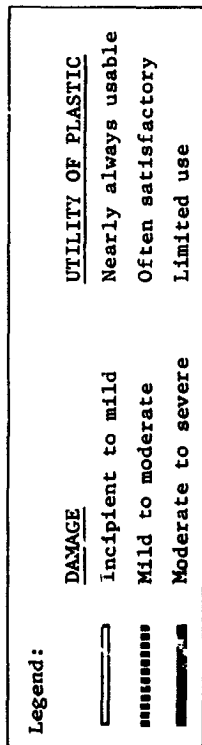


Figure V-63 Relative Radiation Resistance to Thermoplastic Resins

6. Martin Marietta Corporation Radiation Presentation (Viking) 1971.
7. *Viking Piece Part Nuclear Radiation Test Report*. TN-3770162, 1972. Martin Marietta Corporation.
8. J. L. Westrom, D. C. Atorthy: *Design Guidelines for Circuitry In a Nuclear Reactor-Propelled Spacecraft*. Lockheed, 1965.
9. Giulio Q. Varsi: "Radiation Effects on Pseudostable Material for Long-Term Space Mission." *American Nuclear Society*. October 17-21, 1971.

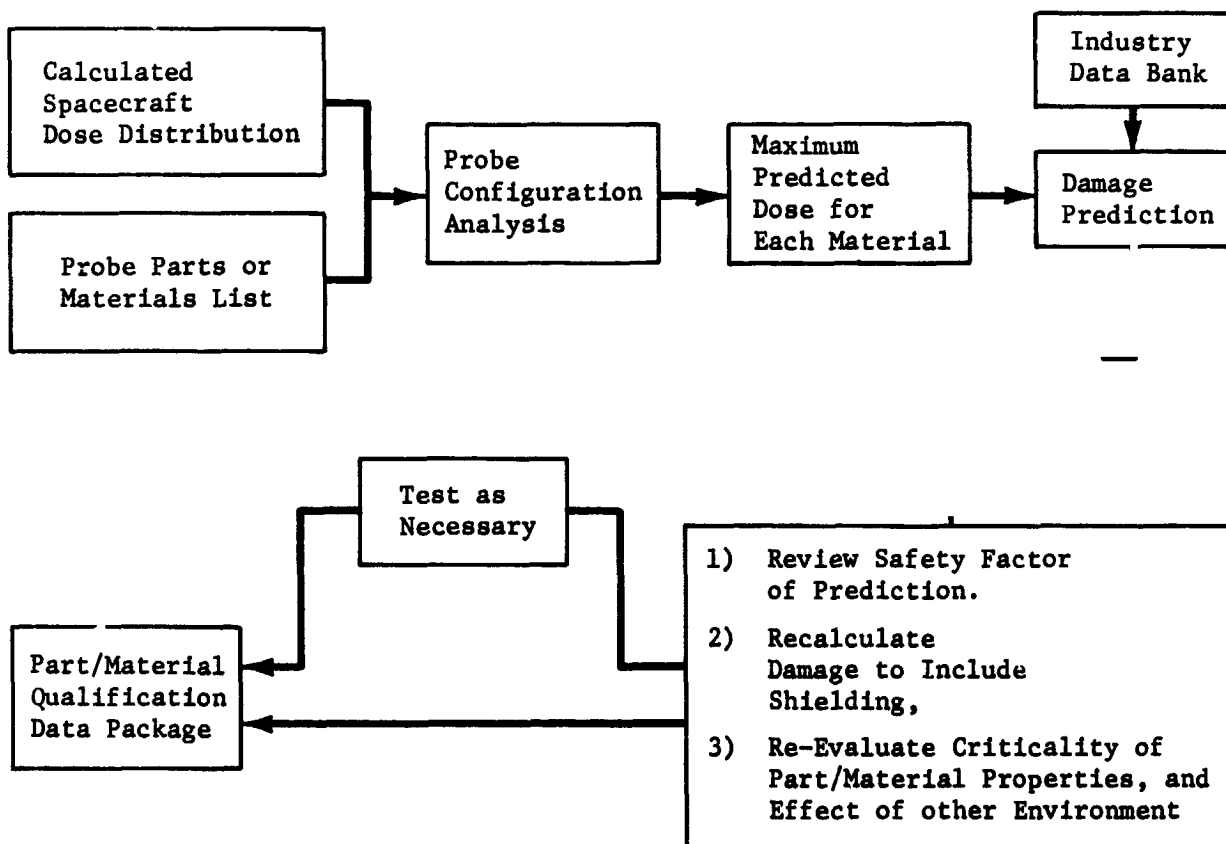


Figure V-64 Entry Probe Parts/Materials Evaluation Plan

## 12. Probe to Spacecraft Integration

During the program parametric analysis, identified in Figure V-1 and further defined in Table V-2, three candidate spacecrafts were considered. The nominal Jupiter probe discussed in Chapter V, Section B is the reference for each of the parametric point designs. This configuration used the Modified Outer Planet Spacecraft (MOPS) and the resulting point designs used either the Pioneer spacecraft or a Martin Marietta generated MOPS. The modifications to the three spacecraft were estimated and combined with the probe to give estimated launch weights as shown in Table V-13.

*Table V-13 Launch Weights for Parametric Point Designs*

Breakdown \ S/C	MOPS	MOPS (MMC)	Pioneer			
	Probe Deflection, lb	S/C Deflection, lb	Probe Deflection, lb	S/C Deflection, lb	Probe Deflection, lb	Shared
Spacecraft	1450	1041	996	547	547	547
S/C Adapter	30	38	38	43	43	43
Probe	339	255	339	253	339	337
S/C Modification	--	--	--	--	--	--
Communications	12	47	47	92	59	86
Cabling	1					
Thermal	2					
Mechanisms	5					
Structures	37	125	0	14	0	13
Propulsion	0					
15% Margin	8	7	7	14	9	13
Launch Weight, lb	1884 lb	1513 lb	1427	949	997	1026

Interface requirements between the probe and a three-axis stabilized spacecraft like the MOPS identified a tradeoff relative to probe tipoff errors at probe separation. Since the probe is spin-stabilized, it is desirable to have the probe spinning just before separation and have the spacecraft point the probe in a known direction. In order to minimize the effect of the tipoff errors, three solutions were considered:

- 1) Addition of a spin table to the spacecraft for probe spinning;
- 2) Spinning the spacecraft itself;
- 3) Making the probe ACS more accurate.

The last alternative was baselined. The probe separation errors are discussed in detail in Chapter V, Section A,7.

### 13. Summary of Parametric Analysis

This data contained in this subsection was used to establish the constraints, summarized in Sections C and D to control the definition of the two alternative Jupiter probes.

The major program parametric analyses are identified in Figure V-1 and further defined in Table V-2. Results of these analyses are as follows.

- 1) *Entry Angle Impact* - Figure V-65 shows the probe weight variations as a function of entry angle for the cool/dense atmosphere and an estimate for the nominal atmosphere. These are based upon a periapsis radius of  $2 R_J$ . A periapsis radius of  $6 R_J$  is shown for comparison. Figure V-66 shows the RF power requirement variation as a function of entry angle.
- 2) *Entry Latitude Impact* - Figures V-67 and V-68 show the probe ejected weight and radiation fluence variation, respectively, as a function of entry latitude. The radiation data was taken from Table II-2 and from similar data for the post-workshop radiation model.
- 3) *Pressure Depth Impact* - Figures V-69 thru V-71 and Table V-14 show the impact of descent depth on science objectives, RF power, and thermal control.
- 4) *Deflection Mode Impact* - Table V-15 shows the  $\Delta V$  requirement variations for the three deflection modes. It is noted that the shared mode is not competitive with the other two.
- 5) *Mission Launch Date Impact* - Figure V-72 shows the payload capability of the T-IIIE/Centaur/Burner II launch vehicle as a function of launch period for the years 1978 thru 1982. In addition, the figure shows various spacecraft/probe combinations.



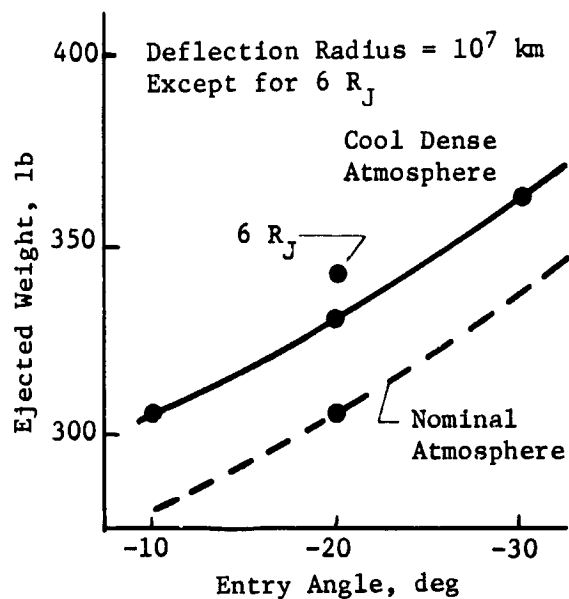


Figure V-65 Weight vs Entry Angle

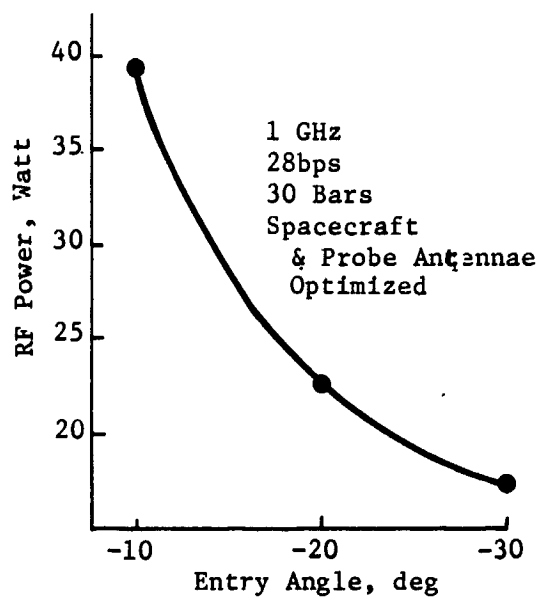


Figure V-66 RF Power vs Entry Angle

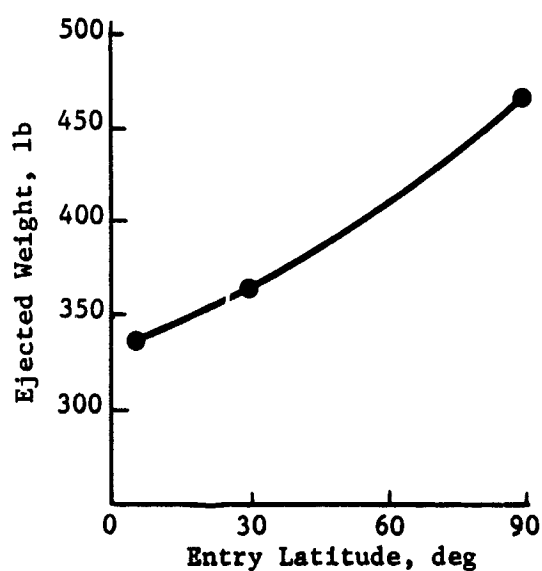


Figure V-67 Weight vs Latitude

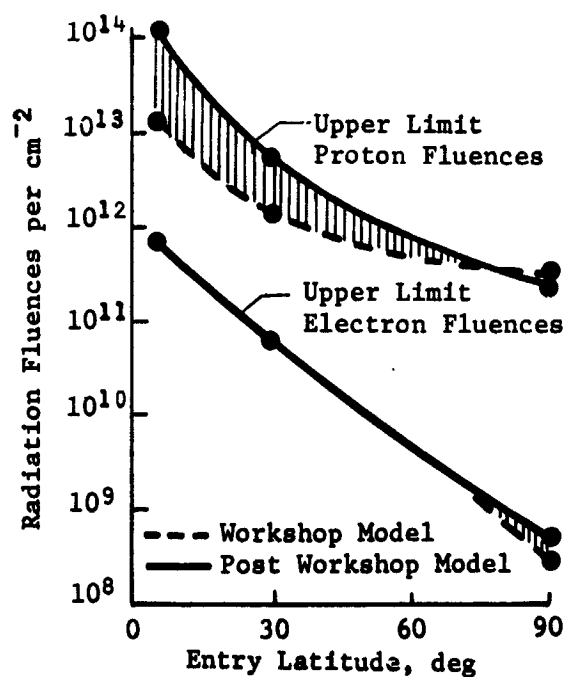


Figure V-68 Radiation vs Latitude

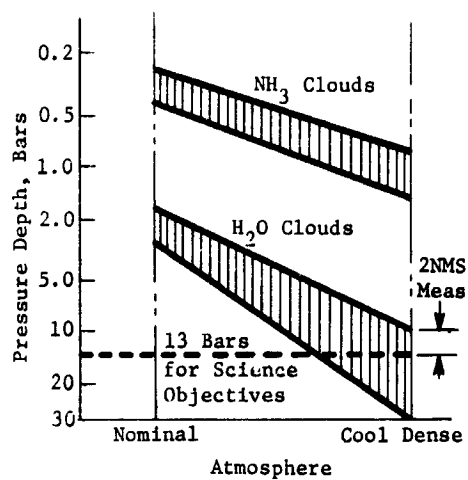


Figure V-69 Pressure Depth for Science Objectives

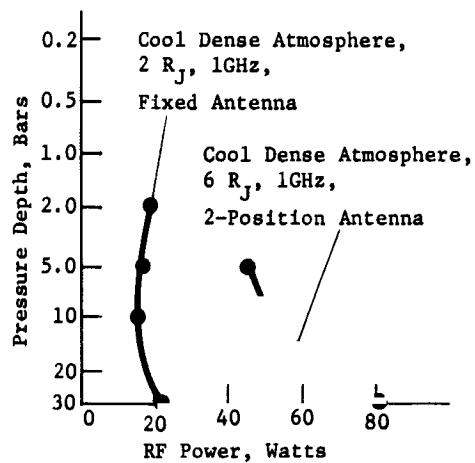


Figure V-70 Pressure Depth vs RF Power

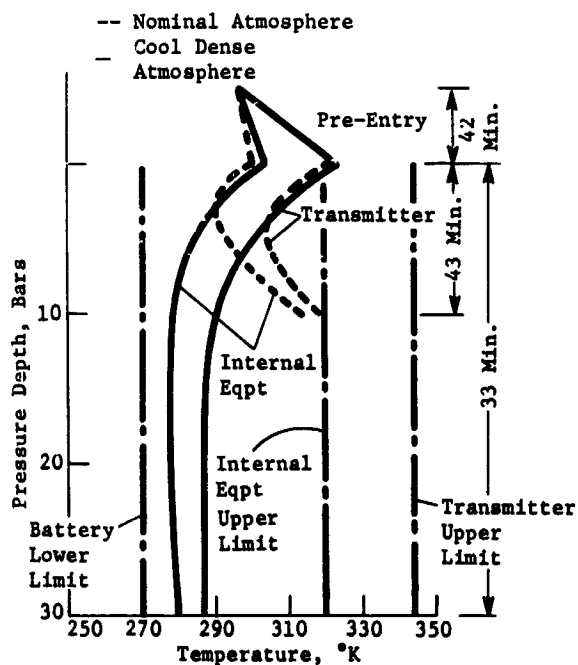


Figure V-71 Pressure Depth Impact on Thermal Control

Table V-14 Pressure Depth vs RF Power

Mission Ref Table V-2	RF Power, W	
	30 bars	10 bars
Point Design No. 1	23	16
Point Design No. 5		12.4
Point Design No. 3	29	20
Point Design No. 8		
2 Position Search	81	52
3 Position Search	36	23
Direct Link	31 400*	19.5 37.5*
*2.3 GHz, All other powers are for 1 GHz		

Table V-15 Deflection Mode Velocity Requirements

Deflection Mode	Probe $\Delta V$ , m/s	Spacecraft $\Delta V$ , m/s	Total $\Delta V$ , m/s
Probe	221	0	221
Spacecraft	0	221	221
Shared	246	201	447

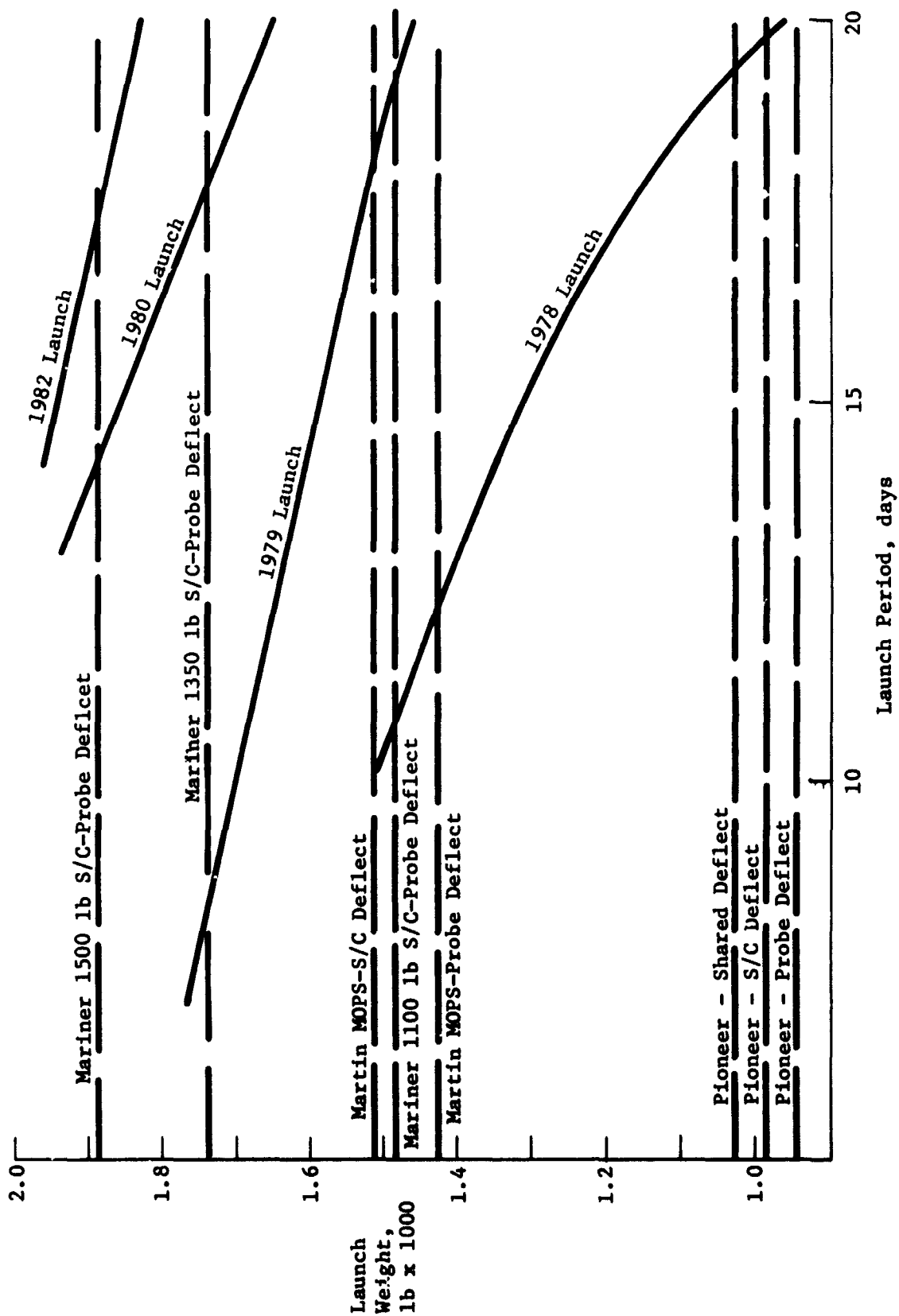


Figure V-72 Spacecraft-Probe-Mission Candidates for the Titan IIIIE/Centaur/Burner II

B. NOMINAL JUPITER PROBE SYSTEM DEFINITION

This nominal Jupiter probe was defined essentially as a reference configuration to assist in the conduct of the parametric analysis of Section A. The constraints for this configuration are:

Mission	Type I for 1979
Entry Angle	-20°
Entry Latitude	5°
Depth of Descent	2 to 30 Bars
Velocity and Pressure	Less than Mach 1 above 100 mb
Science	SAG Exploratory Payload (Viking)
Atmosphere	Cool/Dense
Spacecraft	TOPS
Carrier Mode	Flyby
Periapsis Radius	2 $R_J$
Communication Mode	Relay Link
Deflection Mode	Probe
Radiation Belt Model	Nominal

1. Science Instrumentation and Performance

Many of the mission characteristics of the nominal Jupiter probe were specified in the statement of work. The science instruments were specified to be Viking-derived wherever possible. The characteristics of the resulting nominal Jupiter probe instruments are shown in Table V-16. The temperature gage is the Viking parachute phase instrument, its range of operation is sufficient for Jupiter. Two pressure transducers are necessary to cover the pressure range required: One with a range similar to that of the Viking instrument (0-300 mb); the other with a larger range. The accelerometer triad is the Bell Model IX 3-axis system with pulse rate convertor, with a modification to scale up the flexure for 1600 peak load. Discussions with Bell Aerospace indicate this

is a minor change. The proposed mass spectrometer deviates from the Viking upper atmospheric instrument, but is considered to be a magnetic sector analyzer with a porous leak remote inlet system. The given characteristics are compatible with Viking derivations. (See Chapter III, Section C for further instrument details.)

Table V-16 Nominal Instrument Characteristics (Viking-Derived)

Instrument and Component	Weight, lb	Power, watts	Volume, in. <sup>3</sup>
Temperature Gage (including deployment mechanism)	1.0	1.4	26
Pressure Transducers (2)	1.7	2.8	32
Accelerometer System		2.8	
Triad Sensor	1.3		16
Pulse Rate Converter	2.1		40
Neutral Mass Spectrometer		16.0	
Analyzer	5.0		114
Electronics	6.0		210
Pump	1.0		27
Plumbing and Ballast Tank, 1 liter	1.0		61
Totals	19.1 (8.66 kg)	23.0	526 (86,203 cm <sup>3</sup> )

The nominal Jupiter probe analysis considered only the cool/dense atmosphere and the descent profile was chosen with this assumption. Also, this initial task was to determine how a descent to 30 bars could be performed. The resulting parametric values, which are consistent with the criteria, follow.

Design pressure limit = 30 bars

Main parachute ballistic coefficient = 6.12 slug/ft<sup>2</sup> (18.84 kg/m<sup>2</sup>)

Drogue parachute ballistic coefficient = 1.50 slug/ft<sup>2</sup> (235.5 kg/m<sup>2</sup>)

Separation pressure = 10 bars

Parachute deployment pressure = 92 millibars.

Pressure at first measurement = 111 millibars

The entry and descent times, instrument sampling times, and resulting bit rates are shown in Table V-17. The transmission bit rate is significantly higher than the collection bit rate because the data taken during the 5-minute-acquisition period is stored and must be interleaved with the real time data. Total mission time from entry to 30 bars is 33 min 40 sec. The pressure descent profile is given in Figure V-2 using the appropriate ballistic coefficient. In addition to this, the radius and velocity descent histories are given in Figure V-73.

Table V-17 Nominal Jupiter Probe Instrument Sampling Times and Data Rates

Phase	Instrument	Sampling Times, sec	Collection Bit Rate, bps	Transmission Bit Rate, bps
Entry, 34 sec	Accelerometers			
	Longitudinal	0.1	100	0.0
	Lateral	0.2	50	0.0
	Lateral	0.2	50	0.0
Descent, 2002 sec	Temperature	5	2	2.4
	Pressure	5	2	2.4
	Mass Spectrometer	50	8	9.3
	Accelerometers			
	Turbulence	10	6	7.1
	Stored	0	0	4.0
Science Total				25.2
Engineering and Formatting				2.8
Total				28.0

Table V-18 presents the measurement performance for the nominal Jupiter probe mission. All of the requirements have been satisfied, the numbers in the ziptoned box showing the critical measurements. Note that the mass spectrometer sampling time is given here as 60 sec, and it satisfies the requirements. Thus, the 50 sec used in Table V-17 to calculate the bit rate is conservative.

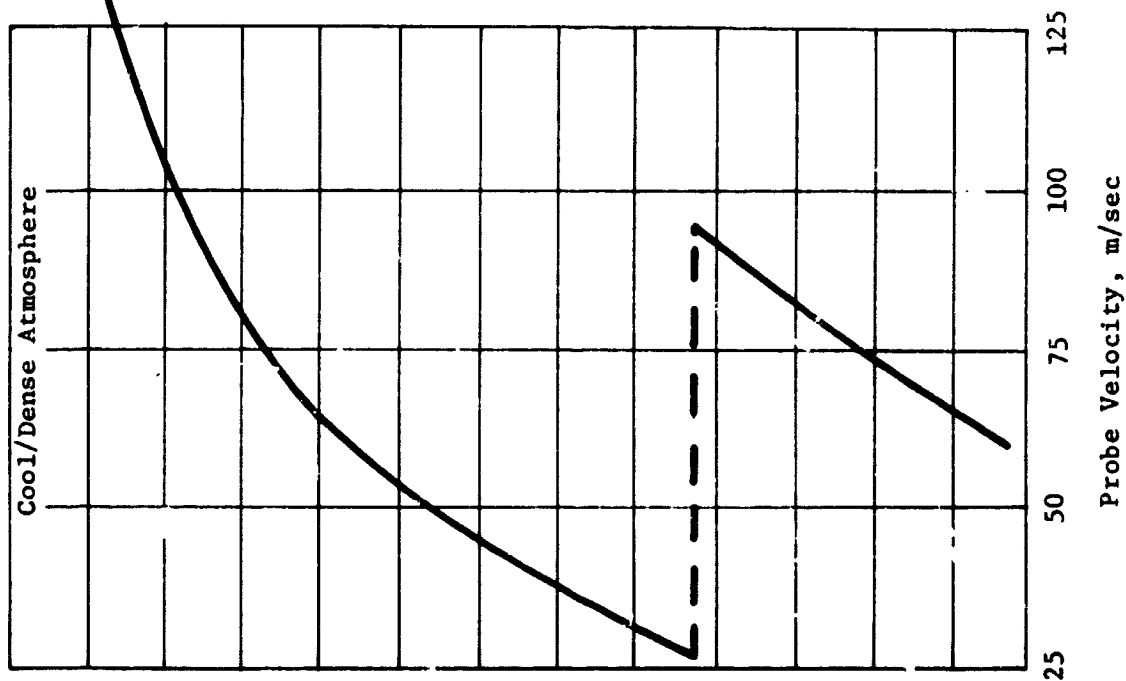
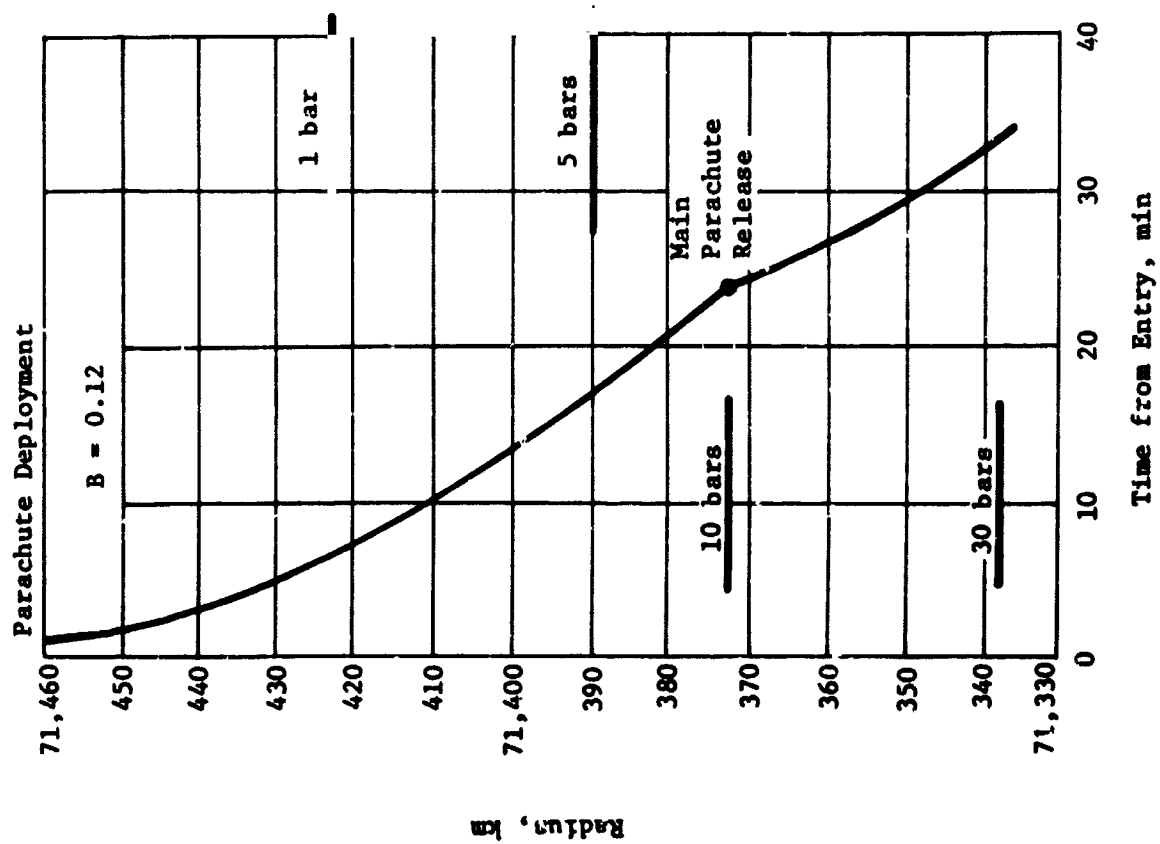


Figure V-73 Time and Velocity vs Descent Radius



Table V-18 Nominal Descent Measurement Performance

Instrument and Measurement	Criteria	Descent Performance (b = 0.12)
Mass Spectrometer		( $\Delta t = 60$ sec)
Minor Constituents	2 per scale height*	4.3 to 18
Cloud Layering	2 inside cloud	<del>2.4</del> in $\text{NH}_3$ 8.0 in $\text{H}_2\text{O}$
H/He Ratio	4 measurements	36 measurements
Isotopic Ratios		
Molecular Weight		
Temperature Gage		( $\Delta t = 5.0$ sec)
Temperature	1 per $^\circ\text{K}$	<del>1.0</del> to 3.7
Cloud Layering	2 inside cloud	23 in $\text{NH}_3$ 92 in $\text{H}_2\text{O}$
Pressure Gage		( $\Delta t = 5.0$ sec)
Pressure	2 per $\text{km}^*$	<del>2.1</del> to 7.3
Turbulence	1 per $\text{km}^*$	2.1 to 7.3
Cloud Layering	2 inside cloud	23 in $\text{NH}_3$ 92 in $\text{H}_2\text{O}$
Accelerometers		( $\Delta t = 10$ sec)
Turbulence	1 per $\text{km}^*$	<del>2.0</del> to 3.6
*Below cloud tops.		

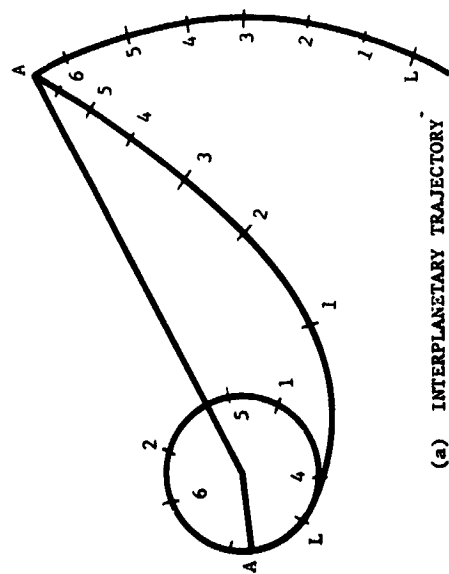
## 2. Mission Definition

The nominal Jupiter probe mission is pictorially described in Figure V-74 and detailed in Table V-19. Important mission design results are summarized in this section.

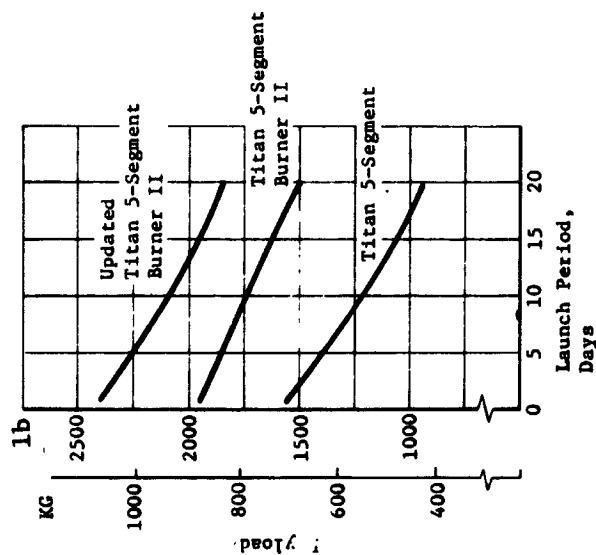
*a. Interplanetary Trajectory Selection* - The interplanetary trajectory is pictured in Figure V-74(a) with 100-day intervals noted. The launch date of November 7, 1979 and arrival date of September 17, 1981 (trip time of 680 days) result in a maximization of the payload weight as discussed in Chapter IV, Section A. As indicated in the figure, the spacecraft arrives at Jupiter shortly before the view to Jupiter is obstructed by the Sun.

*b. Launch Analysis* - The launch analysis is provided in Figure V-74(b). Available payload is plotted against launch period for three sets of launch vehicle performance data: standard data for the Titan 5 Segment vehicle with and without Burner II, plus updated data for the Burner II. For reference, the payload weight (probe, spacecraft, spacecraft modifications, and spacecraft-launch vehicle adapter) is about 1000 lb for a Pioneer mission and 1500 lb for a MOPS mission. Thus, the Burner II option is necessary for a MOPS-type mission to obtain a 20-day launch period. The nominal launch trajectory summarized in Table V-19(a) indicates that the daily launch window and parking orbit coast time are satisfactory.

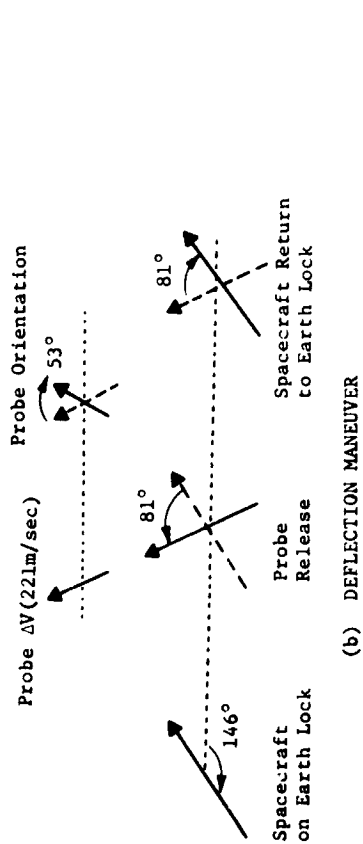
*c. Approach Trajectories* - The approach trajectory is pictured in Figure V-74(a) and summarized in Table V-19(a). The spacecraft trajectory was selected with a periapsis radius of  $2 R_J$  to obtain a good communication geometry between the probe and spacecraft during the probe descent phase. The inclination of  $10^\circ$  (with respect to the orbital plane of Jupiter) was chosen so that the probe entry site defined by a latitude of  $5^\circ$  and an entry angle of  $-20^\circ$  could be achieved with the in-plane deflection. The communication geometry chosen has a lead angle of  $-12.05^\circ$  (probe leading spacecraft at entry) so that the probe aspect angle at the start of descent is  $21^\circ$ , passes through zero during descent, and is  $5^\circ$  at the end of mission (EOM).



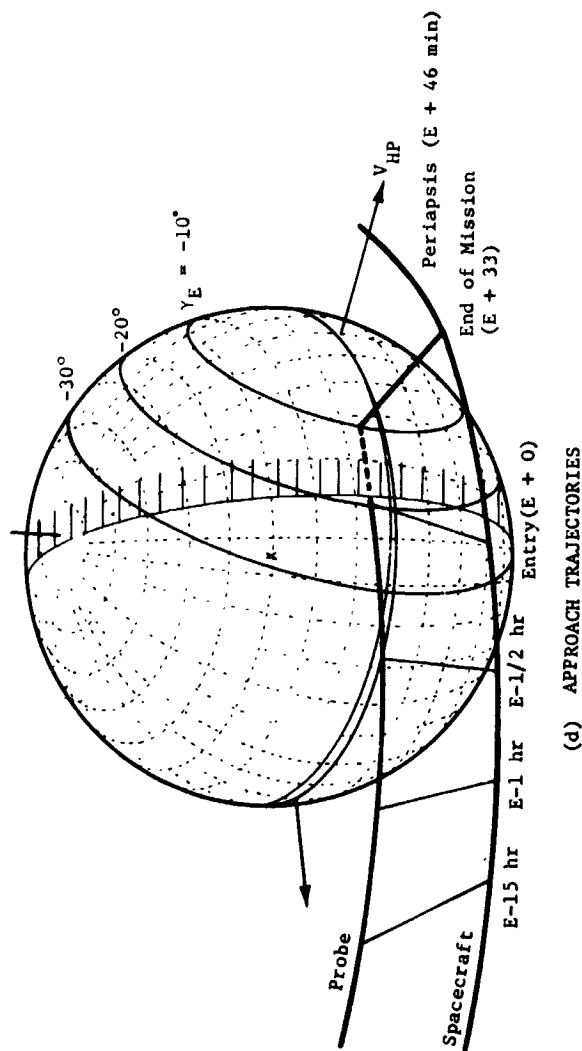
(a) INTERPLANETARY TRAJECTORY



(b) LAUNCH ANALYSIS



(c) DEFLECTION MANEUVER



(d) APPROACH TRAJECTORIES

Figure V-74 Nominal Jupiter Probe Mission Description

Table V-19 Nominal Jupiter Probe Mission Summary

a. Conic Trajectory Data

Interplanetary Trajectory	Launch Trajectory	Arrival Trajectory
Launch Date: 11/7/79 Arrival Date: 9/17/81 Flight Time: 680 days Central Angle: 155°	Nominal C <sub>3</sub> : 93.6 km <sup>2</sup> /sec <sup>2</sup> Nominal DLA: 30.5° Launch Window: 1.17 hr Parking Orbit Coast: 36 min C <sub>3</sub> (10 day): 97.5 km <sup>2</sup> /sec <sup>2</sup> C <sub>3</sub> (20 day): 105 km <sup>2</sup> /sec <sup>2</sup> Azimuth Range: 101.7° - 115°	VHP: 8.474 km/sec RA: 161.3° DEC: 6.81° ZAE: 145.2° ZAP: 141.4° RP: 2 R <sub>J</sub> INC: 10°

b. Deflection Maneuver and Probe Conic

Deflection Maneuver	Probe Conic Definition
Deflection Mode: Probe Deflection Radius: 10 x 10 <sup>6</sup> km Coast Time: 9.75 days ΔV: 221 m/sec Application Angle: 116° Out-of-Plane Angle: 0° Rotation for Probe Release: 81° Probe Reorientation Angle: -53° Spacecraft ΔV from Earth: NA	Entry Angle: -20° Entry Latitude: 5.0 Entry Longitude: 88.9 Lead Time: 45.8 min Lead Angle: -12.05° Probe-Spacecraft Range (Entry): 96,742 km Probe Aspect Angle (Entry): 43.9° Probe Aspect Angle (Descent): 21.0° Probe Aspect Angle (EOM): 4.7°

c. Dispersion Analysis Summary

Navigation Uncertainties	Execution Errors (3σ)	Dispersions (3σ)
Type: Range-Doppler 167-day arc SMAA: 1482 km SMIA: 139 km β: 88° TOF: 54 sec	ΔV Proportionality: 1% ΔV Pointing: 2° Probe Orientation Pointing: 2°	Entry Angle: 1.1° Angle of Attack: 2.5° Down Range: 2.02° Cross Range: 0.80° Lead Angle: 4.4° Lead Time: 7.4 min Entry Time: 8.0 min

d. Entry and Descent Trajectory Summary

Entry Parameters	Descent Parameters	Critical Events	
		Time from Entry	Altitudes above 1 atm
Entry Velocity, km/sec: 60 Entry Altitude, km: 304.6 Entry B, slug/ft <sup>2</sup> : 0.65 kg/m <sup>2</sup> : 102.1 Entry Atmosphere: Cool/Dense Max Deceleration, g: 1500 Max Dynamic Pressure, lb/ft <sup>2</sup> : 2.1 x 10 <sup>4</sup> kg/m <sup>2</sup> : 1.0 x 10 <sup>6</sup>	Descent Atmosphere: Cool/Dense EOM Pressure, bar: 30 Descent B, slug/ft <sup>2</sup> : slug/ft <sup>2</sup> : 0.12 kg/m <sup>2</sup> : 18.84	g = 0.1, sec: 5.5 Max g, sec: 12 M = 0.7, sec: 34 Descent Time, min: 33.3 EOM, min: 33.8	km: 182 km: 65 km: 32 km: -85

d. *Deflection Maneuver* - The probe deflection mode was used for the deflection maneuver for this mission. The deflection maneuver is illustrated in Figure V-74(b) and summarized in Table V-19(b). The deflection radius of 10 million km resulted in a  $\Delta V$  of 221 m/sec and a coast time (time from deflection to probe entry) of 9.8 days. The  $\Delta V$  is applied at an angle of  $116^\circ$  to the approach asymptote and is in the plane of the spacecraft trajectory. The spacecraft must rotate  $81^\circ$  from its Earth-lock attitude of release the probe. After firing the  $\Delta V$ , the probe must precess  $53^\circ$  to obtain the attitude required for zero relative angle of attack.

e. *Dispersion Analysis* - The navigation and dispersion analysis results are summarized in Table V-19(c). The navigation uncertainties have little impact on dispersions at entry even assuming only a standard range and Doppler tracking arc. All the entry parameter dispersions are within satisfactory tolerances. The communication parameter dispersions are discussed in Subsection B.4 of this chapter.

f. *Entry and Descent Trajectories* - Table V-19(d) summarizes the entry and descent phases of the mission. The cool/dense atmosphere model is used for both phases for this mission. The entry phase starts at 304.6 km above the 1 atm pressure level (0 km alt - 71,726 km) and ends at the staging of the aeroshell 34 sec later. During this phase, the peak deceleration of 1500 g is attained. The descent phase starts after staging and lasts until the end of the mission at 30 bars. The total mission time (entry and descent) is 33.8 min.

### 3. System Integration

a. *Functional Sequence* - Figure V-75 shows a pictorial sequence of events which identifies the functions with the equipment and also shows the interface between the probe and spacecraft. Table V-20 shows the sequence of events from launch until spacecraft periapsis for a mission duration of 680 days. After probe separation from the spacecraft, the probe is precessed for a zero angle of attack at entry, then down-moded for coast. The engineering data collected during this period is transmitted to the spacecraft just before shut down. After approximately 9.5 days of coast, the probe is activated by a probe timer. During pre-entry, the subsystems operate to monitor conditions of the probe and to initiate probe functions before entry including the start of science equipment warmup. Near entry, accelerometers sense 0.1 g and 100 g and initiate a program for separating the descent probe from the heat shield and aeroshell.

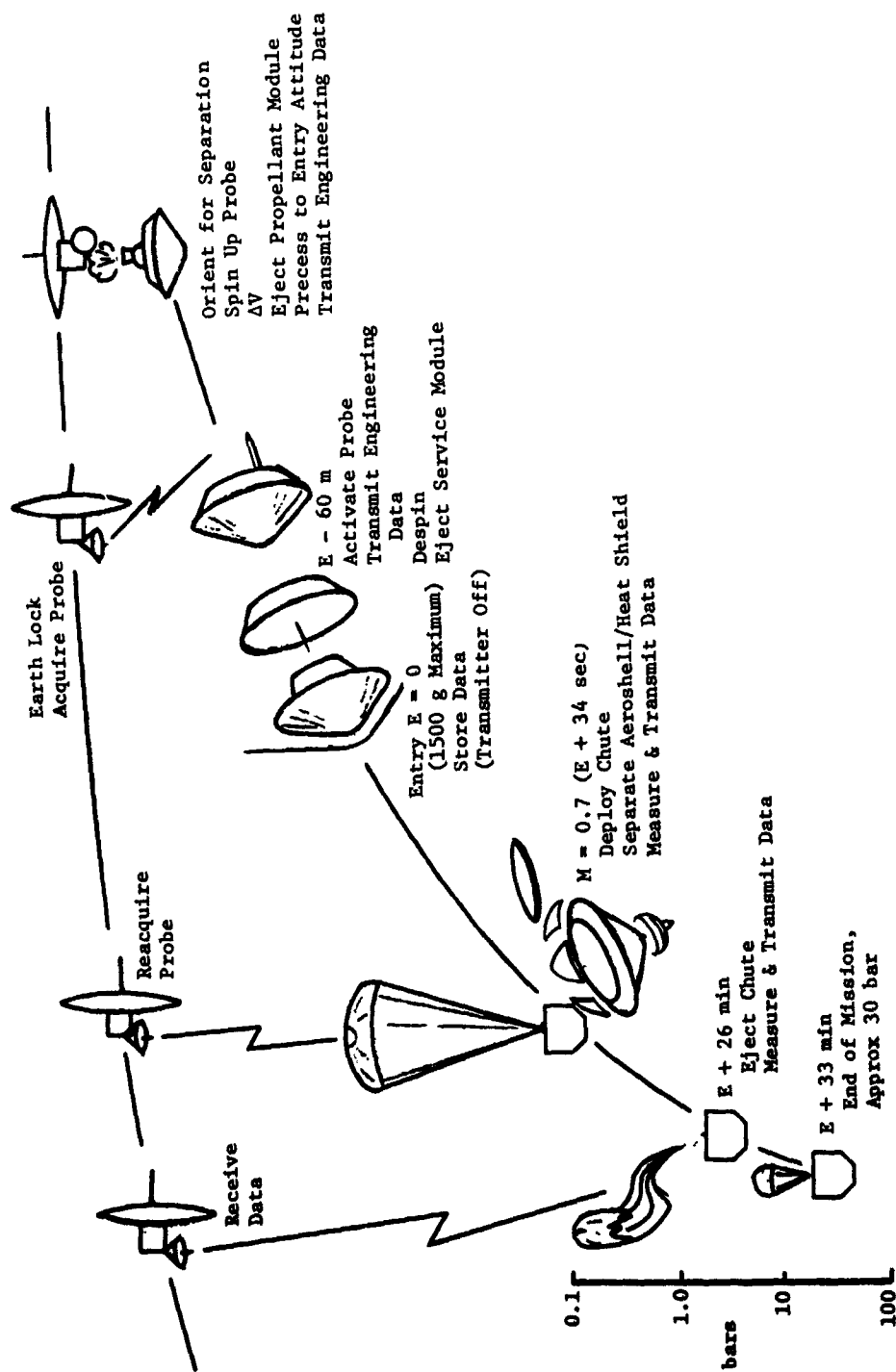


Figure V-75 Pictorial Sequence of Events

Table V-80 Nominal Jupiter Probe Sequence of Events

ITEM	TIME	EVENT
1.	L=0	Launch, November 7, 1979
2.	L+2h	Separate S/C from L/V
3.	L+2h	Cruise
4.	S-6h, 0m, 0s	S/C Power to Probe; Eject Environmental Cover
5.	S-5h, 47m, 0s	Start Probe Checkout
6.	S-0h, 17m, 0s	Probe C/O Complete; Start S/C Orientation for Release
7.	S-0h, 2m, 0s	S/C Orientation to 81° Complete; Activate Probe Data Handling System & Separation Subsystems
8.	(L+670.2d) S=0	Separate
9.	S+0m, 0.5s	Start Probe Spinup to 100 rpm
10.	S+4m, 0s	Probe Spinup to 100 rpm Complete
11.	S+15m, 0s	Apply Probe $\Delta V$ (221 m/sec, 11-sec burn) (900 m min separation)
12.	S+15m, 21s	Eject Probe Deflection Motor; Activate Attitude Propellant Subsystem
13.	S+15m, 31s	Start Probe Precession; Reorient S/C to Earth Lock ( $\sim 81^\circ$ )
14.	S+6h, 13m, 31s	Turn on Transmitter
15.	S+6h, 15m, 31s	Probe Precession Complete ( $\sim 53^\circ$ ); Start Probe Acquisition
16.	S+6h, 16m, 31s	Acquisition Complete; Start Engineering Data Transmission
17.	S+6h, 26m, 31s	Complete Data Transmission; Deactivate Probe Systems
18.	L+670.46d to L+679.94d	Coast
19.	E-1h, 21m, 20s	Enable Entry Battery Ordnance
20.	E-1h, 1m, 20s	Activate Probe Descent Batteries (in aeroshell & descent probe)
21.	E-41m, 10s	Turn Transmitter "On", Data Handling System, Engineering Instrumentation
22.	E-39m, 10s	Start Probe Acquisition
23.	E-35m, 0s	Complete Probe Acquisition; Start Data Transmission; Activate Probe Despin Subsystem
24.	E-25m, 0s	Start Probe Despin to 5 rpm
25.	E-18m, 0s	Probe Despin Complete; Turn on Science Instrument
26.	E-13m, 0s	Eject Service Module; Activate Service Module Deflection Propulsion
27.	E=0	Entry (305 km above 1 atm; $3 \times 10^{-7}$ atm)
28.	E+0m, 5.5s	Probe Transmitter "Off" (0.1 g sensing); Start Recording Accelerometer Data
29.	E+0m, 9.7s	Initiate Probe Descent Program (100 g sensing)
30.	E+0m, 30.5s	Eject Base Cover Quadrants (Mach 0.8)
31.	E+0m, 34s	Deploy Main Parachute (Mach 0.7, $\sim 0.1$ atm); Activate Scientific Ordnance
32.	E+0m, 44s	Release Descent Probe from Entry Probe (switch probe antenna)
33.	E+0m, 54s	Probe Transmitter "On"; Start Probe Acquisition
34.	E+5m, 04s	Probe Acquisition Complete; Start Data Transmission
35.	E+26m, 16s	Release Main Chute and Allow Drogue Chute to Open (10 bar)
36.	E+33m, 40s	End of Design Mission ( $\sim 30$ bar)
37.	(L+680d) E+45m, 45s	S/C Periapsis (2 R <sub>J</sub> ) September 17, 1981

Includes 7-min trajectory uncertainty and is based on a descent ballistic coefficient of 0.12 and 1.50 slug/ft<sup>2</sup> (19/236 kg/m<sup>2</sup>) and 10 bar staging.

b. *Functional Block Diagram* - Figure V-76 shows the interrelationship of the probe subsystems and the electrical interface between the probe and spacecraft during periods before and after separation.

c. *System Data Profile* - Figure V-77 shows the data collection and transmission activities as a function of the five periods of the probe mission. The accumulative data collection is shown along with that stored within the probe and the data transmission rates. It is seen that the storage capacity required is approximately 13K bits and that the maximum transmission rate is 28 bits per second.

d. *System Power Profile* - The system power requirements are shown in Figure V-78 for the five periods of the probe mission.

e. *System Weight Summary* - Table V-21 shows the probe weight breakdown by subsystems which fixes the probe ejection weight of 157.46 kg. In addition, the entry and descent weights are presented.

Table V-21 Nominal Jupiter Probe Weight Summary

Probe Breakdown	Weight	
	kg	lb
Science	8.66	19.1
Power and Power Conditioning	5.91	13.0
Cabling	5.44	12.0
Data Handling	2.13	4.7
Attitude Control	11.76	25.9
Communications	3.61	8.0
Pyrotechnic	6.31	13.9
Structures and Heat Shield	61.92	136.5
Mechanisms	7.71	17.0
Thermal	7.44	16.4
Propulsion (dry)	3.85	8.5
Propellant	12.16	26.8
Engineering Instrumentation	0.00	0.0
15% Margin	20.54	45.30
Ejected Weight	157.46	347.28
Entry Weight	106.34	234.6
Descent Weight	41.93	92.6



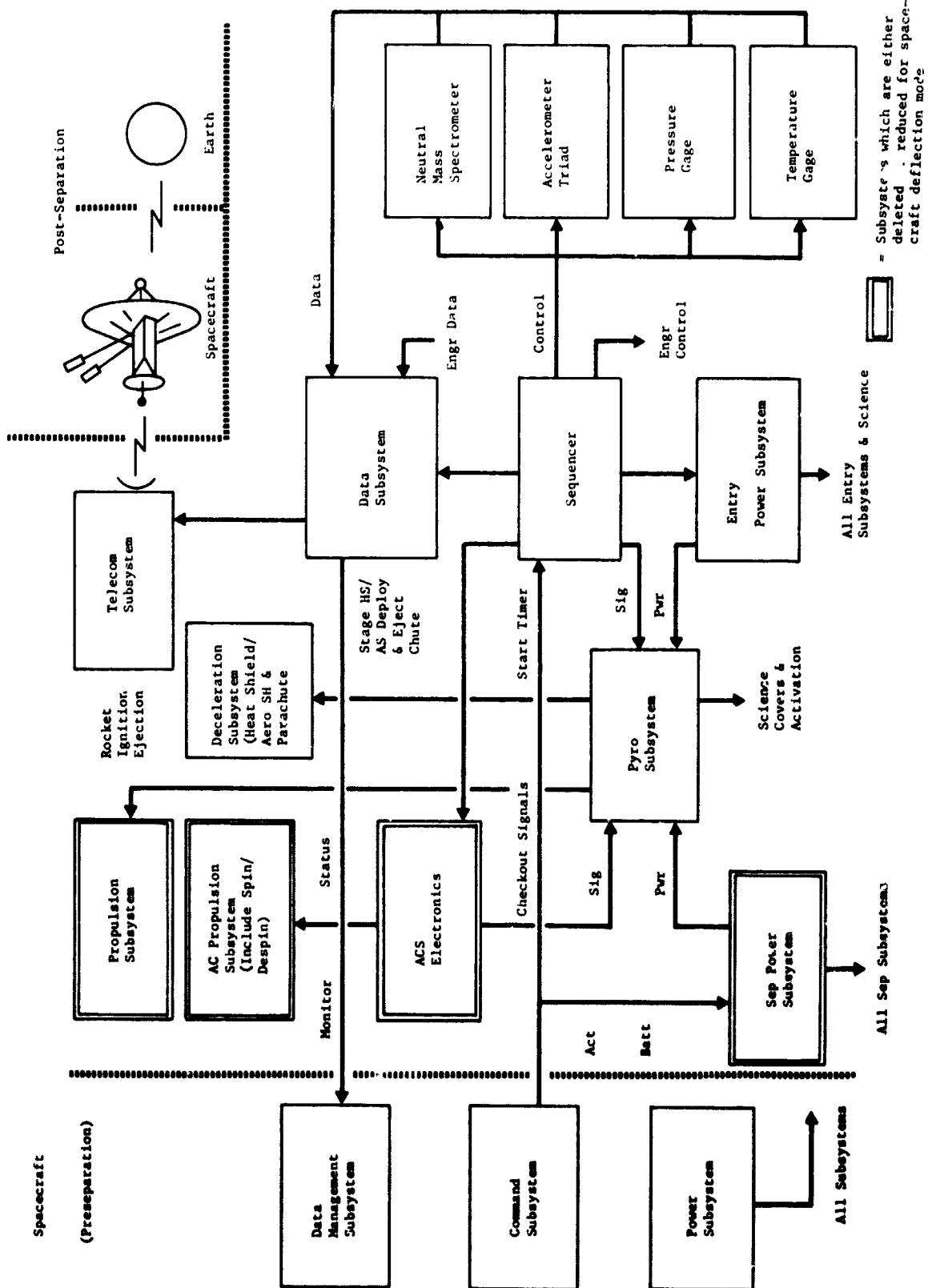


Figure V-76 Functional Block Diagram for the Nominal Jupiter Probe

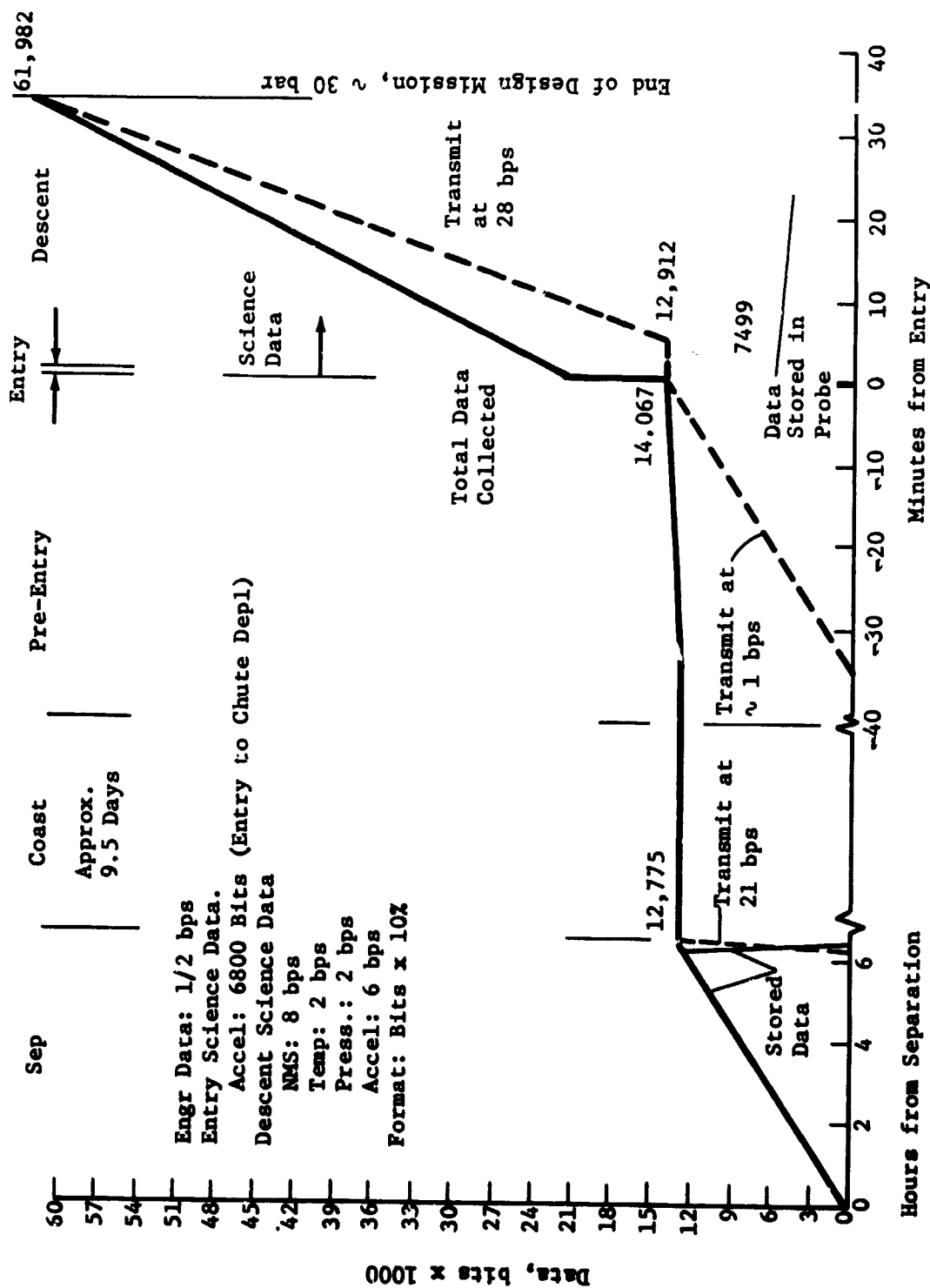


Figure V-77 Data Profile for the Nominal Jupiter Probe

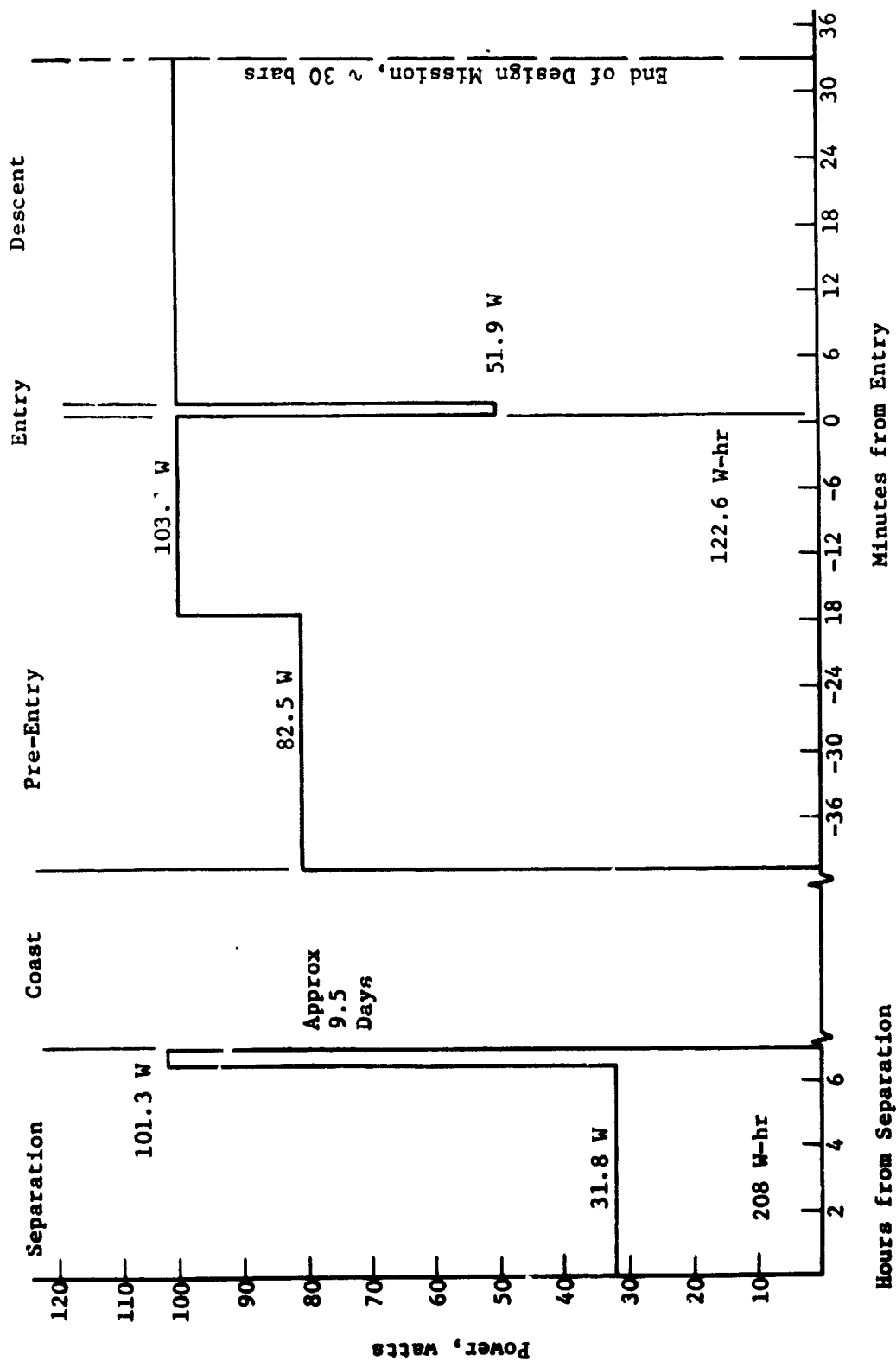


Figure V-78 System Power Profile for the Nominal Jupiter Probe

#### 4. Telecommunications Subsystem

a. *RF Subsystem Definition* - Definition of the telecommunications subsystem for the nominal Jupiter probe system was linked heavily with design of the probe trajectory. The missile optimized communication parameters in order to minimize the RF power required. Many changes were made in periapsis radius, lead time, and ballistic coefficient in order to arrive at a trajectory that places the spacecraft overhead at the end of the mission and minimize several RF power sensitive parameters.

The objective was to have minimum communications range and probe aspect angle at mission completion. These variables are shown in Figures V-79 and V-80 as a function of mission time for the nominal Jupiter mission. Range decreases by approximately  $0.3 R_J$  from entry to mission completion. Increasing range before entry is due to the relative motion of the probe and spacecraft with the probe accelerating ahead of the spacecraft along the trajectory. Probe aspect angle also decreases during probe descent and is at a minimum of  $5.2^\circ$  when a depth of 30 bars is reached in the cool/dense atmosphere model.

Selection of an optimum frequency was also considered while developing the nominal mission. Details of the tradeoffs performed are discussed in Volume III, Appendix A. One of the major contributors to RF loss in the link is attenuation of the Jovian atmosphere. Atmospheric loss for the nominal probe conditions is shown in Figure V-81 as a function of frequency and depth of descent. Atmosphere loss is also a direct function of the angle off zenith. Minimizing probe aspect angle minimized atmosphere loss at a given depth while optimizing probe antenna gain. Both effects improved the RF link conditions. Power requirements relative to 21 W for 1 GHz at entry are shown in Figure V-82. End of mission RF power requirements at S-band are over 1 kW and are greatly reduced as the frequency is lowered. Therefore, the operating frequency for the nominal probe mission was selected at 1 GHz. Antenna size becomes a significant factor below 1 GHz and a lower frequency was not chosen. Parameters of the RF link are depicted in Table V-22 for the nominal mission at 1 GHz. Defining conditions of the RF link are listed in the remarks column and at the bottom of the table. Maximum power is required at mission completion but the trajectory was designed to minimize the level at this worst-case point. The major contributor to increasing RF loss during descent is the atmosphere attenuation.

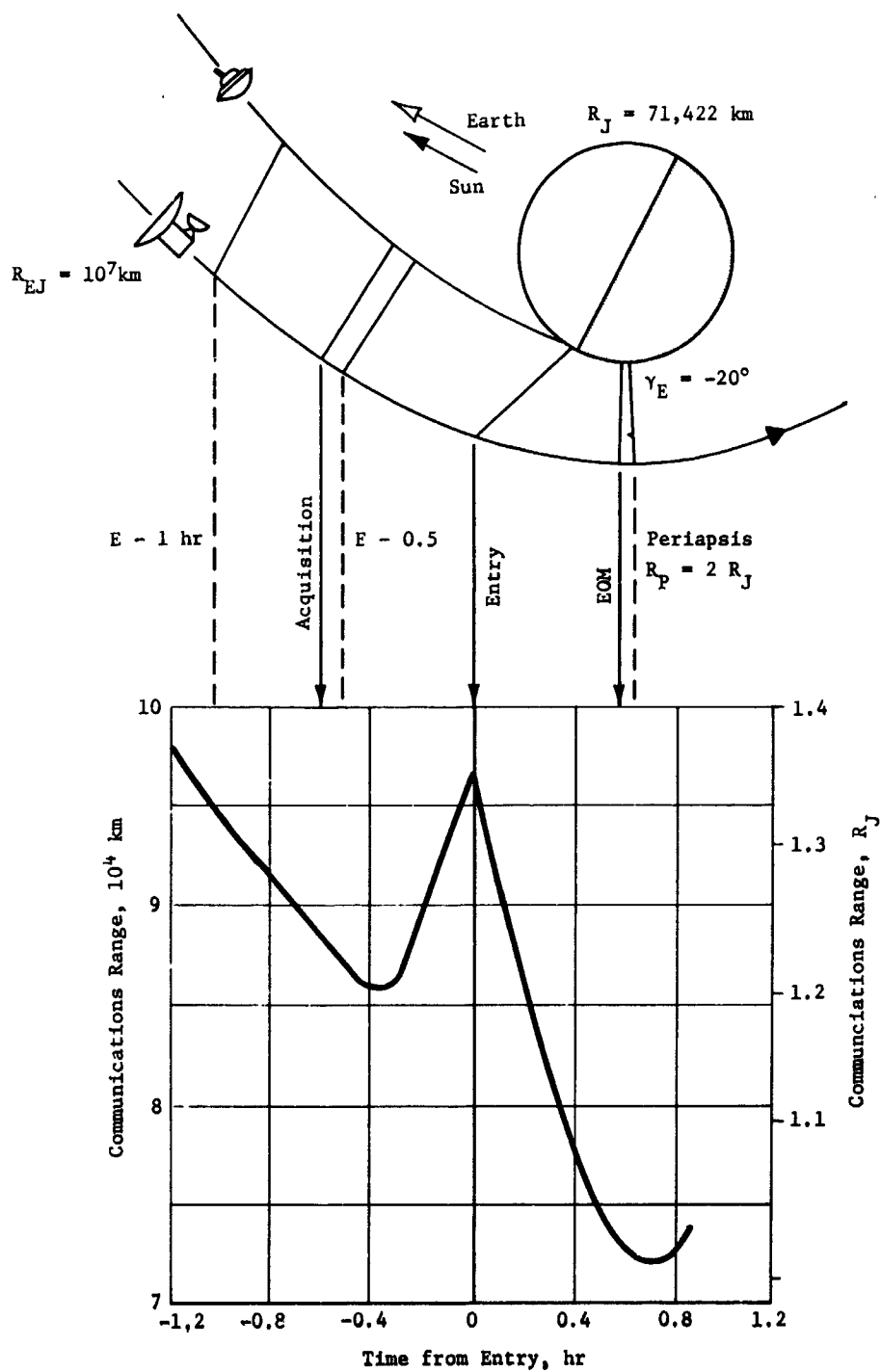
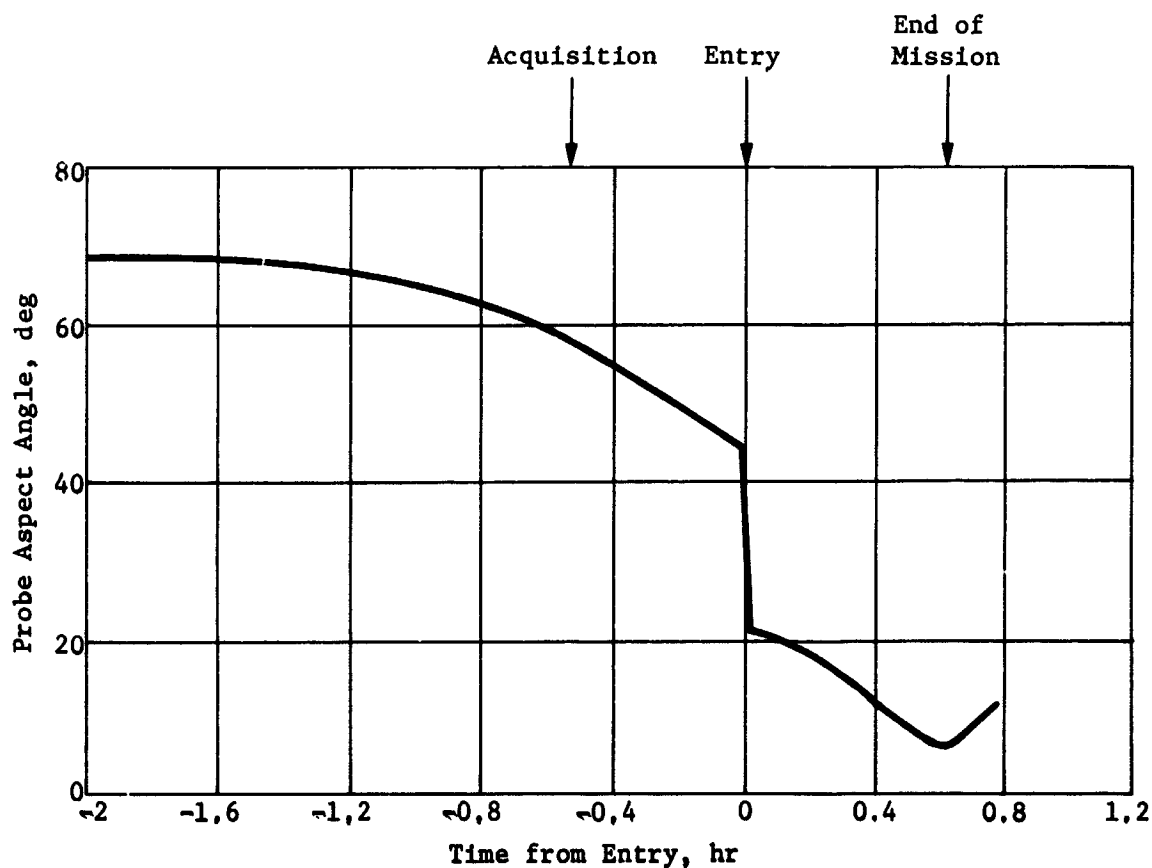
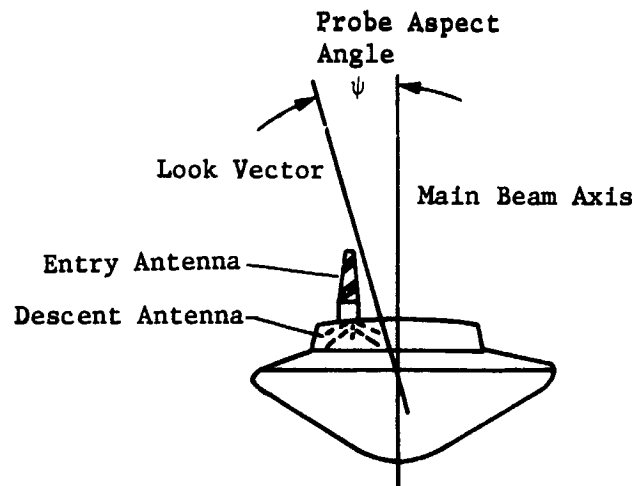


Figure V-79 Probe-to-Spacecraft Communications Range for The Nominal Mission



Conditions:  $R_P = 2 R_J$        $T_L = 46 \text{ min}$   
 $R_{EJ} = 10^7 \text{ km}$        $EOM = 30 \text{ bars (E + 34 min)}$   
 $\gamma_E = -20^\circ$        $\text{Cool/Dense Atmosphere}$

Figure V-80 Nominal Jupiter Probe Aspect Angle

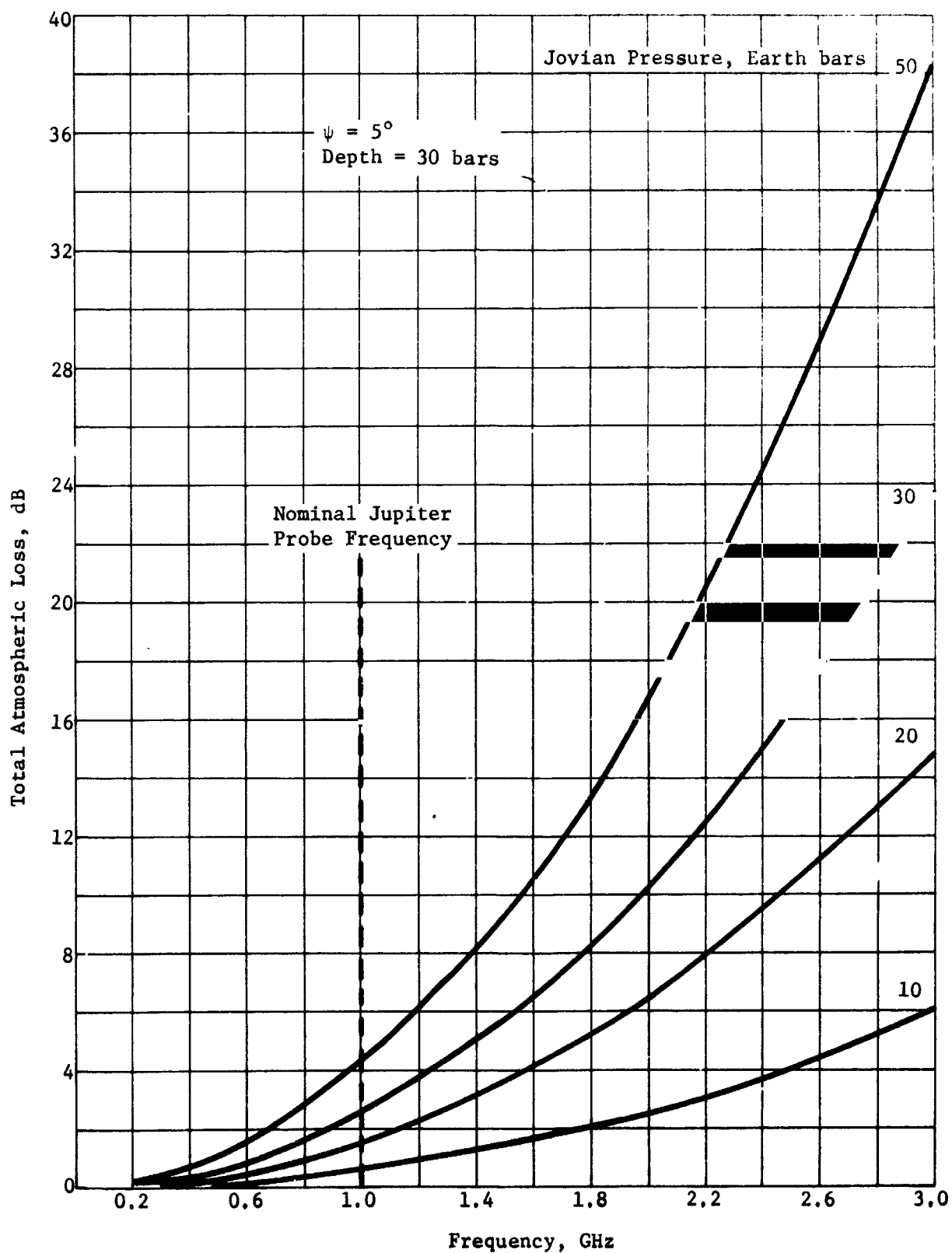


Figure V-81 End of Mission Attenuation for Jupiter Cool/Dense Atmosphere

V-139

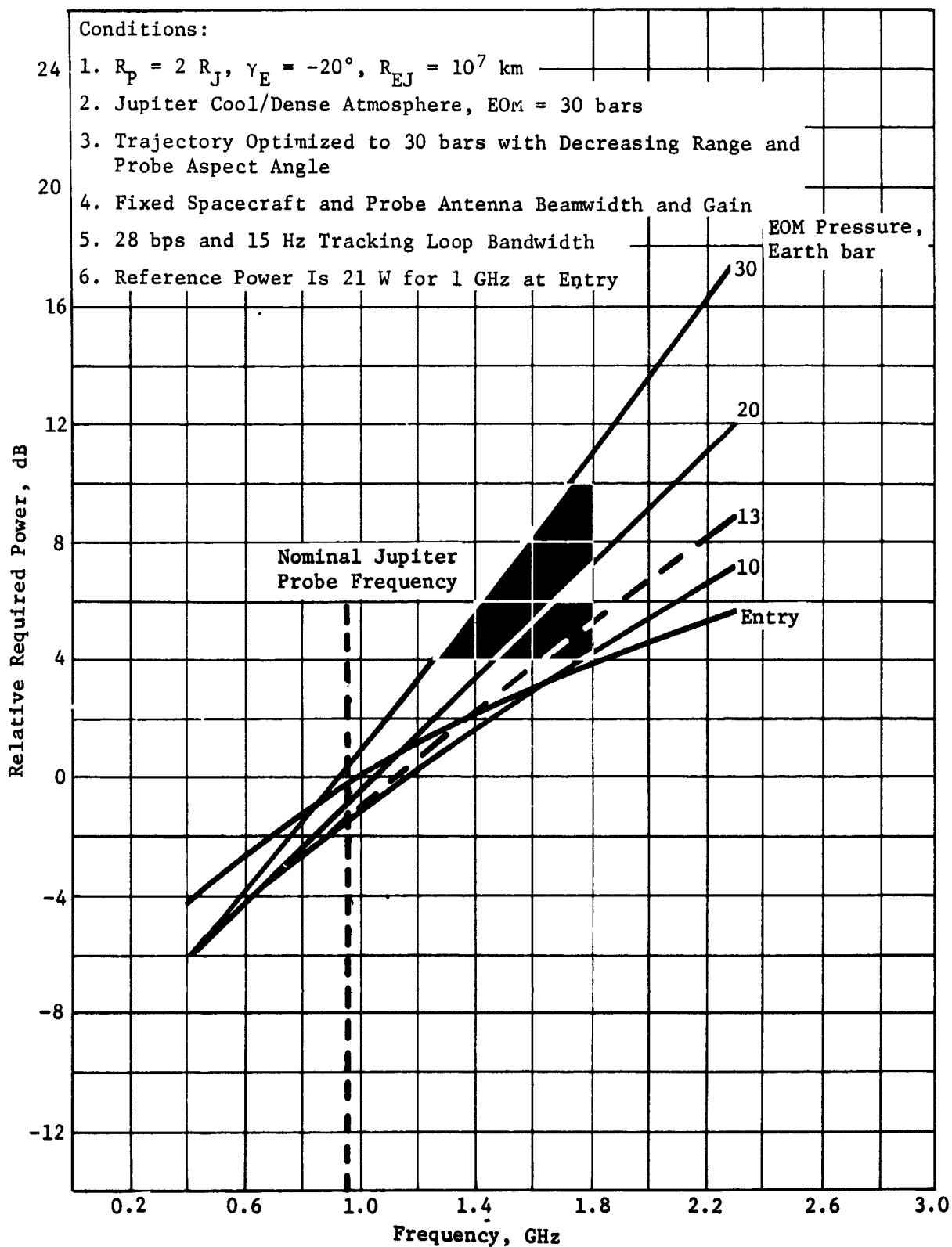


Figure V-82 Relative Power Required for Jovian Descent, Nominal Probe



Table V-22 Probe Telemetry Link Design for the Nominal Jupiter Probe

Parameter	Nominal Value	Adverse Tolerance	Remarks
1. Total Transmitter Power, dBW	14.0	0	25 W
2. Transmitting Circuit Loss, dB	-0.3	0.2	Switch loss: 0.2 dB
3. Transmitting Antenna Gain, dB	5.0	1.4	120° beamwidth
4. Communications Range Loss, dB	-189.7	0.9	$7.33 \times 10^4$ km
5. Planet Atmosphere & Defocus Loss, dB	-2.7	0.2	Cool/dense, 30 bars
6. Polarization Loss, dB	0	0.2	
7. Antenna Pattern Ripple Loss, dB	0	0.2	
8. Receiving Antenna Gain, dB	11.6	4.0	45° beamwidth
9. Receiving Circuit Loss, dB	-0.2	0.2	
10. Net Circuit Loss, $\Sigma(2 \rightarrow 9)$ , dB	-176.3	7.3	
11. Total Received Power (1 + 10), dBW	-162.3	7.3	
12. Receiver Noise Spectral Density, dBW	-197.5	0.5	$T_S = 1280^\circ\text{K}$ , $NF_S = 7.34$ dB
<u>Tracking Tone</u>			
13. Tone Power/Total Power, dB	-5.2	0.4	
14. Received Tone Power (11 + 13), dBW	-167.5	7.7	
15. Tracking Threshold Bandwidth, dB	11.8	0	Bandwidth = 15 Hz
16. Threshold SNR, dB	10.0	0	
17. Threshold Tracking Power (12 + 15 + 16), dBW	-175.7	0.5	
18. Tracking Performance Margin (14 - 17), dB	8.2	8.2	
<u>Data Channel</u>			
19. Data Power/Total Power, dB	-1.6	0.4	
20. Radio System Processing Loss, dB	-1.0	0	
21. Fading Loss, dB	-1.0	0	
22. Received Data Power (11 + 19 + 20 + 21), dBW	-165.9	7.7	
23. Data Bit Rate, dB	14.5	0	28 bps
24. Threshold $E_b N_o$ , dB	8.9	0	
25. Threshold Data Power (12 + 23 + 24), dBW	174.1	0.5	
26. Performance Margin (22 - 25), dB	8.2	8.2	
27. Nominal Less Adverse Value (26 - 26 adv), dB	0		
<u>Conditions:</u> <ol style="list-style-type: none"> <li>1. Worst-Case (EOM) Conditions at 1 GHz</li> <li>2. EOM Probe Aspect Angle, <math>\psi = 5.3^\circ</math></li> <li>3. Coded Noncoherent System with Viterbi Decoding</li> <li>4. Convolutional Encoder, <math>M = 2</math>, <math>V = 2</math>, <math>Q = 8</math></li> <li>5. BER = <math>5 \times 10^{-5}</math> for Binary FSK with <math>K = 8</math> Code</li> </ol>			

The binary FSK requires 25 W of RF power and 28 bps with a tracking tone. A functional diagram of the telecommunications subsystem is shown in Figure V-83. Relative probe positions during the mission are shown by the ellipses in Figure V-84. The ellipses account for trajectory and probe dispersions and represent the nominal positions (triangles) and associated uncertainties. The dispersions are based on a 100-sample Monte Carlo analysis. Elevation angle (cross cone angle) dispersions are very small with the major difference occurring in cone angle. A  $45^\circ$  spacecraft antenna beamwidth provides maximum gain at the points of maximum dispersion. The cone angle decreases during descent and retraces the increasing angle from acquisition to entry. Decreasing cone angle after entry results when the spacecraft overtakes the descending probe.

Table V-23 depicts design details of the RF components that comprise the telecommunications subsystem. Complete details of the components are given in Section A.4 of this chapter. A mechanical RF switch is used because of the high RF power level. A four-arm equiangular spiral antenna on a cone is small enough to be placed on the service module and provide the required butterfly pattern with circular polarization during entry. The descent antenna is a crossed dipole in a cup and attaches to the basecover. A helix antenna on the three-axis stabilized spacecraft provides sufficient coverage for the probe mission when mounted in a fixed position.

*b. Spacecraft Receiver Tracking and Acquisition* - The configuration of the spacecraft receiver is shown in Figure V-85. The following functional description is based on the more detailed discussion to be found in Volume III, Appendix C.

The maximum gain of the IF amplifier under no-signal conditions should be controlled (AGC or spacecraft computer) to provide the proper threshold for the acquisition circuitry. Wideband acquisition filters (A-U-BPF, A-L-BPF) provide initial acquisition at high frequency sweep rates. A narrow band ( $S/N = 20$  dB) filter then provides final acquisition at lower sweep rates. When signal is detected in the narrow band acquisition filter (A-A-BPF), the tracking loop ( $S/N = 10$  dB) is enabled. Analysis has indicated that a maximum frequency error of 7.5 Hz may occur with the expected Doppler rates and instabilities. The local oscillator frequency will be swept with a saw-tooth waveform through the uncertainty region around a preprogrammed expected Doppler shift. After acquisition, the saw-tooth is discontinued but the predicted Doppler shift program will continue to relieve loop stress. In addition to the main frequency tracking loop, the output of the discriminator is used to update the Doppler program, further relieve loop stress and reduce frequency error toward the basic line width of the probe transmitter. Loss of acquisition will result in a narrow band search as long as the signal remains in the wideband acquisition filter. Acquisition will require less than 100 sec and reacquisition approximately 1.2 sec for the nominal Jupiter probe design.

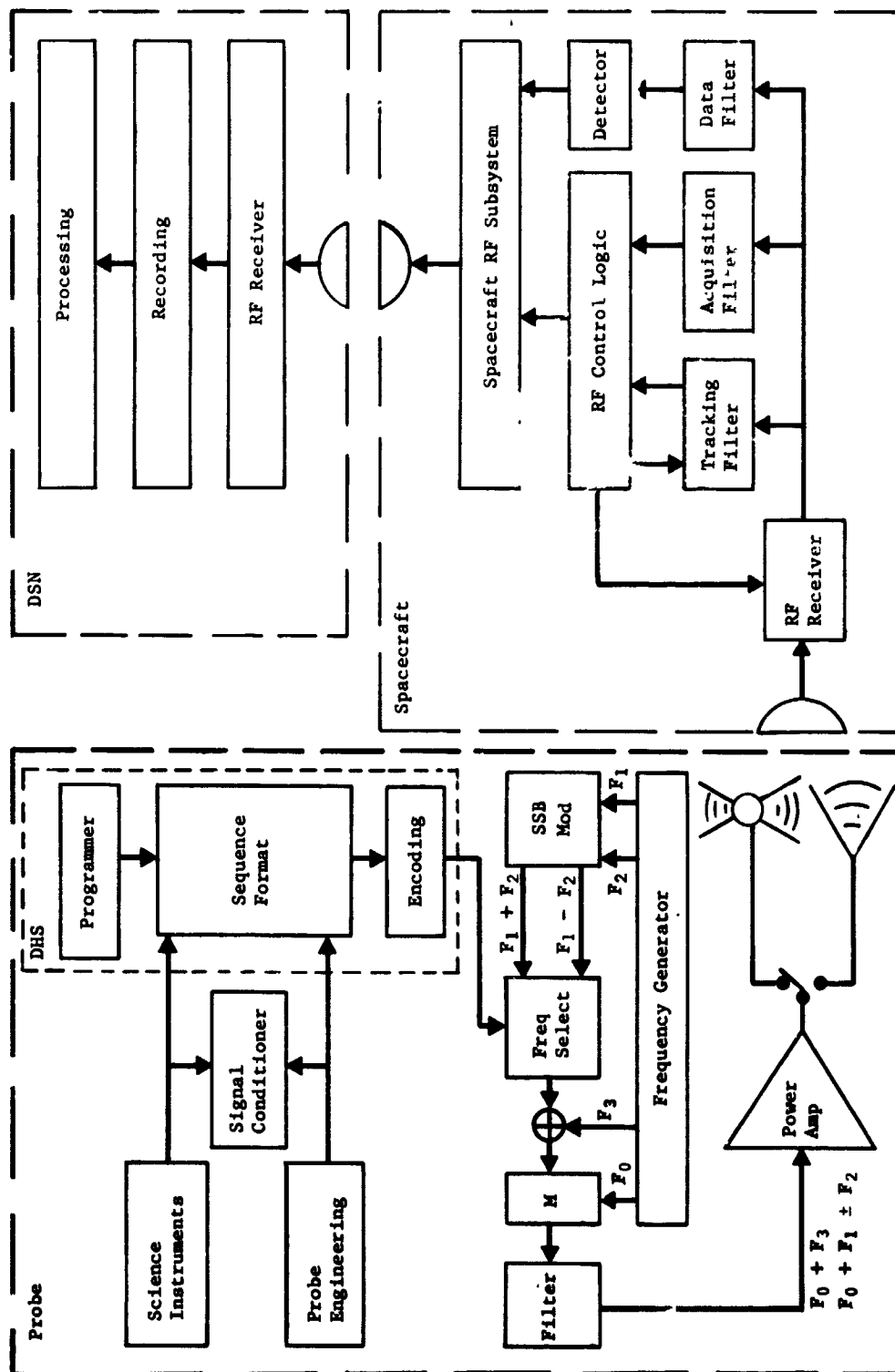


Figure V-83 Communications Functional Diagram

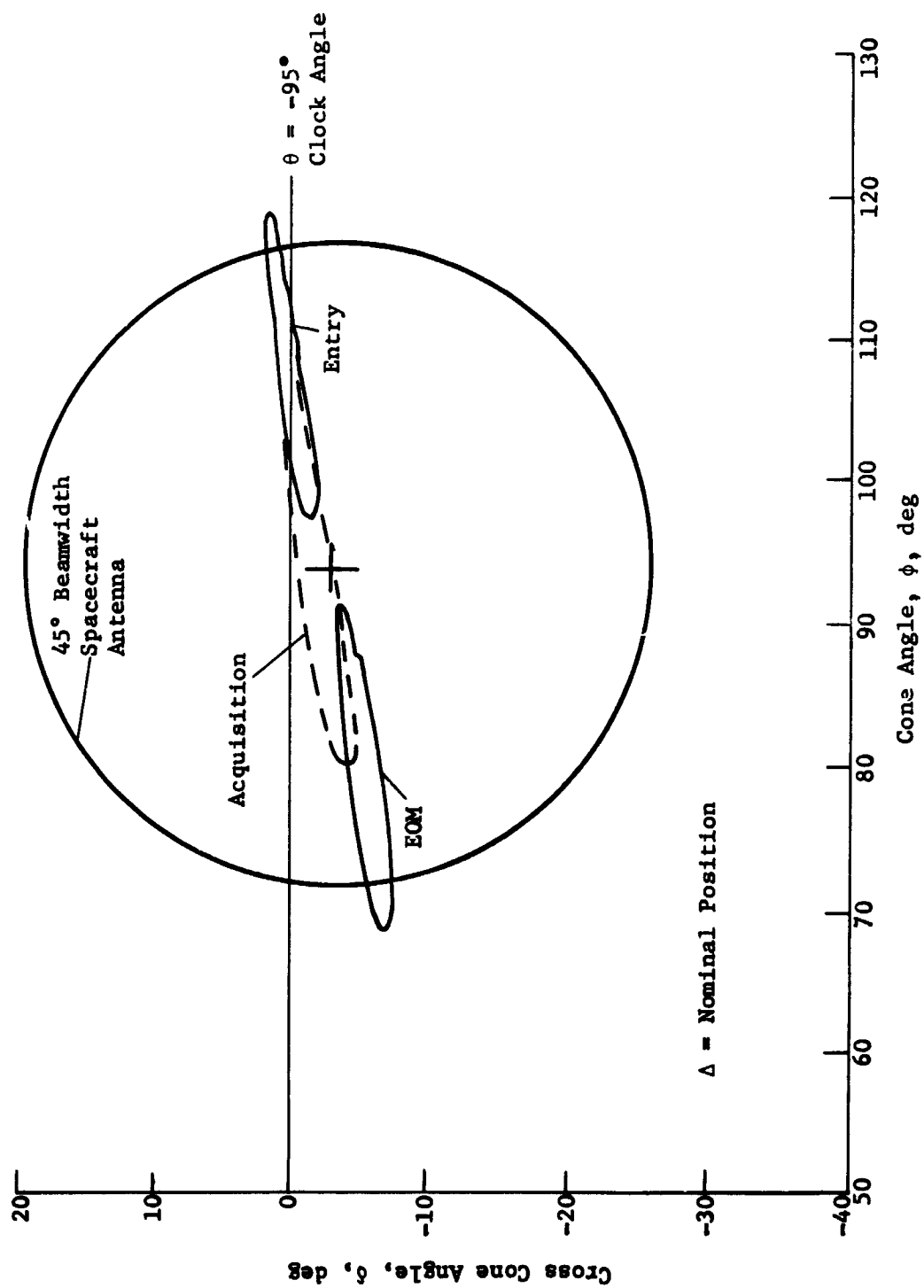


Figure V-84 Spacecraft Antenna Requirements for the Nominal Mission

Table V-23 Telecommunications RF Subsystem for the Nominal Jupiter Probe

CONDITIONS: Planet:Jupiter S/C: TOPS FREQUENCY: 1 GHz BIT RATE: 28 bps			
COMPONENT	CHARACTERISTIC	UNIT	VALUE
Transmitter	RF Power Out	W	25
	Overall Efficiency	%	45
	DC Power in at 28 V dc	W	55
	Total Weight	kg	2.7
		lb	6.0
RF Switch	Type		Mechanical
	Insertion Loss	dB	0.3
	Weight	kg	0.23
		lb	0.5
Entry Antenna	Type		Spiral on Cone
	Main Beam Angle	deg	55
	Beamwidth	deg	35
	Maximum Gain	dB	6.2
	Size (l x diameter)	cm	27 x 22.5
		in.	10.6 x 8.8
	Weight	kg	0.23
Descent Antenna		lb	0.5
	Type		Turnstile in Cup
	Main Beam Angle	deg	0
	Beamwidth	deg	110
	Maximum Gain	dB	5.2
	Size (diameter x h)	cm	18.8 x 7.6
		in.	7.4 x 3.0
Spacecraft Antenna	Weight	kg	0.45
		lb	1.0
	Type		Helix
	Beamwidth	deg	45
	Maximum Gain	dB	12.3
	Size (l x diameter)	cm	51 x 9.5
		in.	20 x 3.75
	Weight	kg	2.27
		lb	5
	Despin		No
	Position Search	sec	1
	Frequency Acquisition	deg	35
	Clock Angle, $\theta$	deg	-94
Spacecraft Receiver	Cone Angle, $\phi$	deg	100
	Noise Temperature	$^{\circ}\text{K}$	300
	Noise Figure	dB	3.1
	DC Power in at 28 V dc	W	3.0
	Weight	kg	0.9
		lb	2.0

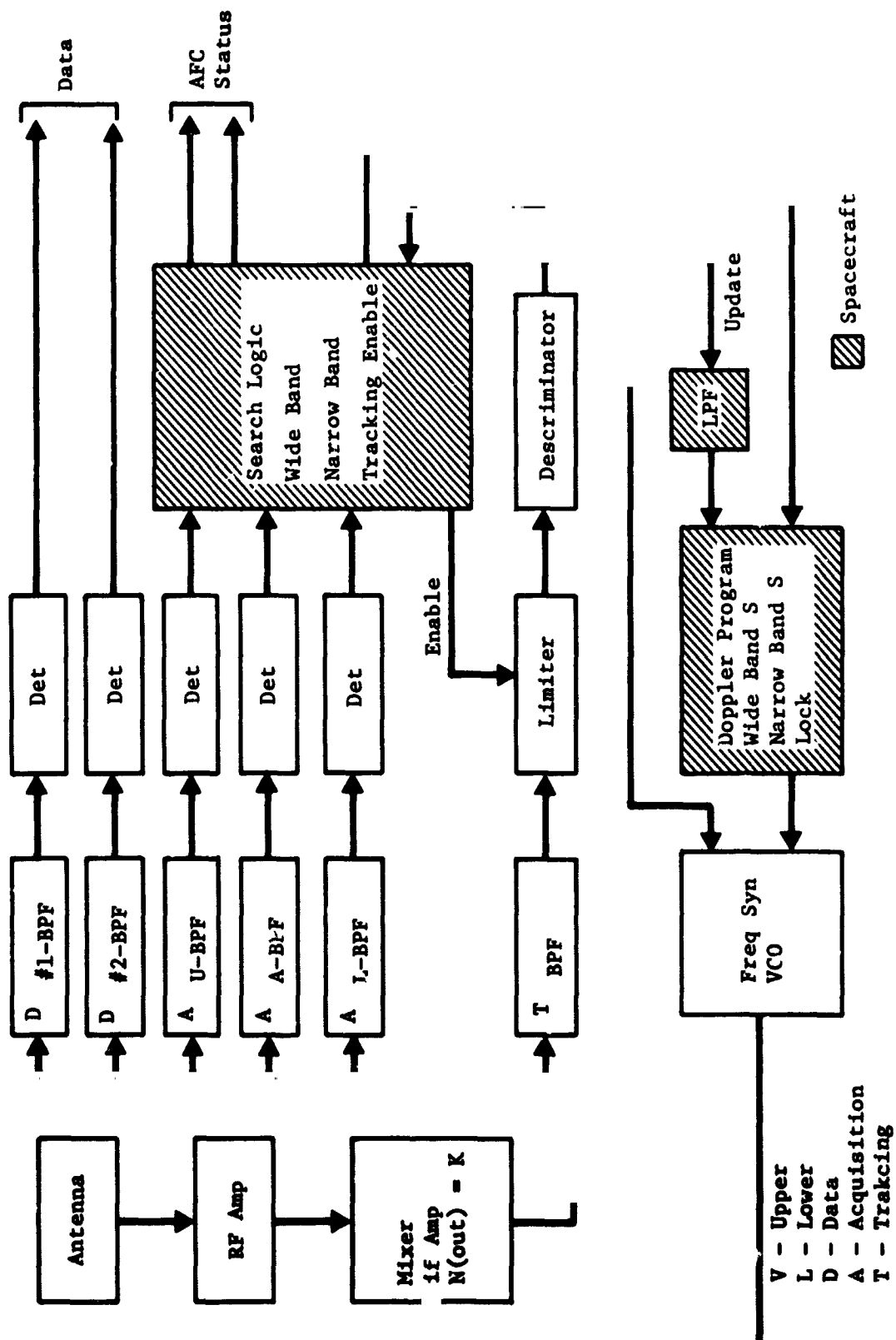


Figure V-85 Acquisition/Tracking/Data/Spacecraft Receiver Diagram

The shaded blocks are portions of the subsystem which conceivably are part of the spacecraft (i.e., spacecraft computer programs and processing). The storage of probe data, which appears to be a desirable option in view of the down-link communications range and coded data rates with soft quantization, will require the capacity of a tape recorder. In the event that this item is not available in the spacecraft system, a dedicated recorder will be required. The remaining items are considered to be probe mission dedicated components. The size weight and power of these electronic components was estimated on the basis of similar (Viking) systems to be

Vol = 11.4x12.7x15.2 cm (4.5x5x6 in.)

Weight = 2.3 kg (5.0 lb)

Power = 7.5 watts.

These numbers are quite flexible and are strongly dependent on the type of electronics, the degree of redundancy, and the structural design.

A dedicated tape recorder would probably be of the air filled type and require 24 watts power and weigh 25 lb. Recently, vendors (RCA, Borg-Warner) have built and proposed for space use tape recorders with these typical physical characteristics.

Vol = 10.2x17.8x36.5 cm (4x7x14 in.)

Weight = 5.9 kg (13.0 lb)

Power = 15 watts.

##### 5. Data Handling Subsystem (DHS)

The functional requirements of the special purpose Data Handling Subsystem is shown in Table V-6. A nominal series of significant events relative to the DHS are listed in Table V-24. The DHS performs only the necessarily centralized functions of timing, sequencing, and formatting. The subsystem is energized twice, by the spacecraft before pre-separation checkout and by the coast timer/bus voltage sensor during the pre-entry period. Once energized, the timer and sequence generator control the probe functions. The DHS receives two additional commands: (1) the accelerometer signals the presence of significant g-level to prevent overloading the memory with useless pre-entry acceleration data; and (2) g-switches provide signals to initiate the descent format. The probe

bus voltage sensor has an additional function in that it provides controls so that the DHS is disabled until full power is on the bus; signals are available to ensure that the internal states of the DHS are properly set. It is assumed that the science instruments will have ten or twelve bit buffer storage outputs to hold the measurements and signal the state of the instrument. Information is shifted from these buffers into the appropriate DHS memory registers. Although this procedure produces some redundancy in the electronics, it facilitates the simultaneous measurements that must be made by the science instruments, and it will also reduce design schedule interference between probe engineering design and changing science objectives. The bridge completion network, analog multiplexer and analog-digital converter are provided for engineering measurements. Standard voltage cell are provided for calibration and measurement purposes. These may be chemical cells or zener diodes. (The difficulty of maintaining a voltage standard for as much as eight years is recognized; however, the probe may be calibrated during preseparation checkout. This will ensure that probe accuracy is approximately equal to the accuracy of the spacecraft.) The data in the DHS buffer storage is then sequenced into the data stream and convolutionally encoded.

Table V-24 Nominal DHS Sequence of Events

Time	Function	Command Source
S - 6 hr	Energize probe power bus and DHS	S/C DHS
	Start timer	S/C DHS
	Exercise probe functions/checkout	S/C DHS, Probe DHS
S - 1 min	Activate probe battery	S/C DHS
S - 0	Separate probe	S/C DHS
S + 0	Perform spinup $\Delta V$ , ACS maneuver	DHS
	Engineering measurements, RF Transmission	
S + 6 hr	Initiate coast shut-down sequence	ACS logic
S + 6 <sup>+</sup> hr	Complete coast shut-down sequence	DHS
E - 85 min	Charge pyrotechnic banks	Coast timer
E - 65 min	Activate descent battery	Coast timer
	Activate DHS timer/sequencer	Bus Voltage Sensor
E - 45 min	Initiate pre-entry sequence	DHS
E + 20 sec	Initiate descent sequence (100 g)	G-switch
	Measure/store science/engineering data	DHS
E - 3 min	Resume transmission of measurements and stored data	DHS



In addition to the science instruments, the DHS controls vehicle pyrotechnics, power, ACS, and RF transmission. Their functions are indicated by the "pyro" and "power" control interfaces. Incoming commands from the accelerometer and g-switches are indicated by the "probe control bilevels."

The physical characteristics are based on estimates of devices required for each function. Included in this estimate are 14-lead flat packs, LSI packages, hybrids, transistors, diodes, resistors, capacitors (small and large tantalum) coils, and transformers. Card surface area was allotted for each device and total surface area calculated. Board thickness of 0.3 in. and density of 0.93 g/cm<sup>3</sup> (0.333 lb/in.<sup>3</sup>) were assumed. These estimates resulted in the following physical characteristics: volume, 2320 cm<sup>3</sup> (142 in.<sup>3</sup>); weight 2.13 kg (4.7 lb); and power, 6.9 watts. The weight of the memory was based on an estimate from Electronic Memories (Division of Electronics Memories and Magnetics Corporation). The estimate for a 7 kb bipolar IC memory (8 kb card) is as follows: volume, 16.5x11.4x0.64 cm (6.5x4.5x0.25 in.); weight, 0.23 kg (0.5 lb); and power 6 watts. This has been used as a basic building block for the cost of memory capacity. The resultant total physical characteristics for the nominal Jupiter probe DHS and memory are: volume, 2575 cm<sup>3</sup> (158 in.<sup>3</sup>); weight, 2.59 kg (5.7 lb); and power, 18.9 watts.

## 6. Power and Pyrotechnic Subsystems

a. *Electrical Power Subsystem* - Power requirements for the probe components are listed in Table V-25. The subsystem design approach for all missions is essentially the same. The functional block diagram of the power and pyrotechnic subsystem is illustrated in Figure V-1. It should be noted that there are two power subsystems: (1) post-separation power subsystem consisting of a primary power source, power conditioning, and essentially hard-wire distribution; and (2) entry power subsystem consisting of a primary power source, separation power filters, and relay power distribution. In addition to the above, there are two long-life, low-drain Hg-Zn batteries to provide power for the Accutron timer and the initial pre-entry pyrotechnic event. The power and pyrotechnic subsystem configuration was based on an evaluation of a study of outer planet probe requirements. Batteries were evaluated on the basis of a nominal Jupiter mission time and temperature profile. This evaluation would not be valid for the application of secondary cells to Saturn and Uranus. Primary batteries were selected and will fly in the dry state until used. The evaluation for the remotely activated cells is considered valid for Saturn and Uranus.

Power for the Accutron timer is provided by a Hg-Zn battery which is required to supply approximately 8 microamperes at 1.6 volts for 30 days. A 40-volt Hg-Zn battery is required to charge two pyrotechnic capacitor banks, hold the charge against leakage for approximately 20 minutes, provide power to operate two or three (detail design dependent) latching relays and some minor pyrotechnic logic. Initial drain of the 40-volt Hg-Zn battery is expected to be approximately 40 milliamperes, dropping rapidly to less than one milliampere as the capacitors charge and leakage decreases. The current will rise again to approximately 10 milliamperes for a fraction of a second at the end of the 20-minute soak period. The Hg-Zn battery size and weight is based on standard catalog cells degraded at 7% per year. Approximately 15% increase in volume and weight was allowed for packaging. The Hg-Zn batteries are located near the RTG heaters where the temperature control is more effective and protection against low temperature conditions is provided.

Table V-25 Nominal Power Requirements

Subsystem Elements	Power (W)	Subsystem Elements	Power (W)
Data Management	6.9	ACS Electronics	2.0
Memory	12.0	Sun Sensor	2.0
Pyrotechnics	0.5	Planet Sensor	1.0
Instrument Engineering	1.0	Mass Spectrometer	14.0
Vehicle Engineering	1.0	Accelerometer	2.8
Accutron Timer	14 $\mu$ (a)	Temperature Gage	1.4
Nutation Damper	(b)	Pressure Gage	1.3
RF Subsystem	14 - 122		
Power Subsystem Efficiency			
Post-Separation	80%	(a) Self contained Hg-Zn Battery	
Entry	90%	(b) No power required	

b. *Pyrotechnic Subsystem* - The pyrotechnic subsystem is similar to designs already applied to several space vehicles such as Mariner and Viking. Specific constraints and devices considered for outer planet probe designs were principally derived from Viking, which has severe restrictions on weight and a radiation environment. The pyrotechnic subsystem consists of power conditioning equipment, relay switching control, control logic, and capacitor banks for high-pulse discharge.

The pyrotechnic control system derives power and initiating signal from several sources.

- 1) Separation events - Initial charging of the capacitor banks and initiation signal are provided by the spacecraft. After the post-separation battery has been activated, power is then derived from the probe post-separation battery.
- 2) Post-separation events - Power is derived from the probe post-separation battery and initiation signals from the probe data management system.
- 3) Pre-entry battery event - Power is derived from 40-volt Hg-Zn battery. This is the only function for this battery which must maintain the capacitors on charge for about 20 min. The initiation signal is derived from the electromechanical (Accutron) timer.
- 4) Pre-entry events - Power is derived from the probe pre-entry battery. Initiation signals are provided by the data management system.

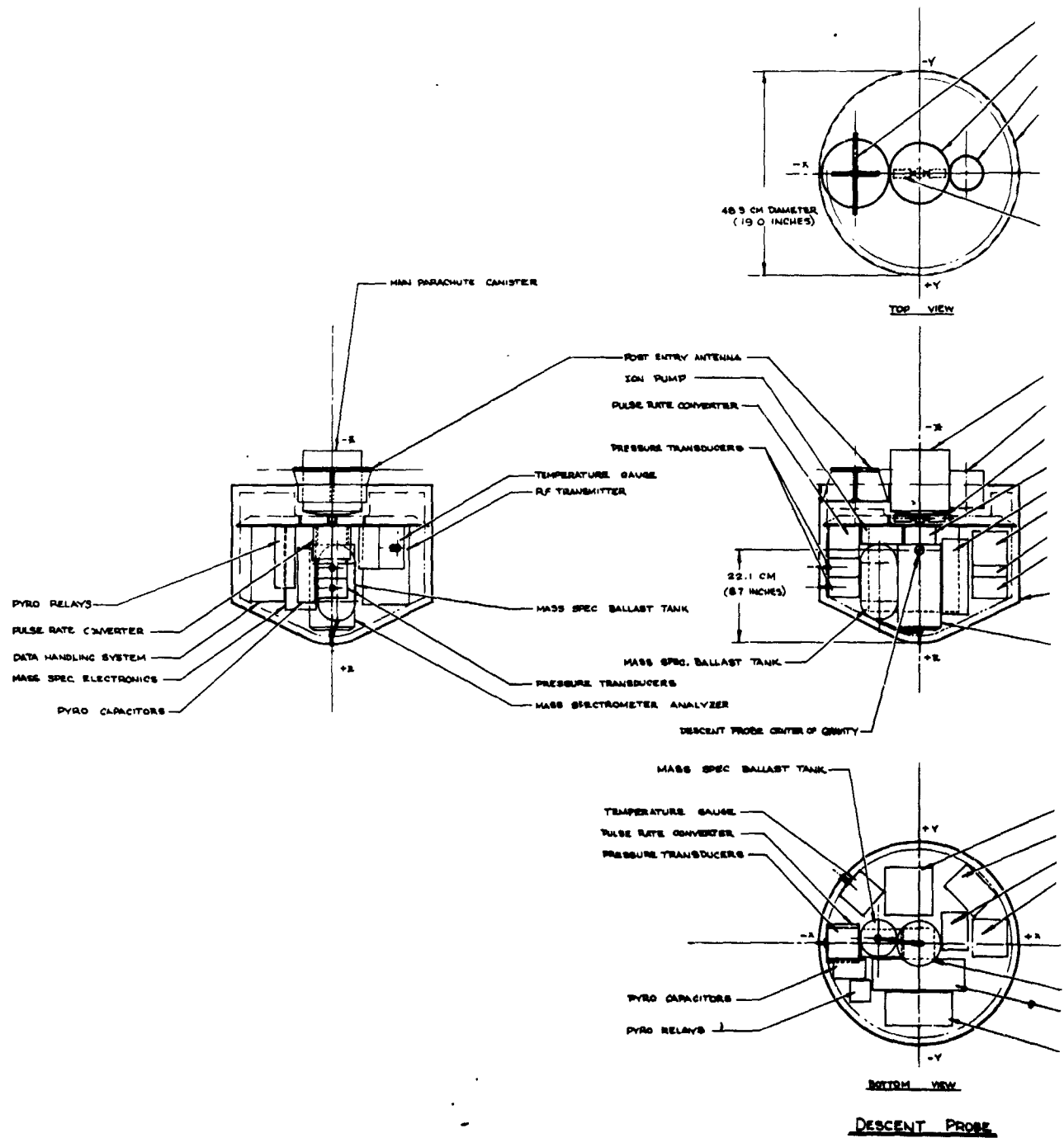
*Power* - Except for the entry battery pyro event, all power conditioning required in the pyrotechnic control subsystem is provided by an internal power supply. Outputs are not regulated and have a tolerance of  $\pm 10\%$ . The outputs consist of two 40-volt windings completely isolated from each other and from all other windings. Power provided for internal use is:

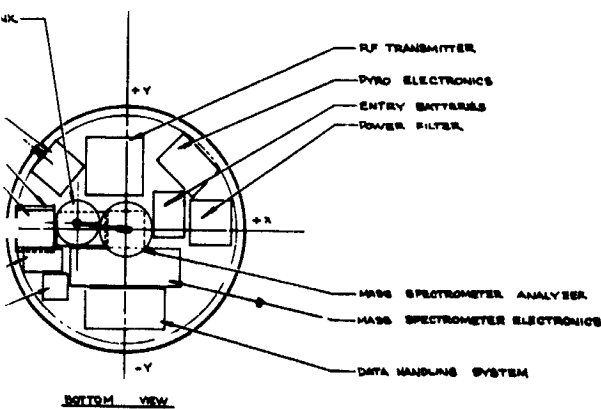
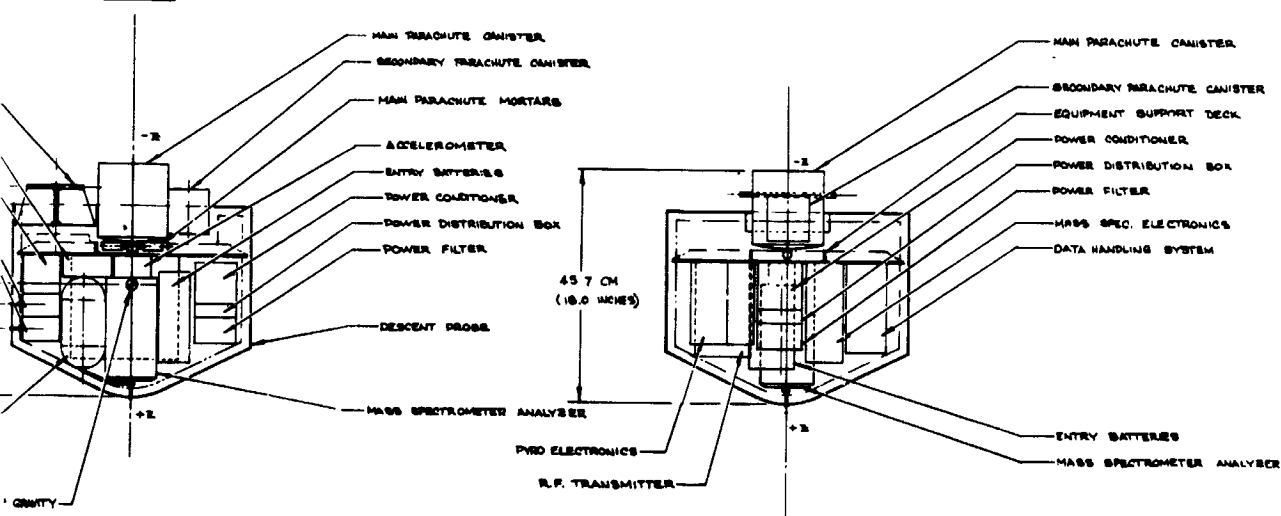
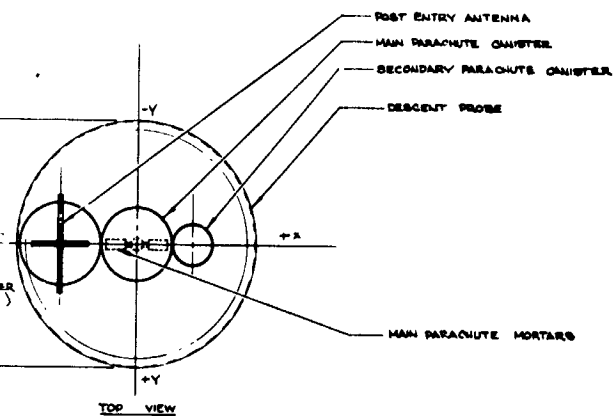
	<u>Volts</u>
Capacitor charging	+40
Relay switching	+28
Logic circuitry	+5
Digital interface circuitry	$\pm 5$

## 8. Structure and Mechanical Subsystem

The objective of the nominal Jupiter probe configuration is to provide environmental protection of the probe functional systems through the entire sequence of space flight, from launch pad lift-off through descent into the Jovian atmosphere. A further configuration objective is to enable efficient accomplishment of the systematic sequential functional probe events of the programmed mission. The probe configuration and structure and mechanical design meeting these objectives are described in this subsection.

*a. Configuration and General Arrangement* - The configuration of the developed nominal Jupiter probe is shown in Figure V-86. This drawing shows, right to left, the three major configurations of the probe as ejected from the spacecraft, the planetary entry configuration, and the descent probe configuration. The ejected configuration has a conical nose cone of  $60^\circ$  half angle with maximum diameter of 0.94 meter (37.0 in.). The descent probe is 0.483 meter (19.0 in.) in diameter and 0.457 meter (18.0) long. The descent probe contains all of the scientific instruments and supporting electronics and electrical gear all mounted on a circular equipment deck. The internal equipment of the entire probe is arranged such as to allow disposal of unneeded components after their functions are accomplished. In that manner, weight at entry (which affects aeroshell and heat shield size and weight) and descent (which affects parachute size and weight) are minimized. The general arrangement of the entire probe is perhaps best explained by reference to Figure V-87 and relating this to the planetary entry sequence of events. As seen in the Figures V-86 and V-87, the probe as ejected from the spacecraft is in a configuration ready for the delta velocity deflection maneuver. The ejected probe is still covered by fore and aft multilayer insulation blanket from the cruise phase thermal protection system, with the delta velocity deflection motor and the attitude control system (ACS) spin nozzles exposed. Immediately following spacecraft separation, the ACS system in the probe service module at the aft end of the probe spins the probe to approximately 10.5 rad/sec (100 rpm) to stabilize the  $\Delta V$  attitude. The solid propellant rocket motor is fired to impart the delta velocity for probe deflection, and is then jettisoned. Thus, the motor is exposed at the aft end for ready jettisoning. The probe is then precessed by pulsed operation of precession nozzles on the service module, with the precession being monitored by Sun and planet sensors mounted on exterior of the service module, and controlled by the ACS system within the service module. The probe continues to spin at 10.5 rad/sec until about an hour before planetary entry, at which time the ACS commands a probe despin maneuver to 0.52 rad/sec (5 rpm) for planetary entry. The service module, having completed its mission, is then jettisoned to lighten the entry weight.





DESCENT PROBE

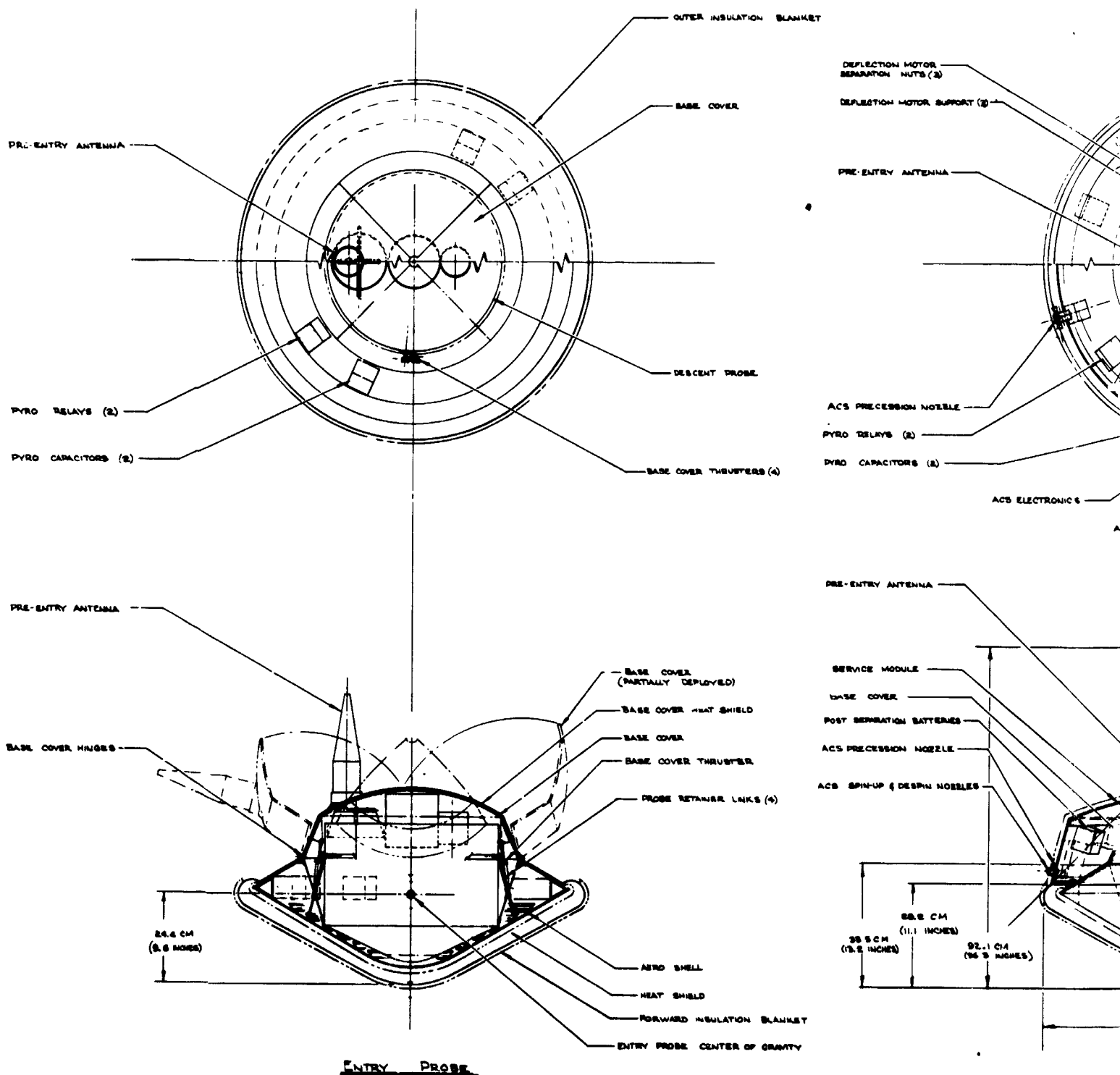
PRE-ENTRY ANTENNA

PYRO RELAYS (

PYRO CAPACITORS

PRE-ENTRY ANT

P-BL COVER HAIRS



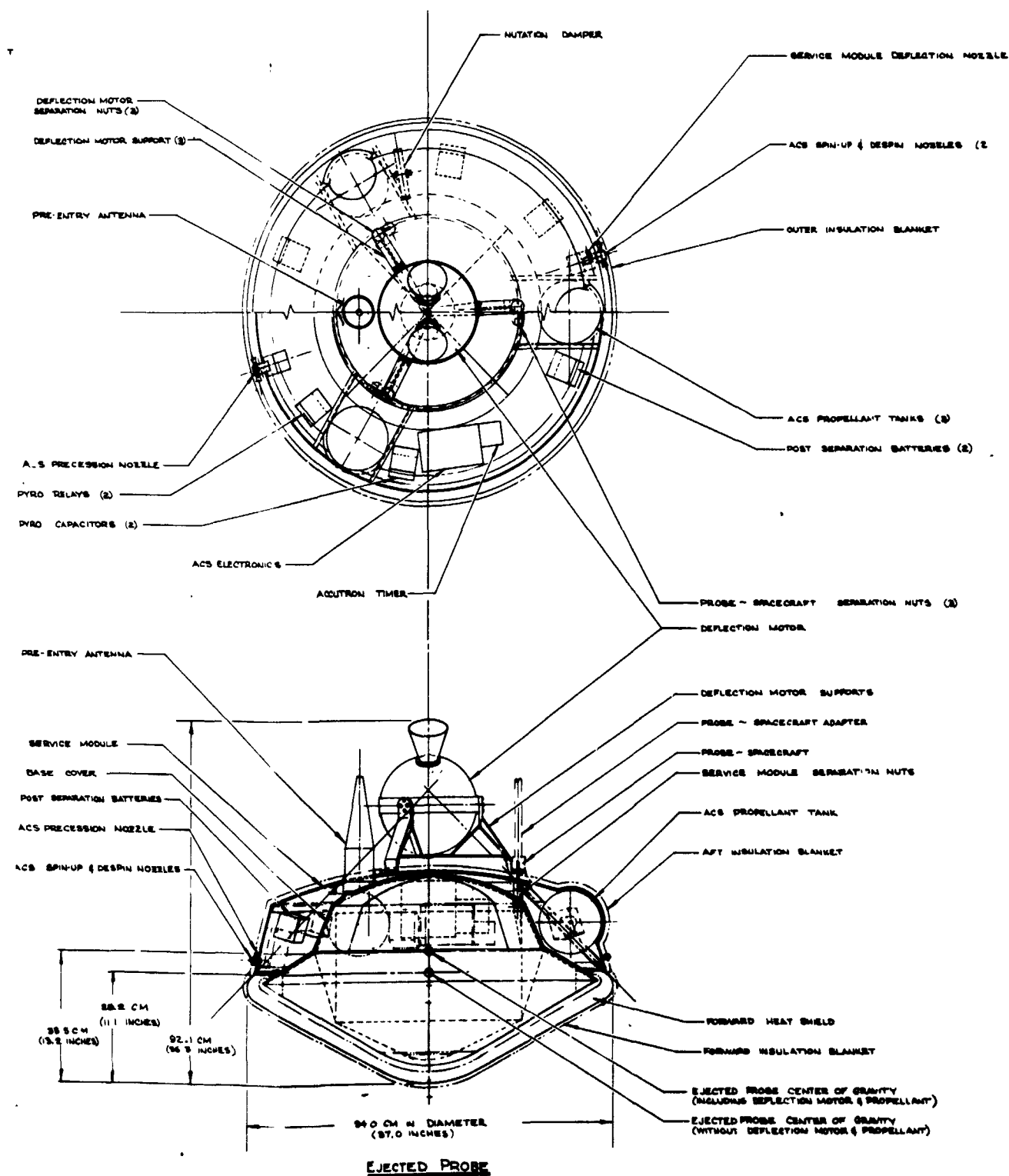


Figure V-86 Jupiter Survivable Probe - Task I Configuration



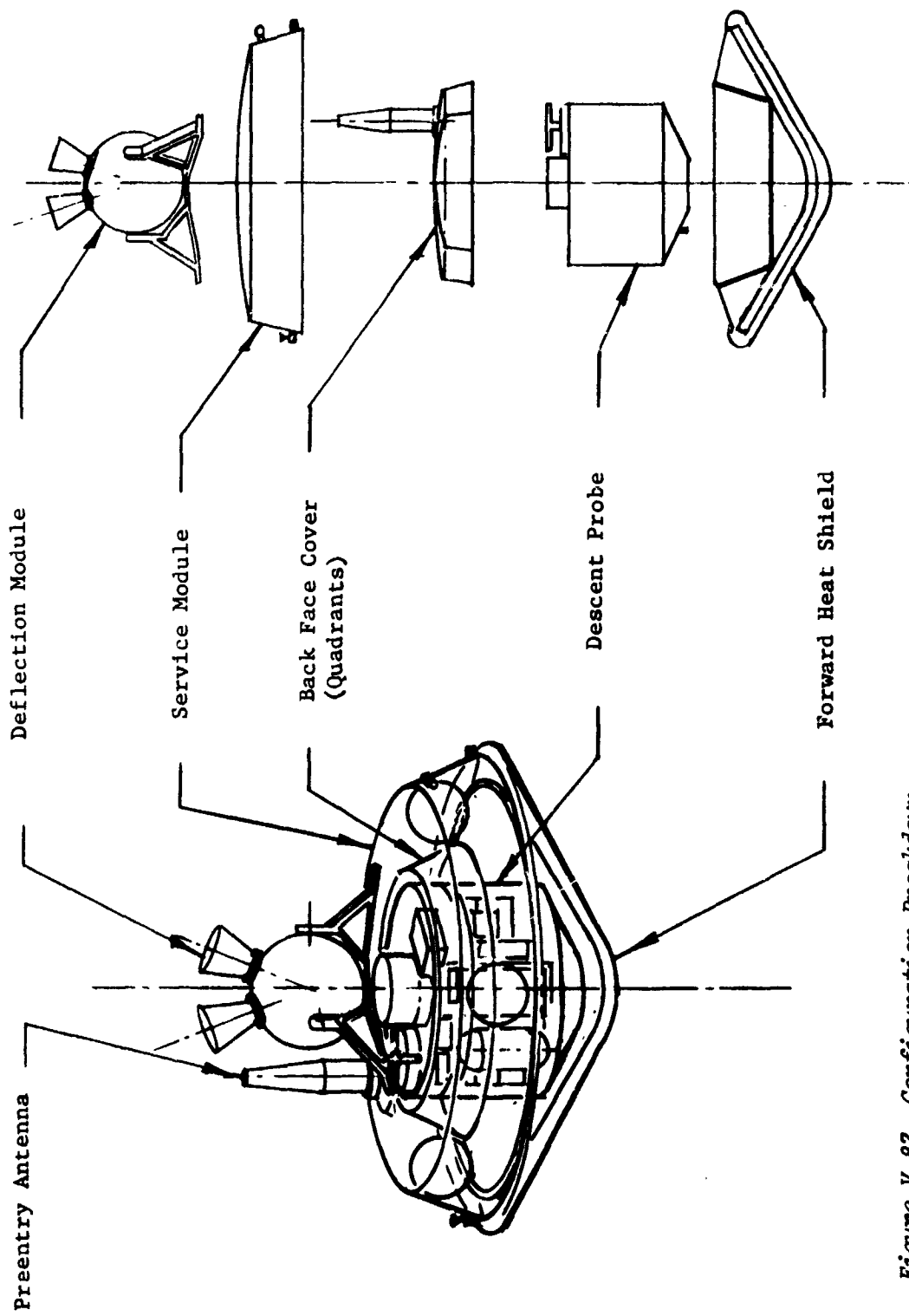


Figure V-87 Configuration Breakdown

The supply has an output capability of approximately 50 watts and a standby power dissipation of 450 mW. Because the supply is essentially in the standby condition at all times, except for approximately 5 sec after each event, the assumed average power requirement is 0.5 W.

- 5) Weight, Volume and Power - The physical characteristics of the electronics, conversion equipment, and filters are based on similar subsystems and engineering estimates. The remote activated batteries were estimated from the weight chart in Appendix G with an assumed 13.7 in.<sup>3</sup>/lb volume. Capacitor banks, pyrotechnic relay control and power distribution (relay) characteristics were based on part count and known volume and weight of the elements. The physical characteristics of these subsystems are summarized in Table V-26. A more complete description of these subsystems may be found in Volume III, Appendix G.

Table V-26 Physical Characteristics of the Pyrotechnic Subsystem

Power Subsystem	Size		Weight	
Post-Separation Battery	1550 cm <sup>3</sup>	(94 in. <sup>3</sup> )	3.13 kg	(6.9 lb)
Entry Battery	924 cm <sup>3</sup>	(56 in. <sup>3</sup> )	1.86 kg	(4.1 lb)
Hg-Zn Battery	10.2x5.1 cm	(4x2 in.)	0.41 kg	(0.9 lb)
Power Conditioning	625 cm <sup>3</sup>	(40 in. <sup>3</sup> )	0.91 kg	(2.0 lb)
Power Distribution	163 cm <sup>3</sup>	(10 in. <sup>3</sup> )	0.45 kg	(1.0 lb)
Power Filters	326 cm <sup>3</sup>	(20 in. <sup>3</sup> )	0.91 kg	(2.0 lb)
<u>Pyrotechnic Subsystem</u>				
Electronics	1223 cm <sup>3</sup>	(75 in. <sup>3</sup> )	0.91 kg	(2.0 lb)
Relays	1497 cm <sup>3</sup>	(91.8 in. <sup>3</sup> )	3.0 kg	(6.6 lb)
Capacitor Banks	1630 cm <sup>3</sup>	(100 in. <sup>3</sup> )	0.84 kg	(1.85 lb)

## 7. Attitude Control Subsystems (ACS)

This design approach makes use of a Sun sensor to measure solar aspect angle and Sun crossing time and a Jupiter sensor to measure Jupiter crossing time. Immediately following the delta velocity impulse maneuver, a preprogrammed series of pulses orients the probe near its final position. Then, after a waiting period of several damper time constants, measurements are made of solar aspect angle and the angle between the Sun and Jupiter, measured about the spin axis of the probe. These measurements are then used to develop subsequent precession programs to finalize the position of the probe.

The Sun sensor measures the angle between the spacecraft spin axis and the Sun. This can be a 9-bit digital output (with the Adcole Corporation instrument) or linear analog output (with the Honeywell Radiation Center instrument). The second axis is determined by the direction of the Sun when the plane containing the instrument's optical axis and the spacecraft spin axis crosses the sun. This is indicated by a pulse output from the Sun sensor. This Sun sensor and its electronics will weigh a maximum of 3.5 lb, and require a maximum of 2 watts, if the instrument is to cover the whole celestial sphere on each revolution about the spacecraft spin axis.

The Jupiter sensor is only required to develop a pulse when Jupiter crosses the optical axis. This device will be a Sun sensor with modified optics and reduced electronics.

The functional block diagram illustrated in Figure V-20 is representative of the electronics for all mission requiring an attitude control system. The functions required of the ACS electronics follow.

- 1) Process the solar aspect angle information. The data output of the solar aspect sensor is generally analog or digital gray code. In either case, this output is converted to binary digital for processing in the logic. The solar aspect output may be used as a measure of nutation by determining the maximum and minimum angles in a given set of measurements.
- 2) The pulse output from the Sun sensor is generated when the Sun crosses the sensors optical axis. Processing of this pulse will consist of establishing the center of the pulse by selecting the point at which the derivative (slope) is equal to zero (maximum amplitude), or averaging the time between preselected amplitudes. The Sun pulse is used to control the sector logic (discussed below) as well as provide attitude information in combination with a similar Jupiter pulse.

- 3) The pulse derived from the Jupiter sensor when the planet crosses the optical axis of the sensor is essentially similar to the Sun pulse described above and processing will be the same.
- 4) Sector logic will be used to establish correct precession jet firing intervals by driving an oscillator (VCO) so that the count register approaches a fixed value for every revolution. The angular position of the probe is determined when this counter reaches a preselected value.

The attitude control logic may be implemented by COSMOS if the state of the art permits. Since this is a critical maneuver, and with this design there is no method by which the success of the maneuver may be evaluated and readjusted by spacecraft or ground command, it is recommended that 100% redundant majority logic be used. The use of COSMOS will alleviate the power penalty that might otherwise be incurred. The Jupiter range at which this maneuver takes place is sufficient to ignore the effects of the Jupiter radiation belts.

The precession pulses will be implemented by pneumatic jets driven by appropriate power amplifiers. The design of these amplifiers should be such that they require low power during the standby condition.

With the constants appropriate to the various probes with dynamic attitude control, it appears that time constants of the order of one hour are feasible with 12-cm diameter viscous damper. Since the period during which the ACS system is required to be active may be as long as 6 hr, this would appear adequate. With a vehicle operating at 5 rpm, the damping period would extend out to 20 hr. This does not present a problem because there is no attitude control system dependent on the damping on missions with this vehicle angular rate. Furthermore, initial nutation would be due only to tipoff rates and approximately seven days are available for damping.

The estimated physical characteristics of the attitude control subsystem follow:

	<u>Size, in.<sup>3</sup></u>	<u>Weight, lb</u>	<u>Power, W</u>
Sun Sensor		3.5	2.0
Jupiter Sensor		2.0	1.0
Electronics	100	3.0	2.0

A more complete discussion of the attitude control subsystem may be found in Volume III, Appendix F of this report.

Thus, at service module jettisoning, the following unneeded hardware is removed: Sun and planet sensor, ACS system including tanks and nutation damper, service module structure and aft insulation, pre-entry antenna, separation system including timer, battery, springs, and pyrotechnic devices. Because all of the above is unneeded for planetary entry, the general arrangement of hardware locates these items in the service module.

Shortly after jettisoning of the service module, the probe enters the Jovian atmosphere. The planetary entry capsule basically consists of the descent probe surrounded by the fore and aft heat shield. The forward heat shield assembly, in turn, consists of a structural aeroshell capped with a graphite heat shield, containing additional hardware needed for entry but not needed for descent. The aft heat shield consists merely of an aft structural shell coated externally with ESA 5500M3 ablator, and a pyrotechnic system for its ejection. After high entry heating and deceleration loadings have passed, the aft head shield is opened and the four quadrants, their attachment hardware, and thrusters are ejected to permit parachute deployment. The main parachute is deployed at approximately Mach 0.7 by means of a pyrotechnic mortar. A ballistic coefficient of  $18.8 \text{ kg/m}^2$  ( $0.12 \text{ slug/ft}^2$ ) for the descent probe on the main parachute provides enough deceleration of the descent probe relative to the forward heat shield to drag the descent probe out of the heat shield. The forward heat shield is thus separated and jettisoned, having a ballistic coefficient sufficiently different from the descent probe to follow a different descent trajectory.

The forward heat shield, having performed the entry mission, carries with it the following items not needed for descent: aeroshell structure and heat shield; descent probe latches, and bands; pyrotechnic capacitors, relays, and squibs; spring cartridges and separation nuts; isotope heaters.

The radioisotope heaters were not really needed for entry, but were needed up to the time of entry; thus they were stowed in both the forward and aft heat shields. Stowage of the above items in the heat shield reduces the remaining weight for the descent probe, and hence the parachute size.

Parachute deployment and descent probe separation from the aeroshell is followed by deployment of a temperature probe through the side of the descent probe and opening of the inlet to the mass spectrometer at the nose of the descent probe. Both are accomplished pyrotechnically.

The last mechanical operation for the probe is to release the main parachute and to deploy a smaller parachute providing a higher ballistic coefficient of  $235 \text{ kg/m}^2$  ( $1.5 \text{ slug/ft}^2$ ) to accelerate the probe final descent.

The descent probe descending on the main parachute is shown in Figure V-87a. The pyrotechnic events for the probe mission are defined in Table V-26a. The interior of the descent probe is lined with a layer of lightweight thermal insulation 0.019 meter (0.75 in.) thick. This insulation serves no purpose during the cruise and coast phase, but protects the interior of the descent probe during parachute descent into the Jovian atmosphere.

*b. Structural Design* - The nominal Jupiter probe is designed to an entry angle of  $20^\circ$  at a latitude of  $5^\circ$ , resulting in an entry deceleration of 1500 g. Thus, the structure of this probe is designed for that level of inertia loading, with the exception of those components that are jettisoned before entry. The delta velocity deflection motor and the service module are both expended and jettisoned before entry. All of the vehicle is designed to a nominal launch environment of 10 g for the launch boost phase of flight.

The Jupiter probe is of high strength 7075-T6 aluminum construction with the exception of the service module structure. This item could also have been designed of aluminum; however, it contains various bulges to clear gas propellant bottles, and can be fabricated cheaper in low quantity production when designed of fiberglass. The equipment deck is designed as a thick disc that is machined in all areas to leave only a network of reinforcing beam sections. The equipment deck is shown in the cutaway drawing of the descent probe in Figure V-88. This approach will accommodate the numerous attachment points supporting the components on the equipment deck, and minimize weight of the deck itself.

The outer cylindrical shell of the descent probe must accept the inertia loads transmitted by the integral beams of the equipment deck, and distribute these loads as uniformly as possible into the descent probe support ring on the aeroshell. (The intent here is to avoid distorting the graphite heat shield any more than necessary, minimizing the potential for cracking the heat shield.) The outer cylindrical shell is designed using 10 equally spaced longerons to accept the loads from the equipment deck and distribute these loads into the probe cylindrical shell. A T-frame at the level of the equipment deck on the cylinder mates with the equipment deck and transfers the deck loads into the longerons.

Table 26a Pyrotechnic Events

<u>Event</u>	<u>Function</u>
1	Activate Probe Battery*
2	Eject Environmental Cover*
3	Separate Probe*
4	Probe Spinup
5	Cease Probe Spinup
6	Ignite Solid Rocket Deflection Motor
7	Eject Deflection Motor
8	Activate Probe Battery
9	Eject Service Module and Activate SM Deflection
10	Eject Base Cover (2 band cutters, 4 thrusters)
11	Deploy Parachute
12	Release Descent Probe from Aeroshell
13	Deploy Temperature Gage and Activate Science (open mass spec port)

\*Signal and power from spacecraft.

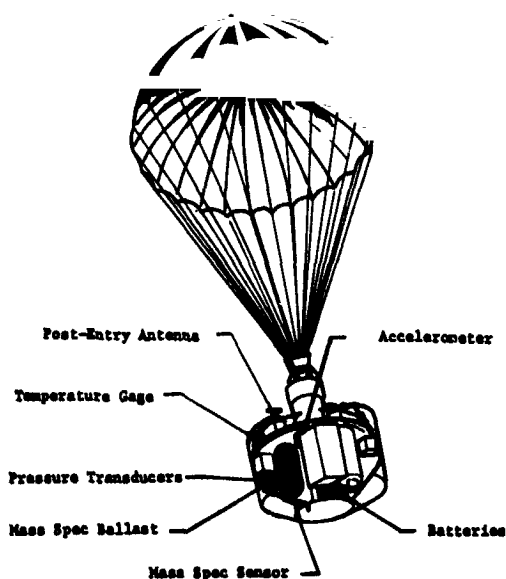
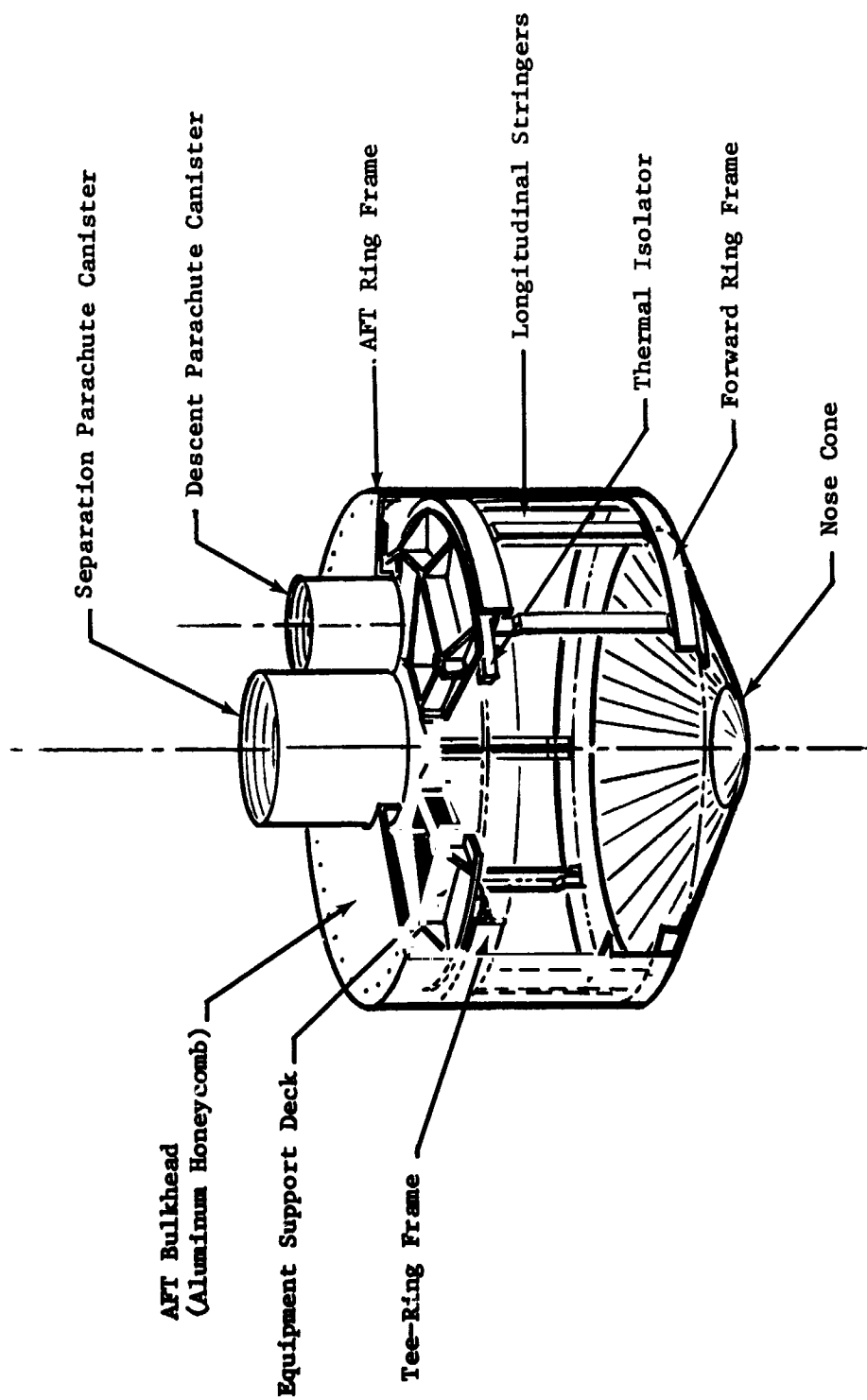


Figure V-87a Probe Descent



**NOTE:** 1. Material: 7075-T6 Aluminum.  
2. Designed By Entry Deceleration Loading.

*Figure V-88 Descent Probe Structure*



This frame is equipped with a thermal standoff ring between the equipment deck and the frame to minimize thermal heat transfer from the deck during descent into the Jovian atmosphere. The aft bulkhead of the descent probe is flat aluminum honeycomb for strength and stiffness. The nose cone of the descent probe is in tension during the high load regime of entry deceleration, and could be designed of minimum gage aluminum for any planetary entry deceleration. However, the structure is exposed to aerodynamic pressure ( $q$ ) values of the order of magnitude of  $4800 \text{ N/m}^2$  (100 psf) at aeroshell separation, is therefore also of ring stiffened monocoque construction. A main load bearing ring frame at the intersection of the nose cone and the cylindrical section provides for load transfer to the aeroshell structure.

The aeroshell structure consists of a ring-stiffened,  $60^\circ$  half-angle cone capped on the nose with spherical segment, having a radius equal to 20% of the base diameter. A triangular ring frame at the base of the cone completes the structure. This configuration is shown in Figure V-89. The design of the aeroshell is based on analysis of the cone as a pressure vessel exposed to external pressure, which is, in fact, the case. A design of a vessel resisting external pressure is governed by buckling criteria; hence the ring-frame design. A saddle ring frame approximately mid-length of the cone adapts the descent probe and introduces the descent probe inertia loads into the aeroshell.

The descent probe is retained in the aeroshell, before separation, by hold-down straps on a clamp ring. One end of the straps attach to the aeroshell and the other end attach to a clamp ring encircling the descent probe cylinder. Pyrotechnic retaining nuts permit the clamp ring to separate and release the descent probe at the appropriate time.

The base cover consists of four quadrants that join together to form a complete enclosure during planetary entry. These quadrants are stiffened quarter panels dovetailing into the adjacent panels to provide partial circumferential structural continuity. They are released by a pyrotechnic retaining nut and opened by four pyrotechnic thrusters. Hinges are provided at the base to retain the quadrants until they are nearly open and then release the quadrants permitting them to tumble away.

The service module, as mentioned earlier, is designed of fiberglass with aluminum ring frame reinforcement. Springs and pyrotechnic nuts provide for jettisoning of the service module.

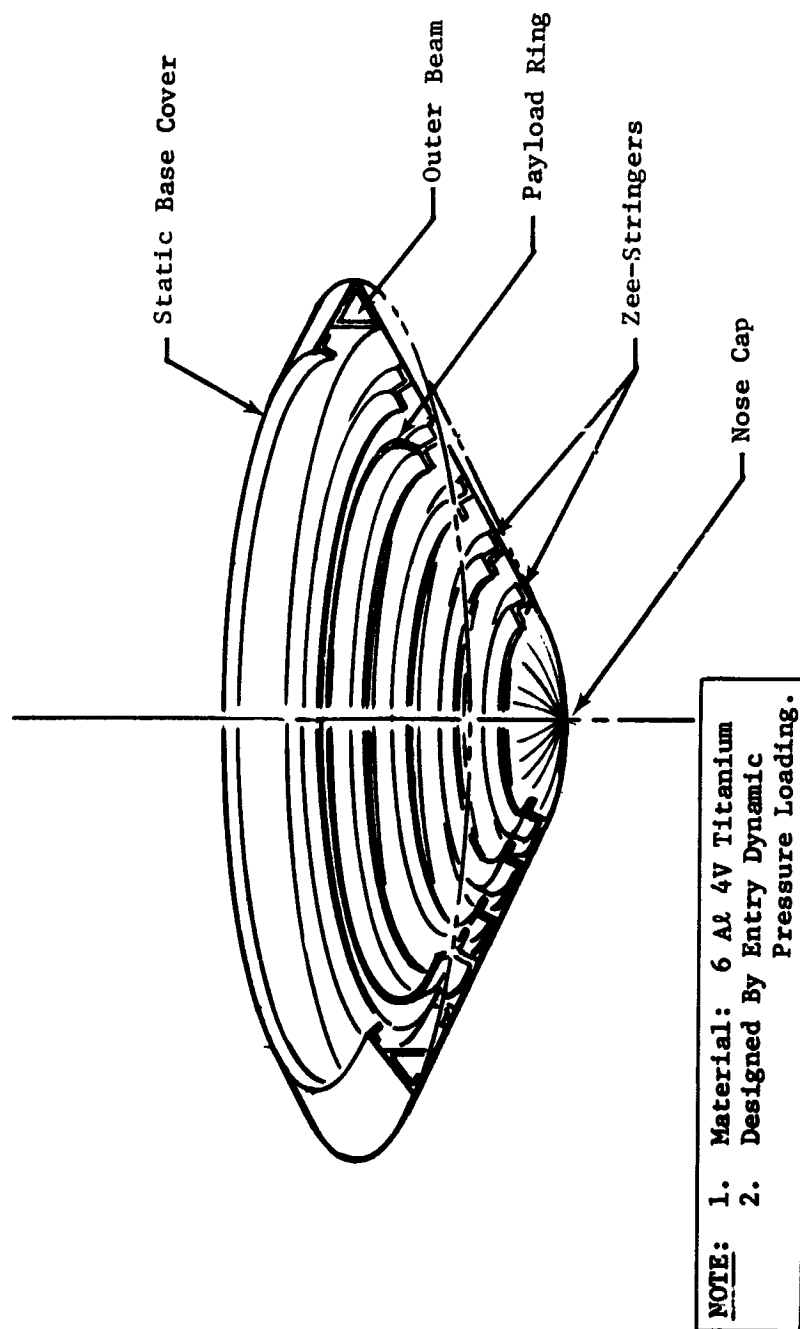


Figure V-89 Aeroshell Structure

c. *Parachute Assembly* - A two-stage descent was used for the nominal Jupiter probe for mission requirements of descent to the 30-bar level. For the two-stage descent, a disc-gap-band configuration was selected for the main parachute, and a flat circular configuration selected for the secondary parachute. A ballistic coefficient of  $18.9 \text{ kg/m}^2$  ( $0.12 \text{ slug/ft}^2$ ) is used for initial descent, and a ballistic coefficient of  $2.36 \text{ kg/m}^2$  ( $1.5 \text{ slug/ft}^2$ ) for the secondary parachute. For a descent probe weight of 43.8 kg (97.0 lbm), the corresponding parachute diameters are 2.46 meters (7.5 ft) and 0.45 meter (1.0 ft), respectively. The proportions of the disc-gap-band parachute selected are:

Disc diameter = 1.59 meters (5.2 ft)

Gap width = 0.088 meter (0.29 ft)

Bandwidth = 0.265 meter (0.85 ft).

The main parachute is programmed to open to Mach 0.7 at 100 millibars of pressure. The main parachute is deployed by a mortar using a pyrotechnic pressure source for ejection. It is stowed before ejection within the mortar folded to a packaging density of  $560 \text{ kg/m}^3$  ( $35 \text{ lbm/ft}^3$ ). The secondary parachute is deployed when the main parachute pulls it from its container. No mortar is used.

d. *Head Shield* - An entry ballistic coefficient of  $100 \text{ kg/m}^2$  ( $0.65 \text{ slug/ft}^2$ ) has been selected for entry of the nominal Jupiter probe into the Jovian atmosphere. This coefficient, combined with a  $20^\circ$  entry angle at  $5^\circ$  latitude, results in a planetary deceleration producing the desired conditions for staging of the descent probe from the heat shield/aeroshell. These resulting conditions at staging are Mach 0.7 at approximately 100 millibars pressure altitude (Ref Fig. V-90). The heat shield for this probe uses a high density (ATJ) graphite ablator material having an intrinsic heat of ablation of  $28 \text{ MJ/kg}$  ( $12,000 \text{ Btu/lbm}$ ). Using data from Figures V-35, V-36 and V-37, the mass fraction of the heat shield including a 2 cm (0.79 in.) carbonaceous backface insulator is shown to be 0.317. This value takes into account a correction factor of 0.88, for the probe diameter of 0.94 meter (37 in.), and a latitude correction factor of 1.01. Thus, the resulting heat shield weight is 29.71 kg (65.50 lbm). Of the weight, 23.14 kg (51.00 lbm) is lost during entry.

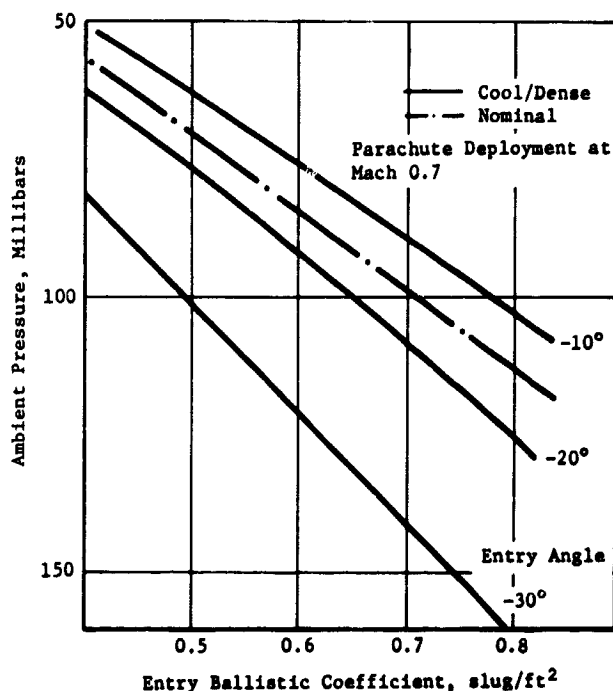


Figure V-90 Relationship of Ballistic Coefficient to Pressure Altitude at  $M = 0.7$

The estimate on heating for the base cover is based on a heating pulse of 2% of the nose cone heating. For a  $20^\circ$  entry angle, the total heating pulse is of the order of  $18.4 \text{ MJ/m}^2$  ( $1620 \text{ Btu/ft}^2$ ), and a heating pulse time is approximately 8 sec. This heating pulse requires  $3.2 \text{ kg/m}^2$  ( $0.65 \text{ lbm/ft}^2$ ) of ESA 5500M3 ablator to protect the base cover.

e. *Mass Properties* - The tabulation of the component weights of the nominal Jupiter probe is shown in Table V-27. It should be noted that component weights are grouped in categories in the table to arrive at a total weight. A 15% contingency factor is applied to the total weight including growth. The weight thus achieved is then reduced sequentially in the remainder of the table to provide weight data for different phases during entry and descent.

It should be noted that in calculating the weight of the entry heat shield, the 15% growth factor of total weight is first removed, and the heat shield mass fraction is multiplied by the reduced number. This is appropriate, because after the heat shield weight is calculated, a 15% growth factor is applied to the heat shield weight in the total vehicle sum. Thus, the 15% factor is not applied twice to the heat shield.

Table V-27 Nominal Jupiter Probe Weight Breakdown

	Weight	
	Kg	Lb
<u>Science</u>		
Temperature Gauge	0.45	1.00
Pressure Transducer	0.77	1.70
Accelerometer	0.59	1.30
Sensor	0.96	2.10
Converter	2.27	5.00
Neutral Mass Spectrometer Analyzer	2.72	6.00
Electronics	0.45	1.00
Pump	0.45	1.00
Ballast Tank	8.66	19.10
<u>Power &amp; Power Conditioning</u>		
Power Conditioner	0.91	2.00
Power Distribution Box	0.45	1.00
Power Filters	0.68	1.50
Entry Batteries	2.09	4.60
Post-Separation Batteries	1.76	3.88
	5.91	12.98
<u>Cabling</u>		
Inner Probe	2.95	6.50
External Structure	2.49	5.50
	5.44	12.00
<u>Data Handling</u>		
Data Handling System & Memory Banks	2.13	4.70
	2.13	4.70
<u>Attitude Control System (less propellant)</u>		
Sun Sensor	1.59	3.50
Planet Sensor	0.91	2.00
ACS System & Tanks	6.67	14.70
Nutation Damper	1.09	2.40
Accutron Timer	0.14	0.30
ACS Electronics	1.36	3.00
	11.76	25.90
<u>Communications</u>		
Pre-Entry Antenna	0.45	1.00
Post-Entry Antenna	0.23	0.50
RF Transmitter	2.70	6.00
RF Switch	0.23	0.50
	3.61	8.00
<u>Pyrotechnic Subsystem</u>		
Pyro Electronics	0.91	2.00
Pyro Capacitors (Probe)	0.27	0.60
Pyro Capacitors (External)	0.57	1.25
Pyro Relays (Probe)	0.77	1.70
Pyro Relays (External)	2.22	4.90
Mercury-Zinc Battery	0.41	0.90
Pyro Squibs	0.71	1.56
Pyro Thruster	0.45	1.00
	6.31	13.91

Table V-27 (cont)

	Weight	
	Kg	Lb
<b>Structures and Heat Shields</b>		
Descent Probe Structure	5.31	11.70
Equipment Support Deck	3.95	8.70
Base Cover	4.31	9.50
Service Module Structures	5.35	11.80
Aeroshell (2 lb for payload ring)	9.30	20.50
Forward Heat Shield	29.71	65.50
Aft Heat Shield	2.18	4.80
Deflection Motor Support	1.81	4.0
	61.92	136.5
<b>Mechanisms</b>		
Separation Spring Cartridges	1.22	2.70
Separation Nuts	0.77	1.70
Pin Puller	0.82	1.80
Latches & Bands	0.91	2.00
Main Parachute	3.72	8.20
Secondary Parachute	0.27	0.6
	7.71	17.00
<b>Thermal</b>		
External Insulation Blanket (forward heat shield)	1.77	3.90
External Insulation Blanket (base cover)	2.27	5.00
Probe Null Insulation (internal)	1.59	3.50
Isotope Heaters	1.81	4.00
	7.44	16.4
<b>Propulsion</b>		
Deflection Motor Cases	3.85	8.50
Deflection Motor Propellant	10.66	23.50
ACS Propellant	1.50	3.30
	16.01	35.30
<b>Total</b>	136.92	301.98
<b>15% Contingency</b>	20.54	45.30
	157.46	347.28
<b>Items Deployed for Despun Weight</b>		
Deflection Motor Supports	1.81	4.00
Separation Spring Cartridges	0.41	0.90
Separation Nuts	0.32	0.70
ΔV Motor Cases	3.85	8.50
Propellant	12.16	26.80
	18.55	40.90
<b>15% Contingency</b>	2.77	6.10
(347.28 - 47.00 = 300.28 lb)	21.32	47.00
157.46 - 21.32 = 136.14 kg		

Table V-27 (concl)

	weight	
	Kg	Lb
<u>Entry Weight</u>		
External Cabling	2.49	5.50
Sun Sensor	1.59	3.50
Planet Sensor	0.91	2.00
ACS System (including tanks)	6.67	14.70
Nutation Damper	1.09	2.40
Accutron Timer	0.14	0.30
Pyro Capacitors	0.32	0.70
Pyro Relays	1.14	2.50
Service Module Structure	5.35	11.80
Separation Spring Cartridge	0.41	0.90
Separation Pin Pullers	0.41	0.90
External Base Cover Insulation Blanket	2.27	5.00
Separation Battery	1.77	3.90
ACS Electronics	1.36	3.00
	<u>25.92</u>	<u>57.10</u>
15% Contingency	<u>3.88</u>	<u>8.60</u>
(300.28 - 65.70 = 234.60 lb)	<u>29.80</u>	<u>65.70</u>
136.14 - 29.80 = <u>106.34 kg</u>		
<u>Post Entry Weight</u>		
Forward Heat Shield Ablated	23.14	51.00
Aft Heat Shield Ablated	1.81	4.00
Insulation Blanket (forward HS)	1.77	3.90
Pre-Entry Antenna	0.45	1.00
	<u>27.17</u>	<u>59.90</u>
15% Contingency	<u>4.08</u>	<u>9.00</u>
(234.60 - 68.90 = 165.70 lb)	<u>31.25</u>	<u>68.90</u>
106.34 - 31.25 = <u>75.09 kg</u>		
<u>Weight on Parachute (Initially)</u>		
Base Cover Quadrants	4.31	9.50
Base Cover Heat Shield (not ablated)	0.36	1.80
Separation Pin Pullers	0.41	0.90
Separation Nuts	0.23	0.50
Isotope Heaters	0.91	2.00
Pyro Thrusters	0.45	1.00
	<u>6.67</u>	<u>14.70</u>
15% Contingency	<u>1.00</u>	<u>2.20</u>
(165.70 - 16.90 = 148.80 lb)	<u>7.67</u>	<u>16.90</u>
75.09 - 7.67 = <u>67.42 kg</u>		
<u>Weight on Parachute (Final)</u>		
Pyro Capacitors	0.27	0.60
Pyro Relays	1.09	2.40
Pyro Squibs	0.72	1.60
Aeroshell	9.30	20.50
Forward Heat Shield (not ablated)	6.58	14.50
Spring Cartridges	0.41	0.90
Separation Nuts	0.22	0.50
Latches and Band	0.91	2.00
Isotope Heaters	0.91	2.00
	<u>20.41</u>	<u>45.00</u>
15% Contingency	<u>3.08</u>	<u>6.8</u>
(148.80 - 51.80 = 97.00 lb)	<u>23.49</u>	<u>51.80</u>
67.42 - 23.49 = <u>43.93 kg</u>		
<u>Final Descent Weight on Secondary Chute</u>		
Main Parachute (canopy & risers)	1.74	3.85
15% Contingency	<u>0.26</u>	<u>0.50</u>
(97.00 - 4.40 = 92.60 lb)	<u>2.00</u>	<u>4.43</u>
43.93 - 2.00 = <u>41.93 kg</u>		

The moment of inertia about the three orthogonal axes of the probe have been computed. For the nominal Jupiter probe, the moment of inertia values are:

$$I_{zz} = 12.2 \text{ kg/m}^2 \text{ (9.0 slug/ft}^2\text{) (spin axis)}$$

$$I_{xx} = 9.5 \text{ kg/m}^2 \text{ (7.0 slug/ft}^2\text{)}$$

The moment of inertia about the spin axis is used for attitude control system sizing. The ratio of  $I_{zz}/I_{xx}$  is an indicator of probe stability about the spin axis and preferably should be a value of 1.20 or higher.

#### 9. Propulsion Subsystem

The propulsion subsystem for the nominal Jupiter probe consists of a spherical solid-propellant rocket motor to provide a mission deflection delta velocity, and a cold gas system to provide the spin-design-precess maneuvers for attitude control. This combination was shown in the parametric studies to be the lightest of the candidate systems, provided that a fixed total impulse for the deflection maneuvers is acceptable.

*a. Deflection Motor System* - The selected solid propellant motor is capable of being stored for long periods of time at temperatures of 256°K to 322°K (0°F to +120°F). The temperature aboard the spacecraft during the long period of cruise has nominally been selected at 291°K (65°F). The preferred operating temperature of the solid propellant motor is over the range of 283°K to 311°K (50°F to 100°F), and both storage and operating temperature are met by the nominal storage temperature aboard the spacecraft.

A dual nozzle configuration has been chosen for the solid propellant motor. This was done to obviate the problem of impinging the spacecraft with solid particles from the exhaust of the probe rocket motor. The configuration of the motor is shown in Figure V-91. It has two nozzles each located 22½° off the centerline of the motor axis. Each nozzle, in turn, is a 15° half-angle cone. With this configuration, the solid particulate of the aluminized propellant will be discharged in a direction that does not intercept the spacecraft. With a separation velocity from the spacecraft of 0.91 m/sec (3 fps) and a coast time of 15 min before igniting the deflection motor, the probe is 0.82 km (2700 ft) from the spacecraft at ignition. This distance, plus pointing of the rocket engine exhaust nozzles, will assure that the spacecraft is undamaged by the rocket engine exhaust.



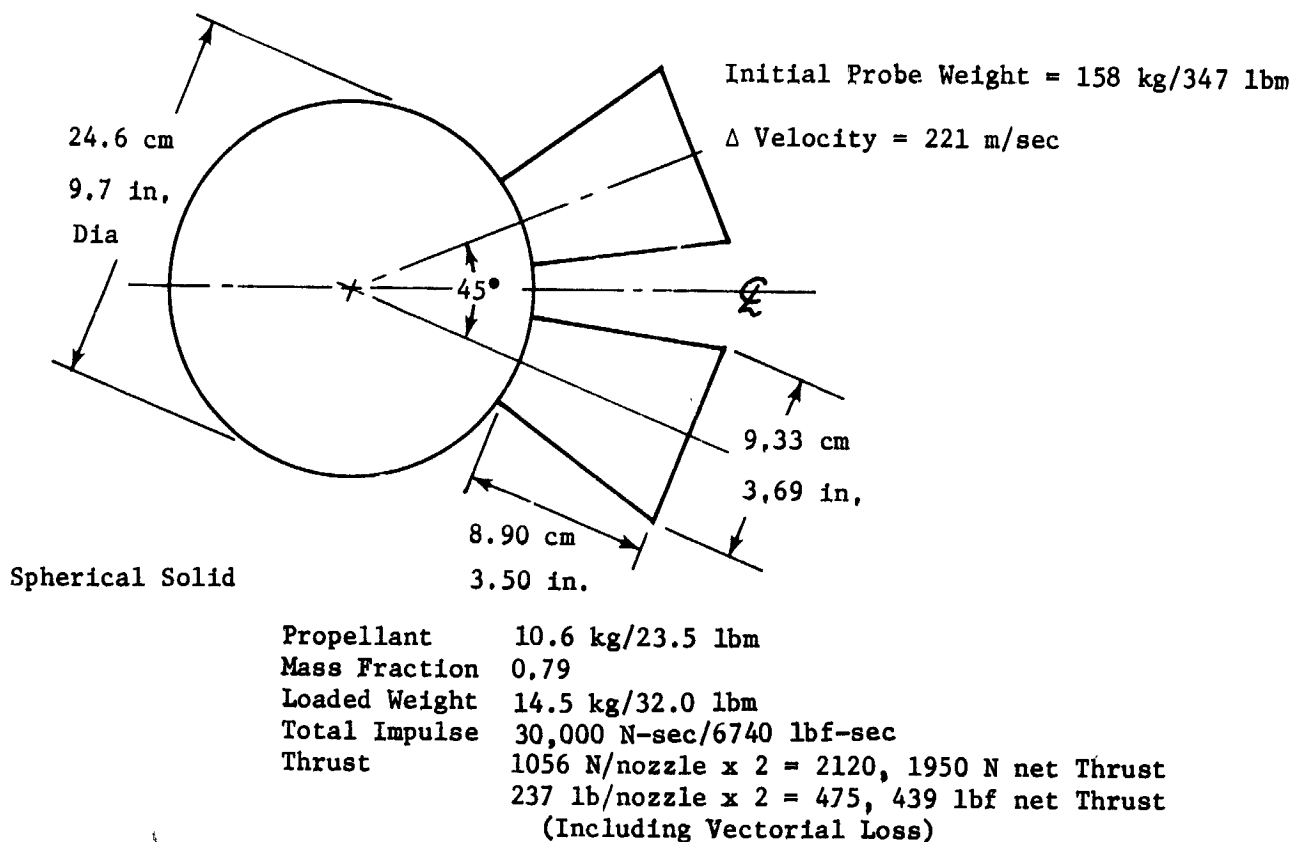


Figure V-91 Deflection Propulsion Motor

The functional requirement for the motor are for the motor to provide a deflection delta velocity of 221 m/sec (725 fps) to a probe weighing 141 kg (312 lbm) not including the weight of the motor. Using a theoretical specific impulse,  $I_{sp} = 287$  sec,

which is achievable with this type of motor, the necessary weight of propellant to provide the delta velocity is 9.8 (21.7 lbm). This value is divided by a propellant mass fraction of 0.79, and a thrust vectorial loss coefficient of 0.924 ( $\cos 22.5^\circ$ ) for the dual nozzles to give the total loaded motor weight of 14.5 kg (32.0 lbm). This weight also includes a weight penalty, above and beyond the mass fraction, of 0.68 kg (1.5 lbm) to account for the extra nozzle. This weight brings the probe total weight up to 157 kg (347 lbm). The motor configuration and characteristics are shown in Figure V-91. It should be noted that for a high performance solid propellant rocket motor, the total impulse of the motor is fairly constant (within 0.75%) over the normal range of usage temperatures, since thrust level and burning time vary in opposite directions with changes in motor temperature. The analysis of the deflection motor is shown in Appendix M.

b. *Attitude Control System* - The attitude control system provides for spinning the probe to approximately 10.5 rad/sec (100 rpm) to stabilize the probe attitude while firing the deflection delta velocity motor. This spin rate also permits precessing the probe from attitude required for the deflection delta velocity to a different heading for planetary entry. For the nominal Jupiter probe, this precession angle is 0.87 rad (51°). The attitude control system must then despin the probe to a rate of approximately 0.52 rad/sec (5 rpm) for entry into the planetary atmosphere. Finally, the attitude control system must impart a delta velocity to the service module of 0.46 m/sec (1.5 fps) for jettisoning of the module.

A cold gas (dry nitrogen) system, shown in Figure V-92, is used for the attitude control of the probe. This system gas is stored at a pressure of approximately  $23.5 \times 10^6 \text{ N/m}^2$  (3400 psi) in three spherical bottles. The entire system is contained within the service module of the probe. The system is placed in operation by opening the pyrotechnic valves to the gas storage bottles. This releases the stored gas through a pressure regulator and through a series pair of normally open pyrotechnic valves. The gas then exits through a pair of spin nozzles on opposite sides of the probe to impart the desired spin. A timer operates the shut off of the gas to the spin nozzle by closing the normally open pyrotechnic valves.

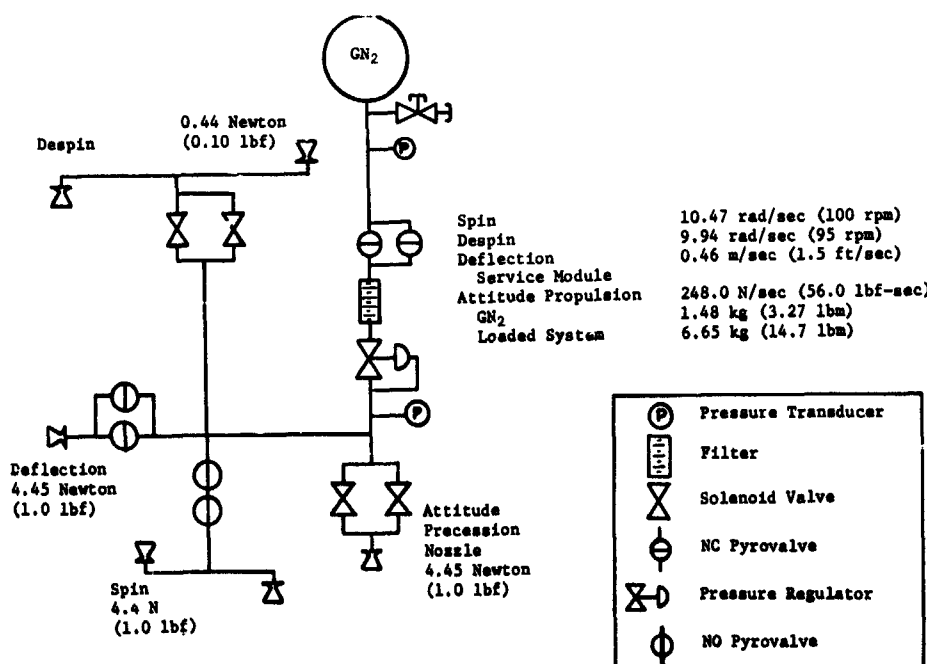


Figure V-92 Jupiter Probe Attitude Control System

To precess the probe through its attitude precession maneuver, the single precession nozzle is pulsed every revolution of the probe by passing nitrogen gas through the two parallel-connected precession valves. The timing and operation of the precession valves is controlled by the ACS electronics, which, in turn, uses intelligence from the Sun and planet sensors for operation. The precession valves are solenoid valves capable of repeated operation.

The despin maneuver is controlled by a pair of nozzles located on opposite sides of the probe and pointed in opposite directions to those of the spin nozzles. The gas is supplied to the despin nozzles through a pair of solenoid valves connected in parallel. A timer controls the despin maneuver by closing the valves to shut off the system.

The service module deflection maneuver to jettison the module is accomplished by opening a pair of parallel-connected pyrotechnic valves to vent the remaining nitrogen gas through the single deflection nozzle.

The pressure regulator is used in the system to provide better control of the spin-despin and precession maneuvers. A plain blowdown system without the regulator could have been used, but this would have made the system more sensitive to loss of gas by leakage over the long time period of the cruise phase of flight. The  $I_{sp}$  of the system is 72 sec.

The component weights breakdown of the system follows:

	<u>kg</u>	<u>lbm</u>
Fill Valves (1)	0.113	0.25
Transducers (2)	0.226	0.50
Squib Valves (6)		1.50
Filters (1)	0.158	0.35
Regulators (1)	0.182	0.40
Solenoid Valves (8)	0.725	1.60
Thrusters, 1 lbf (4)	0.362	0.8
Thruster, 0.1 lbf (2)	0.090	0.2
Lines	<u>0.724</u>	<u>1.6</u>
TOTAL	3.26	7.20

Approximately 1.48 kg (3.27 lb) of gas is provided for the system and the gas is stored in three spherical bottles weighing a total of 1.93 kg (4.25 lb); thus, the total system weight is 6.67 kg (14.72 lbm). The analysis of the ACS system is shown in Appendix F.

#### 10. Thermal Control Subsystems

Thermal control is required to maintain the probe equipment within acceptable temperature limits throughout all phases of the outer planet mission. For the nominal Jupiter probe, the thermal design concept consists of multilayer insulation, thermal coatings, and radioisotope heaters during the spacecraft cruise and probe coast phases. For the entry and descent portions of the mission, the probe relies on sufficient thermal inertia and low density foam insulation protection internal to the probe shell. An integral discussion of the thermal control subsystem design has been previously presented in Section A.10.a. of this chapter.

The pivotal temperature from standpoint of thermal design is the probe temperature at the end of the mission coast phase. For the nominal Jupiter probe (cool/dense atmosphere), the primary thermal problem is one of losing too much thermal energy to the atmospheric environment during descent. The entry temperature, therefore, must be adequate to allow sufficient leeway for probe cooling. Likewise, however, the probe equilibrium temperature during the long duration spacecraft cruise must be safely below the upper allowable battery storage limits.

A probe thermal analysis was performed for the nominal Jupiter probe mission defined. The basic probe configuration consists of a 94 cm diameter probe design with a propulsion system, Sun and planet sensors, and an attitude control system. To analyze the probe's thermal performance, two finite-element thermal math models were constructed for the descent probe, and the coast probe and probe/spacecraft combination. The probe thermal models have been previously discussed (Sections A.10.d and A.10.e of this chapter) and consist of 16 nodes and 23 conductors for the coast probe and probe/spacecraft combination, and 18 nodes and 28 conductors for the descent probe. On the basis of the thermal analysis performed, a complete thermal history of the nominal Jupiter mission has been constructed and is presented in Figure V-93. Determination of the spacecraft cruise and coast temperatures is based on the radioisotope heater power present and the degree of solar energy absorption during the coast phase. The probe temperatures represent the aggregate internal equipment, which includes the service module during cruise and coast, and the RF transmitter when active. The RF transmitter is shown separate from the probe internal equipment due to its high electrical dissipation and relatively small mass.

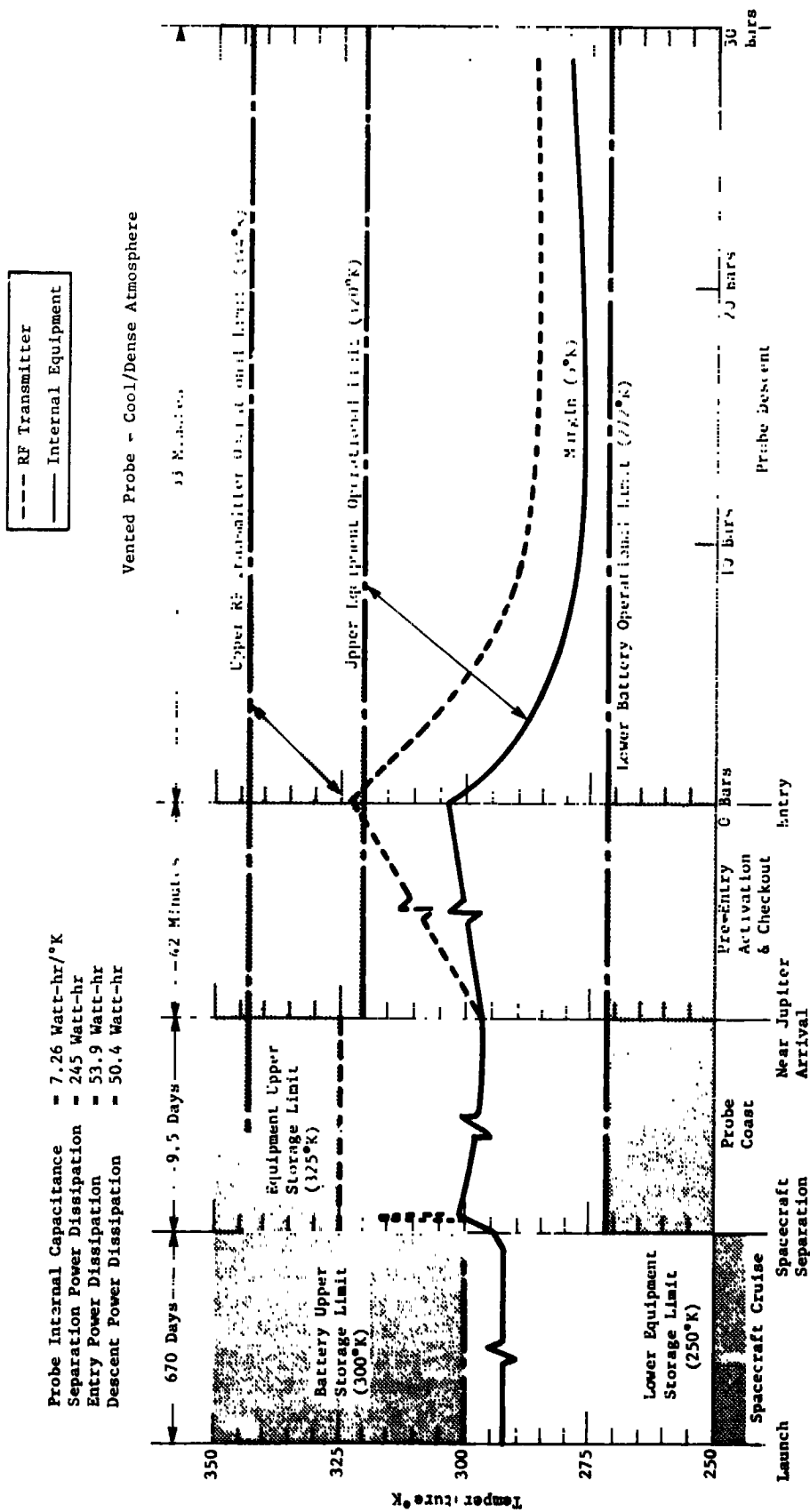


Figure V-83 Launch to Descent Thermal History of the Mariner Jupiter Probe

The results presented show that the thermal design selected is adequate to maintain the probe temperatures within limits under nominal conditions. Sufficient probe thermal mass is present during the cruise and coast phases such that brief excursions of the thermal boundary conditions, such as midcourse corrections or motor firings, should cause only minor variations in probe temperature. Trajectory uncertainties for entry are only seven minutes for the nominal Jupiter mission and would contribute to only slight initial descent probe temperature uncertainty. For descent, the worst-case model atmosphere encounter was considered and conservative foam insulation properties were assumed. The biggest uncertainties in the thermal analysis are the multilayer insulation performance and the coast transient response of the internal equipment inside the descent capsule. Temperature changes required during coast, however, were designed to be small for this mission and the multilayer insulation therefore is the most critical thermal design item.

Since the radioisotope heater output is constant and cannot be changed during the mission, the multilayer performance will have to be accurately determined by thermal tests before final hardware design. Likewise, the repeatability and possible degradation of the probe thermal coatings will have to be carefully evaluated. Since insulation damage by meteroids or micrometeoroids would be catastrophic, an environmental cover is provided during spacecraft cruise. The maximum temperature excursion of the RF transmitter predicted is 18°K which will occur at entry. The aerodynamic entry heating is brief and the aeroshell jettisoned soon after entry protecting the descent capsule.

*a. Cruise and Coast Thermal Control* - Thermal control during the spacecraft cruise and the probe coast phases of the mission is provided by multilayer insulation, thermal coatings, and radioisotope heaters. The multilayer insulation fully encapsulates the probe except for the deflection motor throughout cruise and coast. The deflection motor is equipped with its own thermal blanket and a thermostatically controlled electrical resistance heater powered by the spacecraft. Since the deflection motor is fired immediately after spacecraft separation, the motor insulation blanket is also mounted to the spacecraft. The spacecraft power requirement for the deflection motor will be less than 5 watts provided that the heater is activated in sufficient advance of spacecraft separation (100 days). Any motor temperature in the desired range of the probe temperature is acceptable. Since a "burn to completion" solid has been selected for the deflection maneuver, the temperature selected must be maintained for precise performance.

The multilayer insulation thickness chosen for the nominal Jupiter probe was 1.5 cm or approximately 70 layers of insulation. The insulation thickness was selected to achieve a reasonable compromise between heater power and insulation bulk. The thermal coatings selected were chosen to allow the least degree of temperature change due to probe solar impingement following spacecraft separation. For the nominal Jupiter probe, thermal coating values of  $\alpha/\epsilon = 0.25/0.25$  were selected for the aft section (tail) and a value of  $\epsilon = 0.80$  was chosen for the forward section (nose). The probe/solar aspect angle is considered  $180^\circ$  with solar impingement directly on the aft section of the probe cross section. The solar constant at near-Jupiter was assumed  $54.3 \text{ watt/m}^2$ .

Figure V-94 presents the radioisotope heater power required to maintain respective probe internal temperatures during cruise and coast. Since the probe temperature must be below  $300^\circ\text{K}$  during cruise (upper storage battery limit), 32 watts of radioisotope heater power were selected for nominal mission thermal control providing a  $8^\circ\text{K}$  margin. The correlation of heater power shows that approximately a  $5^\circ\text{K}$  temperature increase can be expected following spacecraft separation. Approximately 245 W/hr of electrical thermal energy are dissipated during separation that will overshoot the probe temperature slightly and cause probe cooling during early coast. In either case, the transient effects in the 9.5-day coast are not significant because of the small temperature changes predicted.

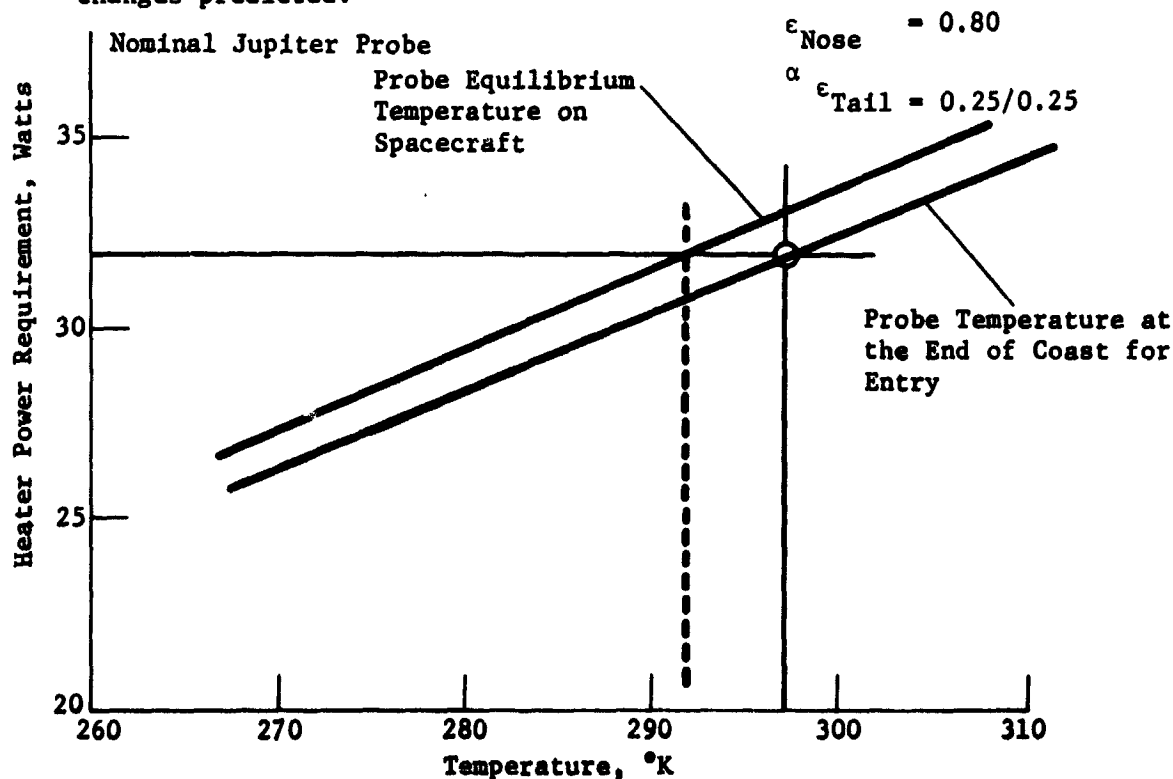


Figure V-94 Radioisotope Heater Sizing Based on Probe Thermal Coating Selection

The environment cover provided during spacecraft cruise is primarily for meteoroid protection, but also provides a coating function for possible solar impingement. The environmental cover coating desired would be  $\alpha/\epsilon \approx 0.20/0.80$  for adequate solar rejection and minimum blockage of probe heat rejection.

*b. Entry and Descent Thermal History* - The complete nominal Jupiter probe thermal history presented in Figure V-93 emphasizes the entry and descent thermal profile. Following launch, the probe is basically in thermal equilibrium and steady-state conditions throughout cruise and coast. Initiated with pre-entry probe activation and checkout, the transient stages of the mission begin. The time between activation and entry is important since the probe is slowly heating because of internal electrical heat dissipation, and the RF transmitter is storing excessive thermal energy because of its standby status. At entry, however, the probe begins the atmosphere descent portion of the mission and the rapid heat losses to the environment become predominant. The transmitter reaches its maximum temperature at entry as does the internal probe equipment.

The power profile used for the nominal Jupiter mission thermal analysis is presented in Figure V-95. This power profile does not reflect the increase in transmitter efficiency which was incorporated for subsequent analyses. The power profile presented includes 80 W of electrical dc power supplied to the transmitter only 20 W of which is radiated as RF power (25% efficiency). Total thermal energy dissipation during pre-entry activation and checkout is 53.9 W/hr and during descent 50.4 W-hr.

The ballistic coefficients chosen for the science return descent were 0.12 slug/ft<sup>2</sup> down to 10 bars pressure with staging to a 1.50 slug/ft<sup>2</sup> ballistic coefficient for the remaining descent to 30 bars pressure. The probe thermal history shown in Figure V-93 presents the descent probe temperature response versus depth of descent pressure. The total descent elapsed time is approximately 33 minutes. Figure V-96 presents the descent atmosphere temperature and pressure profiles based on the above coefficients. At 10 bars the mission is within 7 min of completion.





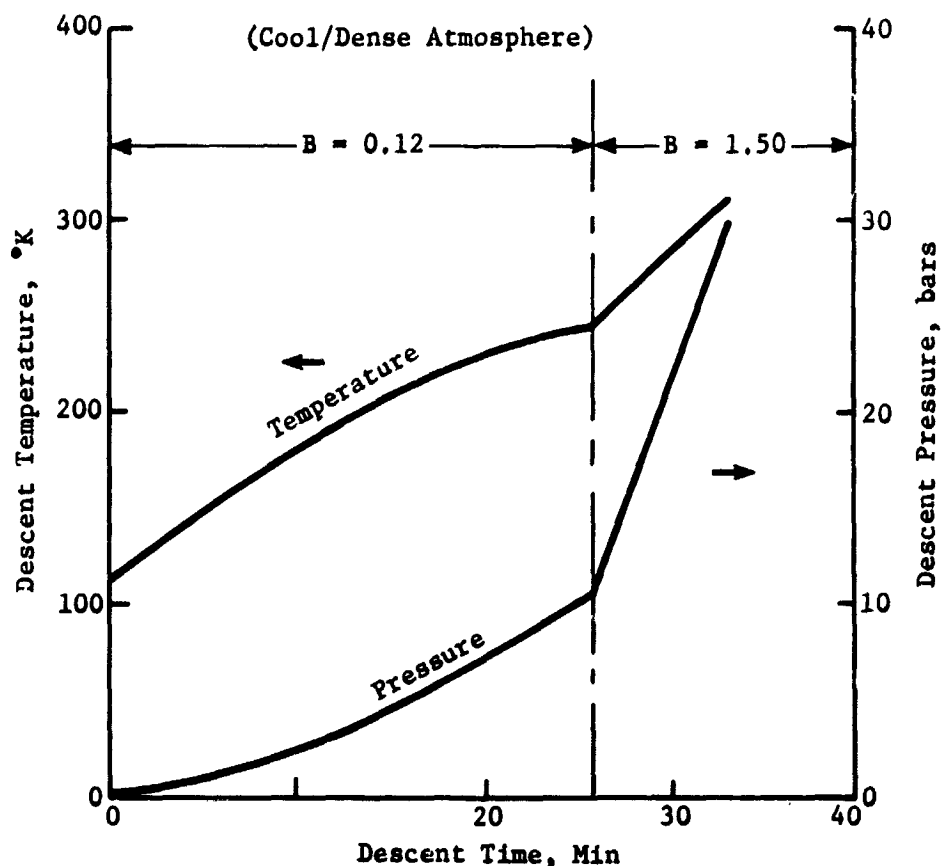


Figure V-96 Nominal Jupiter Mission, Descent Temperature and Pressure Profiles

The probe temperature margins predicted on the basis of probe thermal analysis for the nominal Jupiter mission follow:

Temperature Margin	Spacecraft Cruise Phase, °K	Probe Coast Phase, °K	Entry-Descent Phase, °K
Above Equipment Lower Limit	42	22	55
Below Equipment Upper Limit	8	23	17
Below Transmitter Upper Limit	NA	28	22

c. *Alternative Thermal Control* - The probe thermal history indicates that two possible areas of concern exist from a standpoint of adequate thermal control. The probe equilibrium temperature during coast must be maintained close to the battery upper storage limit (-8°K margin) to eliminate significant probe temperature changes during coast and establish sufficient leeway for the minimum probe temperature experienced during descent (+5°K margin).

To improve coast thermal control, selection of probe thermal coatings with a higher  $\alpha/\epsilon$  ratio would be recommended to increase the probe equilibrium temperature between cruise and coast and thereby allow lower cruise temperatures and increased temperature margin. Since probe coast temperature transients are undesirable for this mission, spacecraft heater power would be required to raise the internal probe temperature to the coast equilibrium before separation.

For improved descent thermal design, the entry temperature can be increased as discussed above, but improvement in probe isolation during descent appears more favorable. The batteries themselves could be isolated with standoffs and insulation, although this is not recommended because of the high entry decelerations and possible violent battery reactions. Other alternatives would be the nitrogen gas environmental control approach discussed in Section A.10.b of this chapter, or the use of improved insulations or filler materials to decrease the internal free convection. Of the possible thermal control alternatives, the  $N_2$  gas system appears to have the most advantages and the best reliability for minimum weight. This approach essentially seals the probe for the first few bars of descent and eliminates the high heat losses experienced during those times.

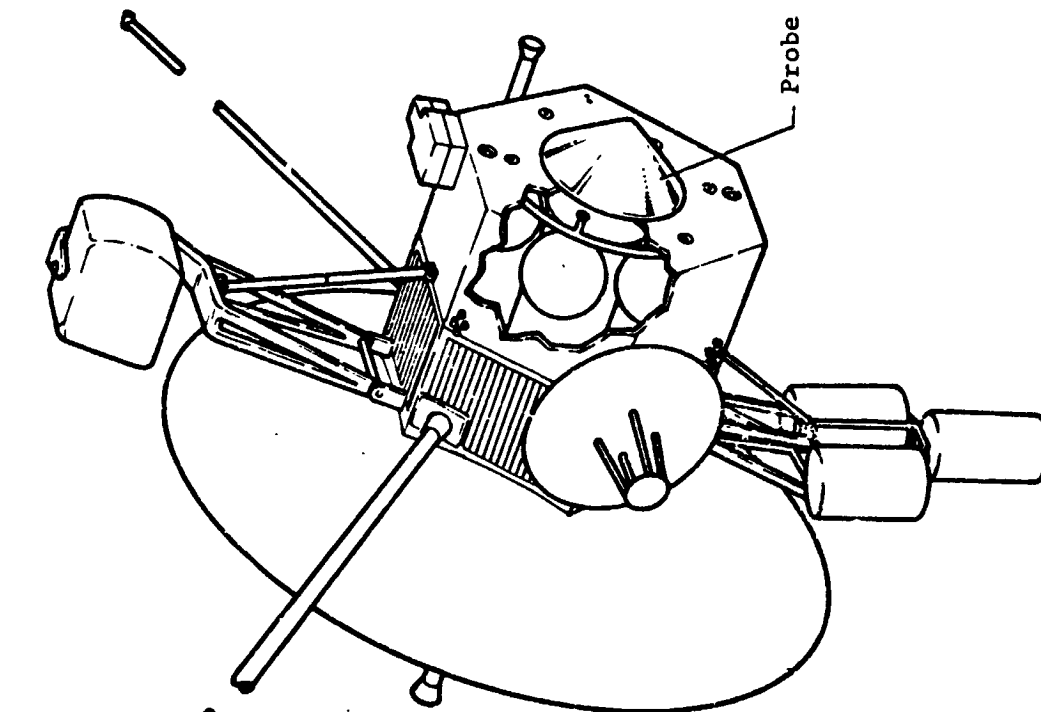
#### 11. Probe to Spacecraft Integration

The integration of the planetary probe with a carrier spacecraft was performed using a Martin Marietta modified outer planet spacecraft (MOPS) as the carrier. The configuration of the spacecraft with the nominal Jupiter probe attached is shown in Figure V-97. The probe is mounted on the aft end (for launch) of the spacecraft, with the probe heat shield pointed away from the spacecraft, providing the proper probe orientation with respect to the spacecraft for later separation. The figure also shows the functional interfaces for the various phases of the mission. Further discussion of the interfaces as well as a description of the spacecraft follows.

*a. Spacecraft Description* - The MOPS (Modified Outer Planet Spacecraft) is a hex-bodied, 3-axis-stabilized vehicle with a JS-77 mission dry weight of 1241.4 lb. For the Jupiter dedicated missions, the dry weight was reduced to 929 lb. The center of the hexagon is hollow and serves as a cradle for the probe. The propulsion system is powered with monopropellant hydrazine that is used by both the ACS and the TCS. A fixed 12-ft diameter high gain antenna provides the communication link with Earth and a smaller, gimbaled antenna tracks the probe. Electrical power is provided by three multihundred-watt RTGs. The baseline payload consists of 130 lb of scientific experiments mounted on extendable booms and a two-axis scan platform. The MOPS is launched on a Titan IIIE/Centaur/Burner II vehicle encased in a standard Viking around.

Probe Weight: 347 lb

Spacecraft Mod (MMC MOPS): 54 lb



**Cruise:**

- Environmental Cover
- T/C Power - 5 W
- Monitor (on Demand)
- 0.5 watts and 80 bits

**Preseparation Checkout:**

- Power - 8 W Ave; 30 W Peak
- Checkout Signals
- Data Monitor - 1400 bits

**Separation:**

- Probe Pointing - 2°
- Battery Activation Signal
- Separation Signal

**Post-Separation:**

- Track Probe
- Receive Data - 30 bps;
- 60 to 80Kbits

*Figure V-97 MOPS Spacecraft/Jupiter Probe Integration*

b. *Structure and Mechanical* - The probe is attached to the spacecraft through a mechanical release joint incorporating a matched set of separation springs. The probe is held in place by means of attachments incorporating explosive nuts for release. Separation is accomplished by firing the pyrotechnic nuts, allowing the probe and spacecraft to be pushed apart. A delta velocity at separation of 0.915 m/sec (3.0 fps) provided by the springs allows a satisfactory separation velocity without excessive angular tip-off rates (actual experience with the Vela satellite indicates that tipoff rates less than 0.0087 rad/sec (0.5 deg/sec) can be achieved using spring separation systems.) It can be shown that the energy to provide a separation velocity of 0.915 m/sec (3.0 fps) for a 155 kg (344 lbm) probe from a 498 kg (1100 lbm) spacecraft is approximately 50.6 N/m (37 ft/lb) (Reference Appendix Q). This level of energy is achievable by three springs weighing 0.089 kg (0.197 lbm) each.

c. *Probe Pre-Separation Checkout* - The pre-separation checkout period should be initiated sufficiently before separation to allow at least two opportunities for ground command. This will require approximately six hours at Jupiter range. During this period, all subsystems will be activated in sequence and interrogated as to decode and implement spacecraft commands and return the diagnostic data. Since each subsystem will be activated for short periods, the spacecraft power required for the DHS. Peak power requirements are determined by DHS power and the maximum power of the individual probe subsystem. If the spacecraft is peak power limited, the probe subsystem may have to be operated in a degraded mode. In addition to the above, the probe may require up to 5 W to heat the deflection motor. The probe post-separation battery is not activated until about one minute before separation. Two critical timing events occur during this period. The Accutron timer, which has a fixed response period, must be started at a time consistent with the predicted entry time. The timing interval is established before launch and cannot be reprogrammed during flight. The post-separation sequence is controlled by timing circuits in the DHS or ACS. The time for the post-separation events is critically related to the separation period (i.e., spinup must occur at  $S + 0.5$  sec). Post-separation probe battery activation and the separation pyrotechnic events are spacecraft functions. The estimated average and peak power required from the spacecraft during pre-separation checkout are 8.0 W and 30 W, respectively.

d. *Relay Link* - The mission profile specifies three communication periods for the nominal probe mission: (1) a brief period at the end of the post-separation activity to provide data on the status of the probe, (2) a low data rate communication period before entry. During the pre-entry period probe data is transmitted on probe and scientific instrument status that may be useful in the ultimate reduction of the descent data, (3) descent data transmission of scientific data.

The post-separation communication has not been evaluated in depth. It has been included in the mission profile as a desirable option which enables the evaluation of the probe/spacecraft link under favorable conditions.

The communications range will be small (55 km) and space loss will be decreased approximately 45 dB over the entry communications range. The spacecraft will exercise the frequency acquisition and tracking functions, check probe frequency (Doppler shift  $\approx 100$  Hz, Doppler rate 0), read and record noise levels in the receiving system for later comparison with measurements in the vicinity of Jupiter.

e. *Pre-Entry Relay Link* - The spacecraft essentially repeats the procedures mentioned above. (1) calibrate spacecraft receiving system noise, establish threshold levels; (2) initiate search mode, (3) start recording when search logic indicates probe has been detected.

The post-separation activity and the pre-entry communication activity will both be performed on the basis of a timed sequence and programs stored on the spacecraft. Since the post-separation and pre-entry communications is linear rather than circularly polarized, it may be necessary to provide logic to receive only one polarization during the pre-entry period. Receiving both polarizations under these conditions would entail a 3 dB loss. Switching to the descent (circularly polarized mode) may be made on a time basis, receiver detection logic, or evaluation of Doppler and Doppler rates. A timed command for descent mode reception should override any logic to ensure that the critical descent data is not compromised.

f. *Descent Communications* - The previously described procedure is repeated in the circularly polarized reception mode. The details of the receiver acquisition and tracking electronics may be found in Volume III, Appendix C. Antenna configurations are discussed in Appendix D.

g. *Data* - The data interface occurs at the output of the receiver demodulator and the frequency tracking loop. The latter provides tracking loop stress data to assist in the scientific data reduction. If the data is to be stored, as appears likely, a tape recorder should be provided. A probe mission dedicated tape recorder would be of the "air filled" type ( $\approx 25$  lb, 25 W). In the 1975-1977 time period, a lighter unit should be available (i.e., 15 lb, 15 W) with good reliability.

h. *Thermal Control* - For thermal control, the spacecraft provides an environmental cover to protect the probe from meteoroid damage. In addition, it provides a low  $\alpha/\epsilon$  thermal coating to minimize probe heating during spacecraft maneuvers when direct solar impingement is possible. Since the deflection delta velocity motor on the probe is external to the probe primary multilayer insulation blanket, the spacecraft will be required to provide an electrical resistance heater and a multilayer insulation blanket to surround the motor. The blanket should be mounted to a lightweight fiberglass frame and would remain with the spacecraft on probe separation. The resistance heater for the deflection motor would require approximately 5 W peak power from the spacecraft and would be thermostatically controlled.

i. *Mass Properties* - The weights data for the MOPS spacecraft and the nominal Jupiter probe is shown in Table V-28.

Table V-28 MOPS Spacecraft/Nominal Jupiter Probe Weight Breakdown

Description	Weight	
	kg	lbm
Structural Subsystems	95.7	211.3
Telecommunications Subsystems	39.4	87.4
Power Subsystems	123.6	273.5
Attitude & Articulation Control	35.4	78.0
Propulsion & Pyrotechnics	25.3	55.9
Control Computer, Command & Timing	31.2	69.0
Measurement Processor	9.1	20.0
Data Storage	9.1	20.0
Control & Conditioning Logic	6.3	14.0
Radiation Shielding	0	0
Science Payload	0	0
Spacecraft Dry Weight	375.6	829.1
Spacecraft Adapter	17.1	37.8
Spacecraft Contingency (15%)	58.9	130.0
Navigation Propellant	13.3	29.4
APS Propellant	3.6	8.0
Probe	157.5	347.3
Probe Support Systems	4.0	8.9
Probe Radio Relay	10.8	23.9
Probe Support System & Radio Relay Contingency	2.2	4.9
Launch Weight	643.1	1419.3



C. PROBE-DEDICATED ALTERNATE JUPITER PROBE SYSTEM DEFINITION

The constraints for this alternative Jupiter probe were the result of the Jupiter parametrics discussed in Section A. In general, this configuration was intended to optimize the probe by reducing its complexity and the radiation field that it would encounter. The general constraints follow.

Mission	Type I in 1979
Entry Angle	-15° (structures designed to -20°)
Entry Latitude	30°
Depth of Descent and Atmosphere	13 bars in cool/dense atmosphere 7.5 bars in nominal atmosphere
Science	SAG exploratory payload (PAET)
Spacecraft	Mariner family
Carrier Mode	Flyby
Periapsis Radius	2 R <sub>J</sub>
Communication Mode	Relay
Deflection Mode	Spacecraft
Ejection Radius	30 x 10 <sup>6</sup> km
Entry Ballistic Coefficient	102 kg/m <sup>2</sup> (0.65 slug/ft <sup>2</sup> )
Descent Ballistic Coefficient	14.1 kg/m <sup>2</sup> (0.09 slug/ft <sup>2</sup> )

1. Science Instrumentation and Performance

The instruments for the Jupiter alternative probe missions were to be selected from a consideration of the PAET vehicle, Viking, and discussions in the previous study. From these sources, Table V-29 presents the instruments and their characteristics. The temperature gage and accelerometer triad system are basically the same for Viking and PAET; thus no change is shown here from the nominal design. However, the PAET pressure transducers, which were selected were significantly smaller in size and slightly lighter in weight. The mass spectrometer on PAET used a quadrupole analyzer, which for a limited range of 1-40 amu, appears to allow packaging in a smaller volume and has a lighter weight than the magnetic sector instrument. The porous leak inlet system is the same as for the nominal; however, since the design pressure level is only 13 bars, a ballast volume of only 0.5 liter is required. Further instrument details are given in Chapter III, Section C.

Table V-29 Alternative Instrument Characteristics

<u>Instrument and Component</u>	<u>Weight, lb</u>	<u>Power, watts</u>	<u>Volume, in.<sup>3</sup></u>
Temperature Gage (Including Deployment Mechanism)	1.0	1.4	26
Pressure Transducers (2)	1.5	1.3	15
Accelerometer System		2.8	
Triad Sensor	1.3		16
Pulse Rate Convertor	2.0		40
Neutral Mass Spectrometer		14.0	
Analyzer (3 in. diameter 8 in. long)	4.0		57
Electronics (5 x 6 x 7 in.)	6.0		210
Pump (3 x 3 x 3 in.)	1.0		27
Plumbing and Ballast Tank (0.5 liter)	1.0		30
Totals	17.8	19.5	421
	(8.08 kg)		(68,950 cm <sup>3</sup> )

Table V-30 Alternative Jupiter Probe-Dedicated Instrument Sampling Times and Data Rates

<u>Phase</u>	<u>Instrument</u>	<u>Sampling Times (sec)</u>	<u>Collection Bit Rate (bps)</u>	<u>Transmission Bit Rate (bps)</u>
Entry (44 sec)	Accelerometers			
	Longitudinal	0.1	100	0
	Lateral	0.2	50	0
	Lateral	0.2	50	0
Descent (2130 sec)	Temperature	3.5	2.9	3.0
	Pressure	3.5	2.9	3.0
	Mass Spectrometer	40.0	10.0	10.5
	Accelerometers			
	Turbulence	10	6.0	6.3
	Stored (Entry)	0	0	4.4
			Science Total	27.2
			Engineering & Formatting	3.2
			Total	30.4

The alternative Jupiter probe analysis considered both the cool/dense and the nominal model atmospheres. The probe is, therefore, designed for worst-case atmosphere conditions. It was stated in Section A.1 of this chapter that selection of a ballistic coefficient and instrument sampling times for the nominal atmosphere would guarantee satisfaction of the criteria in the cool/dense despite having to descend to higher pressures. Thus, the worst-case design is the nominal parameters descending into the cool/dense atmosphere. The values for the parameters are:

Design pressure limit = 13 bars (C/D)

Main parachute ballistic coefficient = 0.09 slug/ft<sup>2</sup> (14.13 kg/m<sup>2</sup>)

Parachute deployment pressure = 92 millibars (C/D)  
or = 86 millibars (nominal)

Pressure at first measurement = 111 millibars (C/D)  
or = 96 millibars (nominal)

No secondary parachute necessary

Total mission time from entry = 36 min, 14 sec.

The entry and descent times, instrument sampling times, and resulting bit rates are shown in Table V-30. The collection bit rate is the rate at which the instrument actually collects the data. The transmission bit rate is slightly higher to allow for interleaving of data stored during acquisition with the real time data for telemetry. The pressure descent profile is given in Figure V-6 using the appropriate ballistic coefficient. In addition, the radius and velocity descent histories are given in Figure V-98 for descent into the cool/dense atmosphere and in Figure V-99 for descent into the nominal atmosphere.

In Table V-31 the mission measurement performance is given for descent profiles using the selected parameters into both atmospheres. The descent parameters have been chosen so as to equalize the performance with the criteria for the nominal atmosphere for each instrument, as shown by the bold faced type, except for the pressure transducers. They have an overriding requirement to sample simultaneously with the temperature gage. In the cool/dense atmosphere, the performance in all cases exceeds the criteria. Note that the mass spectrometer makes 6.0 measurements in the H<sub>2</sub>O cloud as specified by the model; however, only the last 2 measurements are taken in an area where the cloud density is at least 1 mg/l. Ranges are given for those performance numbers that vary during descent, the higher values taken at end of mission where the probe has its lowest velocity.

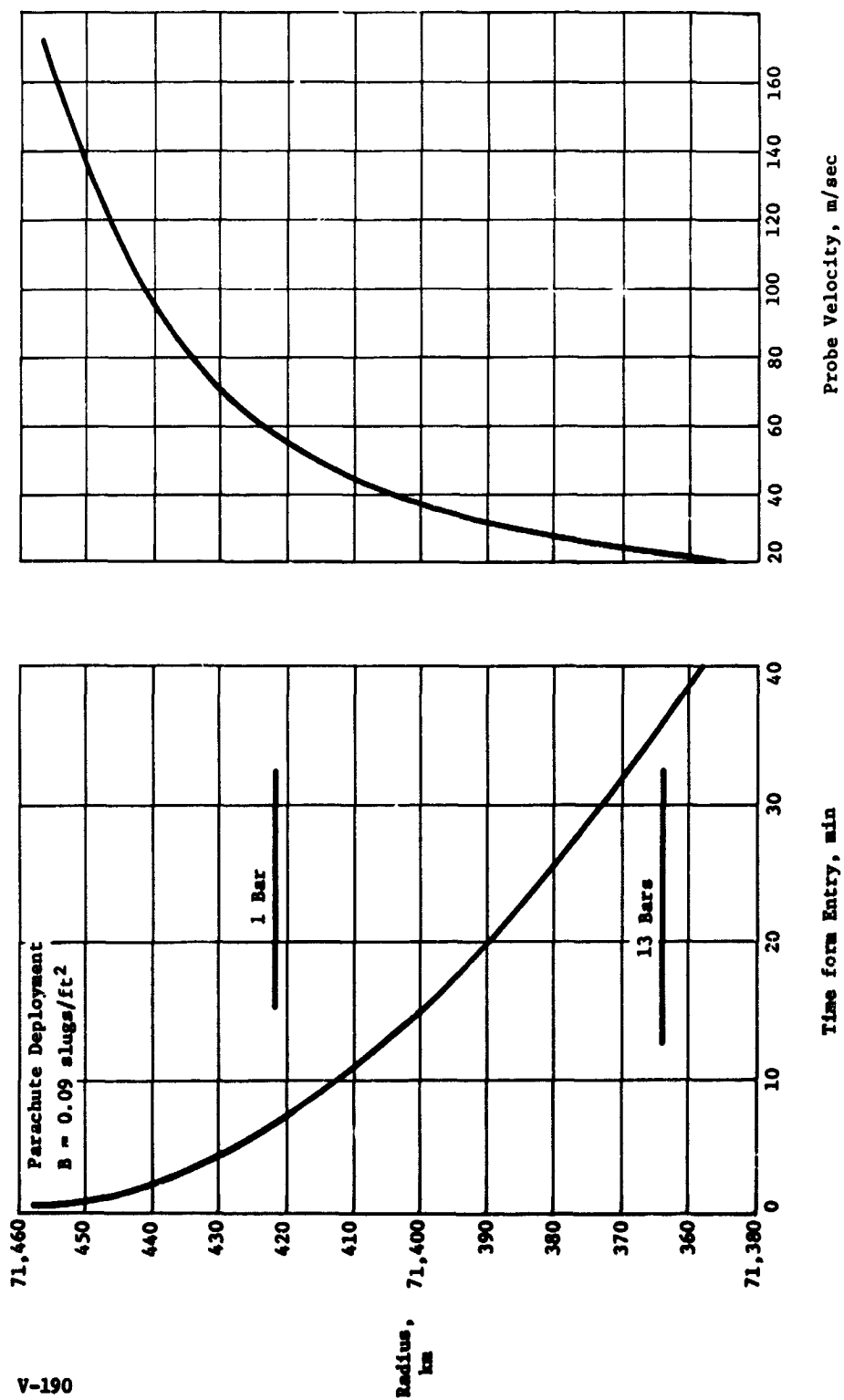


Figure V-98 Time and Velocity vs Descent Radius  
(Cool/Dense Atmosphere)

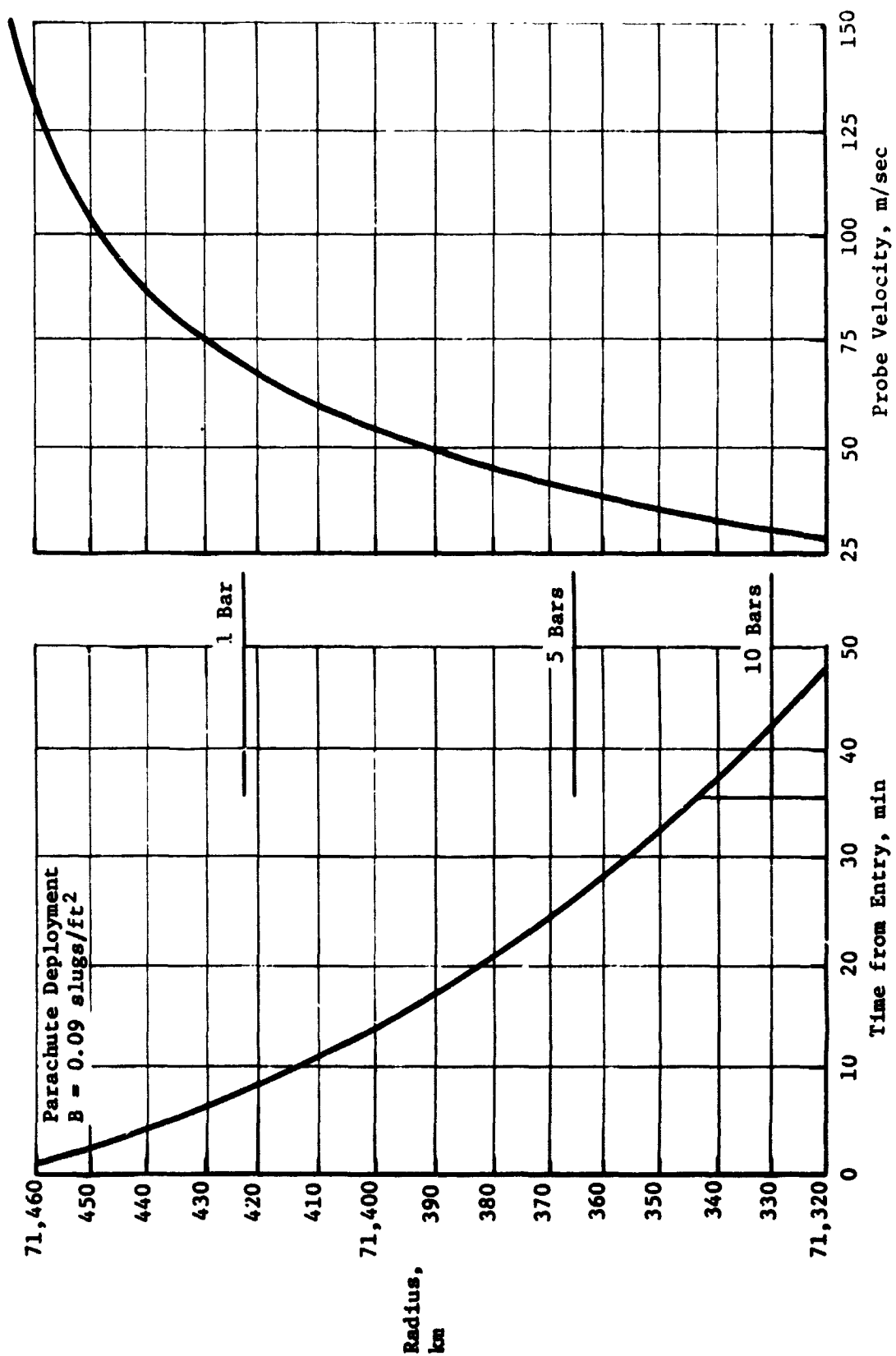


Figure V-99 Time and Velocity Versus Descent Radius (Nominal Atmosphere)

Table V-31 Alternative Descent Measurement Performance in Both Atmospheres

Instrument (At.) and Measurement	Criteria	Descent Performance (B = 0.09)	
		Cool Dense	Nominal
Mass Spectrometer (40 sec) Minor Constituents Cloud Layering	2 per scale height* 2 inside cloud	6.2 to 34 {4.3 in NH <sub>3</sub> 6.0 in H <sub>2</sub> O}	4.6 to 37 [2.0] in NH <sub>3</sub> 7.1 in H <sub>2</sub> O
H/He Ratio Isotopic Ratios Molecular Weight	4 measurements	53 meas (to 13 bars)	53 meas (to 7.5 bars)
Temperature Gage (3.5 sec) Temperature Cloud Layering	1 per °K 2 inside cloud	1.6 to 6.7 {49 in NH <sub>3</sub> 94 in H <sub>2</sub> O}	[1.0] to 4.4 23 in NH <sub>3</sub> 80 in H <sub>2</sub> O
Pressure Gage (3.5 sec) Pressure Turbulence Cloud Layering	2 per km* 1 per km* 2 inside cloud	4.9 to 13 4.9 to 13 {49 in NH <sub>3</sub> 94 in H <sub>2</sub> O}	2.7 to 9.1 2.7 to 9.1 23 in NH <sub>3</sub> 80 in H <sub>2</sub> O
Accelerometers (10 sec) Turbulence	1 per km*	1.8 to 4.6	[1.0] to 3.2
*Below Cloud Tops			

2.

### Mission Definition

The probe-dedicated alternative mission is shown in Figure V-100 and detailed in Table V-32. Important mission design results are summarized in this section.

a. *Interplanetary Trajectory Selection* - The interplanetary trajectory is pictured in Figure V-100(a) with 100-day intervals noted. The launch data of November 7, 1979 and arrival date of September 17, 1981 (trip time of 680 days) result in a maximization of the payload weight as discussed in Chapter IV, Section A. As indicated in the figure, the spacecraft arrives at Jupiter shortly before the view to Jupiter is obstructed by the Sun.

b. *Launch Analysis* - The launch analysis is provided in Figure V-100(b). Available payload is plotted against launch period for three sets of launch vehicle performance data: standard data for the Titan 5 Segment vehicle, with and without Burner II, plus updated data for the Burner II. For reference, the payload weight (probe, spacecraft, spacecraft modifications, and spacecraft-launch vehicle adaptor) is about 1000 lb for a Pioneer mission and 1500 lb for a Mariner mission. Thus, the Burner II option is necessary for a Mariner type mission to obtain a 20 day launch period. The nominal launch window and parking orbit coast time are satisfactory.

c. *Approach Trajectories* - The probe trajectory for this mission was constrained to enter at an entry angle of  $-15^\circ$  and an entry latitude of  $30^\circ$ . To satisfy this requirement, the probe trajectory must be inclined  $50^\circ$  to Jupiter's orbital plane. To establish an effective communication link, the spacecraft was deflected for a  $55^\circ$  inclination. The probe was released on the lower inclination trajectory so that during descent it would rotate through the trace of the spacecraft trajectory. The resulting trajectories are pictured in Figure V-100(d) and summarized in Tables V-32(a) and V-32(b).

d. *Deflection Maneuver* - A spacecraft deflection maneuver was performed at 30 million km and 34.5 days from the planet. The  $\Delta V$  required was 71 m/sec. The implementation sequence is illustrated in Figure V-100(c). The spacecraft rotates  $49^\circ$  off Earth-lock to release the probe. It then rotates  $45^\circ$  further and fires a  $\Delta V$  of 71 m/sec to achieve its desired flyby radius and communication geometry.

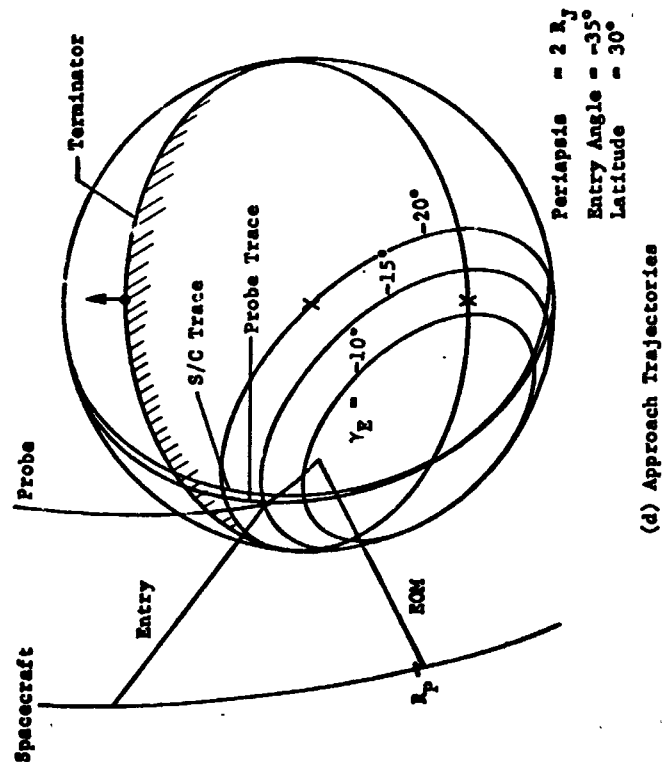
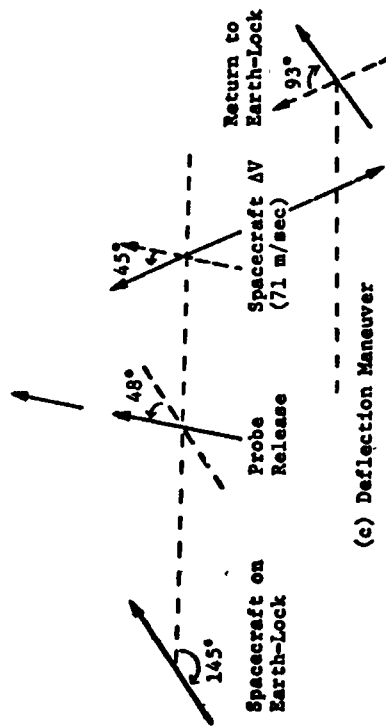
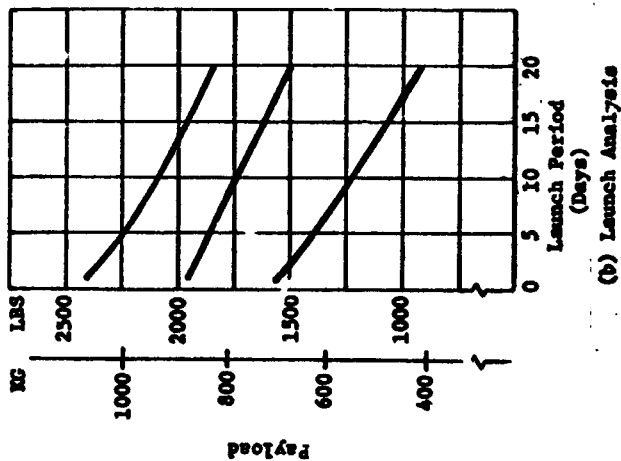
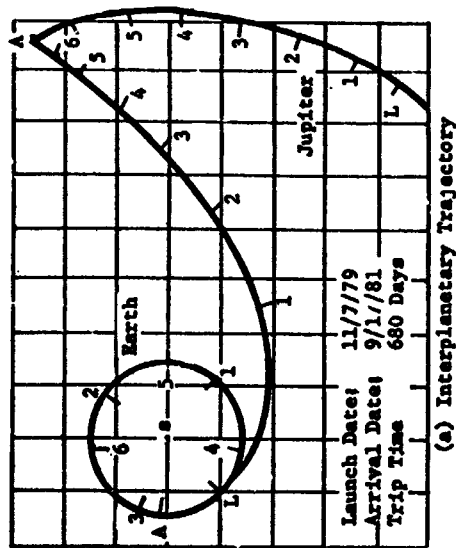


Figure V-100 Probe-Dedicated Alternative Mission Description



Table V-32 Alternative Jupiter Probe - Dedicated Mission Summary

a. Conic Trajectory Data

Interplanetary Trajectory	Launch Trajectory	Arrival Trajectory
Launch Date: 11/7/79 Arrival Date: 9/17/81 Flight Time: 680 days Central Angle: 155°	Nominal C <sub>3</sub> : 93.6 km <sup>2</sup> /sec <sup>2</sup> Nominal DLA: 30.5° Launch Window: 1.17 hr Parking Orbit Coast: 36 min C <sub>3</sub> (10 day): 97.5 km <sup>2</sup> /sec <sup>2</sup> C <sub>3</sub> (20 day): 105 km <sup>2</sup> /sec <sup>2</sup> Azimuth Range: 101.7° - 115°	VHP: 8.474 km/sec RA: 161.3° DEC: 6.81° ZAE: 145.2° ZAP: 141.4° RP: 2 R <sub>J</sub> INC: 55°

b. Deflection Maneuver and Probe Conic

Deflection Maneuver	Probe Conic Definition
Deflection Mode: Spacecraft Deflection Radius: 30 x 10 <sup>6</sup> km Coast Time: 34.5 days ΔV: 71 m/sec Application Angle: 108.6° Out-of-Plane Angle: 5.0° Rotation for Probe Release: +47.6° Probe Reorientation Angle: NA Spacecraft ΔV from Earth: +93.5°	Entry Angle: -15° Entry Latitude: 30.6° Entry Longitude: 109.9° Lead Time: 35.2 min Lead Angle: -12.0° Probe-Spacecraft Range (Entry): 88,287 km Probe Aspect Angle (Entry): 50.6° Probe Aspect Angle (Descent): 22.7° Probe Aspect Angle (EOM): 28.1°

c. Dispersion Analysis Summary

Navigation Uncertainties	Execution Errors (3σ)	Dispersions (3σ)
Type: R, R̄/67 day arc SMAA: 1576 km SMIA: 224 km β: 86° TOF: 122 sec	ΔV Proportionality: 1% ΔV Pointing: 2° Probe Orientation Pointing: 2°	Entry Angle: 1.4° Angle of Attack: 2.5° Down Range: 3.0° Cross Range: 0.1° Lead Angle: 8.2° Lead Time: 100 min Entry Time: 5.72 min

d. Entry and Descent Trajectory Summary

Entry Parameters	Descent Parameters	Critical Events	
		Time from Entry	Altitudes above 1 atm
Entry Velocity, km/sec: 60 Entry Altitude, km: 304.6 Entry B, slug/ft <sup>2</sup> : 0.65 kg/m <sup>2</sup> : 102.1 Entry Atmosphere: Cool/Dense Max Deceleration, g: 1650 Max Dynamic Pressure, lb/ft <sup>2</sup> : 2.3 x 10 <sup>4</sup> kg/m <sup>2</sup> : 1.1 x 10 <sup>6</sup>	Descent Atmosphere: Cool/Dense/Nominal EOM Pressure, bar: 13 Descent B, slug/ft <sup>2</sup> : 0.09 kg/m <sup>2</sup> : 14.13	g = 0.1, sec: 8.5s Max g, sec: 18.0 M = 0.7, sec: 44.0 Descent Time, min: 35.6 EOM, min: 36.1	km: 189 km: 66.8 km: 33.4 km: -57.5

e. *Dispersion Analysis* - The navigation uncertainties are slightly larger in this mission than the previous mission because the deflection radius is slightly increased. Navigation uncertainties still have only a minor contribution to the final dispersions compared to the execution errors. The entry parameter dispersions are provided in Table V-32(C). These dispersions are based on the spacecraft deflection mode. For comparison, a probe deflection mode dispersion analysis was made for the identical conditions and resulted in dispersions ( $3\sigma$ ) of entry angle  $1.9^\circ$ , angle of attack  $2.8^\circ$ , downrange  $4.0^\circ$ , crossrange  $0.7^\circ$ , lead angle  $7.0^\circ$ , lead time 10.0 min, and entry time 11.9 min. The communication parameter dispersions are given in Subsection VC.4.

f. *Entry and Descent* - The entry latitude for the probe-dedicated mission is  $30^\circ$  whereas the nominal mission has an equatorial entry. The effect of entering at a  $30^\circ$  latitude is to increase the g-loading as well as the dynamic pressure by approximately 10%. All other critical parameters remain unchanged from the nominal mission. The nominal entry angle (chosen from science considerations) is  $-15^\circ$ ; however, to accommodate dispersions ( $3\sigma \approx 5^\circ$ ) a value of  $-20^\circ$  is used to determine structural loads. The descent parameters are chosen from a combination of the cool/dense and nominal environments. The worst-case design results when the ballistic coefficient is based upon the nominal atmosphere and the resulting times and pressures determined from the cool/dense model. A summary of the entry and descent parameters is given in Table V-32(d).

### 3. System Integration

a. *Functional Sequence* - Table V-33 shows the sequence of events for this probe system. Compared to the other probe definitions throughout this volume, this probe is less complex because it is not required to provide a  $\Delta V$  and the attitude control subsystem is very simple. The probe separation activities occupy such a short time, i.e. four minutes, that engineering data are not collected and transmitted during this period. Other probe phases are similar to that described in Section B,3.

b. *Functional Block Diagram* - The functional interfaces of this probe are similar to those shown in Figure V-76 except that the propulsion interface does not exist.

c. *System Data Profile* - Figure V-101 shows the data profile for this probe mission. As denoted in the sequence of events above, engineering and science data are collected during pre-entry, entry, and descent.

Table V-33 Sequence of Events for Probe-Dedicated Jupiter Mission

<u>Item</u>	<u>Time</u>	<u>Event</u>
1.	L=0	Launch, November 7, 1979
2.	L+2h	Separate Spacecraft from Launch Vehicle
3.	L+2h to L+670d	Cruise
4.	S-6h, 0m, 0s	Spacecraft Power to Probe; Eject Environmental Cover
5.	S-5h, 47m, 0s	Start Probe Checkout
6.	S-0h, 17m, 0s	Probe Checkout Complete; Start Spacecraft Orientation for Release (47.6°)
7.	S-0h, 2m, 0s	Spacecraft Orientation to 47.6° Complete; Activate Separation Subsystems
8.	(L+645.5d) S=0	Separate
9.	S+0m, 0.5s	Start Probe Spinup to 5 RPM
10.	S+0m, 30s	Start Spacecraft Orientation for $\Delta V$ (45.9°)
11.	S+4m, 0s	Probe Spinup to 4 rpm Complete; Deactivate Probe Systems
12.	S+15m, 30s	Complete Spacecraft Orientation for $\Delta V$ (45.9°)
13.	S+17m, 36s	Apply Spacecraft $\Delta V$ (71m/sec)
14.	S+18m, 0s	Start Reorient Spacecraft to Earth Lock (-93.5°)
15.	S+33m, 0s	Spacecraft Reorientation Complete (-93.5°)
16.	L+645.48d to L+679.94d	Coast
17.	E-0h, 45m, 2s	Enable Entry Battery Ordnance
18.	E-0h, 25m, 2s	Activate Probe Descent Batteries (in descent probe) Turn on Data Handling System, Engineering Instrumentation
19.	E-10m, 22s	Turn on Transmitter
20.	E-9m, 56s	Turn on Science Instruments
21.	E-8m, 42a	Start Probe Acquisition
22.	E-6m, 42s	Complete Probe Acquisition; Start Data Transmission;
23.	E=0	Entry (305 km above 1 atm; $3 \times 10^{-7}$ bars)
24.	E+0m, 8.5s	Probe Transmitter "Off" (0.1 g sensing); Start Recording, Accelerometer Data
25.	E+0m, 14.7s	Initiate Probe Descent Program (100 g sensing)
26.	E+0m, 38.2s	Eject Base Cover Quadrants (Mach 0.8)
27.	E+0m, 44s	Deploy Main Parachute (Mach 0.7, $\sim 0.092$ bars)
28.	E+0m, 54s	Release Descent Probe from Entry Probe (switch probe antenna)
29.	E+0m, 56s	Deploy Temperature Gauge; Release Mass Spectrometer Covers
30.	E+2m, 34s	Probe Acquisition Complete; Start Data Transmission
31.	E+36m, 14s	End of Design Mission ( $\sim 13$ bars)
32.	(L+680d) E+34m, 36s	Spacecraft Periapsis (2 $R_J$ ; September 17, 1981)

Includes 5.7 min trajectory uncertainty and based on a descent ballistic coefficient of 0.09 slug/ft<sup>2</sup>

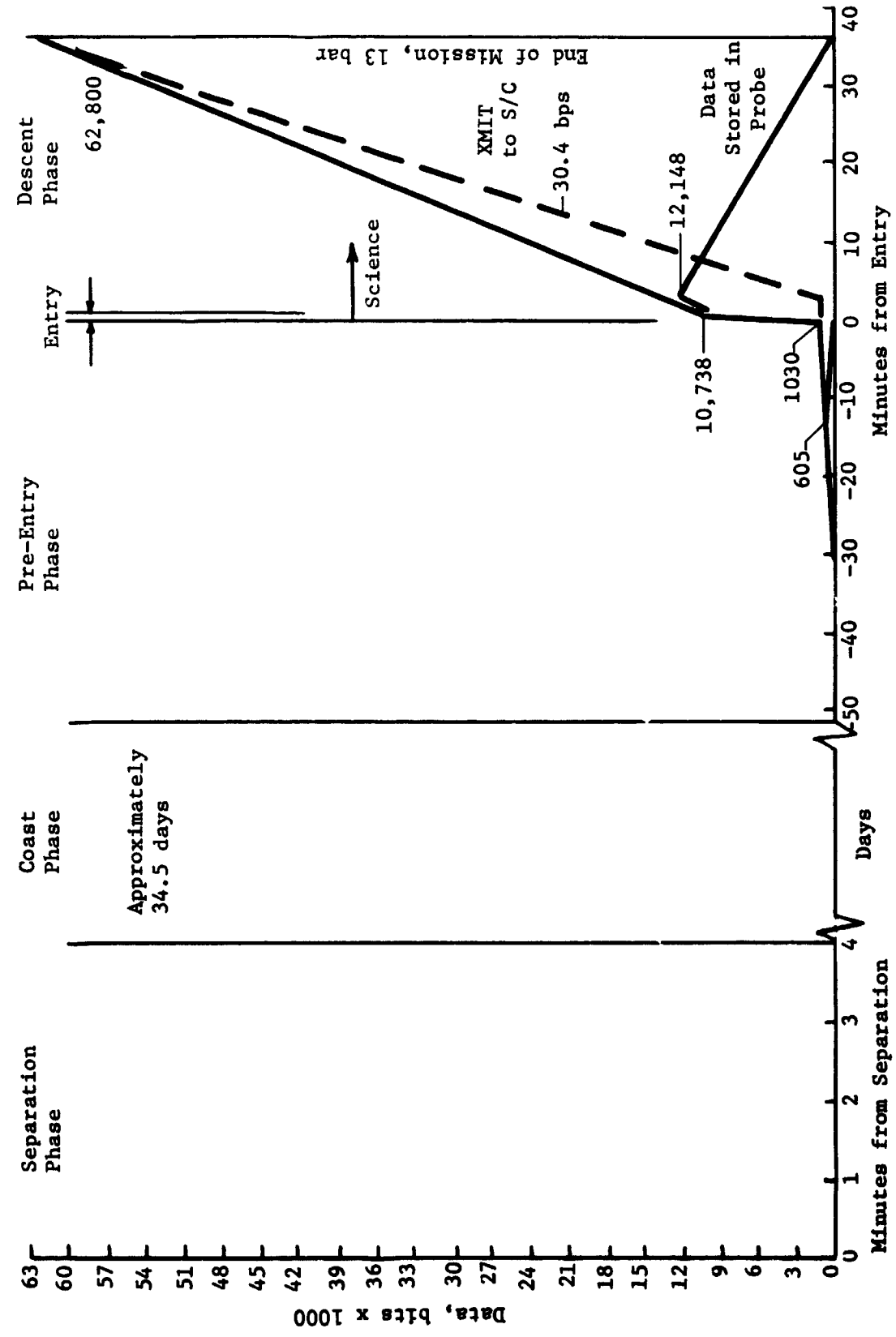


Figure V-101 Data Profile for the Probe-Dedicated Jupiter Mission

d. *System Power Profile* - Figure V-102 shows the power requirements for this probe mission. It is seen that the entry power requirements are very small.

e. *System Weight Summary* - Table V-34 shows the weight breakdown. The ejected weight and entry weight is approximately the same; the difference is the amount of ACS gas used after separation.

Table V-34 *Weight Summary for Probe-Dedicated Jupiter Mission*

Probe Breakdown	Weight	
	<u>kg</u>	<u>lb</u>
Science	8.07	17.8
Power and Power Conditioning	3.15	6.94
Cabling	4.67	10.3
Data Handling	2.59	5.7
Attitude Control (dry)	2.63	5.8
Communications	5.53	12.2
Pyrotechnics	3.54	7.8
Structures and Heat Shield	65.71	144.85
Mechanisms	6.12	13.5
Thermal	8.39	18.5
Propellant (ACS)	.02	0.05
Engineering Instrumentation	0.00	0.0
15% Margin	<u>16.56</u>	<u>36.52</u>
Ejected Weight	126.99	279.96
Entry Weight	126.96	279.90
Descent Weight (final)	42.36	93.41

#### 4. Telecommunications Subsystem

The Jupiter probe-dedicated mission at  $2 R_J$  is very similar to the nominal mission as far as the trajectory and communications geometry are concerned. The probe aspect angle is  $60^\circ$  at acquisition and is optimized to be a minimum during descent. The angle is  $22^\circ$  at the end of entry and  $18^\circ$  at the end of the mission at a depth of 13 bars, as seen in Figure V-103.

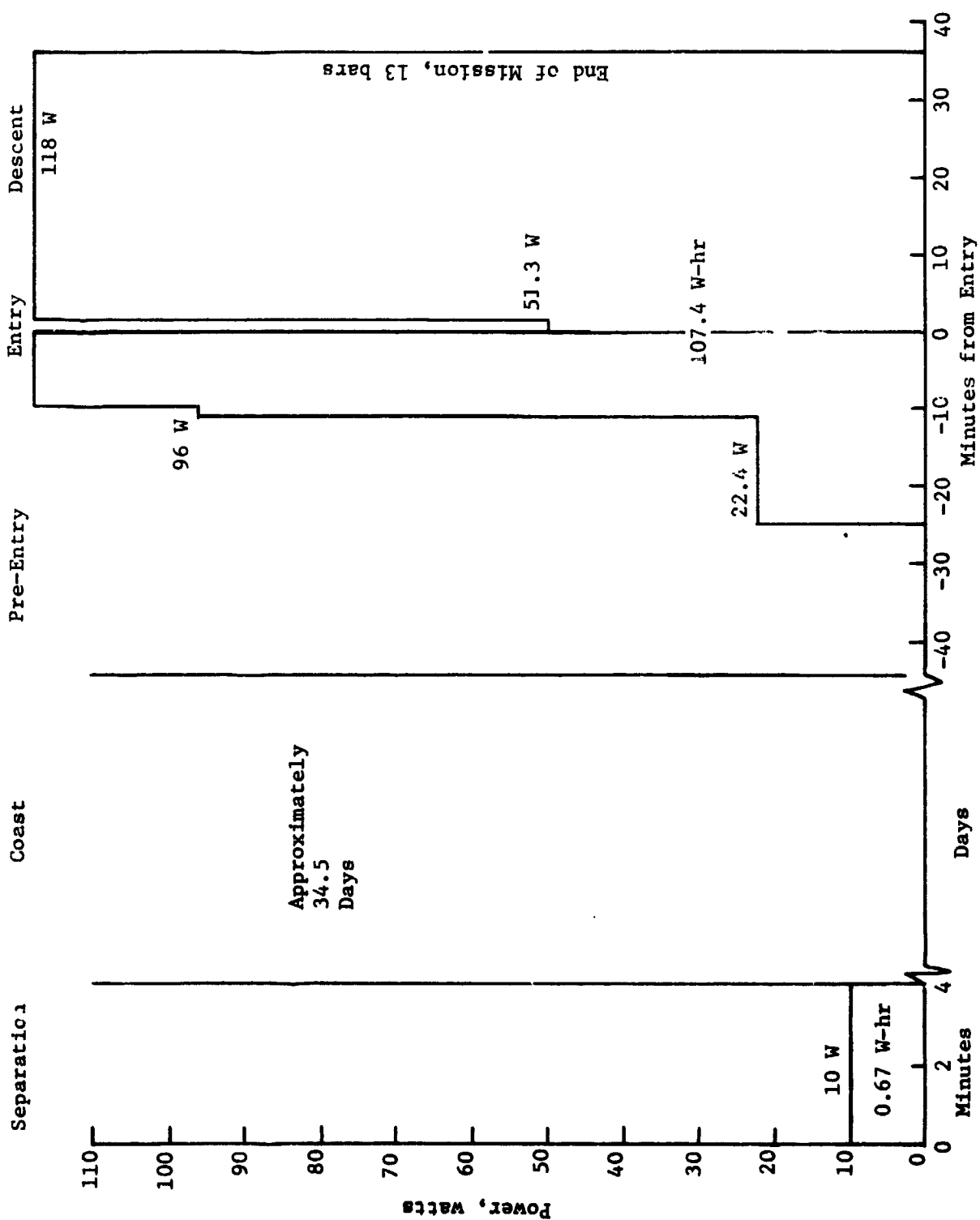


Figure V-102 Power Profile for Probe-Dedicated Jupiter Mission

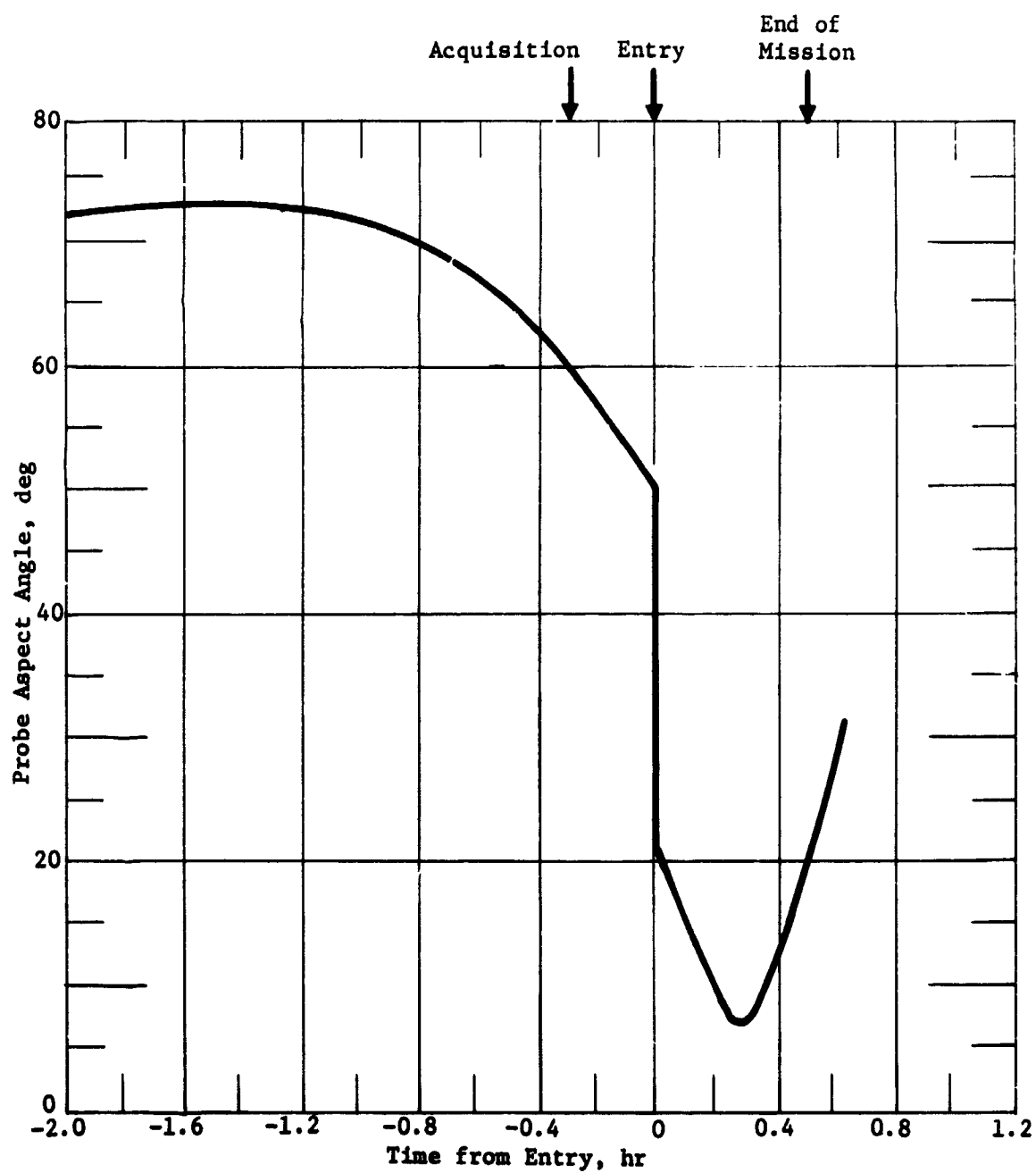


Figure V-103 Probe Aspect Angle for the Jupiter Probe-Dedicated Mission

Probe dispersions are shown in Figures V-104. The uncertainty ellipses are tilted more than usual but variations in cone angle are about the same as for other missions. A 55° beamwidth spacecraft antenna provides maximum gain at the points of maximum dispersion. All the nominal probe positions fall within the 3-dB beamwidth.

Parameters of the RF link are depicted in Table V-35 for the probe-dedicated Jupiter mission at 0.86 GHz. Maximum transmitter power is required at mission completion.

Table V-35a depicts design details of the RF components that comprise the telecommunications subsystem. Complete details of the components are given in Section A.4. 30 W of RF power is required at 0.86 GHz with a bit rate of 30 bps using binary FSK with a tracking tone. A mechanical switch is required at this power level. The entry antenna is an annular slot which is mounted on the base cover. The descent antenna is a turnstile over a cone design which is mounted on the aft bulkhead of the descent probe. The spacecraft antenna is a helix with right-hand-circular polarization and a 55° beamwidth.

An analysis similar to the one performed for the other alternative Jupiter probe mission (Section D, 4) was performed for this mission to determine the effects of increased system noise temperature. Trajectory geometry for the mission is shown in Figure V-105. The spacecraft and probe are within the magnetosphere during the active portion of the mission. Calculations were performed using Equation [C-1], which determines the antenna temperature from the maximum synchrotron temperature plus the planet disk temperature,

$$T_A = T_{BS} + T_{BD} = 0.45 d \lambda^2 + T_{BD} \quad [C-1]$$

where

$T_A$  = antenna temperature, °K

$d$  = path length,  $R_J$

$\lambda$  = wavelength, cm

$T_{BD}$  = planet disk temperature, °K.

Path length,  $d$ , is shown in Figure V-105. A frequency of 1 GHz was chosen and the wavelength,  $\lambda$ , is 30 cm. The disk brightness at 1 GHz is 430 °K using the upper limit curve of Figure B-1 in Vol III, Appendix B. Equation [C-1] reduces to

$$T_A = 405 d + 430. \quad [C-2]$$



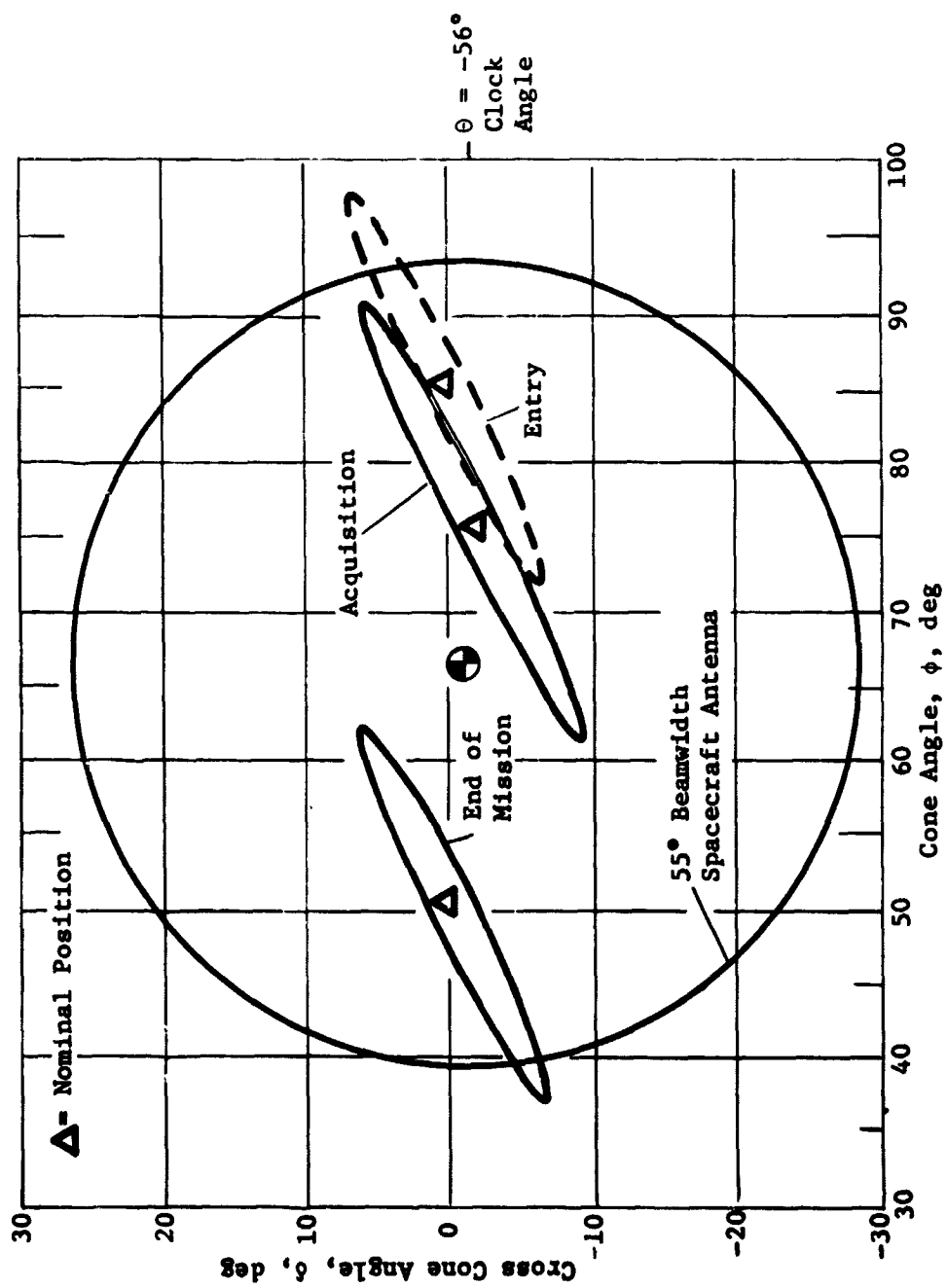


Figure V-104 Spacecraft Antenna Requirements for the Jupiter Probe Dedicated Mission

Table V-35 Probe Telemetry Link Design, Probe Dedicated Jupiter Mission

Parameter	Unit	Nominal Value	Adverse Tolerance	Remarks
Total Transmitter Power	dBW	14.8	0	30 W
Transmitting Circuit Loss	dB	-0.3	0.2	
Transmitting Antenna Gain	dB	4.4	2.2	120° Beamwidth
Communications Range Loss	dB	-188.8	1.1	$7.6 \times 10^4$ km
Planet Atmos & Defocus Loss	dB	-0.8	0.2	Cool/Dense, 13 bars
Polarization Loss	dB	0.0	0.2	
Antenna Pattern Ripple Loss	dB	0.0	0.2	
Receiving Antenna Gain	dB	9.8	3.9	55° Beamwidth
Receiving Circuit Loss	dB	-0.2	0.2	
Net Circuit Loss, $\Sigma$ (2→9)	dB	-175.9	8.0	
Total Received Power (1 + 10)	dBW	-161.1	8.0	
Receiver Noise Spectral Density	dBW	-196.9	0.5	$T_s = 1469^\circ\text{K}$ $NF_s = 7.82$ dB
Tracking Tone				
Tone Power/Total Power	dB	-5.4	0	
Received Tone Power (11+13)	dBW	-166.5	8.0	
Tracking Threshold Bandwidth	dB	11.8	0	Bandwidth = 15 Hz
Threshold SNR	dB	10.0	0	
Threshold Tracking Power (12+15+16)	dBW	-175.1	0.5	
Tracking Performance Margin (14-17)	dB	8.6	8.5	
Data Channel				
Data Power/Total Power	dB	-1.5	0	
Radio System Processing Loss	dB	-1.0	0	
Fading Loss	dB	-1.0	0	
Received Data Power (11+19+20+21)	dBW	-164.6	8.0	
Data Bit Rate	dB	14.8	0	
Threshold $E_b/N_0$	dB	8.9	0	
Threshold Data Power (12+23+24)	dBW	-173.2	0.5	
Performance Margin (22-25)	dB	8.6	8.5	
Nominal Less Adverse Value (26-27 adv)	dB	0.1		
<b>CONDITIONS:</b> 1. Worst Case (EOM) conditions at 0.86 GHz 2. Convolutional Encoder, M=2, V=2, Q=8 3. BER = $5 \times 10^{-5}$ for binary FSK with K=8 code 4. EOM probe aspect angle, $\psi = 28^\circ$ 5. Coded Noncoherent System with Viterbi Decoding				

*Title V-35a Telecommunications RF Subsystem for the Probe-Dedicated Mission*

Conditions: Planet: Jupiter; Spacecraft: Mariner; Frequency: 0.96 GHz; Bit Rate: 30 bps			
<u>Component</u>	<u>Characteristic</u>	<u>Unit</u>	<u>Value</u>
Transmitter	RF Power Out	W	30
	Overall Efficiency	%	45
	DC Power-In at 28 V dc	W	66.7
	Total Weight	kg	2.7
RF Switch		lb	6.0
	Type		Mechanical
	Insertion Loss	dB	0.3
	Weight	kg	2.3
Entry Antenna		lb	0.5
	Type		Annular Slot
	Main Beam Angle	deg	60
	Beamwidth	deg	40
	Max Gain	dB	5.2
	Diameter	cm	43
		in.	17
	Weight	kg	2.1
Descent Antenna		lb	4.7
	Type		Turnstile/Cone
	Main Beam Angle	deg	0
	Beamwidth	deg	120
	Max Gain	dB	5
	Size (diameter x h)	cm	20.3 x 7.6
		in.	8 x 3
	Weight	kg	0.45
Spacecraft Antenna		lb	1.0
	Type		Helix
	Beamwidth	deg	55
	Max Gain	dB	9.6
	Size (diameter x h)	cm	29.6 x 11.1
		in.	11.7 x 4.4
	Weight	kg	1.36
		lb	3.0
	Despin		no
	Position Search		none
	Frequency Acquisition	sec	65
	Clock Angle, $\theta$	deg	-56
	Cone Angle, $\phi$	deg	67
Spacecraft Receiver	Noise Temperature	°K	300
	Noise Figure	dB	3.1
	DC Power-In at 28V dc	W	3.0
	Weight	kg	0.9
		lb	2.0

V-206

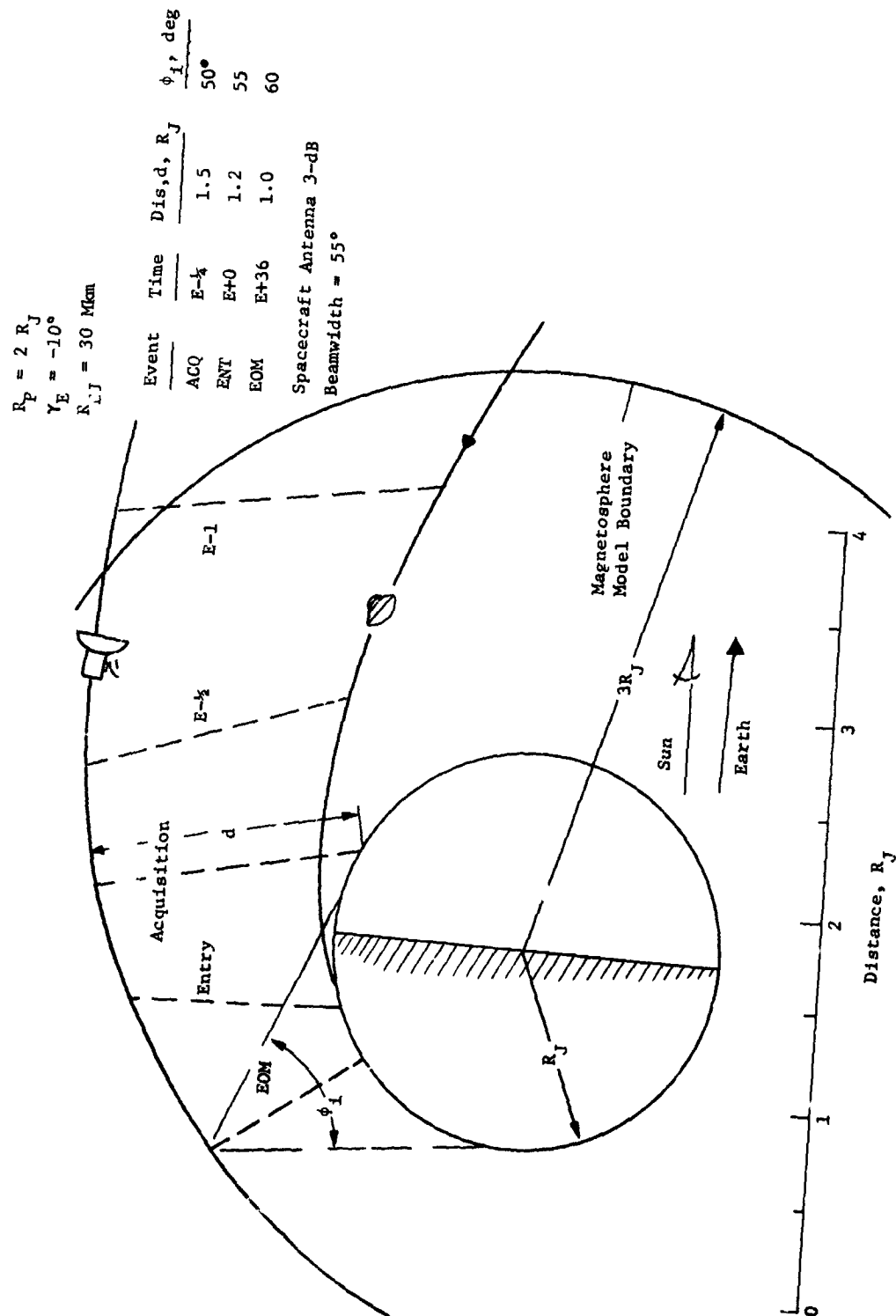


Figure V-105 Trajectory Geometry for the Jupiter Probe-Dedicated Mission

The receiving system noise temperature is the sum of the antenna temperature and the receiver noise temperature. The receiver temperature, from Figure V-11 is 302 °K at 1 GHz which corresponds to a noise figure of 3.1 dB. The receiving system temperature is determined by

$$T_S = T_A + T_R = 405d + 430 + 302$$

$$= 405d + 732 . \quad [C-3]$$

Equation [C-3] was used to compute  $T_S$  at acquisition, entry, and mission completion. The values are shown in Table V-36. The RF link design was based on a constant  $T_S$  of 1280 °K throughout the mission. The difference is negligible for this mission configuration as can be seen in the table. Comparison of the results of the two alternative missions in this area, indicates that system noise temperature is a function of the path length,  $d$ , for a mission. Mission geometries that have a large path length at acquisition in the planet's magnetosphere and do not intersect the planet disk have a large dispersion in antenna temperature before entry. The effect is negligible for the 2  $R_J$  mission but is very significant for the 6  $R_J$  mission as discussed in Section V.D.

Table V-36 System Noise Temperature for the Jupiter Probe-Dedicated Mission at 1 GHz

Time	Event	$T_{BS}$ , °K	$T_{BD}$ , °K	$T_R$ , °K	$T_S$ , °K
E - ½	Acquisition	607	430	302	1339
E - 0	Entry	486	430	302	1218
E + ½	EOM	405	430	302	1137

##### 5. Data Handling Subsystem (DHS)

The data handling subsystem has a slightly reduced function for this spacecraft deflection mode mission. Since the post-separation activity is limited to a few minutes during which the probe is spun up to 5 rpm, the DHS is not activated. The electronic functions during this period will be implemented by a dedicated timer that will be started at separation. The logic and associated circuitry. The final state of the counter will establish the coast shutdown sequence.

The requirements for the DHS during the entry and descent phase are essentially unchanged from the nominal Jupiter probe definition. A description of the analysis and definition of this subsystem may be found in Chapter V Section A.5 of this volume, and Vol III, Appendix H.

#### 6. Power and Pyrotechnic Subsystem

A description of the analysis and preferred configuration of the probe power and pyrotechnic subsystem may be found in Chapter V, Sections A, 6 and A, 7 of this volume, and in Vol III, Appendix G.

The deviation of this subsystem from the nominal Jupiter probe subsystem is in the deletion of the post-separation power conditioning and modification of the battery weights. Power conditioning is not included because the simple post-separation electronics power requirements do not justify the cost and weight of this component. A summary of the physical characteristics of the power and pyrotechnic subsystem follows.

<u>COMPONENT</u>	<u>SIZE/VOLUME</u>	<u>WEIGHT</u>	
		<u>kg</u>	<u>lb</u>
Power			
Separation Battery	3.96 D x 7.52 L cm (1.56 in D x 3 in. L)	0.24	(0.52)
Entry Battery	832 cm <sup>3</sup> (51 in. <sup>3</sup> )	1.68	(3.7)
Power Distribution	163 cm <sup>3</sup> (10 in. <sup>3</sup> )	0.45	(1.0)
Power Filter	326 cm <sup>3</sup> (20 in. <sup>3</sup> )	0.68	(1.5)
Pyrotechnics			
Electronics	1222 cm <sup>3</sup> (75 in. <sup>3</sup> )	0.91	(2.0)
Capacitor Banks	625 cm <sup>3</sup> (40 in. <sup>3</sup> )	0.36	(0.8)
Relay Banks	440 cm <sup>3</sup> (27 in. <sup>3</sup> )	1.14	(2.5)

#### Attitude Control Subsystem -

The mission profile requires the probe to be separated from a three-axis stabilized spacecraft, spinup to 0.5 rad/sec, and maintain pointing accuracy to within 3° of the desired entry orientation. Since spacecraft pointing will have errors less than 1.0°

(30), a requirement for pointing on the probe of less than  $2^\circ$  is sufficient to meet the design goals. The error accumulation caused by tip-off rates during the period from separation to spinup and the iteration of tipoff rates and spinup are discussed in Vol III, Appendix F. The following constraints and attitude errors are appropriate to this mission.

$$W_T = 1/2^\circ/\text{sec} \text{ (tipoff rate)}$$

$$t_p = 0.50 \text{ sec (drift time, separation to spinup)}$$

$$m = 4.07 \text{ Newton-meters (spin torque)}$$

$$W_s = 0.5 \text{ rad/sec (final spin rate)}$$

$$\theta_1 = 0.25^\circ \text{ Error due to tipoff drift}$$

$$\theta_2 = 1.06^\circ \text{ Spinup error due to tipoff rate}$$

$$\theta(p) = 1.19^\circ \text{ Total momentum error}$$

The residual nutation angle will be approximately  $1^\circ$ . This nutation will be effectively damped out during the coast period by the viscous damper which has a time constant of 20 hr at this spin rate. It should be noted that the only disturbances to the probe attitude are magnetic and gravity gradient effects. Magnetic cleanliness practices should be followed at this spin rate although the period in the significant planetary magnetic field is small. Gravity gradient effects are negligible. The attitude control subsystem for this mission consists of the cold gas system, discussed in Section C .9 of this chapter, a minimum of electronics, and a nutation damper.

#### 8. Structural and Mechanical

The probe-dedicated alternative Jupiter probe is a substantially simpler probe than the nominal Jupiter probe presented previously in Section B of this chapter. For this mission, the spacecraft provides the deflection delta velocity maneuver. It leaves the probe in the proper attitude and with the proper trajectory for planetary entry at the time of separation. Thus, the probe does not need a deflection delta velocity motor, nor does it need to be spun up to a spin rate of 10.5 rad/sec (100 rpm) to stabilize the probe for firing of the deflection motor and for precession.

Instead, the probe requires only a spin rate of 0.52 rad/sec (5 rpm) to stabilize its attitude at separation and eliminate drift before planetary entry. Thus, the probe does not have a deflection motor or a service module. The ACS system for the lower spin rate is included within the basic entry probe.

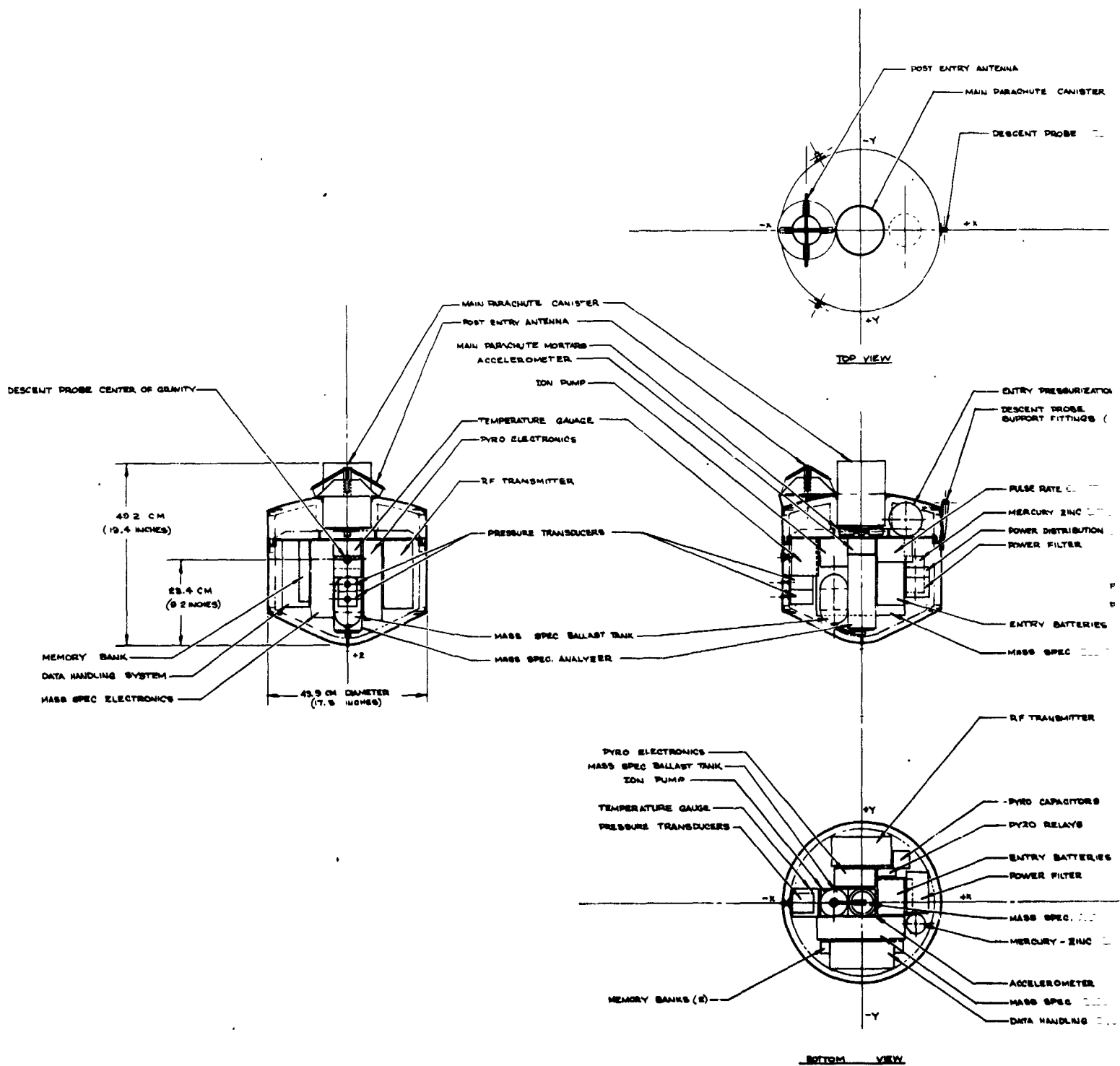
a. *Configuration and General Arrangement* - The configuration of the probe is shown in Figure V-106. The ejected probe is 1.005 m (39.6 in.) in diameter, 0.604 m (23.8 in.) in length, and weighs 126.99 kg (279.96 lbm). Since there is no service module, the ejected probe and entry probe are essentially identical. The descent probe is 0.439 m (17.3 in.) in diameter, .492 m (19.4 in.) in length, and weighs 42.36 kg (93.41 lbm). The scientific complement for the probe is the same as for nominal Jupiter probe, except for the type of neutral mass spectrometer. This unit is approximately .45 kg (1.0 lbm) lighter for the dedicated probe system, and the power and power conditioning equipment is lighter by 2.73 kg (6.04 lbm). Thus, the basic components on the equipment deck are somewhat lighter. A single descent parachute replaces the dual parachute that was used on the nominal Jupiter probe.

The remaining basic difference between this descent probe and that of the nominal Jupiter probe lies in the provisions for a nitrogen atmospheric gas system added to this configuration. This system provides a small nitrogen gas supply which is vented to the inside of the descent probe before descent. The system is added to control descent thermal cooldown of the probe. The function of the system for thermal control is discussed in Section c.10 of this chapter.

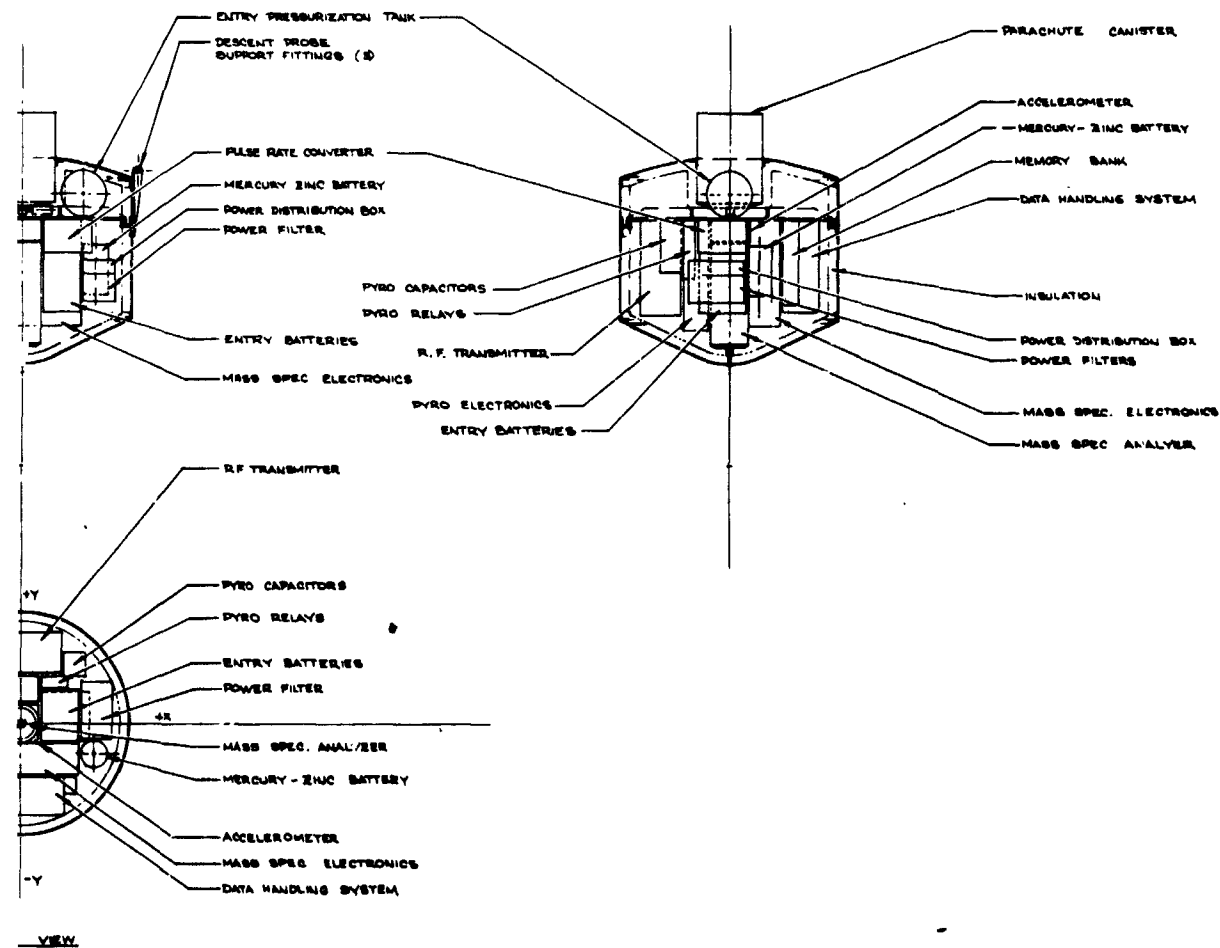
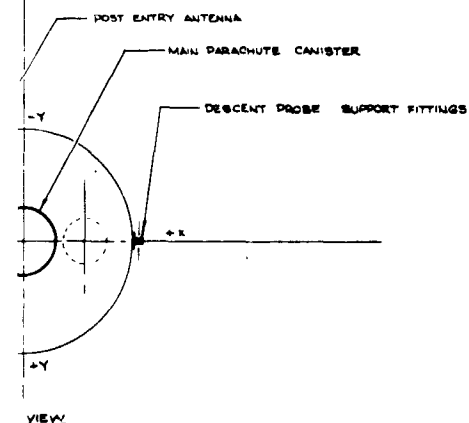
The entry probe is the same configuration as the ejected probe, and consists of the aeroshell/heat shield assembly, the descent probe, the aft heat shield, and the post-separation antenna. The entire probe with the exception of the post-separation antenna is enclosed by a forward and an aft multilayer insulation blanket. The antenna and the insulation blankets are allowed to remain on the entry probe through entry rather than ejecting them. The insulation blanket will burn off during entry, as will a portion of the antenna. The remaining antenna portion is jettisoned during the opening of the aft closure.

Since this probe requires only a very minimal attitude control system, the entire system is located within the entry probe.





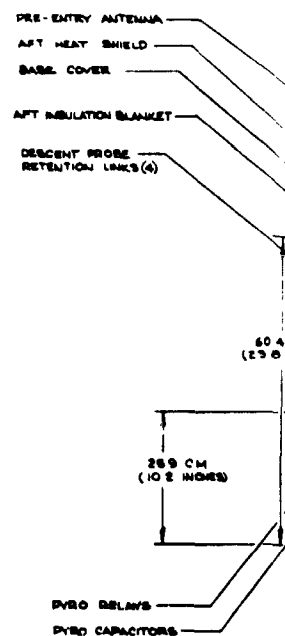
FOLDOUT FRAME )



PYRO RELAYS

PYRO CAPACITORS

DESCENT



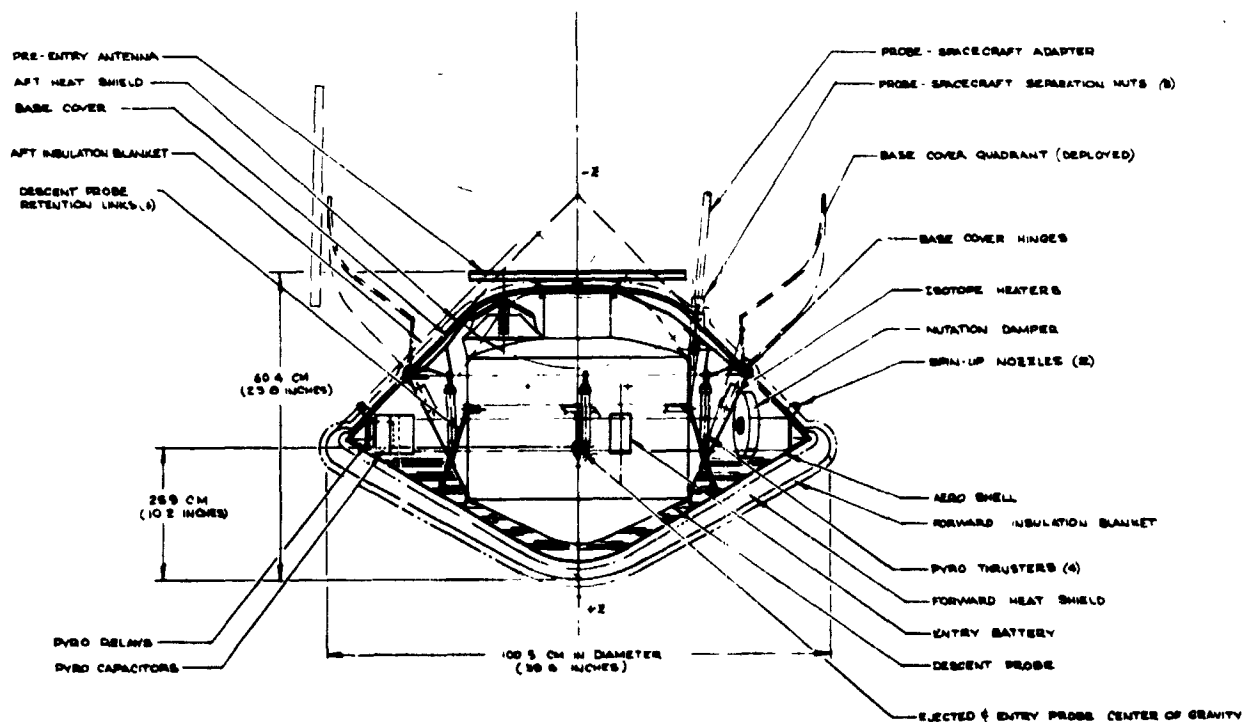
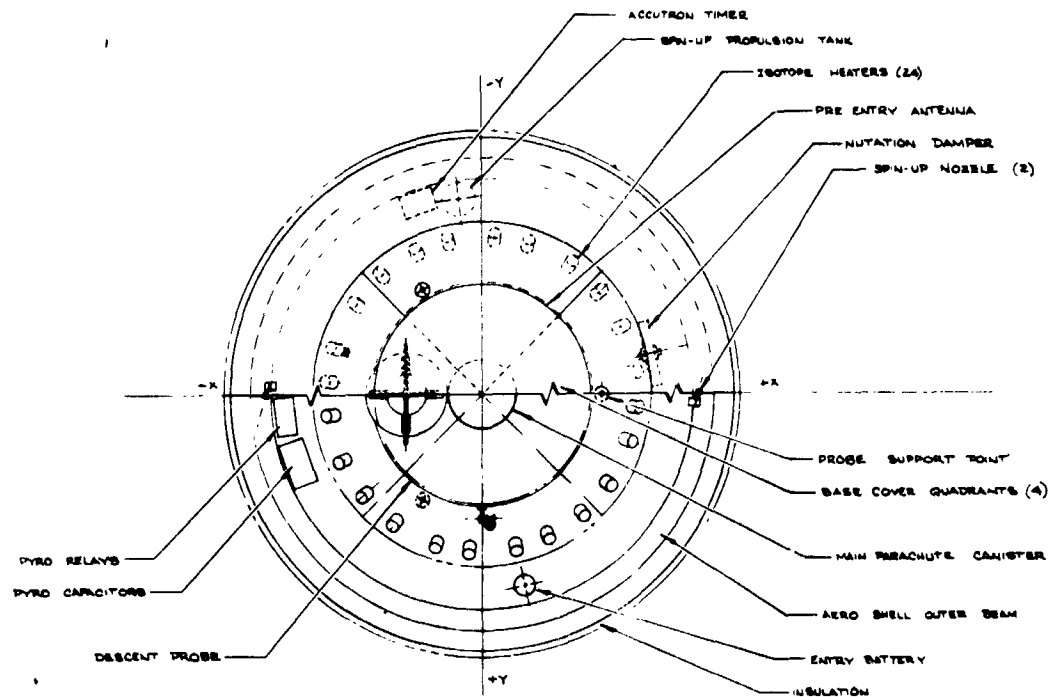
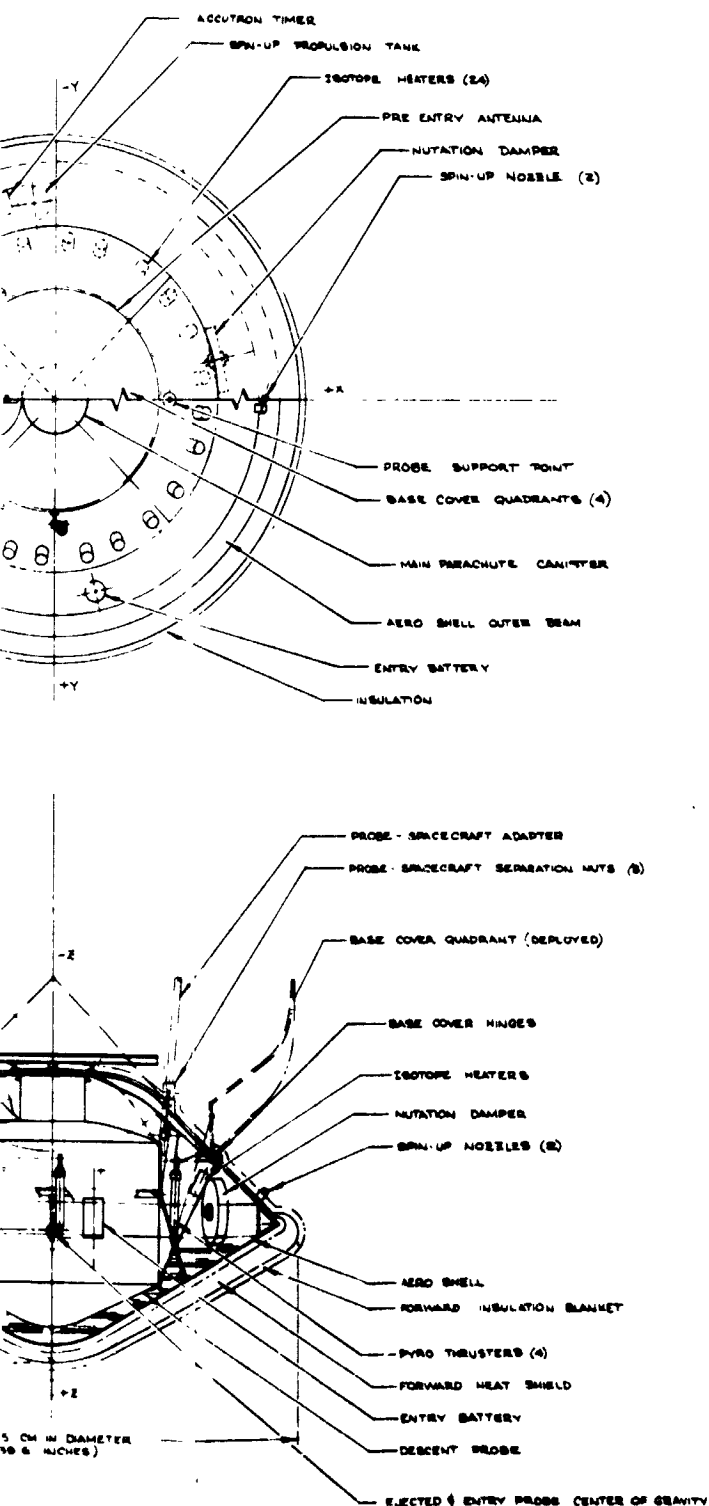


Figure V-106 Alternative Jupiter Pro

EOLDOUT FRAME

FC



RG 100-000 000/12

JUPITER SURVIVABLE PROBE -  
TASK III CONFIGURATION III  
OUTER PLANET ENTRY PROBE STUDY

Figure V-106 Alternative Jupiter Probe-Dedicated Mission Configuration

EOLDOUT FRAME

3

FOLDOUT FRAME

4

V-211 and V-212

b. *Structural Design* - The probe is designed by the structural loadings encountered during entry of the Jovian atmosphere, at an entry angle of  $20^\circ$  at a latitude of  $30^\circ$ , with an entry ballistic coefficient of  $102 \text{ kg/m}^2$  ( $0.65 \text{ slug/ft}^2$ ). These loadings are  $1650 \text{ g}$  peak and a maximum dynamic pressure of  $1.1 \times 10^6 \text{ N/m}^2$  ( $23,000 \text{ lbf/ft}^2$ ). For this probe, the entire vehicle is designed by these loadings plus the acoustic and vibration loadings at launch. There is no service module nor delta velocity motor (which are designed only by launch loads on the nominal Jupiter probe). The aeroshell structure is designed of titanium to provide adequate strength at the heat shield backface temperature. The configuration is ring-frame stiffened skin with a triangular shaped closure frame. A saddle frame accepts the descent probe loads and introduces the loads into the aeroshell.

The descent probe basic structure is identical with the nominal Jupiter probe. It consists of a cylindrical section stiffened by 10 equally spaced longerons to distribute the equipment deck loads into the skin of the probe. The only difference in this cylindrical section is the magnitude of loading ( $1650 \text{ g}$  vs  $1500 \text{ g}$  for the nominal Jupiter probe) and the resultant weight changes. The shape of the aft closure is changed, however. It is a spherical segment to better withstand entry loads.

c. *Parachute Assembly* - A single stage of parachute descent is satisfactory for this probe, which need descend only to 13 bars to satisfy mission requirements. The selected descent ballistic coefficient of  $14.1 \text{ kg/m}^2$  ( $0.09 \text{ slug/ft}^2$ ) for a descent probe weighing  $42.36 \text{ kg}$  ( $93.41 \text{ lbf}$ ) results in a parachute size of  $2.59 \text{ m}$  ( $8.5 \text{ ft}$ ) diameter. This parachute is of the disc-gap-band configuration.

d. *Heat Shield* - An entry ballistic coefficient of  $100 \text{ kg/m}^2$  ( $0.65 \text{ slug/ft}^2$ ) has been selected for entry of the probe into the Jovian atmosphere. This probe enters the planet at a latitude of  $30^\circ$  as compared with essentially equatorial entry for the nominal probe. This change in entry latitude, plus the relocation of probe components from the service module (which is deleted) to the entry probe results in a fairly large heat shield and aeroshell. The heat shield mass fraction for this configuration is  $0.350$  (Fig. V-35). The heat shield weight is  $38.7 \text{ kg}$  ( $85.4 \text{ lbf}$ ), of which  $30.3 \text{ kg}$  ( $66.8 \text{ lbf}$ ) is ablated at entry.

e. *Mass Properties* - The weight tabulation for the components of the probe dedicated mission vehicle are shown in Table V-37. It should be noted again for this weight table that component weights

Table 1-1. Weight Breakdown for the Probe-Selected Alternative Jupiter Probe

	Weight	
	Kg	Lb
<u>Science</u>		
Temperature Gauge	0.45	1.00
Pressure Transducer	0.68	1.50
Accelerometer: Sensor	0.59	1.30
Converter	0.91	2.00
Neutral Mass Spectrometer Analyzer:	1.81	4.00
Electronics	2.72	6.00
Pump	0.45	1.00
Ballast Tank	0.45	1.00
	8.06	17.80
<u>Power &amp; Power Conditioning</u>		
Power Conditioner	-	-
Power Distribution Box	0.45	1.00
Power Filters	0.68	1.50
Entry Batteries	1.78	3.92
Post-Separation Batteries	0.24	0.52
	3.15	6.94
<u>Cabling</u>		
Inner Probe	2.81	6.20
External Structure	1.86	4.10
	4.67	10.30
<u>Data Handling</u>		
Data Handling System	2.14	4.70
Memory Banks	0.45	1.00
	2.59	5.70
<u>Attitude Control System (Less Propellant)</u>		
Sun Sensor	-	-
Planet Sensor	-	-
ACS System and Links	1.41	3.10
Nutation Damper	1.07	2.40
Accutron Timer	0.14	0.30
ACS Electronics	-	-
	2.64	5.80
<u>Communications</u>		
Pre-Entry Antenna	2.13	4.70
Post-Entry Antenna	0.45	1.00
RF Transmitter	2.72	6.00
RF Switch	0.23	0.5
	5.53	12.2
<u>Pyrotechnic Subsystem</u>		
Pyro Electronics	0.91	2.00
Pyro Capacitors (Probe)	0.11	0.24
Pyro Capacitors (External)	0.26	0.56
Pyro Relays (Probe)	0.34	0.75
Pyro Relays (External)	0.79	1.75
Mercury-Zinc Battery	0.41	0.90
Pyro-Squibs (78 at 0.25 lb each)	0.27	0.60
	0.45	1.00
	3.54	7.80
<u>Structures and Heat Shields</u>		
Descent Probe Structure	5.08	11.20
Equipment Support Deck	4.99	11.00
Base Cover	4.38	9.65
Service Module Structure	-	-
Aeroshell (21b for payload ring)	10.43	23.00
Forward Heat Shield (66.8 ablated during entry)	38.74	85.40
Aft Heat Shield	2.09	4.60
Deflection Motor Support	-	-
	65.71	144.85
<u>Mechanisms</u>		
Separation Spring Cartridges (at 0.37 lb)	0.41	0.90
Separation Nuts (at 0.23 lb/.7 + .5)	0.32	0.70
Pin Puller (at 0.3 lb/.9 + .9)	0.41	0.90
Latches and Bands	0.91	2.00
Main Parachute (3.25 in chute & Riser)	4.08	9.0
Secondary Parachute	-	-
	6.13	13.50

Table 7-37 (cont.)

	Weight	
	Kg	Lb
<u>Thermal:</u>		
External Insulation Blanket (Forward Heatshield)	2.00	4.40
External Insulation Blanket (Base Cover)	2.49	5.50
Probe Hull Insulation (Internal)	1.59	3.50
Isotope Heaters	1.81	4.00
Environmental Tank & N <sub>2</sub>	0.50	1.10
	<u>8.39</u>	<u>18.50</u>
<u>Propulsion:</u>		
Deflection Motor Cases		
Deflection Motor Propellant		
ACS Propellant	0.02	0.05
	<u>0.02</u>	<u>0.05</u>
Total	110.47	243.46
15% Contingency	<u>16.56</u>	<u>36.52</u>
	<u>126.99</u>	<u>279.97</u>
1. <u>Pre-Entry Weight</u>		
ACS Propellant	0.02	0.05
15% Contingency	0.01	0.01
(279.96 - 0.06 = 279.90 lb)		
126.99 - .03 = 126.96 kg		
	<u>0.03</u>	<u>0.06</u>
2. <u>Post-Entry Weight</u>		
Forward Heat Shield (Ablated)	30.30	66.80
Aft Heat Shield (Ablated)	2.04	4.50
Forward Insulation Blanket	2.00	4.40
Aft Insulation Blanket	2.50	5.50
Pre-Entry Antenna	2.13	4.70
	<u>38.97</u>	<u>85.90</u>
15% Contingency	<u>5.85</u>	<u>12.9</u>
(279.90 - 38.8 = 181.10 lb)	<u>44.82</u>	<u>98.80</u>
126.96 - 44.82 = 82.14 kg		
3. <u>Weight on Parachute (Initially):</u>		
Base Cover Quadrants	4.36	9.65
Base Cover Heat Shield (Not Ablated)	0.45	1.00
Separation Pin Pullers	0.41	0.90
Separation Nut	0.90	0.20
ACS System	1.41	3.10
Isotope Heaters	0.91	2.00
Pyro Thrusters	0.41	1.00
	<u>8.07</u>	<u>17.85</u>
15% Contingency	<u>1.23</u>	<u>2.68</u>
(181.10 - 20.53 = 160.57 lbs)	<u>9.30</u>	<u>20.53</u>
82.14 - 9.30 = 72.84 kg		
4. <u>Weight on Parachute (Final):</u>		
Pyro Capacitors	0.25	0.56
Pyro Relays	0.79	1.75
Pyro Squibs	0.18	0.40
Aero Shell	10.43	23.00
Forward Heat Shield (Not Ablated)	8.44	18.60
Spring Cartridges	0.41	0.90
Separation Nuts	0.23	0.50
Latches & Bands	0.91	2.00
Isotope Heaters	0.91	2.00
External Cabling	2.49	5.50
Nutation Damper	1.00	2.40
Accutron Timer	0.14	0.30
Separation Battery	0.24	0.52
	<u>26.51</u>	<u>58.71</u>
15% Contingency	<u>3.97</u>	<u>8.76</u>
(160.57 - 67.14 = 93.41 lb)	<u>30.48</u>	<u>67.19</u>
72.84 - 30.48 = 42.36 kg		

are grouped in categories in the table, and a 15% contingency factor is added for arriving at the total weight to account for growth. The weight thus achieved is reduced sequentially in the remainder of the table to provide weight data for the different phases of the mission, from spacecraft separation to entry and descent.

### 9. Propulsion Subsystem

This probe has no deflection delta velocity motor, but does have a minimal attitude stabilization system. The proper entry trajectory and pointing attitude is provided by the spacecraft before probe separation for this configuration. Thus, the ACS system need only provide a probe spinup to 0.52 rad/sec (5 rpm) to stabilize the pointing orientation during the pre-entry coast phase of flight. The schematic for this system is shown in Figure V-107.

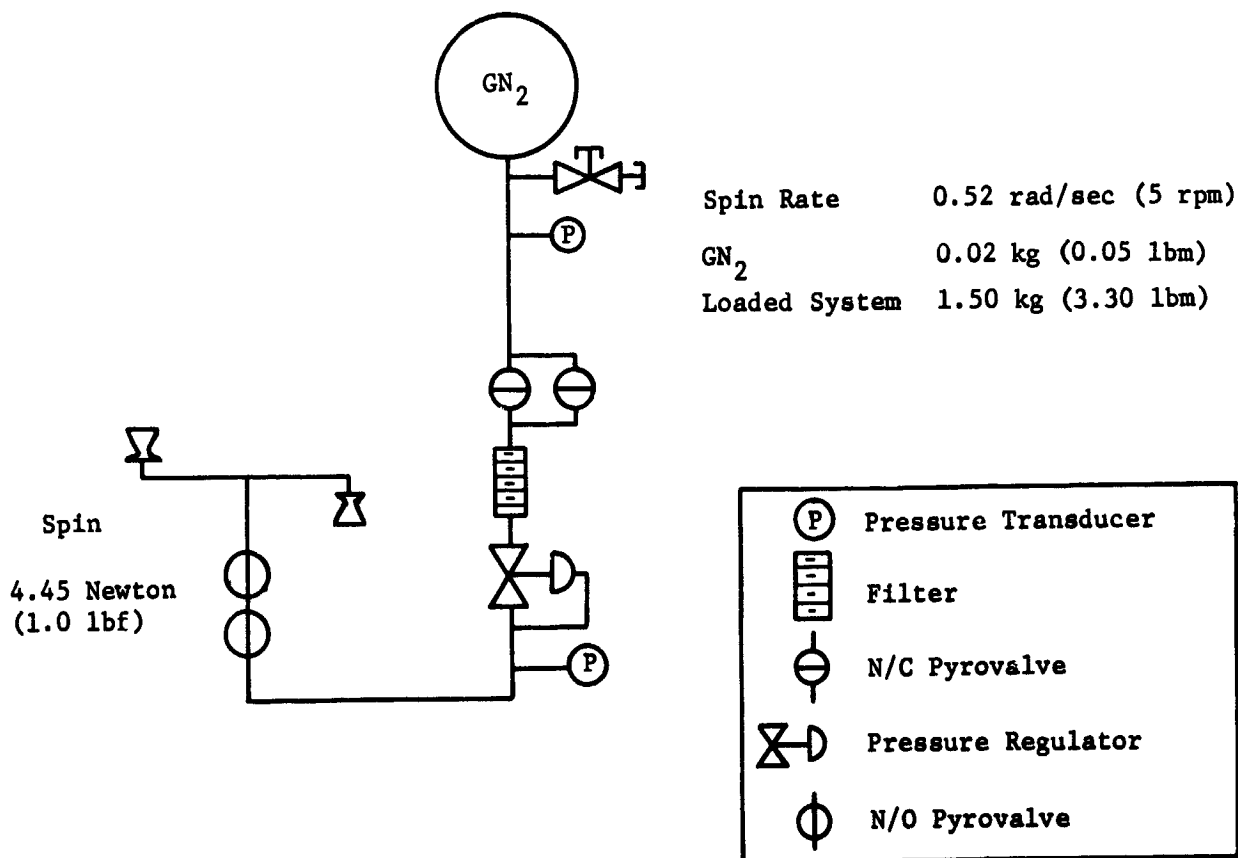


Figure V-107 Attitude Control Subsystem



The weight breakdown of the ACS follows.

		Weight	
		kg	lbm
Component Weights:	Fill Valves (1)	.11	.25
	Transducers (2)	.23	.50
	Squib Valves (4)	.54	1.00
	Filters (1)	.09	.20
	Regulators (1)	.18	.40
	Thrusters, 1 blf (2)	.18	.40
	Lines	.18	.40
Total		1.43 kg	3.15 lbm

The amount of propellant to achieve the spin rate is minute, amounting to only 0.02 kg (0.05 lbm) and the pressure tank weight is 0.04 kg (0.10 lbm). Thus, the total system weight is approximately 1.50 kg (3.30 lbm).

#### 10. Thermal Control Subsystem

*a. General Discussions* - For the probe-dedicated alternative Jupiter probe, the thermal design concept is basically the same as the nominal Jupiter probe mission. Multilayer insulation, thermal coatings, and radioisotope heaters are used for thermal control during spacecraft cruise and probe coast, and the probe thermal inertia coupled with low density foam insulation is used for entry and descent. For the probe-dedicated mission the minimum temperature predicted during descent is marginal (3°K margin above lower limit), and two additional improved probe thermal designs were therefore, investigated. On the basis of those investigations, the addition of nitrogen gas environmental control was included for descent thermal control. For this design, the probe would be purged and sealed with one-bar dry nitrogen gas at launch and equipped with a nitrogen gas supply bottle capable of purging the probe volume to a depth of 2.5 bars during descent. The delta weight and volume added by the N<sub>2</sub> gas supply would be approximately 0.41 kg (1.1 lb) and 0.35 liters based on a storage design pressure 250 bar.

As before, the pivotal temperature for thermal design is the probe temperature at the end of the mission coast phase, which determines the probe entry temperature for descent. Although the probe-dedicated mission considered either a cool/dense or nominal atmosphere encounter and descent, the primary thermal problem remains one of losing too much thermal energy to the atmosphere environment during the cool/dense descent. The probe coast and entry temperatures, therefore, were increased for this mission by using a higher  $\alpha/\epsilon$  thermal coating on the probe and absorbing a higher percentage of solar energy during coast. Because the coast time is longer for this mission (34.5 days), the transient temperature effects following spacecraft separation were of no consequence.

A thermal analysis was performed for the probe-dedicated alternate Jupiter mission probe configuration. The basic probe consists of a 39.6 diameter entry probe design with a minimal ACS spinup system. No probe propulsion capability or Sun and planet guidance sensors are required because by definition, the probe-dedicated mission is a spacecraft deflect mission and a flyby is not required. To analyze the probe's thermal performance, the two finite-element thermal math models previously constructed were utilized. For the spacecraft cruise and coast analysis, the probe service module was eliminated and only the aeroshell and base cover were present.

On the basis of the thermal analysis, a complete thermal history for the probe-dedicated Jupiter mission was constructed and is presented in Figure V-108. The spacecraft cruise and coast temperatures were determined based on the radioisotope heater power supplied and the probe thermal coating. The probe temperature is represented by the internal equipment and the RF transmitter which is shown separately when activated. These results represent the baseline mission thermal history. Figures V-109 and V-110 present the probe thermal history for improved thermal design. Figure V-109 considered a sealed probe for the first 2.5 bars of descent while Figure V-110 considered  $N_2$  gas environment control for the first 2.5 bars of descent.

During cruise and coast, sufficient probe mass is present such that brief excursions of the boundary conditions cause only minor temperature variations. Trajectory uncertainties for the probe-dedicated alternate Jupiter mission are less than six minutes and therefore not thermally significant. As before, the most critical design item is the multilayer insulation performance which should be accurately determined by actual hardware thermal tests. An integral discussion of the thermal control subsystem design has been previously presented in Section A. 10. a and b of this chapter.

Probe Internal Capacitance = 6.33 Watt-hr/°K  
 Separation Power Dissipation = 48.7 Watt-hr  
 Entry Power Dissipation = 28.2 Watt-hr  
 Descent Power Dissipation = 44.6 Watt-hr

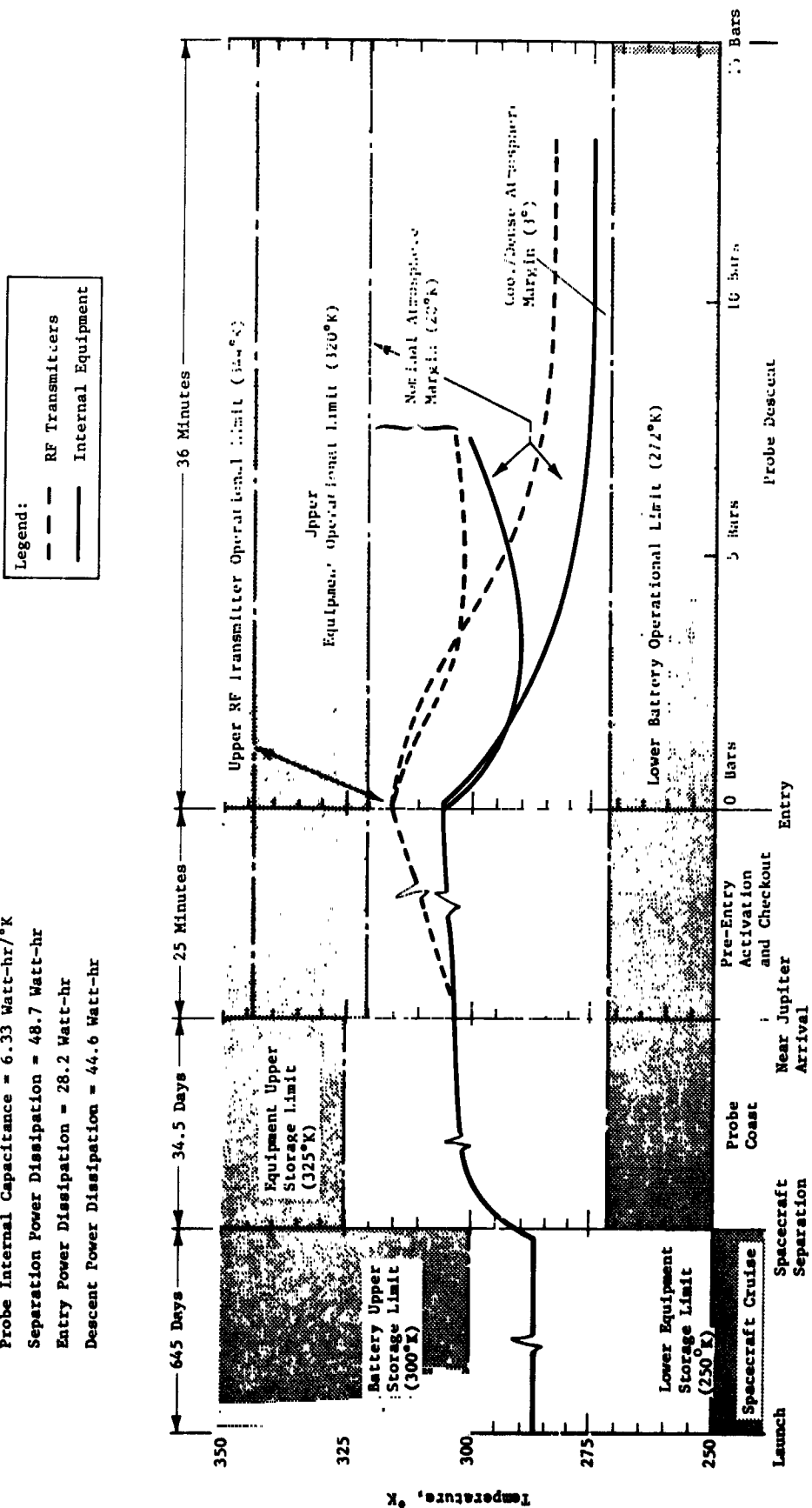


Figure V-108 Launch to Descent Thermal History of Probe-Dedicated Jupiter Mission Probe

Probe Internal Capacitance = 6.33 Watt-hr/°K  
 Separation Power Dissipation = 48.7 Watt-hr  
 Entry Power Dissipation = 28.2 Watt-hr  
 Descent Power Dissipation = 44.6 Watt-hr

Legend:  
 --- RF Transmitter  
 --- Internal Equipment

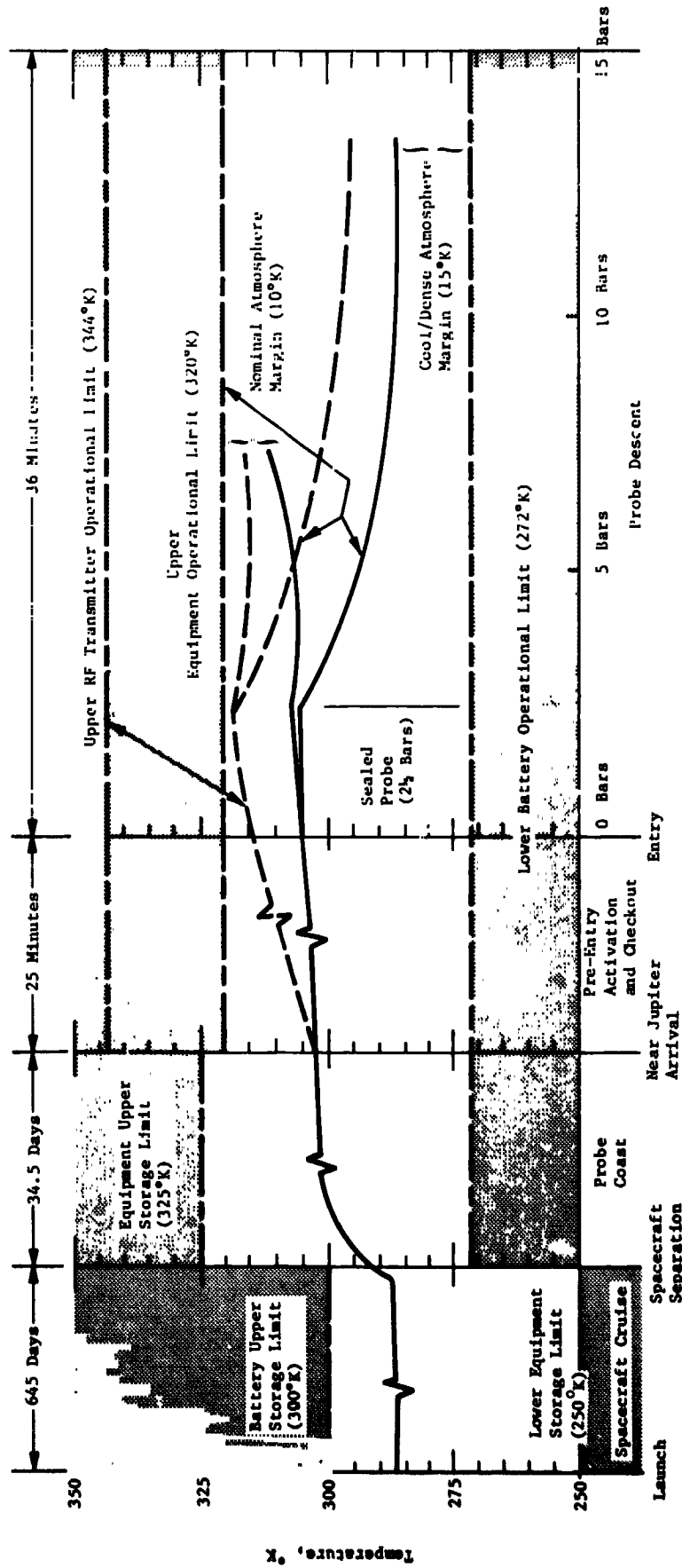


Figure V-109 Launch to Descent Thermal History of Probe-Dedicated Jupiter Mission with Partially Sealed Probe Improved Thermal Control

Probe Internal Capacitance = 6.33 Watt-hr/°K  
 Separation Power Dissipation = 48.7 Watt-hr  
 Entry Power Dissipation = 28.2 Watt-hr  
 Descent Power Dissipation = 44.6 Watt-hr

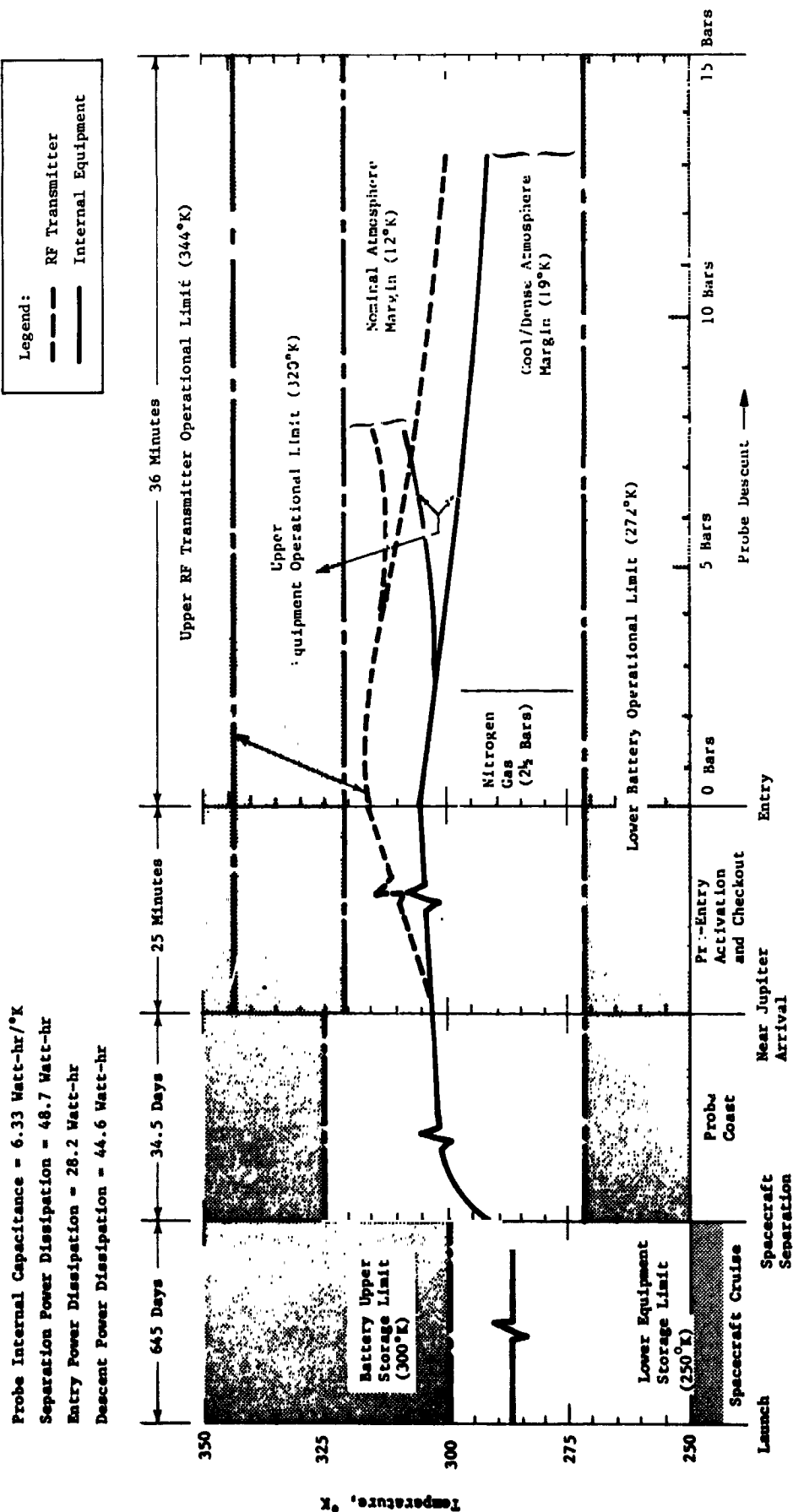


Figure V-110 Launch to Descent Thermal History of Probe-Dedicated Jupiter Mission with Nitrogen Gas Partially Sealed Probe Improved Thermal Control

b. *Cruise and Coast Thermal Control* - The sizing of the radioisotope heaters for the probe-dedicated mission is presented in Figure V-111. Multilayer-insulation thicknesses of 1.5 cm were assumed to achieve a reasonable compromise between insulation bulk and heater power. The probe thermal coatings for this mission were chosen such that a larger temperature increase between spacecraft separation and probe coast equilibrium would occur. A thermal coating value of  $\alpha/\epsilon = 0.62/0.13$  was found to be optimum from a standpoint of temperature delta and isotope heater requirement. Although higher  $\alpha/\epsilon$  ratios are available that would produce more desirable temperature differences, the isotope heat requirement becomes very sensitive to coating emissivity. The actual coating selected is a surface treatment of aluminum with Iridite 14-2. The emissivity value for the probe nose was 0.20.

The results in Figure V-111 show that 18 watts of radioisotope heater power will establish a probe entry temperature (302°K) and maintain a safe probe temperature margin during the long spacecraft cruise phase of the mission (13°K margin below storage limit). The increase in probe temperature following separation is of no consequence since a 34.5-day probe coast period occurs before entry, which will be adequate time to approach thermal equilibrium conditions.

c. *Entry and Descent Thermal History* - The probe-dedicated alternate Jupiter probe thermal design concepts have been presented in Figure V-108 thru V-110. The most desirable of these designs from a standpoint of reliability, minimum weight, and over-all thermal control is the N<sub>2</sub> gas environment concept. It was this design that was chosen for the actual mission probe configuration. Descent results for both the nominal atmosphere and cool/dense atmosphere encounters are presented in Figure V-110.

The power profile used for the descent thermal analysis represented the improved transmitter with an efficiency of 45%. It was mainly this reduction in transmitter power coupled with a decrease in probe mass that makes this mission more critical than the nominal probe mission. In addition, the descent ballistic coefficient defined to accommodate the nominal atmosphere encounter for the probe-dedicated mission is less requiring increased probe exposure to the cooler atmosphere layers during the cool atmosphere encounter.

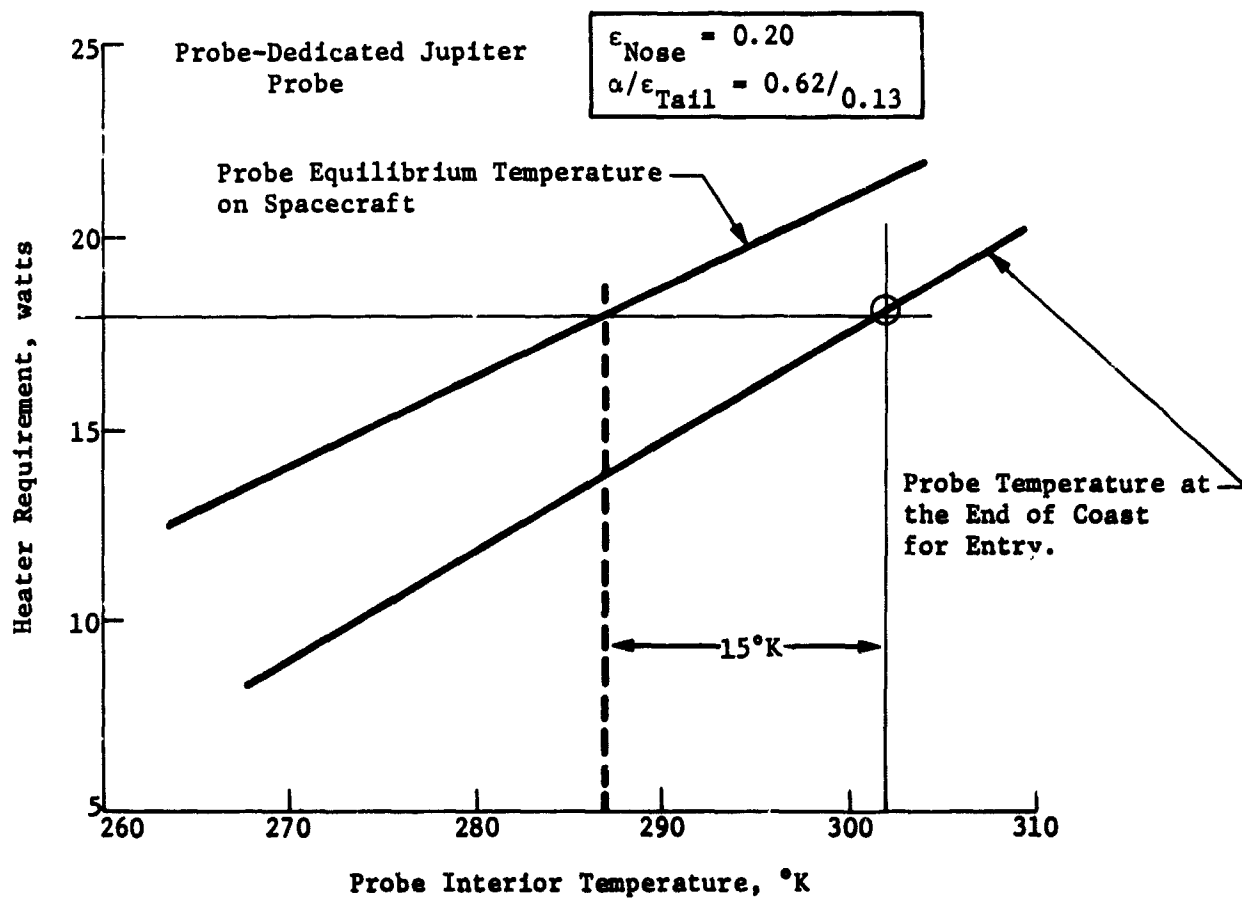


Figure V-111 Radioisotope Heater Sizing Based on Probe Thermal Coating Selection

The descent temperature and pressure profiles for the probe dedicated mission are presented in Figure V-112. This mission requires 36 minutes for descent to 13 bars pressure in a cool/dense atmosphere or to 7.5 bars in a nominal atmosphere. The probe is not staged for the probe-dedicated mission.

Analytical results show that improved thermal design is obtained by using the N<sub>2</sub> gas environmental thermal control concept. The probe temperature margins predicted for identical mission conditions follow.

Temperature Margin	Spacecraft	Probe	Entry-Descent Phase	
	Cruise Phase, °K	Coast Phase, °K	Nominal Design, °K	Improved N <sub>2</sub> Design, °K
Above				
Equipment				
Lower Limit	37	23	3	19
Below				
Equipment				
Upper Limit	13	19	15	12
Below				
Transmitter				
Upper Limit	NA	NA	29	28

#### 11. Probe to Spacecraft Integration

The probe-dedicated alternative Jupiter probe integration with the spacecraft is essentially the same as that described in Section b.11 of this chapter. The differences lie primarily in the weight of the probe itself, and in the power consumption by the probe as supplied from the spacecraft. Since the probe does not have a solid propellant deflection motor, the 5 watts of heater power is not required.



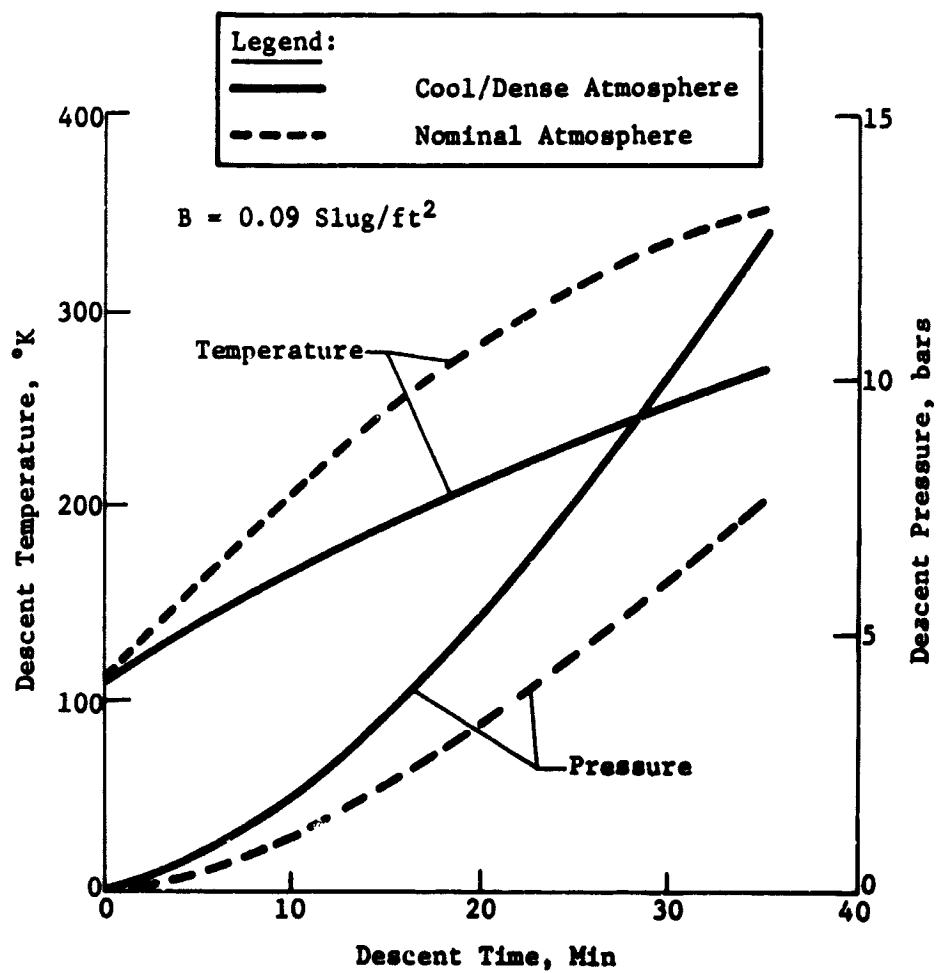


Figure V-112 Probe-Dedicated Mission Descent Temperature and Pressure Profiles

D. SPACECRAFT-RADIATION-COMPATIBLE ALTERNATIVE JUPITER PROBE SYSTEM  
DEFINITION

As for the alternative Jupiter probe discussed in Section C of this chapter, the constraints for this probe were also the results of the Jupiter parametric studies discussed in Section A. This alternative probe mission is intended to optimize the spacecraft usage, i.e., the probe provides the deflection, the encounter is essentially equatorial, and the periapsis radius minimizes the radiation environment for the spacecraft. The constraints follow.

Mission	Type I in 1979
Entry Angle	-15° (structure design to -20°)
Entry Latitude	5°
Periapsis Radius	6 $R_J$
Deflection Mode	Probe

All other constraints are the same as for the probe mission described in Section C.

1. Science Instrumentation and Performance

The major differences between the two alternative probes involve spacecraft probe function trades, and the entry and descent profile and measurement performance are identical. Thus, the discussion given in Section C describes these functions for both alternative Jupiter probe designs. The only difference is in the data rate necessary for engineering and formatting, the science data rate being the same. This is summarized in Table V-38. Consult Section C.1 for further details.

Table V-38 *Radiation Compatible Alternative Jupiter  
Probe Instrument Sampling Times and Data  
Rates*

Phase	Instrument	Sampling Times, sec	Collection Bit Rate, bps	Transmission Bit Rate, bps
Entry, 44 sec	Accelerometers			
	Longitudinal	0.1	100	0
	Lateral	0.2	50	0
Descent, 2130 sec	Temperature	3.5	2.9	3.0
	Pressure	3.5	2.9	3.0
	Mass Spectrometer	40.0	10.0	10.5
	Accelerometers			
	Turbulence	10.0	6.0	6.3
	Stored	0.0	0	4.4
	Science Total			27.2
	Engineering and Formatting			4.5
	Total			31.7

## 2. Mission Definition

The radiation-compatible probe mission is shown in Figure V-113 and detailed in Table V-39. Important mission design results are summarized in this section.

*a. Interplanetary Trajectory Selection* - The interplanetary trajectory is pictured in Figure V-113(a) with 100 day intervals noted. The launch date of November 7, 1979, and arrival date of September 17, 1981 (trip time of 680 days), result in a maximization of the payload weight as discussed in Chapter VI, Section A. As indicated in the figure, the spacecraft arrives at Jupiter shortly before the view to Jupiter is obstructed by the Sun.

*b. Launch Analysis* - The launch analysis is provided in Figure V-113(b). Available payload is plotted against launch period for three sets of launch vehicle performance data: standard data for the Titan 5 Segment vehicle with and without Burner II, plus updated data for the Burner II combination. For reference, the payload weight (probe, spacecraft, spacecraft modifications, and spacecraft launch vehicle adapter) is about 1000 lb for a Pioneer mission and 1500 lb for a Mariner mission. Thus, the Burner II option is necessary for a Mariner-type mission to obtain a 20-day

launch period. The nominal launch trajectory summarized in Table V-39(a) indicates that the daily launch window and parking orbit coast time are satisfactory.

c. *Approach Trajectories* - The approach trajectory is pictured in Figure V-113(d) and summarized in Table V-39(b). The spacecraft flyby radius was selected to be  $6 R_J$  to limit radiation

damage to the spacecraft. Since a low inclination probe trajectory was selected (entry latitude of  $5^\circ$ ), an in-plane deflection maneuver was used. The spacecraft initially leads the probe but because of Jupiter's rapid rotation rate the probe quickly overtakes the spacecraft. The probe aspect angle at the start of descent is  $7.3^\circ$ , passes nearly through zero, and ends at  $10^\circ$  at the end of mission.

d. *Deflection Maneuver* - A probe deflection maneuver is used in this mission at a deflection radius of 30 million km or 35.1 days from Jupiter. The deflection sequence is illustrated in Figure V-113(c). For comparison, a deflection maneuver was targeted at 50 million km. This resulted in a coast time of 61.4 days and a  $\Delta V$  of 152 m/sec to establish the same conditions at entry.

e. *Navigation and Dispersions* - The navigation and dispersion results are pictured in Table V-39(c). Standard Doppler and range tracking is all that is assumed since navigation dispersions are not significant at Jupiter. The entry dispersions are large compared to the other missions with  $3\sigma$  dispersions in entry angle of  $6.0^\circ$ , angle of attack of  $5.6^\circ$ , and entry time of 38.4 min. For comparison, the deflection at 50 million km resulted in dispersions of  $5.8^\circ$ ,  $5.5^\circ$ , and 40.8 min, respectively. The communication parameter dispersions are discussed in Subsection D.4.

f. *Entry and Descent Trajectories* - Table V-39(d) summarizes the entry and descent phases of the mission. The entry phase starts at 304.6 km above the 1 atm pressure level and ends at the staging of the aeroshell, 34 sec later. During this phase, the peak deceleration of 1500 g is attained. The descent phase starts after staging and lasts until the end of mission at 13 bars. The total mission time (entry and descent) is 36.1 min.

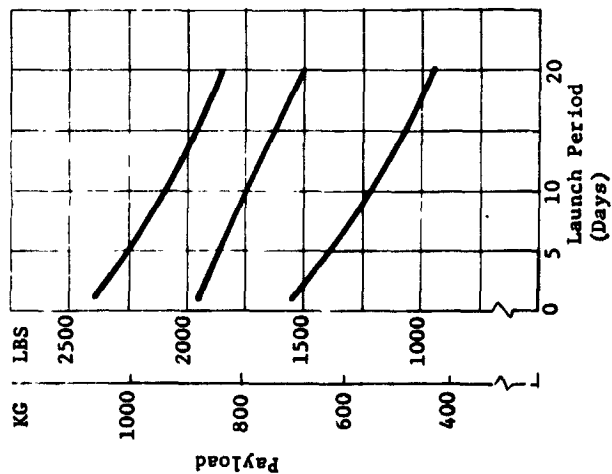
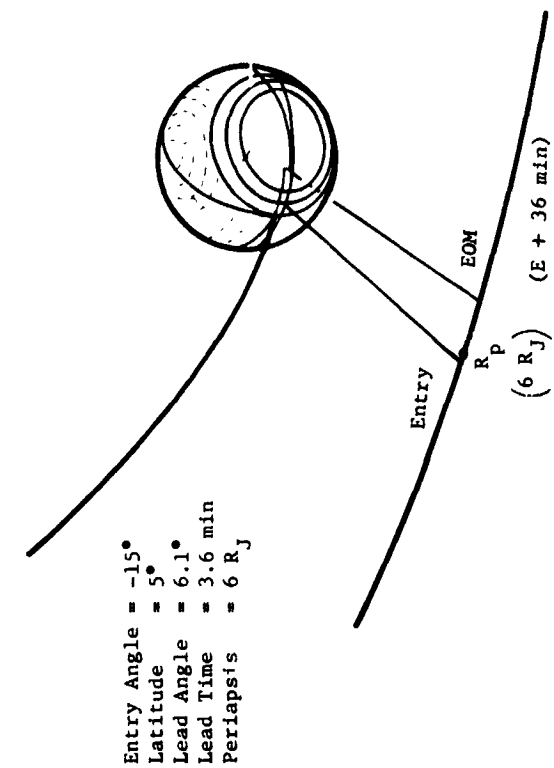
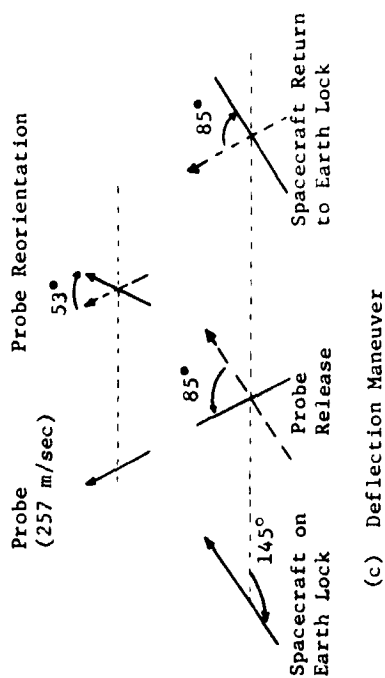
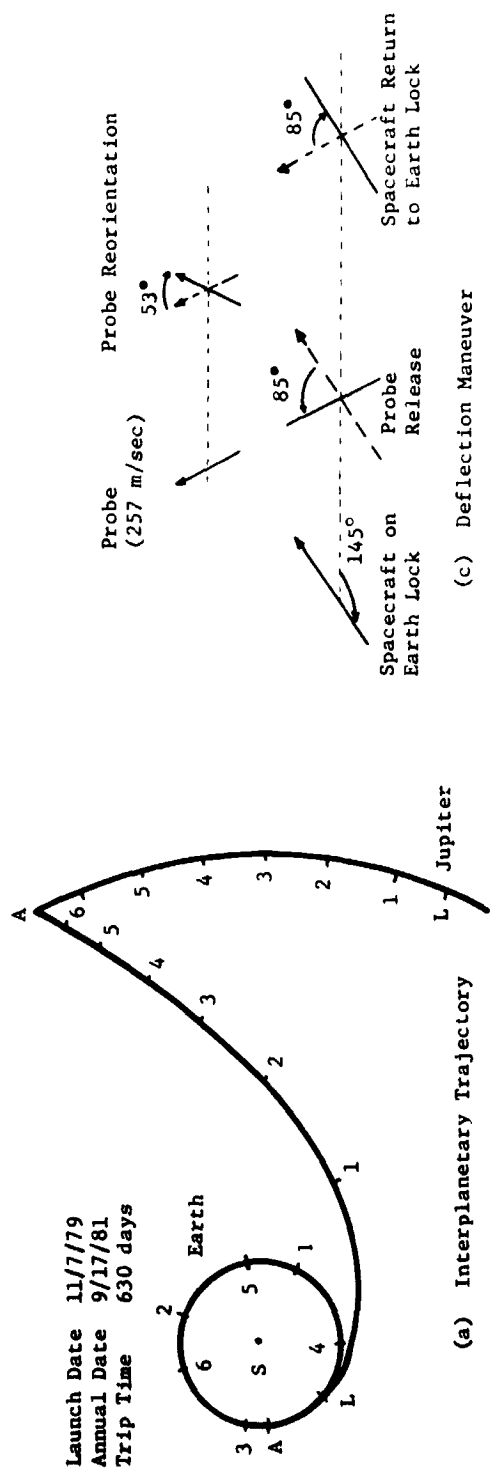


Figure V-113 Radiation-Compatible Alternative Mission Definition

Table V-39 Radiation-Compatible Alternative Mission Summary

a. Conic Trajectory Data

Interplanetary Trajectory	Launch Trajectory	Arrival Trajectory
Launch Date: 11/7/79 Arrival Date: 9/17/81 Flight Time: 680 days Central Angle: 155°	Nominal $C_3$ : 93.6 km <sup>2</sup> /sec <sup>2</sup> Nominal DLA: 30.5° Launch Window: 1.17 hr Parking Orbit Coast: 36 min $C_3$ (10 day): $C_3$ (20 day): Azimuth Range: 101.7° - 115°	VHP: 8.474 km/sec RA: 161.3° DEC: 6.8° ZAE: 145.2° ZAP: 141.4° RP: 6 R <sub>J</sub> INC: 5°

b. Deflection Maneuver and Probe Conic

Deflection Maneuver	Probe Conic Definition
Deflection Mode: Probe Deflection Radius: 30 x 10 <sup>6</sup> km Coast Time: 35.1 days $\Delta V$ : 257 m/sec Application Angle: 119° Out-of-Plane Angle: 0° Rotation for Probe Release: 85° Probe Reorientation Angle: -53° Spacecraft $\Delta V$ from Earth: NA	Entry Angle: -15° Entry Latitude: 5.10 Entry Longitude: 98.8 Lead Time: 3.55 min Lead Angle: 6.11° Probe-Spacecraft Range (Entry): 357,422 km Probe Aspect Angle (Entry): 78.4° Probe Aspect Angle (Descent): 7.3° Probe Aspect Angle (EOM): 10.4°

c. Dispersion Analysis Summary

Navigation Uncertainties	Execution Errors (3 $\sigma$ )	Dispersions (3 $\sigma$ )
Type: Range-Doppler 167-day arc SMAA: 1576 km SMIA: 224 km $\beta$ : 86° TOF: 122 sec	$\Delta V$ Proportionality: 1% $\Delta V$ Pointing: 2° Probe Orientation Pointing: 2°	Entry Angle: 6.02° Angle of Attack: 5.60° Down Range: 11.46° Cross Range: 2.00° Lead Angle: 6.91° Lead Time: 37.4 min Entry Time: 38.4 min

d. Entry and Descent Trajectory Summary

Entry Parameters	Descent Parameters	Critical Events	
		Time from Entry	Altitudes above 1 atm
Entry Velocity, km/sec: 60 Entry Altitude, km: 304.6 Entry B, slug/ft <sup>2</sup> : 0.65 kg/m <sup>2</sup> : 102.1 Entry Atmosphere: Cool/Dense Max Deceleration, g: 1500 Max Dynamic Pressure, lb/ft <sup>2</sup> : 2.1 x 10 <sup>4</sup> kg/m <sup>2</sup> : 1.0 x 10 <sup>6</sup>	Descent Atmosphere: Cool/Dense EOM Pressure, bar: 13 Descent B, slug/ft <sup>2</sup> : slug/ft <sup>2</sup> : 0.09 kg/m <sup>2</sup> : 14.13	g = 0.1, sec: 8.5 Max g, sec: 18 M = 0.7, sec: 44 Descent Time, min: 35.6 EOM, min: 36.1	km: 189 km: 66.8 km: 33.4 km: -57.5

### 3. System Integration

a. *Functional Sequence* - Table V-40 shows the sequence of events for this mission. This sequence in the separation and pre-entry phases is similar to that for the nominal Jupiter probe described in Section B.3 of this chapter because both use the probe deflection mode. For the entry and descent phases, this sequence is identical to that for the other alternative Jupiter probe described in Section C.3 because both have the same post-entry and descent requirements. The entry arrival uncertainty of 38.35 min has a significant effect upon this probe definition because the pre-entry time is extended by this amount and the communication geometry conditions at the time of acquisition (entry - 52 min) requires a two-position search in order to keep the RF power within state-of-the-art capabilities.

b. *Functional Block Diagram* - The functional interfaces are identical to those for the nominal Jupiter probe, shown in Figure V-76.

c. *System Data Profile* - Figure V-114 shows the data profile for this mission. Since the pre-entry antenna is ejected at 43 min before entry, pre-entry engineering data is stored for later transmission. Therefore, the descent storage capability is increased by approximately 2600 bits. It is noted that the nominal Jupiter probe data profile of Figure V-76 did not eject the pre-entry antenna; therefore, pre-entry storage of engineering data was not required. The telecommunications frequency was higher than for this configuration and a different type of antenna was used.

d. *System Power Profile* - Figure V-115 shows the power profile for this probe mission. Note the impact of the entry arrival uncertainty on the pre-entry power requirements.

e. *System Weight Summary* - Table V-41 shows the probe weight summary for this configuration. The ejection weight is 166 kg (365 lb) and the entry weight is 110 kg (243 lb). It is to be noted that this probe is more complex than the alternative Jupiter probe described in Section C; however, the entry weight of this probe is lighter. Two basic reasons account for this difference: (1) the simpler probe is designed for higher deceleration forces, and (2) the simpler probe carries some service module components through entry instead of ejecting them.

Table 1-10 Sequence of Events for a Nominal Mission-Compatibility Jupiter Mission

Item	Time	Event
1	L=0	Launch, November 7, 1979
2	L+2h	Separate Spacecraft from Launch Vehicle
3	L+2h to L+670d	Cruise
4	S-6h, 0m, 0s	Spacecraft Power to Probe; Eject Environmental Cover
5	S-5h, 47m, 0s	Start Probe Checkout
6	S-0h, 17m, 0s	Probe Checkout Complete; Start Spacecraft Orientation for Release (85°)
7	S-0h, 2m, 0s	Spacecraft Orientation to 85° Complete; Activate Probe Data Handling System and Separation Subsystems
8	(L+644.8d) S=0	Separate
9	S+0m, 0.5s	Start Probe Spinup to 100 rpm
10	S+4m, 0s	Probe Spinup to 100 rpm Complete
11	S+15m, 0s	Apply Probe $\Delta V$ (257 m/sec) (900 m Separation)
12	S+15m, 21s	Eject Probe Deflection Motors; Activate Attitude Propulsion Subsystem
13	S+15m, 31s	Start Probe Precession; Reorient Spacecraft to Earth Lock (-85°)
14	S+6h, 13m, 31s	Turn on Transmitter
15	S+6h, 15m, 31s	Probe Precession Complete (-53°); Start Probe Acquisition
16	S+6h, 16m, 31s	Acquisition Complete; Start Engineering Data Transmission
17	S+6h, 26m, 31s	Complete Data Transmission; Deactivate Probe Systems
18	L+642.12d to L+679.93d	Coast
19	E-1h, 23m, 51s	Enable Entry Battery Ordnance
20	E-1h, 3m, 51s	Activate Probe Descent Batteries (in aeroshell and descent probe); Enable Probe Despin; Turn on Data Handling System, Engineering Instrumentation
21	E-54m, 21s	Turn "On" Transmitter
22	E-52m, 21s	Start Probe Acquisition (2 position search)
23	E-49m, 1s	Complete Probe Acquisition; Start Data Transmission
24	E-48m, 51s	Start Probe Despin to 5 rpm
25	E-43m, 51s	Probe Despin Complete
26	E-43m, 21s	Eject Service Module; Activate Service Module Deflection Propulsion; Stop Transmission
27	E-42m, 35s	Turn on Science Instruments
28	E=0	Entry (305 km above 1 atm; $3 \times 10^{-7}$ bar)
29	E+0m, 8.5s	Start Recording Accelerometer Data (0.1g sensing)
30	E+0m, 14.7s	Initiate Probe Descent Program (100 g sensing)
31	E+0m, 38.2s	Eject Base Cover Quadrants (Mach 0.8)
32	E+0m, 44s	Deploy Main Parachute (Mach 0.7, ~0.092 bar)
33	E+0m, 54s	Release Descent Probe from Entry Probe (switch probe antenna); Probe Transmitter "On"; Start Probe Acquisition
34	E+0m, 56s	Deploy Temperature Gage; Release Mass Spectrometer Covers
35	E+2m, 34s	Probe Acquisition Complete; Start Data Transmission
36	E+36m, 14s	End of Design Mission (~13 bar)
37	(L+680d) E+15m, 41s	Spacecraft Periapsis (6 $R_J$ ); September 17, 1981

Includes 38.35-min trajectory uncertainty and is based on a descent ballistic coefficient of 0.09 slugs/ft<sup>2</sup>.



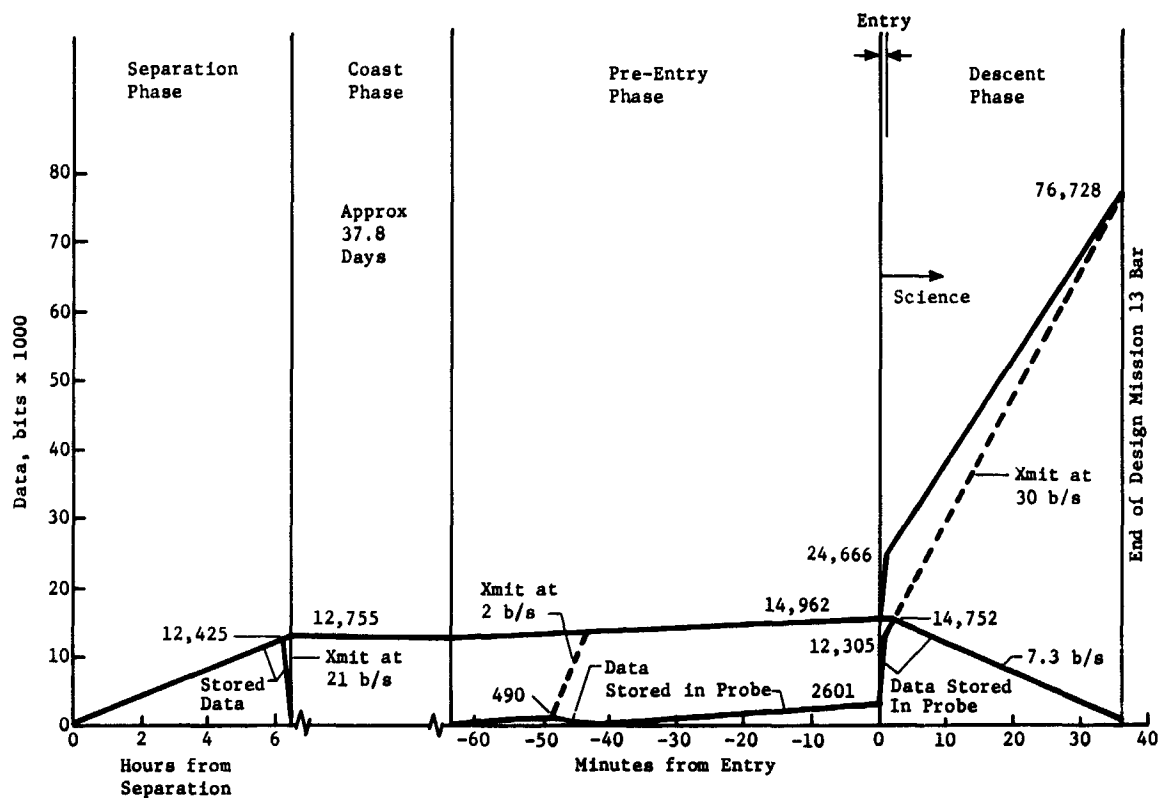


Figure V-114 Data Profile for Spacecraft-Radiation-Compatible Jupiter Mission

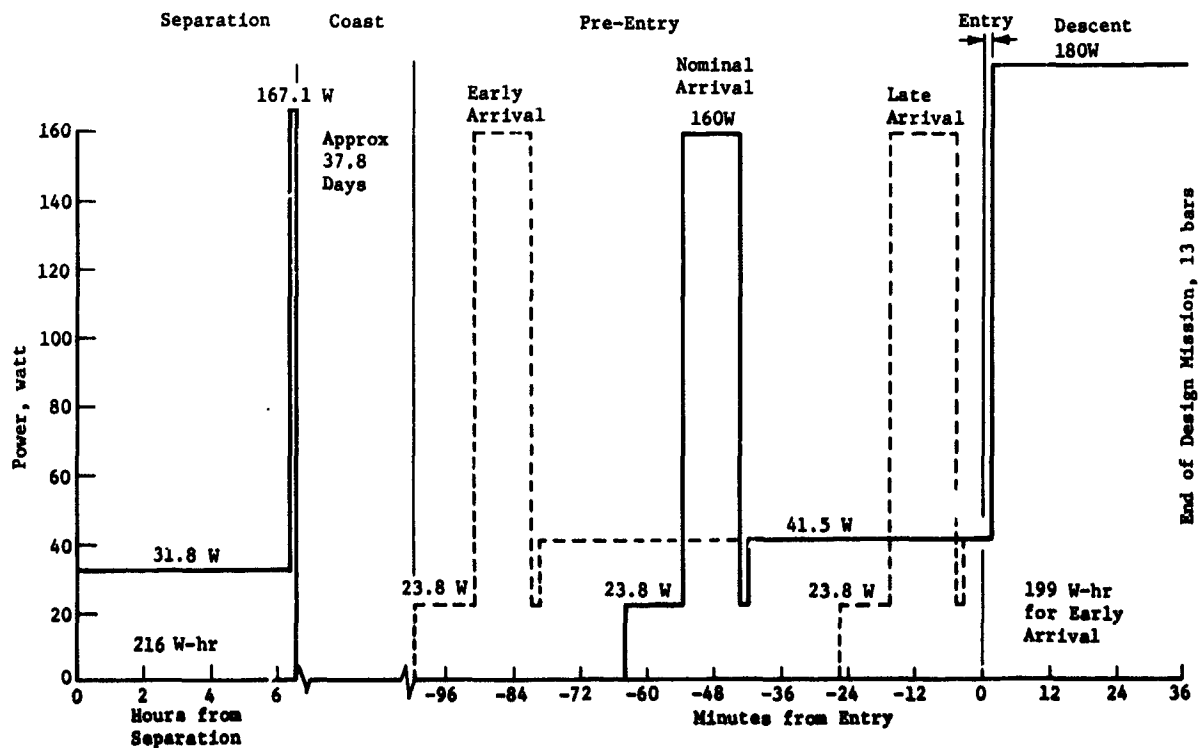


Figure V-115 Power Profile for Spacecraft-Radiation-Compatible Jupiter Mission

Table V-41 Weight Summary for Spacecraft-Radiation-Compatible  
Jupiter Mission

PROBE BREAKDOWN	WEIGHT	
	<u>kg</u>	<u>lb</u>
Science	8.06	17.80
Power and Power Conditioning	6.67	14.70
Cabling	5.67	12.50
Data Handling	2.59	5.70
Attitude Control (dry)	10.26	22.60
Communications	5.96	12.70
Pyrotechnics	6.31	13.91
Structure and Heat Shield	64.22	141.59
Mechanisms	7.98	17.60
Thermal	7.44	16.40
Propulsion (dry)	4.22	9.30
Propellant	14.79	32.60
15% Margin	<u>21.60</u>	<u>47.61</u>
Ejected Weight	155.57	365.02
Entry Weight	110.27	243.12
Descent Weight (final)	46.67	102.91

4. Telecommunications Subsystem

The point design for a 6  $R_J$  mission performed during the parametric studies and described in Section A of this chapter was used as a basis for the spacecraft-radiation-compatible mission. The trajectory is identical in  $R_P$ ,  $R_{EJ}$ ,  $\gamma_E$ , and latitude to point design 8, described in Table V-3. The descent depth has been raised to 13 bars in lieu of 30 bars in the previous case, and the bit rate is increased to 30 bps.

Probe dispersions are similar to the dispersions for point design 8 as shown in Figure V-14. A 20° spacecraft antenna and a descent antenna with a 120° beamwidth were selected; resulting in 55 W of power required at 0.86 GHz. The operating frequency was lowered slightly from 1 GHz because of hardware availability in 1975 at 0.86 GHz for the ATS program, as discussed in detail in Chapter IX, Section A.

parameters of the RF link are depicted in Table V-42 for the radiation compatible Jupiter mission at 0.86 GHz. Maximum transmitter power is required at mission completion. Table V-42A depicts design details of the RF components that comprise the telecommunication subsystem. Design requirements of the components are discussed in detail in Section A.4 of this chapter. RF power of 55 W is required at 0.86 GHz with a bit rate of 30 bps using binary FSK with a tracking tone. A mechanical switch is used at this power level. The entry antenna is an annular slot which is mounted on the service module under the deflection motor. The descent antenna is a turnstile over a cone design which is mounted on the aft bulkhead of the descent probe. The spacecraft antenna is a parabolic dish with right-hand circular polarization and a 20° beamwidth. A two-position sector search technique is required, as discussed for point design 8 in Section A.4 of this chapter. A fixed antenna on the spacecraft without any position and frequency search, requires a beamwidth of 35° and would raise the RF power to over 300 W.

Toward the end of the program, discussion with JPL (Dr. J. Smith) on the Jupiter magnetosphere model resulted in additional analysis to determine noise temperature variations for the missions. As discussed in Volume III, Appendix B, the JPL magnetosphere model for synchrotron noise is dependent upon the distance,  $d$ , within the model for a fixed frequency. The worst-case noise temperature appears to occur when both the magnetosphere and planet disk are within portions of the antenna beam. Since the synchrotron noise is the higher source, it is possible that the system noise temperature could be higher during probe acquisition instead of at entry when the disk is also within the spacecraft antenna 3-dB beam. The possibility of occurrence is dependent upon the trajectory geometry. Therefore, an analysis was performed of the two alternative Jupiter probe missions to determine system noise temperature variations during the mission.

The computer program that calculates RF link parameters uses a constant value for the system noise temperature for each frequency. A variable temperature with time cannot be input into the program. The purpose of the analysis was to determine the effect of variable temperatures on RF signal margin.

Table V-42 Probe Telemetry Link Design, Spacecraft-Radiation-Compatible Jupiter Mission

Parameter	Unit	Nominal Value	Adverse Tolerance	Remarks
Total Transmitter Power	dBW	17.4	0.0	55 W
Transmitting Circuit Loss	dB	-0.3	0.2	
Transmitting Antenna Gain	dB	4.9	1.8	120° Beamwidth
Communications Range Loss	dB	-202.3	1.0	3.6x10 <sup>5</sup> km
Planet Atmos & Defocus Loss	dB	-0.7	0.2	Cool/Dense, 13 bars
Polarization Loss	dB	0.0	0.2	
Antenna Pattern Ripple Loss	dB	0.0	0.2	
Receiving Antenna Gain	dB	18.7	3.0	20° Beamwidth
Receiving Circuit Loss	dB	-0.2	0.2	
Net Circuit Loss, $\Sigma$ (2-9)	dB	-179.9	6.8	
Total Received Power (1+10)	dBW	-162.5	6.8	
Receiver Noise Spectral Density	dBW	-196.9	0.5	$T_s = 1469^\circ\text{K}$ $NF_s = 7.82 \text{ dB}$
Tracking Tone				
Tone Power/Total Power	dB	-5.2	0	
Received Tone Power (11+13)	dBW	-167.7	6.8	
Tracking Threshold Bandwidth	dB	11.8	0	Bandwidth = 15 Hz
Threshold SNR	dB	10.0	0	
Threshold Tracking Power (12+15+16)	dBW	-175.1	0.5	
Tracking Performance Margin (14-17)	dB	7.4	7.3	
Data Channel				
Data Power/Total Power	dB	-1.5	0	
Radio System Processing Loss	dB	-1.0	0	
Fading Loss	dB	-1.0	0	
Received Data Power (11+19+20+21)	dBW	-166.0	6.8	
Data Bit Rate	dB	14.8	0	
Threshold $E_b/N_o$	dB	8.9	0	
Threshold Data Power (12+23+24)	dBW	-173.2	0.5	
Performance Margin (22-25)	dB	7.2	7.3	
Nominal Less Adverse Value (26-26 adv)	dB	0.0		
<b>CONDITIONS:</b> <ol style="list-style-type: none"> <li>1. Worst-Case (EOM) Conditions at 0.86 GHz</li> <li>2. Coded Noncoherent System with Viterbi Decoding</li> <li>3. Convolutional Encoder, M=2, V=2, Q=8</li> <li>4. BER = <math>5 \times 10^{-5}</math> for Binary FSK with K=8 code</li> <li>5. Spacecraft Antenna in 2-position search</li> <li>6. EOM Probe Aspect Angle is 10.5°</li> </ol>				

Table V-42a Telecommunications RF Subsystem for the Spacecraft-Radiation-Compatible Jupiter Mission

CONDITIONS: Planet: Jupiter S/C: Mariner Frequency: 0.86 GHz Bit Rate: 30 bps			
COMPONENT	CHARACTERISTIC	UNIT	VALUE
Transmitter	RF Power Out	W	55
	Overall Efficiency	%	45
	DC Power-In at 28 V dc	W	122
	Total Weight	kg	2.72
	lb	lb	6.0
RF Switch	Type		Mechanical
	Insertion Loss	dB	0.3
	Weight	kg	0.45
		lb	1.0
Entry Antenna	Type		Annular Slot
	Main Beam Angle	deg	85
	Beamwidth	deg	40
	Maximum Gain	dB	5.2
	Diameter	cm	43
		in.	17
	Weight	kg	2.1
		lb	4.7
Descent Antenna	Type		Turnstile/Cone
	Main Beam Angle	deg	0
	Beamwidth	deg	120
	Maximum Gain	dB	5.0
	Size (diameter x h)	cm	20.3 x 7.5
		in.	8 x 3
	Weight	kg	0.45
		lb	1.0
Spacecraft Antenna	Type		Parabolic Dish
	Beamwidth	deg	20
	Maximum Gain	dB	18.3
	Size	cm	128
		in.	50.5
	Weight	kg	4.54
		lb	10.0
	Despin		No
	Position Search		2
	Frequency Acquisition	sec	50 (at each position)
	Clock Angle, $\theta$	deg	101
	Cone Angle, $\phi$	deg	59 and 79
Spacecraft Receiver	Noise Temperature	*K	300
	Noise Figure	dB	3.1
	DC Power-In at 28 V dc	W	3.0
	Weight	kg	0.9
		lb	2.0

Trajectory geometry for the 6  $R_J$  mission is shown in Figure V-116.

Magnetosphere distance is shown for selected times. At acquisition (E-1h), only synchrotron noise is present. At E-0.5h,  $d$  is the largest without the planet limb being visible within the 20-deg spacecraft antenna pattern. At E-1/3h, the planet limb enters the spacecraft antenna pattern and maximum synchrotron model depth,  $d$ , occurs. At E-1/4h, the planet disk fills a major portion of the antenna pattern and  $d$  has decreased. From entry to the end of mission, the disk is totally within the antenna pattern and  $d$  is constant, as seen in the tabulation in Figure V-115. The angular apparent diameter,  $\phi_1$ , is also given in the figure to relate the amount of planet disk included in the 3-dB beamwidth of the spacecraft antenna. It is only coincidental that the spacecraft antenna beamwidth is equal to the angle subtended by the planet. Spacecraft antenna beamwidth is determined by relative probe position dispersions from acquisition to mission completion.

The spacecraft parabolic dish antenna has an axial pattern with a  $\sin u/\pi$  distribution about the pattern axis. For acquisition when only the magnetosphere is viewed by the antenna, Equation [D-1] is used with  $d_1$  shown in Figure V-117. Equation [D-1] relates the maximum synchrotron temperature. For partial planet intercept with the limb intersecting the 3-dB antenna pattern, the disk and magnetosphere temperatures are proportional to the solid angle ratio as seen in Figure V-117. With the planet completely in the background of the antenna, the total noise temperature is the sum of a constant disk temperature and a magnetosphere noise that is a function of  $d$ , as seen in Figure V-117. Thus, we have the following relationships to describe antenna noise temperatures from two independent noise sources, one being range dependent with distance,  $d$ , measured in  $R_J$ :

a. *No Disk Intersection (synchrotron noise only)*

$$T_A = T_{BS} = \frac{0.45 D_1 \lambda^2}{R_J} = C d_1 \quad [D-1]$$

b. *Partial Planet Intersection (disk and synchrotron noise)*

$$T_A = C(d_2 + d_3) \left[ \frac{\Omega_b - \Omega_1}{\Omega_b} \right] + C d_2 \left( \frac{\Omega_1}{\Omega_b} \right) + T_{BD} \left( \frac{\Omega_1}{\Omega_b} \right) \quad [D-2]$$

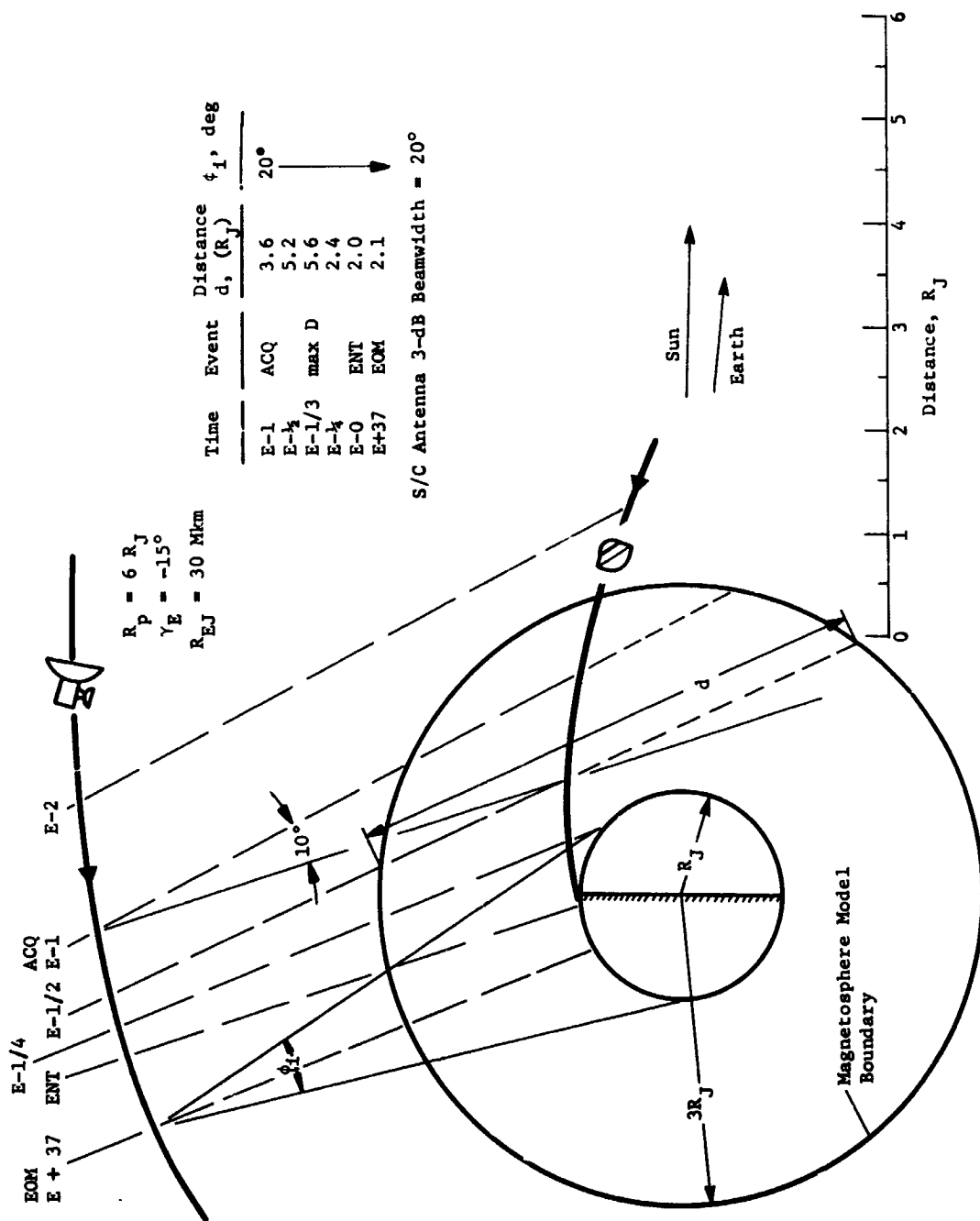


Figure V-116 Trajectory Geometry for the Spacecraft Radiation-Compatible Mission

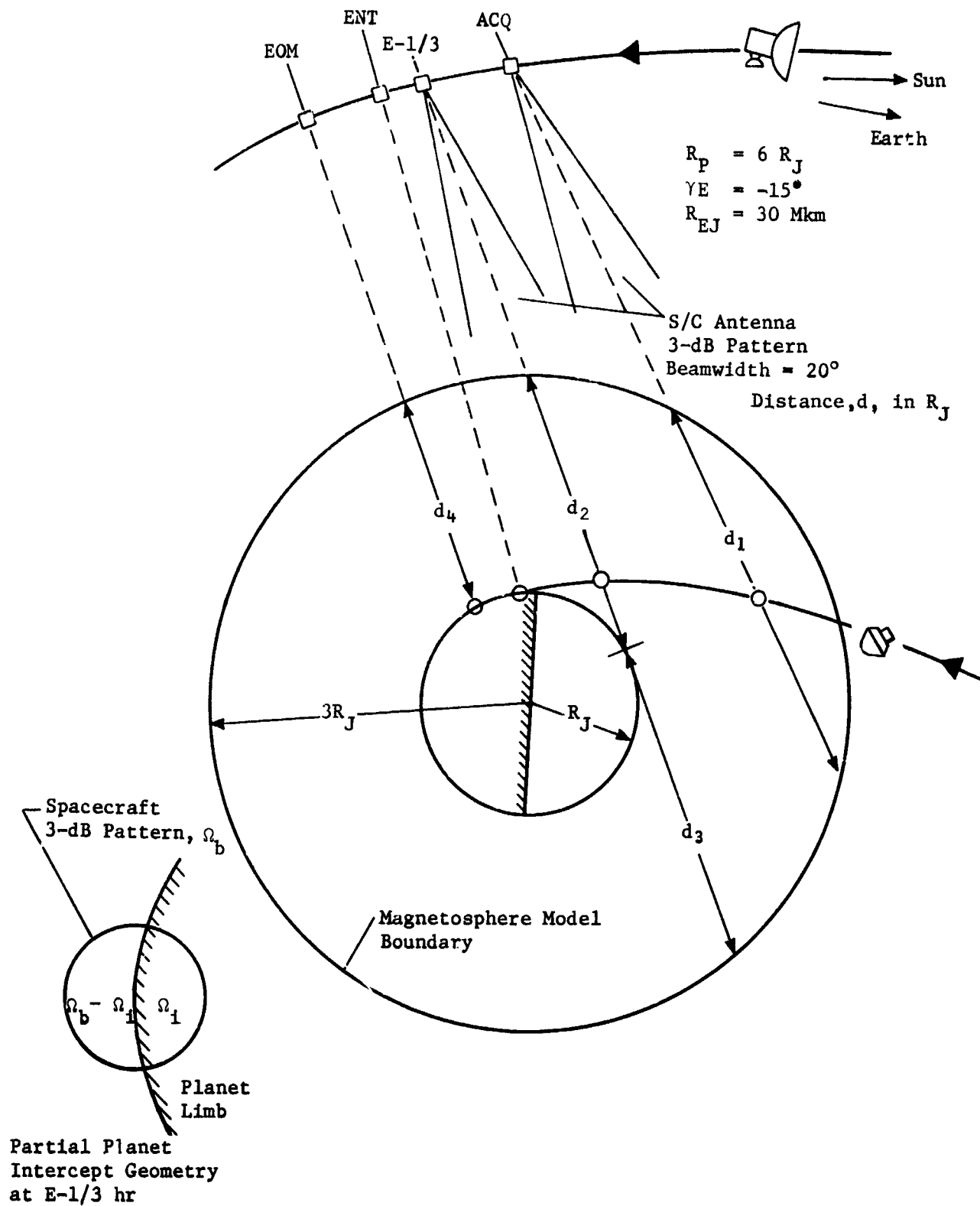


Figure V-117 Jovian Magnetosphere Noise Temperature Distance Geometry



c. Total Intersection (planet in background)

$$T_A = C d_4 + T_{BD} \quad [D-3]$$

where

C = brightness temperature constant for fixed frequency ( $\lambda$  = constant),  $= 0.45 \lambda^2$

d = path length, in  $R_J$ , defined in Figure V-117

$\Omega_b$  = antenna pattern solid angle,  $\text{rad}^2 = (3\text{-dB beamwidth, rad})^2$

$\Omega_i$  = portion of solid angle from planet limb, see Figure V-117,  $\text{rad}^2$

Results of using Equations [D-1] through [D-3] for the mission, as depicted in Figure V-116, are shown in Figure V-118 for 1 GHz. The antenna temperature peaks at E-1/2h when  $d_1$  is maximum without any of the antenna pattern being intersected by the planet limb. Synchrotron noise decreases and disk noise increases as entry is approached. At entry, the full planet disk is in view by the spacecraft antenna. Distance  $d_4$  increases only slightly from entry to mission completion. At 1 GHz, the receiver noise temperature (Figure V-11) is 302°K. System noise temperature, as required by the RF link program is the sum of the variable antenna temperature and receiver front-end temperature. As mentioned previously, the computer program only accepts a constant systems noise temperature for computation of receiver noise spectral density. The value used at 1 GHz for the mission was 1280°K. The scale on the right of Figure V-118 relates the relative systems noise temperature difference with 1280°K as a reference.

In conclusion, a detailed analysis to determine the actual antenna noise temperature variation with mission time should be performed for planets with a magnetosphere that has a high noise temperature in the UHF region. As seen in Figure V-118, significant errors exist if a constant value is used for missions with variable periaapsis. The values used for d in Equations [D-1] and [D-3] are dependent on whether the spacecraft intersects the magnetosphere model or not. A constant temperature at a fixed frequency should not be used for a mission if the RF power required is close to the upper power limit. As seen for the mission used in Figure V-118, the systems noise temperature is 2.7 dB higher before entry than the value used to calculate the RF link. The RF power required at acquisition is 61 W caused by aspect angle and the low gain pre-entry antenna.

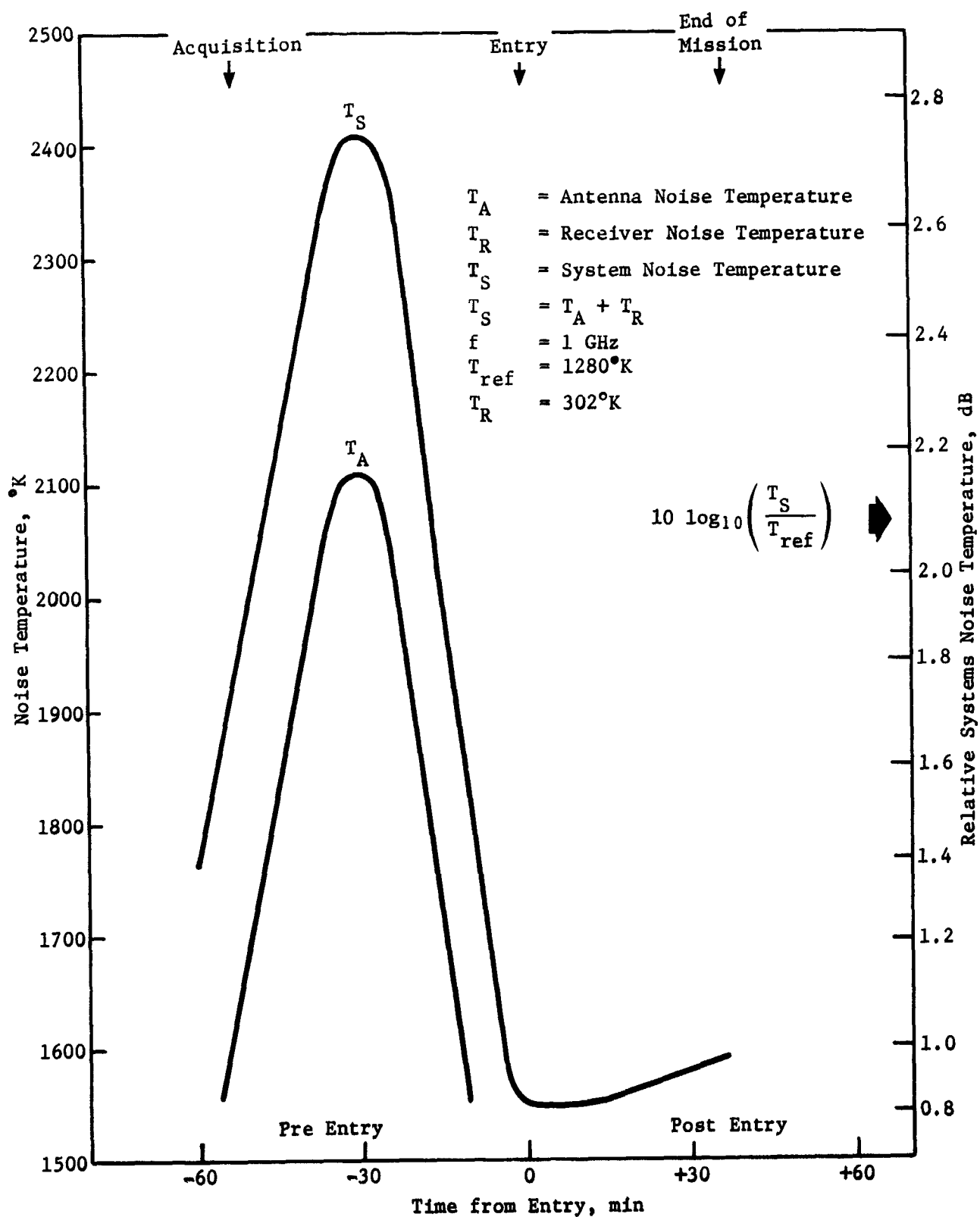


Figure V-118 Radiation-Compatible Mission Noise Temperature

The mission is designed with a constant system noise temperature of 1280°K and a total RF power of 55 W, based upon end-of-mission conditions. The effects of increased noise temperature, as seen in Figure V-118, increases the RF link power at E-30m to 1.86 (2.7 dB) times 61 W or 114 W. Since only 55 W is available, the signal margin is -3.2 dB at E-30m, due primarily to increased antenna noise temperature and probe aspect angle.

The RF power level of 55 W at 0.86 GHz is approaching the projected 1975 state-of-the-art upper limit for deep space transmitters. Therefore, it is impractical to design the mission for the severe pre-entry conditions. The systems advantages of having pre-entry communications must be weighed against the large entry antenna size and weight and the fact that data will be lost during random time intervals of pre-entry when the link margin is driven below zero by the increased system noise temperature.

5. Data Handling Subsystem

The configuration and functions of the data handling subsystem are unchanged from the design of the nominal Jupiter probe, with the exception of minor modifications of sequence and format. (See Sections A.5 and B.5 of this chapter and Vol III, Appendix H.)

6. Power and Pyrotechnic Subsystems

The configuration of the power and pyrotechnic subsystems is unchanged from the nominal Jupiter probe with the exception of battery size and weight. (See Sections A.6 and B.6 of this chapter and Vol III, Appendix G.) These physical characteristics are:

Ag-Zn	Post-separation Battery	6.9 lb	94 in. <sup>3</sup>
Ag-Zn	Entry Battery	6.4 lb	87 in. <sup>3</sup>
Hg-Zn	Pyrotechnic Battery	0.9 lb	1.0x0.5x3 in.

The remotely activated Ag-Zn batteries are based on power consumption for this mission. The change in the dimensions of the Hg-Zn battery is based on later catalog information than was available during nominal Jupiter probe definition.

## 7. Attitude Control Subsystem - Electronics

The electronics configuration and functions for this subsystem are unchanged from the nominal Jupiter probe design. (See Sections A.7 and B.7 of this chapter and Vol III, Appendix F.)

## 8. Structures and Mechanical Subsystem

The spacecraft-radiation-compatible Jupiter probe is very similar in appearance and arrangement to that of the nominal Jupiter probe. This probe, like the nominal Jupiter probe, provides its own deflection maneuver to place the probe on the proper entry trajectory. Thus, it has a full complement of propulsion system components. Like the probe-dedicated mission probe, only a single parachute is used for descent into the Jovian atmosphere.

*a. Configuration and General Arrangement* - The configuration of the probe for the spacecraft-radiation-compatible Jupiter mission is shown in Figure V-119. The ejected configuration has a conical nose cone of 60° half angle with maximum diameter of 0.954 meters (37.6 in.), and weight 165.57 kg (365.02 lbm). The descent probe is 0.47 meters (18.5 in.) in diameter and 0.463 meters (18.2 in.) long. It weighs 46.67 kg (102.91 lbm). The descent probe contains all of the scientific instruments and supporting electronics and electrical gear, all mounted on a circular equipment deck. The scientific instrument complement is identical to that of the probe-dedicated mission; however, mission requirements result in different support electrical weight.

The entry ballistic coefficient, which sizes the aeroshell/heat shield assembly, is 102 kg/m<sup>2</sup> (0.65 slug/ft<sup>2</sup>). The ballistic coefficient, which sizes the descent probe parachute size, is 14.1 kg/m<sup>2</sup> (0.09 slug/ft<sup>2</sup>). The probe has a service module to provide the spin-despin-precess maneuver and provides a cold gas propellant supply adequate to spin to 10.45 rad/sec (100 rpm), precess through a 0.94 rad (53.5°) angle, and despin to 0.52 rad/sec (5 rpm), as well as deflect the service module at jettisoning. The service module is jettisoned just shortly before planetary entry.

Shortly after jettisoning the service module, the probe enters the Jovian atmosphere. The planetary entry capsule basically consists of the descent probe surrounded by the fore and aft heat shield. The forward heat shield assembly, in turn, consists of a Titanium structural aeroshell capped with a graphite heat shield, and containing additional hardware needed for entry. The aft heat shield consists merely of an aft structural shell coated externally with ESA 550QM3 ablator, and a pyrotechnic system for its ejection.

After high entry heating and deceleration loadings have passed, the aft heat shield is opened and the four quadrants, their attachment hardware and thrusters are ejected to permit parachute deployment. The parachute is deployed at approximately Mach 0.7 by means of a pyrotechnic mortar, providing both the deceleration to separate the descent probe from the heat shield, and the desired descent rate into the Jovian atmosphere. The interior of the descent probe is lined with a layer of lightweight thermal insulation 0.019 meter (0.75 in.) thick. This provides protection against heat loss during descent into the Jovian atmosphere.

Basically, the probe configuration and events are identical to those of the nominal Jupiter probe.

*b. Structural Design* - The structure of the probe is governed by entry angle of  $20^\circ$  at a latitude of  $5^\circ$ , resulting in an entry deceleration of 1500 g. The peak entry dynamic pressure is approximately  $1.13 \times 10^6 \text{ N/m}^2$  (23,500 psf), and this value converts to a local pressure normal to the nose cone of approximately  $1.56 \times 10^6 \text{ N/m}^2$  (225 psi). The descent probe and aeroshell base cover structural weight is governed by the 1500 g deceleration, while the aeroshell itself is designed by normal pressure on the nose cone. The descent probe and aeroshell base cover are designed to high strength 7075-T6 aluminum, while the aeroshell is designed of 6Al-4V titanium alloy. An aluminum aeroshell would be slightly lighter; however, the thermal transient time phasing of aeroshell temperature as compared with peak load has not been completely resolved; until this is resolved by refined analysis, the backface temperature of the heat shield is assumed to be too high for aluminum design. The aeroshell for this probe and that for the probe-dedicated mission are designed to this criteria.

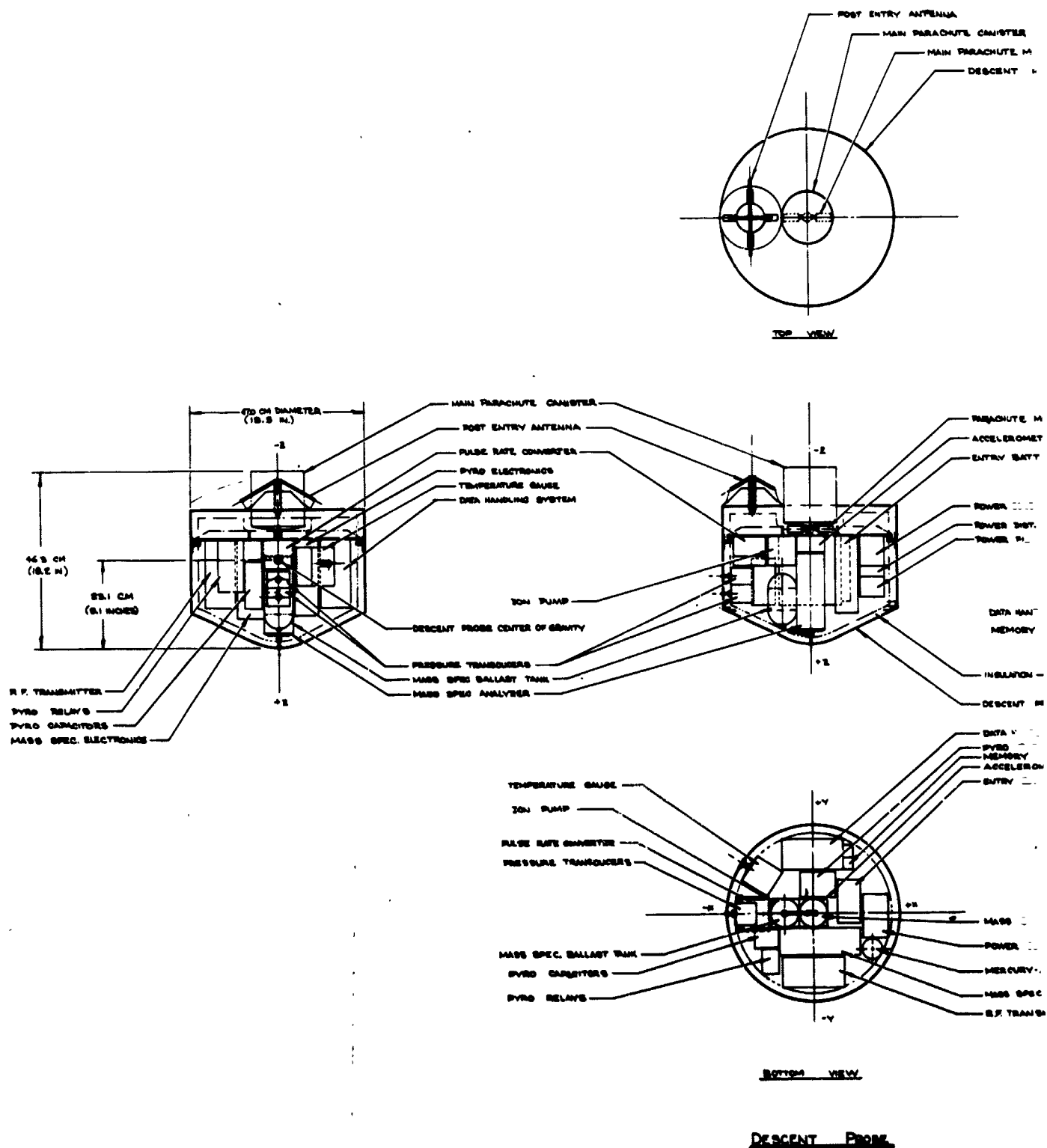
The type of structural design is common for all Jupiter probes; i.e., the aeroshell is ring-frame stiffened monocoque. The descent probe uses a multilongeron stiffened cylinder for basic load transfer. The equipment deck is a machined, thick disk with a residual network of intersecting beams for equipment support. The base cover is a simple stiffened shell since it supports only its own inertial loads plus those of the base cover ablator. The service module is a ring frame stiffened fiberglass shell, which encounters only launch loads plus some lesser deflection maneuver loads.

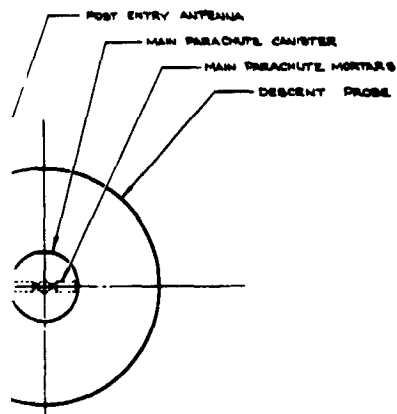
c. *Parachute Assembly* - A single parachute provides the force for separating the descent probe from the aeroshell, and the proper descent ballistic coefficient for planetary descent. A ballistic coefficient of  $14.1 \text{ kg/m}^2$  ( $0.09 \text{ slug/ft}^2$ ) selected for this probe combined with a probe descent weight of  $46.7 \text{ kg}$  ( $102.91 \text{ lbm}$ ) results in a parachute size roughly the same as that for the probe-dedicated mission, approximately  $2.74 \text{ m}$  ( $9.0 \text{ ft}$ ). This parachute is a disc-gap-band configuration. It is programmed to open at Mach 0.7 at approximately  $0.092 \text{ bar}$  pressure. It is deployed by a pyrotechnic mortar.

d. *Heat Shield* - An entry ballistic coefficient of  $100 \text{ kg/m}^2$  ( $0.65 \text{ slug/ft}^2$ ) has been selected for entry of the nominal Jupiter probe into the Jovian atmosphere. This coefficient, combined with a  $20^\circ$  entry angle at  $5^\circ$  latitude, results in a planetary deceleration producing the desired conditions for staging of the descent probe from the heat shield/aeroshell. These resulting conditions at staging are Mach 0.7 at approximately  $92 \text{ mb}$  pressure. Using data from Figure V-35, the mass fraction of the heat shield including a  $2\text{-cm}$  ( $0.79\text{-in.}$ ) carbonaceous backface insulator is shown to be 0.317. This value takes into account a correction factor of 0.88, for the probe diameter of  $0.94 \text{ meters}$  ( $37 \text{ in.}$ ), and a latitude correction factor of 1.01. Thus, for a probe weight of  $110.3 \text{ kg}$  ( $242.12 \text{ lbm}$ ) at entry, the resulting heat shield weight is  $30.5 \text{ kg}$  ( $67.20 \text{ lbm}$ ). Of the weight,  $23.1 \text{ kg}$  ( $51.0 \text{ lbm}$ ) is lost during entry.

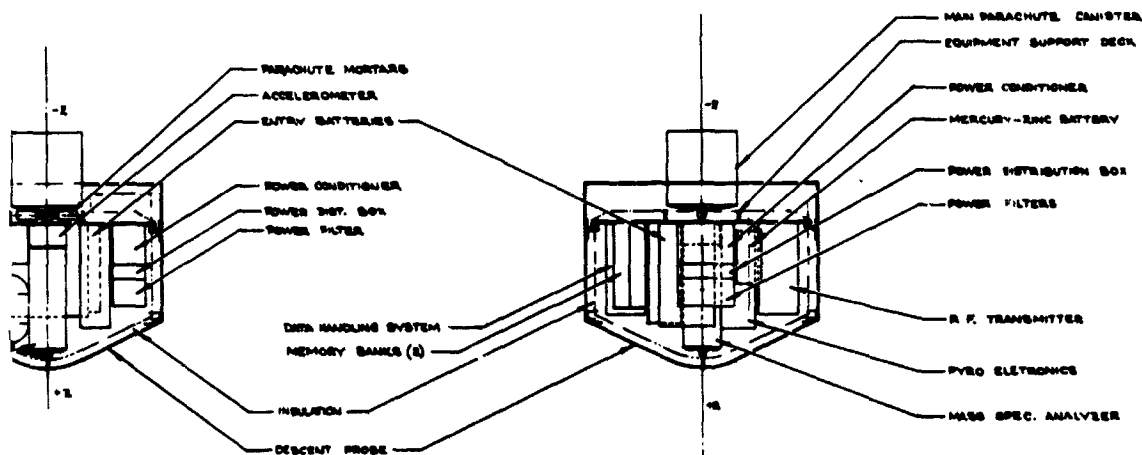
The heating for the base cover is estimated based on a heating pulse of 2% of the nose cone heating. For a  $20^\circ$  entry angle, the total heating pulse is of the order of  $18.4 \text{ MJ/m}^2$  ( $1620 \text{ Btu/ft}^2$ ), and a heating pulse time of approximately 8 sec. This heating pulse requires  $3.2 \text{ kg/m}^2$  ( $0.65 \text{ lbm/ft}^2$ ) of ESA 550M3 ablator to protect the base cover.

e. *Mass Properties* - The weight tabulation for the components of the spacecraft-radiation-compatible probe is shown in Table V-43. In reviewing these weights and comparing them with the weights data for the probe-dedicated mission, it is interesting to note that for this mission, the probe at separation, and again at planetary descent, is heavier than for the probe-dedicated mission; however, for planetary entry configuration, the situation is reversed. The probe-dedicated probe is heavier at entry due to two factors: (1) for the radiation-compatible mission the heat shield mass fraction is 0.317 compared to 0.350 for the probe-dedicated mission at  $0.52 \text{ rad}$  ( $30^\circ$ ) latitude entry; (2) the probe-dedicated mission has no service module, and that probe carries through entry the following components which are jettisoned in the case of the spacecraft-radiation-compatible mission probe--ACS system and electronics, Accutron timer, external base cover insulation blanket, separation battery, pre-entry antenna, and nutation damper. These factors combined increase both the size and weight of the spacecraft-radiation-compatible probe for entry.





TOP VIEW

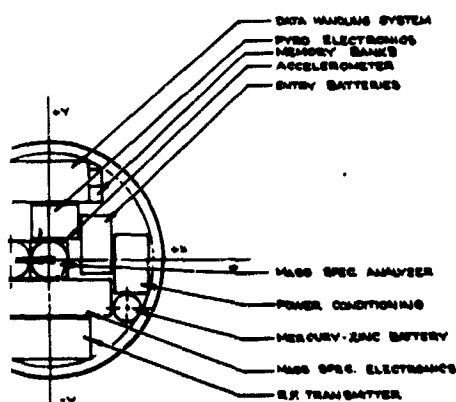


POST ENTRY ANTENNA

ACCELEROMETER

MAIN PARACHUTE  
POST ENTRY ANTENNA

DESCENT PROBE REFLECTION U



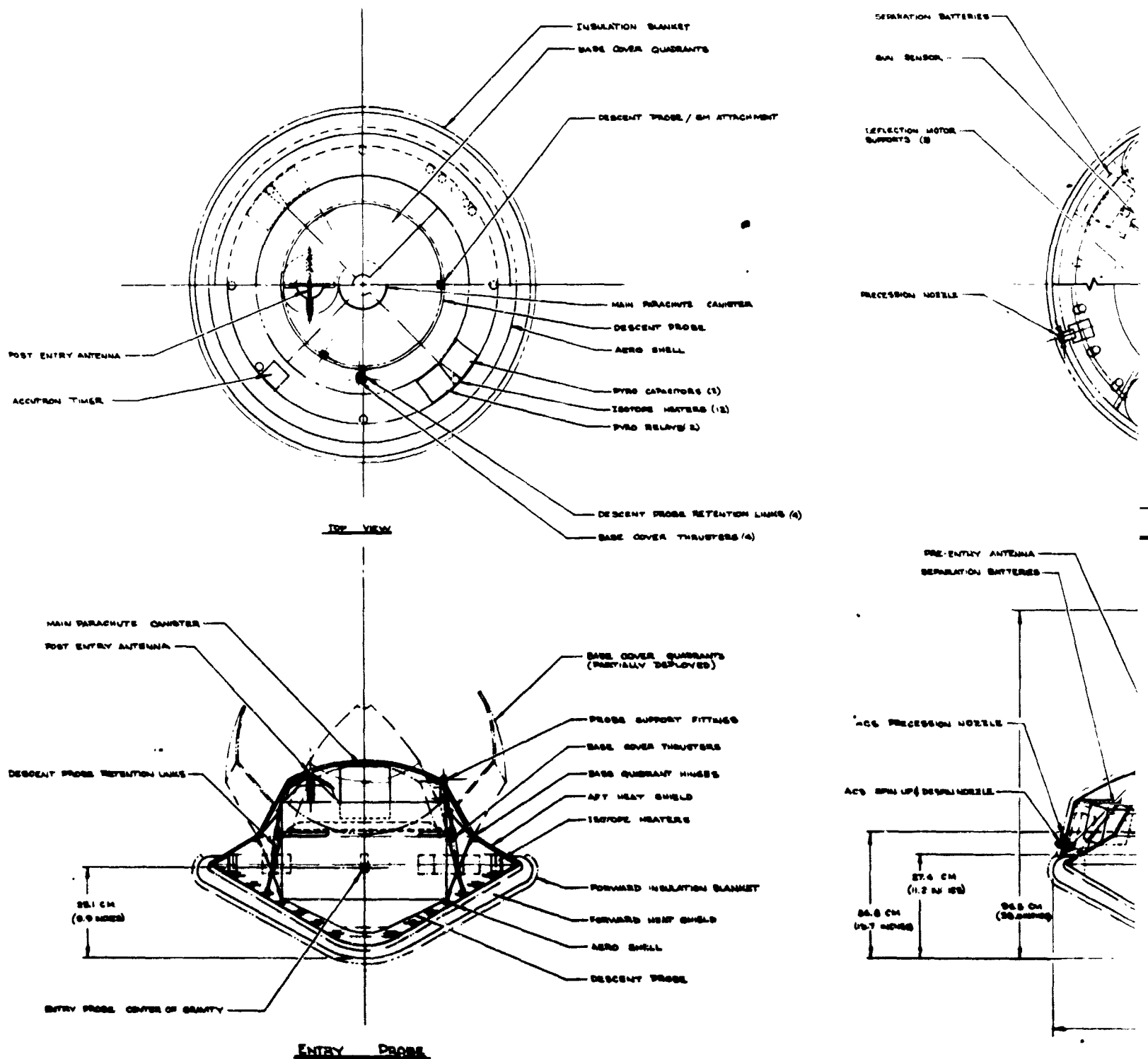
0.1 CM  
(0.0 INCH)

ENTRY PROBE CENTER

BOTTOM VIEW

ENTRY PROBE





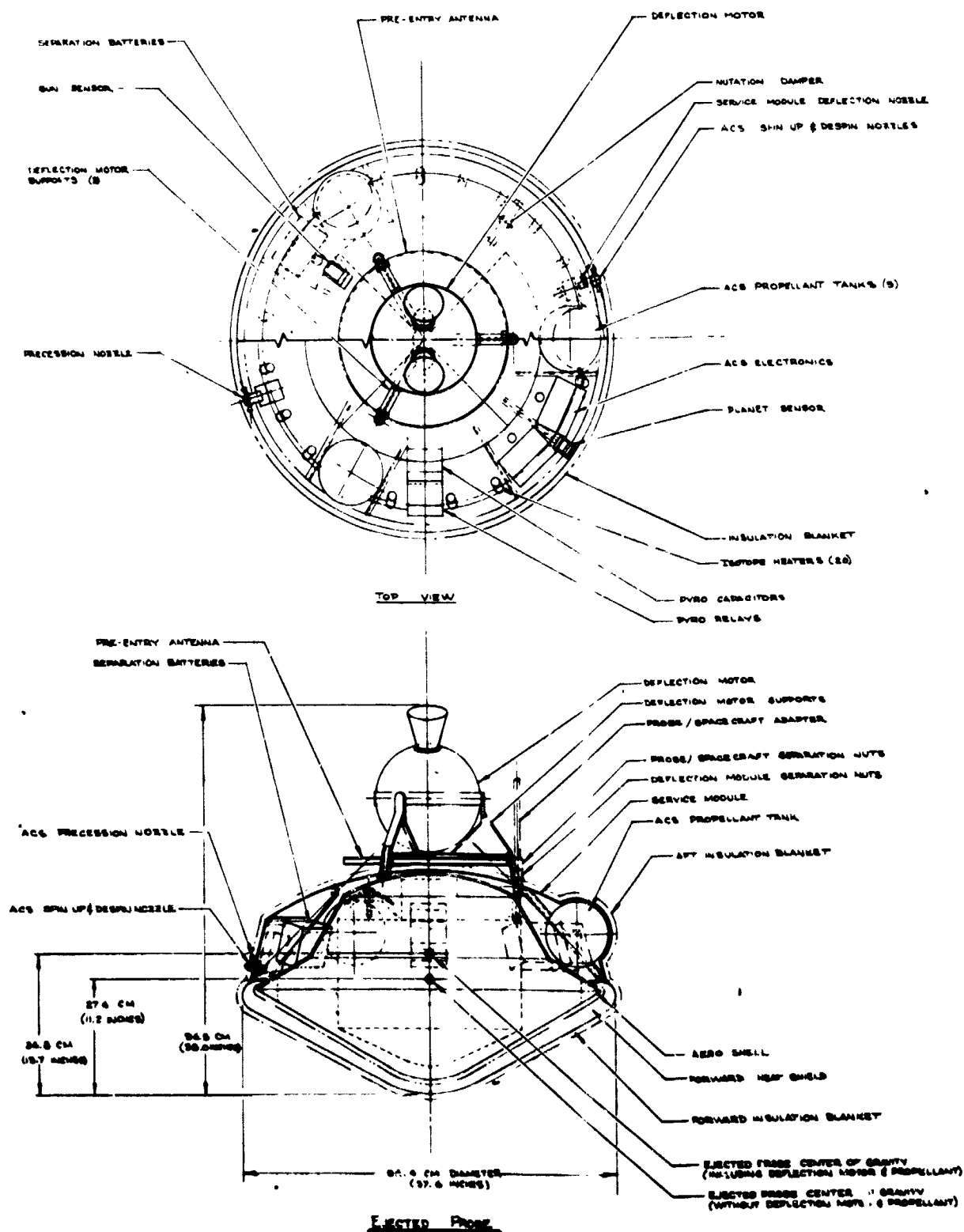


Figure V-119 Probe Definition of Spacecraft-Radiatio

DEFLECTION MOTOR

MUTATION DAMPER

SERVICE MODULE DEFLECTION NOZZLE

ACS SPIN-UP & DESPIN NOZZLES

ACS PROPELLANT TANKS (3)

ACS ELECTRONICS

PLANET SENSOR

INSULATION BLANKET

ISOTOPE HEATERS (20)

PYRO CAPACITORS

PYRO RELAYS

DEFLECTION MOTOR

DEFLECTION MOTOR SUPPORTS

PROBE / SPACECRAFT ADAPTER

PROBE / SPACECRAFT SEPARATION NUTS

DEFLECTION MODULE SEPARATION NUTS

SERVICE MODULE

ACS PROPELLANT TANK

AFT INSULATION BLANKET

AERO SHELL

FORWARD HEAT SHIELD

FORWARD INSULATION BLANKET

EJECTED PROBE CENTER OF GRAVITY  
(INCLUDING DEFLECTION MOTOR & PROPELLANT)

EJECTED PROBE CENTER OF GRAVITY  
(WITHOUT DEFLECTION MOTOR & PROPELLANT)

U.S. COSA. 0455 5/6/78

PARING MADE TO COORDINATION

JUPITER SURVIVABLE PROBE - TASK III  
CONFIGURATION II - OUTER PLANET  
ENTRY PROBE SYSTEM STUDY -

V-119 Probe Definition of Spacecraft-Radiation-Compatible Jupiter Mission

V-247 and V-248

EOLDOUT FRAME

4

Table V-43 Weight Breakdown for Spacecraft-Radiation-Compatible Jupiter Probe

	Weight	
	Kg	Lb
<u>Science</u>		
Temperature Gauge	0.45	1.00
Pressure Transducer	0.68	1.50
Accelerometer	0.59	1.30
Sensor	0.91	2.00
Converter	1.81	4.00
Neutral Mass Spectrometer Analyzer	2.72	6.00
Electronics	0.45	1.00
Pump	0.45	1.00
Ballast Tank	8.06	17.80
<u>Power and Power Conditioning</u>		
Power Conditioner	0.91	2.00
Power Distribution Box	0.45	1.00
Power Filters	0.45	1.00
Entry Batteries	3.08	6.80
Post Separation Batteries	1.77	3.91
	6.67	14.70
<u>Cabling</u>		
Inner Probe	3.18	7.00
External Structure	2.49	5.50
	5.67	12.50
<u>Data Handling</u>		
Memory Bank	2.14	4.7
	0.45	1.0
	2.59	5.7
<u>Attitude Control System (less propellant)</u>		
Sun Sensor	1.59	3.5
Planet Sensor	0.91	2.0
ACS System & Tanks (3 tanks 8 in. diam)	5.17	11.4
Nutation Damper	1.09	2.4
Accutron Timer	0.14	0.3
ACS Electronics	1.36	3.0
	10.26	22.6
<u>Communications</u>		
Pre-Entry Antenna	2.13	4.7
Post-Entry Antenna	0.45	1.0
RF Transmitter	2.73	6.0
RF Switch	0.45	1.0
	5.96	12.7
<u>Pyrotechnic Subsystem</u>		
Pyro Electronics	0.91	2.00
Pyro Capacitors (Probe)	0.27	0.6
Pyro Capacitors (External)	0.56	1.25
Pyro Relays (Probe)	0.78	1.7
Pyro Relays (External)	2.22	4.9
Pyro Squibs	0.71	1.56
Pyro Thrusters at (.25 lb each)	0.45	1.00
Mercury Zinc Battery	0.41	0.90
	6.31	13.91

Table V-42 (cont)

	Weight	
	Kg	Lb
<u>Structures and Heat Shields</u>		
Descent Probe Structure	5.09	11.2
Equipment Support Deck	5.07	11.15
Base Cover	4.47	9.85
Service Module Structures	5.35	11.8
Aeroshell (2 lb for payload ring)	9.86	21.75
Forward Heat Shield (51 lb ablated during entry)	30.48	67.2
Aft Heat Shield (4 lb ablated during entry)	2.09	4.64
Deflection Motor Support	1.81	4.0
	64.22	141.59
<u>Mechanisms</u>		
Separation Spring Cartridges (at 0.37 lb)	1.22	2.70
Separation Nuts (at 0.23 lb)	0.77	1.7
Pin Puller (at 0.3 lb)	0.82	1.8
Latches & Bands	0.91	2.0
Main Parachute	4.26	9.4
	7.98	17.60
<u>Thermal</u>		
External Insulation Blanket (forward heat shield)	1.77	3.9
External Insulation Blanket (base cover)	2.27	5.0
Probe Hull Insulation (internal)	1.59	3.5
Isotope Heaters	1.81	4.0
	7.44	16.4
<u>Propulsion</u>		
Deflection Motor Cases	4.22	9.3
Deflection Motor Propellant	13.29	29.3
ACS Propellant	1.50	3.3
	19.01	41.9
Total	143.97	317.41
15% Contingency	21.60	47.61
	165.57	365.02
<u>Items Deployed for Despin Weight</u>		
Deflection Motor Supports	1.81	4.0
Separation Spring Cartridges	0.41	0.9
Separation Nuts	0.32	0.7
Δ V Motor Cases	4.22	9.3
Propellant	14.79	32.6
	21.55	47.5
15% Contingency	3.22	7.1
(365.02 - 54.6 = 310.42 lb)	24.77	54.6
165.57 - 24.77 = 140.80 kg		

Table V-43 (concl)

	Weight	
	Kg	Lb
<u>Entry Weight</u>		
External Cabling	2.49	5.5
Sun Sensor	1.59	3.5
Planet Sensor	0.91	2.0
ACS System (including tanks)	5.17	11.4
Nutation Damper	1.09	2.4
Accutron Timer	0.14	0.3
Pyro Capacitors	0.32	0.7
Pyro Relays	1.13	2.5
Service Module Structure	5.35	11.8
Separation Spring Cartridge	0.41	0.9
Separation Pin Pullers	0.71	0.9
External Base Cover Insulation Blanket	2.27	5.0
Separation Battery	1.77	3.9
ACS Electronics	1.36	3.0
Pre Entry Antenna	2.13	4.7
	<u>26.54</u>	<u>58.5</u>
15% Contingency	<u>3.99</u>	<u>8.8</u>
(310.42 - 67.3 = 243.12 lb)	<u>30.53</u>	<u>67.3</u>
140.80 - 30.53 = <u>110.27</u> kg		
<u>Post Entry Weight</u>		
Forward Heat Shield Ablated	23.59	52.0
Aft Heat Shield Ablated	1.81	4.0
Insulation Blanket (forward heat shield)	<u>1.77</u>	<u>3.9</u>
	<u>27.17</u>	<u>59.9</u>
15% Contingency	<u>4.08</u>	<u>8.99</u>
(243.12 - 68.89 = <u>174.23</u> lb)	<u>31.25</u>	<u>68.89</u>
110.27 - 31.25 = <u>79.02</u> kg		
<u>Weight on Parachute (initially)</u>		
Base Cover Quadrants	4.47	9.85
Base Cover Heat Shield (not ablated)	0.36	0.8
Separation Pin Pullers	0.41	0.9
Separation Nuts	0.23	0.5
Isotope Heaters	0.91	2.0
Pyro Thrusters	<u>0.45</u>	<u>1.0</u>
	<u>6.83</u>	<u>15.05</u>
15% Contingency	<u>1.03</u>	<u>2.28</u>
(174.23 - 17.33 = <u>156.90</u> lb)	<u>7.86</u>	<u>17.33</u>
79.02 - 7.86 = <u>71.16</u> kg		
<u>Weight on Parachute (final)</u>		
Pyro Capacitors	0.27	0.6
Pyro Relays	1.09	2.4
Pyro Squibs	0.73	1.6
Aero Shell	9.86	21.75
Forward Heat Shield (not ablated)	6.89	15.2
Spring Cartridges	0.41	0.9
Separation Nuts	0.23	0.5
Latches & Band	0.91	2.00
Isotope Heaters	<u>0.91</u>	<u>2.00</u>
	<u>21.30</u>	<u>46.95</u>
15% Contingency	<u>3.19</u>	<u>7.04</u>
(156.90 - 53.99 = <u>102.91</u> lb)	<u>24.49</u>	<u>53.99</u>
71.16 - 24.49 = <u>46.67</u> kg		

It is noted in Table V-43 that component weights are grouped in categories, and a 15% contingency factor is added for arriving at the total weight to account for growth. The weight thus achieved is reduced sequentially in the remainder of the table to provide weight data for the different phases of the mission, from spacecraft separation to entry and descent.

#### 9. Propulsion Subsystem

The propulsion subsystem for the probe is almost identical to that for the nominal Jupiter probe except for the required deflection maneuver delta velocity requirement, which requires a somewhat different size motor. This mission requires a deflection maneuver of 256.5 m/sec (842 fps) as compared with a requirement of 221 m/sec (725 fps) for the nominal Jupiter probe.

*a. Deflection Motor System* - A spherical solid propellant rocket motor is provided for the probe. This motor uses an aluminized solid propellant (described as the baseline propellant in Appendix M) and has a dual nozzle configuration to avoid the problem of exhaust impingement on the carrier spacecraft at separation. The motor is ignited after the probe has coasted away from the spacecraft for 900 sec, with a relative separation velocity of approximately 1 m/sec (3 fps), for a separation distance somewhat less than 1 km.

The functional requirement for the motor is provision of deflection delta velocity of 256.5 m/sec (842 fps) to a probe weighing 148 kg (326.4 lbm), not including the weight of the motor. Using a theoretical specific impulse,  $I_{sp}$ , of 287 sec, the necessary weight of propellant to provide the delta velocity is 12.4 kg (27.4 lbm). This value is divided by a propellant mass fraction of 0.80, and a thrust vectorial loss coefficient of 0.924 ( $\cos 22\frac{1}{2}^\circ$ ) for the dual nozzles to give the total loaded motor weight of 17.5 kg (38.6 lbm). This weight also includes a weight penalty, above and beyond the mass fraction, of 0.68 kg (1.5 lbm) to account for the extra nozzle. The configuration of the deflection motor is similar to that shown in Section B.9 of this chapter.

*b. Attitude Control Subsystem* - The attitude control subsystem provides for spinning the probe to approximately 10.5 rad/sec (100 rpm) to stabilize the probe attitude while firing the deflection delta velocity motor. This spin rate also permits precessing the probe for attitude required for the deflection delta velocity to a different heading for planetary entry. This precession angle is 0.93 rad (53.5°). The attitude control system must then despin

the probe to a rate of approximately 0.52 rad/sec (5 rpm) for entry into the planetary atmosphere. Finally, the attitude control system must impart a delta velocity to the service module of 0.46 m/sec (1.5 fps) for jettisoning the module.

A cold gas (dry nitrogen) system, contained within the service module, is used for the attitude control of the probe. The operation of the system and its components are identical to those of the nominal Jupiter probe described in Section B.9 of this chapter.

#### 10. Thermal Control Subsystem

*a. General Discussions* - The thermal control required for the spacecraft-radiation-compatible probe is the same as for the nominal Jupiter mission, and thermal analysis shows that this design is adequate for the desired probe performance (Figure V-120). The probe design requirements are not as critical as the probe-dedicated alternative probe since the weight and transmitter power are increased due to the 6  $R_J$  communication distance and the relatively long pre-entry standby power requirement.

As for all missions, the pivotal design temperature is the probe temperature established at the beginning of entry. Analysis shows that with an entry temperature of 300°K, a 15°K margin can be created for both the minimum equipment temperature experienced during a cool/dense atmosphere descent encounter and the maximum equipment temperature experienced during a nominal atmosphere encounter.

To analyze the probe's thermal performance, the two finite-element math models previously discussed were used. The basic probe consists of a (95.4 cm) diameter entry design, the configuration being similar to the nominal Jupiter probe since probe propulsion is present for deflection. As before, a separate thermal blanket must be provided for the deflection motor as well as an electrical resistance heater powered by the spacecraft.

Trajectory uncertainties for the spacecraft-radiation-compatible probe are relatively high ( $\pm 38$  min) and would have caused considerable thermal control problems if the transmitter had not been turned off following service module ejection. Since the transmitter is deactivated, probe entry temperature uncertainties are only  $\pm 3^\circ\text{K}$ . An integral discussion of the thermal control subsystem design has been previously presented in Section A.10.a of this chapter.



Probe Internal Capacitance = 8.93 watt-hr/°K  
 Separation Power Dissipation = 244 watt-hr  
 Entry Power Dissipation = 66.6 watt-hr  
 Descent Power Dissipation = 73.8 watt-hr

Note: Mission trajectory uncertainties are high for the spacecraft-radiation-compatible Jupiter probe (±38.35 min at entry) and result in probe entry temperature band uncertainty of ±3°K.

Legend:  
 --- RF Transmitter  
 — Internal Equipment

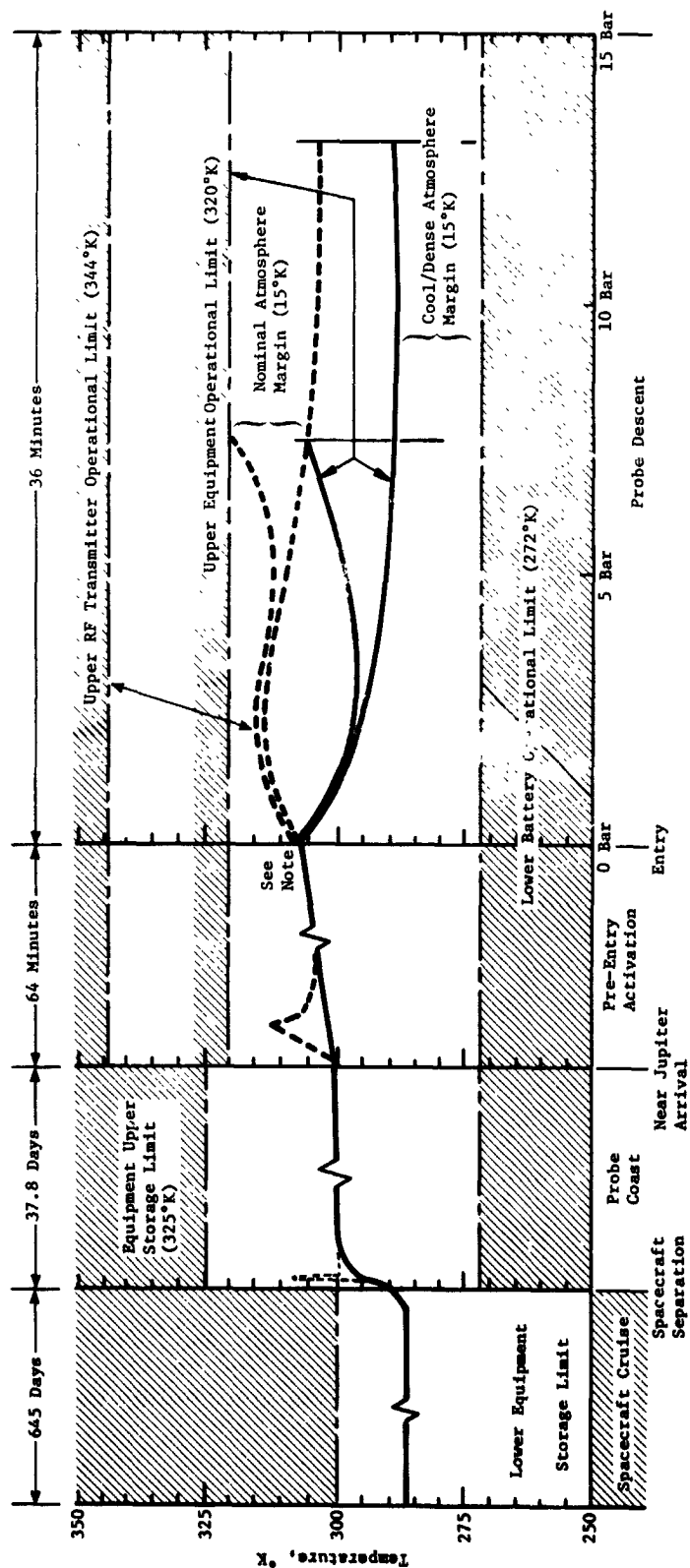


Figure V-120 Launch to Descent Thermal History of Spacecraft-Radiation-Compatible Alternative Jupiter Probe.

- b. *Cruise and Coast Thermal Control* - The thermal coatings used for the spacecraft-radiation-compatible probe are the same as the probe-dedicated mission. Since the probe temperatures during coast will have sufficient time to reach equilibrium, better thermal design is afforded using a spacecraft cruise equilibrium temperature of 286°K.

The correlation of radioisotope heater to probe temperature is presented in Figure V-121. Since the spacecraft-radiation-compatible probe requires probe deflection and a service module, slightly more radioisotope heater power is required for this mission than for the probe-dedicated mission (20 W). The probe aft thermal coating is aluminum Iridite 14-2 surface treatment with values of  $\alpha/\epsilon = 0.62/0.13$ .

c. *Entry and Descent Thermal History* - The spacecraft-radiation-compatible probe mission thermal history is presented in Figure V-120. These results show that adequate thermal control is provided for this mission and no thermal problems are envisioned. The power profile used for the descent analysis again represented improved transmitter efficiency (45%). The ballistic coefficient for this mission is the same as the probe-dedicated Jupiter mission, and the temperature-pressure probe descent profiles are presented in Figure V-122.

Results for the spacecraft-radiation-compatible Jupiter mission indicate that the following probe temperature margins are expected. Note that the entry-descent upper and lower equipment temperature margins are in balance (15°K).

TEMPERATURE MARGIN	SPACECRAFT CRUISE PHASE, °K	PROBE COAST PHASE, °K	ENTRY-DESCENT PHASE, °K
Above Equipment Lower Limit	36	26	15
Below Equipment Upper Limit	14	25	15
Below Transmitter Upper Limit	NA	36	24

#### 11. Probe to Spacecraft Integration

The spacecraft-radiation-compatible mission probe integration with the spacecraft is essentially the same as that described in Section B.11 of this chapter.

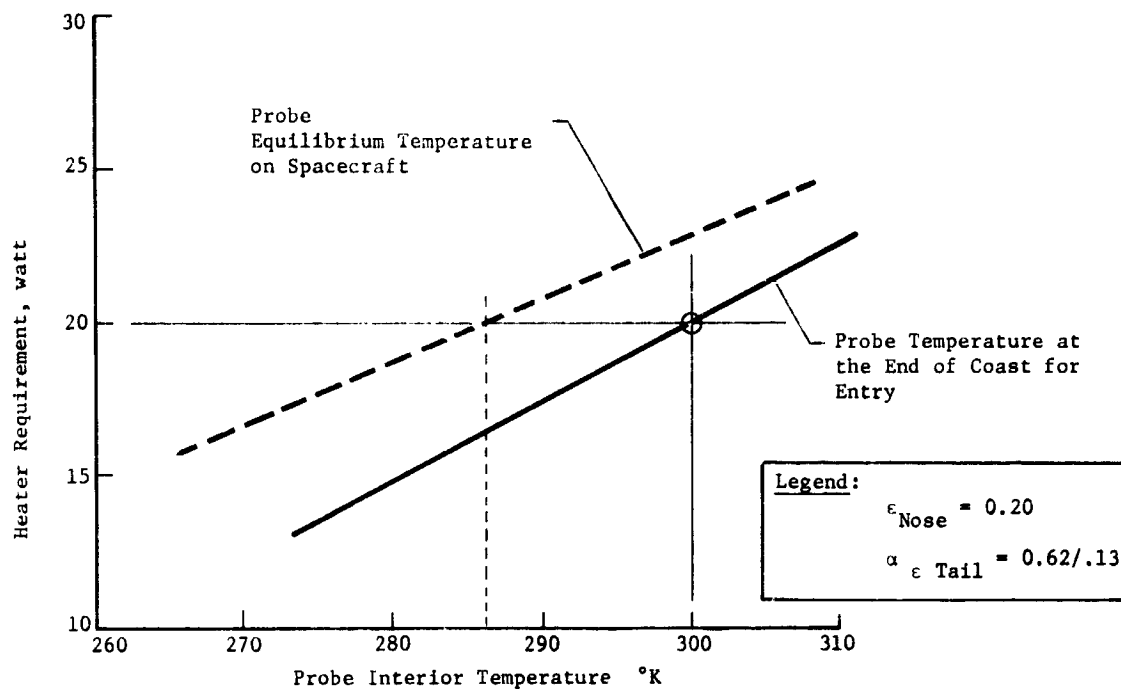


Figure V-121 Radiosotope Heater Sizing Based on Thermal Coating Selection Probe

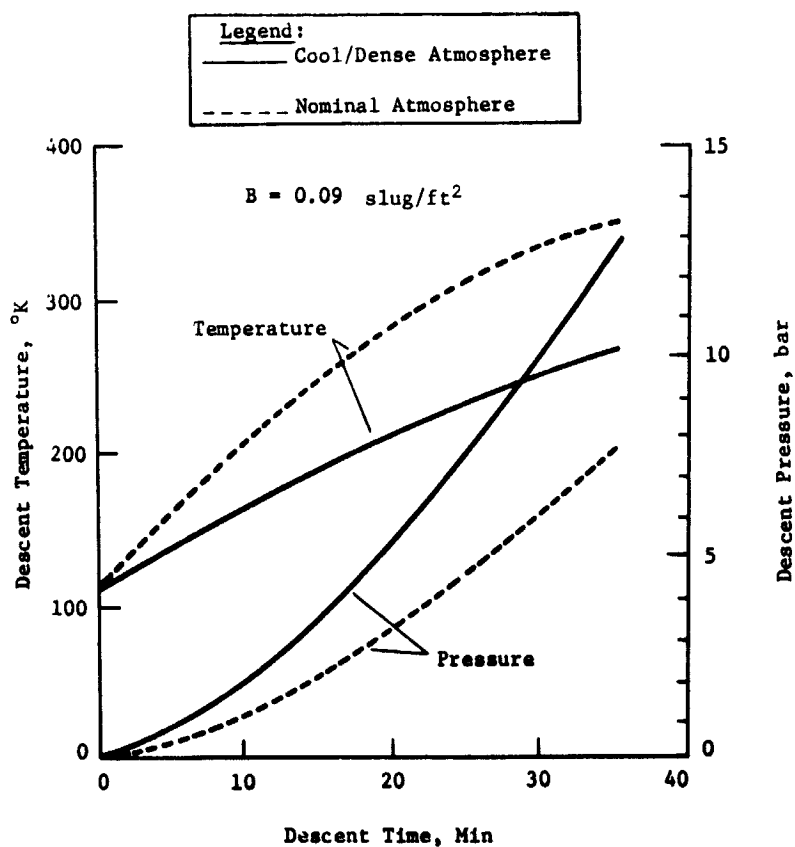


Figure V-122 Mission Descent Temperature and Pressure Profiles

## VI. SATURN STUDIES

At the beginning of the contract, the multiple planet studies involved Saturn, Uranus, and Neptune. Five different missions for each planet were evaluated to identify the encounter parameters, and two representative missions were selected for further applications. The initial five Saturn missions were: JSP 78, SUN 81-82, SUN 82-83, SUN 84, and JS 77. The two selected for in-depth analyses are the SUN 82-83 and the JS 77. The initial objectives were to identify the changes to the Jupiter probe functional requirements for Saturn atmospheric entry. Similar effort was included for the planets Uranus and Neptune. Jupiter probe changes for these three planet applications were then to be used to define a joint usage Uranus/Neptune probe. At the mid-term oral presentation, the emphasis was revised to define a Saturn probe and to assess its applicability for Uranus atmospheric entry. Some of the parametric effort was begun for the original five missions and is reported in this chapter.

The revised combined objectives of the Saturn studies, also discussed in this chapter, and those for Uranus (Section VII), then, are to define a Saturn probe and identify changes required for Uranus application. The Saturn parametric and general analysis also considered the major impact for use at Uranus.

### A. PARAMETRIC ANALYSIS

The analyses are centered primarily in the mission and science areas and consider the five missions previously mentioned as well as the high inclination JS 77 mission for a Titan encounter.

#### 1. Science Performance Analysis

The parametrics for Saturn and Uranus are both given in this section because of the commonality of much of the data. The analyses performed for these two planets benefited greatly from those performed for Jupiter, given in Chapter V, Section A.1, and thus are more limited in scope.

a. *Descent Profile Parametrics* - The major parametrics performed for both Saturn and Uranus were to establish descent profiles in both atmospheres, using as many common parameters as possible that would satisfy the objectives of the mission by making the necessary measurements within the criteria. The parameters involved are the parachute ballistic coefficient, the sample rate for each of the instruments, and the total descent time. The design limit pressure, initially a variable, was selected at 7 bars (discussion in Chapter III, Section D.2). The descent time becomes a constraining factor for Uranus because of the planet's rotation vector lying near its orbital plane and the equator. The spacecraft's trajectory lies near the ecliptic plane. The probe, upon entering, rotates upward with the planet, away from the spacecraft, and the time available for good communications is shortened. Good geometry is available for no more than about 50 minutes of descent time.

The statement of work specified consideration of the nominal model atmospheres of both planets. Figure VI-1 shows the variation in pressure descent profile with changes in parachute ballistic coefficient. The parachute is deployed 78.5 sec after entry at about 110 km altitude and 48 millibars of pressure. The first descent computer run made was at  $0.10 \text{ slug/ft}^2$  ( $15.7 \text{ kg/m}^2$ ), which was near the optimal value for Jupiter descent. However, the descent time to 10 bars in Saturn's atmosphere was 134 min, which presents intolerable communications and thermal control problems. Also, the amount of data collected was several times that which was necessary for satisfactory mission performance. The range of ballistic coefficients that resulted in satisfactory descent times was that from  $0.50 \text{ slug/ft}^2$  ( $78.5 \text{ kg/m}^2$ ) to  $1.00 \text{ slug/ft}^2$  ( $157 \text{ kg/m}^2$ ).

Figure VI-2 shows a similar set of parametric pressure descent profiles for Uranus. Here the parachute is deployed 54.5 sec after entry, which corresponds to an altitude of about 30 km and a pressure of 33 millibars. Again, one descent computer run was made near the Jupiter optimum ballistic coefficient with the same extensive time results as for Saturn. The range of values for reasonable descent times was about the same as that for Saturn. A summary of descent times versus ballistic coefficient is given in Figure VI-3.

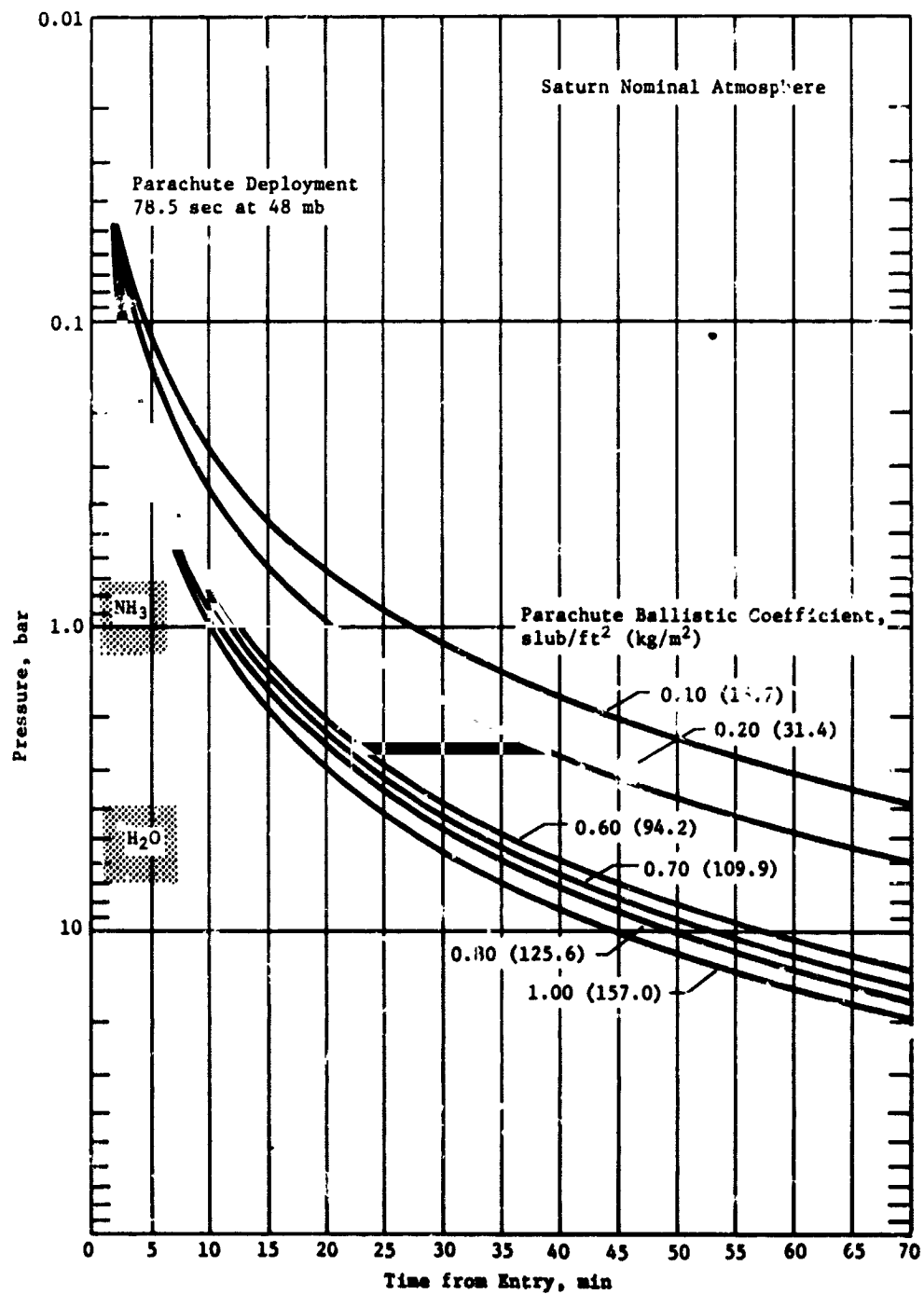


Figure VI-1 Saturn Pressure Descent Profile Parameters

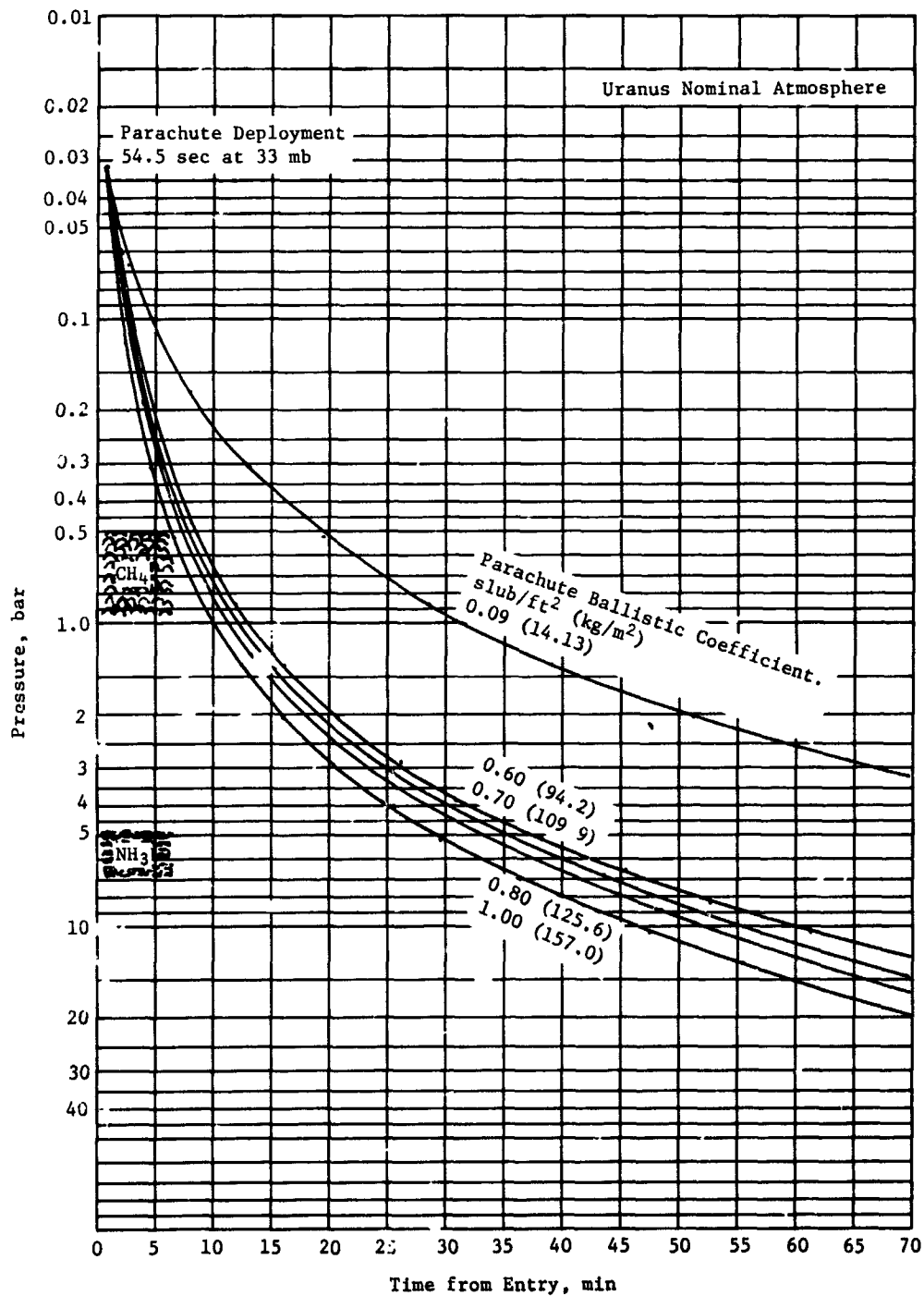


Figure VI-2 Uranus Pressure Descent Profile Parameters

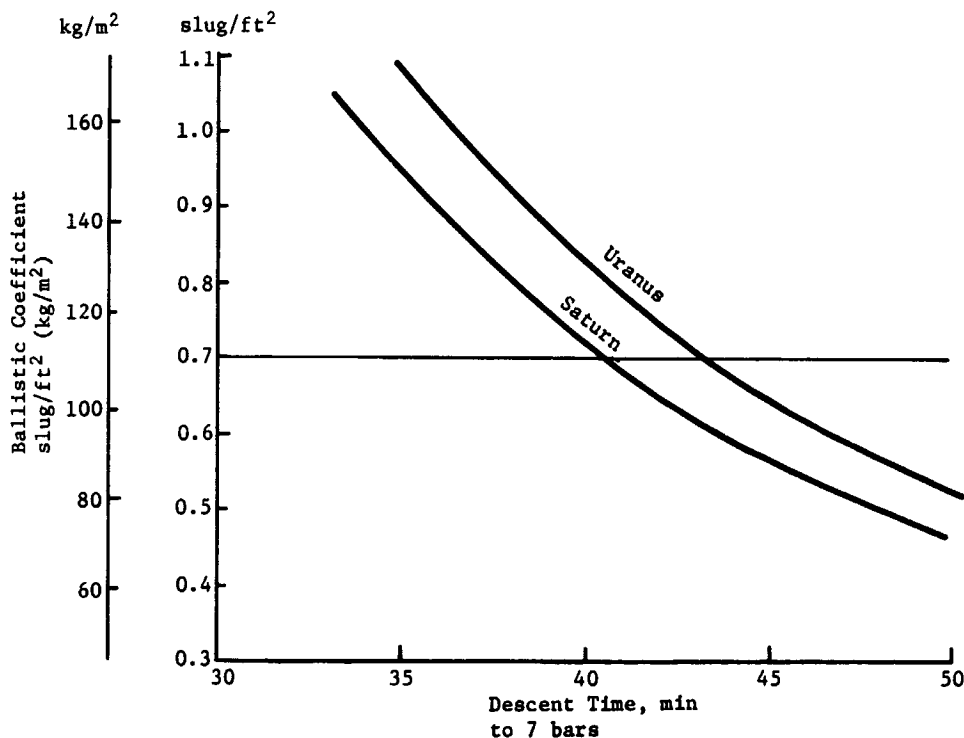


Figure VI-3 Descent Time for Saturn and Uranus vs Ballistic Coefficient

With the descent times narrowing the range, consideration of the instruments sampling times and measurement performance can enable the selection of a particular design ballistic coefficient. Figure VI-4 shows the sampling time parametrics as a function of ballistic coefficient and the same four measurements and criteria that were important for Jupiter considerations. Again, the temperature gage performance is checked against criteria at the point where the temperature begins increasing, and the pressure gage and accelerometers at the top of the first cloud. The mass spectrometer performance is measured inside the first cloud, which is the ammonia cloud for Saturn beginning at 0.727 bars, and the methane cloud for Uranus beginning at 0.49 bars.

In the case of Jupiter, it was the temperature gage and mass spectrometer that governed the selection of the design ballistic coefficient, whereas with Saturn, it is the pressure gage and turbulence accelerometers. Note from (a) and (c) of Figure VI-4 that with a 4-sec sampling time, the pressure gage just meets the criteria at a ballistic coefficient of 0.7 slug/ft<sup>2</sup>, while the temperature gage is obtaining 1.24 meas/°K, almost 25% more than required. Also, at the same ballistic coefficient and a sampling time of 8 sec, the turbulence accelerometers [(d) of Fig. VI-4] also just meet the criteria. The mass spectrometer makes 2.8 measurements in the ammonia cloud, which is satisfactory.



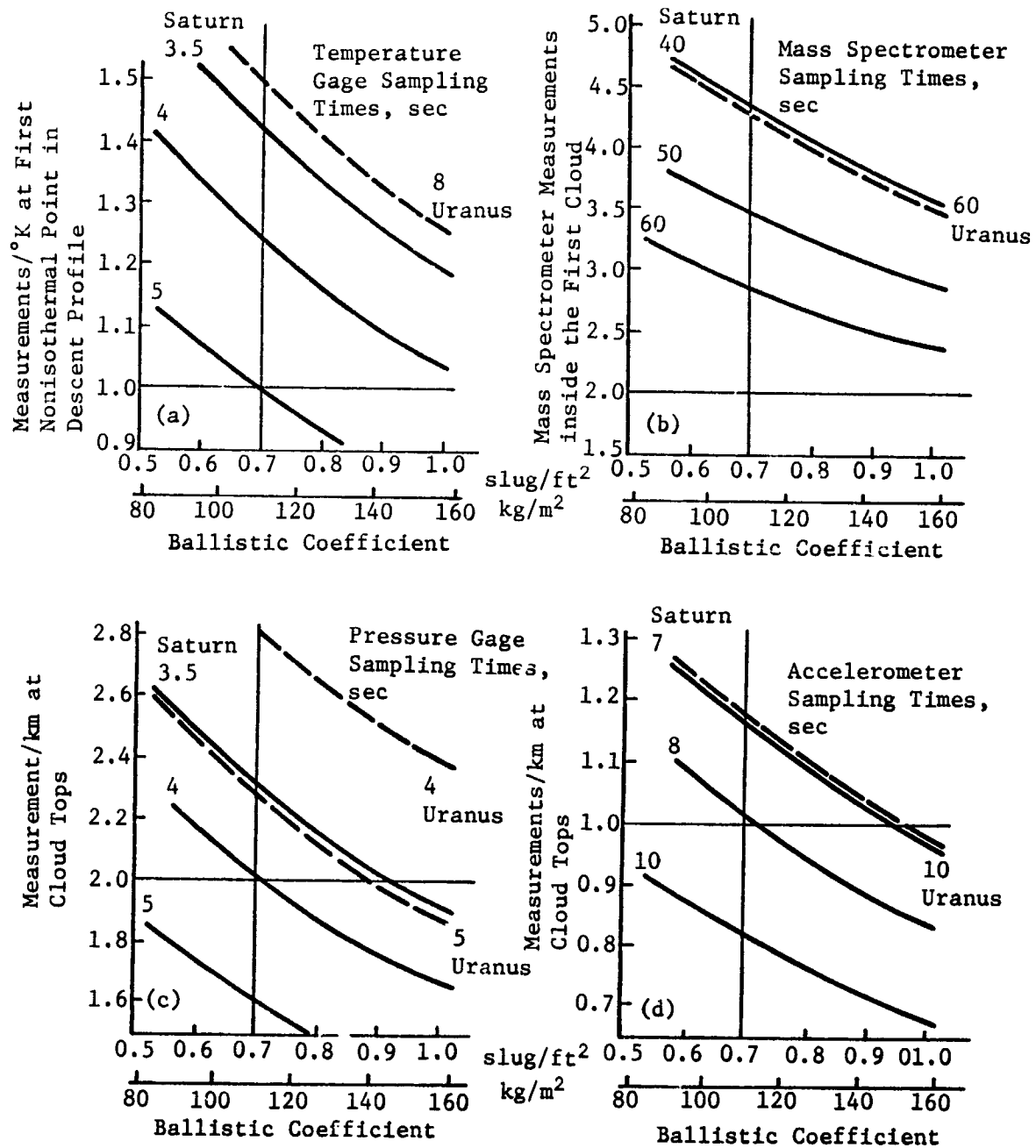


Figure VI-4 Instrument Sampling Time Effects on Measurement Performance for Saturn and Uranus

For Uranus, the measurement data is greatly increased, as shown by the dashed lines for the sampling times that were analyzed that were within the range of Figure VI-4. However, they were allowed to remain the same as Saturn for commonality, and the performance requirements are satisfied.

*b. Entry Accelerometer Performance* - The primary function of the accelerometer triad is to collect the entry g-load information with sufficient accuracy to be able to reproduce the g-curve, in particular the sharp maximum point on the curve with the data. This can be used to reconstruct the atmosphere, as described in Chapter III, Section C. However, the g-load may go from 10% of its peak value through peak and back to 10% in only a few seconds; thus, an analysis was made to ensure that the axial accelerometer sampling rate of 5 samples/sec would give an adequate number of points along the curve to reproduce the steep slope.

Figure VI-5 is a plot of the expected g-load curves based on each of the Saturn and Uranus nominal atmospheres and calculated by an entry dynamics computer program. Superimposed upon this are marks that represent individual axial accelerometer measurements of 0.2 sec each. This is only half as fast as the design required at Jupiter, because the peak g-load is only 350 to 360 g compared to 1500 g. Note that while the peaks are about the same, the Uranus peak occurs earlier. This is because of the steeper entry angle.

## 2. Mission Analysis

The detailed mission analysis parametric data is provided in Chapter IV. This section summarizes the important design considerations for probe missions to Saturn.

*a. Interplanetary Trajectory Selection* - The interplanetary trajectories considered for Saturn missions were either Jupiter flybys (JS 77, JSP 78) or solar electric propulsion trajectories (SUN 81, 82, 83). The interplanetary trajectories for these candidate missions are given in Chapter IV, Section G. The trip time from Earth to Saturn is typically  $3\frac{1}{4}$  years for either type mission. Direct flights to Saturn are marginally possible at best for payload weights discussed in this study for the 1978-82 time period.

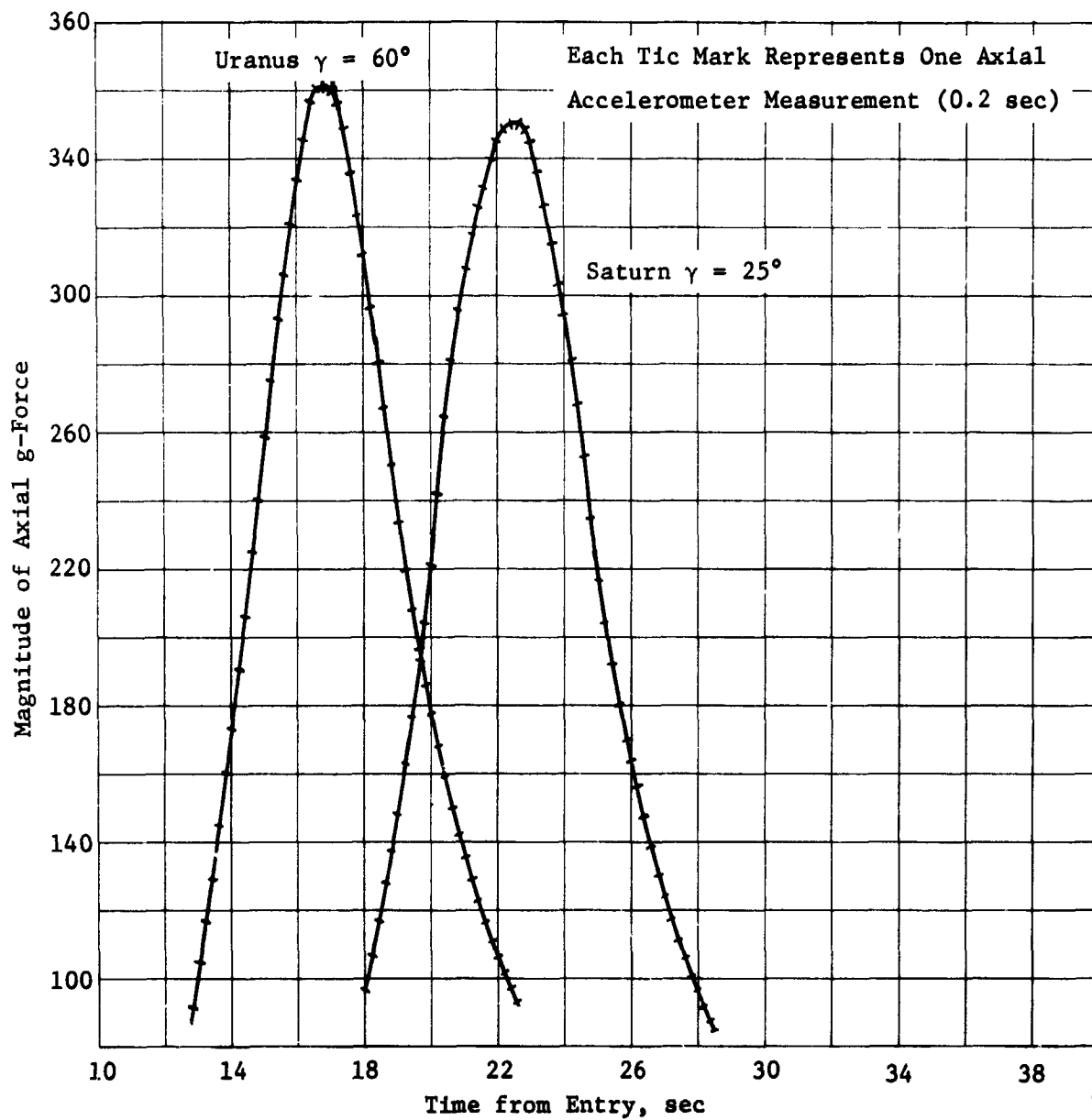


Figure VI-5 Saturn and Uranus Entry Accelerometer Performance

b. *Approach Trajectory Selection* - As at Jupiter, the optimal probe-spacecraft geometry would have the probe entering on the equator with the spacecraft flyby in the same plane. The optimal flyby radius at Saturn is about  $2.5 R_S$  (Fig. IV-11). With this flyby, it is possible to keep the spacecraft approximately over the probe during the probe descent. For the JS 77 mission, involving a Titan encounter, the flyby radius is  $2.33 R_J$  with a highly inclined orbit.

c. *Navigation and Guidance Results* - The approach orbit determination at Saturn is less effective than at Jupiter, because the Saturn ephemeris uncertainties are approximately twice those of Jupiter. The navigation is further degraded at Saturn on the JS 77 mission because the geocentric declination of Saturn during the encounter period is very near zero. Thus, with Doppler and range measurements, the uncertainty ellipse (1 $\sigma$ ) is characterized by a semi-major axis (SMAA) of 2200 km. Adding QVLBI measurements reduces the SMAA to 1100 km; adding optical tracking reduces the value to 500 km.

d. *Deflection Maneuver Parametrics* - The deflection maneuver trends indicated for Jupiter also apply at Saturn. Reasonable deflection radii at Saturn are from 10 to 30 million km. Thus, for a spacecraft periapsis radius of  $2 R_S$  the  $\Delta V$  requirements decrease from 140 to 70 to 47 m/sec as the deflection radius is increased from 10 to 20 to 30 million km, respectively. For a spacecraft flyby radius of  $6 R_S$  the corresponding  $\Delta V$  become 620 to 300 to 200, respectively.

e. *Dispersion Parametrics* - For Saturn missions, the navigation uncertainties become significant relative to the deflection maneuver execution errors in terms of dispersions. This is in contrast to the situation at Jupiter where execution errors dominated the dispersions. Thus, at Saturn the  $3\sigma$  uncertainties in entry time, entry angle, angle of attack, and lead angle are 4.50/6.58 min, 2.79°/3.41°, 1.66°/3.75°, and 2.50°/3.25°, respectively, where the numerator is the uncertainty contributed by navigation uncertainties (80 days tracking of Doppler range) alone and the denominator is the total uncertainty resulting from both navigation uncertainties and deflection execution errors.

f. *Entry Trajectory Parametrics* - The selection of an entry ballistic coefficient that results in satisfactory staging conditions (deceleration to  $M = 0.7$  above 100 mb) for entry angles of from  $-10^\circ$  to  $-30^\circ$  was investigated. Any ballistic coefficient less than  $156.0 \text{ kg/m}^2$  ( $1.0 \text{ slug/ft}^2$ ) was identified as adequate.

The peak  $g$  experienced at entry angles of  $-10^\circ$ ,  $-20^\circ$ , and  $-30^\circ$  are 105, 240, and 355, respectively, in the nominal atmosphere. Entering at higher latitudes increases the peak  $g$  loading as the relative velocity is increased. A polar entry increases the  $g$  loading by approximately 30%. Parametric analysis has shown that the  $g$  loading is essentially independent of ballistic coefficient.

The maximum aerodynamic loading ( $q$ ) is a function of ballistic coefficient. Entering with a ballistic coefficient of  $1.0 \text{ slug/ft}^2$  at entry angles of  $-10^\circ$ ,  $-20^\circ$ , and  $-30^\circ$  results in max  $q$  of 2000, 7000, and 11,000 psf, respectively, in the nominal atmosphere. The dynamic pressure increases linearly with ballistic coefficient.

### 3. System Integration

The constraints that control the Saturn parametric effort for the revised multiple planet objectives are:

- 1) Mission: Define a Saturn mission using JPL's high inclination trajectory for a Titan encounter such that the spacecraft and probe do not penetrate Saturn's rings.
- 2) Spacecraft: Mariner family in a flyby mode
- 3) Deflection Mode: Probe
- 4) Atmosphere: Nominal Saturn
- 5) Science Payload: SAG Exploratory Payload (PAET)

### 4. Telecommunications Subsystem

General results of the parametric study performed for Jupiter were used to define the telecommunications subsystem for Saturn. The operating frequency, established for Jupiter at 0.86 GHz, applies to the Saturn mission. Binary FSK modulation is used with the same characteristics as for the Jupiter missions.

Microwave attenuation of the nominal Saturn atmosphere is shown in Figure VI-6. Attenuation at 7 bars and 1 GHz is 0.5 dB and is very close to the loss at the same conditions in the Jovian cool/dense atmosphere. Saturn atmospheric loss is slightly lower than the loss for Jupiter as the pressure is increased. Therefore, atmospheric loss for Saturn to depths up to 10 bars is very close to the atmospheric loss encountered in the Jovian cool/dense atmosphere.

The system noise temperature was determined for Saturn based on information provided with the study by JPL (Ref 1). The thermal disk brightness temperature (Ref 1, Table IV) is shown in Figure VI-7 as a function of decimetric frequency. The disk temperature curve shown is the upper limit values from ten separate measured observations. The increase in brightness temperature with increasing wavelength is entirely due to thermal radiation from the atmosphere of Saturn. Observations are within the thermal model limits proposed by Gulkis and McDonough with ammonia mixture ratios of  $10^{-4}$  and  $5 \times 10^{-4}$  (Ref 2).

Radioastronomy measurements have not verified the existence of a magnetosphere around Saturn. An atmospheric thermal source can be responsible for all of the characteristics of the UHF radiation, with the exception of linear polarization reported by Rose *et al.* in 1963, which has not been confirmed by subsequent observations. Comparative discussions with respect to Jupiter indicate the possibility that Saturn could possess a trapped radiation belt that should be considered by probe mission designs. The belt would be similar to Jupiter's, but weaker in strength. The rings of Saturn interfere with the formation of a belt interior to  $2.3 R_S$  (the radius of the outer ring). Haffner (Ref 3) discusses the magnetosphere of Saturn and assumes a Van Allen belt with typical dipole characteristics. The size of the belt is not known, but should be between 3 and  $4 R_S$  when compared with Earth and Jupiter. The high inclination trajectory at  $2.3 R_S$  will miss the rings, but would be within the magnetosphere.

The synchrotron brightness temperature of Saturn is given in the monograph (Ref 1) as

$$T_{BS} = (0.2 \pm 0.2) \lambda^2 \quad \text{[VI-1]}$$

with

$T_{BS}$  = synchrotron brightness temperature, °K

$\lambda$  = wavelength, cm =  $30/f$

$f$  = frequency, GHz

VI-11

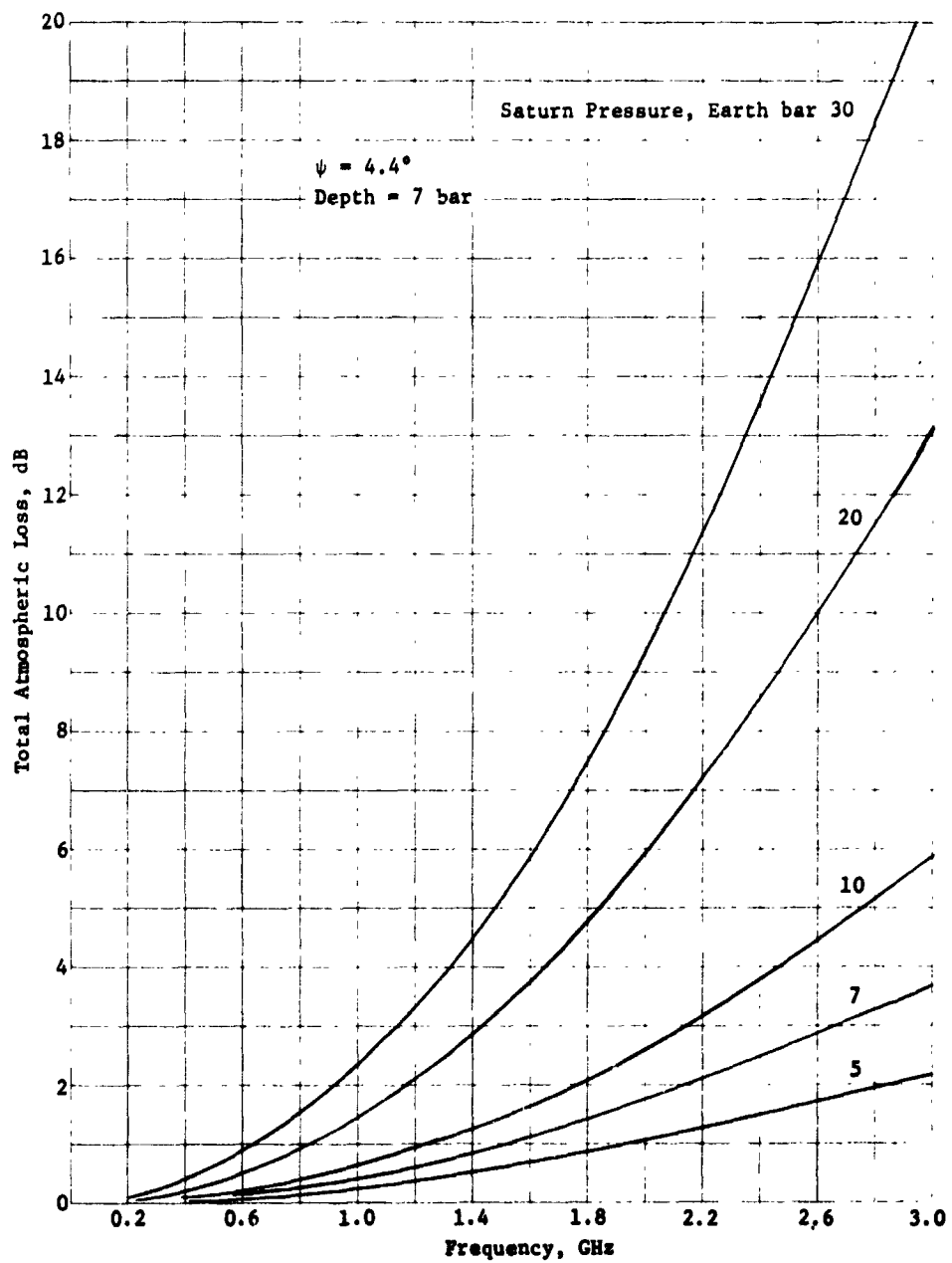


Figure VI-6 End of Mission Attenuation for Saturn Nominal Atmosphere

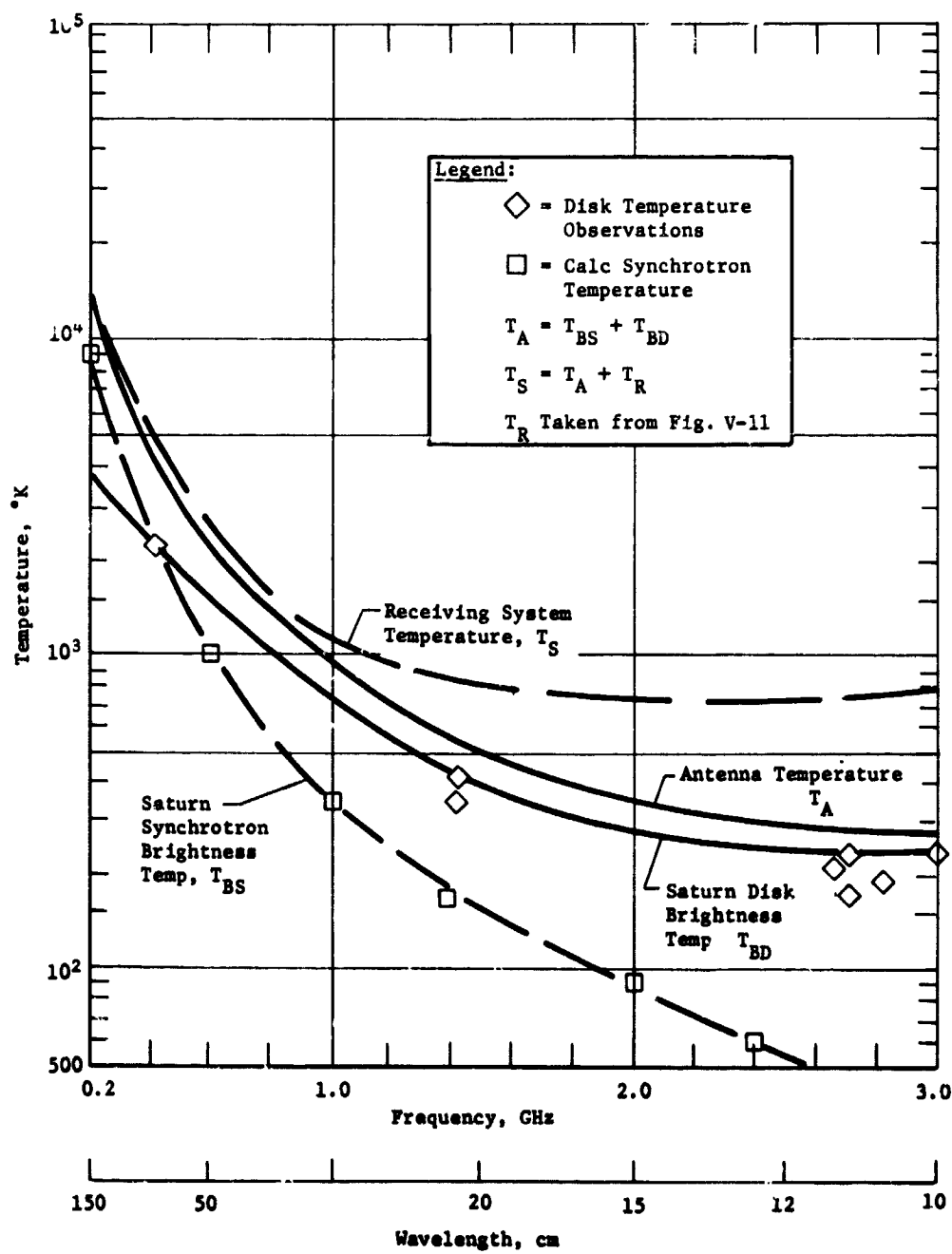


Figure VI-7 Spacecraft Receiving System Noise Temperature for Saturn Mission



The synchrotron temperature is independent of path length since a model is not defined as is the case for Jupiter; it is only a function of frequency. Equation [VI-1] is plotted in Figure VI-7 as a function of frequency. The spacecraft antenna noise temperature is the sum of disk and synchrotron temperatures. The noise temperature of the receiving system, shown in the figure, is the sum of the antenna temperature and the receiver front-end noise temperature based upon the average curve shown in Figure V-11. As seen in Figure VI-7, the system noise temperature rises sharply below 1 GHz due to synchrotron and thermal disk noise. It is fairly constant at approximately 750°K between 1.6 and 3 GHz, rising slightly near 3 GHz from increased noise figure of the receiver. Variations in the system noise temperature are similar to the Jupiter probe dedicated mission and will be 0.2 dB or less from acquisition to mission completion. The planet disk is in the background of the spacecraft antenna at acquisition and distance in the magnetosphere is  $1.75 R_J$ . The path length decreases to  $1.2 R_J$  at mission completion.

Adjustments in spacecraft lead time were made in order to optimize probe-to-spacecraft range and probe aspect angle. Communications range is shown in Figure VI-8. Increasing range before entry is due to the relative motion of the probe and spacecraft with the spacecraft moving ahead of the probe along the trajectory. Maximum range occurs at entry and decreases by  $0.3 R_J$  at mission completion.

Periapsis occurs after the mission is over (7-bar level reached) at one hour after entry.

Probe aspect angle as a function of mission time is shown in Figure VI-9. As seen in the figure, the objective of having minimum probe aspect angle approximately at mission completion is achieved. Final RF power requirements were low enough that it was not necessary to adjust lead time to make end of mission and minimum aspect angle coincide exactly. The probe aspect angle is  $10^\circ$  when the descent antenna is energized and  $5^\circ$  at mission completion.

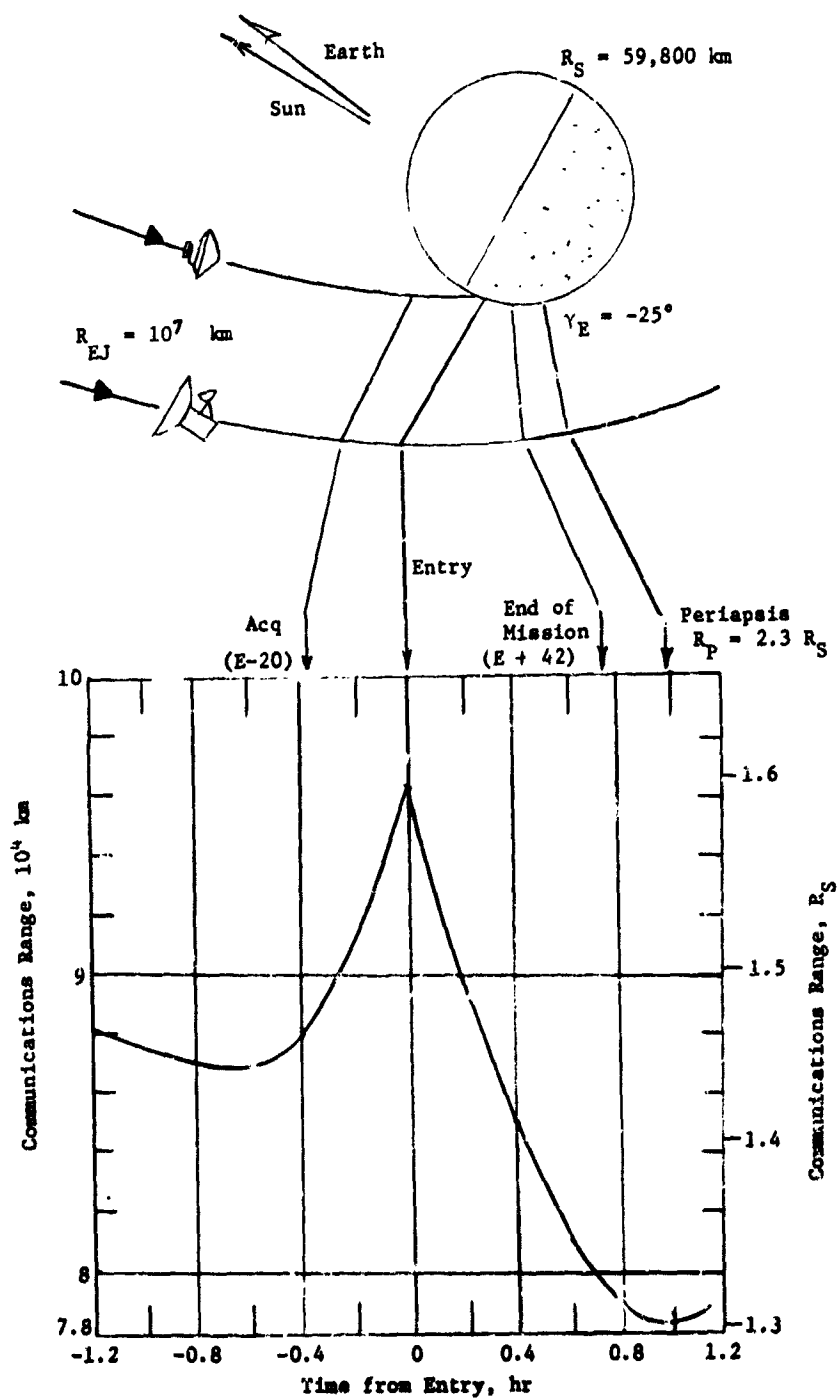
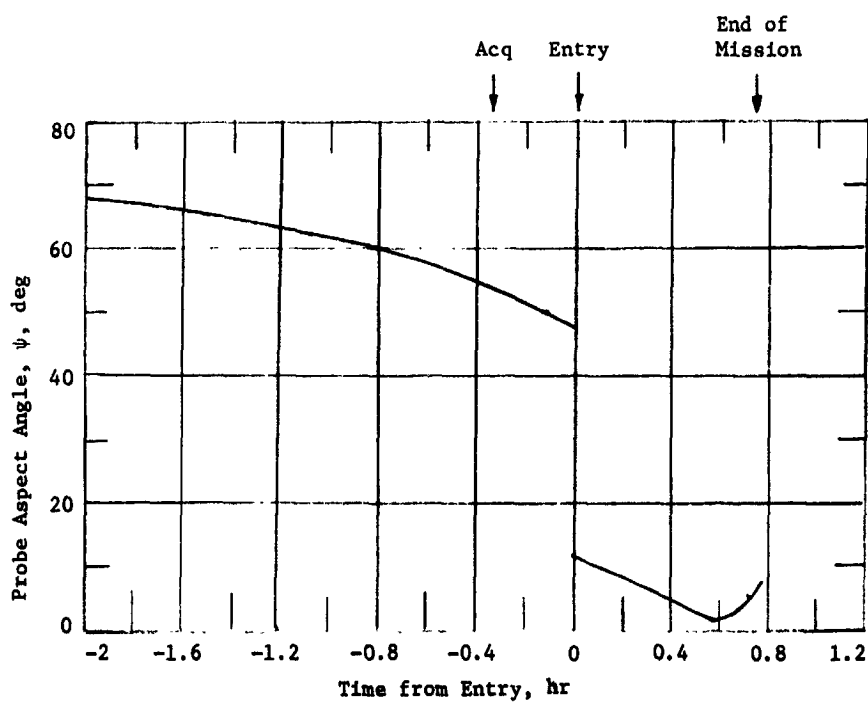
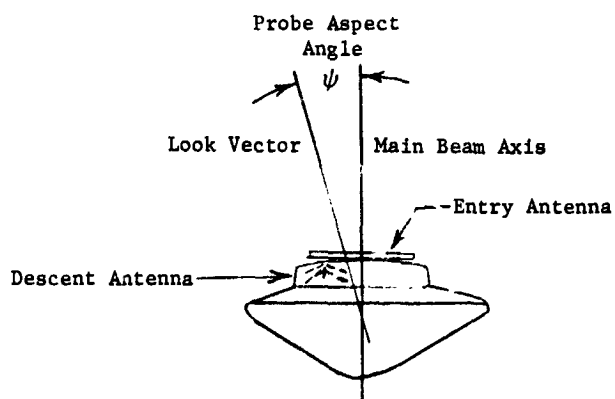


Figure VI-8 Probe-to-Spacecraft Communication Range for the Saturn Mission



Conditions:  $R_P = 2.3 R_S$   
 $R_{EJ} = 10^7$  km  
 $\gamma_E = -25^\circ$

$T_L = 56$  min  
 EOM = 7 bar (E + 42 min)  
 Nominal Atmosphere

Figure VI-9 Saturn Probe Aspect Angle

Relative probe positions during the mission (Fig. VI-10) are shown by the ellipses, which account for trajectory and probe dispersions and represent the nominal positions (triangles) and associated uncertainties. The dispersions are based on a 100-sample Monte Carlo analysis. Elevation angle (cross cone angle) dispersions are very small with the major difference occurring in cone angle. A 35° spacecraft antenna beamwidth provides maximum gain at the points of maximum dispersion. The cone angle decreases during descent and retraces the increasing angle from acquisition to entry. Decreasing cone angle after entry results from the spacecraft pulling ahead of the descending probe. The ellipse shown for entry represents the actual entry dispersions, and is used because it is slightly larger than the nominal entry dispersions. The spacecraft antenna is positioned to cover descent with the high-gain portions of the beam. Nominal positions at entry and mission completion are within the 3-dB beamwidth points and a 35° beam provides maximum gain at the points of maximum ellipse dispersion even though they are outside the 3-dB points.

Parameters of the RF link are depicted in Table VI-1 for the Saturn mission at 0.86 GHz. Defining conditions of the RF link are listed in the remarks column and in the note at the bottom of the table. Maximum RF power is required at mission completion because atmosphere losses increase with depth, as seen in Figure VI-1.

5. Data Handling Subsystem

The data handling subsystem analysis is essentially identical to that for the nominal Jupiter probe subsystem. Minor modifications of the time sequence and data format will occur, but do not influence the parametric or analytic approach. For discussion of these alternatives, refer to Chapter V, Section A.5 of this volume and Vol III, Appendix H.

6. Power and Pyrotechnic Subsystem

The power and pyrotechnic subsystem analysis is essentially identical to that for the nominal Jupiter probe subsystem. Minor modifications of battery weight and size will occur. For discussion of the parametric and analytic considerations, refer to Chapter V, Section A.6 of this volume and Vol III, Appendix G.

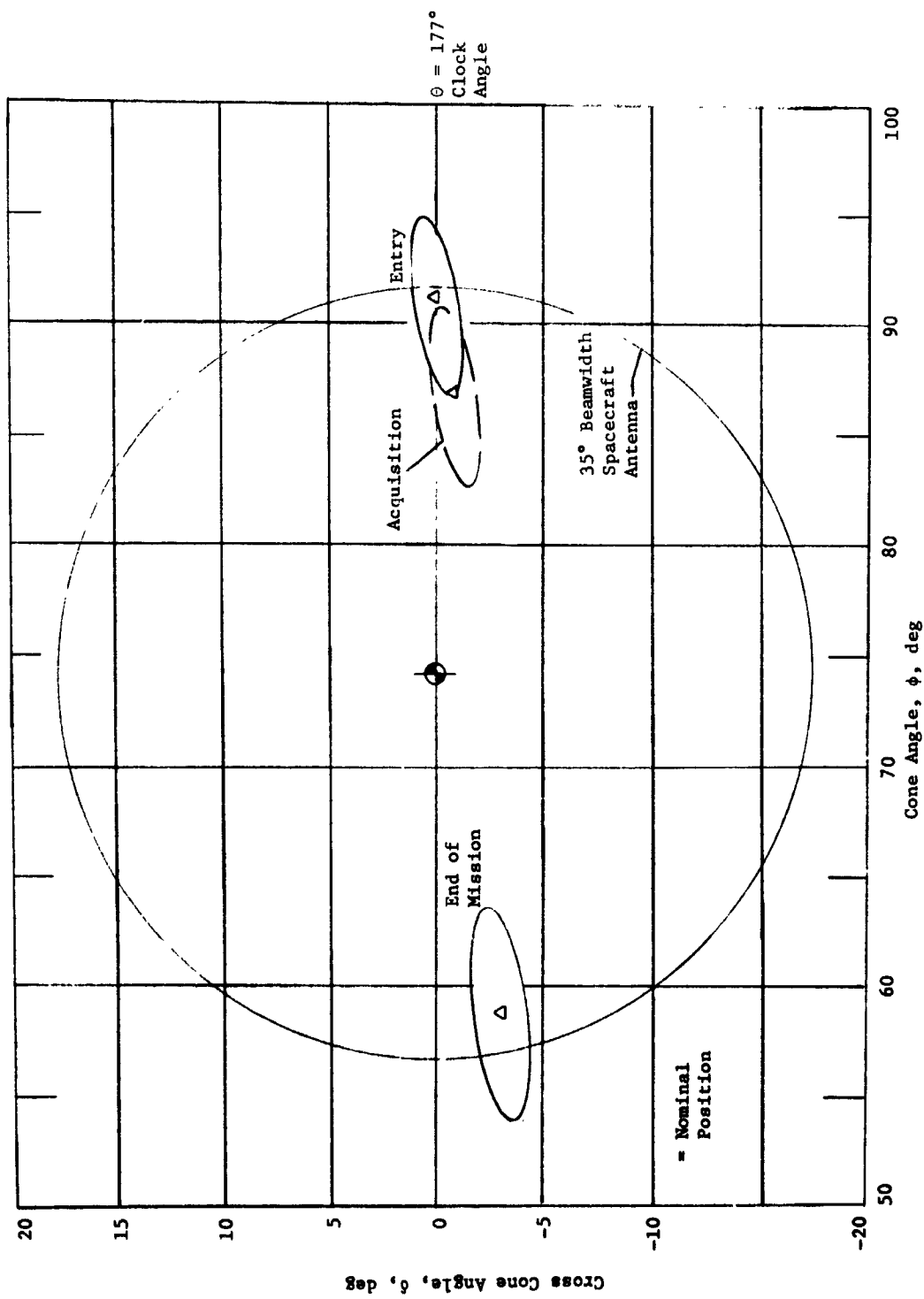


Figure VI-10 Spacecraft Antenna Requirements for the Saturn Mission

Table VI-1 Probe Telemetry Link Design Table for the Saturn Probe

Parameter	Nominal Value	Adverse Tolerance	Remarks
1. Total Transmitter Power, dBW	8.1	0	6.5 W
2. Transmitting Circuit Loss, dB	-0.3	0.2	Switch Loss: 0.2 dB
3. Transmitting Antenna Gain, dB	6.0	1.8	90° Beamwidth
4. Communications Range Loss, dB	-189.2	0.4	8 x 10 <sup>4</sup> km
5. Planet Atmosphere & Defocus Loss, dB	-0.3	0.2	Nominal, 7 atm
6. Polarization Loss, dB	0	0.2	
7. Antenna Pattern Ripple Loss, dB	0	0.2	
8. Receiving Antenna Gain, dB	13.8	4.0	35° Beamwidth
9. Receiving Circuit Loss, dB	-0.2	0.2	
10. Net Circuit Loss, $\Sigma$ (2+9), dB	-170.2	7.2	
11. Total Received Power (1 + 10), dBW	-161.9	7.2	
12. Receiver Noise Spectral Density, dBW	-196.5	0.5	$T_S = 1600^\circ K$ $NF_S = 8.12$ dB
Tracking Tone			
13. Tone Power/Total Power, dB	-5.1	0	
14. Received Tone Power (11 + 13), dBW	-167.0	7.2	
15. Tracking Threshold Bandwidth, dB	11.8	0	15 Hz Bandwidth
16. Threshold SNR, dB	10.0	0	
17. Threshold Tracking Power (12 + 15 + 16), dBW	-174.7	0.5	
18. Tracking Performance Margin (14 - 17), dB	7.7	7.7	
Data Channel			
19. Data Power/Total Power, dB	-1.7	0	
20. Radio System Processing Loss, dB	-1.0	0	
21. Fading Loss, dB	-1.0	0	
22. Received Data Power (11 + 19 + 20 + 21), dBW	-165.6	7.2	
23. Data Bit Rate, dB	14.2	0	26 bps
24. Threshold $E_b/N_o$ , dB	8.9	0	
25. Threshold Data Power (12 + 23 + 24), dBW	-173.4	0.5	
26. Performance Margin (22 - 25), dB	7.7	7.7	
27. Nominal Less Adverse Value (26 - 26 adv), dB	0		
Conditions: 1. Saturn JS-77 Mission 2. Worst-Case (EOM) conditions at $f = 0.86$ GHz 3. Convolutional Encoder, $M = 2$ , $V = 2$ , $Q = 8$ 4. BER = $5 \times 10^{-5}$ for binary FSK with $K = 8$ code			

7. Attitude Control Subsystem

The attitude control subsystem analysis is essentially identical to that for the nominal Jupiter probe subsystem. The most significant parameters that are modified are the Sun/probe and Saturn/probe ranges which affect the sensor capability. Review of state-of-the-art sensor capability indicates that present solar aspect sensors have sufficient sensitive range to provide adequate performance at Saturn distance solar density (MSC-04568: *Evaluation Test Report for Precision Digital Solar Aspect Sensor*. June 1971). The planet sensor may require additional optics. For a discussion of the attitude control subsystem parametrics and analysis, refer to Chapter V, Section A.7 of this volume and Vol III, Appendix F.

8. Structures and Mechanical

The parametric structural studies performed for the Jupiter probe, and reported in Chapter V, Section B.8, are applicable to the Saturn probe provided that the proper parameters are observed. The aeroshell weights data, however, apply only to a conical nose shape, and not to the blunt nose configuration.

The aft cover of the entry probe was evaluated parametrically for weight of ablator heat shield required versus planet entry angle. This data is reported in Section B.8 of this chapter.

Two configurations of the Saturn entry probe were evaluated for comparison of effects of heat shield shape. This data also are reported in Chapter VI, Section B.8.

9. Propulsion Subsystem

The propulsion parametric data presented in Chapter V, Section A.9 is applicable to the Saturn probe.

10. Thermal Control Subsystems

a. *General Discussions* - For Saturn, thermal control must be provided to ensure that all probe systems will be maintained within acceptable temperature limits. Like Jupiter, the primary thermal problem is one of losing too much thermal energy during the atmospheric descent phase of the mission and exceeding the allowable primary battery lower limit described in Chapter V, Section A.10.c. The selection of and approach to the thermal control subsystem is the same as the Jupiter probes design, and consists of the following:

#### Cruise/Coast Phase Thermal Control

- 1) Radioisotope Heaters
- 2) Multilayer Insulation
- 3) Environmental Cover
- 4) Thermal Coatings
- 5) Deflection Motor Blanket and Heater

#### and Entry/Descent Phase Thermal Control

- 1) Graphite Ablator and Aeroshell Insulator
- 2) Low Density Internal Foam Insulation
- 3) Nitrogen Gas Environmental Control

A schematic of the basic thermal control subsystems has been presented and discussed (Fig. V-41). The pivotal temperature is the probe temperature at the end of the mission coast phase. This temperature must be high so that the probe will have sufficient thermal inertia to survive the critical heat losses during descent. For the Jupiter probe, radioisotope heaters maintain the probe temperature safely below maximum battery storage temperatures during cruise, and then thermal coatings were selected for solar heating of the probe approximately 15°K following spacecraft separation. With the Saturn probe, however, the solar flux has reduced to 15 W/m<sup>2</sup> and thermal coatings are now just sufficient to maintain the probe at the cruise equilibrium temperature. Better thermal protection, therefore, must be provided during descent because the obtainable entry temperature will be lower than during the Jupiter missions.

*b. Cruise/Coast Probe Thermal Control*-- Thermal control during spacecraft cruise and probe coast is supplied by multilayer insulation, thermal coatings, and radioisotope heaters. To determine the radioisotope heater requirement, a thermal analysis was performed using the finite-element thermal model previously discussed in Chapter V, Section A.10.e. Based on the Iridite 14-2 aluminum coating, the analysis shows that 18 watts of heater power will be adequate to maintain the desired probe temperature during cruise, but that the probe temperature during coast will be 2°K cooler than the probe cruise temperature since the low solar energy available is small. The results generated to size the radioisotope heaters are presented in Figure VI-11. A detailed discussion of the cruise/coast thermal analysis has been presented in Chapter V, Section A.10.d.



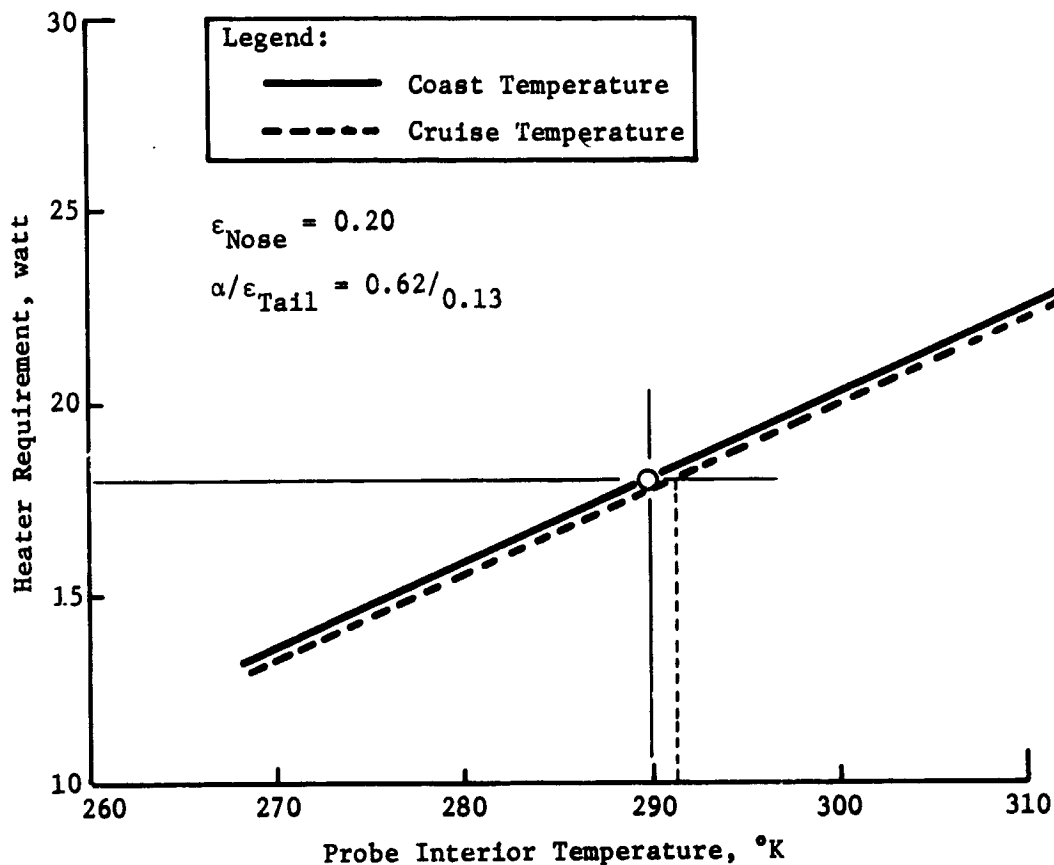


Figure VI-11 Radioisotope Heater Requirement and Probe Coast Equilibrium Temperature for Saturn Probe

c. *Descent Probe Thermal Control* - Thermal control for the atmosphere descent portion of the mission relies on the probe/coast entry temperature, internal foam insulation and sufficient probe thermal inertia to survive the descent environment encountered. For Saturn, only the nominal atmosphere and vented probe design were considered. The model atmospheres for Saturn are presented in Figure VI-12. On the basis of the ballistic coefficient chosen for the science return descent portion of the mission (0.70 slug/ft<sup>2</sup>), the probe descent temperature and pressure profiles for the Saturn mission are presented in Figure VI-13.

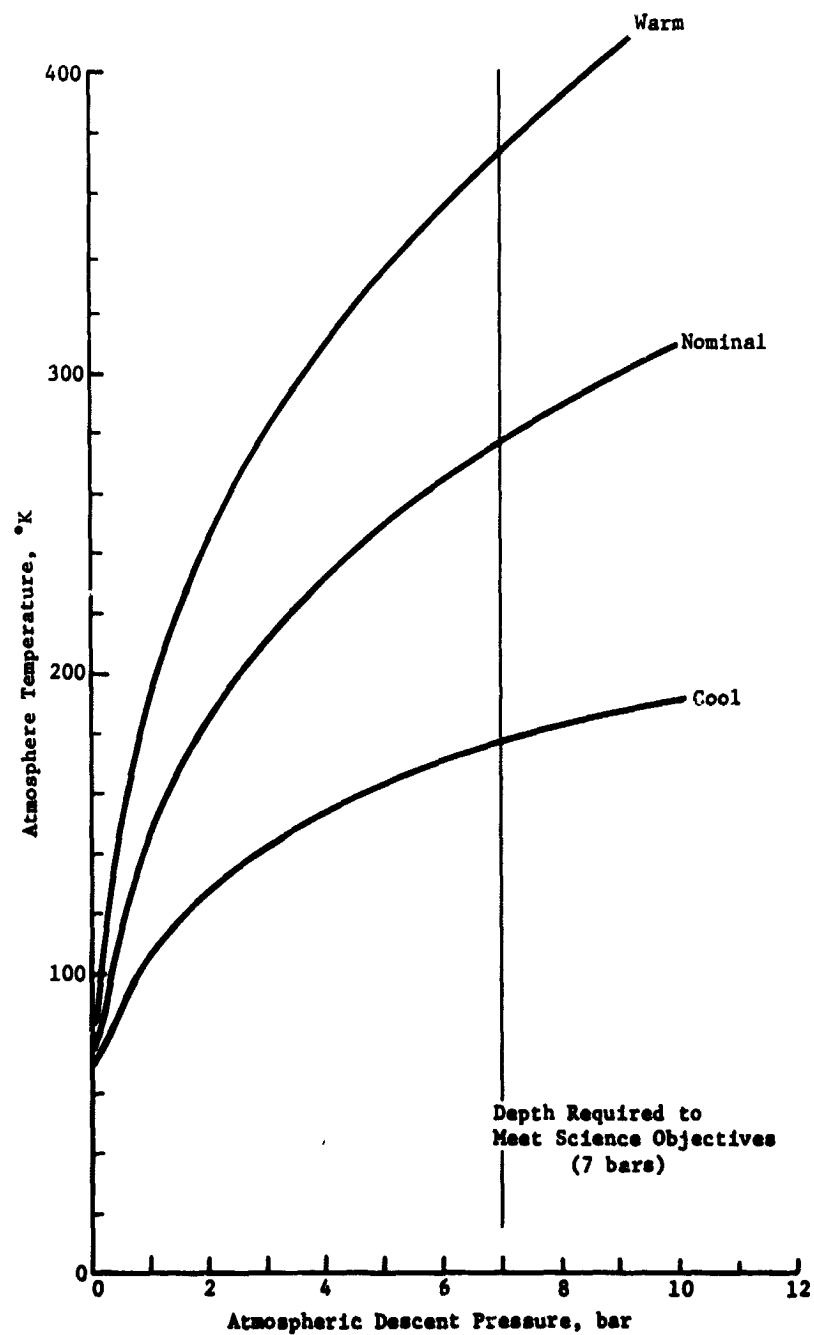


Figure VI-18 Saturn Atmospheric Models Temperature vs Descent Pressure

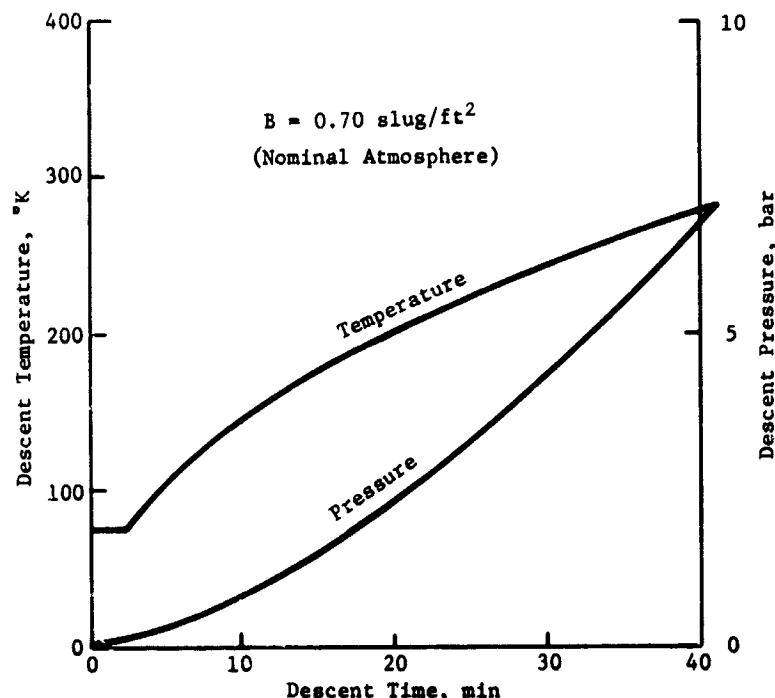
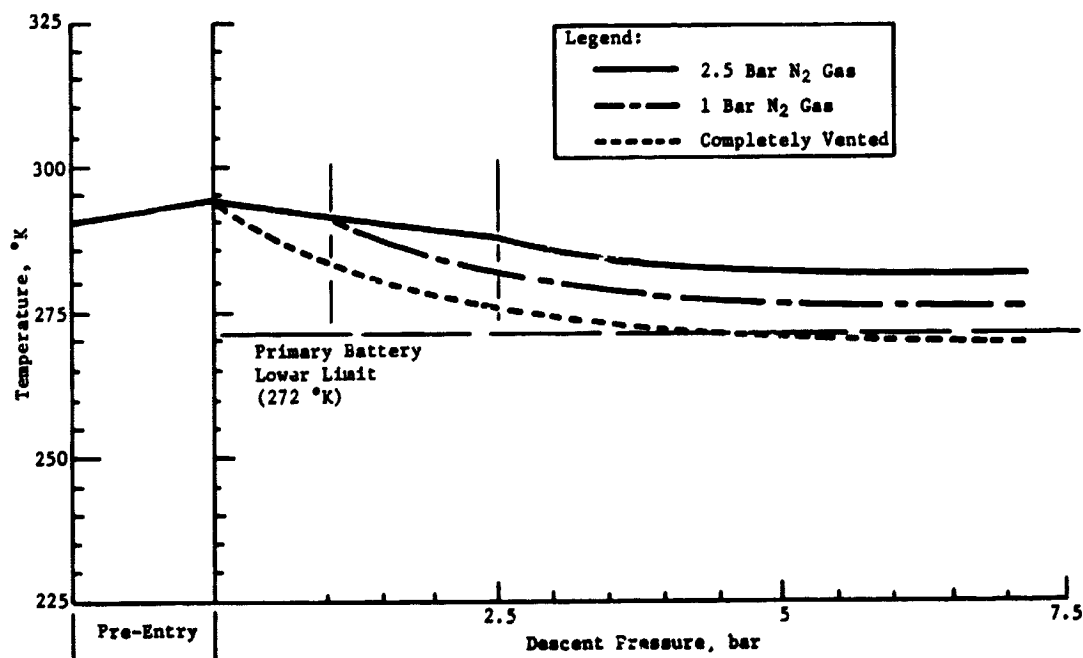


Figure VI-13 Nominal Saturn Mission Descent Temperature and Pressure Profiles

To determine the Saturn probe descent thermal response, a thermal analysis was performed using the finite-element thermal math model presented and discussed in Chapter V, Section A.10.e. Results for the descent analysis are shown in Figure VI-14. These results show that due to the low probe entry temperature, sufficient probe inertia is not available to survive the temperature specifications during descent. The nitrogen gas environmental control concept was chosen as a likely alternative for thermal control. The delta weight and volume added by an  $N_2$  gas supply is approximately 0.41 kg and 0.35 liters. The use of the  $N_2$  gas system to 2.5 bars pressure during descent increases the minimum probe descent temperature approximately 12°K. A second likely alternative could be the use of electrical battery-supplied heater power for the battery. This concept had been ruled out for Jupiter because even for the cool/dense atmosphere a need for a battery heater was not identified. For Saturn, however, the investigation of the nominal atmosphere alone indicates that thermal problems will exist and the use of battery heating would be desirable. In addition, the entry decelerations for Saturn are not as severe as for Jupiter, and the internal probe free convection is significantly less (planet gravity 42% of Jupiter) which makes this concept more desirable.



*Figure VI-14 Saturn Probe Descent Parametric Thermal Response*

The improvement in probe descent thermal performance due to the N<sub>2</sub> gas environmental control concept is shown from a standpoint of instantaneous probe heat leak in Figure VI-15. It is interesting to note that to compensate for the N<sub>2</sub> gas improvement by heater power would require approximately 70 watt-hr of electrical energy or about 2.8 lb of batteries for Saturn. However, this heater power could be concentrated at the batteries themselves thereby increasing the reliability of battery thermal control. For the Jupiter probe-dedicated alternative mission, approximately 120 watt-hr of electrical energy would have been required to compensate for the N<sub>2</sub> gas system (Chapter V, Section C.10).

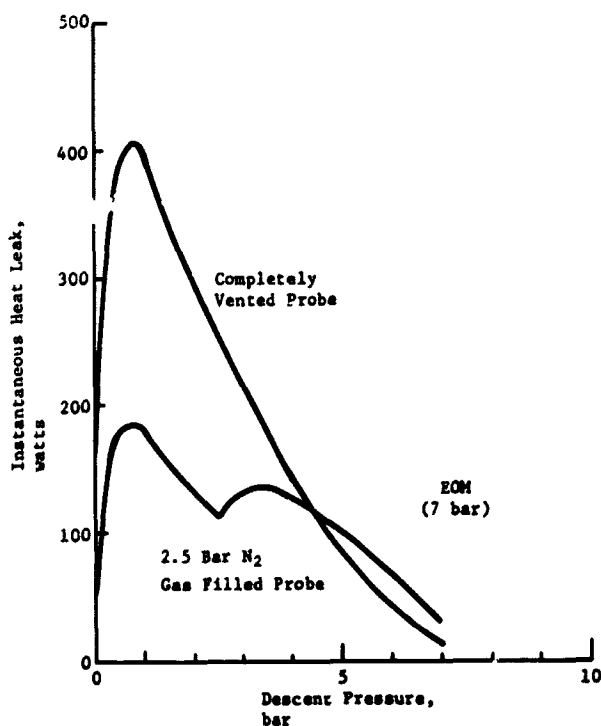


Figure VI-15 *Instantaneous Saturn Probe Atmospheric Heat Leak*

11. Summary of Saturn Parametric Analysis

A summary of the Saturn parametric analysis results follow:

Mission Times to Saturn	3½ yr
Optimal Flyby Radius at Saturn	2.5 R <sub>S</sub>
Flyby Radius for JST	2.33 R <sub>S</sub>
One Sigma Navigation Uncertainty w/QVLBI	1100 km
Three Sigma Dispersions (max)	
Entry Time	6.58 min
Entry Angle	3.41°
Angle of Attack	~ 75°
Lead Angle	3.25°
Entry Ballistic Coefficient	<156 kg/m <sup>2</sup>
Depth of Descent for Science Objectives	7 bar
Descent Ballistic Coefficient for Science Objectives	19 kg/m <sup>2</sup>
Descent Time	Approximately 40 minutes

12. References

1. *The Planet Saturn (1970)*, Preliminary NASA Space Vehicle Design Criteria (Environment), NASA SP-XXXX, to be published, pp 28 through 33.
2. S. Gulkis and T. R. McDonough: "The Microwave Spectrum of Saturn." *ICARUS*, Vol 10, 1969, pp 421 through 427.
3. J. W. Haffner: "Magnetospheres of Jupiter and Saturn." *AIAA Journal*, Vol 9, No. 12, December 1971, pp 2422 through 2427.

B. SATURN PROBE SYSTEM DEFINITION

This probe system used the alternative Jupiter probe approach, defined in Chapter V, Sections C and D, but adjusted for a Saturn entry. The general constraints follow.

Mission	JPL's JS 77 High Inclination Trajectory for a Titan Encounter
Entry Angle	-25° (structure designed to -30°)
Depth of Descent	7 bar
Atmosphere	Nominal
Science	SAG Exploratory Payload (PAET)
Spacecraft	Mariner Family
Carrier Mode	Flyby
Periapsis Radius	2.33 R <sub>S</sub>
Communication Mode	Relay
Deflection Mode	Probe
Entry Ballistic Coefficient	0.65 slug/ft <sup>2</sup> (102 kg/m <sup>2</sup> )
Ballistic Coefficient for Heat Shield Removal	0.12 slug/ft <sup>2</sup> (19 kg/m <sup>2</sup> )
Descent Ballistic Coefficient	0.7 slug/ft <sup>2</sup> (110 kg/m <sup>2</sup> )

## 1. Science Instrumentation and Performance

The instruments for the Saturn probe are identical to those for the Jupiter alternative probe and the characteristics are given in Table V-29. They are discussed in Chapter V, Section C and in Chapter III, Section C.1. The only difference would be a modification of the range of the temperature gage and possibly entry accelerometers for the colder atmosphere and lower g-load.

The descent profile parametrics were discussed in Section A.1 of this chapter. The results are:

Design Limit Pressure = 7 bars

Parachute Ballistic Coefficient =  $0.70 \text{ slug/ft}^2$  ( $109.9 \text{ kg/m}^2$ )

Parachute Deployment Pressure = 48 millibars

Pressure at First Measurement = 57 millibars

Total Mission Time from Entry = 41 min, 43 sec.

The entry and descent times, instrument sampling times, and resulting bit rates are shown in Table VI-2. The transmission bit rates for descent are slightly higher than the collection bit rates because the descent data collected during probe acquisition by the S/C must be stored and later interleaved with real time data for transmission. The pressure descent profile is given in Figure VI-1 using the appropriate ballistic coefficient.

In Table VI-3, the mission measurement performance is given for descent with the above parameters. All of the requirements have been satisfied, the bold face numbers showing the governing measurement.

Table VI-2 Saturn Probe Instrument Sampling Times and Data Rates

Phase	Instrument	Sampling Times, sec	Collection Bit Rate, bps	Transmission Bit Rate, bps
Entry, 78.5 sec	Accelerometers			
	Longitudinal	0.2	50	0
	Lateral	0.4	25	0
	Lateral	0.4	25	0
Descent, 2425 sec	Temperature	4	2.5	2.6
	Pressure	4	2.5	2.6
	Mass Spectrometer	60	6.7	7.0
	Accelerometers			
	Turbulence	8	7.5	7.8
	Stored	0	0	3.4
Science Total				23.4
Engineering and Formatting				2.9
Total				26.3

Table VI-3 Saturn Probe Descent Measurement Performance

Instrument, $\Delta t$ and Measurement	Criteria	Descent Performance, $B = 0.70 \text{ slug/ft}^2$
Mass Spectrometer, 60 sec Minor Constituents Cloud Layering  H/He Ratio Isotopic Ratios Molecular Weight	2 per scale height* 2 inside cloud  4 measurements	6.4 to 28 2.8 in $\text{NH}_3$ 13.1 in $\text{H}_2\text{O}$  41
Temperature Gage, 4 sec Temperature Cloud Layering	1 per $^\circ\text{K}$ 2 inside cloud	1.2 to 4.8 46 in $\text{NH}_3$ 196 in $\text{H}_2\text{O}$
Pressure Gage, 4 sec Pressure Turbulence Cloud Layering	2 per km* 1 per km* 2 inside cloud	2.0 to 4.3 2.0 to 4.3 46 in $\text{NH}_3$ 196 in $\text{H}_2\text{O}$
Accelerometers, 8 sec Turbulence	1 per km*	1.0 to 2.2
*Below cloud tops.		



## 2. Mission Definition

The Saturn mission upon which the system design is based is described in Figure VI-16 and summarized in Table VI-4. Important mission design results are discussed in this section.

*a. Interplanetary Trajectory Selection* - The interplanetary trajectory for this mission is based on the JST mission--a JS 77 mission including an encounter with Titan. The trajectory is pictured in Figure VI-16(a) and detailed in Table VI-4(a). The trajectory arrives at Jupiter 1.6 yr after launch and passes by at a periapsis radius of  $5.8 R_J$ . The flight time to Saturn is 3.4 yr and the flyby radius at Saturn is  $2.3 R_S$ . Titan is encountered 18 hr before arrival at Saturn.

*b. Launch Analysis* - The results of the launch analysis are given in Figure VI-16(b) and Table VI-4(a). The available payload weight (probe, spacecraft, spacecraft-to-launch vehicle adaptor) is plotted against launch period for three sets of performance data. The slight decrease in available payload relative to the previous Jupiter missions is due to the fact that the interplanetary trajectory was selected to satisfy the requirements of the entire JST mission and not to optimize payload weight.

*c. Approach Trajectories* - The approach trajectories are illustrated in Figures VI-16(d) and (e) and summarized in Table VI-4(a) and (b). The spacecraft flyby radius of  $2.3 R_S$  was selected to permit the encounter with Titan, but is compatible with an effective communication link. Thus, the nominal values of the probe aspect angle begin at  $12.42^\circ$ , reach a minimum value of  $1.86^\circ$ , and end at  $4.05^\circ$  as the faster moving spacecraft overtakes the probe. This is most clear in Figure VI-16(d) where the view is from a point nearly normal to the spacecraft orbit plane. The location of Saturn's rings relative to the probe and spacecraft trajectories is indicated in Figure VI-16(e).

*d. Deflection Maneuver* - A probe deflection maneuver was used for this mission. The deflection radius of  $10.15 \times 10^6$  km was selected to give a  $\Delta V$  of 170 m/sec to obtain an identical deflection motor for the Saturn and Uranus missions. The deflection sequence is illustrated in Figure VI-16(c) and detailed in Table VI-4(b).

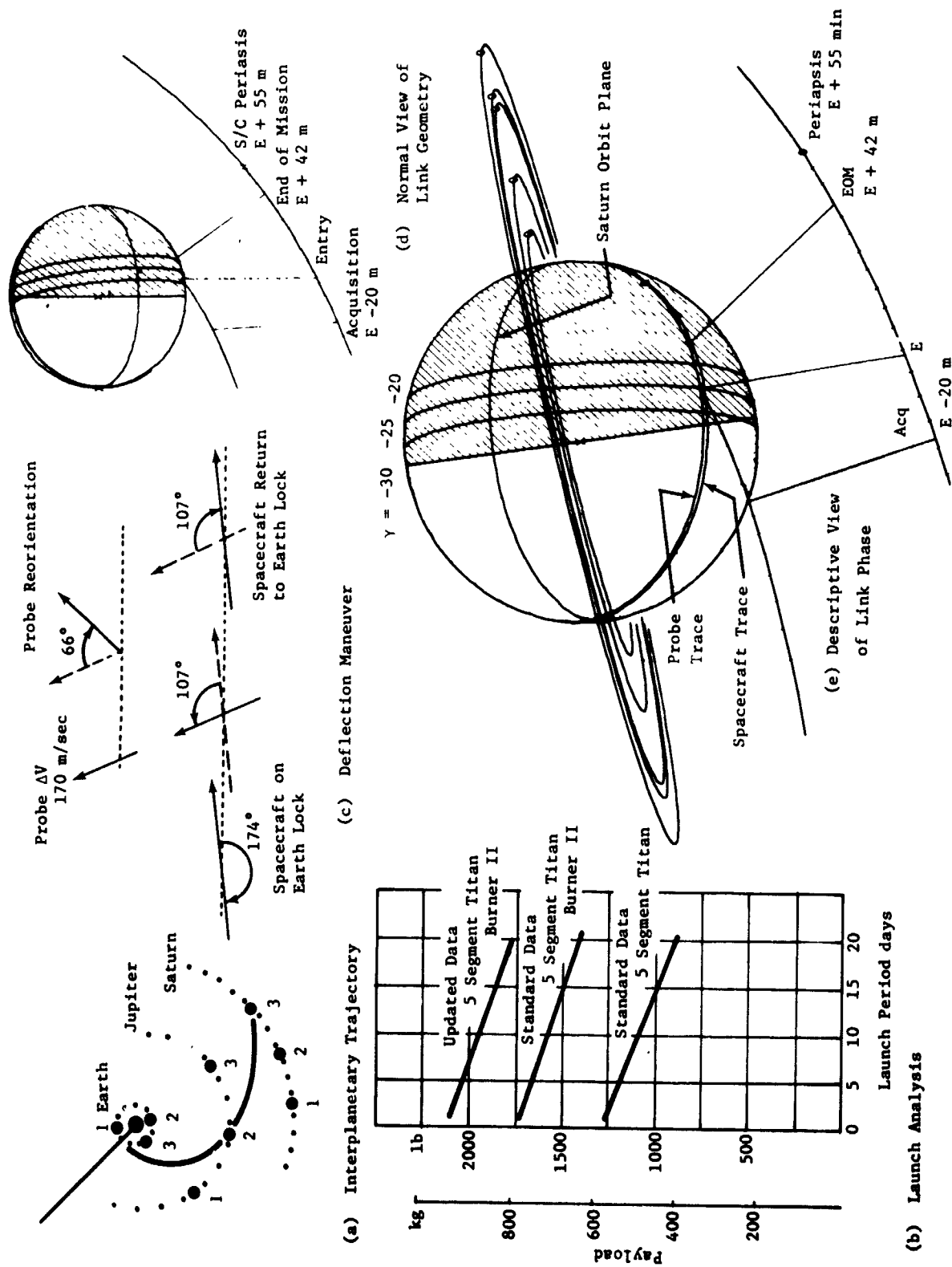


Figure VI-16 Saturn Mission Description

Table VI-4 Saturn Mission Summary

a. Conic Trajectory Data

Interplanetary Trajectory	Launch Trajectory	Arrival Trajectory
Launch Date: 9/4/77 Arrival Date: 2/16/81 Flight Time: 1261 days Central Angle: 207.3	Nominal $C_3$ : 99 km <sup>2</sup> /sec <sup>2</sup> Nominal DLA: 27.6° Launch Window: Parking Orbit Coast: $C_3$ (10 day): 102 km <sup>2</sup> /sec <sup>2</sup> $C_3$ (20 day): 107 km <sup>2</sup> /sec <sup>2</sup> Azimuth Range:	VHP: 13.66 km/sec RA: 195.28° DEC: 2.54° ZAE: 173.6° ZAP: 169.1° RP: 2.31 $R_S$ INC: 52.44°

b. Deflection Maneuver and Probe Conic

Deflection Maneuver	Probe Conic Definition
Deflection Mode: Probe Deflection Radius: 10.15 x 10 <sup>6</sup> km Coast Time: 8.02 days $\Delta V$ : 170 m/sec Application Angle: 105° Out-of-Plane Angle: 2° Rotation for Probe Release: 107° Probe Reorientation Angle: -66° Spacecraft $\Delta V$ from Earth: NA	Entry Angle: -25° Entry Latitude: -50.3° Entry Longitude: 102.2° Lead Time: 55.8 min Lead Angle: -7.63 Probe-Spacecraft Range (Entry): 96,305 km Probe Aspect Angle (Entry): 48.2° Probe Aspect Angle (Descent): 12.42° Probe Aspect Angle (EOM): 4.05°

c. Dispersion Analysis Summary

Navigation Uncertainties	Execution Errors (3 $\sigma$ )	Dispersions (3 $\sigma$ )
Type: Range/Doppler 80 day arc SMAA: 2178 km SMIA: 760 km $\delta$ : 89° TOF: 40 sec	$\Delta V$ Proportionality: 1% $\Delta V$ Pointing: 2° Probe Orientation Pointing: 2°	Entry Angle: 5.04° Angle of Attack: 4.00° Down Range: 12.70° Cross Range: 1.57° Lead Angle: 5.43° Lead Time: 5.18° Entry Time: 7.59 min

d. Entry and Descent Trajectory Summary

Entry Parameters	Descent Parameters	Critical Events	
		Time from Entry	Altitudes above 1 atm
Entry Velocity, km/sec: 37.1 Entry Altitude, km: 491 Entry B, slug/ft <sup>2</sup> : 0.65 kg/m <sup>2</sup> : Entry Atmosphere: Nominal Max Deceleration, g: 350 Max Dynamic Pressure. lb/ft <sup>2</sup> : 7.0 x 10 <sup>3</sup> kg/m <sup>2</sup> : 3.3 x 10 <sup>5</sup>	Descent Atmosphere: Nominal EOM Pressure, bar: 7.0 Descent B, slug/ft <sup>2</sup> : slug/ft <sup>2</sup> : 0.7 kg/m <sup>2</sup> : 109.9	g = 0.1, sec: 3.0 Max g, sec: 22.5 M = 0.7, sec: 78.5 Descent Time, min: 40.4 EOM, min: 41.7	km: 444 km: 158 km: 100

e. *Navigation and Dispersions* - The navigation and dispersion summary is provided in Table VI-4(c). The spacecraft uncertainties are based on using range/Doppler measurements over an 80-day tracking arc. The SMAA would be reduced by half by using QVLBI measurements. The navigation uncertainties have an approximately equal contribution to dispersions as execution errors. The entry dispersions are rather large but are tolerable.

f. *Entry and Descent Trajectories* - Table VI-4(d) summarizes the entry and descent phases on the mission. Both phases of the mission were simulated using the nominal atmosphere. The entry phase starts 491 km above the 1 atm pressure level (0 km alt = 59,800 km) and ends with the staging of the aeroshell 78.5 sec later. During this phase, a peak deceleration of 350 g is attained 19.0 sec after entry. The descent phase starts after staging of the aeroshell and continues through the end of mission at 7.0 bar. The total descent time is 40.4 min.

#### System Integration

a. *Functional Sequence* - Table VI-5 shows the sequence of events for the Saturn probe mission. This is similar to the sequence for the spacecraft-radiation-compatible Jupiter mission discussed in Chapter V, Section D; the primary difference is related to the main chute deployment. The entry and descent ballistic coefficients are essentially the same. Therefore, in order to remove the descent probe from the heat shield/aeroshell, a main parachute is deployed for approximately 15 sec and then released to allow the drogue chute to open.

b. *Functional Block Diagram* - The functional interfaces are identical to those discussed for the nominal Jupiter probe (Chapter V, Section B).

c. *System Data Profile* - Figure VI-17 shows the data profile for the Saturn probe and is similar to that for the spacecraft-radiation compatible Jupiter probe. The storage capacity is approximately 12,400 bits and the transmitted data rate is approximately 21 bps during separation, 2 bps during pre-entry, and 26.3 bps during entry.

d. *System Power Profile* - Figure VI-18 shows the power profile for the Saturn probe. It is similar to that discussed in Chapter V, Section D for the alternative Jupiter probe, except that the entry time uncertainties are much less for the Saturn probe.

Table VI-5 Sequence of Events for the Saturn Probe

ITEM	TIME	EVENT
1.	L=0	Launch, September 4, 1977
2.	L+2h	Separate Spacecraft from Launch Vehicle
3.	L+2h to L+1253.46d	Cruise
4.	S-6h, 0m, 0s	Spacecraft Power to Probe; Eject Environmental Cover
5.	S-5h, 47m, 0s	Start Probe Checkout
6.	S-0h, 17m, 0s	Probe Checkout Complete; Start Spacecraft Orientation for Release
7.	S-0h, 2m, 0s	Spacecraft Orientation to 107° Complete; Activate Probe Data Handling System & Separation Subsystems;
8.	(L+1253.59d) S=0	Separate Probe
9.	S+0m, 0.5s	Start Probe Spinup to 100 rpm
10.	S+4m, 0s	Probe Spinup to 100 rpm Complete
11.	S+15m, 0s	Apply Probe $\Delta V$ (170 m/sec) (900 m Separation)
12.	S+15m, 21s	Eject Probe Deflection Motors; Activate Attitude Propulsion Subsystem
13.	S+15m, 31s	Start Probe Precession; Reorient Spacecraft to Earth Lock (-107°)
14.	S+6h, 13m, 31s	Turn on Transmitter
15.	S+6h, 15m, 31s	Probe Precession Complete (-66°); Start Probe Acquisition
16.	S+6h, 16m, 31s	Acquisition Complete; Start Engineering Data Transmission
17.	S+6h, 26m, 31s	Complete Data Transmission; Deactivate Probe Systems
18.	L+1253.86d to L+1261.53d	Coast
19.	E-0h, 53m, 0s	Enable Entry Battery Ordinance
20.	E-0h, 33m, 0s	Activate Probe Descent Batteries (In Aeroshell & Descent Probe) Enable Probe Despin; Turn on Data Handling System, Engineering Instrumentation
21.	E-0h, 22m, 20s	Turn "On" Transmitter
22.	E-0h, 20m, 20s	Start Probe Acquisition
23.	E-0h, 18m, 40s	Complete Probe Acquisition; Start Data Transmission;
24.	E-0h, 18m, 30s	Start Probe Despin to 5 rpm
25.	E-0h, 13m, 30s	Probe Despin Complete
26.	E-0h, 13m, 0s	Eject Service Module; Activate Service Module Deflection Propulsion; Transmitter "Off"
27.	E-0h, 11m, 10.5s	Turn on Science Instruments
28.	E=0	Entry (491 km above 1 atm; $\sim 10^{-7}$ bar)
29.	E+0h, 0m, 2s	Start Recording Accelerometer Data (0.1 g Sensing)
30.	E+0h, 0m, 20.5s	Initiate Probe Descent Program (100 g Sensing)
31.	E+0h, 0m, 22.5s	Maximum G = 350 for $-25^\circ \gamma_E$
32.	E+0h, 1m, 25s	Eject Base Cover Quadrants (Mach 0.8)
33.	E+0h, 1m, 18.5s	Deploy Main Parachute (Mach 0.7 $\sim$ 0.048 bars)
34.	E+0h, 1m, 28.5s	Release Descent Probe from Entry Probe (Switch Probe Antenna) Probe Transmitter "On"; Start Probe Acquisition.
35.	E+0h, 1m, 30.5s	Deploy temperature Gauge; Release Mass Spectrometer Covers
36.	E+0h, 3m, 33.5s	Release Main Chute and Deploy Drogue Chute.
37.	E+0h, 3m, 8.5s	Probe Acquisition Complete; Start Data Transmission
38.	E+0h, 41m, 43.5s	End of Design Mission ( $\sim$ 7 bars)
39.	(L+1261.61d) E+55m, 54s	Spacecraft Periapsis (2.33 Rs); February 16, 1981
Includes 8.0 min Entry Trajectory uncertainty and based on a descent ballistic coefficient of 0.7 slug/ft <sup>2</sup> (110 kg/m <sup>2</sup> ).		

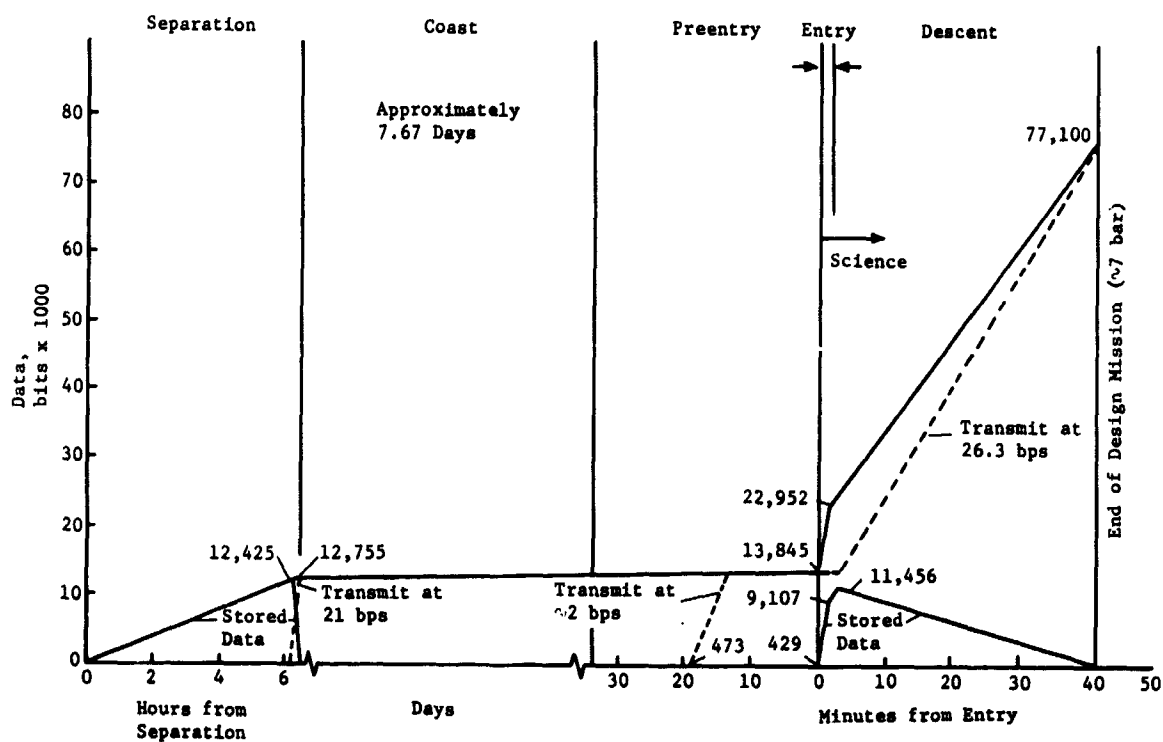


Figure VI-17 Data profile for Saturn Probe

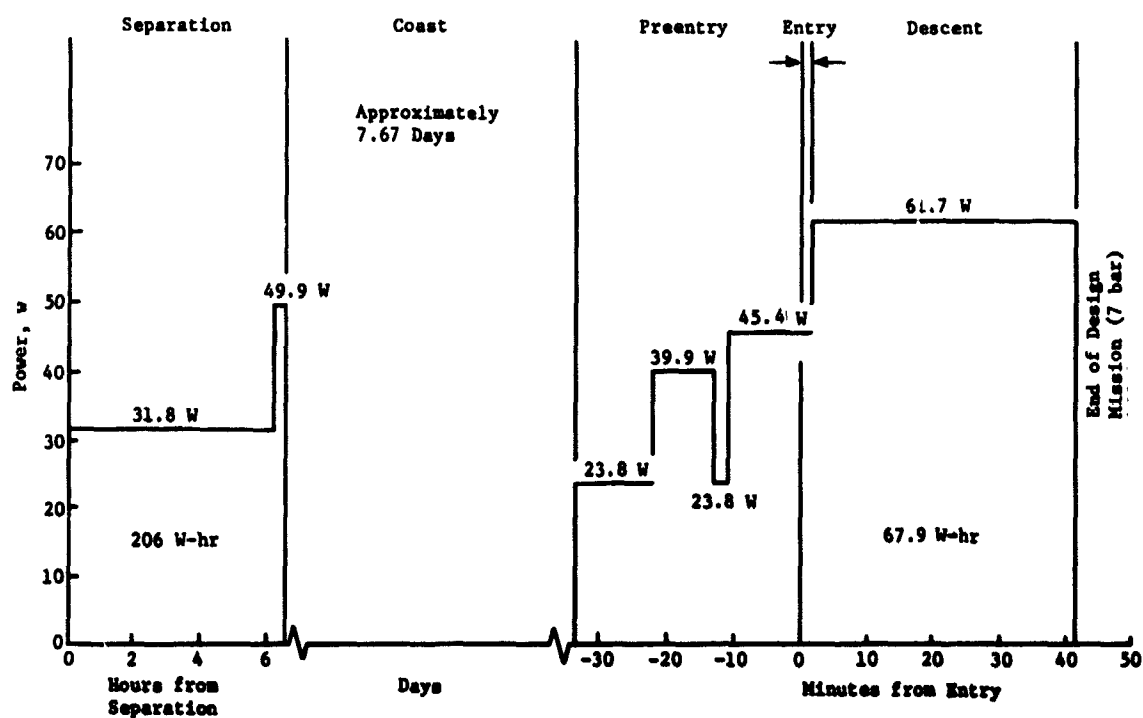


Figure VI-18 Power Profile for Saturn Probe

e. *System Weight Summary* - Table VI-6 presents the weight summary for the Saturn probe. The entry weight of 76.39 kg is approximately 34 kg lighter than the entry weight for the spacecraft-radiation-compatible Jupiter probe. The significant differences are in the heat shield and deceleration forces.

Table VI-6 *Weight Summary for the Saturn Probe*

Probe Breakdown	Weight	
	kg	lb
Science	8.07	17.80
Power and Power Conditioning	6.18	13.65
Cabling	4.85	10.70
Data Handling	2.59	5.70
Attitude Control (dry)	10.25	22.60
Communication	5.40	11.90
Pyrotechnics	4.23	9.32
Structure and Heat Shield	34.30	75.61
Mechanisms	7.57	16.70
Thermal	6.71	14.80
Propulsion (dry)	2.65	5.85
Propellant	7.10	15.65
15% Margin	<u>14.99</u>	<u>33.04</u>
Ejected Weight	114.90	253.32
Entry Weight	76.39	168.40
Descent Weight (final)	36.44	80.33

#### 4. Telecommunications Subsystem

Table VI-7 depicts design details of the RF components which comprise the telecommunications subsystem. Design requirements are discussed in Section A of this chapter. Complete details of the components are given in Chapter V, Section A.4. 6.5 W of RF power is required at 0.86 GHz with a bit rate of 26 bps using binary FSK with a tracking tone. A solid-state switch may be used at this power level. The entry antenna is an annular slot which is mounted on the service module under the deflection motor. The descent antenna is a turnstile over a cone design which is mounted on the aft bulkhead of the descent probe. The spacecraft antenna is a helix with right-hand circular (RHC) polarization and a 35° beamwidth. The descent antenna is also RHC polarized but the entry slot antenna has linear polarization. Cross polarization losses occur during entry but the link margin is high enough to overcome the loss. The spacecraft receiver is conventional solid-state design with a noise figure of 3.1 dB.

#### 5. Data Handling Subsystem

The configuration and functions of the data handling subsystem are unchanged from the design of the nominal Jupiter probe with the exception of minor modifications of sequence and format (Chapter V, Sections A.5 and B.5 of this volume and Vol III, Appendix H).

#### 6. Power and Pyrotechnic Subsystem

The configuration of the power and pyrotechnic subsystem is unchanged from the nominal Jupiter probe except for battery size and weight (Chapter V, Sections A.6 and B.6 of this volume and Vol III, Appendix G). These physical characteristics are:

Ag-Zn	Post-Separation Battery	94 in. <sup>3</sup>	6.9 lb
Ag-Zn	Entry Battery	35.6 in. <sup>3</sup>	2.6 lb
Hg-Zn	Pyrotechnic Battery	1 × 0.5 × 3 in.	0.9 lb

The remotely activated Ag-Zn batteries are based on power consumption for this mission. The change in the dimensions of the Hg-Zn battery is based on later catalog information that was available during the nominal Jupiter probe definition.



Table VI-7 Telecommunications RF Subsystem for the Saturn Mission

CONDITIONS: Planet: Saturn S/C: Mariner Frequency: 0.86 GHz Bit rate: 26 bps			
COMPONENT	CHARACTERISTIC	UNIT	VALUE
Transmitter	RF Power Out	W	6.5
	Overall Efficiency	%	45
	DC Power-in at 28 V dc	W	14.5
	Total Weight	kg	2.72
RF Switch		lb	6.0
	Type		Solid State
	Insertion Loss	dB	0.3
	Weight	kg	0.1
Entry Antenna		lb	0.2
	Type		Annular Slot
	Main Beam Angle	deg	55
	Beamwidth	deg	30
	Max Gain	dB	5.2
	Diameter	cm	43.2
		in.	17
	Weight	kg	2.1
Descent Antenna		lb	4.7
	Type		Turnstile/Cone
	Main Beam Angle	deg	0
	Beamwidth	deg	90
	Max Gain	dB	6.0
	Size (diameter x h)	cm	20.3 x 7.6
		in.	8 x 3
Spacecraft Antenna	Weight	kg	0.45
		lb	1.0
	Type		Helix
	Beamwidth	deg	35
	Max Gain	dB	13.5
	Size (l x diameter)	cm	73.2 x 11.1
		in.	28.8 x 4.4
	Weight	kg	2.72
		lb	6.0
	Despin		No
	Position Search		1
	Frequency Acquisition	sec	41
	Clock Angle, $\theta$	deg	177
	Cone Angle, $\phi$	deg	74
Spacecraft Receiver	Noise Temperature	°K	300
	Noise Figure	dB	3.1
	DC Power-in at 28 V dc	W	3.0
	Weight	kg	0.9
		lb	2.0

7. Attitude Control Subsystem - Electronics

The electronics configuration and functions for this subsystem are unchanged from the nominal Jupiter probe design (Chapter V, Sections A.7 and B.7 in this volume and Vol III, Appendix F).

8. Structural and Mechanical

The Saturn probe is the smallest of the configurations evaluated; this is due to the less hostile (from a structural standpoint) entry environment. The planetary entry decelerations are lower, resulting in lower structural weights. The heat shield mass fraction is also less, and this, combined with the reduced structural weight, produces a probe design weighing substantially less than the Jupiter configurations.

The probe is required to provide a deflection maneuver delta velocity, attitude stabilization, and attitude reorientation between the trajectory deflection maneuver and entry. Thus, the probe configuration propulsion system includes a delta velocity motor and an attitude control system.

a. *Configuration and General Arrangement (Blunt Nose)* - Two configurations of the Saturn probe were evaluated. Configuration 1 uses the blunt entry nose cone shape recommended by the heat shield analysis results.\* The other configuration evaluated (Configuration 2) uses the same 1.04 rad (60°) half angle nose cone as that used for the Jupiter entry probes. Each configuration used the respective heat shield mass fraction recommended by M Tauber.\* The heat shield diameters are shown to be almost identical for the two configurations. This is due to the drag coefficients being very close for the two nose shapes. The hypersonic drag coefficient for the blunt nose is  $C_D = 1.57$  while the comparable coefficient for the conical nose cone is  $C_D = 1.51$ .

---

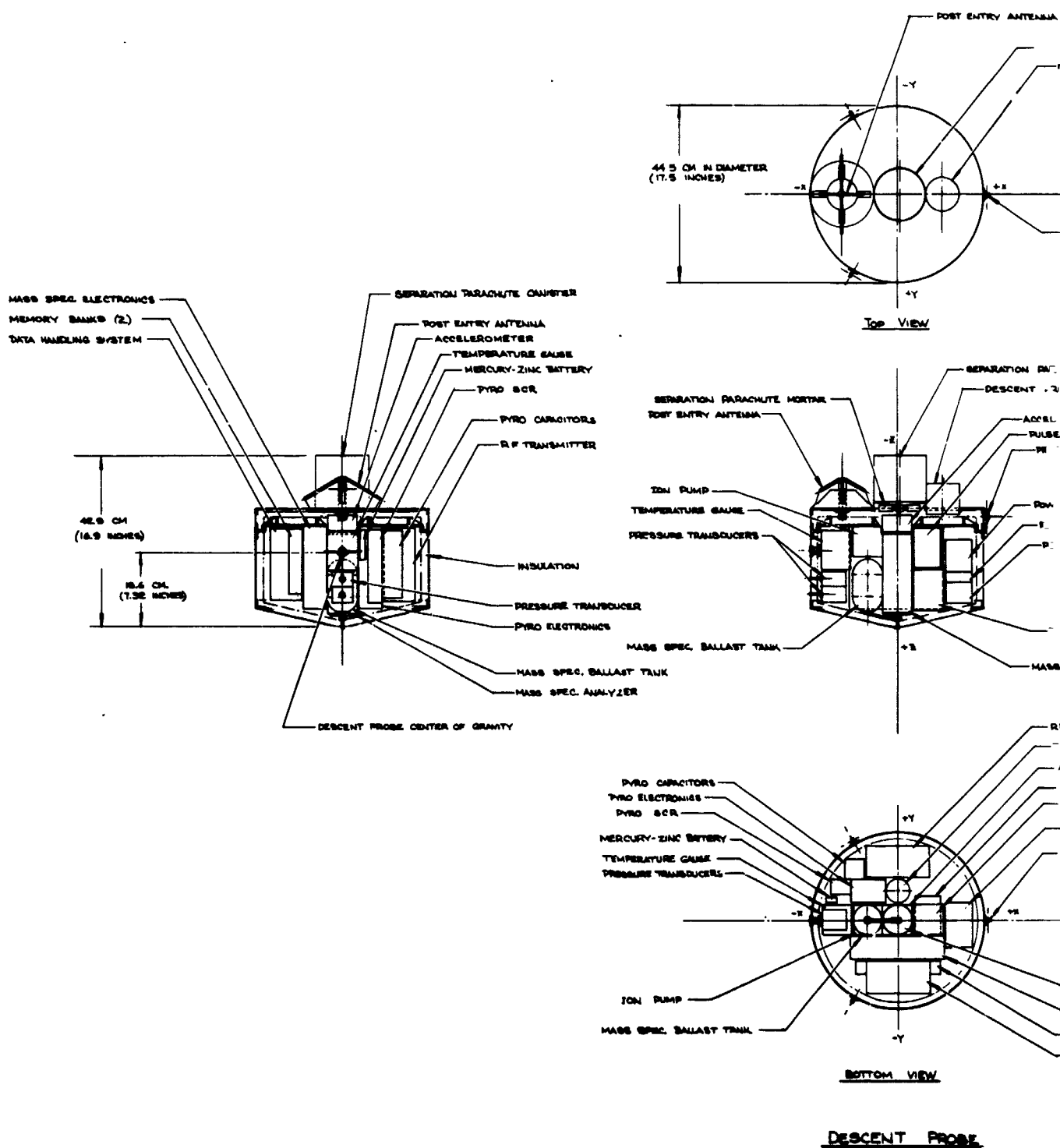
\*M. E. Tauber: *Heat Protection for Atmospheric Entry into Saturn, Uranus, and Neptune*. Preprint No. ASS-71-145, 17th Annual Meeting, American Astronautical Society, June 28, 30, 1971.

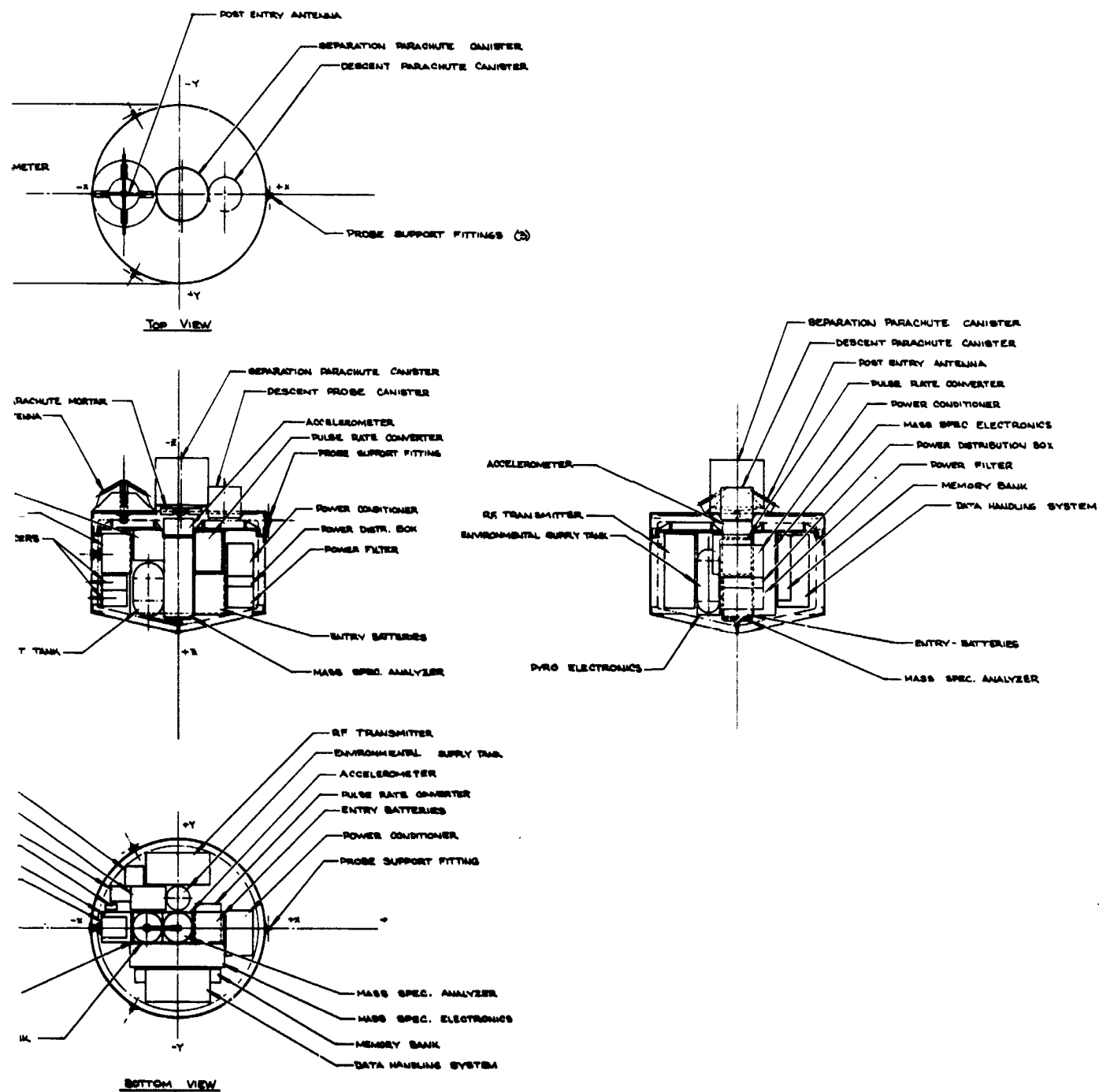
The Configuration 1 Saturn probe is shown in Figure VI-19. Generally speaking, this configuration is much like the Jupiter probes except for the changes necessary to accept the blunt shape of the aeroshell/heat shield assembly. This blunt nose shape of the aeroshell forces the descent probe nose to be blunted also, resulting in the inlet of the mass spectrometer being forced aft. The net result is that the mass spectrometer and the accelerometer above it are forced aft with respect to the equipment support deck. For this configuration, the equipment support deck incorporates a center hole permitting the accelerometer to project through and above the deck. This, in turn, forces the main parachute mortar further aft on the probe. The aeroshell for this configuration is kept as small in cross-section thickness as possible, to minimize the transfer of equipment location in the descent probe.

The ejected probe as separated from the spacecraft is 0.786 m (31.0 in.) in diameter, 0.803 m (31.6 in.) long including the deflection motor, and weighs 107.92 (237.88 lbm). The entry probe length is shortened to 0.482 m (19.0 in.) and the weight decreased to 67.63 kg (149.12 lbm), with the separation of the deflection motor and the service module before entry. The descent probe is 0.445 m (17.5 in.) in diameter, 0.429 m (16.9 in.) long, and weighs 37.33 kg (82.35 lbm). The descent probe is vented to the atmosphere during descent. The scientific instrument component complement is the same as that for the probe-dedicated Jupiter mission and for the spacecraft-radiation-compatible mission probes. The arrangement of these components and the supporting electrical and electronic components of the probe are shown on the figure.

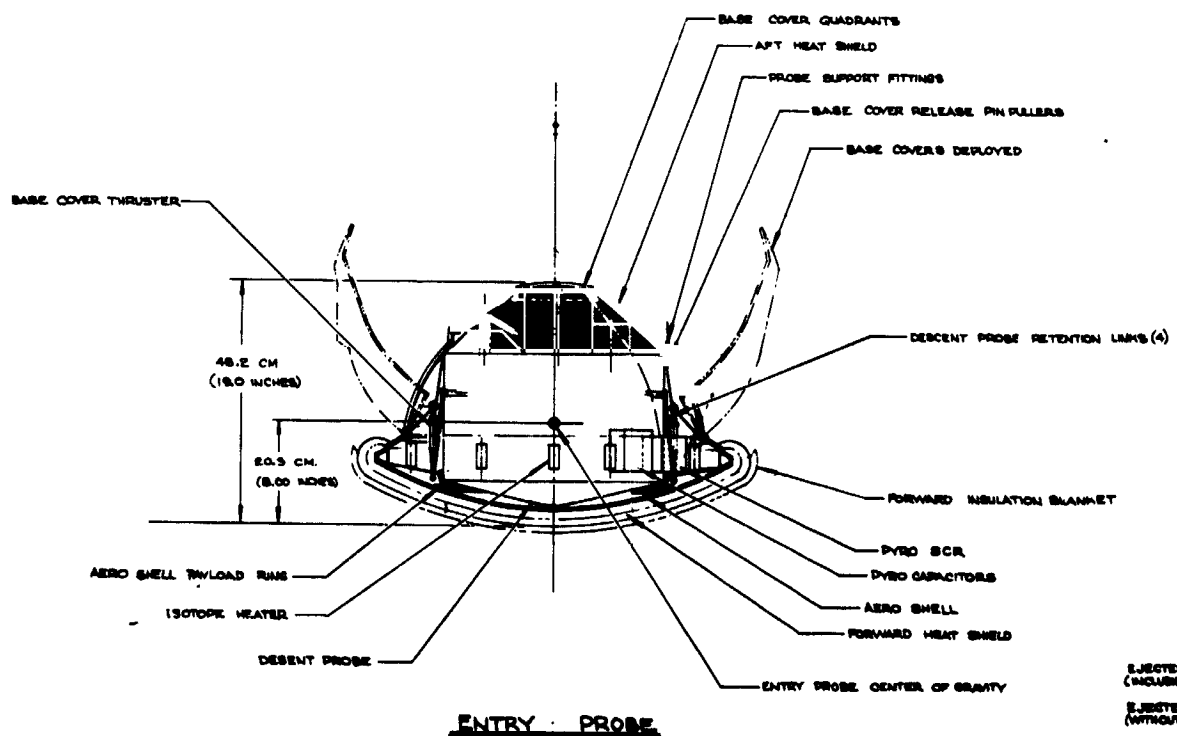
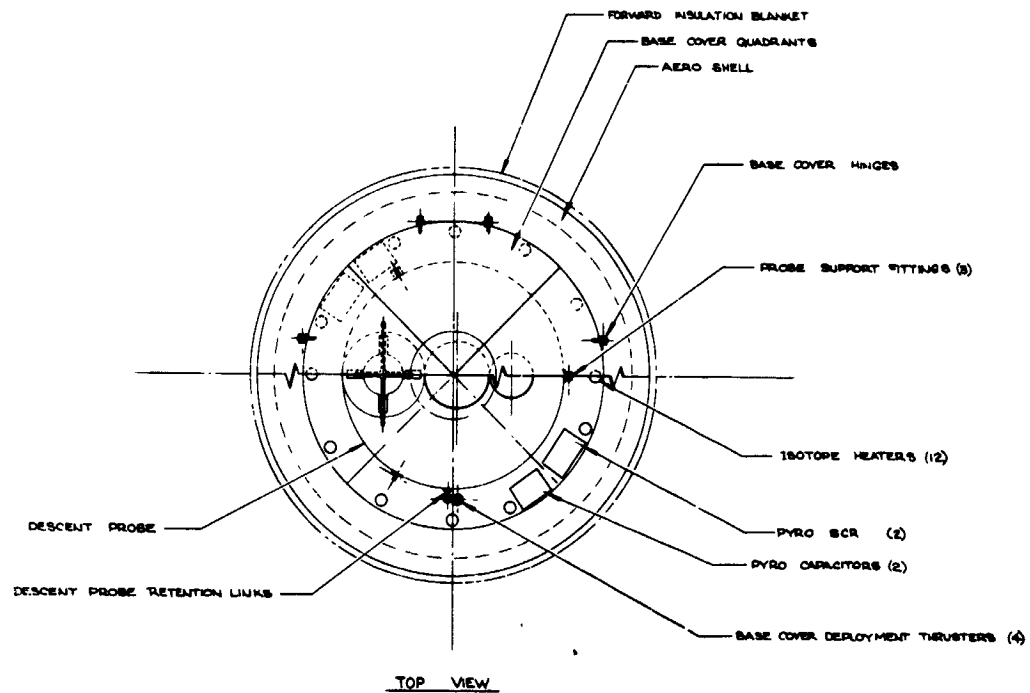
A service module provides for the attitude control of the probe after separation from the carrier spacecraft, and contains the attitude control propulsion and electronic subsystems. The service module is jettisoned after performing the probe spin-despin-precession maneuver. The aft end of the service module interfaces with the pre-entry antenna and the deflection maneuver motor. The deflection motor is jettisoned after the deflection maneuver. The pre-entry antenna is jettisoned along with the service module.

A dual parachute system is provided for this probe. This was done to provide separation of the descent probe from the aeroshell at staging. The descent parachute ballistic coefficient is too high to drag the descent probe from the aeroshell. Hence, a second larger parachute is used to provide a low ballistic coefficient for separation, and then jettisoned.





DESCENT PROBE



EJECTED PROBE CENTER OF GRAVITY (INCLUDING DEFECTION MOTOR)  
EJECTED PROBE CENTER OF GRAVITY (WITHOUT DEFECTION MOTOR)

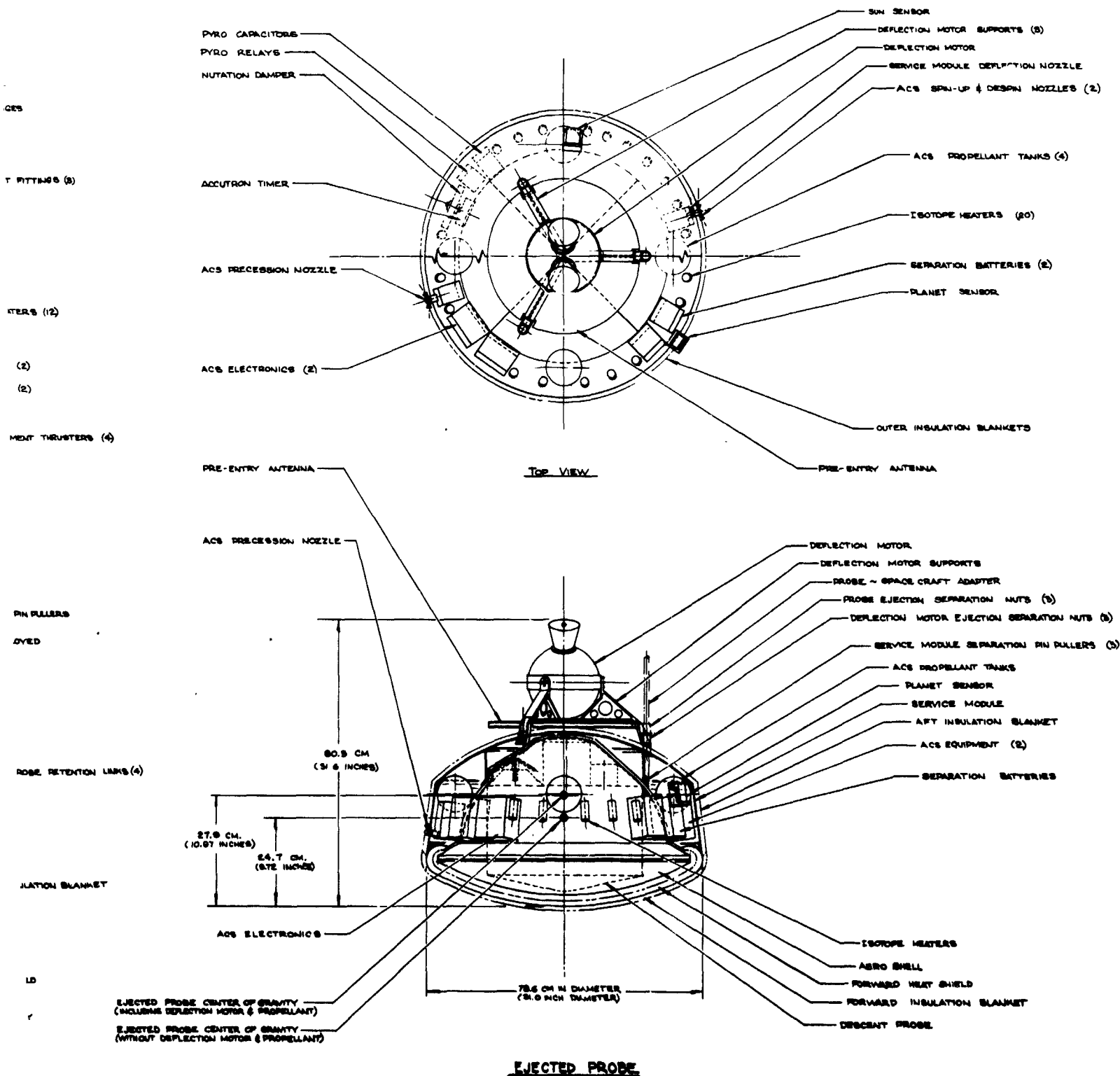
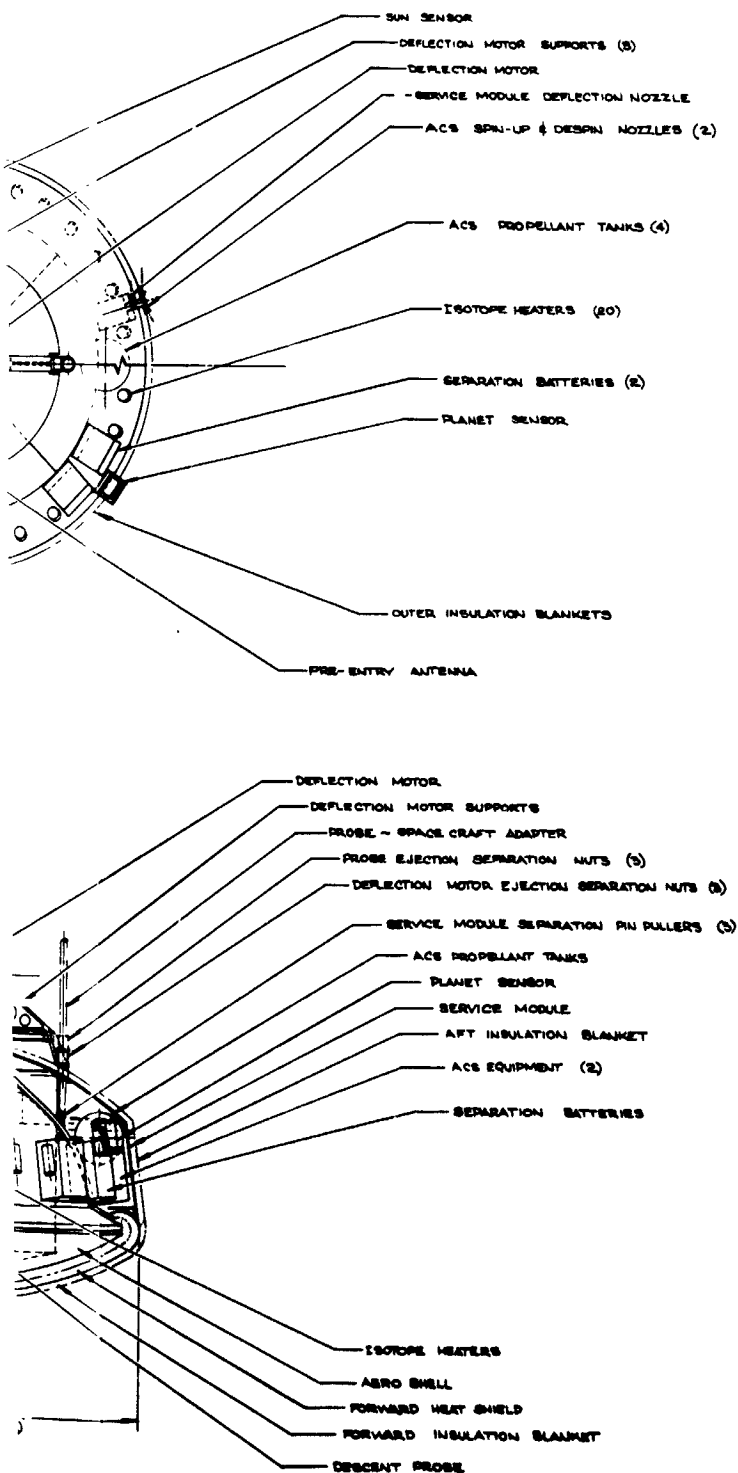


Fig.

FOLDOUT FRAME 4

FOLDOUT



R.E. COOK, 405 4427

REPT 100-100000-100-100

STURN SURVIVABLE PROBE -  
TASK V CONFIGURATION I  
OUTER PLANET ENTRY PROBE GRAB

Figure VI-19 Saturn Probe Configuration

VI-41 and VI-42

FOLDOUT FRAME



b. *Configuration and General Arrangement (Conical Nose)* - The second Saturn probe configuration investigated used a 1.04 rad (60°) half angle conical aeroshell/heat shield structure. Although the heat shield mass fraction is slightly larger than that for the blunt nose cone of Configuration 1, the conical aeroshell offers packaging advantages for the descent probe, and was thus investigated. The general arrangement of Configuration 2 is shown in Figure VI-20. For this configuration, the aeroshell structural arrangement is similar to that of the Jupiter probes. The nose of the descent probe is allowed to project forward into the aeroshell at approximately a 1.05 rad (60°) half angle cone, permitting the equipment arrangement to be less cramped and similar to that of the Jupiter probes. This packaging arrangement is a little cleaner than Configuration 1.

The aft cover for both configurations is designed like that of the Jupiter probes. The base cover is designed in quadrants that open after entry and are jettisoned by means of pyrotechnic thrusters. The Configuration 2 ejected probe as separated from the spacecraft is 0.786 m (31.0 in.) in diameter, 0.825 m (32.5 in.) long including the deflection motor, and weighs 114.9/kg (253.32 lbm). The entry probe length is shortened to 0.51 m (20 in.) and the weight decreased to 76.39 kg (168.40 lbm), with the separation of the deflection motor and the service module before entry. The descent probe is 0.445 m (17.5 in.) in diameter, 0.435 m (17.1 in.) long, and weighs 36.44 kg (80.33 lbm) pyrotechnic thrusters.

c. *Structural Design* - The Saturn probe is designed for entry at either the planet Saturn or Uranus. The entry conditions are close enough for the two planets that no appreciable structural weight penalty is involved in designing for the worst case. An entry deceleration of 380 g is encountered at Uranus as compared with 350 g at Saturn. Likewise, the planetary entry peak dynamic pressure occurs at Uranus. The peak dynamic pressure at Uranus of  $35.4 \times 10^4 \text{ N/m}^2$  (7400 lbf/ft<sup>2</sup>) compares with  $33.5 \times 10^4 \text{ N/m}^2$  (7000 lbf/ft<sup>2</sup>) for Saturn for the respective missions. Thus, the entry probe with the exception of the aeroshell is designed to 380 g deceleration loads. The aeroshell is designed by the normal pressure on the nose cone, which is a function of nose cone shape, and the peak dynamic pressure at planetary entry. The dynamic pressure at Uranus, which is slightly higher than at Saturn, is used for design.

The descent probe configuration is similar to that of the Jupiter probe, using a machined plate with integral stiffening beams for the equipment deck, and a probe sidewall using 10 longerons to transfer the deck load into the probe shell.

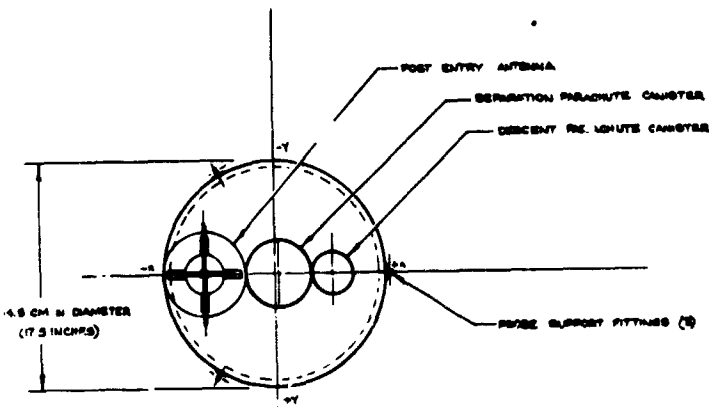
The nose cone aeroshell structure for Configuration 1 is a point design using a waffle-type structure. The aeroshell would be stretch-formed to a spherical segment, and chemically milled after forming to leave a grid work of intersecting reinforcing webs. Analyses show that an aeroshell having reinforcing webs approximately 0.63 cm (0.25 in.) high and fabricated of titanium would have approximately the same weight as the ring reinforced conical aeroshell.

The aeroshell structure of the Configuration 2 Saturn probe uses the ring-frame stiffened cone design of the Jupiter probes. The parametric data generated for Jupiter aeroshell structure, and presented in Chapter V, A.8 may be used for calculating the weight of the structure.

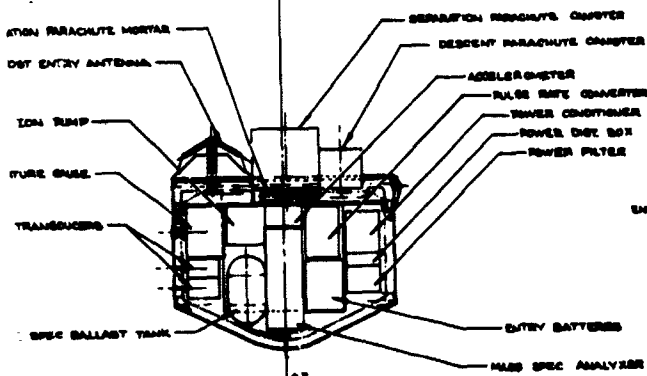
a. *Parachute Assembly* - A two-stage deceleration is supplied for the Saturn descent probe. This arrangement is necessary because of the high ballistic coefficient provided for descent into the atmospheres of Saturn and Uranus. The selected ballistic coefficient for descent is  $110 \text{ kg/m}^2$  ( $0.7 \text{ slug/ft}^2$ ). The spent aeroshell/heat shield assembly has a ballistic coefficient of  $43.5 \text{ kg/m}^2$  ( $0.25 \text{ slug/ft}^2$ ) after separation, and it is readily apparent that the descent parachute will not pull the descent probe away from the aeroshell. However, once the descent probe is on the descent parachute, it will outrun the aeroshell assembly. The same parachute configurations are satisfactory for use on either of the two Saturn probe designs investigated.

The ballistic coefficient for the separation parachute has been arbitrarily selected as half that of the spent aeroshell, or  $B = 21 \text{ kg/m}^2$  ( $0.12 \text{ slug/ft}^2$ ). This value provides reasonable relative deceleration of the descent probe to that of the aeroshell. For a value of dynamic pressure of  $1700 \text{ N/m}^2$  ( $36 \text{ lbf/ft}^2$ ), the relative deceleration is approximately 5 g, ample to provide separation.



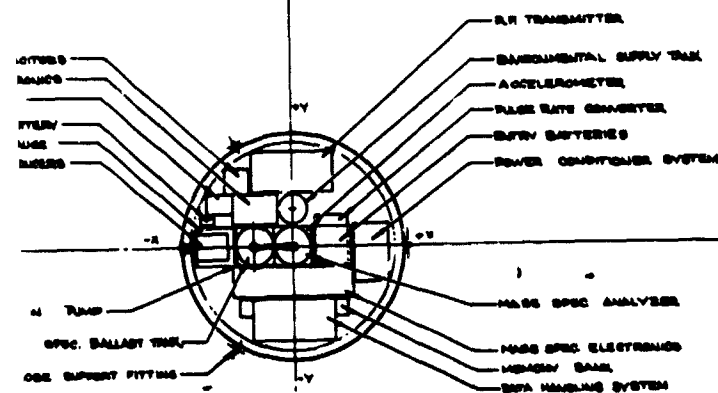


TOP VIEW



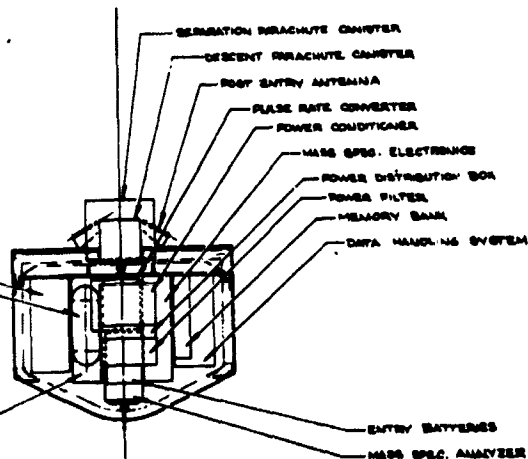
RF TRANSMITTER  
ENVIRONMENTAL SUPPLY TANK

ENTRY BATTERIES  
MASS SPEC. ANALYZER

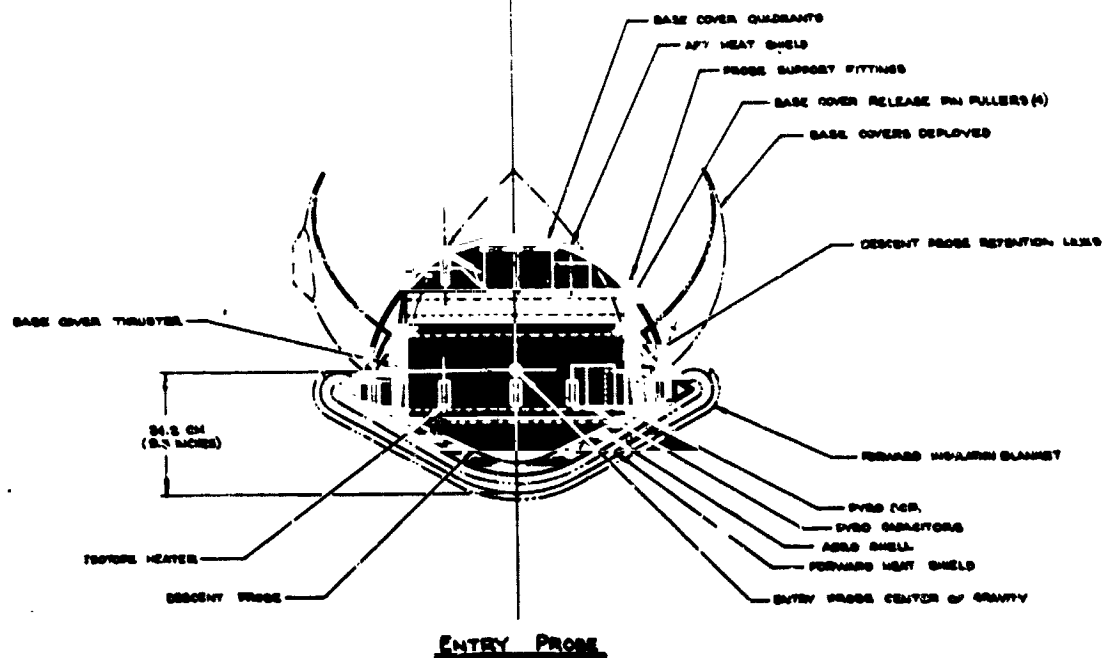
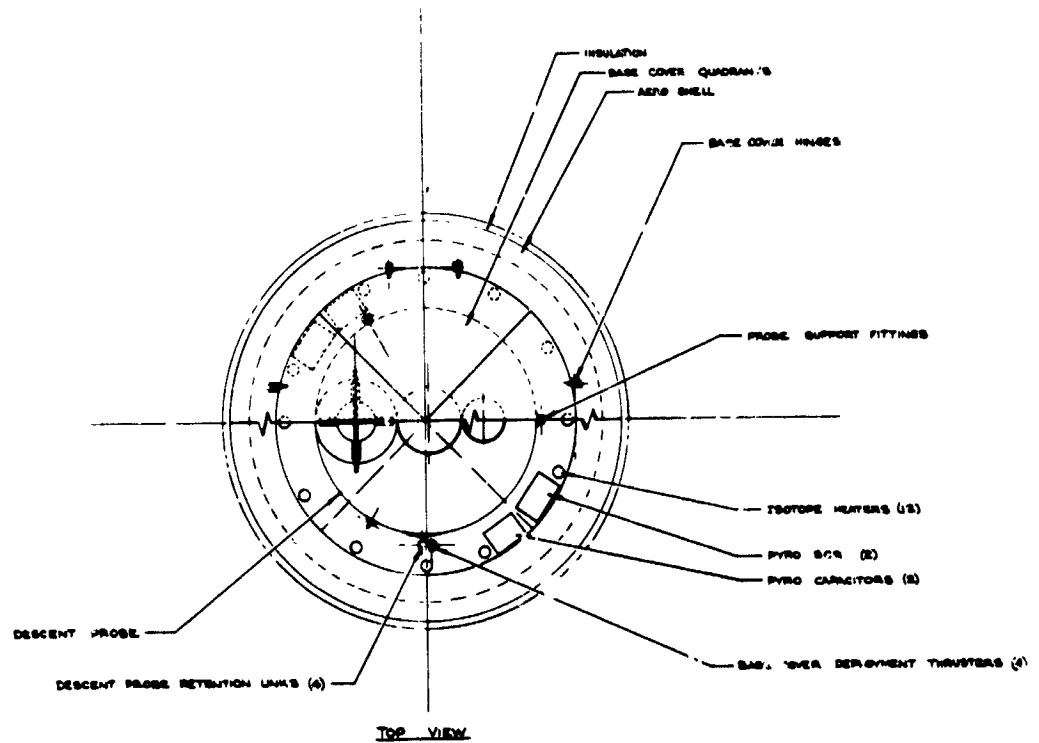


BOTTOM VIEW

DESCENT PROBE



ENTRY BATTERIES  
MASS SPEC. ANALYZER



QUADRANTS  
11

- BASE COVER HINGES

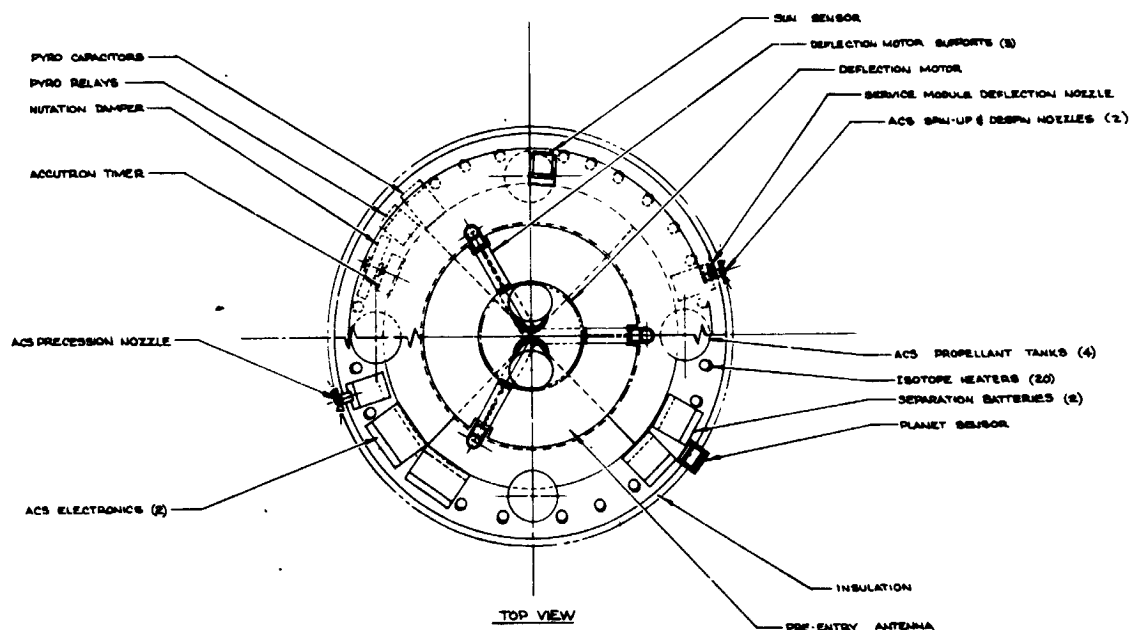
PROBE SUPPORT FITTINGS

ISOTOPE HEATERS (12)

PYRO SCR (2)

PYRO CAPACITORS (8)

BASE COVER DEPLOYMENT THRUSTERS (4)



LD  
PROBE FITTINGS

COVER RELEASE PIN PULLERS (4)

BASE COVERS DEPLOYED

DESCENT PROBE RETENTION LINKS

FORWARD INSULATION BLANKET

PYRO SCR

PYRO CAPACITORS

AERO SHELL

FORWARD HEAT SHIELD

PROBE CENTER OF GRAVITY

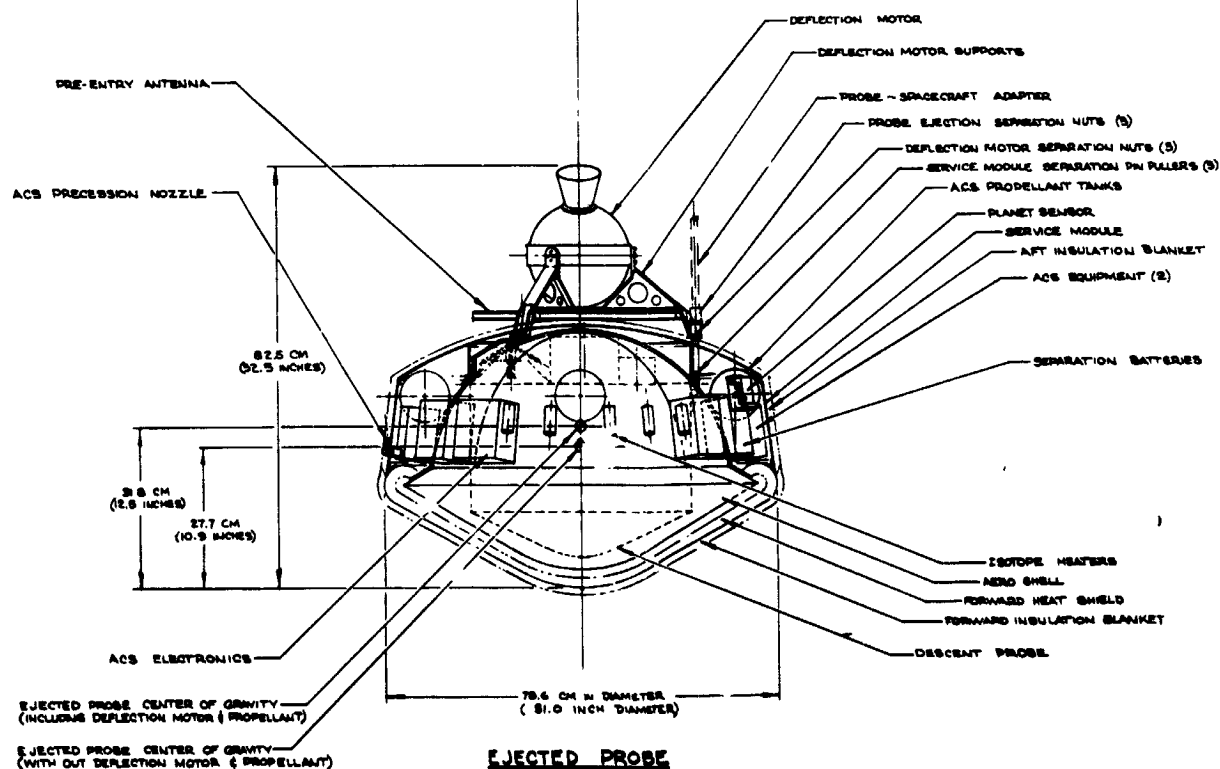
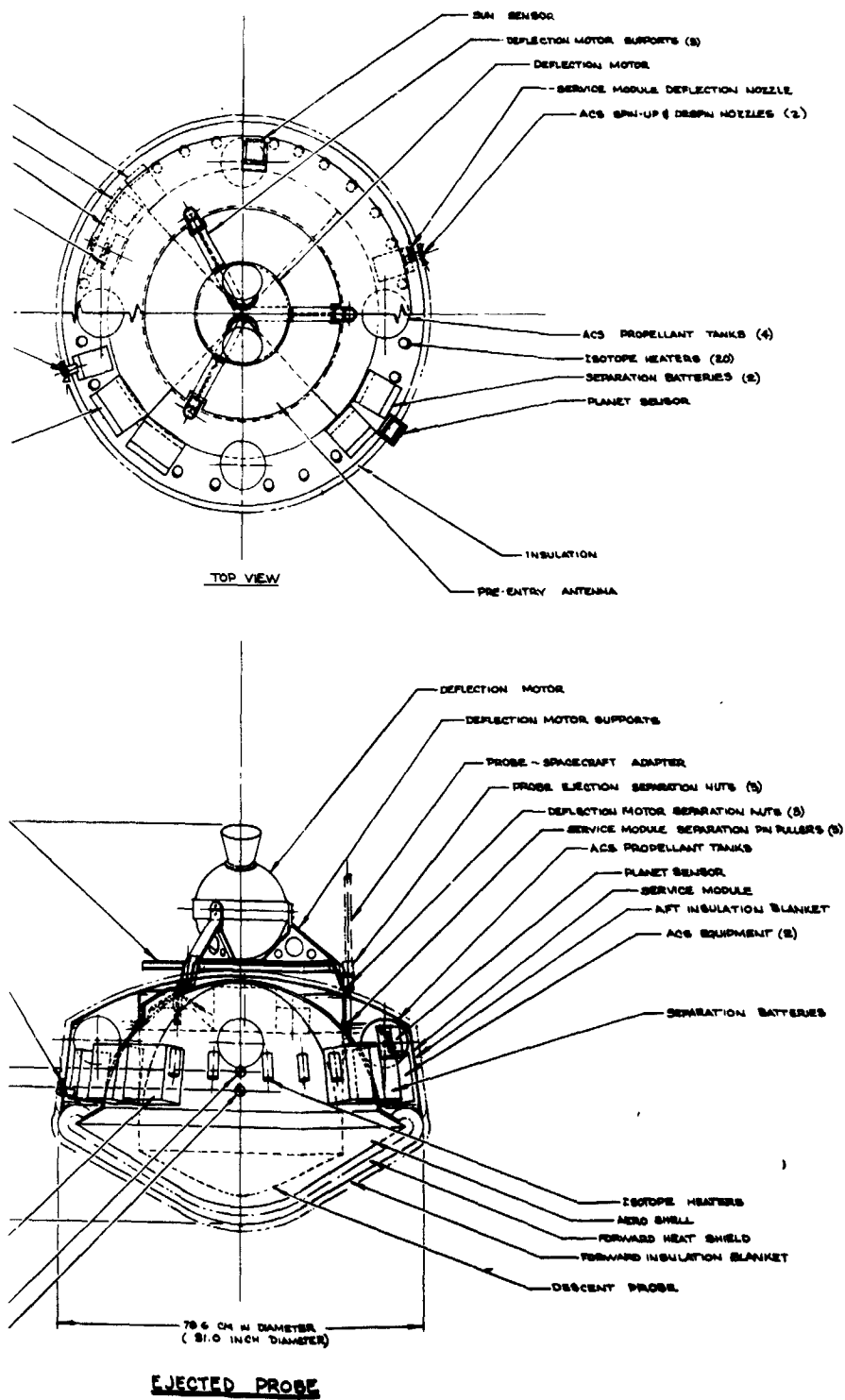


Figure VI-20



U.S. ORIGIN 000 4/2/72

WORTH RESEARCH & DEVELOPMENT

SATURN SURVIVABLE PROBE -  
TASK 2 CONFIGURATION 2  
OVER PLANET ENTRY PROBE STUDY

Figure VI-20 Alternative Saturn Probe Configuration

OUT FRAME 4

FOLDOUT FRAME 5

VI-45 and VI-46

The separation parachute is selected using the above ballistic coefficient and a descent probe mass of 37.2 kg (2.55 slug). This results in a parachute size of 2.1 m (6.8 ft) in diameter. This parachute is a disc-gap-band configuration. The parachute is deployed by a pyrotechnic mortar, and released after separation.

The descent parachute has a ballistic coefficient of  $110 \text{ kg/m}^2$  ( $0.7 \text{ slug/ft}^2$ ). For a descent probe weight of 37.2 kg (2.55 slug), this results in a parachute diameter of 0.67 m (2.2 ft). For parachutes this small, the drag of the entry probe body cannot be ignored. The probe body accounts for a fair percentage of the total drag. The above parachute diameter takes the probe body drag into account. The descent probe is a flat circular parachute.

*e. Heat Shield* - The nose cone heat shield design has been developed using heat shield mass fraction data developed by M. Tauber. These mass fractions are shown in Figures VI-21 and VI-22 for Saturn and Uranus entries. The mass fraction data for Saturn has been used for design of the probe heat shield since this is the more severe case. From Figure VI-21, it is seen that the heat shield mass fraction for the blunt body nose cone for a Saturn entry angle of  $30^\circ$  is 0.145. The mass fraction for the  $1.04 \text{ rad}$  ( $60^\circ$ ) conical nose and a Saturn entry angle of  $30^\circ$  is higher, approximately 0.215. The former (blunt body) results in a heat shield weight of approximately 8.93 kg (19.68 lbm) for configuration 1. Configuration 2 conical nose has a heat shield weight of approximately 14.2 kg (31.4 lbm). Therefore, the delta heat shield weight of between the two configurations is 5.27 kg (11.72 lbm).

The base cover heat shield for the probe is based on a heat pulse of 2% of the nose cone heat pulse. The methodology of determining the base cover heat shield is the same as that presented in the heat shield discussion of Chapter V, Section A.8. The heat pulse data to enter the ablator analysis is presented in Table VI-8 for the planets Saturn and Uranus. The resulting ablator protection required is presented in Table VI-9.

The base cover protection selected is that for the planet Saturn, the more severe of the two planets. The ablator material selected is ESA 3560, which is a filled silicone material reinforced with fiberglass honeycomb.



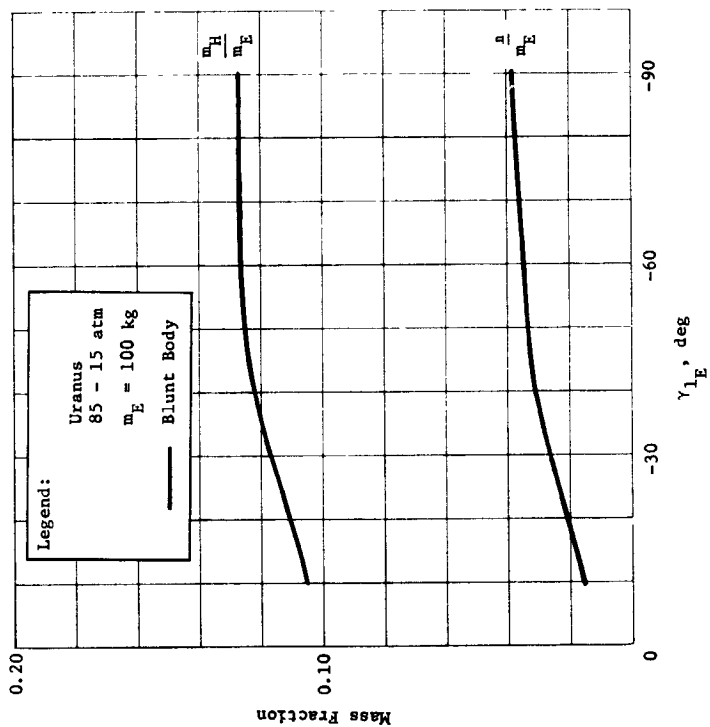


Figure VI-22 Heat Shield Mass Fraction vs Entry Angle for Planet Uranus

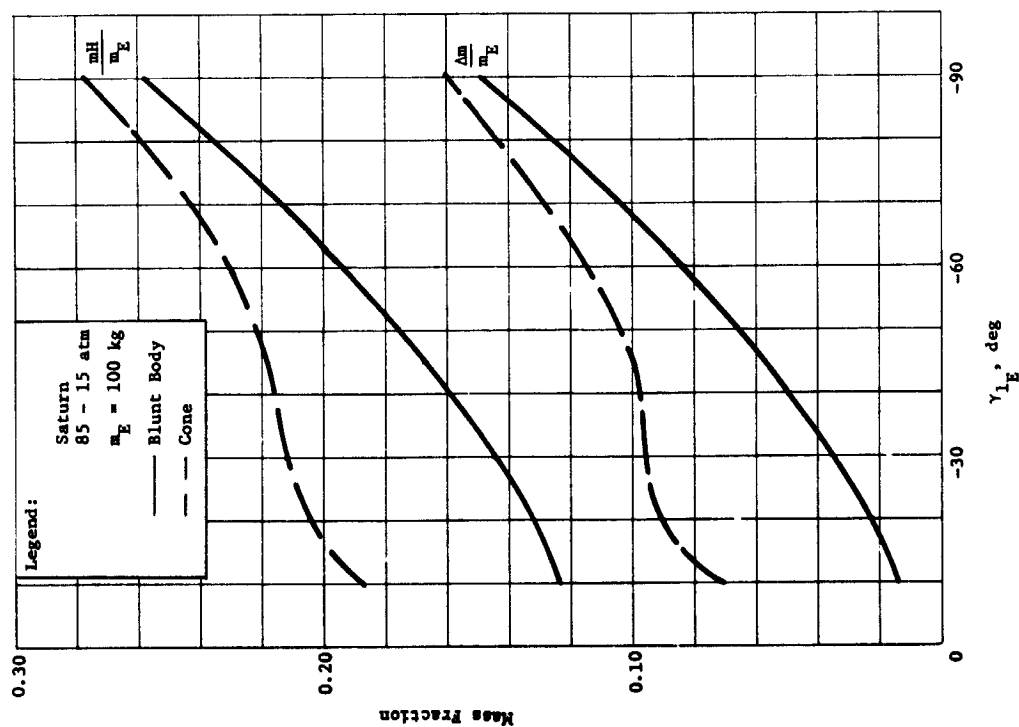


Figure VI-21 Heat Shield Mass Fraction vs Entry Angle for Planet Saturn

Table VI-8 Heat Pulse Data for Base Cover Ablator Analysis

Planet	$\gamma_E$	Peak HTG Rate, $\frac{\text{Btu}}{\text{ft}^2\text{-sec}}$	Total Heat, $\frac{\text{Btu}}{\text{ft}^2}$	Time of HTG Pulse, sec
Saturn	-60	158	475	
	-30	96.7	392	8.1
	-20	68.0	370	10.9
	-10	35.0	280	16.0
Uranus	-60	105.0	270	5.15
	-30	66.7	198	5.95
	-20	35.0	148	8.45
	-10	10.5	111	21.0

Table VI-9 Unit Weight of Ablator Required to Protect Base Cover Structure to 300°F Maximum during Planetary Entry

Planet	$\gamma_E$	Carbon Phenolic	ESA 5500-MB	ESA 3560	SLA 561	Quartz Phenolic
Saturn	-30	1.10	0.61	0.28		1.04
	-20	1.24	0.68	0.32		1.18
	-10	1.44	0.79	0.37	0.19	1.36
Uranus	-30	0.92	0.51	0.23		0.87
	-20	1.04	0.57	0.27	0.14	0.99
	-10	1.50	0.83	0.39	0.20	1.42

f. *Mass Properties* - The weight tabulation for the components of the Configuration 1 Saturn/Uranus probe are presented in Table VI-10.

Table VI-10 Weight Breakdown for the Saturn Probe (Configuration 1)

	Weight	
	Kg	Lb
<u>Science</u>		
Temperature Gauge	0.45	1.00
Pressure Transducer	0.68	1.50
Accelerometer	0.59	1.30
Sensor	0.91	2.00
Converter	1.81	4.00
Neutral Mass Spectrometer Analyzer	2.72	6.00
Electronics	0.45	1.00
Pump	0.45	1.00
Ballast Tank	8.06	17.8
<u>Power and Power Conditioning</u>		
Power Conditioner	0.91	2.00
Power Distribution Box	0.45	1.00
Power Filters	0.81	1.80
Entry Batteries	1.29	2.85
Post Separation Batteries	2.31	5.1
Mercury-Zinc Battery (Pyro)	0.41	.90
	6.18	13.65
<u>Cabling</u>		
Inner Probe	2.82	6.20
External Structure	2.04	4.50
	4.86	10.70
<u>Data Handling</u>		
Electronics	2.13	4.7
Memory Banks	0.45	1.0
	2.58	5.7
<u>Attitude</u>		
Sun Sensor	1.59	3.5
Planet Sensor	0.91	2.0
ACS System and Tanks	4.63	10.2
Nutation Damper	1.09	2.4
Accutron Timer	0.14	.3
ACS Electronics	1.36	3.0
	9.72	21.4
<u>Communications</u>		
Pre-entry Antenna	2.13	4.70
Post-entry Antenna	0.45	1.0
RF Transmitter	2.72	6.0
RF Switch	0.10	0.20
	5.40	11.90
<u>Pyrotechnic Subsystem</u>		
Pyro Electronics	0.91	2.00
Pyro Capacitors (Probe)	0.23	.5
Pyro Capacitors (External)	0.45	1.0
Pyro Relay (26) (External Ser Mod)	0.74	1.64
SCR (26) Probe	0.37	0.81
SCR (26) Aero Shell	0.37	0.81
Pyro Squibs	0.71	1.56
Pyro Thruster	0.45	1.00
	4.23	9.32
<u>Structures and Heat Shields</u>		
Descent Probe Structure	3.12	6.88
Equipment Support Deck	2.34	5.15
Base Cover	3.86	8.50
Service Module Structures	3.68	8.1
Aeroshell (2 lb for Payload Ring Added)	4.27	9.4
Forward Heat Shield (4.37 lb ablated during entry)	8.93	19.68
Aft Heat Shield (4.0 lb ablated during entry)	1.21	2.68
Deflection Motor Support	1.59	3.5
	29.00	63.89

Table VI-10 (cont)

	Weight	
	Kg	Lb
<u>Mechanisms</u>		
Separation Spring Cartridges	1.23	2.70
Separation Nuts	0.64	1.4
Pin Puller	0.82	1.8
Latches and Bands	0.91	2.0
Descent Parachute	0.41	0.9
Separation Parachute	3.43	7.56
	7.44	16.36
<u>Thermal</u>		
External Insulation Blanket (Forward Heatshield)	1.23	2.7
External Insulation Blanket (Base Cover)	1.59	3.5
Probe Hull Insulation (Internal)	1.59	3.5
Isotope Heaters 2 - 2	1.82	4.0
Environmental N <sub>2</sub> tanks	0.50	1.1
	6.73	14.8
<u>Propulsion</u>		
Deflection Motor Cases	2.50	5.50
Deflection Motor Propellant	6.13	13.50
ACS Propellant	1.06	2.33
	9.69	21.33
Total	93.84	206.85
15% Contingency	14.08	31.03
	107.92	237.88
<u>Items Deployed for Despun Weight</u>		
Deflection Motor Supports	1.59	3.5
Separation Spring Cartridges	0.18	0.4
Separation Nuts	0.32	0.7
ΔV Motor Cases	2.50	5.5
Propellant	7.19	15.85
	11.78	25.93
15% Contingency	1.77	3.90
(237.88 - 29.83 = 208.05 lb)	13.55	29.83
107.92 - 13.55 = 94.37 kg		
<u>Entry Weight</u>		
Preentry Antenna	2.13	4.7
External Cabling	2.04	4.5
Sun Sensor	1.59	3.5
Planet Sensor	0.91	2.0
ACS System (including tanks)	4.63	10.02
Nutation Damper	1.09	2.4
Accutron Timer	0.14	0.3
Pyro Capacitors	0.23	0.5
Pyro Relays	0.74	1.64
Service Module Structures	3.68	8.1
Separation Spring Cartridge	0.41	0.9
Separation Pin Pullers	0.41	0.9
External Base Cover Insulation Blanket	1.59	3.5
Separation Battery	2.31	5.1
ACS Electronics	1.36	3.0
	23.25	51.24
15% Contingency	3.49	7.69
(208.05 - 58.93 = 149.12 lb)	26.74	58.93
94.37 - 26.74 = 67.63 kg		
<u>Post Entry Weight</u>		
Forward Heat Shield Ablated	1.98	4.37
Aft Heat Shield Ablated	0.86	1.90
Insulation Blanket (Forward H.3)	1.23	2.7
	4.07	8.97
15% Contingency	0.61	1.34
(149.12 - 10.31 = 138.81 lb)	4.68	10.31
67.63 - 4.68 = 62.95 kg		

Table VI-10 (concl)

	Weight	
	Kg	Lb
<u>Weight on Parachute (Initially)</u>		
Base Cover Quadrants	3.86	8.5
Base Cover Heat Shield (not ablated)	0.35	0.78
Separation Pin Pullers	0.41	0.9
Separation Nuts	0.23	0.5
Isotope Heaters	0.91	2.0
Pyro Thrusters	0.45	1.0
	<u>6.21</u>	<u>13.68</u>
15% Contingency	0.93	2.05
(138.81 - 15.73 = 123.08 lb)	<u>7.14</u>	<u>15.73</u>
62.95 - 7.14 = 55.81 kg		
<u>Weight on Parachute (Final)</u>		
Separation Parachute	1.09	2.4
Pyro Capacitors	0.23	0.5
Pyro SCR	0.37	0.81
Pyro Squibs	0.72	1.6
Aero Shell	4.26	9.4
Forward Heat Shield (not ablated)	6.95	15.31
Spring Cartridges	0.41	0.9
Separation Nuts	0.23	0.5
Latches & Band	0.91	2.00
Isotope Heaters	0.91	2.00
	<u>16.08</u>	<u>35.42</u>
15% Contingency	2.41	5.31
(123.08 - 40.73 = 82.35 lb)	<u>18.49</u>	<u>40.73</u>
55.81 - 18.49 = 37.32 kg		

## 9. Propulsion Subsystem

The propulsion subsystem for the Saturn/Uranus probe consists of a spherical solid propellant motor to provide the deflection maneuver delta velocity, and a cold gas attitude control propulsion system. The deflection motor provides a delta velocity of 170 m/sec (557 fps) for the deflection maneuver. The attitude control system provides sufficient cold gas (nitrogen) propellant to spin the probe to 10.5 rad/sec (100 rpm), precess the probe through an angle of  $66^\circ$ , despin to an angular rate of 0.52 rad/sec (5 rpm), and finally impart a delta velocity of 0.46 m/sec (1.5 fps) to deflect the service module at jettisoning of the module. These systems are described in the following paragraphs.

*Deflection Motor* - The deflection motor for the Saturn probe is the smallest of those investigated for the various planetary probes. The configuration of the motor is similar to that defined in Chapter V, Section B.9. This motor is 20.3 cm (8.0 in.) in diameter and weighs 8.9 kg (19.6 lbm). It is a spherical solid propellant motor using, like the other motor designed, a dual nozzle to avoid particulate impingement on the carrier spacecraft at motor ignition. The motor is designed to impart a velocity of 170 m/sec (557 fps) to a probe weighing 114 kg (252 lbm). The delta velocity of 170 m/sec is applicable to either the planet Saturn or Uranus, since these planets can use a common deflection delta velocity. The probe weight is also common for either planet, thus permitting the motor design to be compatible for entry in either planet.

*Attitude Control System* - The attitude control system for the Saturn planet is smaller than the other probes investigated, having a moment of inertia of approximately  $6.6 \text{ kg/m}^2$  ( $5.0 \text{ slug/ft}^2$ ). Thus, for a given spinup rate, less total impulse is required. However, the spin-despin-precess nozzles have a smaller moment arm due to the probe smaller size. This parameter partially offsets the gain of reduced moment of inertia. The net result is a small reduction in gas weight and gas container weight for the ACS system. The functional diagram is similar to that defined in Chapter V, Section B.9.

The precession maneuver at Saturn is 1.15 rad ( $66^\circ$ ) while that required at Uranus is only 0.42 rad ( $24^\circ$ ). The cold gas supply is based on the larger of the two precession angles, such that the common probe may be used to enter either planet. The spinup rate before performing the deflection maneuver is the same as that applied to other probes, namely 10.5 rad/sec (100 rpm).

Likewise, the despin maneuver is 10.0 rad/sec (95 rpm), and the service module deflection maneuver is 0.46 m/sec (1.5 fps). The total propellant gas requirement for the above maneuvers is 1.05 kg, 2.33 lbm, and the gas container weight is 1.37 kg (3.02 lbm) for a total system weight of 5.7 kg (12.6 lbm).

#### 10. Thermal Control Subsystem

A probe thermal analysis was performed for the nominal Saturn probe mission defined. The basic probe configuration consisted of a 78.6 cm diameter entry probe design with probe propulsion, Sun and planet sensors, and an attitude control system. On the basis of the thermal analysis, a complete thermal history of probe was constructed and is presented in Figure VI-23. These results show that the thermal design selected is adequate to maintain the probe temperatures within limits throughout the mission specified. Trajectory uncertainties for this mission are 8 min, which is small from a thermal control standpoint. In addition, the RF transmitter power required for Saturn is small (6.5 watts RF); consequently no transmitter thermal problems would be expected. For the descent to 7 bars, the N<sub>2</sub> gas environment control to 2.5 bars pressure was selected for optimum design.

The probe temperature margins predicted for the Saturn probe mission are:

<u>Temperature Margin</u>	<u>Spacecraft Cruise, °K</u>	<u>Probe Coast, °K</u>	<u>Entry &amp; Descent, °K</u>
Above Equipment Lower Limit	42	18	9
Below Equipment Upper Limit	8	25	27
Below Transmitter Upper Limit	--	38	47

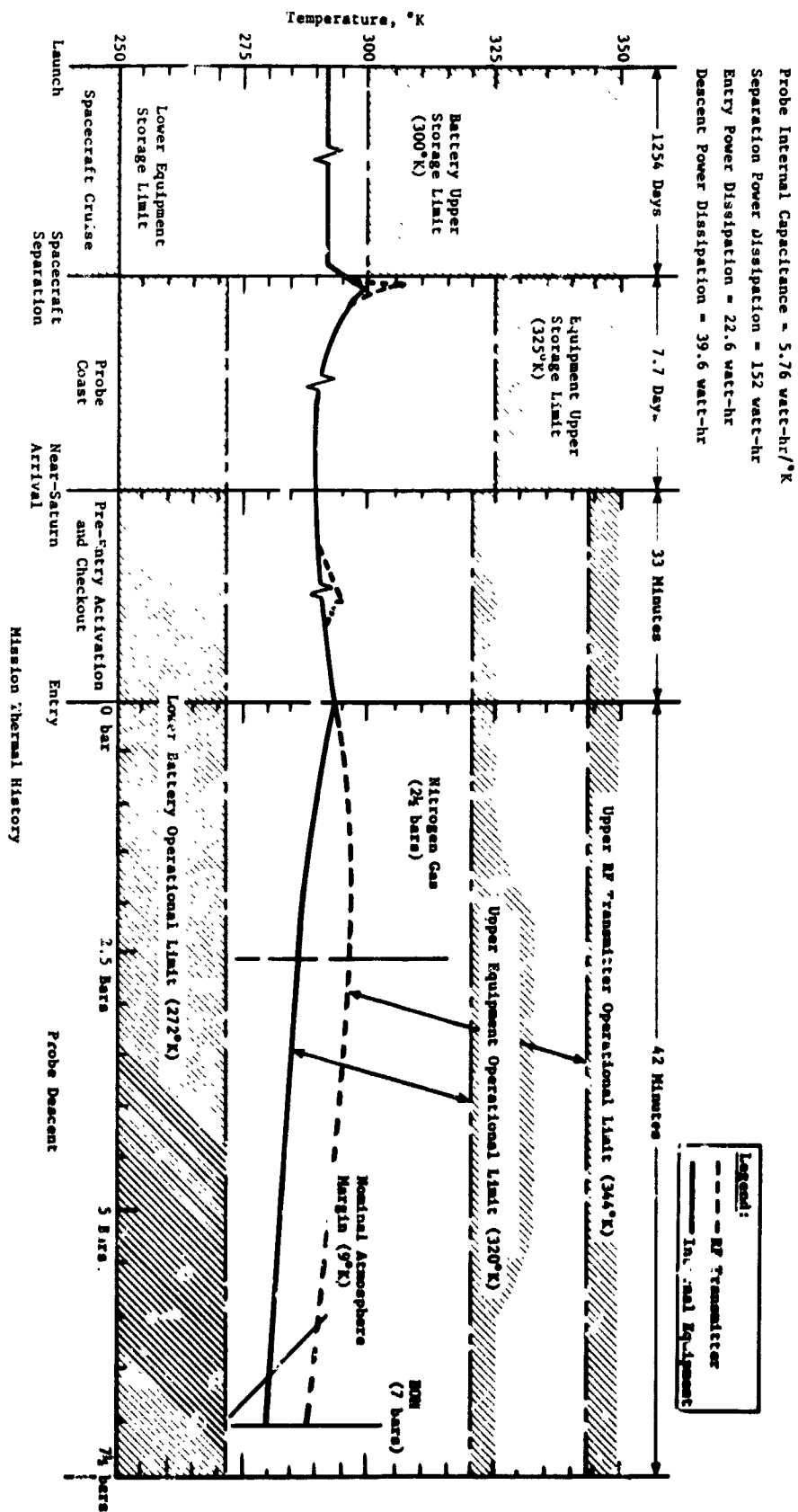


Figure VI-23 Launch to Descent Thermal History of the Saturn Probe



## 11. Spacecraft Integration

The Saturn probe has been studied for integration with the JPL Mariner Spacecraft, Configuration 2 (JPL Drawing No. 10054478). This spacecraft configuration is shown in Figure VI-24.

The integration of the Saturn probe and the Mariner spacecraft must have minimal impact on the mission and operation of the spacecraft. The probe is positioned on the spacecraft to provide for proper ejection, minimum effect on the spacecraft subsystems and least amount of modification of the original spacecraft concept.

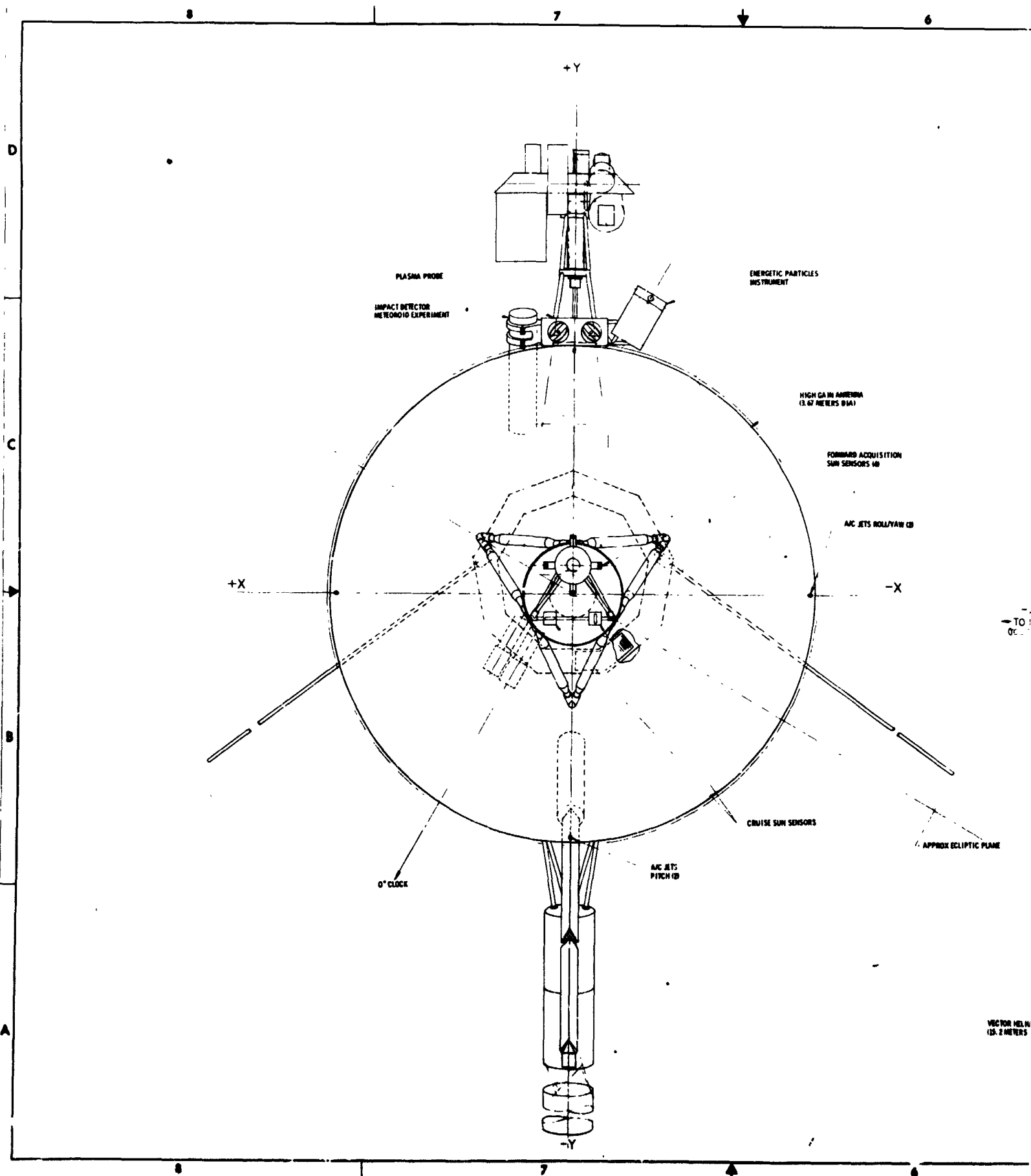
The probe is mounted on the aft end of the spacecraft with its centerline angled  $31^\circ$  to the spacecraft center line, away from the trajectory correction motor. The probe is supported by tubular trusses from the center cavity of the equipment bay module permitting the deflection motor to nest into that cavity.

The probe integration with this spacecraft is shown in Figure VI-25. The probe shown in the figure is actually the alternative Saturn probe using a  $1.04$  rad ( $60^\circ$ ) half angle nose cone, rather than the blunt nose primary configuration. The installation would be essentially the same for either probe configuration, since there are only minor differences in the probes.

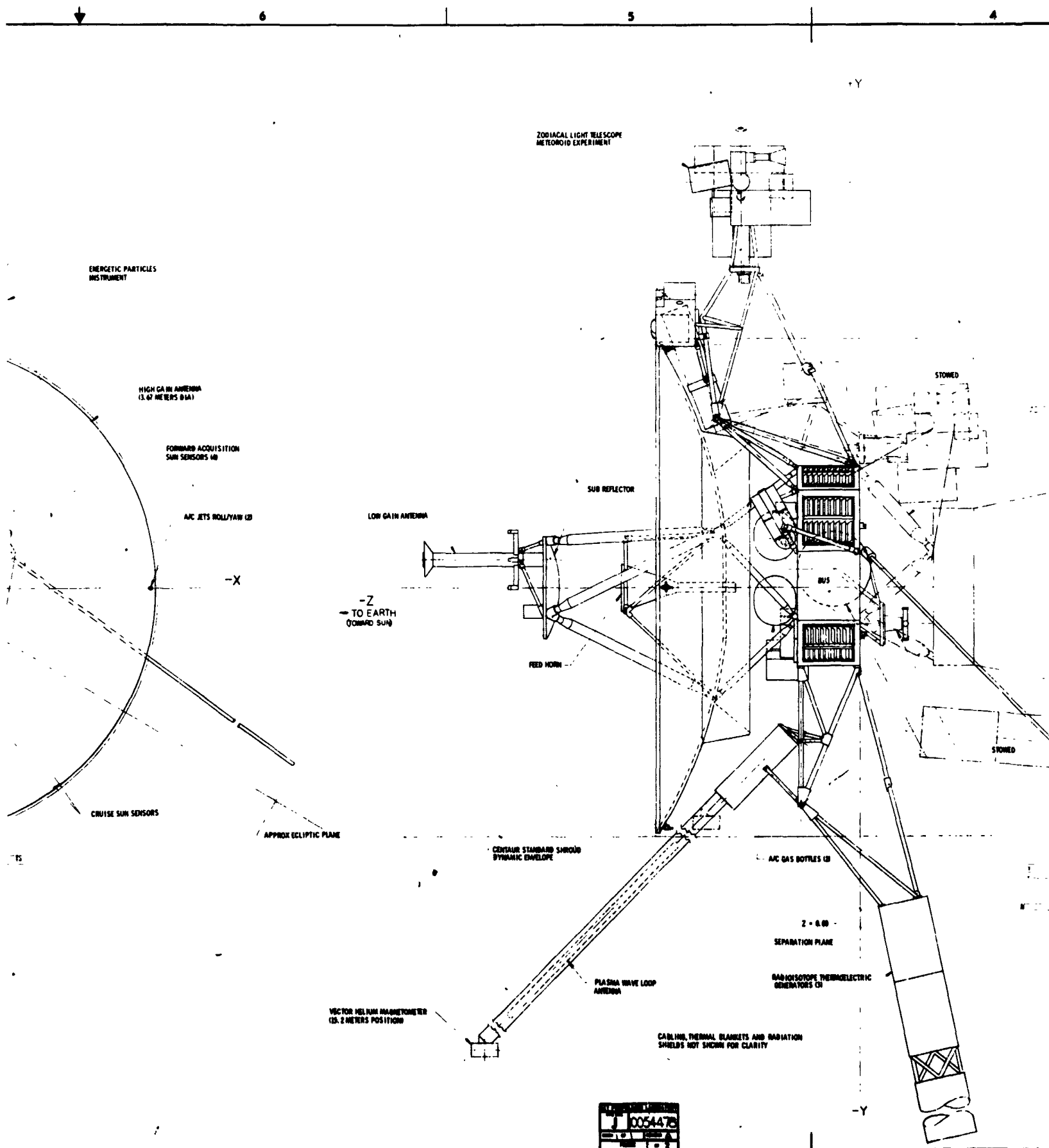
The probe is mounted so that it partially intrudes into the volume of the polygon basic body of the spacecraft. This is done to minimize the center of gravity shift of the spacecraft-plus-probe configuration as compared with that of the spacecraft-only configuration. It is mounted on the end of the spacecraft opposite the spacecraft communication antenna, so that the probe is pointed away from the Sun during most of the cruise portion of flight. This permits better thermal control of probe during the cruise phase.

Certain changes are necessary for the Mariner spacecraft to locate the probe as shown in Figure VI-25. These changes are:

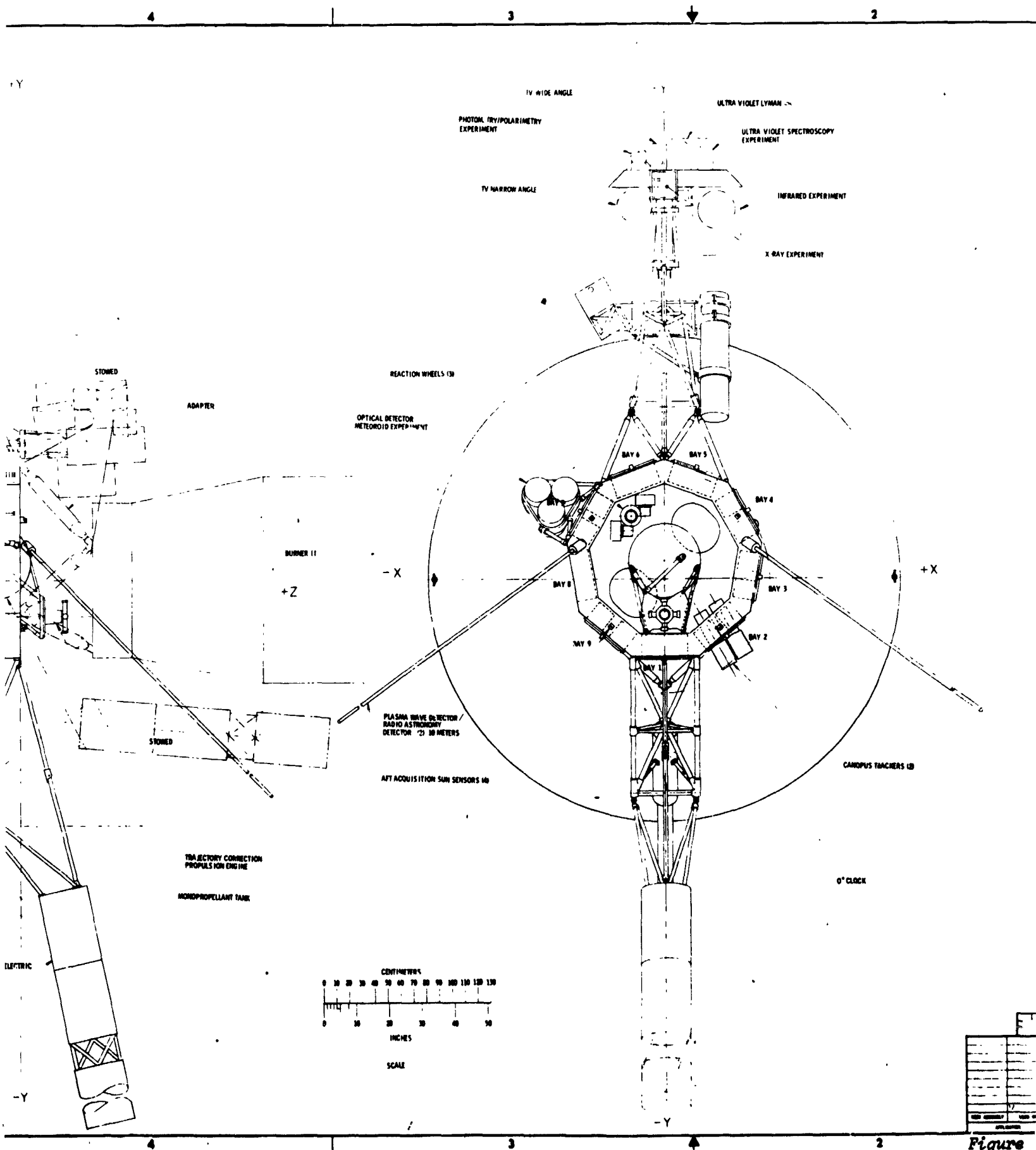
- 1) Move spacecraft propellant tank forward;
- 2) Move the spacecraft trajectory motor aft;
- 3) Relocate the ACS propellant bottles slightly outboard;
- 4) Provide an adapter structure for probe support;
- 5) Lengthen the spacecraft-to-Burner II support truss.



FOLDOUT FRAME



FOLDOUT FRAME 2



1	2	3	4
5	6	7	8
9	10	11	12
13	14	15	16
17	18	19	20
21	22	23	24
25	26	27	28
29	30	31	32
33	34	35	36
37	38	39	40
41	42	43	44
45	46	47	48
49	50	51	52
53	54	55	56
57	58	59	60
61	62	63	64
65	66	67	68
69	70	71	72
73	74	75	76
77	78	79	80
81	82	83	84
85	86	87	88
89	90	91	92
93	94	95	96
97	98	99	100

Figure

FOLDOUT FRAME 3

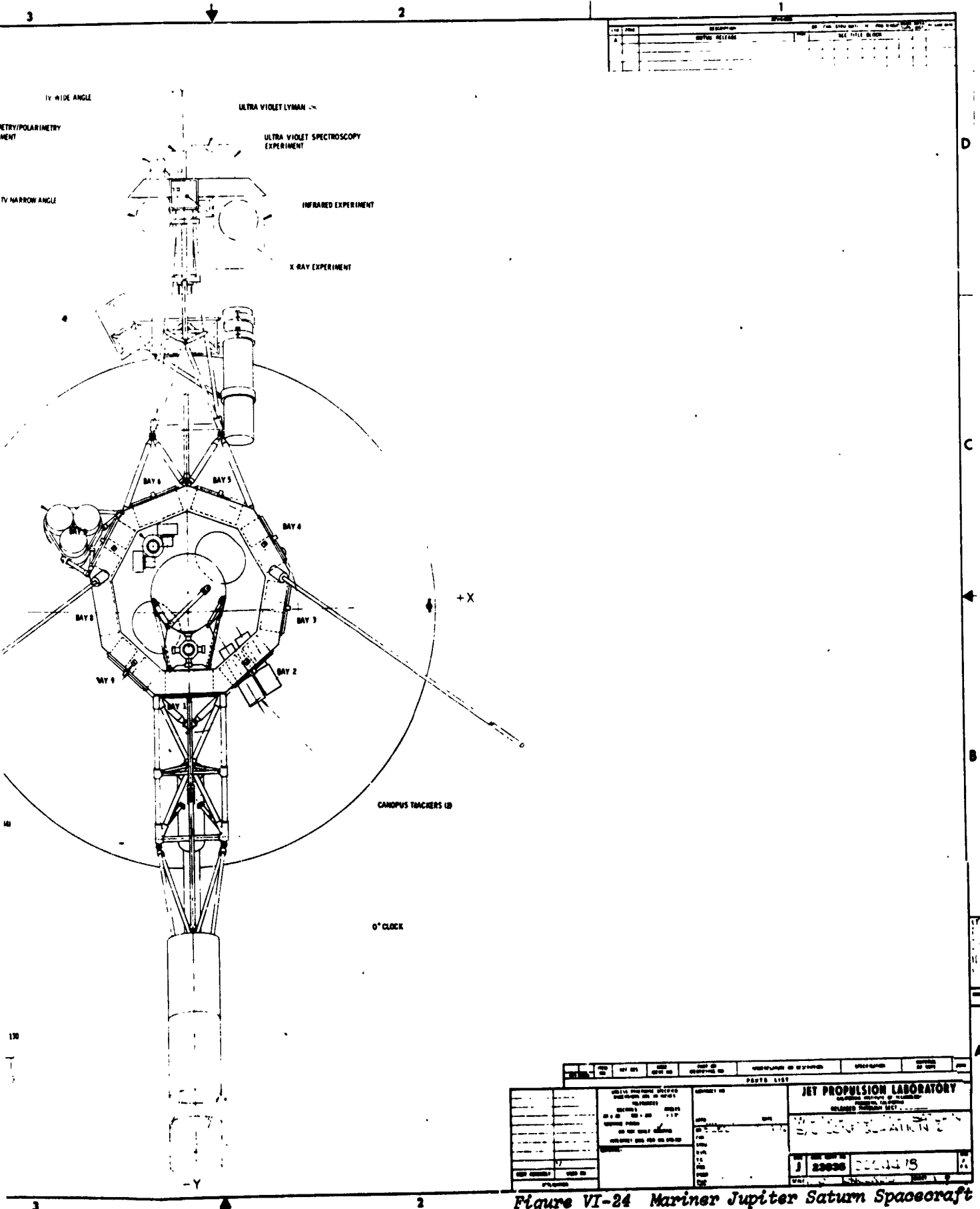
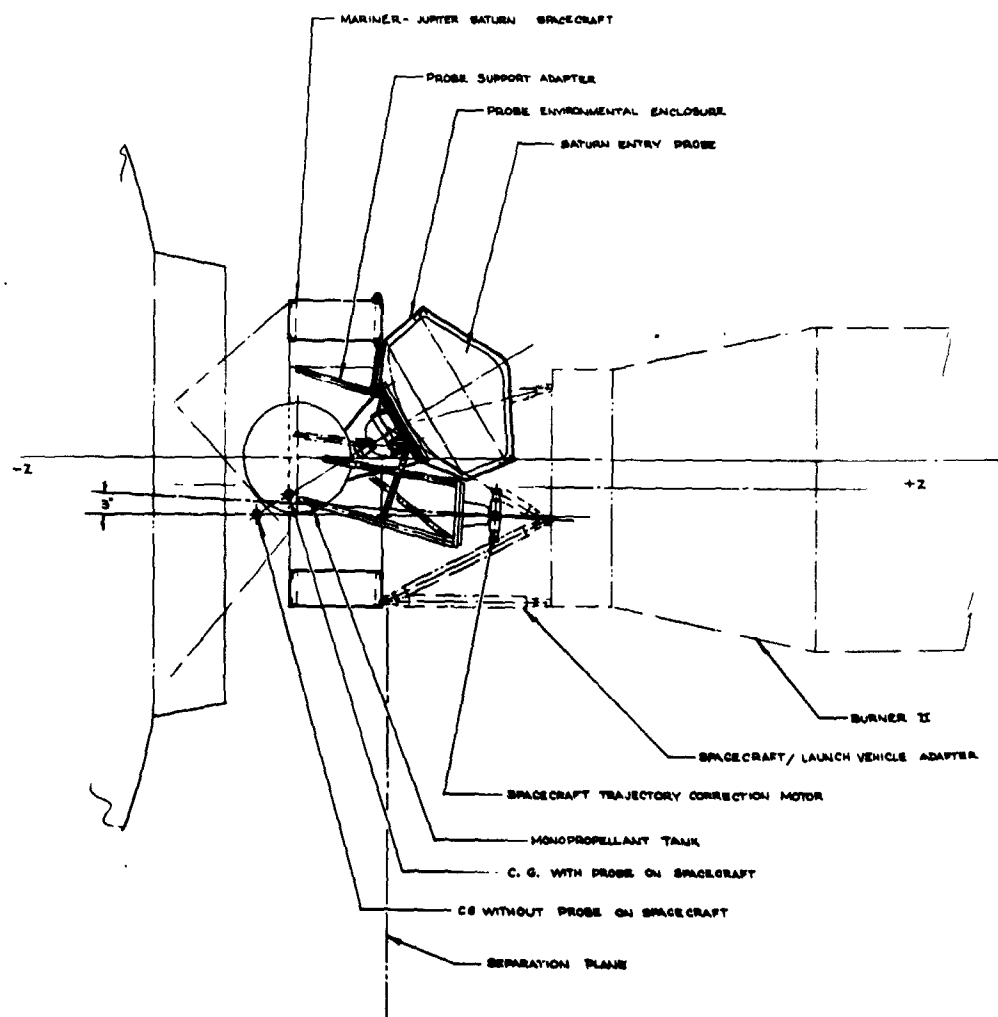


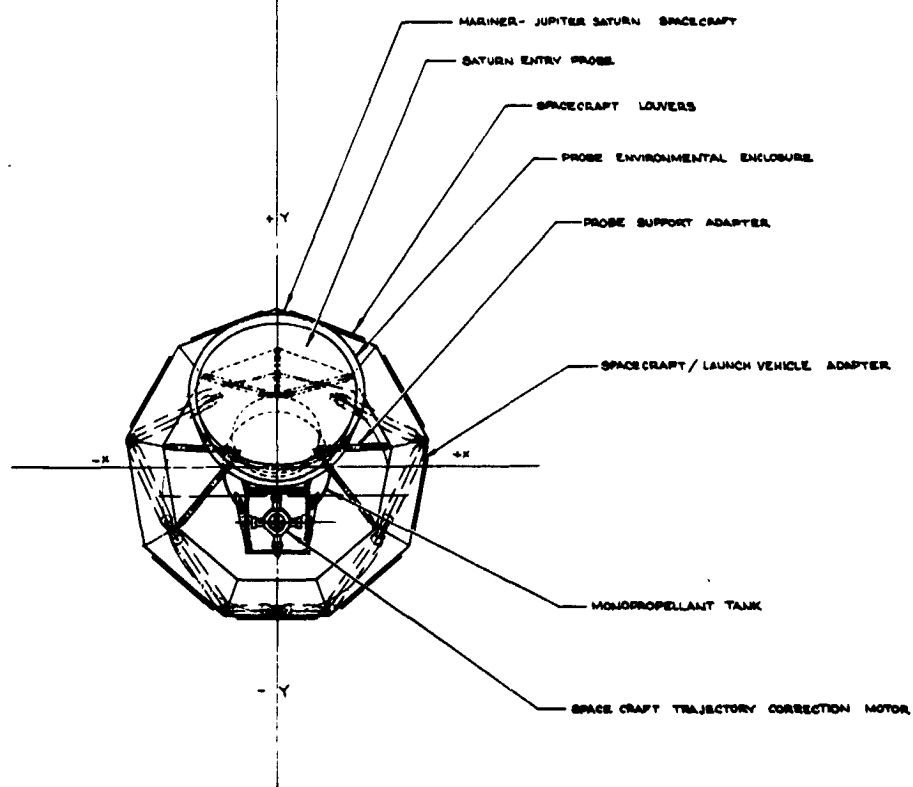
Figure VI-24 Mariner Jupiter Saturn Spacecraft VI-57 and VI-58

ME 3

FOLDOUT FRAME 4



FOLDOUT FRAME



1/1 170K 400 64/72

SATURN SURVIVABLE PROBE (MARINER-  
JUPITER SATURN SPACECRAFT  
INTERFACED ARRANGEMENT - SUPER

Figure VI-25 Spacecraft Probe Integration Configuration

VI-59 and VI-60

EOLDOUT FRAME 2

The spacecraft propellant tank was moved approximately 30.5 cm (12 in.) forward, toward the high gain antenna, to provide clearance for inserting the probe into the spacecraft polygon cavity. The ACS propellant tanks were moved outboard only far enough to permit clearance for the relocated spacecraft propellant tank.

The spacecraft trajectory correction motor was moved 19 cm (7.5 in.) aft to reduce the exhaust impingement on the probe environment enclosure, requiring an 45.7 cm (18 in.) increase to the supporting truss between the motor and the monopropellant tank. The spacecraft support adapter on Burner II was lengthened from 57.2 cm (22.5 in.) to 85 cm (33.5 in.) to maintain the clearance between Burner II and the payload hardware.

In relocating the trajectory motor, the motor pointing angle was also changed 0.05 rad ( $3^\circ$ ) outboard so that the nominal thrust vector was half way between the location of the spacecraft-only center of gravity and that of the combined spacecraft plus probe. Thus, the thrust vector location is a compromise, but probably acceptable.

The mounting angle of the probe on the spacecraft is such that the extended centerline of the probe passes through the center of gravity of the spacecraft. This is deemed necessary to minimize tipoff rates at spacecraft/probe separation. With this arrangement, the separation spring force thrust vector passes through the center of gravity of both bodies and thus should produce zero (or low) tumbling rates at separation. Another approach would be to fold some of the spacecraft instrumentation booms to vary the spacecraft center of gravity at probe separation, thus permitting more flexibility in possible probe pointing attitudes; however, this causes increased spacecraft complexity.

A multiple spring system has been selected for separation of the probe from the spacecraft. Analysis and test for the Air Force Vela satellite show that this is an acceptable technique resulting in separation tipoff rates less than 0.008 rad/sec (0.5 deg/sec). The analysis of separation springs for this application, supplying 0.91 m/sec (3 fps) separation velocity, is presented in Appendix Q.

An environmental cover protects the probe while on the spacecraft. This is a aluminum shell of approximately 0.050 gage aluminum.

The environmental enclosure completely encapsulates the probe and provides thermal and meteoroid protection while the probe is attached to the spacecraft. This enclosure is attached to the probe support trusses. The aft end of the enclosure is deployable for the probe ejection from the spacecraft.

The electrical and electronic modifications are the same as in Chapter V, Section B.11.



## VII. URANUS STUDIES

As was denoted in Chapter VI, the initial Uranus study objectives were revised. The present objectives for the Uranus studies are to (1) influence the Saturn Probe system definition so that few changes are necessary for its use at Uranus and (2) to identify the necessary changes for Uranus application.

### A. PARAMETRIC ANALYSIS

The Uranus parametric analysis are centered around the mission and science areas. The five missions which were considered at the beginning of the contract (JUN 79, JUN 80, SUN 81-82, SUN 82-83, and SUN 84) will be discussed in this chapter, as well as the JU 79 mission that is to influence the Saturn probe definition in Chapter VI.

#### 1. Science Performance Analysis

The parametrics for Uranus are included with those for Saturn in Chapter VI, Section A.1. These parametrics include the descent profile and entry accelerometer performance analysis.

#### 2. Mission Analysis

The detailed mission analysis parametric data was provided in Chapter IV where side-by-side comparisons of mission design studies for the different planets may be made. This chapter summarizes the important results for Uranus probe missions.

*a. Interplanetary Trajectory Selection* - The interplanetary trajectories to be considered for Uranus were specified as either Jupiter swingbys (JUN 79, 80) or Saturn swingbys using solar electric propulsion (SUN 81, 82, 83). The interplanetary trajectories for these missions are summarized in Chapter IV, Section G. The trip times to Uranus are about 6.5 years for the JUN 79, 6.9 years for the JUN 80, 7.2 years for the SUN 81 and 82, and 7.5 years for the SUN 83.

*b. Approach Trajectory Selection* - The selection of the approach trajectories at Uranus is complicated by the fact that the approach velocity is generally about normal to the planet equator, thereby making equatorial flybys impossible (Fig. IV-32). Therefore, if the spacecraft flyby is in the ecliptic plane, the probe should be deflected below the spacecraft trace so that as the probe rotates with the planet it will pass through the spacecraft trace. Generally, an effective relay link geometry then has the spacecraft on the same radius ray as the probe halfway through the probe descent.

*c. Navigation and Guidance Results* - The ephemeris uncertainties at Uranus are characterized by values about ten times worse than those at Saturn. This results in severe navigational problems during the approach orbit determination. The impact plane uncertainty ellipse (one-sigma) has a semi-major axis (SMAA) of 9400 km using range/doppler measurements. This led to impractical entry dispersions. Therefore, optical navigation was included during the approach orbit determination, resulting in a SMAA of 1300 km.

*d. Deflection Maneuver Parametrics* - The general deflection trends indicated for Jupiter also apply to Uranus. Because of the relatively small mass of Uranus, the deflection may be made closer to Uranus than at Jupiter or Saturn. Thus, deflection  $\Delta V$  magnitudes of 180, 90, and 60 m/sec are required for deflection radii of 5, 10, and 15 million km for a  $3 R_N$  flyby radius. These numbers are increased to 410, 205, and 145 m/sec, respectively, for a  $6 R_N$  periapsis radius.

*e. Dispersion Parametrics* - The navigation uncertainties are so large at Uranus that they dominate the entry dispersions instead of the execution errors. Thus, at Uranus, the three sigma dispersions in entry time, entry angle, angle of attack, and lead angle are 22.54/22.89 min, 4.44°/6.08°, 1.75°/3.37° and 3.79°/6.60°, respectively, where the numerator is the uncertainty contributed by navigation uncertainties alone (assuming optical navigation), and the denominator is the net uncertainty contributed by both navigation uncertainties and deflection maneuver execution errors. If Earth-based tracking only is used, one probe out of 100 will miss the planet (-60 deg nominal entry angle), pointing up the necessity for using optical tracking. Because of the large dispersions at Uranus, it is important to enter at steeper entry angles than at Jupiter or Saturn. If the nominal entry angle were -15° and Earth-based tracking were used, 41 probes out of 100 cases would miss the planet.

f. *Entry Trajectory Parameters* - The selection of an entry ballistic coefficient, which results in satisfactory staging conditions (deceleration to  $M = 0.7$  above 100 mb) for entry angles of from  $-10^\circ$  to  $-60^\circ$ , was investigated. Any ballistic coefficient less than  $156.0 \text{ kg/m}^2$  ( $1.0 \text{ slug/ft}^2$ ) was identified as adequate.

The peak g experienced at entry angles of  $-20^\circ$ ,  $-40^\circ$ , and  $-60^\circ$  are 100, 250, and 370, respectively, in the nominal atmosphere. The encounter at Uranus is such that entry with rotation is not possible.

The maximum aerodynamic loading q is a function of ballistic coefficient. Entering with a ballistic coefficient of  $1.0 \text{ slug/ft}^2$  at entry angles of  $-20^\circ$ ,  $-40^\circ$ , and  $-60^\circ$ , results in max q of 3500, 8000, and 11500 psf, respectively, in the nominal atmosphere. The dynamic pressure increases linearly with ballistic coefficient.

### 3. System Integration

The system level constraints that control the Uranus parametrics are:

- 1) Mission -JU-79;
- 2) Atmosphere -Nominal Uranus.

All other constraints such as spacecraft, deflection mode, and science payload are the same as for Saturn as discussed in chapter VI, Section A.3.

### 4. Telecommunications Subsystem

The telecommunications subsystem design for the Saturn mission was used for the Uranus mission to determine feasibility and any required changes. The design goal was to have a subsystem design that can be used for a mission to Saturn or Uranus with a minimum of hardware changes.

Microwave attenuation of the nominal Uranus atmosphere is shown in Figure VII. Comparison with the nominal Saturn atmosphere attenuation (Figure VI-6) shows that the loss is greater for Uranus for depths greater than 10 bars. Atmosphere loss is approximately equal for 10 bars and, for the design end-of-mission depth of 7 bars, Saturn has a slightly greater loss. In conclusion, the atmosphere losses are very similar at 0.86 GHz to the design depth of 7 bars.

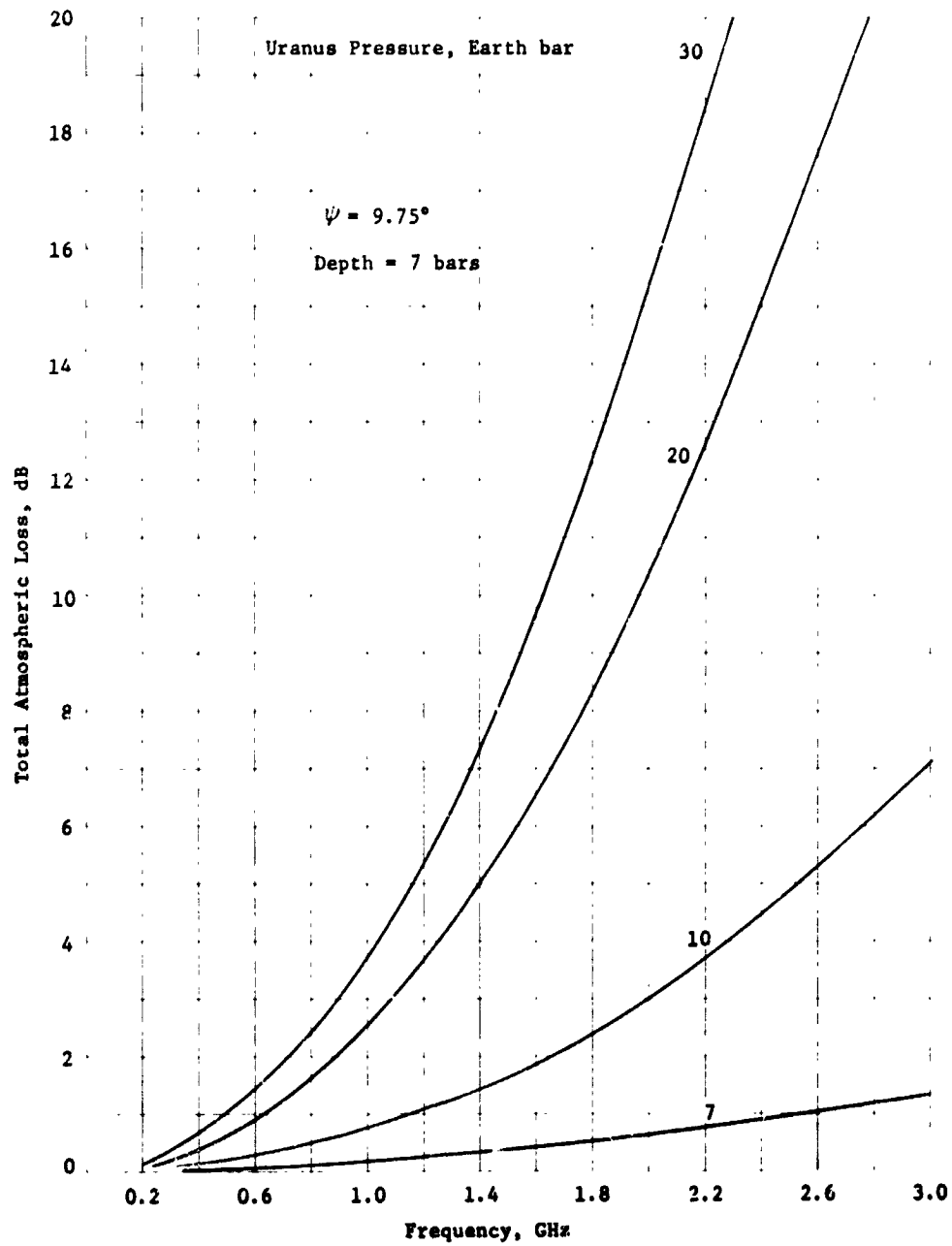


Figure VII-1 End of Mission Attenuation for Uranus Nominal Atmosphere

Data on the noise temperature of Uranus was not provided on the contract and a literature search yielded no useful results. Contact with Dr. J. Smith at JPL resulted in preliminary information on thermal noise. Uranus does not appear to have any magnetosphere. Therefore, the planet disk is the only source of UHF noise. Information from JPL indicates a constant disk temperature of 300°K from thermal sources, which is not a function of frequency. The receiving system noise temperature is the sum of the disk brightness temperature of 300°K, which is the antenna temperature, and the receiver front-end noise temperature from Figure V-11. The system temperature is shown in Figure VII-2 as a function of frequency. The characteristic increase in antenna temperature as frequency is decreased below 2 GHz is absent because the disk temperature is frequency-invariant. This data is considered by JPL to be preliminary and the disk temperature probably is a function of frequency as is the case for Jupiter and Saturn.

Probe-to-spacecraft range is shown as a function of time in Figure VII-3. As seen in the sketch at the top of the figure, range increases before entry as the probe moves ahead of the spacecraft. Maximum range occurs at entry and decreases by 0.5  $R_J$  at mission completion. Periapsis occurs 168 min after entry, which is long after the mission is completed.

Probe aspect angle as a function of time is shown in Figure VII-4. The angle at acquisition is less than 20°, which is smaller than for any other mission. Therefore, a butterfly antenna pattern is not required for the entry antenna, but an endfire (axial) pattern is needed. The angle continues to decrease during descent and rises slightly at mission completion. The maximum descent aspect angle is 14° succeeding entry.

Relative probe positions during the mission are shown in Figure VII-5 by the ellipses. The figure represents the nominal positions (triangles) and associated trajectory and probe dispersions (ellipses). The dispersions are based on a 100-sample Monte Carlo analysis. Elevation (cross cone) angle dispersions are approximately 5°. Large changes in cone angle occur for this mission due to the trajectory geometry as seen at the top of Figure VII-3. Cone angle changes are smaller for Uranus than for Saturn. The minimum spacecraft antenna beamwidth that could be used for this mission is 25°, but the 35° beamwidth that was selected for Saturn was also used for Uranus in accordance with the ground rules. The antenna is positioned in space at the boresight position shown in Figure VII-5

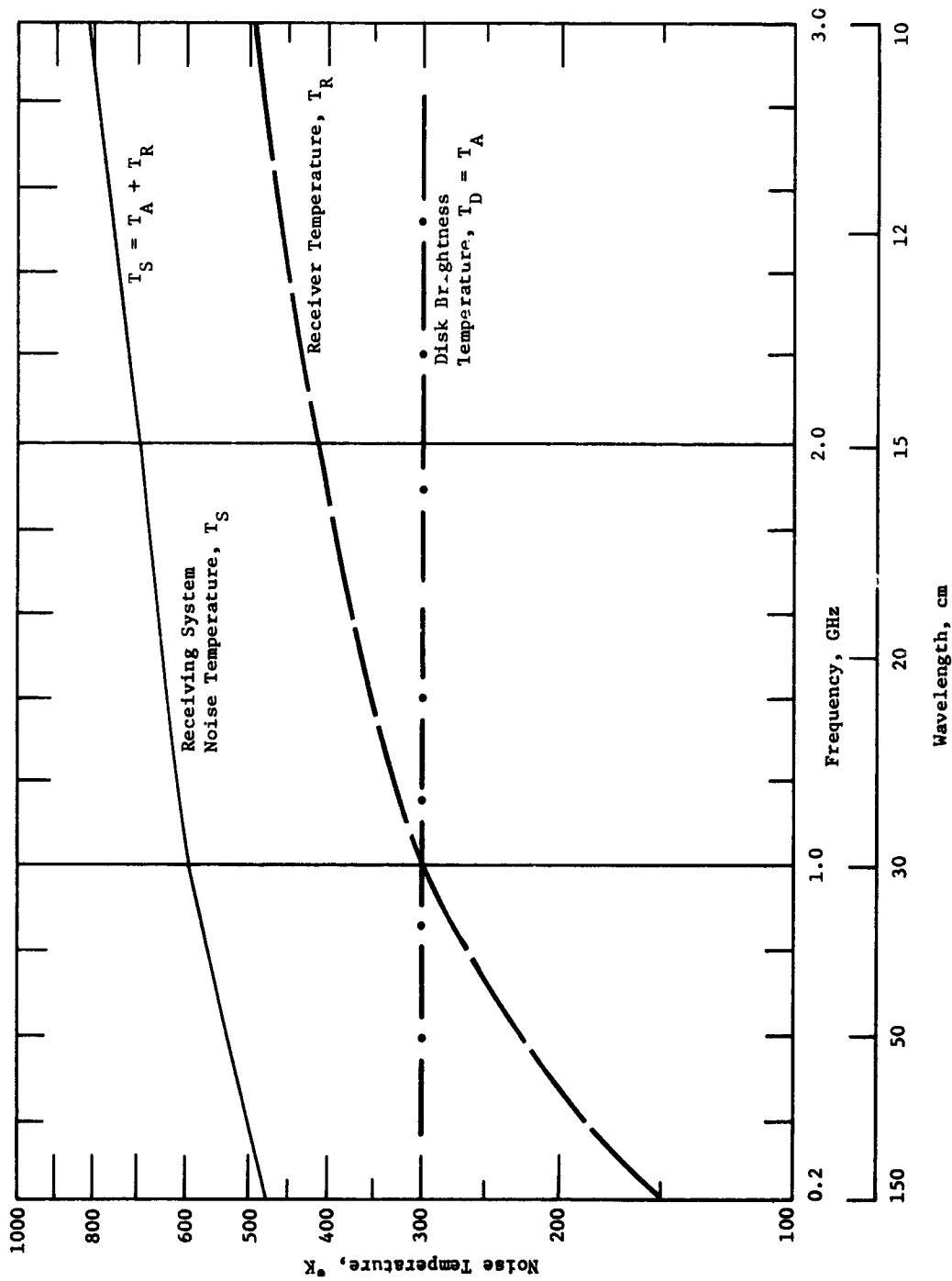


Figure VII-2 Spacecraft Receiving System Noise Temperature for the Uranus Mission

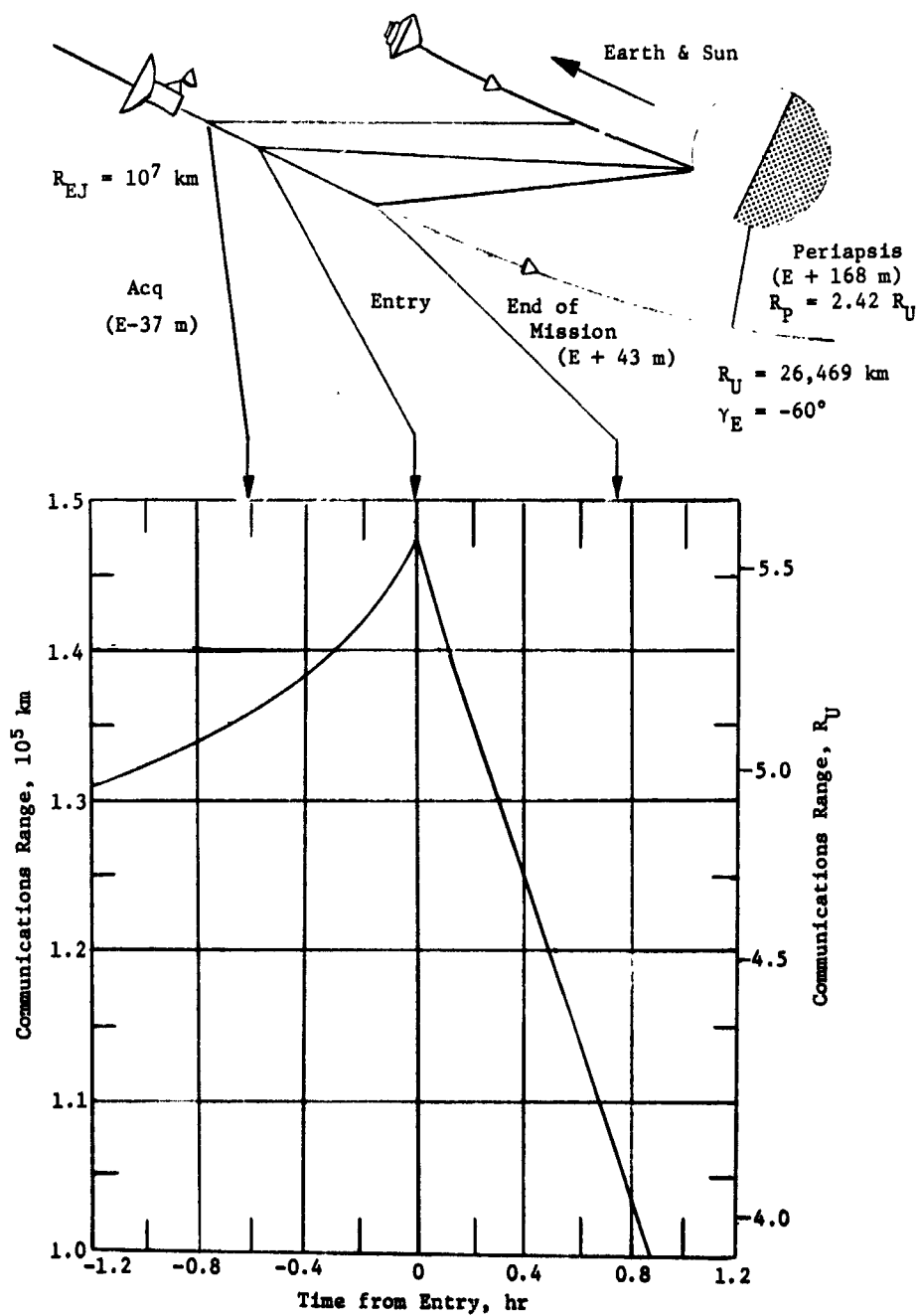


Figure VII-3 Probe-to-Spacecraft Communications Range for the Uranus Mission

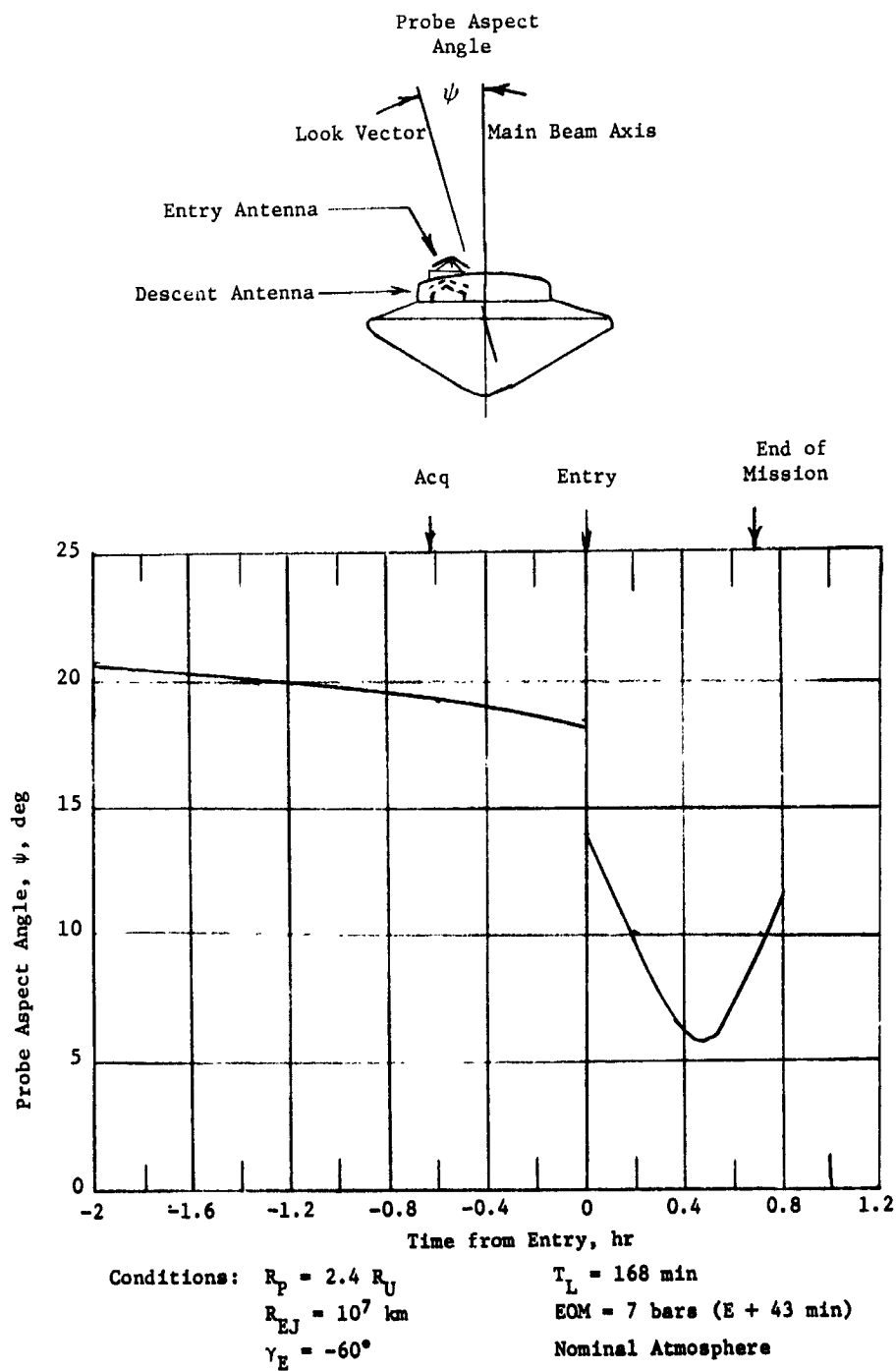


Figure VII-4 Uranus Probe Aspect Angle



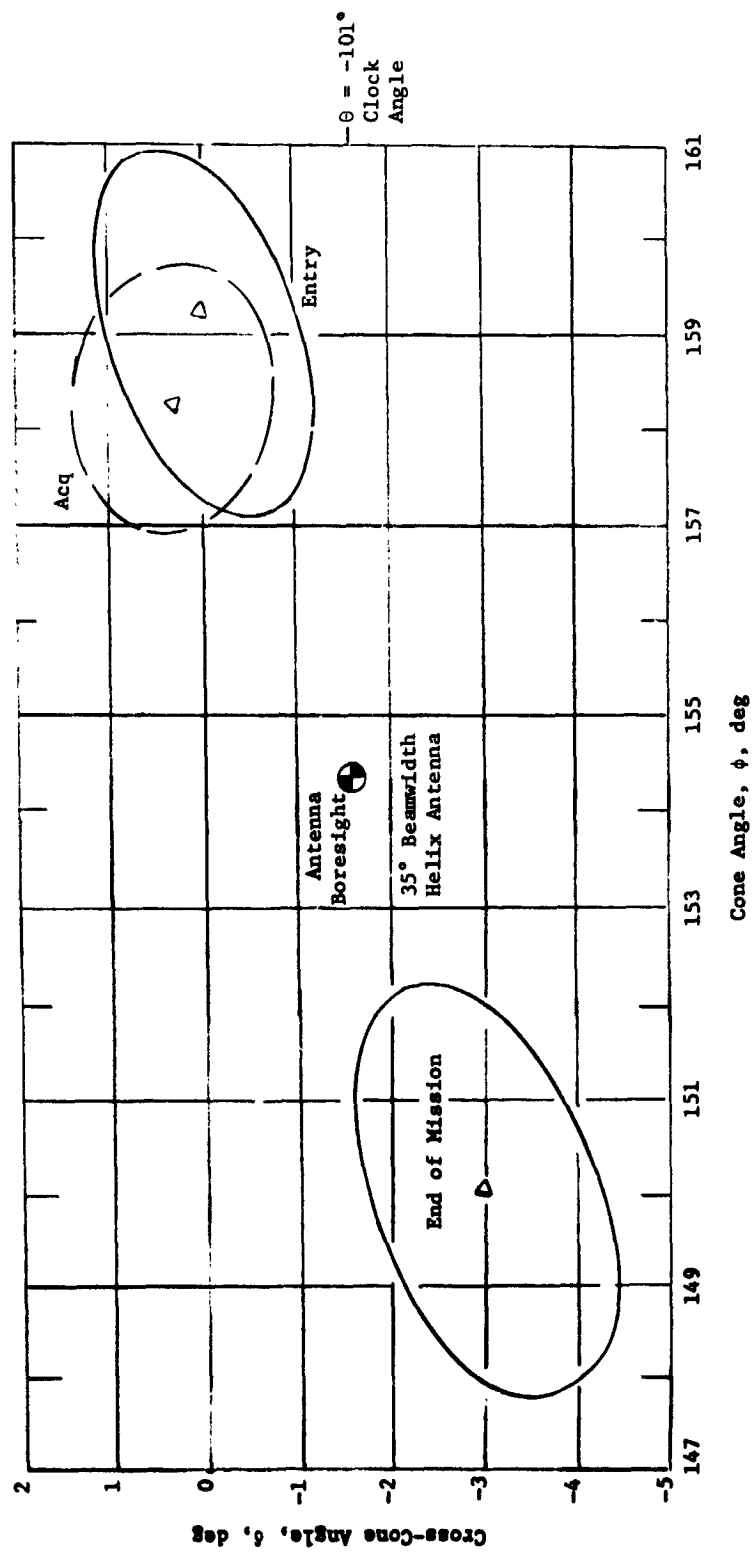


Figure VII-5 Spacecraft Antenna Requirements for the Uranus Mission

Parameters of the RF link are shown in Table VII-1. Defining conditions are based on the Saturn mission shown in Table VI-1. Major differences in the link parameters are the space loss, system noise temperature, and the fact that worst-case RF power requirements occur at entry for Uranus instead of typically at the end of the mission. End of mission power requirements are only 3.5 W. Using the Saturn probe and spacecraft antennas with lower gains did not create severe power requirements, and the only hardware change necessary is the entry antenna for Uranus that must be changed to an axial beam antenna with a beamwidth of 90°. This results in both entry and descent antennas having the same gain and beamwidth requirements; two identical antennas may be employed.

#### 5. Data Handling Subsystem

The analysis of the data handling subsystem is essentially unchanged from the nominal Jupiter probe. Functional requirements remain the same with the exception of minor modifications to sequence and format to conform with the mission profile. For a discussion of DHS selection and configuration, refer to Chapter V, Sections A.5 and B.5 of this volume and Vol III, Appendix H.

#### 6. Power and Pyrotechnic Subsystem

The power and pyrotechnic subsystem configuration remains unchanged from the nominal Jupiter probe (Vol II, Chapter V, A.6 and A.7; Vol III, Appendix G) with the exception of the battery size and weight.

Ag-Zn Post-Separation Battery	94.5 in. <sup>3</sup>	6.9 lb
Ag-Zn Entry Battery	47 in. <sup>3</sup>	3.3 lb
Hg-Zn (Pyrotechnic) Battery	1 x 1 x 3 in.	1.62 lb

The remotely activated Ag-Zn battery characteristics are based on the power consumption required for this mission. The Hg-Zn battery supplies the same load as the nominal Jupiter probe but has an assumed degradation of 7%/year. This assumption may be questioned since valid data is not available on this battery. Because life tests of this length are not desirable and perhaps not feasible; if qualification is to be achieved before launch other approaches may be considered. These consist of (1) the use of an RTG of Pacemaker design with modifications to increase output voltage, (present output power, size, and weight are compatible with coast timer and

Table VII-1 Probe Telemetry Link Design for the Uranus Probe

<u>Parameter</u>	<u>Unit</u>	<u>Nominal Value</u>	<u>Adverse Tolerance</u>	<u>Remarks</u>
1. Total Transmitter Power	dBW	8.1	0	6.5 W
2. Transmitting Circuit Loss	dB	-0.3	0.2	Switch Loss: 0.2dB
3. Transmitting Antenna Gain	dB	5.6	2.4	90° Beamwidth
4. Communications Range Loss	dB	-194.5	1.0	$1.47 \times 10^5$ km
5. Planet Atmosphere & Defocus Loss	dB	0	0.2	Entry
6. Polarization loss	dB	0	0.2	
7. Antenna Pattern Ripple Loss	dB	0	0.2	
8. Receiving Antenna Gain	dB	13.8	1.7	35° Beamwidth
9. Receiving Circuit Loss	dB	-0.2	0.2	
10. Net Circuit Loss, $\Sigma(2+9)$	dB	-175.6	6.1	
11. Total Received Power (1 + 10)	dBW	-167.5	6.1	
12. Receiver Noise Spectral Density	dBW	-200.9	0.5	$T_s = 590^\circ\text{K}$ $NF_s = 4.8$ dB
<u>Tracking Tone</u>				
13. Tone Power/Total Power	dB	-5.0	0	
14. Received Tone Power $\Sigma(11 + 13)$	dBW	-172.5	6.1	
15. Tracking Threshold Bandwidth	dB	11.8	0	15 Hz Bandwidth
16. Threshold SNR	dB	10.0	0	
17. Threshold Tracking Power (12 + 15 + 16)	dBW	-179.1	0.5	
18. Tracking Performance Margin (14-17)	dB	6.6	6.6	
<u>Data Channel</u>				
19. Data Power/Total Power	dB	-1.7	0	
20. Radio System Processing Loss	dB	-1.0	0	
21. Fading Loss	dB	-1.0	0	
22. Received Data Power (11 + 19 + 20 + 21)	dBW	-171.2	6.1	
23. Data Bit Rate	dB	14.2	0	26 bps
24. Threshold $E_b N_o$	dB	8.9	0	
25. Threshold Data Power (12 + 23 + 24)	dBW	-177.8	0.5	
26. Performance Margin (22-25)	dB	6.6	6.6	
27. Nominal Less Adverse Value (26-26 adv)	dB	0		
<u>Conditions:</u> Uranus JU 79 Mission Worst Case (Entry) conditions at $f = 0.86$ GHz Convolutional Encoder, $M = 2$ , $V = 2$ , $Q = 8$ BER = $5 \times 10^{-5}$ for Binary FSK with $K = 8$ code				

pyrotechnic requirements.); (2) development of a 30-day wet stand remote activated battery. Item (2) would be a lower cost development program and provides opportunity for communication and updating on the probes position during the coast period. Both concepts would have future applications in the outer planet missions.

7. Attitude Control Subsystem

The configuration of the attitude control subsystem is unchanged from the nominal Jupiter probe definition. Two detail modifications will be required; (1) the sensors will require additional optics because of the extreme solar range; (2) the geometry for this mission places the Sun  $4^\circ$  off the spin axis of the probe in the entry orientation. The sequence of attitude maneuver will consist of (1) preprogrammed series of pulses to place the spin axis near the sun line; (2) closed-loop precession to complete alignment of the spin axis with the Sun-probe vector; (3) open-loop preprogrammed precession to obtain the  $4^\circ$  offset from the Sun-probe vector. The final maneuver will use the planet sensor to control the sector logic and will contain errors caused by nutation effects and total impulse prediction. However, large percentage errors would be allowable for the small angular precession required. The attitude control subsystem is discussed in more detail in Chapter V, Sections A.7 and B.7 in this Volume and Vol III, Appendix F.

8. Structures and Mechanical

The parametric data reported for Saturn probes as reported in Chapter VI, Section A.8 are applicable to the Uranus probe.

9. Propulsion

The propulsion parametric data reported for the Jupiter probes and reported in Chapter V, Section A.9 are applicable to Uranus.

10. Thermal Control Subsystems

a. *General Discussions* - The Uranus probe is basically identical to the Saturn probe definition (Chapter VI). For Uranus, thermal control must be provided and for this planet, the heat losses experienced during atmospheric descent become very critical. The planetary model atmospheres are presented in Figure VII-6 and show

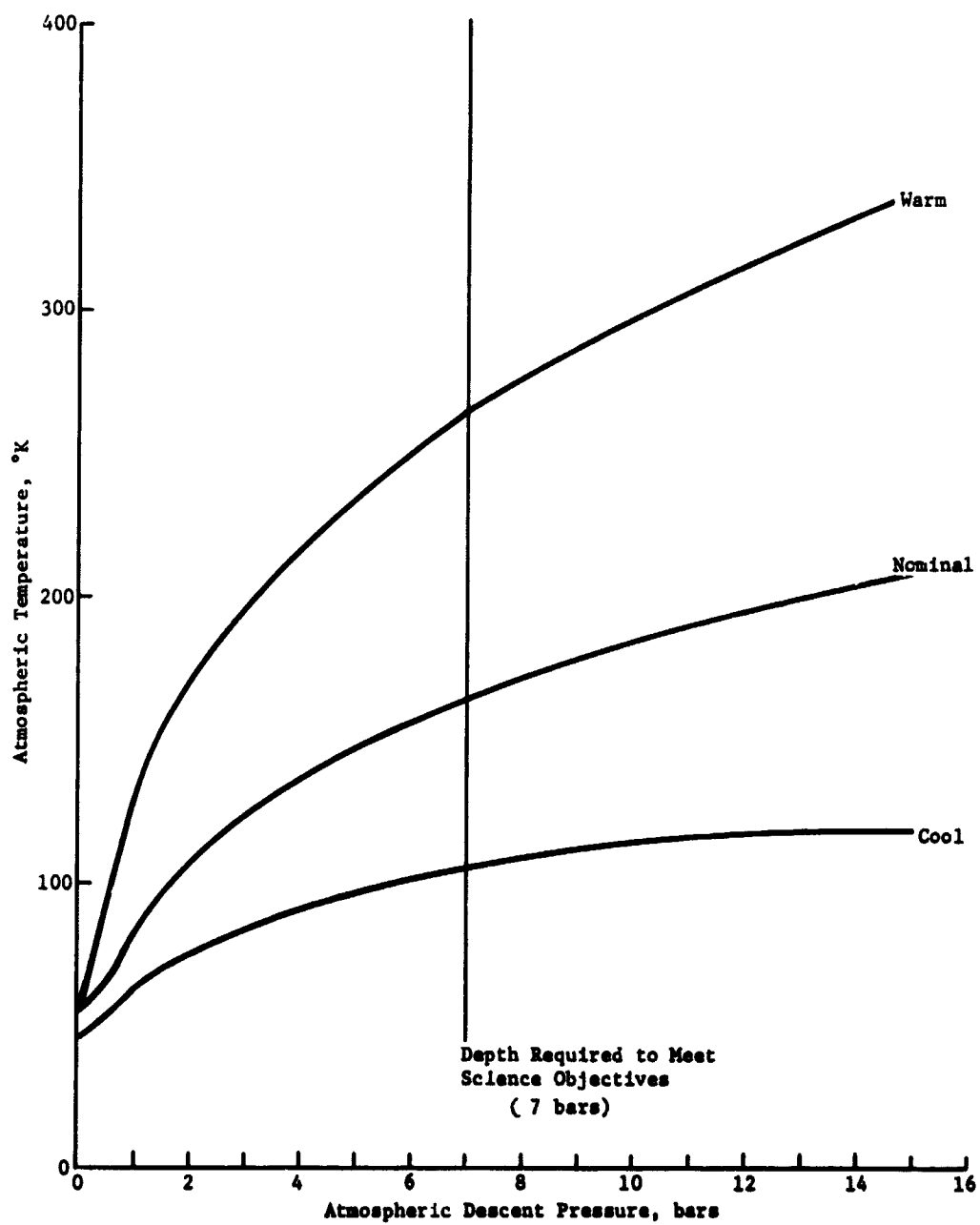


Figure VII-6 Uranus Atmospheric Models,  
Temperature vs Descent Pressure

that the atmospheric temperatures expected will be significantly below those studied for Jupiter and Saturn. The thermal control for Uranus includes:

Cruise/Coast Phase Thermal Control

- 1) Radioisotope Heaters
- 2) Multilayer Insulation
- 3) Environmental Cover
- 4) Thermal Coatings
- 5) Deflection Motor Blanket and Heater

Entry/Descent Phase Thermal Control

- 1) Graphite Ablator and Aeroshell Insulator
- 2) Low Density Internal Foam Insulation
- 3) Nitrogen Gas Environment Control
- 4) Battery Thermal Control Heaters

*b. Cruise/Coast Probe Thermal Control* - For cruise and coast, the thermal design is the same as Saturn with 18 watts for radioisotope heaters being required. After spacecraft separation, however, the solar energy is significantly less than Saturn, and the probe coast temperature will decrease 8°K. Figure VII-7 presents the Uranus cruise/coast radioisotope parametric results. The solar flux at Uranus is assumed to be  $3.7 \text{ w/m}^2$ .

*c. Descent Probe Thermal Control* - Thermal control for the atmospheric descent portion of the Uranus mission is critical because of the very cold atmosphere encounter. The descent temperature and pressure profiles are presented in Figure VII-8. For the thermal design, the 2.5 bar nitrogen gas system was analyzed versus the completely vented probe. For both designs, the probe temperature exceeded the lower allowable limit for battery operation, and for the completely vented probe the probe temperature also exceeded the lower limit desired for electronic equipment operation (Fig. VII-9).

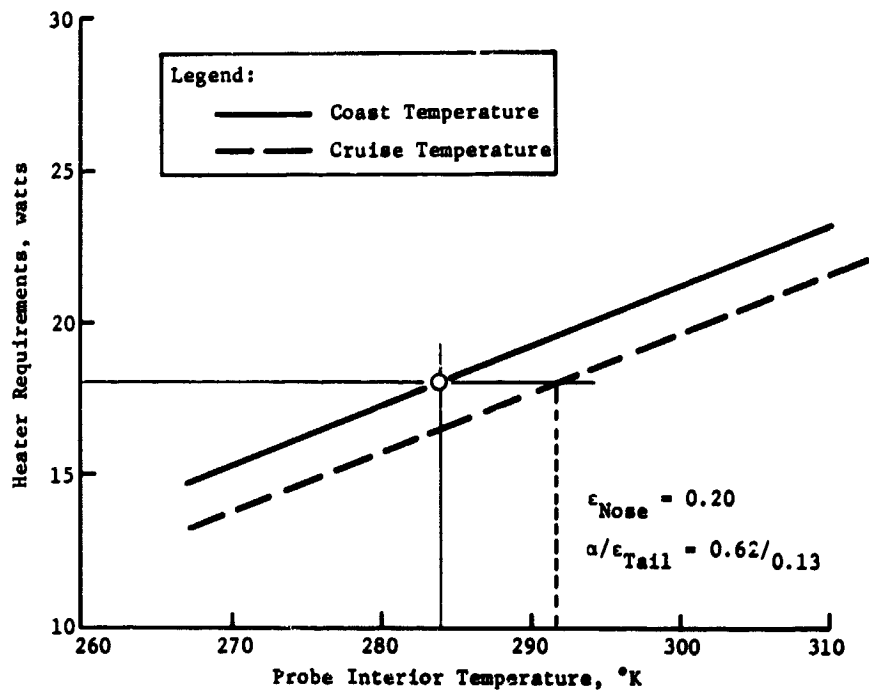


Figure VII-7 Radiosotope Heater Requirement and Probe Coast Equilibrium Temperature for the Uranus Probe

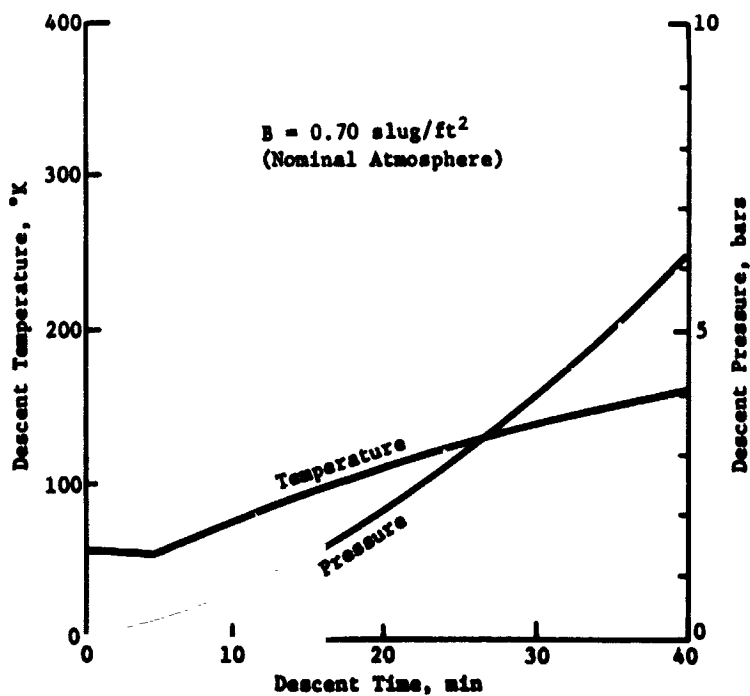


Figure VII-8 Nominal Uranus Mission Descent Temperature and Pressure Profiles

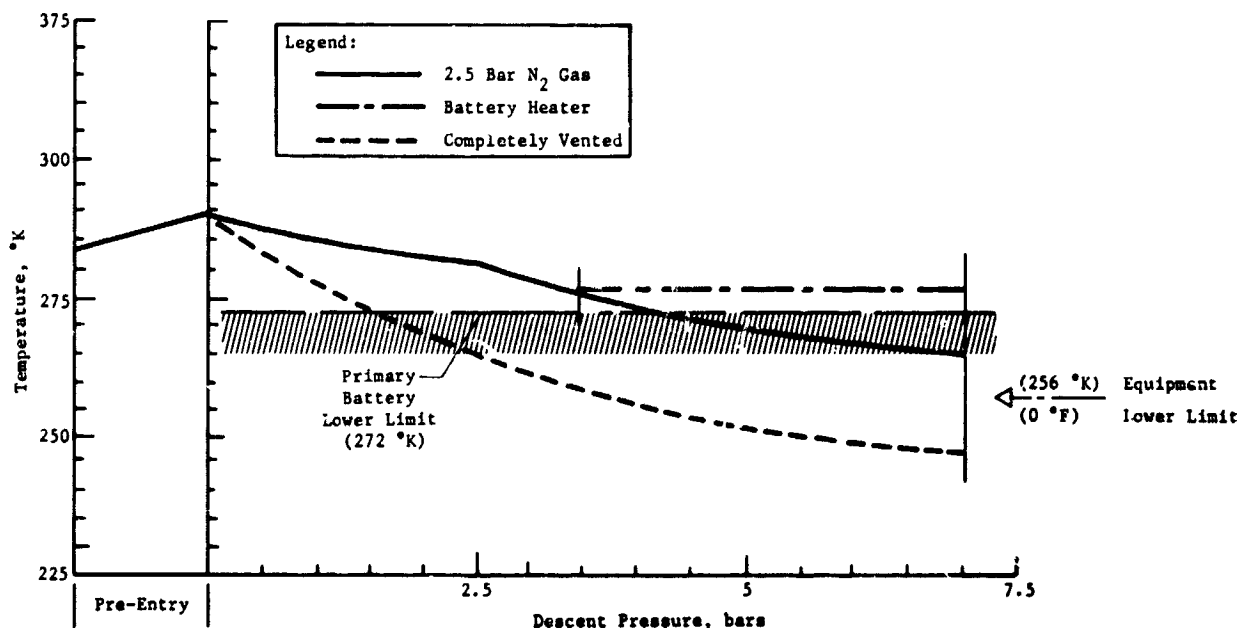


Figure VII-9 Uranus Probe Descent Parametric Thermal Response

For the Uranus probe both nitrogen gas environmental control and additional battery thermal control by thermostatically controlled electrical heating will be required. As shown in Figure VII-10, the electrical energy required to maintain the battery approximately 5°K above its recommended lower limit would require 12 watt-hr of energy and 50 watts of peak power. To maintain the entire probe 5°K above the battery limit would require approximately 65 watt-hr of energy, resulting in 1.2 kg (2.6 lb) of batteries. If the N<sub>2</sub> gas system was additionally eliminated, another 120 watt-hr of additional battery power would be required resulting in a total delta of 3.3 kg (7.4 lb) of batteries. Figure VII-11 presents the Uranus probe instantaneous heat leak during descent for both the N<sub>2</sub> gas system probe and a completely vented probe descent. Note that this heat leak must be balanced by probe internal heat dissipation or a drop in the probe internal temperature.



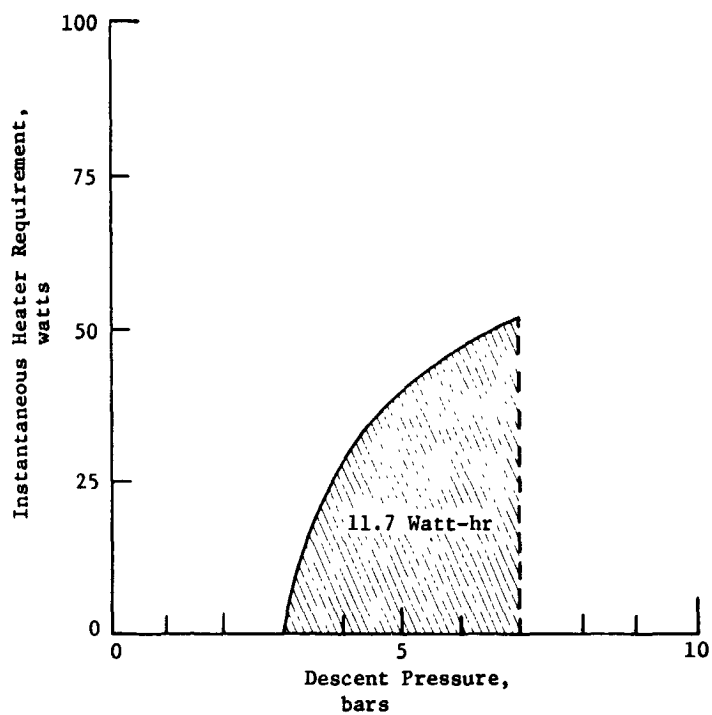


Figure VII-10 Uranus Probe Instantaneous Battery Heating Requirement

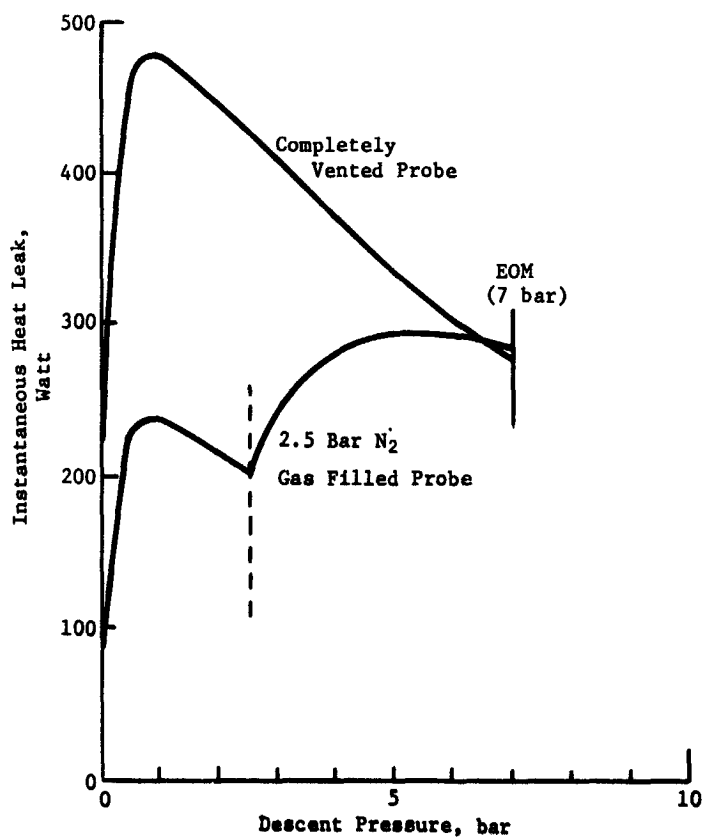


Figure VII-11 Uranus Probe Instantaneous Probe Atmospheric Heat Leak

11. Uranus Parametric Analysis Summary

The Uranus parametric analysis summary was presented with the Saturn analysis in Chapter VI, Section A, particularly in the science area. Analysis results unique to Uranus are:

Mission	6.5 years for JUN 79 to 7.5 years for SUN 83
Approach	Ecliptic with probe de- flected below the space- craft
One Sigma Navigation Uncertainty with Optical Tracking	1300 km
Three Sigma Dispersions (Max)	
Entry Time	22.89 min
Entry Angle	6.08°
Angle of Attack	3.37°
Lead Angle	6.60°
Entry Ballistic Coefficient	< 156 kg/m <sup>2</sup>
Depth of Descent for Science Objectives	7 bars
Descent Ballistic Coefficient for Science Objectives	1.9 kg/m <sup>2</sup>
Descent Time	Approximately 40 min

B. SATURN PROBE APPLICABILITY FOR URANUS

The object of this section is to determine the applicability of the Saturn probe, as defined in Chapter VI, Section B, for atmospheric entry into Uranus, and to identify changes only where the

Saturn probe fails to meet the requirements. In such areas where the Saturn probe more than meets the requirements at Uranus, optimization is not considered. The general constraints for the Uranus application are:

Mission	JU 79
Entry Angle	-60° (Structures Designed to -65°)
Atmosphere	Nominal
Science	SAG Exploratory Payload (PAET)
Spacecraft	Mariner Family
Carrier Mode	Flyby
Periapsis Radius	2.42 $R_u$
Communication Mode	Relay
Deflection Mode	Probe
Entry Ballistic Coefficient	102 kg/m <sup>2</sup> (0.65 slug/ft <sup>2</sup> )
Ballistic Coefficient for Heat Shield Removal	19 kg/m <sup>2</sup> (0.12 slug/ft <sup>2</sup> )
Descent Ballistic Coefficient	110 kg/m <sup>2</sup> (0.7 slug/ft <sup>2</sup> )

1. Science Instrumentation and Performance

The instruments for the Uranus probe are identical to those for the Jupiter alternative probe and the characteristics are given in Table V-29. They are discussed in Chapter V, Section C.1 and in Chapter III, Section C.1. The only difference would be a modification of the range of the temperature gage and possible entry accelerometers for the colder environment and lower g load, respectively.

The descent profile parameters were discussed in Section A.1 of Chapter VI. The results are:

Design Limit Pressure = 7 bars

Parachute Ballistic Coefficient =  $109.9 \text{ kg/m}^2$  ( $0.70 \text{ slug/ft}^2$ )

Parachute Deployment Pressure = 33 millibars

Pressure at First Measurement = 39 millibars

Total Mission Time from Entry = 43 min, 58 sec

The entry and descent times, instrument sampling times, and resulting bit rates are shown in Table VII-2. Transmission bit rates are larger than collection because the data stored during acquisition must be interleaved with real time data and telemetered. The pressure descent profile is given in Figure VI-2 using the appropriate ballistic coefficient.

In Table VII-3, the mission measurement performance is given for descent with the above parameters. All of the requirements have been satisfied, exceeding the criteria in order to keep the instrument sampling times the same as for Saturn.

## 2. Mission Definition

The Uranus mission upon which the systems design is based is illustrated in Figure VII-12 and summarized in Table VII-4. Important characteristics of the mission design are described in this section.

*a. Interplanetary Trajectory* - The interplanetary trajectory for this mission is based on the JUN 79 trajectory. For this mission, the flight time to Jupiter is 1.6 yr with a flyby radius at Jupiter of  $9.9 R_J$ . The total flight time to Uranus is 6.5 yr. The flyby radius at Uranus was selected to be  $2.42 R_U$  to be consistent with the JUN 79 mission. Thus, if the spacecraft continues past Uranus, it will encounter Neptune after a total flight time of 10.3 yr.

*b. Launch Analysis* - Available payload weight is plotted against the launch period for three sets of launch performance data in Figure VII-12(b). It should be noted that the Burner II stage is required if the Titan III/5-Segment vehicle is to be used for the launch vehicle.

*c. Approach Trajectories* - A front and top view of the Uranus encounter is provided in Figures VII-12(d) and (e). The spacecraft trajectory was selected to be consistent with the JUN 79 mission

Table VII-2 Uranus Probe Instrument Sampling Times and Data Rates

Phase	Instrument	Sampling Times (sec)	Collection Bit Rate (bps)	Transmission Bit Rate (bps)
Entry (54.5 sec)	Accelerometers			
	Longitudinal	0.2	50	0
	Lateral	0.4	25	0
	Lateral	0.4	25	0
Descent (2583 sec)	Temperature	4	2.5	2.6
	Pressure	4	2.5	2.6
	Mass Spectrometer	60	6.7	7.0
	Accelerometers			
	Turbulence	8	7.5	7.8
	Stored	0	0	<u>2.2</u>
			Science Total	22.2
			Engineering & Formatting	<u>3.1</u>
			Total	25.3

Table VII-3 Uranus Probe Descent Measurement Performance

Instrument ( $\Delta t$ ) and Measurement	Criteria	Descent Performance (slug/ft <sup>2</sup> )
Mass Spectrometer, 60 sec Minor Constituents Cloud Layering  H/He Ratio Isotopic Ratios Molecular Weight	2 per scale height* 2 inside cloud  4 measurements	5.2 to 29 { 4.0 in CH <sub>4</sub> 8.5 in NH <sub>3</sub>  44 to 7 bars
Temperature Gage, 4 sec Temperature Cloud Layering	1 per °K 2 inside cloud	2.9 to 7.9 { 48 in CH <sub>4</sub> 113 in NH <sub>3</sub>
Pressure Gage, 4 sec Pressure Turbulence Cloud Layering	2 per km* 1 per km* 2 inside cloud	2.5 to 6.8 2.5 to 6.8 { 48 in CH <sub>4</sub> 113 in NH <sub>3</sub>
Accelerometers, sec Turbulence	1 per km*	1.2 to 2.7

\*Below cloud tops.

as explained above. The probe entry angle of  $-60^\circ$  was selected to obtain an entry site well on the Sun-lit side of the planet. The probe was deflected so that at about the middle of descent, the spacecraft was nearly over the probe. This results in a link geometry quite different from the other missions.

d. *Deflection Maneuver* - A probe deflection maneuver was used to establish the above defined link geometry and acquire the entry side. A deflection radius of  $9.75 \times 10^6$  km was used in order to obtain the same  $\Delta V$  requirements (170 m/sec) as the Saturn mission. The implementation sequence is pictured in Figure VII-12(c). The rotation angles are all quite small.

e. *Navigation and Dispersions* - This design mission is required to assume optical tracking because standard Earth-based tracking results in extreme dispersions. This is caused by the fact that Uranus' ephemeris uncertainties are about ten times more severe than those at Saturn. The navigation results provided in Table VII-4(c) are consistent with Saturn including optical tracking along with standard Earth-based tracking. Even with the optical tracking, the navigation uncertainties dominate the execution errors in determining dispersions. The dispersions are now quite reasonable but the subsystems can still be designed to accommodate them. The 3 $\sigma$  entry footprint is pictured in Figure VII-12d.

f. *Entry and Descent Trajectories* - Table VII-4(d) summarizes the entry and descent phases of the mission. Both phases were simulated using the nominal atmospheric model. The entry phase starts at 531 km above the 1 atm pressure level (0 km alt = 26,468 km radius) and ends with the staging of the aeroshell 54.5 sec later. During this phase, a peak deceleration of 357 g is attained 19.0 sec after entry. The descent phase starts after staging of the aeroshell and continues through the end of mission at 7.0 bars. The total descent time is 43.1 min.

### 3. System Integration

a. *Functional Sequence* - Table VII-5 shows the sequence of events for the Uranus probe. Except for the 23-min uncertainty in the entry arrival time which shows up in the pre-entry times, this is very close to the Saturn sequence discussed in Chapter V, Section B.

b. *Functional Block Diagram* - The functional interfaces for the Uranus probe are identical to those for the Saturn probe.

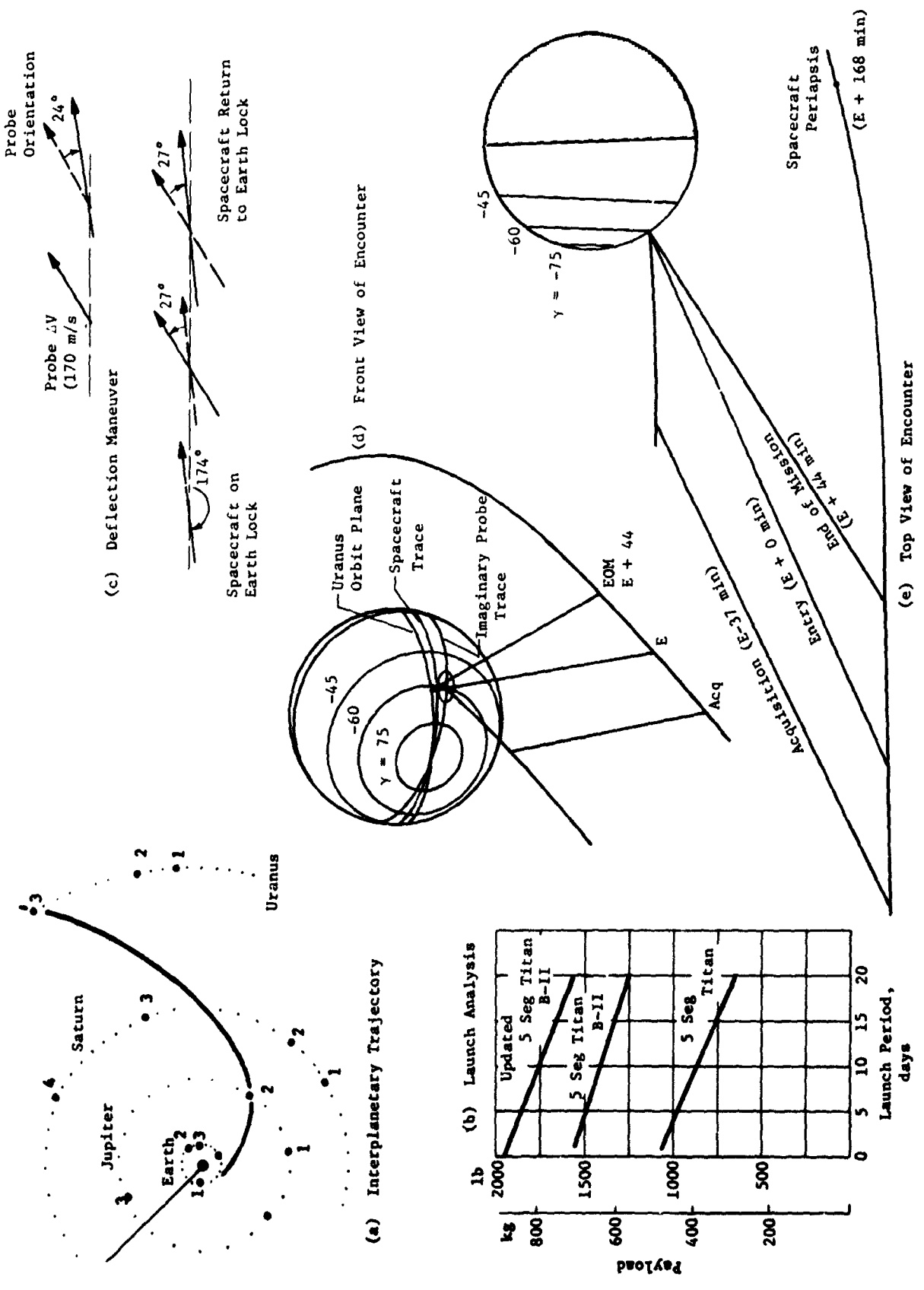


Figure VII-12 Uranus Mission Description



Table VII-4 Uranus Mission Summary

a. Conic Trajectory Data

Interplanetary Trajectory	Launch Trajectory	Arrival Trajectory
Launch Date: 11/6/79 Arrival Date: 5/19/86 Flight Time: 2386 days Central Angle: 212.2	Nominal $C_3$ : 102 km <sup>2</sup> /sec <sup>2</sup> Nominal DLA: 27.0° Launch Window: 4 hr Parking Orbit Coast: 40 min $C_3$ (10 day): 107 km <sup>2</sup> /sec <sup>2</sup> $C_3$ (20 day): 113 km <sup>2</sup> /sec <sup>2</sup> Azimuth Range: $\Sigma_L = 10^\circ - 110^\circ$	VHP: 13.62 km/sec RA: 255.1° DEC: -29.9° ZAE: 174.14° ZAP: 175.32° RP: 2.42° INC: 98.02°

b. Deflection Maneuver and Probe Conic

Deflection Maneuver	Probe Conic Definition
Deflection Mode: Probe Deflection Radius: $9.75 \times 10^6$ km Coast Time: 8.06 days $\Delta V$ : 170 m/sec Application Angle: 33° Out-of-Plane Angle: 9.1° Rotation for Probe Release: 27.3° Probe Reorientation Angle: -24.3° Spacecraft $\Delta V$ from Earth: NA	Entry Angle: -60° Entry Latitude: 53.98° Entry Longitude: 284.17° Lead Time: 168.3 min Lead Angle: -12.07° Probe-Spacecraft Range (Entry): 146,843 km Probe Aspect Angle (Entry): 18.03° Probe Aspect Angle (Descent): 13.91° Probe Aspect Angle (EOM): 7.61°

c. Dispersion Analysis Summary

Naviation Uncertainties	Execution Errors (3 $\sigma$ )	Dispersions (3 $\sigma$ )
Type: Optical/30 day Tracking arc SMAA: 1277 km SMIA: 424 km $\beta$ : TCF: 440 sec	$\Delta V$ Proportionality: 1X $\Delta V$ Pointing: 2° Probe Orientation Pointing: 2°	Entry Angle: 6.08° Angle of Attack: 3.37° Down Range: 8.46° Cross Range: 8.04° Lead Angle: 6.60° Lead Time: 1.69 min Entry Time: 22.89 min

d. Entry and Descent Trajectory Summary

Entry Parameters	Descent Parameters	Critical Events	
		Time from Entry	Altitudes above 1 atm
Entry Velocity, km/sec: 25 Entry Altitude, km: 531 Entry B, slug/ft <sup>2</sup> : 0.65 kg/m <sup>2</sup> : Entry Atmosphere: Nominal Max Deceleration, g: 357 Max Dynamic Pressure, lb/ft <sup>2</sup> : $7.4 \times 10^3$ kg/m <sup>2</sup> : $3.5 \times 10^5$	Descent Atmosphere: Nominal EOM Pressure, bar: 7.0 Descent B, slug/ft <sup>2</sup> : 0.7 kg/m <sup>2</sup> : 109.9	g = 0.1, sec: 4.0 Max g, sec: 17.0 M = 0.7, sec: 54.5 Descent Time, min: 43.1 EOM, min: 44.0	km: 444 km: 138 km: 78.6

Table VII-5 Sequence of Events for the Jovian Probe

Item	Time	Event
1.	L = 0	Launch, November 6, 1979
2.	L + 2h	Separate Spacecraft from Launch Vehicle
3.	L + 2h to L + 3171.5d	Cruise
4.	S - 6h, 0m, 0s	Spacecraft Power to Probe; Eject Environmental Cover
5.	S - 5h, 47m, 0s	Start Probe Checkout
6.	S - 0h, 17m, 0s	Probe Checkout Complete; Start Spacecraft Orientation for Release
7.	S - 0h, 2m, 0s	Spacecraft Orientation to 27° Complete; Activate Probe Data Handling System & Separation Subsystems;
8.	L + 2377.94d S = 0	Separate Probe Start Probe Timer
9.	S + 0m, 0.5s	Start Probe Spinup to 100 rpm
10.	S + 4m, 0s	Probe Spinup to 100 rpm Complete
11.	S + 15m, 0s	Apply Probe ΔV (170 m/sec) (900m Separation)
12.	S + 15m, 21s	Eject Probe Deflection Motors; Activate Attitude Propulsion Subsystem
13.	S + 15m, 31s	Start Probe Precession; Reorient Spacecraft to Earthlock (-27°)
14.	S + 6h, 13m, 31s	Turn on Transmitter
15.	S + 6h, 15m, 31s	Probe Precession Complete (-24°); Start Probe Acquisition
16.	S + 6h, 16m, 31s	Acquisition Complete; Start Engineering Data Transmission
17.	S + 6h, 26m, 31s	Complete Data Transmission; Deactivate Probe Systems
18.	L + 2378.21d to L + 2385.84d	Coast
19.	E - 1h, 7m, 54s	Enable Entry Battery Ordnance
20.	E - 0h, 47m, 54s	Activate Probe Descent Batteries (In Aeroshell & Descent Probe) Enable Probe Despin; Turn on Data Handling System, Engineering Instrumentation
21.	E - 0h, 37m, 14s	Turn "On" Transmitter
22.	E - 0h, 35m, 14s	Start Probe Acquisition
23.	E - 0h, 33m, 34s	Complete Probe Acquisition; Start Data Transmission;
24.	E - 0h, 33m, 24s	Start Probe Despin to 5 rpm
25.	E - 0h, 28m, 24s	Probe Despin Complete
26.	E - 0h, 27m, 54s	Eject Service Module; Activate Service Module Deflection Propulsion; Transmits "Off"
27.	E - 0h, 26m, 47s	Turn on Science Instruments
28.	E = 0	Entry (532 km above 1 atm; $1.3 \times 10^{-7}$ bars)
29.	E + 0h, 0m, 3.5s	Start Recording Accelerometer Data (0.1 g Sensing)
30.	E + 0h, 0m, 8s	Initiate Probe Descent Program (100 g Sensing)
31.	E + 0h, 0m, 17s	Maximum G = 357 for -60° $\gamma_E$
32.	E + 0h, 0m, 49.55	Eject Base Cover Quadrants (Mach 0.8)
33.	E + 0h, 0m, 54.5s	Deploy Main Parachute (Mach 0.7 ~ 0.033 bars)
34.	E + 0h, 1m, 5s	Release Descent Probe from Entry Probe (Switch Probe Antenna) Probe Transmitter "On"; Start Probe Acquisition
35.	E + 0h, 1m, 7s	Deploy Temperature Gage; Release Mass Spectrometer Covers
36.	E + 0h, 1m, 10s	Release Main Chute and Deploy Drogue Chute
37.	E + 0h, 2m, 45s	Probe Acquisition Complete; Start Data Transmission
38.	E + 0h, 43m, 58.5s	End of Design Mission (~ 1 bars)
39.	L + 2386d(E + 2h, 48m, 12s)	Spacecraft Periapsis (2.42 R <sub>J</sub> ); May 19, 1986
Includes 22.9 min Entry Trajectory uncertainty and based on a descent ballistic coefficient of 0.7 slug/ft <sup>2</sup> (110 kg/m <sup>2</sup> )		

c. *System Data Profile* - Figure VII-13 shows the data profile for the Uranus probe. The stored data is the same as that for Saturn and the data transmission rates are the same as for Saturn, except during descent the rate is 1 bps less for Uranus.

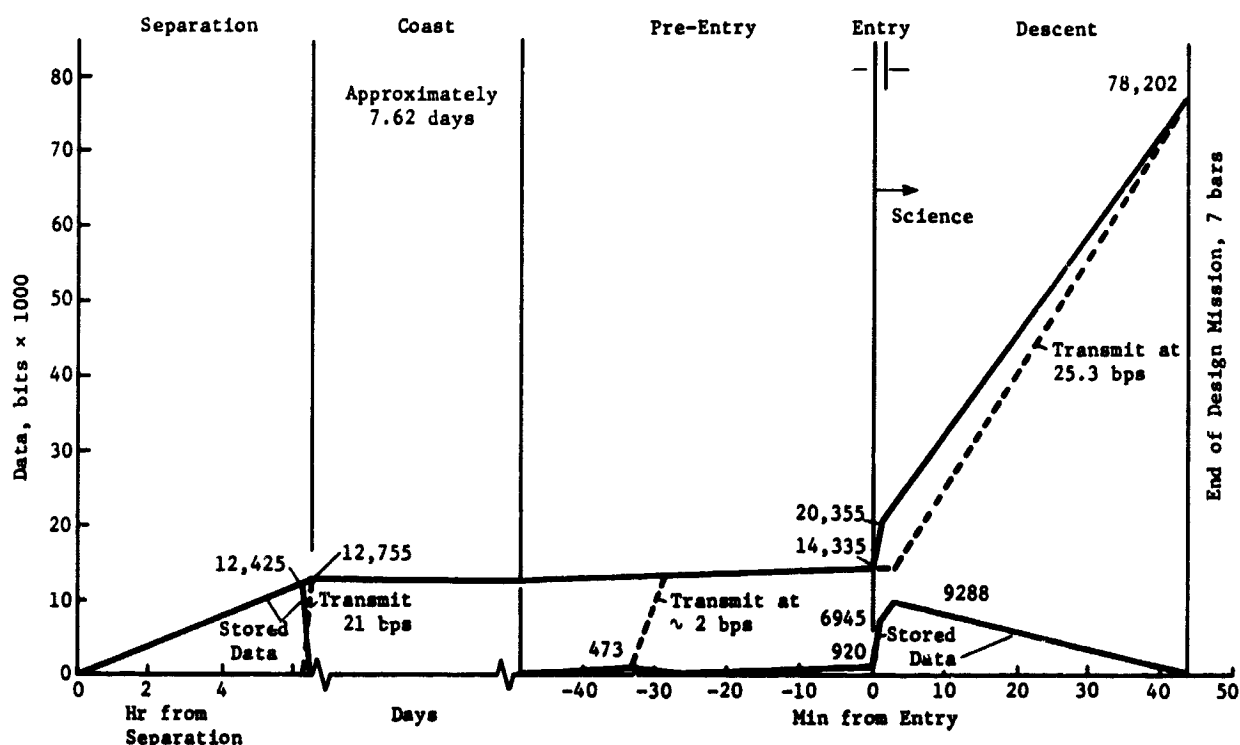


Figure VII-13 Data Profile for the Uranus Probe

d. *System Power Profile* - Figure VII-14 shows the power profile for the Uranus probe. Like the spacecraft-radiation-compatible Jupiter probe (Chapter V, D), the arrival uncertainty at Uranus has an impact on the power profile; however, the total watt-hr capacity is so small that the Uranus descent battery is no more than 0.23 kg (0.5 lb) heavier than the Saturn descent battery. The thermal control subsystem requires an added descent battery of approximately 12 watt-hr for heaters.

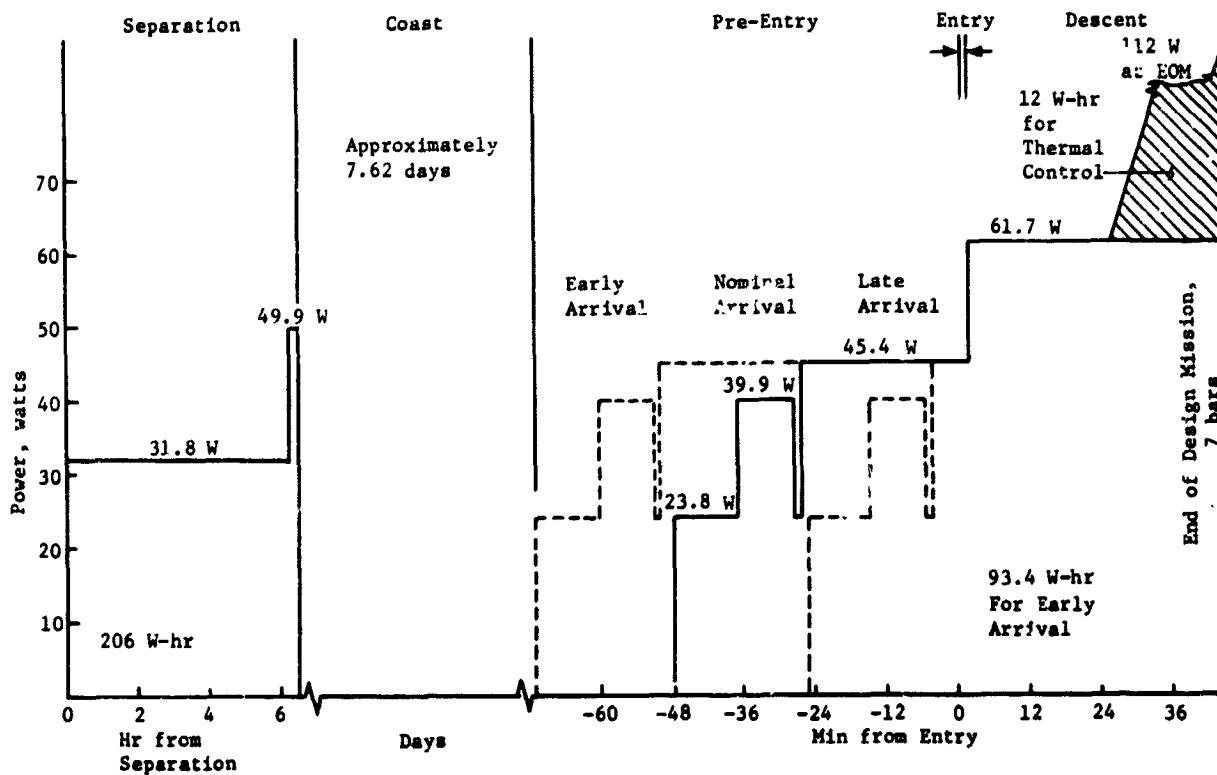


Figure VII-14 Power Profile for the Uranus Probe

a. System Weight Summary - Table VII-6 shows the Uranus weight summary as a delta to the Saturn probe.

Table VII-6 Uranus Probe Weight Summary

Parameter	Uranus Weight*, kg(lb)
Aeroshell Structure	+ 0.09 (+0.20)
Equipment Deck Structure	+ 0.11 (+0.25)
Outer Structure	+ 0.11 (+0.25)
Added Preentry Antenna & 3-position Coax Switch	+ 0.57 (+1.25)
Entry & Descent Battery	+ 0.32 (+0.70)
Added Thermal Control Battery for Descent	+ 0.18 (+0.40)
15% Margin	+ 0.21 (+0.46)
<b>Total</b>	<b>+ 1.59 (3.51)</b>

\*Delta Weight Relative to a Saturn Probe

f. *Saturn/Uranus Probe Comparisons* - Table VII-7 shows the comparisons between the Saturn (Configuration 2) and Uranus probes.

Table VII-7 *Saturn/Uranus Probe Comparisons*

Parameter	Saturn	Uranus
Probe $\Delta V$ , m/sec	170	170
$R_{EJ}$ ( $\times 10^6$ km)	10.15	9.75
Entry Ballistic Coefficient, $kg/m^2$	102	102
Descent Ballistic Coefficient, $kg/m^2$	110	110
Max Deceleration g	350 for $-30^\circ \gamma_E$	320 for $-65^\circ \gamma_E$
Descent Depth, bars	7	7
End of Mission, Entry +	41m, 43.5s	43m, 58.5s
Heat Shield Design Mass Fraction	0.215	0.126
Data Storage, bits	12,400	12,400
Descent Data Rate, bps	26.3	25.3
RF Power at 0.86 GHz, w	6.5	6.4
For same Spacecraft Antenna		
Descent Battery, watt-hr	68	93 + 12 for Thermal
Pre-Entry Antenna	Flat Type	Turnstile/Flared Cone
Thermal Control	Partially Sealed	Partially Sealed with an Added Descent Battery
Ejected Weight, Kg (lb)	115 (253)	} See Table VII-6
Entry Weight, Kg (lb)	76 (168)	
Descent Weight, Kg (lb)	36 (80)	
Heatshield Diameter, m (in.)	0.79 (31)	
Descent Probe Diameter m (in.)	0.445 (17.5)	

4. Telecommunications Subsystem

Table VII-8 depicts design details of the RF components which comprise the telecommunications subsystem for the Uranus mission. Design requirements are discussed in Section A of this chapter. Complete details of the components are given in Chapter V, Section A.4. 6.5 W of RF power is required at 0.86 GHz with a bit rate of 26 bps using binary FSK with a tracking tone. The subsystem hardware design is identical to the Saturn mission except for the entry antenna which must be changed to a 90° axial beam. Identical antennas may be employed for both entry and descent for this mission.

5. Data Handling Subsystem

The DHS for Saturn and Uranus are essentially identical in configuration and function. The dissimilarities are slight differences in timing, sequence, and format during the entry and descent phase of the mission. These dissimilarities could be eliminated by the use of a programmable memory (core, plated wire) or by including dual banks of sequence and format control logic. The desired mission could then be selected by ground-controlled programming power switching.

6. Power and Pyrotechnic Subsystem

The power and pyrotechnic subsystem for Saturn and Uranus are essentially identical in configuration. The only significant dissimilarity consists of the entry/descent (Ag-Zn) battery size and the Hg-Zn (pyrotechnics) battery size. These dissimilarities could be eliminated with negligible cost in weight by using the Uranus-design batteries.

7. Attitude Control Subsystem

The ACS subsystem for Saturn and Uranus are similar in configuration. The principle differences are (1) sensor design for lower solar intensity at Uranus and (2) ACS logic. The dissimilarity (1) could be eliminated by the use of two Sun sensors appropriately mounted for the two missions and the use of a Uranus planet sensor which would perform equally well for Saturn. The changes in the logic [(2) above] would be implemented by DHS control or the use of two sets of logic. The additional electronics would represent a minor increase in weight. The logic and sensor not in use on the selected mission would be removed from the power bus by a latching relay during prepreparation checkout and would not require additional power.

Table VII-8 Telecommunications RF Subsystem for the Uranus Mission

Conditions: Planet - Uranus; Spacecraft - Mariner; Frequency - 0.86 GHz; Bit Rate - 26 bps			
Component	Characteristic	Unit	Value
Transmitter	RF Power Out	W	6.5
	Overall Efficiency	%	45
	DC Power in at 28 V dc	W	14.5
	Total Weight	kg	2.72
		lb	6.0
RF Switch	Type		Solid State
	Insertion Loss	dB	0.3
	Weight	kg	0.1
		lb	0.2
Entry Antenna	Type		Turnstile/Cone
	Main Beam Angle	deg	0
	Beamwidth	deg	90
	Max Gain	dB	6
	Size (dia x h)	cm	20.3 x 7.6
		in.	8 x 3
	Weight	kg	0.45
Descent Antenna		lb	1.0
	Type		Turnstile/Cone
	Main Beam Angle	deg	0
	Beamwidth	deg	90
	Max Gain	dB	6
	Size (dia x h)	cm	20.3 x 7.6
		in.	8 x 3
Spacecraft Antenna	Weight	kg	0.45
		lb	1.0
	Type		Helix
	Beamwidth	deg	35
	Max Gain	dB	13.8
	Size (1 x dia)	cm	73.2 x 11.1
		in.	28.8 x 4.4
	Weight	kg	2.72
		lb	6.0
	Despin		no
	Position Search		1
	Frequency Acquisition	sec	25
	Clock Angle, $\theta$	deg	-101
	Cone Angle, $\phi$ deg	deg	154.3
Spacecraft Receiver	Noise Temperature	°K	300
	Noise Figure	dB	3.1
	DC Power in at 28 V dc	W	3.0
	Weight	kg	0.9
		lb	2.0

## 8. Structures and Mechanics

The entry conditions selected for the planet Uranus result in a deceleration load of 380 g, as compared with 350 g for entry into the atmosphere of Saturn. This small difference is reflected in a delta weight in the equipment support deck of the probe of approximately 0.11 kg (0.25 lbm). The delta weight for the probe outer structure is approximately 0.11 kg (0.25 lbm). The delta weight for the aeroshell base cover is insignificant.

The aeroshell weight is designed by the peak dynamic pressure at entry. Entry at Uranus results in a dynamic pressure of  $36 \times 10^4$  Newtons/m<sup>2</sup> (7400 lbf/ft<sup>2</sup>) as compared with  $34 \times 10^4$  Newtons/m<sup>2</sup> (7000 lbf/ft<sup>2</sup>). The delta weight for the aeroshell is approximately 0.09 kg (0.20 lbm) to accommodate the difference in pressure acting on the nose cone. Thus, it is apparent that the total structural weight is affected by less than 0.45 kg (1.0 lbm) for entering one planet versus the other. This value is insignificant, and the probe design for the joint planet entry is based on the higher loads encountered at Uranus.

*Heat Shield* - Unlike the design of the structure, the most severe heat shield requirements are for the planet Saturn. The 1.13 rad (65°) entry angle at Uranus requires a heat shield mass fraction of only 0.126 and would result in a heat shield weight of 7.82 kg (17.3 lbm). For the 0.52 rad (30°) entry angle at Saturn, the heat shield mass fraction is 0.145. The heat shield weight for Saturn is therefore 9.0 kg (19.9 lbm). The penalty paid for using the Saturn heat shield to enter Uranus is, therefore, 1.2 kg (2.6 lbm), based on both having a blunt nose configuration.

## 9. Propulsion

The delta velocity required for the deflection maneuver is essentially identical for either Saturn or Uranus. The same motor configuration is thus used for either planet. This motor is discussed in Chapter VI, Section B.9.

The precession maneuver for the probe to enter Uranus is only 0.42 rad (24°). The ACS propellant to perform this precession maneuver is 0.141 kg (0.311 lbm) as compared to 0.388 kg (0.856 lbm) for the precession angle for Saturn. Thus 0.247 kg (0.545 lbm) of ACS cold gas propellant could be saved, or a total system weight (propellant plus tank) of 0.57 kg (1.25 lbm) could be saved for a Uranus-only probe design.



#### 10. Thermal Control Subsystem

A probe thermal analysis was performed for the nominal Uranus probe mission. The basic probe configuration was the same as the Saturn probe and included probe propulsion, Sun and planet sensors, and an attitude control system. On the basis of the thermal analysis, a complete thermal history for the Uranus probe was constructed and is presented in Figure VII-15. These results show that the thermal design is critical for this mission because of the low probe entry temperature (284°K) and the very cold planetary atmosphere anticipated. To provide adequate thermal protection for this mission, both N<sub>2</sub> gas environmental control and thermostatically controlled electric heater power is recommended (Section A.10.c of this chapter). The N<sub>2</sub> gas provides adequate probe temperature control until approximately 3 bars pressure (approximately 25 min after entry) after which time battery heating would be required. The heater power requirement to maintain the battery at 5°K above its allowable lower operating limit would be approximately 12 watts-hr of energy with 50 watts peak power required at the end of the design mission. Electrical heating should not be required for any additional probe equipment.

The probe temperature margins predicted for the Uranus probe mission are:

<u>Temperature Margin</u>	<u>Spacecraft Cruise, °K</u>	<u>Probe Coast, °K</u>	<u>Entry Descent, °K</u>
Above Equipment Lower Limit	42	12	5
Below Equipment Upper Limit	8	25	30
Below Transmitter Upper Limit	NA	38	52

#### 11. Probe to S/C Intergration

Integration of the Uranus probe with the Mariner Jupiter Saturn Spacecraft is discussed in Chapter VI, Section B.11 for Saturn. The only unique requirement for the Uranus probe is that optical tracking of the planet is required by the spacecraft to reduce the navigation. Uncertainties are discussed in Section B.2 of this chapter.

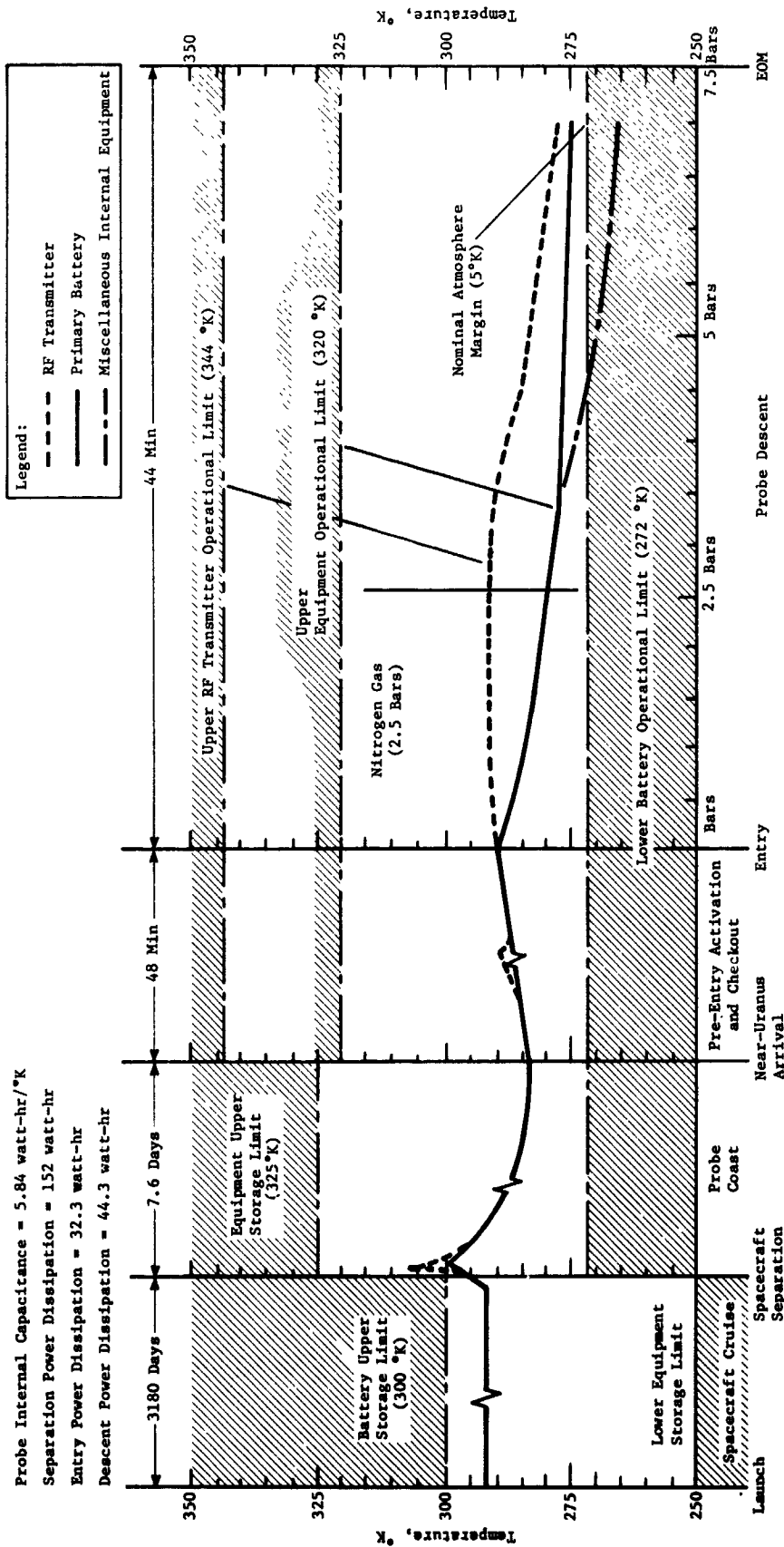


Figure VII-15 Launch to Descent Thermal History of the Uranus Probe

## VIII. NEPTUNE STUDIES

As mentioned in Chapter VI, Saturn Studies, the initial Neptune study objectives were revised. The present objectives deemphasize the Neptune studies; however, parametric analysis using the five initial missions was initiated especially in the mission and science areas. The missions discussed in this chapter are: Jun 79, Jun 80, Sun 81-82, Sun 82-83, and Sun 84.

### A. SCIENCE ANALYSIS

The instruments for Neptune can be identical with those for the other planets, with a possible modification in the ranges of the temperature gage and entry accelerometers. The peak g load is about 200 g, which is similar to Mars entry. The instrument's characteristics are given in Table V-29.

Parametrics were not generated for Neptune descent either in ballistic coefficient or instrument sampling times. However, with the goal of using the same probe for Saturn, Uranus, and Neptune entries, Figure VIII-1 shows a pressure descent profile for a ballistic coefficient of 0.7 slug/ft<sup>2</sup> (109.9 kg/m<sup>2</sup>). The parachute is deployed at 20 millibars, which occurs 91 sec after entry. The design limit pressure from Chapter III, Section D, is 20 bars. The descent time from parachute deployment to end of mission is only 48.4 min despite having started higher in pressure and having to go to greater depths of penetration. This approximate agreement with the descent times of the other planets allows for greater commonality of design.

Using the same instrument sampling times, Table VIII-1 presents the descent measurement performance for this descent profile. All the criteria have been satisfied. The performance values are approximately the same as for Uranus, except for the mass spectrometer measurements in the NH<sub>3</sub> cloud. Note that this is the only mission described in this report where the number of measurements in the second cloud was less than in the first. This is because the second cloud (NH<sub>3</sub>) has a very small pressure (and altitude) differential and exists near the design pressure limit. However, the performance is satisfactory.

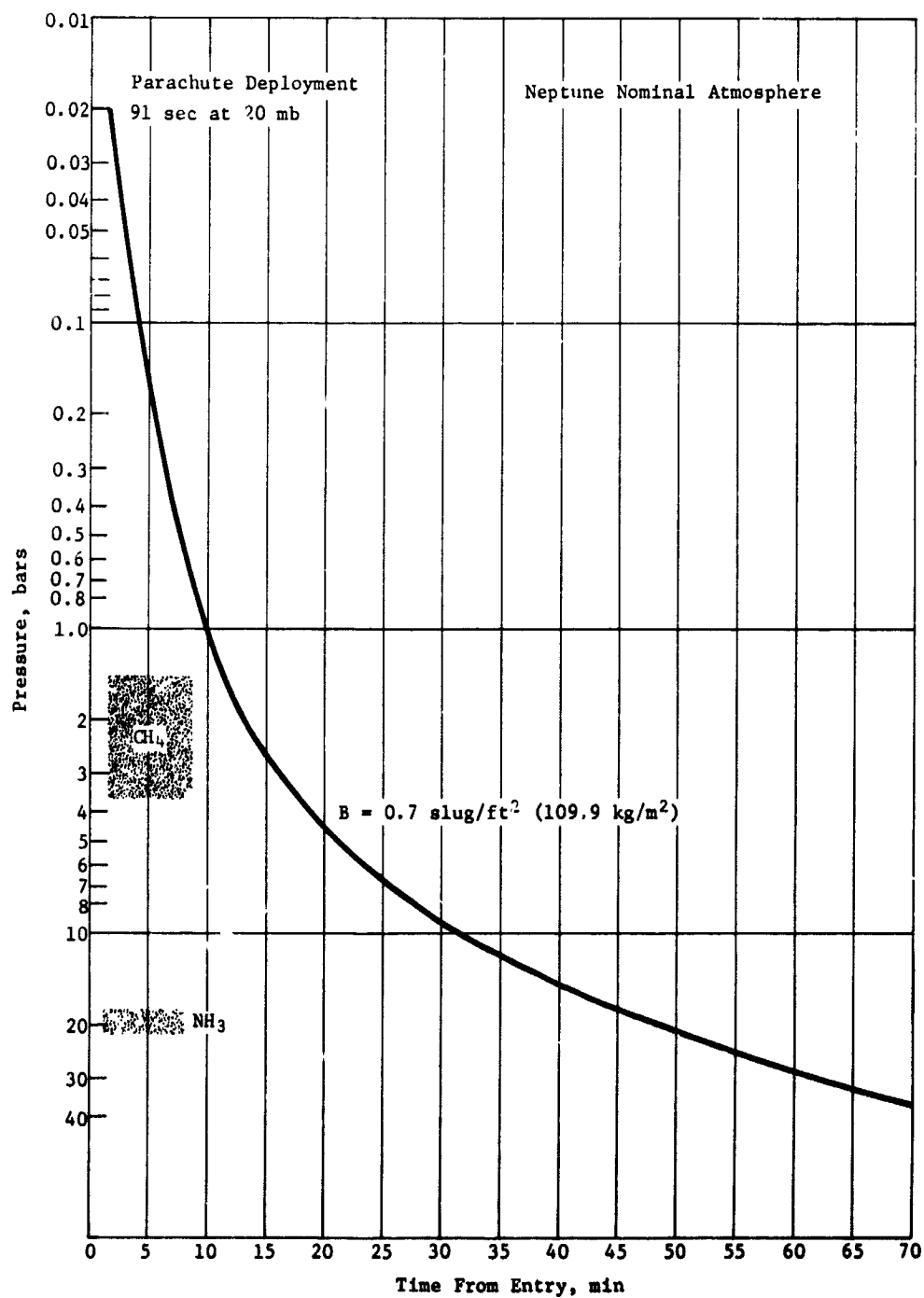


Figure VIII-1 Neptune Pressure Descent Profile

VIII--

Table VIII-1 Neptune Probe Descent Measurement Performance

<u>INSTRUMENT, <math>\Delta t</math> and MEASUREMENT</u>	<u>CRITERIA</u>	<u>DESCENT PERFORMANCE, <math>B = 0.70</math></u>
Mass Spectrometer, 60 sec		
Minor Constituents	2 per scale height*	5.5 to 30
Cloud Layering	2 inside cloud	$\left\{ \begin{array}{l} 6.1 \text{ in } \text{CH}_4 \\ 4.3 \text{ in } \text{NH}_3 \end{array} \right.$
H/He Ratio Isotopic Ratios Molecular Weight	4 measurements	44 to 20 bars
Temperature Gage, 4 sec		
Temperature	1 per $^\circ\text{K}$	2.7 to 9
Cloud Layering	2 inside cloud	$\left\{ \begin{array}{l} 94 \text{ in } \text{CH}_4 \\ 50 \text{ in } \text{NH}_3 \end{array} \right.$
Pressure Gage, 4 sec		
Pressure	2 per km*	4.3 to 10.4
Turbulence	1 per km*	4.3 to 10.4
Cloud Layering	2 inside cloud	$\left\{ \begin{array}{l} 94 \text{ in } \text{CH}_4 \\ 50 \text{ in } \text{NH}_3 \end{array} \right.$
Accelerometers, 8 sec		
Turbulence	1 per km*	1.7 to 4

\*Below cloud tops

## B. MISSION ANALYSIS PARAMETRICS

The detailed mission analysis parametrics are given in Chapter IV where parallel discussions of the different planets are provided. This chapter briefly summarizes the results at Neptune. The mission analysis effort at Neptune was limited to a study of the deterministic characteristics of Neptune missions. A typical Neptune mission is illustrated in Figure VIII-2.

*a. Interplanetary Trajectory Selection* - The interplanetary trajectories to Neptune considered in this study included the JUN 79 and 80 swingbys and the SUN 81, 82, and 83 solar electric propulsion/swingby missions. The total flight times to Neptune are 10.3 and 11.4 yr for the JUN missions and 11.1, 11.6, and 12.6 for the SUN missions respectively. The interplanetary trajectories are pictured in Chapter IV, Section G.

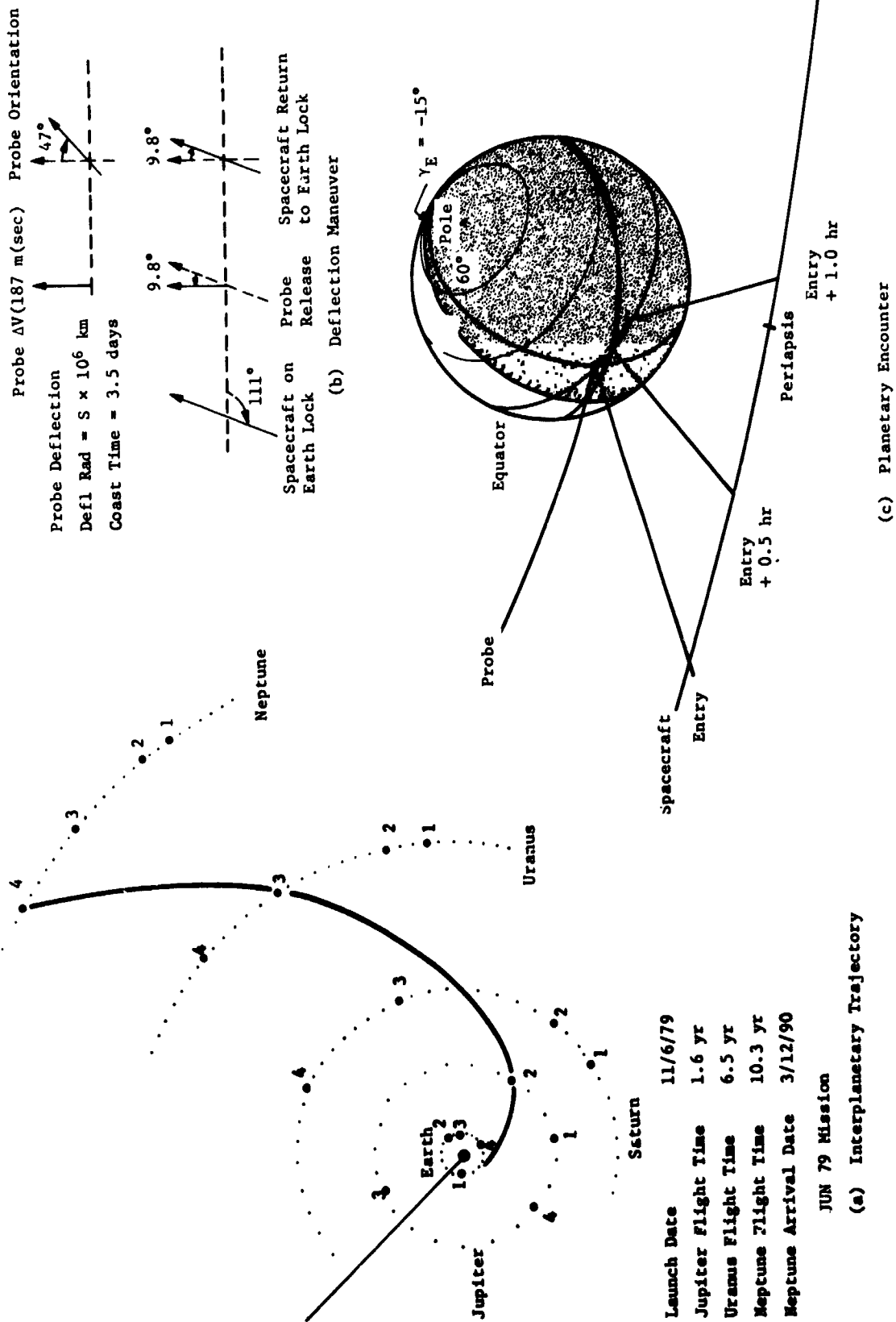


Figure VIII-2 Neptune Mission (JUN 79)

b. *Launch Analysis* - The launch analysis is identical to that given in Chapter VII, Section B.2b for the Uranus phase of the same interplanetary trajectory.

c. *Approach Trajectories* - The optimal relay link geometry at Neptune would have a probe entry site on the equator and a low inclination spacecraft flyby trajectory. The spacecraft periapsis radius should be about  $5 R_N$  for optimal rotation rate matching (Fig. IV-11).

d. *Deflection Parametrics* - Reasonable deflection radii appear to be in the range 5 to 15 million km from the planet. For an entry angle of  $-20^\circ$ , the  $\Delta V$  requirements go from 190 to 90 to 60 m/sec as the deflection radius increases from 5 to 10 to 15 million km for a spacecraft periapsis radius of  $3 R_N$ . The  $\Delta V$  requirements become 410, 210 and 150 m/sec, respectively as the periapsis is increased to  $6 R_N$ .

e. *Navigation and Dispersions* - No specific navigation studies were made at Neptune; however, it is possible to make general observations from extrapolations of existing data. The ephemeris uncertainties at Neptune are characterized by a position uncertainty of about 3000 km. This is to be compared with values at Saturn of 1000 km and 10,000 km at Uranus. Therefore, it is to be expected that navigation uncertainties would play a major role in generating dispersions. Steep entry angles and possibly optical tracking would therefore be advisable for Neptune missions.

f. *Entry Trajectories* - Generally, the entry trajectories at Neptune are similar to those at Saturn or Uranus. The selection of an entry ballistic coefficient less than  $156.0 \text{ kg/m}^2$  ( $1.0 \text{ slug/ft}^2$ ) results in satisfactory staging conditions (deceleration to  $M = 0.7$  above 100 mb) for entry angles from  $-10^\circ$  to  $-40^\circ$ . Figure IV-18 illustrates the relevant trades.

The peak decelerations for Neptune missions are about 200 g's for  $\gamma = -20^\circ$  and 300 g's for  $\gamma = -30^\circ$ . (See Figure IV-24). The maximum dynamic pressure varies from 3000 to 10,000 psf as the entry increases from  $-10^\circ$  to  $-30^\circ$  for a ballistic coefficient of  $156.0 \text{ kg/m}^2$  ( $1.0 \text{ slug/ft}^2$ ).

C. NEPTUNE PARAMETRIC ANALYSIS SUMMARY

The results of the Neptune analysis are tabulated.

Mission Time to Neptune	10.3 yr for JUN 79 to 12.6 yr for SUN 83
Optimal Flyby Radius at Neptune	Approximately $5 R_N$
Entry Ballistic Coefficient	$< 156 \text{ kg/m}^2$
Peak Deceleration	200 g at $-20^\circ \gamma$ to 300 g at $-30^\circ \gamma$
Depth of Descent for Science Objectives	20 bars
Descent Ballistic Coefficient for Science Objectives	$110 \text{ kg/m}^2$ ( $0.7 \text{ slug/ft}^2$ )
Descent Time	Approximately 48 min



## IX. PROGRAM EVALUATION

This chapter discusses the feasibility of a probe system in terms of hardware availability, and identifies the commonality of constraints and hardware for Jupiter, Saturn, and Uranus missions and for Neptune missions to a limited extent.

### A. FEASIBILITY

After defining the nominal Jupiter probe (Chapter V, Section B), various Air Force, NASA, and other programs were researched to determine components that were available for probe implementation. Results of this effort are contained in this chapter.

#### 1. Electrical/Electronic Subsystems

a. *Telecommunications* - Major hardware components include the probe transmitter, probe and spacecraft antennas, RF switch, and spacecraft receiver. Vendor contact was made to determine feasibility of design and availability of hardware in the 1975 time period.

Philco-Ford Corporation (Western Development Labs) at Palo Alto, California; EMR Telemetry, Sarasota, Florida; and Conic Corporation, San Diego, California, were contacted to determine transmitter state of the art for the 1975 and upper limits on RF power. Philco-Ford is developing a transmitter for the Applications Technology Satellite (ATS-F&G) to be used in 1973. The transmitter operates at 0.86 GHz with an RF power of 80 W and an overall efficiency of 45%. The unit weighs 2.7 kg (6 lb) and uses solid-state construction. The unit is nonpressurized and will be qualified to the deep-space environment. Several other vendors are also developing a solid-state capability (Ref A-1 and A-2).

EMR Telemetry presently has transmitters available at S- and L-bands with characteristics shown in Table IX-1. They operate on  $28 \pm 4$  Vdc and have a frequency stability of  $\pm 0.0015\%$ . The transmitters are designed for missile and aircraft applications and withstand shock levels of 55 g and an acceleration of 32 g. Operating temperature ranges are  $-20^{\circ}\text{C}$  to  $+70^{\circ}\text{C}$ . EMR uses hybrid thick and thin film approaches for transmitter microcircuits such as operational amplifiers, crystal oscillators, and RF amplifiers. The power amplifier uses tubes to develop the final power.

Table IX-1 LMR Transmitter Characteristics

FREQUENCY, GHz	RF POWER, W	WEIGHT, kg	SIZE, cm <sup>3</sup>
2.2 to 2.3	25	4.5	2600
1.4 to 1.5	50	7.3	6900

Conic Corporation has transmitters for S- and L-bands with maximum RF power consistent with Table IX-1. All solid-state construction is used with an efficiency of 30%. A 10-W unit can be packaged in an envelope 9x6x4 cm (3.5x2.3x1.6 in.) and weighs 1.5 kg (3 lb). Conic did not expect any significant increase in overall efficiency above 40% by 1975. This is consistent with other investigators (Ref A-3). An RF power level of 50 W at an efficiency of 30% would result in an input power of 165 W. For battery operation, the size and energy requirements would be very large. Conic recommends using antennas with high gain in order to reduce the RF power requirements.

Requirements for the spacecraft receiver are straightforward and extremely low noise levels are not required. A solid-state receiver using transistors or tunnel diode amplifiers is feasible. Conic Corporation also has space-qualified receivers available. Receivers are solid-state and packaged in 380 cm<sup>3</sup>. Environmental conditions satisfied include an operating temperature range from -40 to +70°C, 20 g vibration, 50 g shock, and 100 g acceleration. The package weighs 0.9 kg (2 lb) and operates on 28 ± 4 Vdc with a maximum input current of 40 ma.

RF link calculations require a value for the system noise temperature. The system temperature includes the noise temperature of the receiver front-end (RF amplifier). Noise figures, which are a function of noise temperature as seen in Chapter V, Section A.4, were determined for the 1972 state of the art. Sources for tunnel diodes and transistors include Texas Instruments, Bell Telephone Labs, and KMC Semiconductor Corporation (Ref A-4). Developers do not anticipate solid-state devices to have improved noise figures in the next five years because parametric amplifiers are now being space qualified for low noise requirements (Ref A-5). The effective noise temperature and noise figure are shown for tunnel diode and transistor amplifiers in Figure IX-1. The data are based on the sources mentioned. Silicon transistors have a noise figure that is 1 dB better at 1 GHz than germanium, but is approximately equal at S-band (2.3 GHz). Tunnel diodes have a noise figure of 3 dB for frequencies up to S-band. An average curve is constructed by adding 1 dB to the minimum noise temperature at each frequency. The average curve was used as the receiver effective noise temperature,  $T_R$ , in Chapter V, Section A.4.

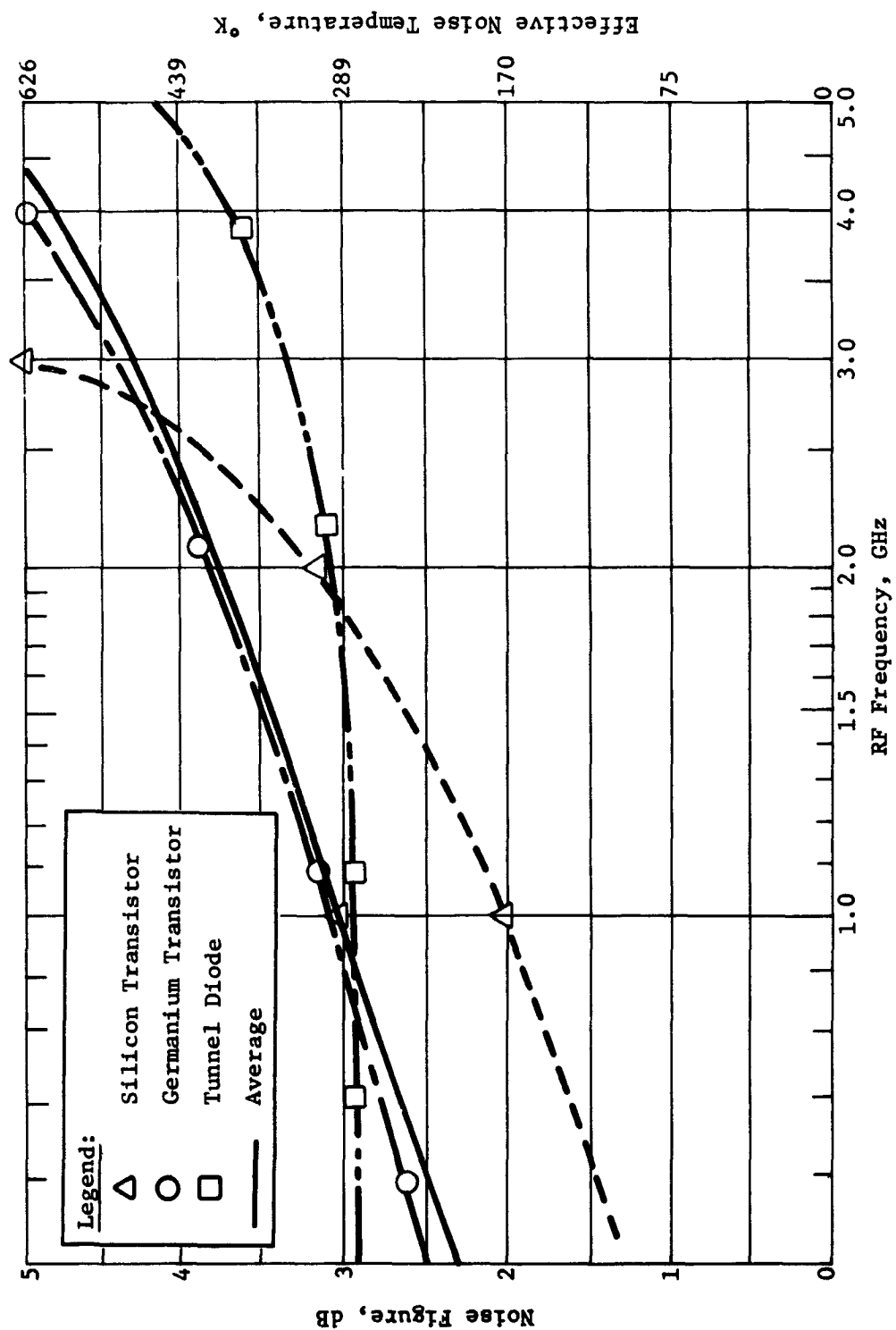


Figure IX-1 1979 Noise Figure State of the Art for Tunnel Diodes and Transistor Amplifiers

The spacecraft antenna for narrow beamwidths is a parabolic dish antenna of conventional design. For missions that require high gain, a dish antenna provides a compact design. Circular polarization is required. This is accomplished by using a feed that consists of crossed dipoles in a cup. Several vendors that can provide a dish with a circular feed as required are available. Missions that require a spacecraft antenna with a wide beamwidth and low gain can use a helical antenna. A helix provides circular polarization and is a conventional design that is often used on spacecraft. Custom designs can be provided by several vendors.

The antenna on the probe for pre-entry and entry use must have a butterfly pattern, which results from the probe aspect angle before entry. The antenna should also have circular polarization to avoid additional loss caused by cross polarization. The entry antenna selected for 1 GHz was a four-arm equiangular spiral on a cone. The antenna design is conventional and construction is straightforward.

For other probe missions, the frequency was lowered to 0.86 GHz and the conical antenna is too large to be placed on the probe. An annular slot antenna was selected to be used for the entry design at this frequency. It is 43 cm (17 in.) in diameter and only 1.9 cm (0.75 in.) thick and is placed under the deflection motor. The main drawback to this design is that the antenna is linearly polarized and cross-polarization losses will exist for look vectors located off the main beam axis. Annular slot antennas are very popular for airborne use in communications, IFF, DME, and TACAN systems. Several vendors manufacture annular slot antennas and the design is not complicated. Printed circuit feed techniques are also common.

The descent antenna on the probe is also of two designs depending on the mission and frequency. For the nominal Jupiter probe mission at 1 GHz, a crossed dipole in a cup was chosen. For circular polarization, the dipoles are unequal in length. The longest dipole is 18.75 cm (7.4 in.) long; the antenna is 7.6 cm (3 in.) deep. This configuration was placed into the baseplate of the probe. For the alternative Jupiter probe missions, the frequency was lowered to 0.86 GHz and the antenna increased in size to 21.8x8.84 cm (8.6x3.5 in.) and could not be placed on the probe because of its larger size. Another design was selected that is more compact and provides circular polarization with the required pattern. The crossed dipole in a cup was replaced with a modification developed by Martin Marietta for the Viking program. It is a turnstile design over a flared cone. The Viking model is shown in Figure IX-2.

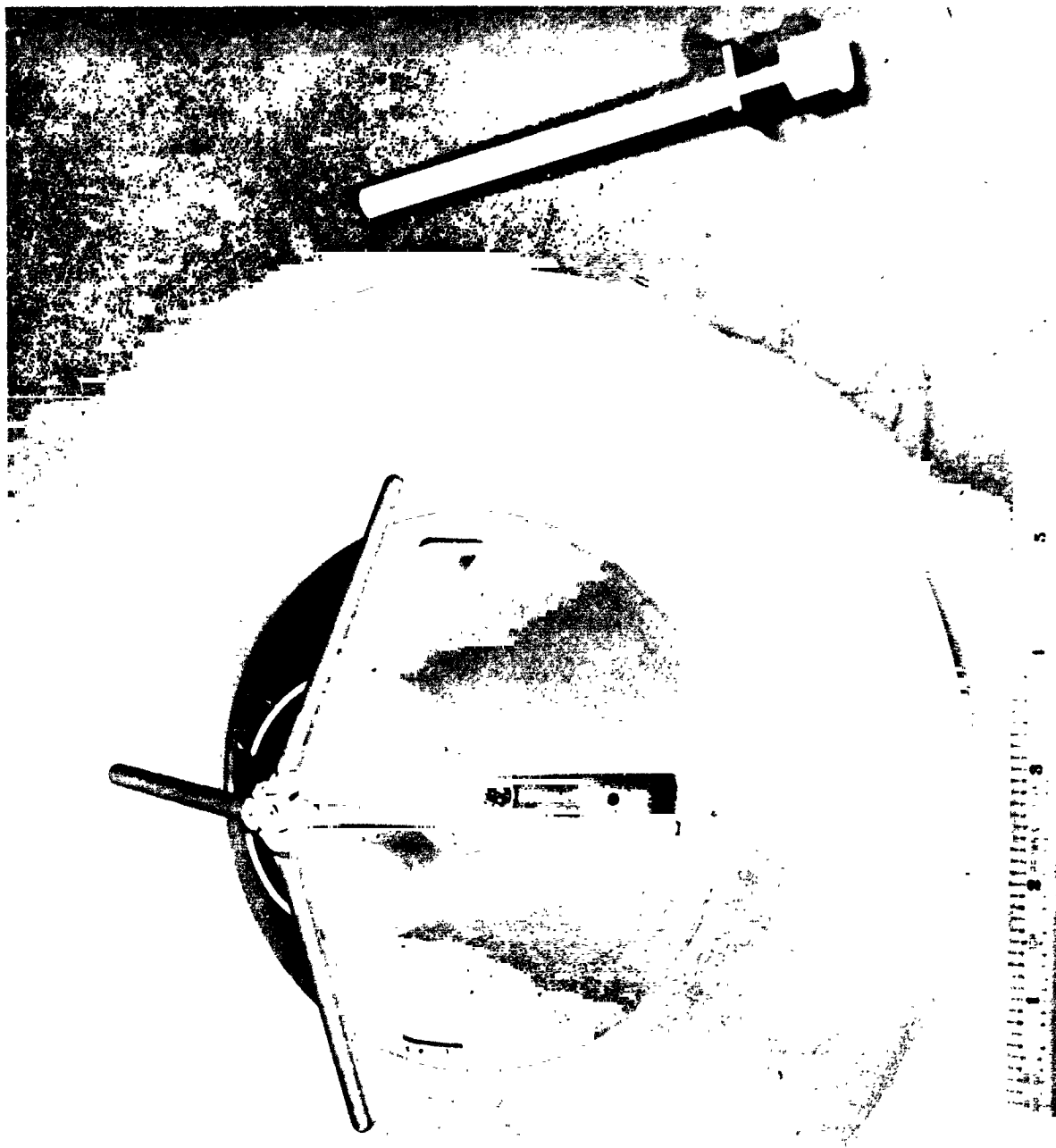


Figure IX-2 Turnstile/Cone Descent Antenna

The large baseplate seen in the figure is required on the Viking lander to reduce backlobes and would not be required for the probe design. For circular polarization, the turnstile arms are unequal. The antenna shown in Figure IX-2 has linear polarization and operates at 1 GHz. For the probe descent antenna at 0.86 GHz, the same design techniques would be employed as are being used by Martin Marietta to develop this antenna for the Viking program.

The transmitter must be switched during planet entry from the entry antenna to the descent antenna. An RF coaxial switch was selected to perform this function. For RF power levels up to 20 W, a solid-state switch may be used; above 20 W, a mechanical switch is required. Several vendors were contacted to determine typical characteristics. This is a routine performance for space vehicles, and RF switches are the most reliable way to transfer RF power from one antenna to the other. Typical electrical and mechanical characteristics are:

#### ELECTRICAL CHARACTERISTICS

Type - SPDT, make before break  
 Isolation - >50 dB  
 Insertion Loss - 0.3 dB Maximum  
 SWR - 1.25:1  
 Switching Time - 10 msec  
 Impedance - 50 ohm  
 RF Connectors - TNC or N.

#### MECHANICAL CHARACTERISTICS

Maximum Power, W	Switch Type	Weight		Volume	
		kg	lb	cm <sup>3</sup>	in. <sup>3</sup>
50	Mechanical	0.45	1.0	786	48
30	Mechanical	0.23	0.5	443	27
25	Mechanical	0.23	0.5	443	27
10	Solid state	0.10	0.2	295	18

Several vendors provide space-qualified units with the above characteristics. The units weigh variable amounts depending on construction, as seen above. Diodes used in solid-state switches can switch RF power up to 20 W reliably, and are currently in production. PIN diodes are being used to develop high-power (>50 W) microstrip switches but are only in early development stages at this time (Ref A-6). Mechanical switching using solenoids is the preferred method for high RF power in a vacuum environment at the present time. High power diode switches could be space-qualified by 1975.

Communications system comparisons were made between the Survivable Jupiter Probe and the following programs:

- 1) Viking
- 2) Venus Pioneer
- 3) Mariner (MM-69 and MM-71)
- 4) Mariner Venus-Mercury (MVM-73)
- 5) LES-8 and LES-9
- 6) SOLRAD High
- 7) DSCS-II
- 8) Advanced Civilian SATCOMs.

1) *Viking* - From a communications system viewpoint, the Survivable Probe has a greater similarity to Viking, which consists of an Orbiter vehicle and a Lander, than any other system studied. The Orbiter is quite similar to Mariner, being capable of transmitting either 10 W or 20 W at S-band. Modulation is PCM/PSK/PM, and data is transmitted to Earth on a 58-in. diameter high-gain antenna.

The Radio Relay System (RRS) consists of a 400-MHz AM command downlink (Orbiter-to-Lander) and a binary FSK/FM 400-MHz uplink (Lander-to-Orbiter). The lander transmits 4 W at 400 MHz. A 20-W S-band link is also provided for transmitting data directly from the lander to Earth, with a 30-in. antenna pointed toward Earth. The 400-MHz data link transmits data only to the Orbiter, where it is detected, stored, and transmitted to Earth on the Orbiter transmitter. No coding is used on the Lander-to-Orbiter link and the 400-MHz binary FSK data are detected on the Orbiter before retransmission to Earth via the S-band link. Block coding is used in the Orbiter-to-Earth and Lander-to-Earth S-band data links. No coding is used in the Lander-to-Orbiter FSK link.

Checkout of the Viking lander, which is under command control from the ground, is made by the Viking bus before the separation and landing maneuver.

2) *Venus Pioneer* - The Venus Pioneer vehicle is capable of launching several probes, each designated for landing in a particular geographic area of Venus. Two types of probes are employed; a large probe and a small probe. Both probes transmit data only at S-band and the signals are received only at Earth; i.e., there is no relay link. Modulation is PCM/PSK/PM on the large probe, and M-ary FSK for the small probe.

The large probe transmits 10 W at a rate 1/2 convolutional code. Probe antenna gain is 7.0 dB. The small probe transmits 2 W M-ary FSK, although M is not specified. Possibilities include  $M = 32$  with convolutional coding. Since Venus Pioneer is still in a proposal stage, many of these detailed parameters have not as yet been specified.

As in the case of the Survivable Jupiter Probe, Venus Pioneer requires a blackout memory for recording sensor measurements made during the time when no communication is possible because of RF blackout. In both cases, memory requirements are nominally a few thousand bits for the blackout period. Memory can be of the MOS-type for Venus Pioneer; however, for the case of Jupiter, where radiation levels are so extremely high, it is probable that a bipolar solid-state memory will be required.

The Venus Pioneer vehicle itself will have a switchable 1, 5, or 10 W S-band transmitter, with a 19-dB gain antenna. The power output level is switched on Earth command.

3) *Mariner (MM-69 and MM-71)* - Mariner Mars 1969 (flyby) and Mariner Mars 1971 (Orbiter) were selected as typical of the Mariner vehicle capabilities. No probes are launched from these vehicles. Power output is 10 or 20 W (TWT) at S-band and a 40-in. antenna is used on the spacecraft. Block coding is used on the data transmitted from the spacecraft. Modulation is PCM/PSK/PM.

4) *Mariner Venus-Mercury (MVM-73)* - Mariner Venus-Mercury is a modified Mariner vehicle having much in common with earlier Mariners so far as the communications system is concerned. Power output is 10 or 20 W at S-band (TWT), with block coding of the telemetry data. The high gain antenna diameter is 48 in. on MVM and an X-band transmitter is added for occultation experiments. Power output is 200 W at X-band (8415 MHz), which is also transmitted on the high gain antenna.



5) *LES-8 and LES-9* - These are experimental communications satellites designed by Lincoln Laboratories for DOD as survivable communications satellites in the event of a nuclear attack. Earth-to-satellite communications will be at UHF, and a satellite-to-satellite data link will be employed to permit global coverage without the necessity of intermediate ground relay links. Both millimeter waves and lasers will be tested for the satellite-to-satellite relay. Orbiter will be synchronous but inclined orbits, elliptical orbits; orbital maneuvers are also possible to ensure survival.

The choice of UHF for ground-to-satellite communications was made to simplify antenna design on the spacecraft and to permit the use of blast hardened antennas. Use of microwave absorbers on the satellite to reduce detectability is also listed as a possibility.

6) *SOLRAD High (SOLRAD 11)* - The SOLRAD High or SOLRAD 11 mission is a series of NRL solar observation satellites designed to operate at an altitude of 69,000 nautical miles to provide continuous monitoring of solar activity in real time from a point outside the range of the Earth's magnetosphere. These satellites will be three-axis stabilized and will be launched on the same vehicles as the LES-8 and LES-9 satellites.

7) *DSCS-II* - The Defense Satellite Communication System, Phase II (DSCS-II) is a military communications satellite system using PCM/PSK/PM modulation, with coding. The frequency is X-band, and total bandwidth is 410 MHz. Up to 1300 channels can be handled simultaneously. The satellites are spin-stabilized at about 60 rpm, but the antennas are despun mechanically. Over 350 W of power is provided by solar cells with rechargeable batteries being used to provide continuous power through any eclipse. Two Earth-coverage horn antennas are used along with two pencil beam (4-ft diameter) parabolic antennas. Gain of 16.8 dB is provided by the horn antenna and 33 dB by the parabolas (2.5° beamwidth). Lifetime of the DSCS-II satellites is designed to be in excess of 5 years.

8) *Advanced Civilian SAT COMs* - A number of civilian communications satellites are now under development, from which it is possible to speculate with a fair degree of accuracy concerning the pattern of future communication satellite capabilities over the next decade. Intelsat IV, Intelsat V, and other more advanced developments, will feature higher frequency operation (up to several hundred GHz), polarization diversity, digital modulation, improved multiple station access techniques, and multiple spot

beam antennas. Most of these satellites will have 3-axis stabilization with high power, directionally controlled solar cell arrays. Designs employing as many as 10-spot beam antennas and several kilowatts of prime power solar arrays are now under consideration.

From a communications system point of view, none of the programs examined is very similar to the Survivable Jupiter Probe. Viking is the closest, yet there are important differences. The Viking Lander, for example, is capable of two-frequency operation, one frequency being a direct Earth link. The Viking relay link, however, does employ binary FSK/FM, and data are stored on the Orbiter before transmission to the ground at a lower data rate.

Venus Pioneer includes the launching of probes, but the probe communications link is direct from probe-to-Earth with no relay. The 210-ft DSN antennas on Earth can be used at S-band during this time period. The attractive feature of the direct link is that it simplifies the spacecraft equipment and the signal acquisition problem because the more complex equipment can be made available on the ground. A direct Jupiter-to-Earth link was investigated during program parametric analysis and found to be impractical at S-band because excessive RF power requirements.

As an alternative to the direct data link, and to simplify equipment on the spacecraft, it is possible that a simple amplifier and frequency translation technique be considered for the spacecraft relay. In this arrangement, the signal is not detected on the spacecraft, but the total frequency uncertainty bandwidth is simply amplified and retransmitted to the ground. This relay technique is used on Intelsat IV.

#### References -

- A-1 J. D. Adams: "Capability of a Projected 1975 Airborne Solid-State Phased-Array Radar." *The Microwave Journal*, Vol 14, No. 9, September 1971, pp 23-34.
- A-2 R. T. Davis: "Wescon's Technical Sessions Stress Trends in Solid-State Devices." *Microwaves*, Vol 10, No. 8, August 1971, pp 41-49.
- A-3 R. E. Koeper: "Solid-State at Microwave Frequencies." *Electrical Design News*, Vol 14, No. 19, October 1969, pp 45-52.
- A-4 T. S. Saad: *Microwave Engineer's Handbook*, Vol 2, Artech House, 1971, pp 166.
- A-5 C. L. Cuccia: "The Paramp Finally Comes of Age." *The Microwave Journal*, Vol 14, No. 8, August 1971, pp 6-8.
- A-6 S. D. Choi: "High-Power Microstrip RF Switch." *JPL Quarterly Technical Review*, Vol 1, No. 3, October 1971, pp 110-124.

b. *Data Handling Subsystem* - The data handling subsystem design may be implemented with flight-qualified off-the-shelf electronic IC and piece parts. The configuration of the system and detailed dynamic requirements are well within the state of the art and could be manufactured by numerous vendors.

c. *Power and Pyrotechnic Subsystems* - The evaluation of power sources for the Outer Planet Entry Probe resulted in the selection of remotely activated silver-zinc batteries for this application. Battery shelf life (dry) has been established as adequate for this purpose. Cells have been held in storage for periods up to 90 months at temperatures less than 80°F and have been activated with no significant degradation. A study has been made of the availability of two types of cell construction--the duplex pile design and the standard design cell--which are applicable to this program. The latter has had extensive use in this country in missile silos and launch vehicles; the duplex pile construction is more common in torpedo and proximity-fused ordnance and is, in general, more shock-resistance than the standard design. Energy density shown is consistent with actual rating at lower (~1 hr) discharge rates.

#### Pile Construction Batteries

Eagle Picher	Type 4379, 1.3 in. deep x 2.15 in. long Piston Activation, 0.7 amp x 5 min 28 ± 15% volts, 35 W-hr/lb Contract from ALC 29 ECM Package, Navy, Johnsville (1969)
Eagle Picher	SAMSO Contract F04694-67-C-0118 28 Volts, 2.3 amp x 12 min, 1.5 in. deep x 3 in. long Weight, 0.547 lb, 35 W-hr/lb (1969)
General Electric	Phase I Contract (Sub to Lockheed) Development, 2 to 5 amp-hr 30 to 50 W-hr/lb, 3 to 5 W-hr/in. <sup>3</sup> (two year development program)

It should be noted that remotely activated batteries are normally used in short life wet stand applications, i.e., 5 to 30 min, and cell separator material is selected to achieve rapid activation. Furthermore, many separator materials, i.e., cellophane, are not compatible with the expected radiation environment in the vicinity of Jupiter. The probe power system does not require rapid activation but does require an approximate 6-hr wet stand life.

In addition to these considerations, the external outgassing products of the usual remotely activated battery designs would not be permissible on a probe when the atmospheric sampling instruments are functioning. This may be reduced by altering the chemical composition of the plates and by providing sufficient volume in the activation mechanism or battery case to contain residual gas.

The modifications to a remotely activated battery design which would alleviate these problems will consist of lead or mercuric oxide additives to the cell plates and the use of an irradiated cross-linked separator material. In addition, the design of the fill mechanism must provide protection from intercell shorts in the fill manifold. These design solutions are within the state of the art and have been applied to battery design. Some testing will be required of the final probe battery design, but should involve only a short, i.e., 6 to 12 hr, wet stand life test since the dry battery shelf life is established.

d. *Attitude Control Subsystem* - The configuration of the attitude control subsystem makes use of technology and design approaches that have been applied to several programs, designed and qualified by numerous vendors. Table IX-2 is a sampling of pertinent programs and vendors.

Table IX-2 Attitude Control System Availability

Component	Source*	Applications*
Sensors	Adcole Honeywell	Tiros, Itos, OAO
Sector Logic	Ball Brothers CDC	ATS-3, OSO-H, IMP-F, ATS F/G
Electronics	(Many)	Space-Qualified Parts
Nutation Damper	RCA TRW	Tiros, Vela, LES
Pneumatics	GE Martin Marietta	Mariner '71, Viking Orbiter '75
*Not limited to these sources or applications.		

## 2. Mechanical and Structural Subsystems

A component search for developed hardware suitable for use in the outer planet probes reveals ready availability of certain components directly applicable to the probes. In other instances, the technology exists but components developed to that technology do not quite fit the requirements of the probe. There exists commercial components that could probably accomplish the program requirements with added development and/or qualification. Listed in this section are the results of a review providing examples of feasible hardware for the first two categories.

In the mechanical engineering area, certain subsystems are not included because they are unique and must be designed and developed for the program. Examples are the structure, parachute subsystems, insulation blankets, certain mechanical components, and propulsion subsystem plumbing.

A listing of those components and subsystems that may be acquired as a result of previous development are shown in Tables IX-3 thru IX-6 for thermal control, mechanisms, and propulsion.

It is anticipated that many essentially "off the shelf" components will be available for use on the program. Examples are the isotope heater, separation nuts, cold gas system valves, filters, pressure regulator, and pressure transducers. The solid deflection motor must be developed for this particular application, based upon existing technology.

Table IX-3 Thermal Control

COMPONENT	FUNCTIONAL REQUIREMENTS	POTENTIAL SUPPLIERS	CANDIDATE COMPONENTS	REMARKS
Heater	Provide Thermal Energy to Maintain Probe Temperature during Cruise and Coast. Meet Safety Requirement	TRW, Redondo Beach	Pioneer 1-watt Heater	Pioneer heater units required 2 years from go-ahead to completion. Unit is presently ready for flight.  (A 15-watt heater also was developed for the Apollo program but was not considered as desirable from a flexibility standpoint as the 1-watt units.)  1-watt heater radiation field is 1.4 m/hr at 25 cm from surface.

Table IX-4 Mechanical Subsystem Components

COMPONENT	FUNCTION	REQUIREMENTS	POTENTIAL SOURCE
Separation Nut	Probe-Spacecraft Separation	Load - 3100 lb Operating Temperature - 0 to +40°F	<u>Viking</u> - Separation nut, PD 3300009-001 Maximum Operating Temperature - -90 to +200°F Allowable Limit Load - 6560 lb
	Deflection Module Probe Separation	Load - 500 lb Operating Temperature - -80 to +40°F	<u>Mariner</u> - Separation Nut, SN 7322-2 Maximum Operating Temperature - -125 to +200°F Allowable Limit Load - 4050 lb
	Service Module Probe Separation	Load - 2,200 lb Operating Temperature - -80 to +45°F	
	Forward Heat Shield Probe Separation	Load - 2000 lb Operating Temperature - +75 to 125°F	
Pin Puller	Base Cover Probe Separation	Load - 5000 lb Operating Temperature - +80 to 200°F	<u>Viking</u> - Pin Puller, PD 5000009 Maximum Operating Temperature - -90 to +2000°F Allowable Limit Load - 2500 lb
	Parachute Staging	Load - 3460 lb Operating Temperature - -40 to -16°F	<u>Mariner</u> - Pin Puller, SP1200 Maximum Operating Temperature - ±300°F Allowable Limit Load 7500 lb  <u>Conax</u> - Pin Puller Model, 1808 Maximum Operating Temperature - -65 to +160°F Allowable Limit Load = 2000 lb
Power Cartridge	Operate - Separation Nuts and Pin Pullers	Withstand Radition 1x10 in. 3-Mev Electrons ( $4.8 \times 10^5$ eng/g) 1x10 in. 20-Mev Protons ( $3.2 \times 10^6$ eng/g)  Operating Temperature - -80 to +200°F	<u>Viking</u> - Initiator, PD 5000006 Maximum Operating Temperature - ±200°F Radiation Tolerance  <u>Mariner</u> - Cartridge P. C. Series Maximum Operating Temperature - ±300°F Radiation Tolerance Gamma Radiation of $10^5$ eng/g

Table IX-5 Deflection Propulsion Solid Propellant Motor

FUNCTIONAL REQUIREMENTS	POTENTIAL SUPPLIERS	CANDIDATE(S)
Total Impulse - 7,750 lbf sec ±0.7%	Hercules	New design required, but state of the art exists to provide a motor with an $I_{sp}$ of 287 and a mass fraction = 0.76. An intermediate motor is required between the Thiokol TE-M-541: $I_t = 3,075$ lbf sec, $I_{sp} = 287$ lbf sec/lbm, Mass Fraction = 0.81 and the Thiokol TE-M-516: $I_t = 2,000$ lbf sec, $I_{sp} = 288$ lbf sec/lbm, Mass Fraction = 0.86.
Thrust - 500 lbf	Thiokol	
Two Canted Nozzle	Aerojet	
Minimum Weight	Atlantic Research	
Space Storable for 800 Days	UTC	

Table IX-6  $GH_2$  Cold Gas System Component Selection

COMPONENT	FUNCTIONAL REQUIREMENTS	POTENTIAL SUPPLIER	CANDIDATE COMPONENTS	REMARKS
Storage Vessel	Pressure - 3500 psi Volume - 330 in. <sup>3</sup> Temperature - -60 to +120°F Leakage - <10 <sup>-6</sup> sec He/sec Maximum at Design Pressure	Pressure Systems, Inc. Airite Aerojet Menasco Arde Tavco, Inc. Fansteel	Fansteel: Part No. 107519 113 in. <sup>3</sup> Capacity at 4000 psi 6 in. Diameter 6A2-4V Weight, 1.3 lbm (Use 3 vessels, load to 3400 psi)	Gas Storage Vessel for Vela Hotel
Isolation Valve (N/C Pyrotechnic)	Pressure - 3500 psi Leakage - <10 <sup>-6</sup> sec He/sec at Design Pressure (internal & external) Temperature - -40 to +120°F Flowrate - 0.015 lbm/sec at 200 psi	Pyronetics Holex Conax Pelmecc Cartridge Act Devices	Pyronetics: New Design New Design Required for High Pressure	Modified Version of MM-71 Pyro Valve
Servicing Valve	Pressure - 3500 psi Leakage - <10 <sup>-6</sup> sec He/sec at Design Pressure (internal & external)	Pyronetics Sterer AIRsearch J. C. Carter	Pyronetics, P/N 1916 (modified) 3/8 in. Size	Used by both Hughes & IRW in Several Spacecraft Applications
Filter	Pressure - 3500 psi Flowrate - 0.015 lbm/sec Filtration - 10 micron absolute Leakage - <10 <sup>-5</sup> scc/sec	Sterer Futurecraft Vacco Wintec	Vacc, S51-81847-2 Stacked Etched Discs	Used on Surveyor
Pyrotechnic Thruster	Pressure - 100 psi Flowrate - N/C, 0.015 lbm/sec N/O, 0.003 lbm/sec Leakage - <10 <sup>-5</sup> scc He/Sec (internal & external)	Pyronetics Holex Conax Piemec Cartridge Act. Devices	Pyronetics P/N 1399 (N/O) P/N 1400 (N/C)	Updated Version of Valves Used on MM-71 and Planned for VO-75

Table IX-6 (concl)

COMPONENT	FUNCTIONAL REQUIREMENT	POTENTIAL SUPPLIER	CANDIDATE COMPONENTS	REMARKS
Pressure Regulator	Pressure - Inlet, 3500 to 200 psi Outlet, 50 $\pm$ 5 psi Flowrate - 0.15 lbm/sec at 200 psi Temperature - -40 to +120°F Leakage - <10 <sup>-5</sup> scc He/sec (internal & external)	National Water Lift Fairchild-Hiller Carleton Sterer Wright	National Water Lift P/N 6890 Sterer Martin Marietta Spec PD-4800164	Qualified under Minuteman III PBP Program. Similar to Unit Used on Titan Transtate ACS. Qualified under Skylab Program for Use in Astronaut Maneuvering Unit
Power Cartridges (for Pyro Valves)	Temperature - -40 to +120°F Firing Current - <5 amp Nuclear Radiation Fluence of 1.34 x 10 <sup>11</sup> 3 Mev Electrons & 7.88 x 10 <sup>10</sup> 20 Mev Protons	Hi-Shear	Hi-Shear 'C-27-007	Qualified under JPL Spec 31192 for Interplanetary Flight
Solenoid Thruster Valves	Pressure - 100 psia Flowrate - Precession, 0.015 lbm/sec Precession, 0.015 lbm/sec Despin, 0.003 lbm/sec Cycles - <1000 Pulse Width - <20 m/sec Leakage - <10 <sup>-5</sup> scc He/sec (internal & external) Temperature - -40 to +120°F	Parker Carleton Sterer Wright Allen Valcor Stratos-Western Futurecraft	Stratos-Western P/N 683000 Wright - P/N 16/80 Futurecraft Martin Marietta Spec PD-4700178	Qualified for the OAO program & for GN-ACS. Coaxial Solenoid-Operated. Qualified under Skylab Program for Use in the Astronautic Maneuvering Unit.
Relief Valve	Pressure - Cracking, 150 psi Reseat, 120 psi Flowrate - <10 <sup>-4</sup> scc He/sec (internal & external) Temperature - -40 to +120°F	Calmec W. O. Leonard Parker Carleton M. C. Manufacturing Sterer	Calmec P/N 1039-591/503	Qualified under the MOL Program by DAC. Will Handle Regulator Fail-Open Flow at Maximum Tank Pressure
Pressure Transducer	Pressure - 0 - 3500 psi 0 - 100 psi Temperature - -40 to +120°F Leakage - <10 <sup>-6</sup> scc He/sec at Design Pressure	Statham Gulton Data Sensors BLH Bourns Servonics Transonics	Statham, Model PA 493: Variety of Ranges from 0-15 to 0-4000 psi, Built in Amplifier w/0-15 V dc Output Weight, ~0.30 lbm Servonics: Model 2101 Variety of Ranges to 0-20,000 psi	Widely Used Because of High Accuracy Reliability to Withstand Overpressure. May Need Modification for 0-5000 psi Range. Improved Version of Model 2091 Transducer Used in Apollo Program



## B. COMMONALITY

Throughout the study, it was noticeable that some constraints and some hardware appeared in more than one application. Of course, during the Saturn and Uranus studies, the intent was to use as much common equipment and parameters as possible. However, in other areas, such as the telecommunications analysis, the frequency used throughout the study was 0.86 GHz. In addition, the entry ballistic coefficient was  $0.65 \text{ slug/ft}^2$  ( $102 \text{ kg/m}^2$ ), which provided the probe deceleration to less than  $M = 1$  near 0.100 bars for all missions. Commonality was considered in the cases of Jupiter, Saturn, Uranus, and to a limited extent, Neptune.

### 1. Science Definition

The probe science commonality is summarized in Table IX-7 for all four planets. The instruments can be the same in their basic characteristics (weight, size, power, etc), except perhaps for extra structural strength that might be required to withstand Jupiter entry. The ranges of the temperature gage and entry accelerometers will require adjustment for each of the respective planets. The sampling times are common for Saturn, Uranus, and Neptune; however, changes are required for Jupiter. This is also true for the descent ballistic coefficient, which translates into parachute size and weight. The initial parachute, used for removing the descent probe from the aeroshell and slowing it to terminal velocity, can be common across all planets. There is some variation in both the total mission time and science data rate, but generally the differences are small enough so that from a science standpoint, similar data handling, power, and telecommunications systems could be used. Finally, the criteria upon which to judge the performance is the same for all planets because their atmospheres are all similar.

### 2. Mission Analysis

Detailed comparisons of mission analysis commonality and contrast for missions to the four planets under consideration are provided in Chapter IV. A summary of these results are listed in Table IX-8 where similar missions to the planets are compared.

In terms of mass and size, Jupiter is by far the largest, followed by Saturn; Uranus and Neptune are fairly similar. The rotation rates of the four planets are approximately the same so that the angular displacement for a probe during descent at any planet will be about the same if the descent times are equal.

Table IX-7 Comparison of Science Mission Characteristics

	JUPITER	SATURN	URANUS	NEPTUNE
<b>Instruments -</b>				
Basic Characteristics	Table V-29	Same	Same	Same
Temperature Gage Range	100-400 °K	70-350 °K	50-250 °K	40-190 °K
Accelerometer Range	1600 g	360 g	360 g	200 g
Sampling Times: Temperature & Pressure	3.5 sec	4 sec	4 sec	4 sec
NMS	40 sec	60 sec	60 sec	60 sec
Turb Accel	10 sec	8 sec	8 sec	8 sec
<b>Descent Parachute System -</b>				
Initial Chute Ballistic Coef	14-19 kg/m <sup>2</sup>	14-19 kg/m <sup>2</sup>	14-19 kg/m <sup>2</sup>	14-19 kg/m <sup>2</sup>
Descent Chute Ballistic Coef	14-19 kg/m <sup>2</sup>	110 kg/m <sup>2</sup>	110 kg/m <sup>2</sup>	110 kg/m <sup>2</sup>
Science Data Rate	30.4 bps	26.3 bps	25.3 bps	~ 29 bps
Parachute Deployment Pressure	0.092 bar	0.048 bar	0.033 bar	0.020 bar
End Mission Pressure	13 bars	7 bars	7 bars	20 bars
Total Mission Time from Entry	36.2 min	41.7 min	44.0 min	48.4 min
<b>Performance Criteria</b>	Table III-3	Same	Same	Same

Table IX-8 Comparison of Similar Missions at Candidate Planets

	Jupiter	Saturn	Uranus	Neptune
Planetary Constants				
Gravitational Constant, $10^6 \text{ km/sec}^2$	126.7	37.93	5.788	6.891
Distance from Sun, AU	5.22	9.57	19.26	30.17
Equatorial Radius, km	71,422	59,800	26,468	24,857
Escape Velocity, km/sec	60	37	22	25
Rotation Rate, deg/hour	36.3	34.5	33.2	28.3
Sphere of Influence*, $10^6 \text{ km}$	48.1	54.8	51.8	87.0
Typical Interplanetary Trajectory				
Flight time, yr	1.8	3.3	6.5	10.3
$V_{HP}$ , km/sec	10.0	13.7	13.6	15.5
ZAP, deg	150.7	169.7	175.5	166.1
ZAE, deg	161.4	173.6	174.3	167.9
Approach Orbit Determination				
Ephemeris Uncertainty, km	500	1000	10000	3000
Geocentric Declination, deg	0(6/81)	0(2/81)	24(6/86)	--
Control SMAA (range/Doppler), km	1500	2200	9500	--
Planetary Encounter				
$V_{HP}$ , km/sec	10.6	13.7	13.6	15.5
Optimal Spacecraft Periapsis, $R_p$	2.7	2.5	3.5	5.0
Deflection Radius, $10^6 \text{ km}$	10-50	10-30	5-15	5-15
Deflection $\Delta V^3(R_p = 2.0 R_J, \gamma = -20^\circ, \text{ m/sec}$	200-45	150-45	140-45	150-50
Coast time, days	9.8-61.4	7.0-22.8	4.1-12.6	3.5-11.5
Planetary Entry				
Entry Ballistic Coefficient, $\text{kg/m}^2$	102.1	102.1	102.1	102.1
Peak Deceleration for $\gamma = -20^\circ$ , g	1500	250	110	200
Maximum Dynamic Pressure for $\gamma = -20^\circ$ , $-20^\circ, 10^5 \text{ nt/m}^2$	10	2.1	1.1	1.9
<p>Sphere of influence radius is that for the Laplacian model defined by <math>r_{SI} = r_D \left( \frac{m_p}{m_s} \right)^{2/5}</math></p> <p>These flight times assume swingby trajectories such as JS 77 or JUN 79</p> <p>These parameters are given for the two limits of deflection radius for the typical missions</p> <p>Values quoted refer to nominal atmosphere model except for Jupiter where cool/dense model is used.</p>				

The flight times to the different planets are important as these impact reliability considerations for hardware. The flight times quoted are for direct missions to Jupiter and for swingby missions to the other planets. The increases in flight times of the missions to the more distant planets are significant. The approach velocities are important as these parameters affect the values of coast times. The approach velocities at the outer planets are higher than at Jupiter because following the Jupiter swingby, the trajectories are significantly accelerated.

The approach orbit determination is critical as it affects the dispersions which the mission and system design must accommodate. Key parameters in the effectiveness of the approach orbit determination are the planet ephemeris uncertainty and the geocentric declination during approach. The Uranus ephemeris uncertainty is the largest, followed by Neptune, Saturn, and Jupiter. The Jupiter and Saturn encounters selected have low geocentric declinations, which lead to degraded accuracy. For comparison purposes, the semimajor axis (SMAA) of the control uncertainty ellipse in the impact plane are listed for range/Doppler tracking. The SMAA for the Jupiter and Saturn uncertainties could be reduced to about half the listed values if QVLBI were used. A significant result is the large uncertainty at Uranus. The magnitude of this error seriously compromises the Uranus probe mission and suggests that optical tracking be required on the Uranus mission.

The planetary encounter phases of the missions are also compared in Table IX-8. The optimal spacecraft periapsis radii are given for rotation rate matching for probes entering at the equator. The deflection radius may be chosen to obtain identical deflection  $\Delta V$  requirements at all the planets. This generally requires larger deflection radii at Jupiter and Saturn than at Uranus and Neptune. The coast times are also larger at Jupiter and Saturn, caused not only by the larger deflection radius, but also by the lower approach velocities.

The planetary entry conditions are compared in Table IX-8 for entry angles of  $-20^\circ$  at each planet. The most hostile environment is that at Jupiter. The entries at the other planets are generally similar. If steeper entry angles at Uranus and Neptune are used (to stay on the light side of those planets or to reduce the effects of entry dispersions), very similar entry characteristics are encountered at Saturn, Uranus, and Neptune.

### 3. Telecommunications

The salient characteristics of the telecommunications system are presented in Table IX-9. The frequency selection for the nominal Jupiter probe (1.0 GHz) was the result of trade studies of power required versus antenna size and currently available designs. Later information and antenna studies indicate that a reevaluation of this mission would result in a selection of 0.86 GHz for this mission also. The selection of this specific frequency (0.86 GHz) is due to the current availability of several point designs in the 0.4 GHz to 2.3 GHz range, the continuous decrease in link losses with frequency, and practical antenna size. The transmitting antenna size is a controlling factor in the frequency selection. The high RF power required by the radiation-compatible mission necessitated the use of the lowest frequency feasible on the probe. The increase of pre-entry antenna size at the lower frequency (0.86 GHz) resulted in mechanical interference between the antenna and the velocity impulse thruster. There was also concern that the rocket motor plume could damage the antenna. Consequently, a design change was made from the spiral-on-cone antenna mounted beside the rocket motor to a flat annular slot antenna mounted beneath the rocket motor. The thruster is ejected before RF transmission and will not interfere with the relay link operation. The annular slot antenna is linearly polarized, which is not desirable, but it does not create a major problem because the attitude of the probe during pre-entry is sufficiently well known so that the spacecraft may select the known polarization during this period. The transmitting antenna patterns for Jupiter nominal probe-dedicated and Saturn show considerable similarity. The geometries for the radiation-compatible and Uranus have probe antenna pointing (pre-entry) almost 90° apart. The pre-entry antenna for Uranus is radically different in that it is a single lobe rather than the butterfly pattern required for the other missions. The descent antennas are all circularly polarized with a single lobe centered along the spin axis. It is reasonable to expect that the descent antenna could be made identical for all missions. The receiving antenna for the radiation-compatible mission is markedly different from the other mission, not only because of beamwidth, but also because of the two-position search required. The increased space loss for this mission requires high gain at the spacecraft and large probe dispersions necessitate a search program. The bit rates shown on the chart were used for link analysis and do not reflect exact mission requirements.

Table IX-3 Telecommunications Subsystem Characteristics

MISSION	JUPITER NOMINAL	RADIATION COMPATIBLE	PROBE DEDICATED	SATURN	URANUS
RF Frequency, GHz	1.0	0.86	0.86	0.86	0.86
RF Power, W	25	55	30	6.5	6.5
Transmitter Antenna, deg	35 at 55 Sp/Cn 110 T/Cp	40 at 85 An/Slt 120 T/Cn	40 at 60 An/Slt 120 T/Cn	30 at 55 An/Slt 90 T/Cn	90 at 0 T/Cn 90 at 0 T/Cn
Receiver Antenna Beamwidth, deg	Helix 40	Parabola 20	Helix 55	Helix 35	Helix 35
Spacecraft	MOPS	Mariner	Mariner	Mariner	Mariner
Bit Rate, bps	28	30	30	26	26
Spacecraft Antenna Position Search	1	2	1	1	1
Frequency Acquisition Time, sec	35	50	65	41	25
<b>Legend:</b>					
Sp/Cn	Spiral on Cone	T/Cn	Turnstile on Cone		
An/Slt	Annular Slot	T/Cp	Turnstile in Cup		

Acquisition time is a function of transmitter power and Doppler rate. The acquisition times shown reflect specific signal-to-noise ratios at the receiver, and consequently the differences across the chart show differences in Doppler rate. A design common to all missions would have to meet the worst-case environment (65 sec, probe-dedicated). However, a common design would probably have higher transmitter power for most missions and acquisition time could be reduced by increasing sweep rate. If the spacecraft receiver can be programmed, the acquisition time for the Jupiter Nominal, Saturn, Uranus could be reduced from that shown on the chart.

As seen in Table IX-9, telecommunication subsystem components are similar for all missions except the radiation-compatible ( $6 R_J$ ).

Telecommunication subsystem design for a common probe for Jupiter, Saturn, and Uranus would have the following characteristics: frequency of 0.86 GHz; 30-W transmitter with binary FSK and a bit rate of 30 bps; probe acquisition 65 sec maximum; fixed helix antenna on the spacecraft without despun platform; and a beamwidth of  $55^\circ$ ;  $40^\circ$  annular slot and  $120^\circ$  turnstile/cone pre-entry antennas, and  $120^\circ$  turnstile/cone descent antenna connected to the transmitter via a three-position solid-state RF switch. The additional pre-entry antenna (turnstile/cone) is required to cover Uranus entry as discussed in detail in Chapter VII, Section A.

#### 4. Data Handling Subsystem

The configuration and functional requirements of the DHS do not change for the missions considered. (Refer to Appendix H for discussion of functional requirements.) Each mission does require a modification of event times, although the ordering of events remains the same. A common design for all missions would require numerous circuit changes to the sequence logic, or a separate sequencer for each mission. The sequencing function could be switched by commanding power control latching relays, or manually, during the prelaunch period.

A development cycle in which there are a significant number of alternative missions or for which the precise details of the selected mission are not resolved, represents a severe environment for the "hard wired" subsystem. If these circumstances are anticipated, the optimum approach for the entry probes would incorporate an adaptive approach to sequencing. This does not change the basic decentralized configuration approach to the probe DHS, but will replace the majority of the ROM functions by nonvolatile programmable memory registers and associated sequencing logic.

Furthermore, in consideration of the modifications required for commonality in the attitude control system, it is logical to provide programmable functions for ACS sequencing and command. The degree to which portions of the ACS subsystem should be incorporated into the DHS should be evaluated with respect to the following considerations:

- 1) The unique or special purpose properties of the ACS logic is such that a decrease in reliability can occur by adding circuitry to the central DHS which provides no function during the entry and descent phase, but can contribute to failure modes;
- 2) The ACS operates in a relatively radiation-free environment and more efficient redundant electronics, i.e., COSMOS, may be used in this subsystem;
- 3) The ACS may be programmed with volatile memory registers during the pre-separation checkout period through a hardwire link to the spacecraft;
- 4) There are, at present, only two differing ACS sequences.

In consideration of the above factors, the preferred approach for a DHS design that includes commonality requirements for Jupiter, Saturn, and Uranus would require the following modifications of the nominal Jupiter probe:

- 1) Programmable sequencer;
- 2) ACS interface would include-
  - a) attitude commands,
  - b) sequence selection commands.

#### 5. Power and Pyrotechnic Subsystem

The power and pyrotechnic subsystem for all missions have few dissimilarities. The only mission that differs significantly is the probe-dedicated mission which has limited post-separation activity. The difference is due primarily to the choice of deflection mode rather than a mission requirement. The power subsystem configurations for the spacecraft deflect mode missions can support the probe-dedicated mission but would not be an optimum design from the standpoint of cost and weight. The variation of the salient characteristics of this subsystem are tabulated.



Table IX-10 Commonality Comparisons

Component	Jupiter Nominal	Radiation- Compatible	Probe- Dedicated	Saturn	Uranus	Commonality Requirements
Post-Separation Battery, W-hr	208	216	0.67	206	206	216
Entry Battery, W-hr	123	199	107	68	93	199
Power Condi- tioning, kg	0.91	0.91	0	0.91	0.91	0.91
Pyrotechnics, kg	5.2	5.2	2.8	3.2	3.2	5.2

The variation of the pyrotechnic weights is due to the substitution of SCRs for relays in the Saturn and Uranus design and the decreased number of pyrotechnic events in the probe-dedicated design. A design that would be compatible for all missions is given in the "commonality requirement" column. It should be recognized that this comparison does not reflect a specific effort to develop a detailed common design. Preferred configurations were used for the subsystem and are essentially identical.

#### 6. Attitude Control Subsystem

The ACS electronic designs for the missions considered are similar in configuration. The detailed functional differences are:

- 1) The attitude maneuver between the delta velocity impulse vector and the entry orientation will vary with the trajectory. Commonality may be achieved by including separate sets of control data or controlling the ACS by a programmable DHS.
- 2) The attitude maneuver at Uranus will follow a different sequence due to the trajectory which places the Sun-probe vector within 4° of the entry orientation spin vector. Commonality may be achieved by including separate sets of control data/ logic or by controlling the ACS with a programmable DHS.
- 3) The sensors at Uranus will require increased optics due to the decreased solar intensity. Furthermore, the field of view and probably the sensitive element configuration will be different for Uranus. Commonality can be achieved by increased optics on the planet sensor and the use of two Sun sensors.

- 4) The probe-dedicated mission requires only a timing logic for spinup. The ACS subsystem for the probe/deflect mission could perform the spinup function for the probe-dedicated mission with appropriate change in control logic as indicated in items 1) and 2).

## 7. Structures Subsystem

Generally speaking, each planetary probe has its own peculiarities affecting the size and/or weight of the total probe configuration. Additionally, the inertia and aerodynamic forces of entry vary from planet to planet and those loads affect the structural weight of a given probe. Since design and fabrication of structures to suit a specific application is an easily accomplished task, it does not really warrant penalizing one probe mission to use structural hardware from another mission. An exception to this is the structural hardware for a probe to enter the planets Saturn and Uranus. For delivery of the same set of scientific instruments to those two planets, the structural hardware can be the same without paying a significant weight penalty. The entry conditions are quite similar as discussed in Chapter VII, Section B.8.

## 8. Propulsion Subsystem

*a. Deflection Motor* - The propulsion requirements to provide the desired delta velocity for entry to the planets Uranus and Saturn are very close; in fact, a common rocket motor providing a delta velocity of 170 m/sec (557 fps) has been selected for the Saturn/Uranus probe. This same motor is not appropriate for the Jupiter probe, unless it proves satisfactory to perform the deflection maneuver further away from the planet Jupiter. (The deflection maneuver radius is inversely proportional to the maneuver delta velocity.) The Saturn/Uranus deflection motor, if used on the Jupiter probe, would produce a deflection velocity of approximately 120 m/sec (390 fps) for the probe. This compares with a desired deflection velocity of 256 m/sec (842 fps) for the Jupiter probe.

*b. Attitude Control Subsystem* - The requirements for attitude control subsystems of the probes investigated are not very different. The amount of propellant for the spin-despin-precess maneuver for the Saturn and Uranus probes is almost identical, and is increased by 40% for the typical Jupiter probe. The amount of propellant for the Saturn/Uranus probe is approximately 1.06 kg (2.33 lbm) as compared to approximately 1.48 kg (3.27 lbm) for Jupiter. Thus, a weight penalty of approximately 0.42 kg (1.0 lbm) for nitrogen gas would be involved in making the system common to all

missions. This translates into a total weight penalty for the Saturn/Uranus probe, including propellant, storage bottle, and heat shield mass fraction penalty, of approximately 1.22 kg (2.7 lbm).

Another approach would be to use a varying number of gas storage bottles. If the bottle size were selected so that two bottles, containing 0.53 kg (1.16 lbm) of nitrogen gas each, were adequate for Saturn/Uranus, then use of three bottles for Jupiter would result in 1.58 kg (3.48 lbm) supply. This is an excess of 0.095 kg (0.21 lbm) of nitrogen gas for Jupiter. The resulting total weight penalty for Jupiter, including propellant, storage bottle, and heat shield mass fraction effects, is 0.32 kg (0.71 lbm).

The remainder of the ACS propulsion system would be common for all probes.

#### 9. Thermal Control Subsystem

The thermal control subsystem defined for the outer planet probe missions was basically the same for all planets investigated. The use of radioisotope heaters, multilayer insulation, and thermal coatings establishes the probe equilibrium temperatures during spacecraft cruise and the independent probe coast phases of the mission. Depending upon the individual probe size and multilayer insulation blanket penetrations, the required amount of radioisotope heater power was determined based on the desired cruise temperature. A cruise temperature safely below the upper battery storage temperature, but a maximum, was desired for all missions.

During coast, the probe temperature is determined by solar energy available and the probe thermal coating. For all missions it was desired to have a probe temperature rise following spacecraft separation. The thermal coating selected for the Jupiter mission (Iridite 14-2) with values of  $\alpha/\epsilon = 0.62/0.13$  allowed a probe temperature increase on the order of 15°K and was considered optimal from a standpoint of the isotope heater power sensitivity to emissivity. Although probe temperature rises are not predicted for Saturn or Uranus, the Jupiter thermal coating is still desirable. Since probe heat losses will increase due to the loss of the environmental cover at separation, the small solar energy available does tend to stabilize the probe coast temperature at Saturn and minimize the drop at Uranus. Lower coating emissivity values, however, would not be recommended.

The thermal design concept for probe descent thermal control is the same for all missions. The use of low density foam insulation is universal to all the probe designs and is required to isolate the probe to some extent from the descent atmospheric environment. The vented probe configuration was also selected for all missions, not from a thermal standpoint, but for improved packaging efficiencies and the savings of structural weight. The thermal design of the descent probe relied on sufficient probe mass and thermal inertia to maintain the probe within acceptable temperature limits during descent.

Some probe missions, particularly Saturn and Uranus, require additional thermal control to offset low entry temperatures and the colder atmosphere encounters possible. For these anticipated cold temperature critical missions, two alternative thermal control concepts were considered. The first was the use of a nitrogen gas bottle to purge the probe early in descent and delay the insulation degradation caused by the predominantly He/H<sub>2</sub> atmospheric gases. A second concept was simply the use of additional battery power to supply heat, electrically, to the batteries themselves during the later portions of the atmospheric descent phase. Of the two alternative improved thermal control concepts, the use of the N<sub>2</sub> gas supply is recommended for the Jupiter probe-dedicated mission and both the Saturn and Uranus missions. In addition, the use of battery power electrical heating is recommended for the more hostile Uranus probe mission.

It must be noted, however, that honest probe design must recognize the large uncertainties associated with probe thermal control. Since little is known as to the exact thermal nature of the planetary atmospheres that will be encountered and actual hardware operation, the reliability of a universal thermal control subsystem should be considered, which would include a limited application of both a nitrogen gas purge system and auxiliary heater power for critical components during all outer planet probe missions.

#### 10. Commonality Summary

There is maximum use of commonality between the Saturn and Uranus probes, as discussed in Chapter VII, Section B. Additional use of commonality among the Jupiter, Saturn, and Uranus probes is tabulated.

Entry Ballistic Coefficient	102 kg/m <sup>2</sup> (0.65 slug/ft <sup>2</sup> )
Initial Descent Coefficient	14 to 19 kg/m <sup>2</sup>
Data Rate	30 bps maximum

Data Storage (except for probe-dedicated mission)	12.4 k bits
Frequency	0.86 GHz
DHS	Identical with a Programmable Sequence
Thermal Control Subsystem	Isotope Heaters, Insulation, and Thermal Coatings
ACS Propulsion (except for probe-dedicated mission)	Identical Except for Quantity of Gas
ACS Electronics	Similar
Descent Time	36 to 48 min